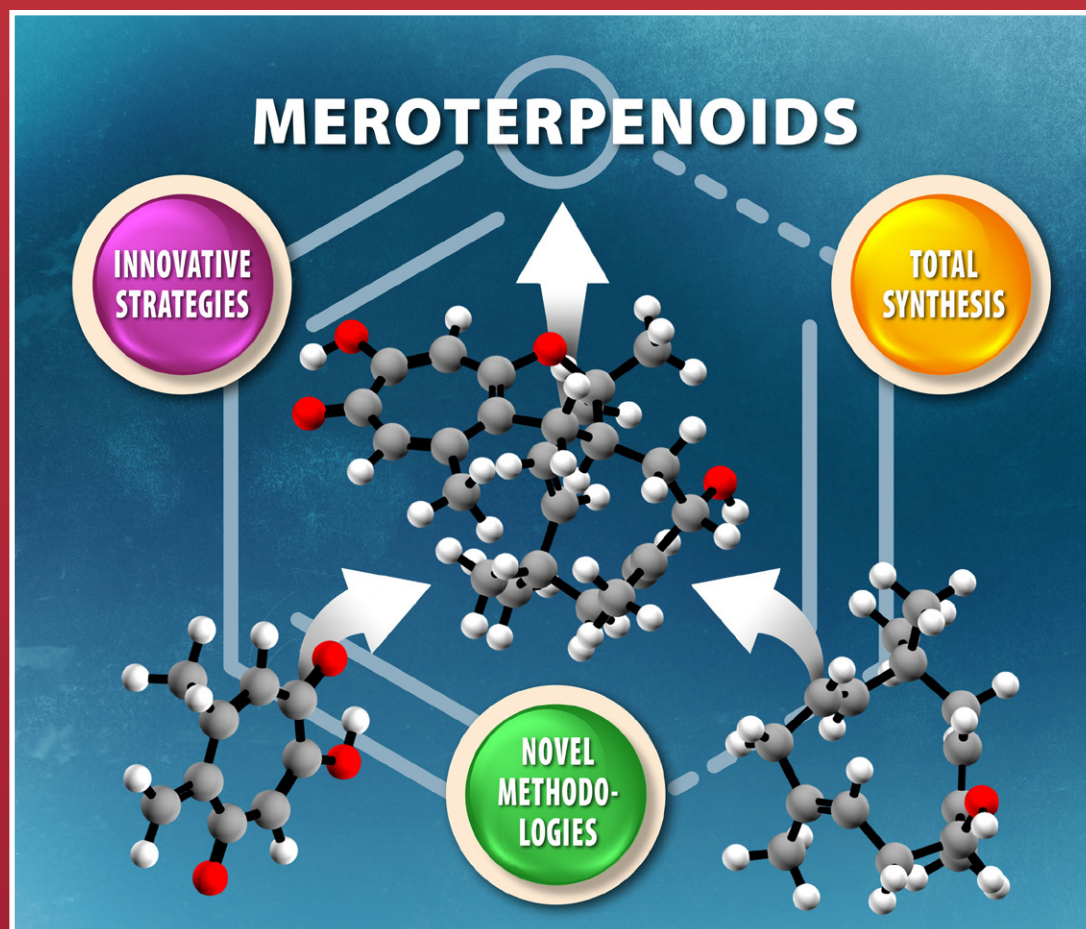




# Acta Chimica Slo Acta Chimica Slo Slovenica Acta C

2



68/2021

---

## EDITOR-IN-CHIEF

**KSENIJA KOGEJ**

University of Ljubljana, Faculty of Chemistry and Chemical Technology, Večna pot 113, SI-1000 Ljubljana, Slovenija  
E-mail: ACSi@fkk.uni-lj.si, Telephone: (+386)-1-479-8538

## ASSOCIATE EDITORS

**Alen Albreht**, National Institute of Chemistry, Slovenia  
**Aleš Berlec**, Jožef Stefan Institute, Slovenia  
**Janez Cerkovnik**, University of Ljubljana, Slovenia  
**Mirela Dragomir**, Jožef Stefan Institute, Slovenia  
**Ksenija Kogej**, University of Ljubljana, Slovenia  
**Krištof Kranjc**, University of Ljubljana, Slovenia

**Matjaž Kristl**, University of Maribor, Slovenia  
**Franč Perdih**, University of Ljubljana, Slovenia  
**Aleš Podgornik**, University of Ljubljana, Slovenia  
**Helena Prosen**, University of Ljubljana, Slovenia  
**Irena Vovk**, National Institute of Chemistry, Slovenia

## ADMINISTRATIVE ASSISTANT

**Marjana Gantar Albreht**, National Institute of Chemistry, Slovenia

---

## EDITORIAL BOARD

**Wolfgang Buchberger**, Johannes Kepler University, Austria  
**Alojz Demšar**, University of Ljubljana, Slovenia  
**Stanislav Gobec**, University of Ljubljana, Slovenia  
**Marko Goličnik**, University of Ljubljana, Slovenia  
**Günter Grampp**, Graz University of Technology, Austria  
**Wojciech Grochala**, University of Warsaw, Poland  
**Danijel Kikelj**, University of Ljubljana  
**Janez Košmrlj**, University of Ljubljana, Slovenia  
**Blaž Likozar**, National Institute of Chemistry, Slovenia  
**Mahesh K. Lakshman**, The City College and  
The City University of New York, USA

**Janez Mavri**, National Institute of Chemistry, Slovenia  
**Friedrich Sreinc**, University of Minnesota, USA  
**Walter Steiner**, Graz University of Technology, Austria  
**Jurij Svete**, University of Ljubljana, Slovenia  
**Ivan Švancara**, University of Pardubice, Czech Republic  
**Jiri Pinkas**, Masaryk University Brno, Czech Republic  
**Gašper Tavčar**, Jožef Stefan Institute, Slovenia  
**Christine Wandrey**, EPFL Lausanne, Switzerland  
**Ennio Zangrando**, University of Trieste, Italy

---

## ADVISORY EDITORIAL BOARD

### Chairman

Branko Stanovnik, Slovenia

### Members

Udo A. Th. Brinkman, The Netherlands  
Attilio Cesaro, Italy  
Vida Hudnik, Slovenia  
Venčeslav Kaučič, Slovenia

Željko Knez, Slovenia  
Radovan Komel, Slovenia  
Stane Pejovnik, Slovenia  
Anton Perdih, Slovenia  
Slavko Pečar, Slovenia  
Andrej Petrič, Slovenia  
Boris Pihlar, Slovenia  
Milan Randić, Des Moines, USA

Jože Škerjanc, Slovenia  
Đurđa Vasić-Rački, Croatia  
Marjan Veber, Slovenia  
Gorazd Vesnaver, Slovenia  
Jure Zupan, Slovenia  
Boris Žemva, Slovenia  
Majda Žigon, Slovenia

---

*Acta Chimica Slovenica* is indexed in: *Academic Search Complete*, *Central & Eastern European Academic Source*, *Chemical Abstracts Plus*, *Chemical Engineering Collection (India)*, *Chemistry Citation Index Expanded*, *Current Contents (Physical, Chemical and Earth Sciences)*, *Digitalna knjižnica Slovenije (dLib.si)*, *DOAJ*, *ISI Alerting Services*, *PubMed*, *Science Citation Index Expanded*, *SciFinder (CAS)*, *Scopus* and *Web of Science*. Impact factor for 2019 is IF = 1.263.



Articles in this journal are published under the  
Creative Commons Attribution 4.0 International License

### Izdaja – Published by:

**SLOVENSKO KEMIJSKO DRUŠTVO – SLOVENIAN CHEMICAL SOCIETY**  
Naslov redakcije in uprave – Address of the Editorial Board and Administration  
Hajdrihova 19, SI-1000 Ljubljana, Slovenija  
Tel.: (+386)-1-476-0252; Fax: (+386)-1-476-0300; E-mail: chem.soc@ki.si

### Izdajanje sofinancirajo – Financially supported by:

National Institute of Chemistry, Ljubljana, Slovenia  
Jožef Stefan Institute, Ljubljana, Slovenia  
Faculty of Chemistry and Chemical Technology, University of Ljubljana, Slovenia  
Faculty of Chemistry and Chemical Engineering, University of Maribor, Slovenia

Slovensko kemijsko društvo  
Slovenian Chemical Society

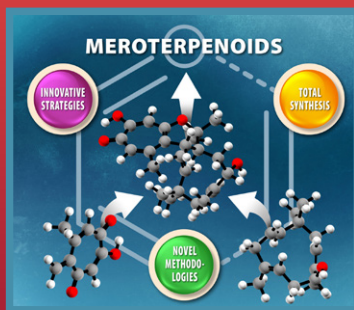


*Acta Chimica Slovenica* izhaja štirikrat letno v elektronski obliki na spletni strani <http://acta.chem-soc.si>. V primeru posvečenih številk izhaja revija tudi v tiskani obliki v omejenem številu izvodov.

*Acta Chimica Slovenica* appears quarterly in electronic form on the web site <http://acta.chem-soc.si>. In case of dedicated issues, a limited number of printed copies are issued as well.

Transakcijski račun: 02053-0013322846 Bank Account No.: SI56020530013322846-Nova Ljubljanska banka d. d., Trg republike 2, SI-1520 Ljubljana, Slovenia, SWIFT Code: LJBA SI 2X

Oblikovanje ovitka – Design cover: KULT, oblikovalski studio, Simon KAJTNA, s. p. Grafična priprava za tisk: OSITO, Laura Jankovič, s.p.

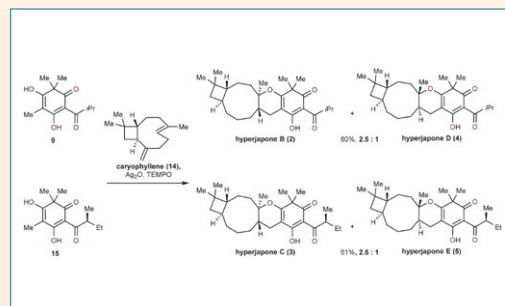


## FEATURE ARTICLE

247–267 Feature Article

### Recent Chemical Methodology Advances in the Total Synthesis of Meroterpenoids

Jan Petrovčič, Chad Nicholas Ungarean and David Sarlah

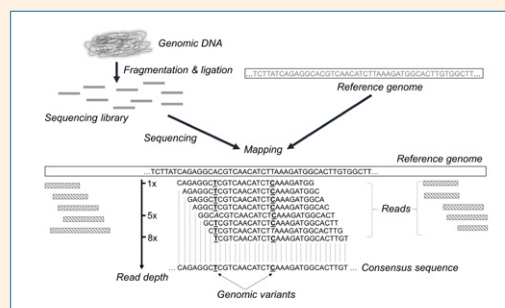


## REVIEW

268–278 Biochemistry and molecular biology

### Sequencing of Nucleic Acids: from the First Human Genome to Next Generation Sequencing in COVID-19 Pandemic

Borut Furlani, Katarina Kouter, Damjana Rozman and Alja Videtič Paska

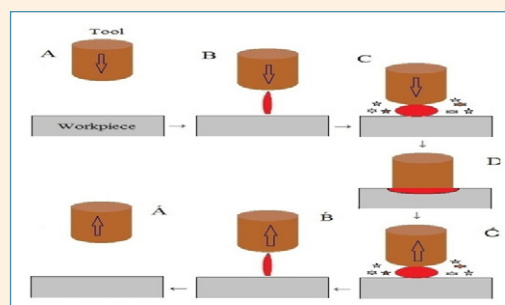


## SCIENTIFIC PAPER

279–288 Materials science

### Study of Electrical Discharge Machining Parameters on Stainless Steel Using Copper Tool Electrode and Its Effect on the Structure and Electrochemical Properties

Mozhgan Karimi, Sayyed Ahmad Nabavi-Amri and Ahmad Soleymanpour

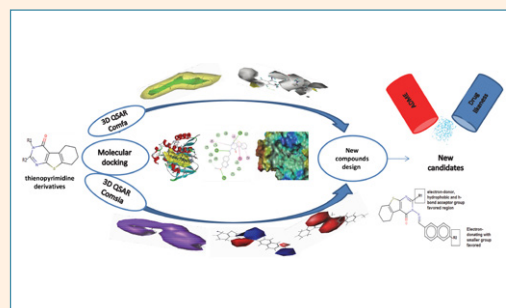


289–303

Chemical, biochemical and environmental engineering

## Combined 3D-QSAR and Molecular Docking Analysis of Thienopyrimidine Derivatives as *Staphylococcus aureus* Inhibitors

Mebarka Ouassaf, Salah Belaidi, Saida Khamouli, Houmam Belaidi and Samir Chtita

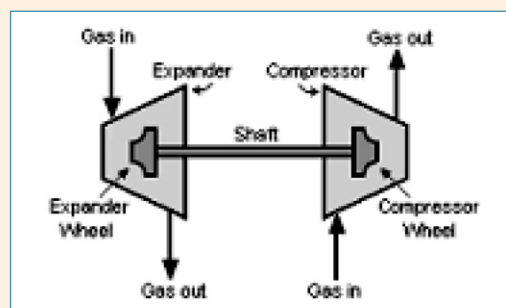


304–312

Chemical, biochemical and environmental engineering

## Exergy Analysis of a Turbo Expander: Modeling and Simulation

Adel El-Husseiny, Rania Farouq, Hassan A. Farag and Yehia El Taweel

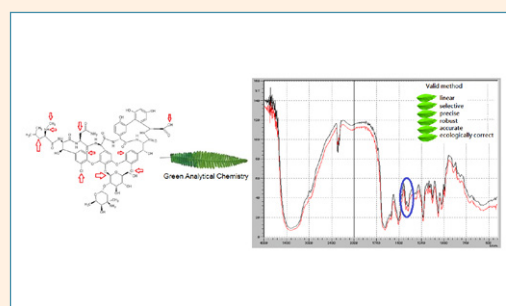


313–319

Analytical chemistry

## A New and Ecological Method to Quantify Vancomycin in Pharmaceutical Product by Infrared Spectrometry

Patrícia Aleixa do Nascimento, Ana Carolina Kogawa and Hérica Regina Nunes Salgado

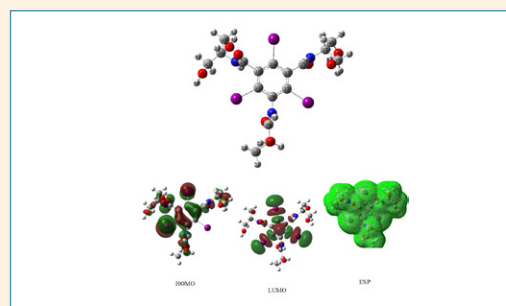


320–331

Inorganic chemistry

## Theoretical B3LYP Study on Electronic Structure of Contrast Agent Iopamidol

Fatma Genç, Sedat Giray Kandemirli and Fatma Kandemirli

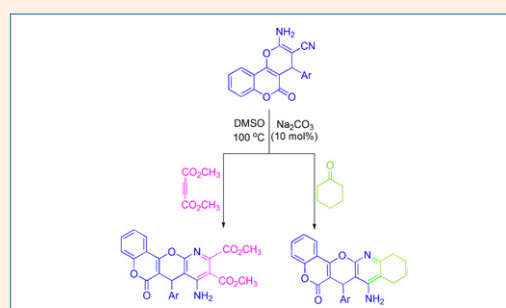


332–340

Organic chemistry

## Efficient and Facile Synthesis of Chromenopyrano[2,3-*b*]pyridine Derivatives Catalyzed by Sodium Carbonate

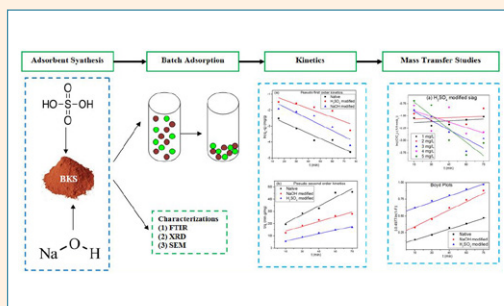
Raziyeh Keshavarz, Mahnaz Farahi and Bahador Karami



341–354 Chemical, biochemical and environmental engineering

## Application of Chemically Modified Industrial Slag to As(III) Adsorption from Wastewater: Kinetics and Mass Transfer Analysis

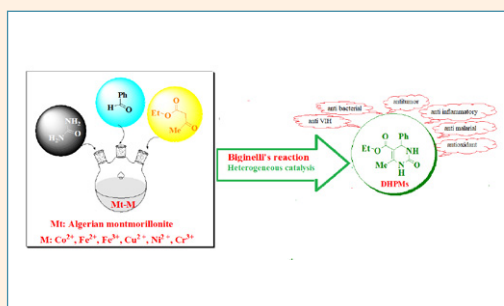
Arijit Dutta Gupta, Vivek Jaiswal, Vivek Bhadauria and Harinder Singh



355–362 Organic chemistry

## Effect of the Exchanged Cation in an Algerian Montmorillonite Used as a Heterogeneous Catalyst for Biginelli Reaction

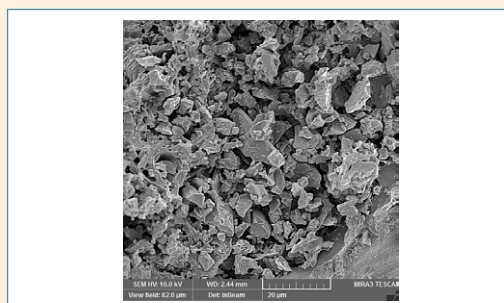
Fatiha Belferdi, Farida Bouremmad, Shalima Shawuti and Mehmet Ali Gulgun



363–373 Chemical, biochemical and environmental engineering

## Methylene Blue Dye Removal from Aqueous Media Using Activated Carbon Prepared by Lotus Leaves: Kinetic, Equilibrium and Thermodynamic Study

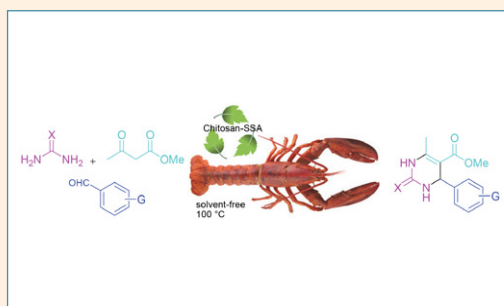
Roya Salahshour, Mehdi Shanbedi and Hossein Esmaeili



374–386 Organic chemistry

## Chitosan-silica Sulfate Nano Hybrid: An Efficient Biopolymer Based-heterogeneous Nano Catalyst for Solvent-free Synthesis of 3,4-Dihydropyrimidine-2(1H)-one/thiones

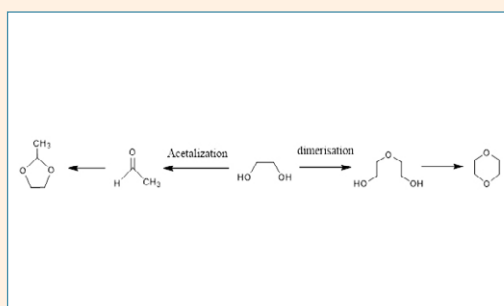
Somayeh Behrouz, Masoome Nazar Abi and Mohammad Amin Piltan



387–394 General chemistry

## Catalysis, Kinetic and Mechanistical Studies for the Transformation of Ethylene Glycol by Alumina and Silica Gel under Autogenous Pressure and Solvent-free Conditions

Taoufik Rohand and Kiyoshi Tanemura

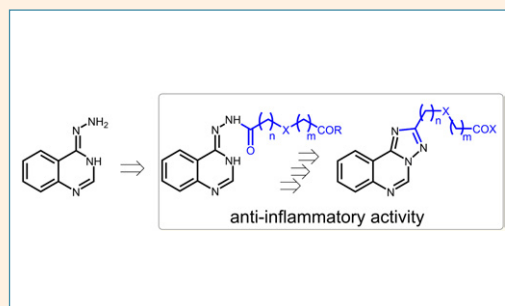


395–403

Organic chemistry

## Quinazoline-containing Hydrazydes of Dicarboxylic Acids and Products of Their Structural Modification: A Novel Class of Anti-inflammatory Agents

Nataliia Krasovska, Viktor Stavytskyi, Inna Nosulenko, Oleksandr Karpenko, Oleksii Voskoboinik, and Serhii Kovalenko

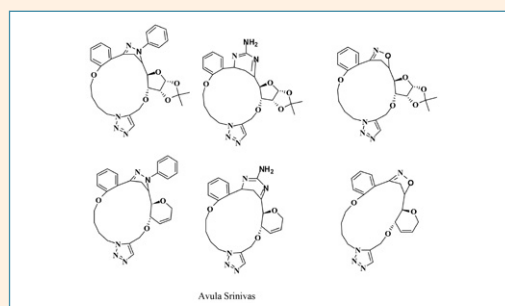


404–413

Organic chemistry

## Synthesis and Anticancer Activity of Triazole Linked Macrocycles and Heterocycles

Avula Srinivas and Enugala Kalyan Rao

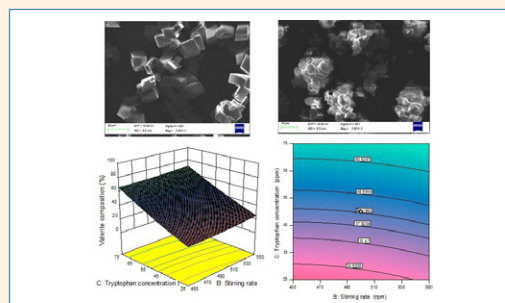


414–425

Chemical, biochemical and environmental engineering

## Effects of Tryptophan on the Polymorphic Transformation of Calcium Carbonate: Central Composite Design, Characterization, Kinetics, and Thermodynamics

Sevgi Polat, Tuba Nur Ozalp-Sendur and Perviz Sayan

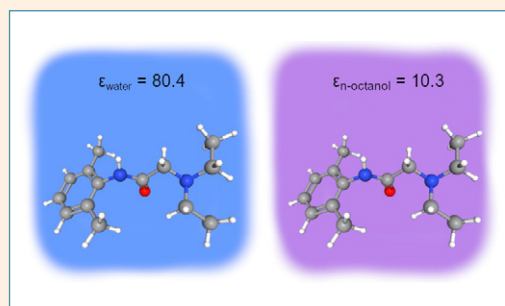


426–432

Biomedical applications

## Local Anesthetics Transfer Across the Membrane: Reproducing Octanol-Water Partition Coefficients by Solvent Reaction Field Methods

Hana Kavcic, Nejc Umek, Domen Pregeljic, Neli Vintar and Janez Mavri

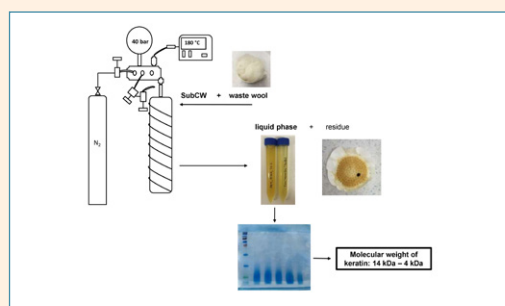


433–440

Chemical, biochemical and environmental engineering

## Isolation of Keratin from Waste Wool Using Hydrothermal Processes

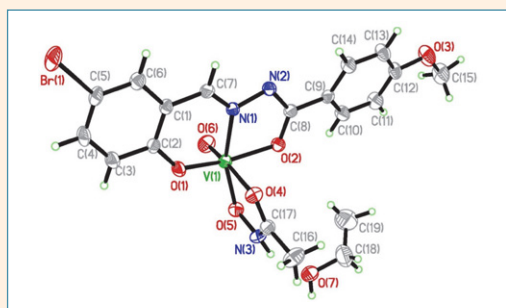
Aleksandra Verdnik, Maja Čolnik, Željko Knez and Mojca Škerget



441–446 Inorganic chemistry

## Synthesis, X-Ray Crystal Structures and Catalytic Epoxidation of Oxidovanadium(V) Complexes with Aroylhydrazone and Ethyl Maltolate Ligands

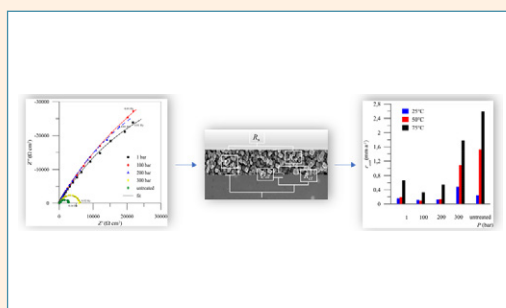
Dong-Hui Zou, Min Liang and Wei Chen



447–457 Materials science

## Impact of High Temperature and Pressure to Steel Passivation in CO<sub>2</sub> Atmosphere

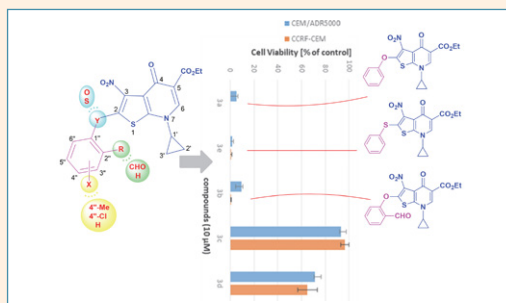
Mojca Slemnik



458–465 Organic chemistry

## Synthesis and Cytotoxicity of Thieno[2,3-*b*]Pyridine Derivatives Toward Sensitive and Multidrug-Resistant Leukemia Cells

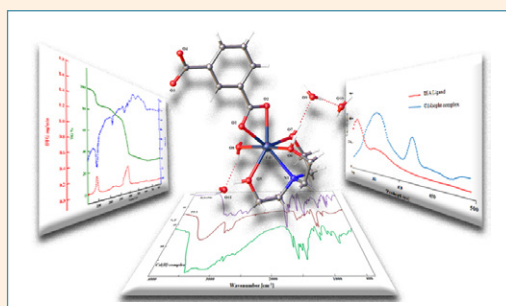
Salah A. Al-Trawneh, Amer H. Tarawneh, Anastassiya V. Gadetskaya, Ean-Jeong Seo, Mohammad R. Al-Ta'ani, Samir A. Al-Taweel and Mustafa M. El-Abadelah



466–474 Inorganic chemistry

## A Novel Cd(II) Isophthalate Complex with Triethanolamine: Crystal Structure, Fluorescence and Antimicrobial Activity

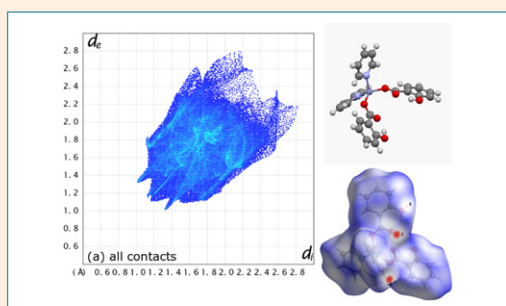
Zuhal Yolcu, Sinem Yurtcan and Meryem Çitlakoglu



475–482 Inorganic chemistry

## New Zinc Coordination Compound with Simple Salicylato and Pyridine Ligands: Synthesis, Crystal Structure and Hirshfeld Surface Analysis

Nives Kitanovski and Marta Počkaj



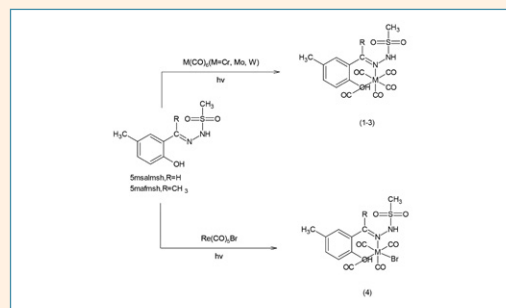
# SHORT COMMUNICATION

483–487

Inorganic chemistry

## Investigation of Photochemical Reactions of some Metal Carbonyls with N'-(2-Hydroxy-6-Methylbenzylidene) Methanesulfonyhydrazide and 5-Methyl-2-Hydroxyacetophenonemethanesulfonylhydrazone

Sema Sert



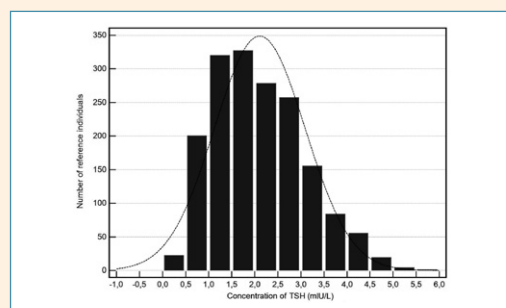
# TECHNICAL PAPERS

488–493

Analytical chemistry

## First Estimation of Reference Intervals for Thyroid-Stimulating Hormone and Thyroid Hormones in Slovenian Population

Adrijana Oblak, Ajda Biček, Edvard Pirnat, Katja Zaletel and Simona Gaberšček

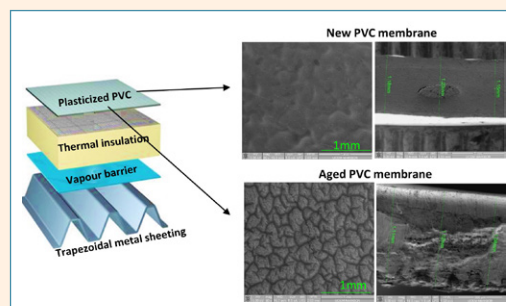


494–504

Materials science

## Degradation of Plasticized Poly(1-chloroethylene) Waterproofing Membranes used as a Building Material

Gregor Kravanja, Andrej Ivanič and Samo Lubej



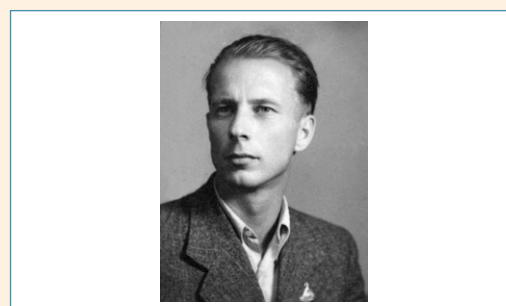
# DRUŠTVENE VESTI

S45–S65

Chemical education

## Boris Krajnc in drugi kemiki na dachauskih procesih

Marko Dolinar





Feature article

# Recent Chemical Methodology Advances in the Total Synthesis of Meroterpenoids

Jan Petrovčič,<sup>2</sup> Chad Nicholas Ungrean<sup>2</sup> and David Sarlah<sup>1,2,\*</sup><sup>1</sup> Roger Adams Laboratory, Department of Chemistry, University of Illinois at Urbana-Champaign, 600 S Mathews Avenue, Champaign, IL 61801, USA<sup>2</sup> Dipartimento di Chimica Organica, Università di Pavia, Via Taramelli 12, 27100 Pavia, Italy\* Corresponding author: E-mail: sarlah@illinois.edu,  
Tel.: (217) 244-9154

Received: 05-07-2021

## Abstract

Heterogeneity of meroterpenoids arising from their dual biosynthetic origins is constantly provoking synthetic chemists to utilize their ingenuity and revise their retrosynthetic logic. By studying recent publications on meroterpenoid synthesis, tremendous advances in the field of synthetic organic chemistry can be witnessed. This feature article covers some of the most intriguing total syntheses and synthetic studies towards the meroterpenoid class of natural products from the last five years.

**Keywords:** Meroterpenoids, total synthesis, natural products, tactics, strategies

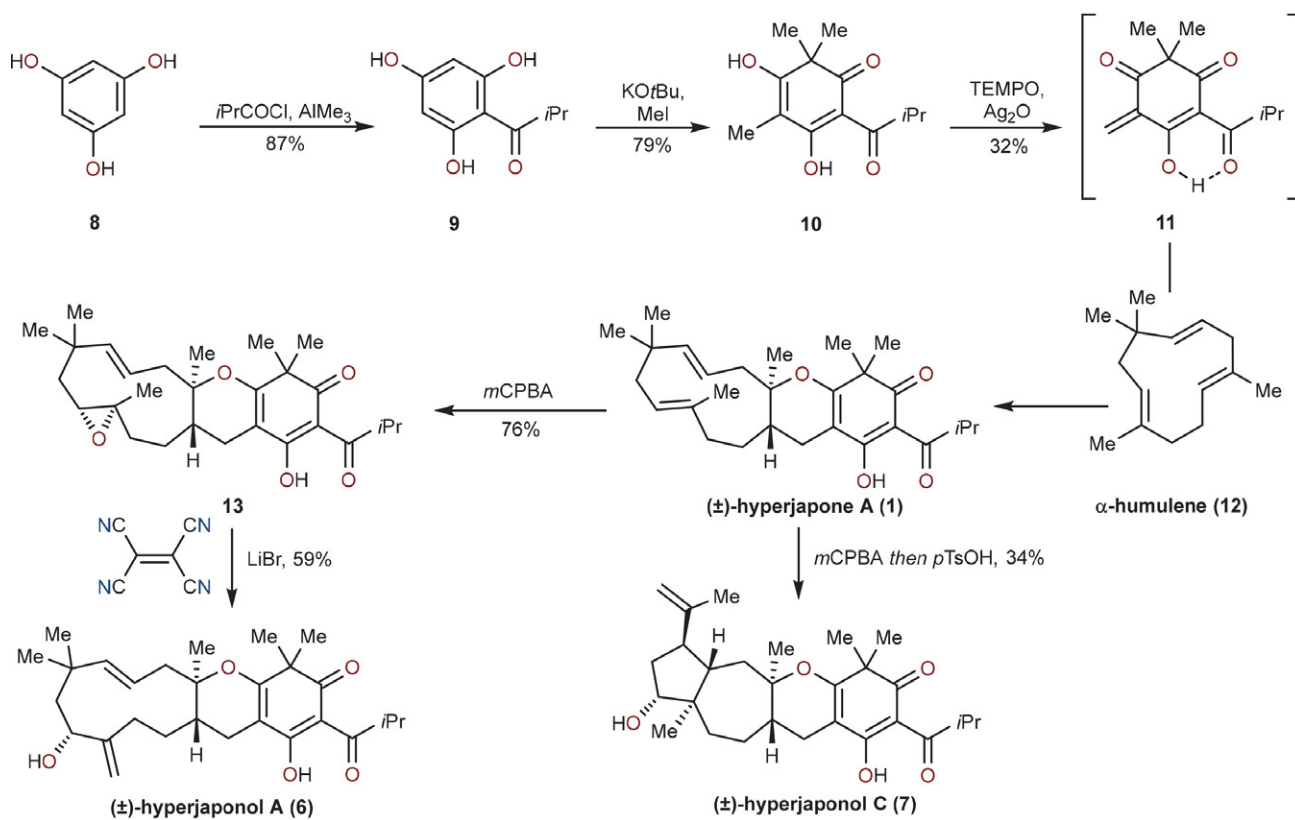
## 1. Introduction

Meroterpenoids represent a family of natural products that originate from the combination of the Greek word *meros*, meaning part, and terpenoids, which are natural isoprene-derived compounds. Their structural diversity stems from their hybrid terpenoid and polyketide biosynthetic roots. Numerous new meroterpenoids are isolated each year from natural sources, which requires the employment and advancement of modern synthetic organic chemistry to effectively obtain sufficient quantities of newly isolated meroterpenoids for more detailed studies. The purpose of this review is to highlight the most efficient modern chemical tools and strategies that have been developed to access different classes of meroterpenoids since 2015. Supplemental and complementary to this work is a vast array of literature covering various aspects of meroterpenoid chemistry. For example, isolation and structure elucidation of fungal meroterpenoids has been reviewed by Geris.<sup>1</sup> The work of Abe<sup>2</sup> describes their biosynthetic origins and work of Kijjoo<sup>3</sup> focuses on their biological properties. A more specific review on biosynthesis as well as chemical synthesis of fungal meroterpenoids breviones has been published by Macías.<sup>4</sup> Additionally, a conceptionally similar survey on meroterpenoids from *Streptomyces* bacteria

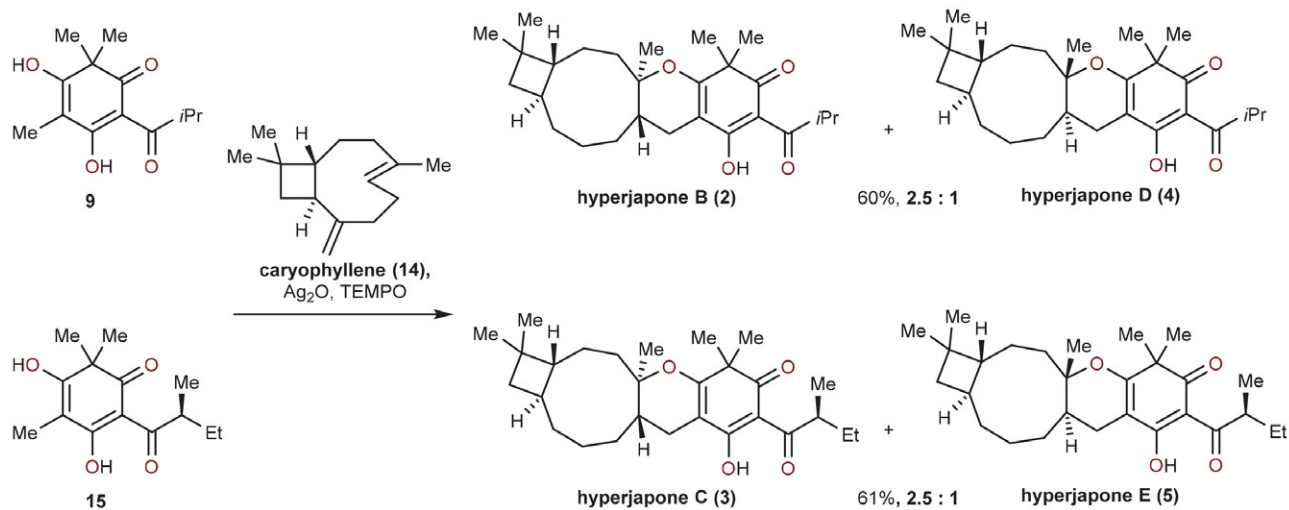
has been disclosed earlier this year jointly by Moore and George.<sup>5</sup> In contrast, other reviews focus exclusively on synthetic efforts toward specific classes of meroterpenoids. Reviews by Ōmura<sup>6</sup> and Gordaliza<sup>7</sup> cover  $\alpha$ -pyrone and quinone/hydroquinone containing meroterpenoids, respectively. Due to the fascination of chemists with certain meroterpenoids like hyperforin (from polyprenylated acylphloroglucinol – PPAP – class), several total syntheses have been published and thoroughly reviewed by Richard.<sup>8</sup> Therefore, the aforementioned topics will be omitted from this feature article.

### 1. 1. George's Total Syntheses of Hyperjaponones (2016)

Meroterpenoids hyperjaponones A–E (1–5), isolated from *Hypericum japonicum*, were prepared in three steps by George's group in 2016 (Schemes 1 and 2).<sup>9</sup> Through subsequent derivatizations they were also able to access to hyperjaponols A (6) and C (7) as well as two other meroterpenoids that have yet to be isolated from natural sources. The synthesis commenced from phloroglucinol (8), which was acylated under classical Friedel–Crafts conditions with isobutyryl chloride to furnish ketone 9. This material was dearomatized through trimethylation with



**Scheme 1.** George's biomimetic total syntheses of (±)-hyperjaponone A (**1**), (±)-hyperjaponols A (**6**) and C (**7**). *m*CPBA = *meta*-chloroperoxybenzoic acid. TEMPO = (2,2,6,6-tetramethylpiperidin-1-yl)oxyl.

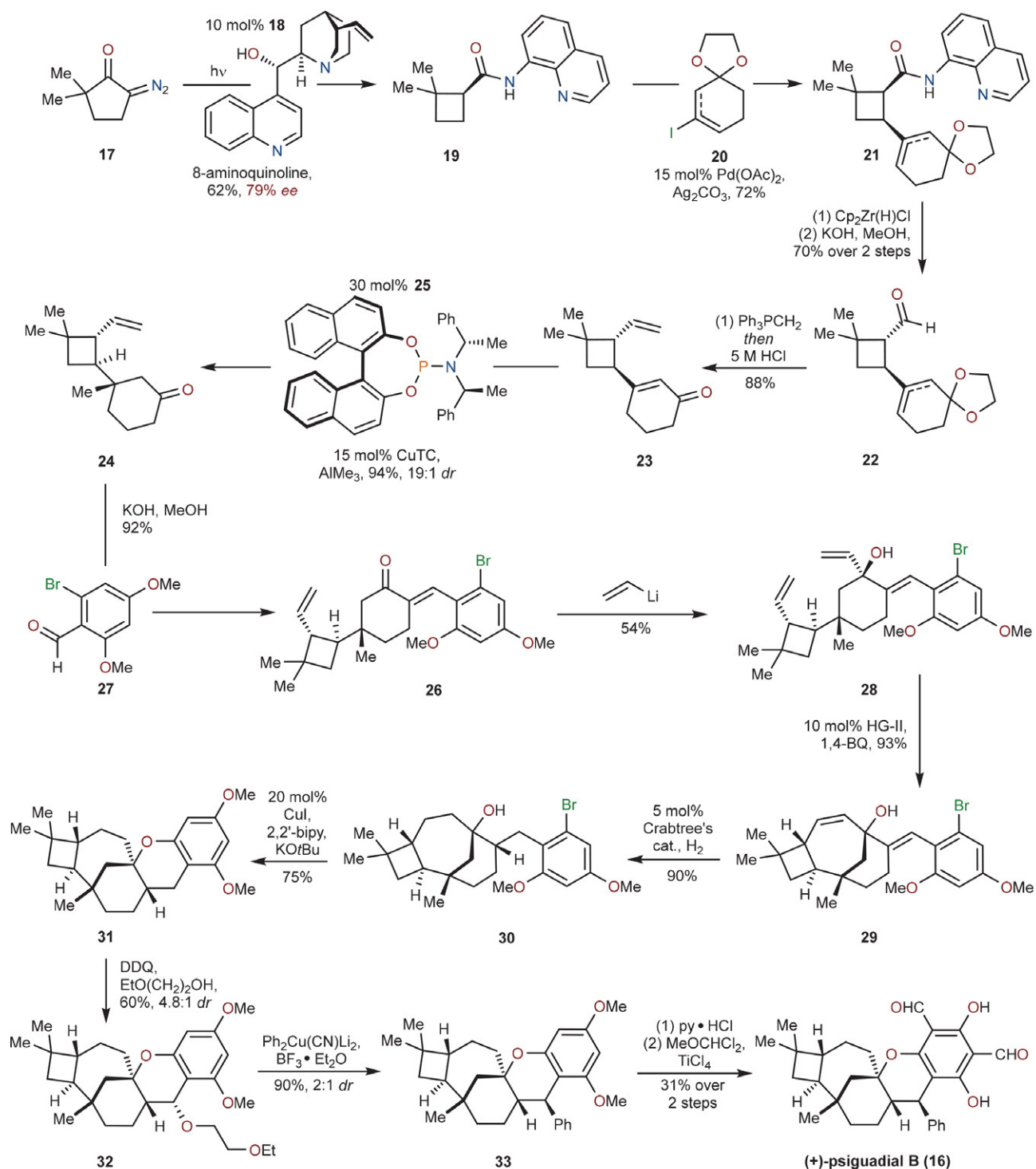


**Scheme 2:** George's biomimetic total syntheses of hyperjaponones B (**2**), C (**3**), D (**4**) and E (**5**). TEMPO = (2,2,6,6-tetramethylpiperidin-1-yl)oxyl.

methyl iodide to **10**; subsequent oxidation with TEMPO and Ag<sub>2</sub>O lead to *in situ* formation of reactive quinone methide **11**, which reacted with α-humulene (**12**) in the same pot to arrive at racemic hyperjaponone A (**1**). This natural compound was divergently taken forward: diastereoselective epoxidation of the trisubstituted olefin with *m*CPBA followed by treatment of the isolable epoxide **13** with ei-

ther tetracyanoethylene π-Lewis acid or *p*-toluenesulfonic Brønsted acid gave racemic hyperjaponols A (**6**) and C (**7**), respectively.

In addition to humulene (**12**), caryophyllene (**14**) was also a competent substrate for the hetero-Diels–Alder key step, ultimately providing a 2.5:1 mixture of hyperjaponones B (**2**) and D (**4**) (Scheme 2). Notably, the same ra-

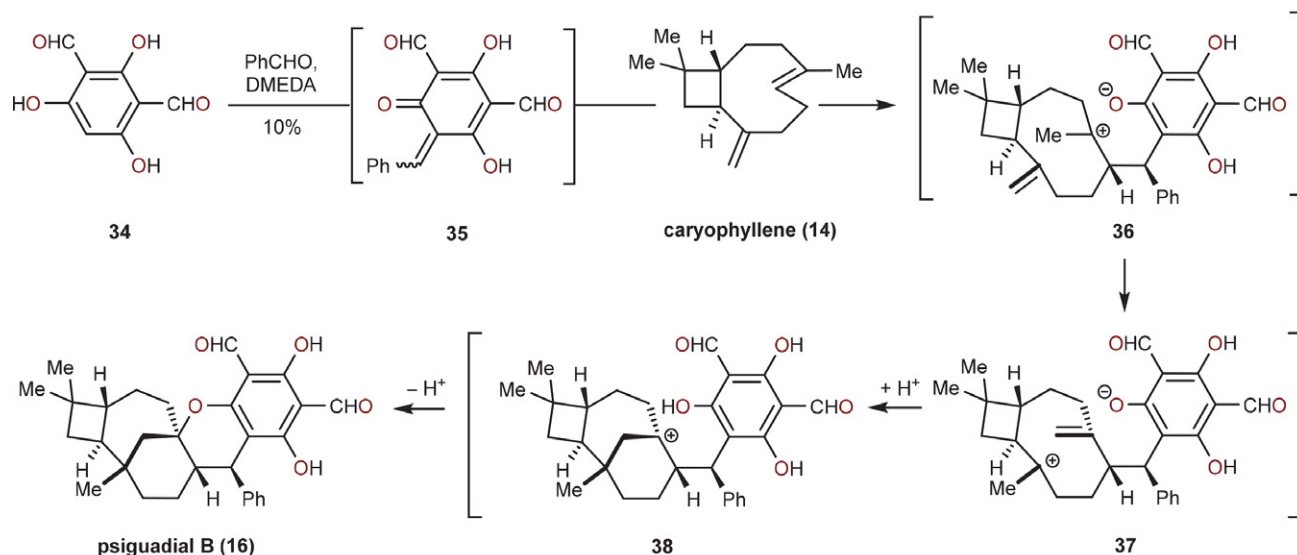


**Scheme 3:** Reisman's enantioselective total synthesis of (+)-psiguadial B (**16**). 2,2'-bipy = 2,2'-bipyridine. Cp = cyclopentadienyl. DDQ = 2,3-dichloro-5,6-dicyano-1,4-benzoquinone. HG = Hoveyda-Grubbs. py = pyridine. TC = thiophene-2-carboxylate.

tio of hyperjapones C (**3**) and E (**5**) was obtained when **15**, derived from *S*-2-methylbutyric acid chloride, was reacted with caryophyllene (**14**) in the presence of TEMPO and Ag<sub>2</sub>O. The authors attributed the observed product ratios to a 3:1 thermodynamic distribution of β $\alpha$  and ββ caryophyllene conformers present in solution.

## 1. 2. Riesman's Total Synthesis of (+)-Psiguadial B (2016)

Plant extracts used in traditional medicine contain a myriad of biologically active compounds with *Psidium guajava* following suit accordingly. Among other compounds,



**Scheme 4:** Cramer's biomimetic total synthesis of psiguadial B (**16**). DMEDA = *N,N'*-dimethylethylenediamine

the meroterpenoid psiguadial B (**16**) was also produced, which was prepared for the first time in its enantiopure form by Reisman's group in 2016 (Scheme 3).<sup>10</sup> To begin the synthesis, the authors recognized  $\alpha$ -diazo-2,2-dimethylcyclopentanone (**17**) as a starting point. It served as a suitable material for the first key step of a photochemical Wolff rearrangement followed by asymmetric ketene trapping. Stereochemical outcome of this transformation with 8-aminoquinoline nucleophile was governed by a chiral (+)-cinchonine (**18**) catalyst. Thereafter, a second key step – palladium catalyzed  $C(sp^3)$ -H alkenylation of intermediate **19** – was executed with 3-iodocyclohex-2-en-1-one derived vinyl iodide **20** as a partner, which provided the *cis*-decorated cyclobutene **21**. The amide directing group was then transformed to the *cis*-aldehyde (not shown) under reductive conditions with  $Cp_2Zr(H)Cl$ , which was isomerized to the thermodynamically more stable *trans*-aldehyde **22** under basic conditions. The addition of methylene triphenylphosphorane to **22** effectively installed the pendant vinyl group, and subsequent ketal deprotection yielded enone **23**. The quaternary stereocenter in **24** was formed with high levels of diastereoselectivity using conjugate addition. A combination of trimethyl aluminum, catalytic amounts of copper thiophene carboxylate and chiral phosphoramidite ligand **25** were invaluable for its success. Conjugated enone **26** was constructed *via* an intermolecular aldol condensation with aromatic aldehyde **27**, and direct 1,2-addition of vinyl lithium gave rise to tertiary allylic alcohol **28**. The latter underwent a subsequent ring closing metathesis catalyzed by Hoveyda–Grubbs second-generation catalyst. Reduction of the two olefins in **29** and consequential installation of an additional stereocenter was accomplished by hydrogenation using Crabtree's catalyst. Tertiary alcohol and aryl bromide moieties in intermediate **30** participated in an intramolecular, copper-catalyzed

*O*-arylation reaction. Benzylic oxidation of **31** and subsequent reaction with ethoxy ethanol gave **32**, which reacted with higher-order cuprate  $Ph_2Cu(CN)Li_2$  in the presence of boron trifluoride etherate to yield **33**. Ultimately, pyridinium hydrochloride mediated demethylation to the penultimate material, which then underwent Rieche formylation, completed the total synthesis of (+)-psiguadial B (**16**).

### 1. 3. Cramer's Total Synthesis of Psiguadial B (2017)

In the year following Reisman's landmark psiguadial B total synthesis, a second total synthesis was disclosed by Cramer's group in which they accomplished a biomimetic, one-pot synthesis (Scheme 4).<sup>11</sup> In a remarkable reaction cascade, they merged commercially available caryophyllene (**14**), benzaldehyde and bisformylphloroglucinol (**34**) fragments to obtain gram quantities of the desired product. Their approach differs from that of Reisman's in the early introduction of two formyl moieties on the arene portion of the cycloaddition partner. Careful reaction optimization revealed that *N,N'*-dimethylaminoethane (DMEDA) in polar yet weakly nucleophilic HFIP sufficiently promoted the anticipated ionic pathway. A clever ozonolysis workup allowed for a simple recrystallization as the only purification needed in the sequence. Ozone selectively oxidized exocyclic double bonds of side products originating from undesired hetero-Diels–Alder reactivity between *ortho*-quinone methide **35** and the trisubstituted olefin in **14**. Additionally, calculations provided an insight into the intriguing mechanism of the aforementioned ionic cascade: it is proposed that initially formed mixture of *ortho*-quinone methides **35** undergoes Michael addition with caryophyllene (**14**). Proton transfer of tertiary carbocation **36** into intermediate **37** enabled a cationic cycliza-

tion to give **38**. The final six-membered ring of the natural product was forged by an intramolecular phenol trapping.

#### 1. 4. Maimone's Total Synthesis of Berkeleyone A (2016)

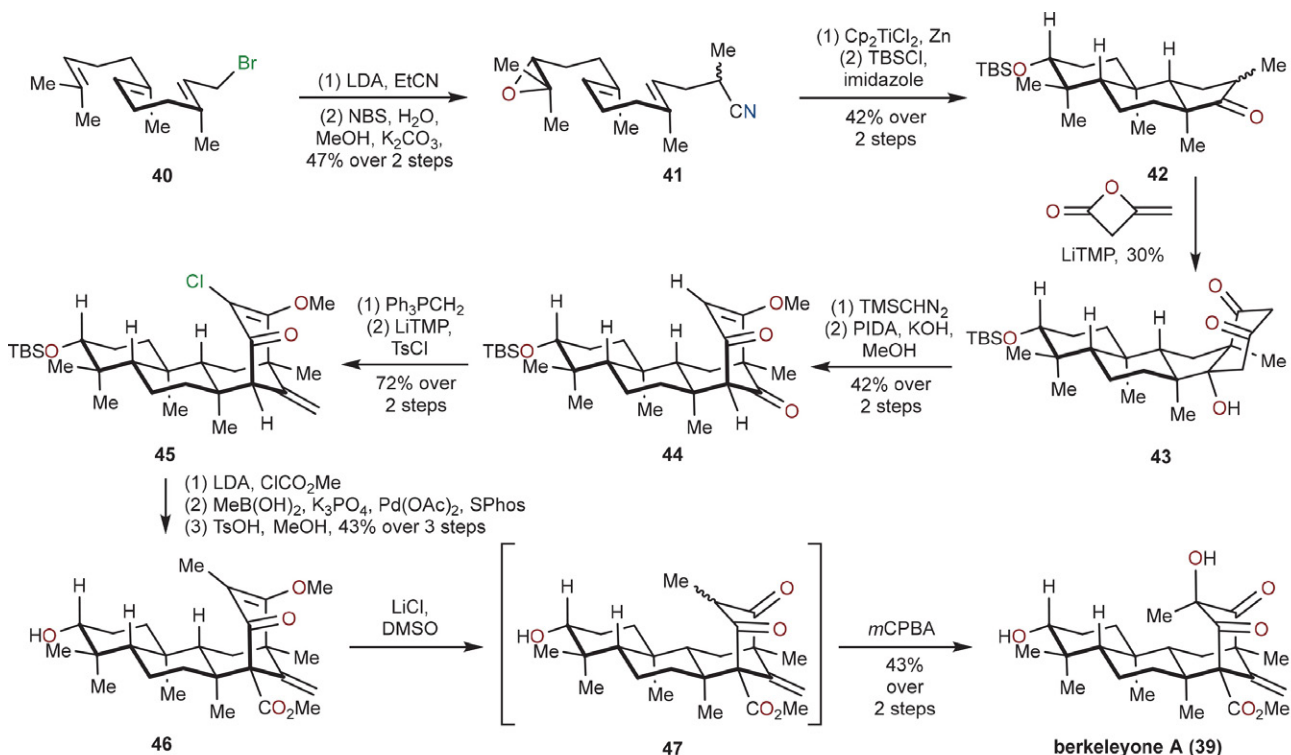
Isolated from extremophilic fungi of the infamous Berkeley Pit lake, berkeleyone A (**39**) is a meroterpenoid with a highly decorated bicyclo[3.3.1]nonane core. Besides its appealing structure, interest in this compound stems from its caspase-1 inhibitory activity as well as its potential to serve as a lead compound for further structure-function studies. To date, two groups have undertaken and completed this formidable synthetic challenge, both in 13 steps and racemic fashion.

The first synthesis of berkeleyone A (**39**) was completed by Maimone's group (Scheme 5).<sup>12</sup> Farnesyl bromide (**40**) was selected as a commercially available starting material, and was used for *C*-alkylation of propionitrile anion. The terminal alkene in alkylated propionitrile (not shown) was then epoxidized *via* a two-step, one-pot bromohydrin formation and subsequent oxirane closing. Treatment of epoxide **41** with titanocene dichloride and zinc triggered a radical polyene cyclization with the nitrile terminating group. The former transformed to an imine which was hydrolyzed during following workup. Secondary alcohol from epoxide opening was silylated with TB-

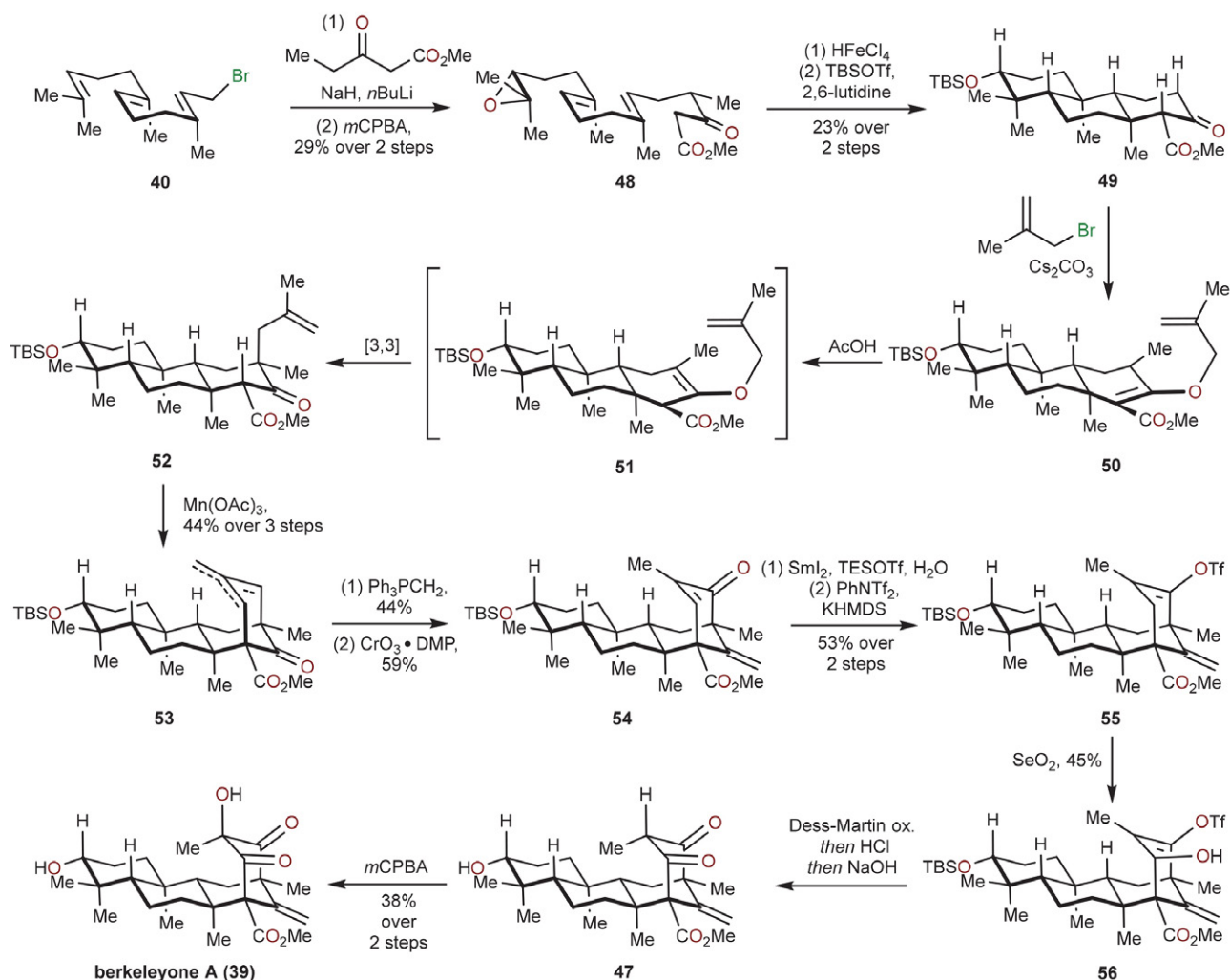
SCl and imidazole. A higher oxidation state variation of the Robinson annulation reaction was performed on the lithium enolate of **42** with diketene to forge the final requisite six-membered ring, notably with high levels of diastereoselectivity. This key step is a testimony to the practicality of the aforementioned methodology that was developed by the same group for the total synthesis of hyperforin.<sup>13</sup> The 1,3-diketone motif in **43** was then chemoselectively *O*-methylated using TMS-diazomethane, and subsequent oxidative ring expansion was induced with PIDA under basic conditions to furnish the core (**44**) of berkeleyone A. Olefination under classical Wittig conditions was followed by chlorination with LiTMP and TsCl. A challenging bridgehead deprotonation with LiTMP enabled acylation with methyl chloroformate. The installed chlorine in **45** was leveraged for Suzuki coupling to introduce the methyl group with silyl deprotection yielding **46**. Krapcho-type demethylation in the presence of a methyl ester gave the penultimate precursor **47** to berkeleyone A, which was immediately oxidized with *m*CPBA to furnish the desired natural product.

#### 1. 5. Newhouse's Total Synthesis of Berkeleyone A (2017)

The Newhouse group took a similar polyene cyclization approach for construction of berkeleyone A (**39**)



**Scheme 5:** Maimone's total synthesis of berkeleyone A (**39**). Cp = cyclopentadienyl. DMSO = dimethylsulfoxide. LDA = lithium diisopropylamide. *m*CPBA = *meta*-chloroperoxybenzoic acid. NBS = *N*-bromosuccinimide. PIDA = phenyliodine(III) diacetate. SPhos = 2-dicyclohexylphosphino-2',6'-dimethoxybiphenyl. TBS = *tert*-butyldimethylsilyl. TMP = tetramethylpiperidide. TMS = trimethylsilyl. Ts = tosyl.



**Scheme 6:** Newhouse's total synthesis of berkeleyone A (**39**). Ac = acetyl. DMP = 3,5-dimethylpyrazole. *mCPBA* = *meta*-chloroperoxybenzoic acid. TBS = *tert*-butyldimethylsilyl. Tf = triflyl.

(Scheme 6).<sup>14</sup> Their synthetic sequence also commenced with farnesyl bromide (**40**), which was used to alkylate methyl 3-oxopentanoate dianion. Chemoselective epoxidation using *mCPBA* in the presence of two other trisubstituted alkenes and  $\beta$ -ketoester moiety yielded terminal epoxide **48**. Using this compound, they showcased the first example of epoxide initiated,  $\beta$ -ketoester terminated, polar polyene cyclization with  $\text{HFeCl}_4$  acting as a Brønsted acid. The cyclized product **49** was treated with 3-bromo-2-methylpropene in the presence of cesium carbonate. Acetic acid solution of *O*-allylated **50** was heated to 120 °C. [3,3]-Claisen rearrangement of intermediate **51** with transposed exocyclic double bond provided the key *C*-allylated intermediate **52** for the manganese-mediated SET oxidation and subsequent radical cyclization onto the pendant 1,1-disubstituted double bond. The mixture of alkene isomers **53** (unified structure shown) reacted with methylene triphenylphosphorane in a Wittig olefination reaction. Allylic oxidation of the newly formed endocyclic methylene groups was achieved using Corey's procedure with

chromium trioxide 3,5-dimethylpyrazole complex ( $\text{CrO}_3\text{-DMP}$ ). The resulting enone **54** was reduced in a 1,4-fashion using  $\text{SmI}_2$  and *in situ* formed triflic acid, which is a complementary approach to more traditional methodologies. The authors demonstrated the feasibility of allylic oxidation of vinyl triflates, as **55** was successfully oxidized to **56**. The 1,3-diketone moiety in **47** was revealed following Dess–Martin periodinane (DMP) oxidation and hydrolysis of the vinyl triflate. Oxidation of **47** with *mCPBA* completed the total synthesis of berkeleyone A (**39**).

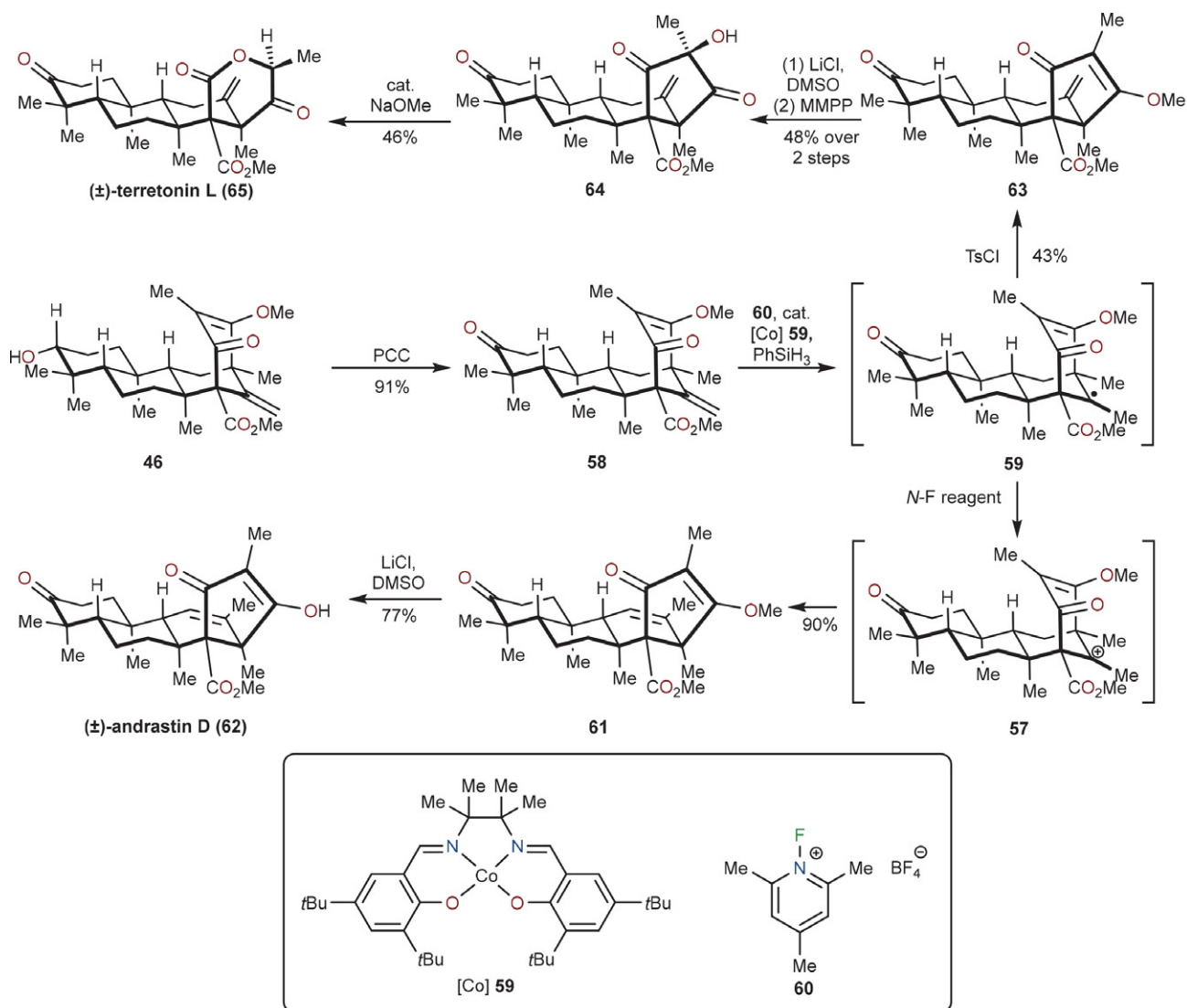
## 1. 6. Newhouse's and Maimone's Syntheses of Terretonin L and Andrastin D (2017)

Having individually completed the total syntheses of berkeleyone A (**39**), the Newhouse and Maimone groups collaborated to further explore the chemistry of natural products containing the berkeleyone framework. Their goal was to access members of the andrastin and terretonin classes of meroterpenoids (Scheme 7).<sup>15</sup> They envi-

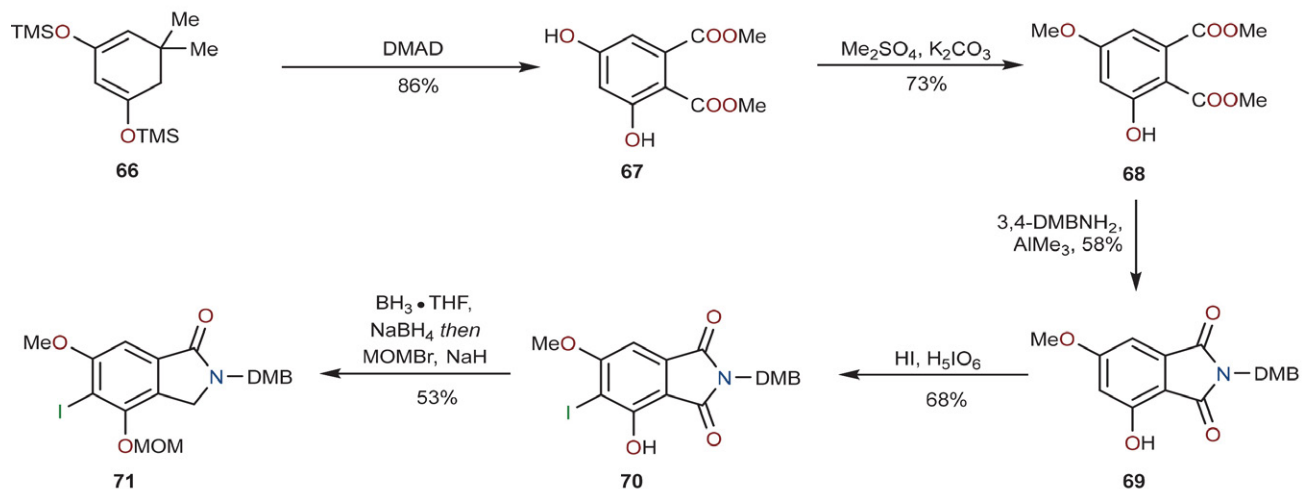
sioned that carbocation **57** would serve as a key intermediate and would give rise to the andrastin and terretinin skeletons. Experimentally, it was shown that the carbocation **57** had to be generated from **58** *via* oxidation of the corresponding tertiary radical **59**. Simple protonation of exocyclic double bond with various Brønsted acids was not feasible for achieving the same goal. Starting from the antepenultimate intermediate **46** (used in Maimone's synthesis of berkeleyone A) PCC oxidation gave compound **58**. This key intermediate required oxidation to arrive at the aforementioned carbocationic species. Inspiration for this transformation came from an alkene hydroalkoxylation methodology developed by Shigehisa. It allows for a variety of unactivated mono-, di- and trisubstituted alkenes to be hydroalkoxylated with primary, secondary, tertiary, or benzylic alcohols in a Markovnikov fashion.<sup>16</sup> Gratifyingly, treatment with catalytic cobalt(II) salen-type complex **59** and phenylsilane in the presence of

*N*-fluoro-2,4,6-trimethylpyridinium tetrafluoroborate (**60**) formed the desired intermediate **57** *in situ*, which rearranged to **61**. Subsequent Krapcho-type demethylation gave racemic andrastin D (**62**).

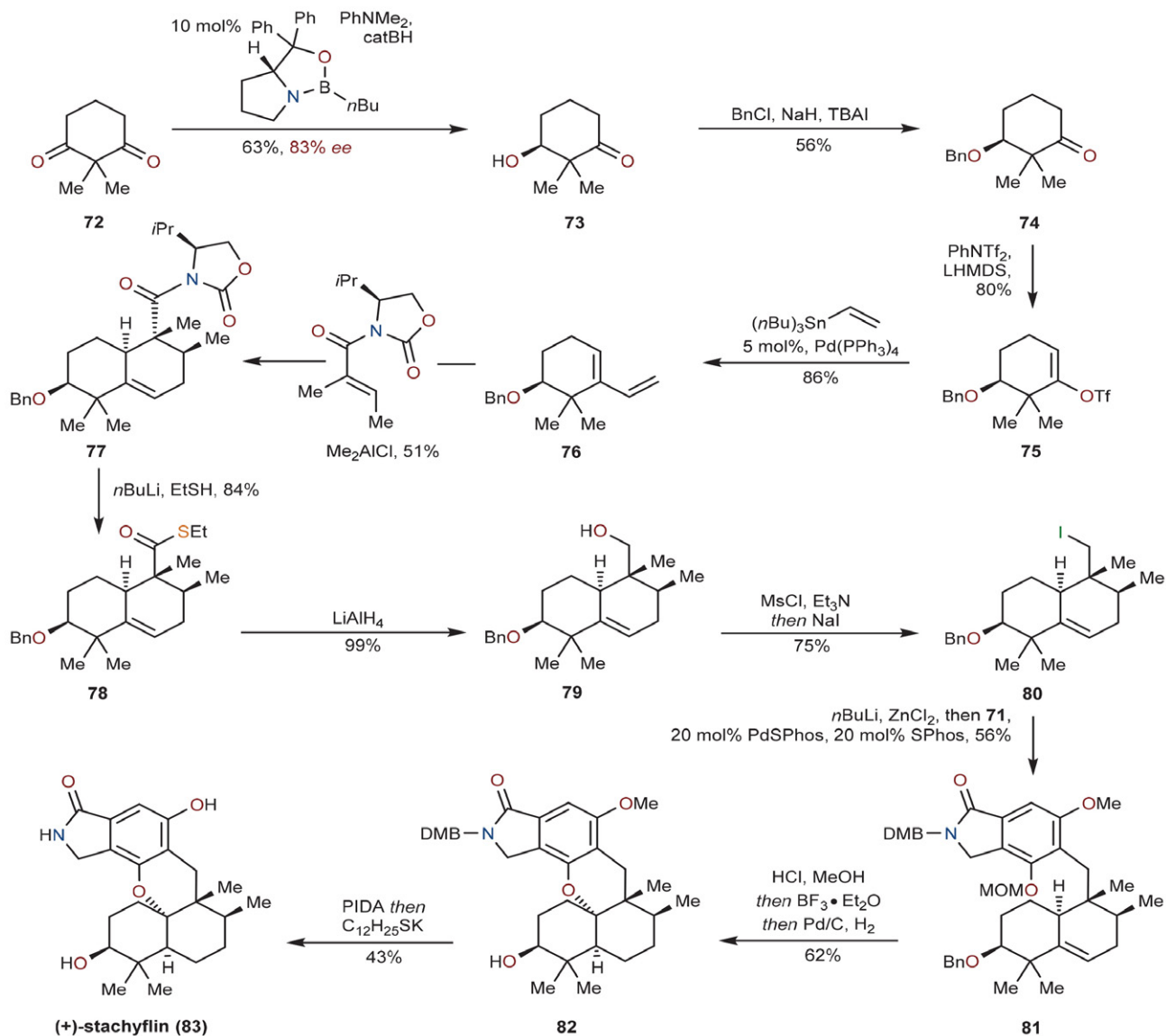
While **63** could be observed in reaction mixtures during the optimization of transformation from **58** to **61**, further screening was required to favor its formation. This observation is consistent with computational results indicating the exocyclic alkene to be less thermodynamically favored in comparison with the endocyclic isomer. Stemming from Carreira's work with radical hydrochlorination, employment of tosyl chloride proved to be crucial in altering the selectivity towards **63**.<sup>17</sup> After the *in situ* formation of the same radical **59** and a homoallyl-type rearrangement, hydrogen atom abstraction from the more sterically accessible methyl group gave rise to **63**. Subsequent Krapcho-type demethylation and magnesium monoperoxyphthalate (MMPP) oxidation yielded the penultimate pre-



**Scheme 7:** Newhouse's and Maimone's racemic total syntheses of terretinin L (**65**) and andrastin D (**62**). DMSO = dimethyl sulfoxide. MMPP = magnesium monoperoxyphthalate. PCC = pyridinium chlorochromate(VI).



**Scheme 8:** Magauer's synthesis of coupling partner 71. DMAD = dimethyl acetylenedicarboxylate. DMB = 3,4-dimethoxybenzyl. MOM = methoxymethyl.



**Scheme 9:** Magauer's asymmetric total synthesis of (+)-stachyflin (83). Bn = benzyl. cat = catechol. Ms = mesyl. PIDA = phenyliodine(III) diacetate. Sphos = 2-dicyclohexylphosphino-2,6'-dimethoxybiphenyl. TBAI = tetrabutylammonium iodide.



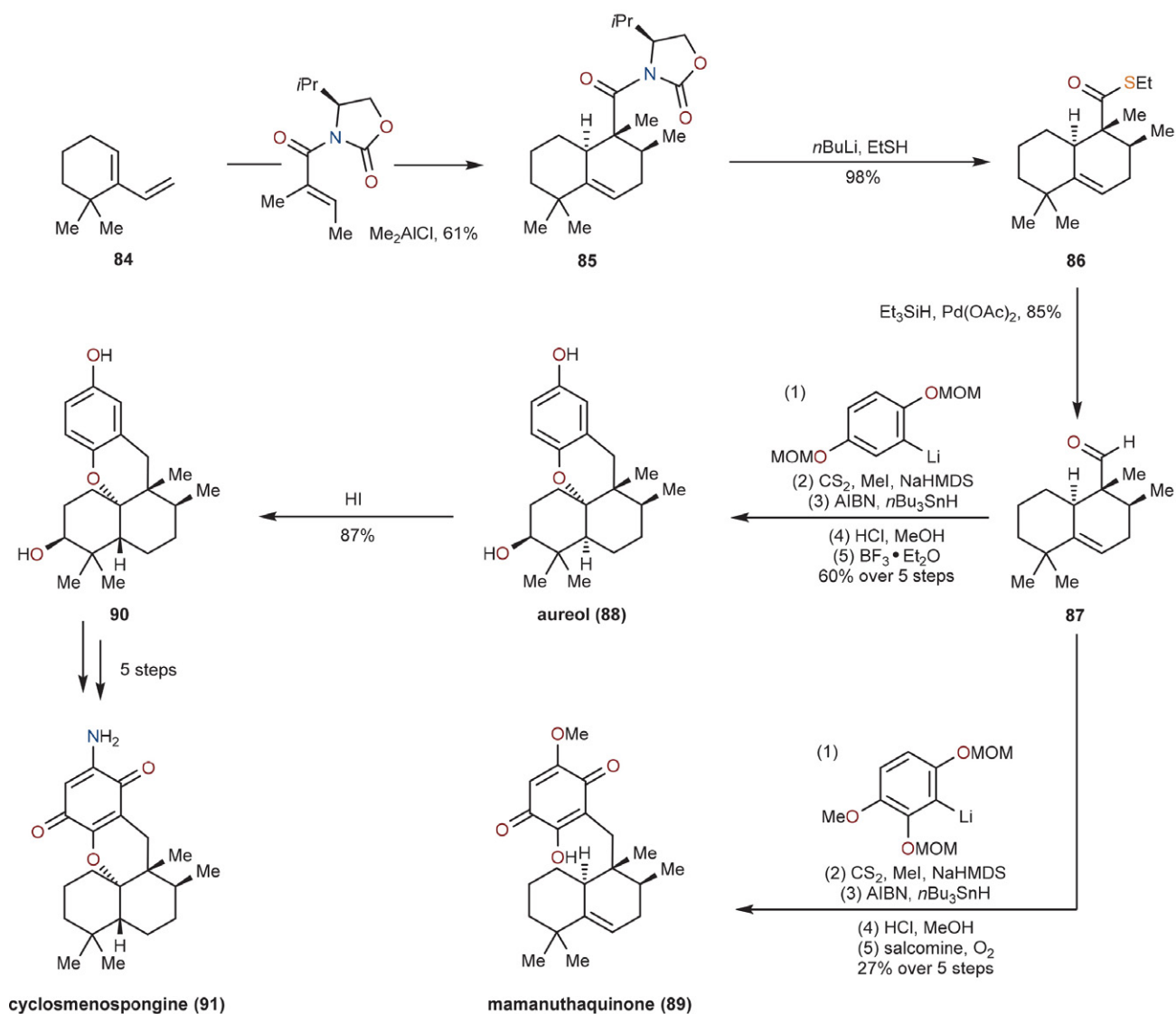
cursor **64**. Treatment with catalytic amounts of sodium methoxide induced a retro-Claisen/esterification cascade and completed the synthesis of racemic terretonin L (**65**).

### 1. 7. Magauer's Total Synthesis of (+)-Stachyflin (2017)

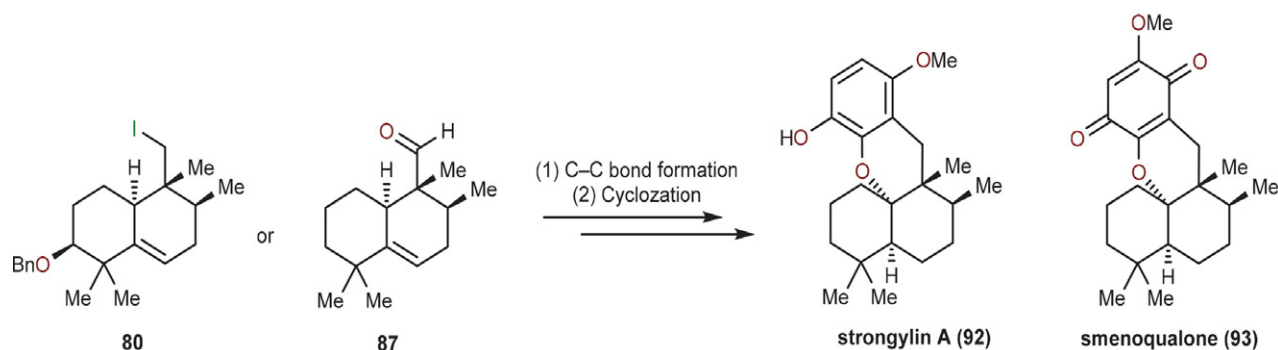
Six natural and 15 unnatural tetracyclic meroterpenoids were prepared in a single study by Thomas Magauer's group in late 2017.<sup>18</sup> All these natural products were derived from simple precursors such as dimedone, cyclohexanone or cyclohexa-1,3-dione in an asymmetric, modular fashion. Their synthetic approach enabled access to a library of compounds of which thorough biological screening was performed and ultimately demonstrated the potential for improving the potency of natural products. Dime-

done *bis*-silyl enol ether **66** was reacted with DMAD in an Alder–Rickert reaction. Expulsion of isobutene and concomitant silyl deprotection delivered resorcinol derivative **67** (Scheme 8). Methylation with dimethyl sulfate controllably formed **68**, which was followed by AlMe<sub>3</sub>-mediated imide formation with 3,4-dimethoxybenzyl amine (3,4-DMBNH<sub>2</sub>). Treatment of imide **69** with a mixture of hydroiodic and periodic acid resulted in electrophilic iodination of the phenol moiety. Finally, aryl iodide **70** was regioselectively reduced, and the remaining free phenol was MOM protected to yield the first coupling fragment **71**.

The second coupling fragment was prepared in the following manner (Scheme 9). First, 2,2-dimethylcyclohexa-1,3-dione (**72**) underwent enantioselective CBS reduction. The secondary hydroxyl group in **73** was benzylated, and the ketone **74** was transformed into vinyl



**Scheme 10:** Magauer's asymmetric total syntheses of aureol (**88**), cyclosmenospongine (**91**) and mamanuthaquinone (**89**). AIBN = azobisisobutyronitrile. HMDS = hexamethyldisilazane. MOM = metoxymethyl.



**Scheme 11:** Magauer's asymmetric total synthesis of stronglylin A (**92**) and smenoqualone (**93**)

triflate **75**. Stille coupling was utilized to prepare diene **76**, which was later employed in a remarkable auxiliary controlled *exo*-selective Diels–Alder reaction to give **77**. Evans valine-derived auxiliary was removed with *in situ* formed lithium ethanethiolate and the resulting thioester **78** was reduced with lithium aluminum hydride to the primary alcohol **79**. Next, the iodide **80**, obtained *via* a mesylation and substitution, underwent lithium halogen exchange. Transmetalation with  $\text{ZnCl}_2$  gave Negishi coupling partner, which in the presence of PdSPhos underwent unification with aryl iodide **71** to give **81**. Deprotection of the MOM group under acidic conditions enabled  $\text{BF}_3 \cdot \text{Et}_2\text{O}$ -mediated cyclization, and hydrogenolysis of benzyl group gave **82**. Two deprotection steps effectively revealed the free lactam and phenol motifs and completed the asymmetric total synthesis of (+)-stachylin (**83**).

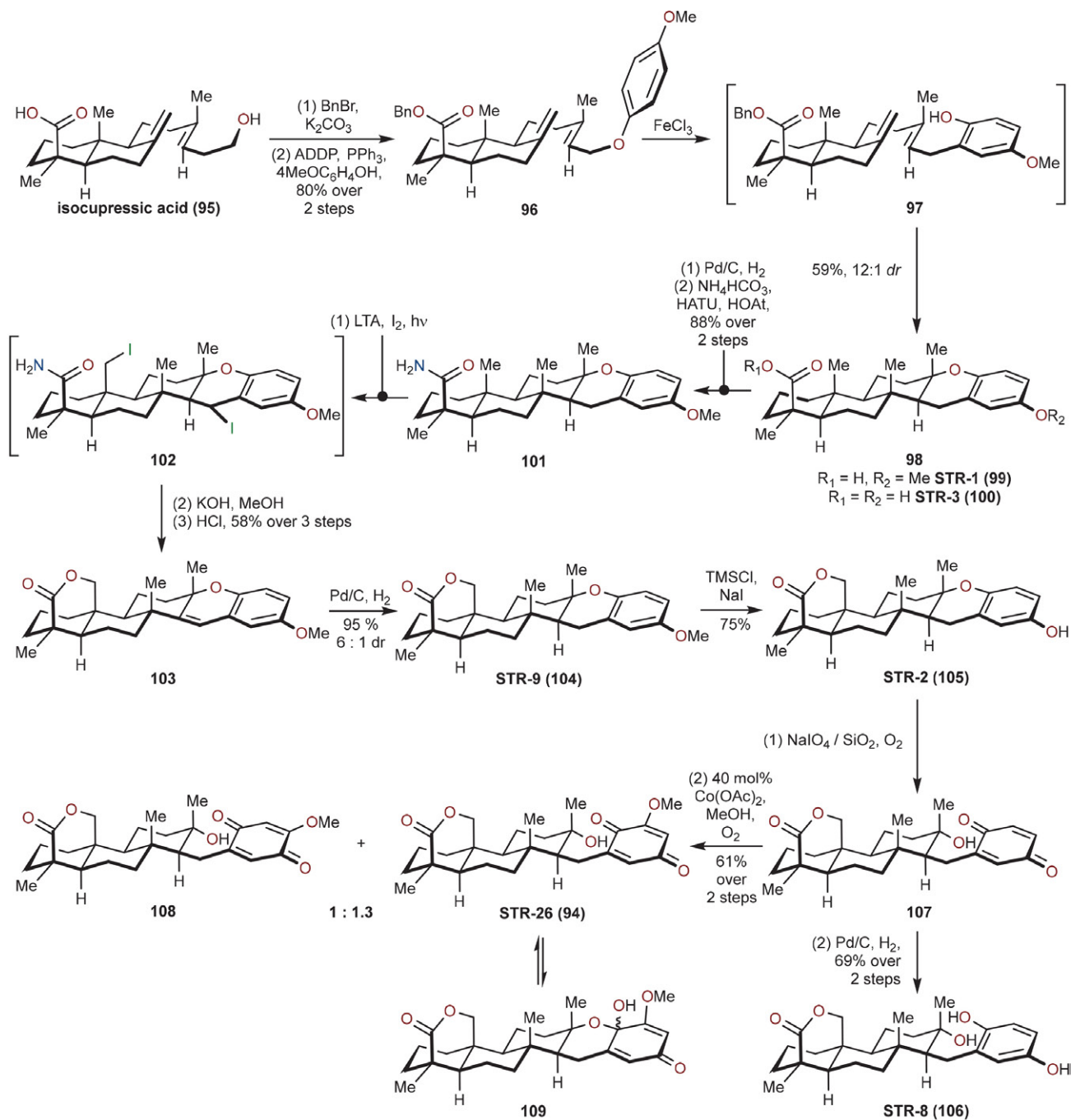
Three additional natural products were analogously made from diene **84** in which the benzyloxy group was absent (Scheme 10). A similar Diels–Alder reaction gave cycloadduct **85** and removal of the chiral auxiliary yielded the thioester **86**; this was converted into the corresponding aldehyde **87** *via* Fukuyama reduction. The 1,2-addition of two different aryllithiums was followed by Barton–McCombie radical deoxygenation and MOM deprotection.  $\text{BF}_3 \cdot \text{Et}_2\text{O}$ -mediated cyclization under kinetic control gave aureol (**88**) and hydroquinone oxidation gave mamanuthaquine (**89**), respectively. The *cis*-fused decalin core of aureol (**88**) could be isomerized into the thermodynamically more favored *trans*-decalin core of **90** using hydroiodic acid. The same group also showed that *trans*-decalin **90** could be transformed into cyclospenone (**91**) in five steps.<sup>19</sup>

Intermediates **80** and **87** proved to be extremely versatile since C–C bond forming reactions, either through Negishi coupling or 1,2-addition of aryllithiums, provided precursors for similar cyclization reactions. These ultimately gave rise to stronglylin A (**92**), smenoqualone (**93**) and 15 other unnatural tetracyclic meroterpenoids with either *cis*- or *trans*-decalin systems (Scheme 11).

## 1. 8. Poulsen's Syntheses of Stronglyphorines (2018)

In a related pair of publications, Poulsen's group disclosed divergent syntheses of seven natural products from the stronglyphorine family of meroterpenoids (Scheme 12).<sup>20,21</sup> The carbon skeleton of this class of bioactive compounds was accessed through a unique iron(III) mediated rearrangement/cyclization cascade and  $\text{C}(\text{sp}^3)\text{-H}$   $\delta$ -lactonization. Development of a novel, catalytic, oxidative quinone heterofunctionalization method was necessary for the completion of the total synthesis of the STR-26 (**94**). Isocupressic acid (**95**) served as a gateway to stronglyphorines; this starting material was isolated from the bark and needles of the *Ponderosa* pine tree.

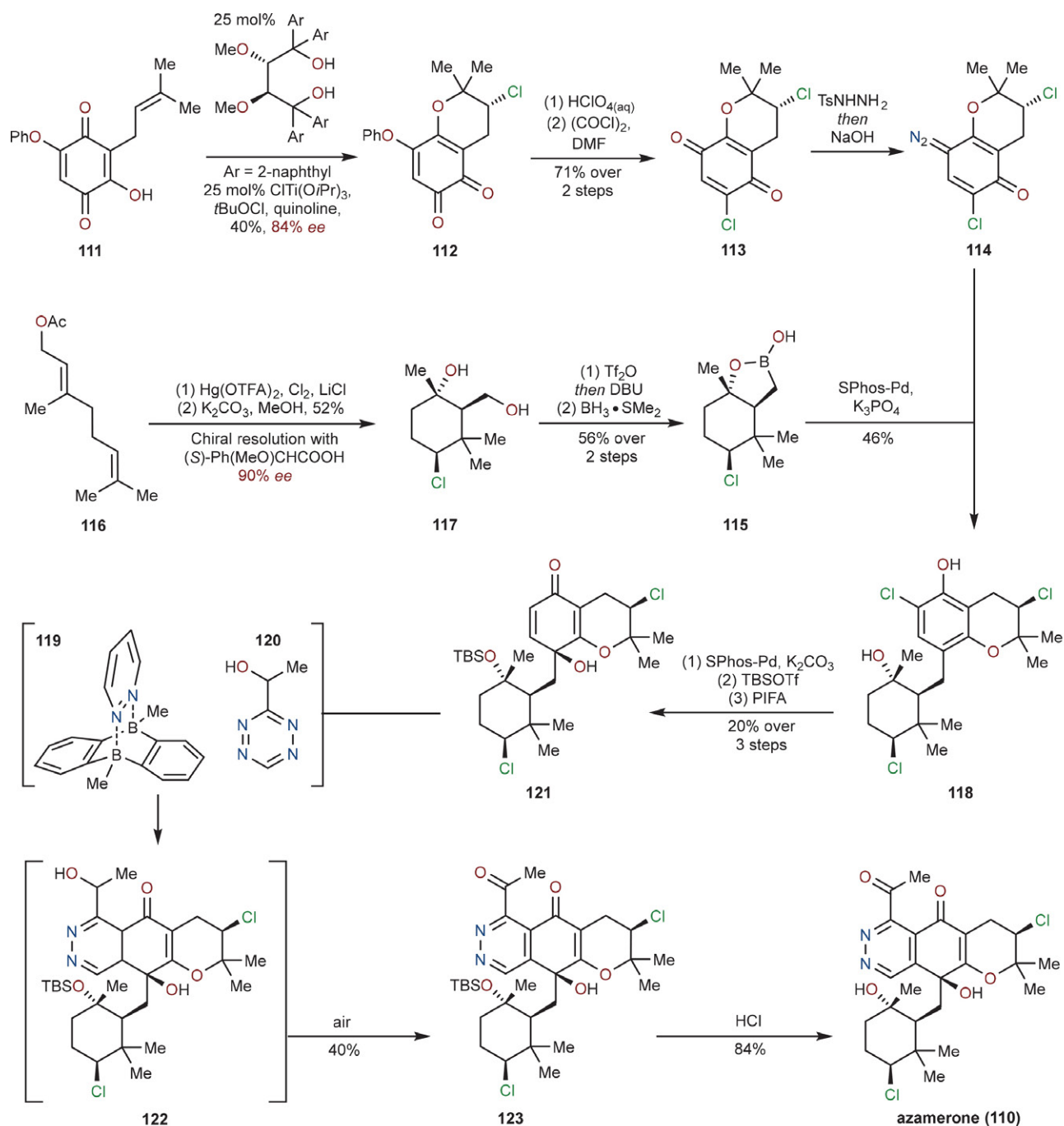
The initial idea of direct phenol C-alkylation with an **95**-derived electrophile was abandoned as it would require laborious preparation of suitable organometallic species and thus an alternative solution was sought. Simple benzyl ester formation and Mitsunobu etherification with *p*-methoxyphenol set the stage for a formal [1,3]-rearrangement (**96** to **97**) and cyclization (**97** to **98**). Both transformations were efficiently promoted by the same Lewis acid ( $\text{FeCl}_3$ ). *Ortho*-selective phenol C-alkylation was therefore achieved through the intermediacy of O-alkylated product **96**. Debonylation of **98** with palladium on carbon gave STR-1 (**99**) and further demethylation with pyridinium chloride at elevated temperatures gave STR-3 (**100**). Alternatively, amide formation with HATU in the presence of 1-hydroxy-7-azabenzotriazole (HOAt) furnished **101**, which was then exposed to *in situ* formed AcOI, generated from lead tetraacetate (LTA) and elemental iodine under UV light. This protocol was able to selectively oxidize the  $\gamma$ -methyl substituent in the presence of an electron-rich arene, even with competing benzylic oxidation. Lactonization *via* amide hydrolysis and dehydroiodination of **102** yielded unsaturated intermediate **103**. The styrene moiety was diastereoselectively hydrogenated with palladium on carbon and *in situ* formed TMSI successfully demethylated STR-9 (**104**) to give STR-2 (**105**). STR-8 (**106**) was prepared from STR-2 (**105**) by oxidative opening of the chromane system with  $\text{NaIO}_4$  and



**Scheme 12:** Poulsen's semisyntheses of stronglyphorines. ADDP = 1,1'-(azodicarbonyl)dipiperidine. Bn = benzyl. HATU = 1-[bis(dimethylamino)methylene]-1H-1,2,3-triazolo[4,5-b]pyridinium 3-oxide hexafluorophosphate. HOAt = 1-hydroxy-7-azabenzotriazole. LTA = lead tetraacetate. TMS = trimethylsilyl.

molecular oxygen with further hydrogenation of the 1,4-benzoquinone motif. Transiently formed 1,4-benzoquinone **107** could be exposed to oxidative heterofunctionalization conditions using  $\text{Co(OAc)}_2$  to give STR-26 (**94**) alongside its constitutional isomer **108** in a 1.3:1 ratio.

The former is in equilibrium with two diastereomeric hemiketals **109**. Catalytic oxidative heterofunctionalization methodology deserves a special mention as it enables controlled functionalization of 1,4-benzoquinone and its derivatives with oxygen, nitrogen and sulfur nucleophiles.



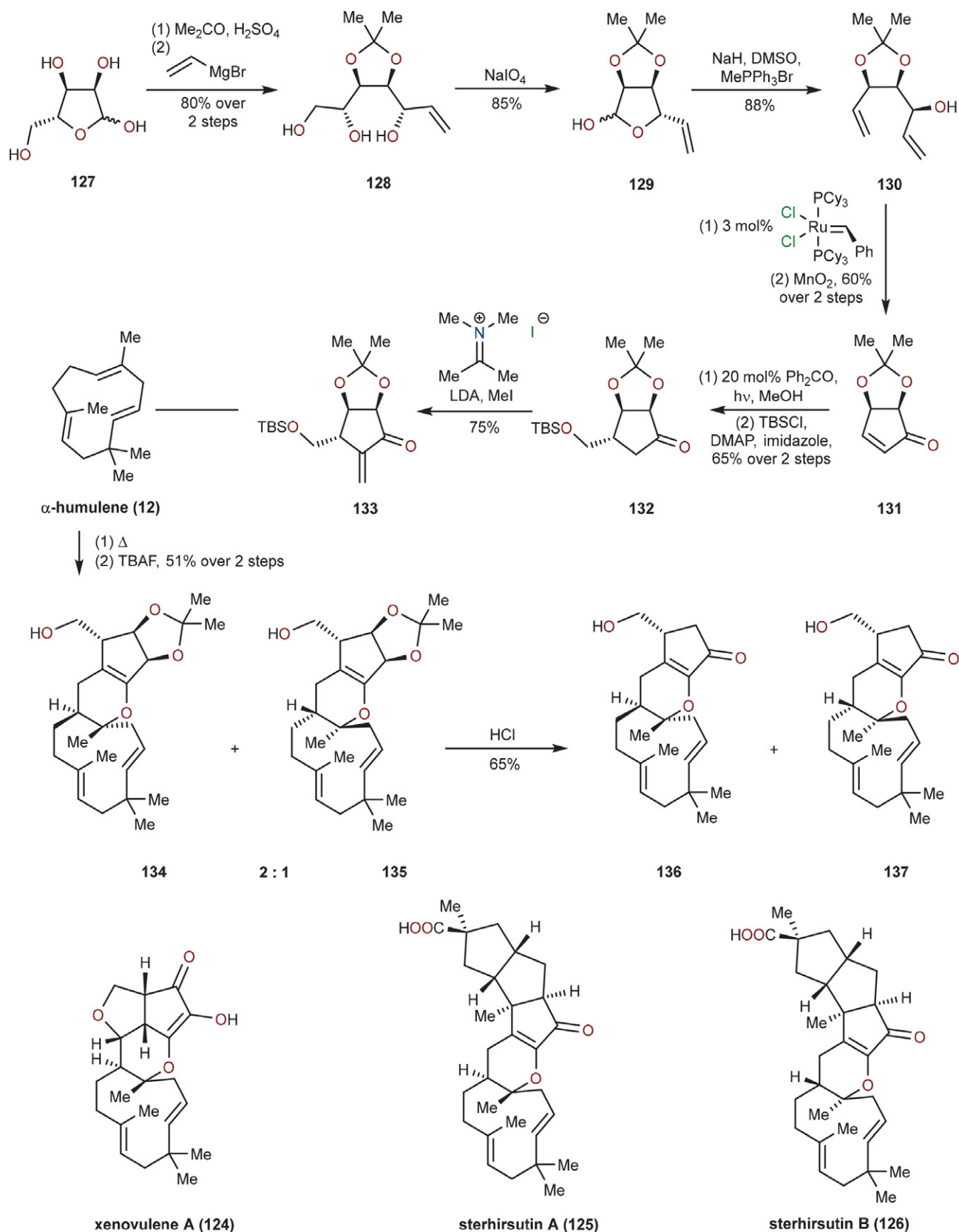
**Scheme 13:** Burns' asymmetric total synthesis of azamerone (**110**). DBU = 1,8-diazabicyclo[5.4.0]undec-7-ene. DMF = *N,N*-dimethylformamide. PIFA = phenyliodine(III) bis(trifluoroacetate). Sphos = 2-dicyclohexylphosphino-2',6'-dimethoxybiphenyl. TBS = *tert*-butyldimethylsilyl. Tf = triflyl. TFA = trifluoroacetate.

## 1. 9. Burns' Total Synthesis of Azamerone (2019)

Azamerone (**110**) presents as a fascinating chlorinated natural product containing a phthalazinone core from the napyradiomycin subset of meroterpenoids. Its biogenesis can be traced back to an  $\alpha$ -diazoketone motif-containing intermediate (not shown) (Scheme 13).<sup>22</sup> The first enantioselective chemical synthesis of azamerone (**110**)

was published in early 2019 by Burns' group, whose work contributes to the development of enantioselective chloroetherification methods of nonstabilized olefins. Key features of the synthetic route include a two-step mimic of halopolyene cyclizations and Suzuki coupling with a quinone diazide.

Azamerone (**110**) was traced back to prenylated hydroxyquinone **111**, which was prepared in four steps from



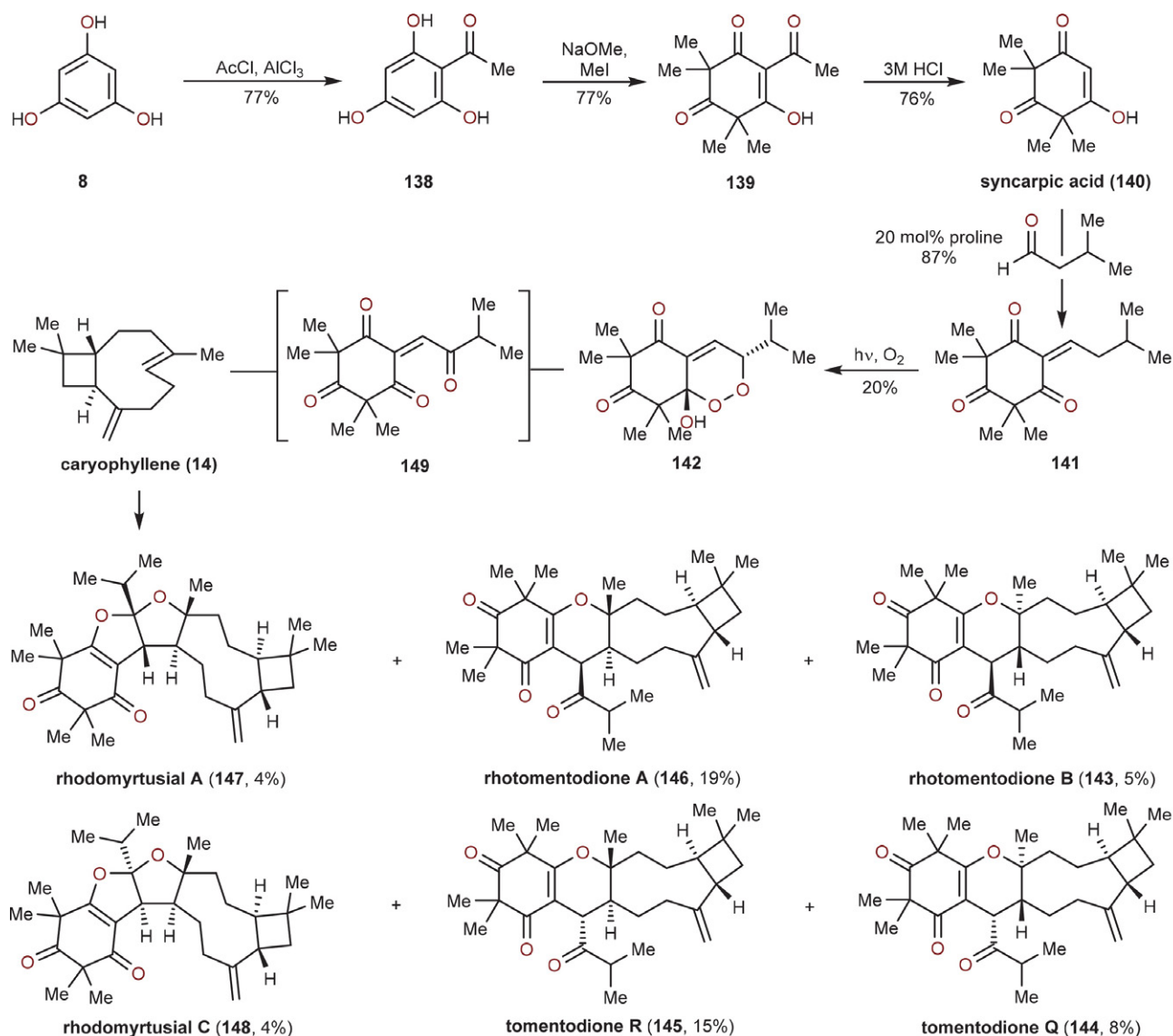
**Scheme 14:** Kirschning's biomimetic synthesis of 5,6,11-tricycle. Cy = cyclohexyl. DMAP = 4-dimethylaminopyridine. DMSO = dimethyl sulfoxide. LDA = lithium diisopropylamide. TBAF = tetrabutylammonium fluoride. TBS = *tert*-butyldimethylsilyl.

catechol. Developed for this purpose, titanium mediated enantioselective intramolecular chloroetherification of **111** gave benzochloropyran **112**, which was later hydrolyzed with aqueous perchloric acid and chlorinated with a mixture of oxalyl chloride and DMF. The decomposition of the corresponding tosyl hydrazone from **113** gave diazo compound **114**, which was used directly without purification in the subsequent Suzuki coupling reaction. The other coupling partner, boronic hemiester **115**, was prepared from geranyl acetate (**116**). Mercury trifluoroacetate-mediated polyene cyclization, acetate deprotection and chiral resolution *via* ester formation with (*S*)- $\alpha$ -methoxyphenylacetic acid gave enantioenriched intermediate **117**. Triflation, DBU-promoted elimination and hydroboration were needed to complete the synthesis of **115**. Suzuki coupling (yielding **118**) was followed by palladium-catalyzed dechlorination, silyl protection of the tertiary alcohol and PIFA oxida-

tion. Bis-boron complex **119** was then employed to catalyze the inverse electron demand Diels–Alder reaction between tetrazine **120** and **121**. Following [4+2]-retrocycloaddition and nitrogen expulsion, dihydropyridazine **122** underwent spontaneous aromatization and benzylic alcohol oxidation to give silyl protected azamerone **123**. Acidic deprotection of the remaining silyl protecting group with aqueous hydrochloric acid furnished the desired natural product **110**.

## 1. 10. Kirschning's Studies Towards 5,6,11-Tricyclic Meroterpenoids (2019)

Meroterpenoids xenovulene A (**124**), sterhirsutin A (**125**), and sterhirsutin B (**126**) share a similar 5,6,11-tricyclic core despite being isolated from different fungi (Scheme 14). Work done by Kirschning's group marks another milestone in the exploration of hetero-Diels–Alder



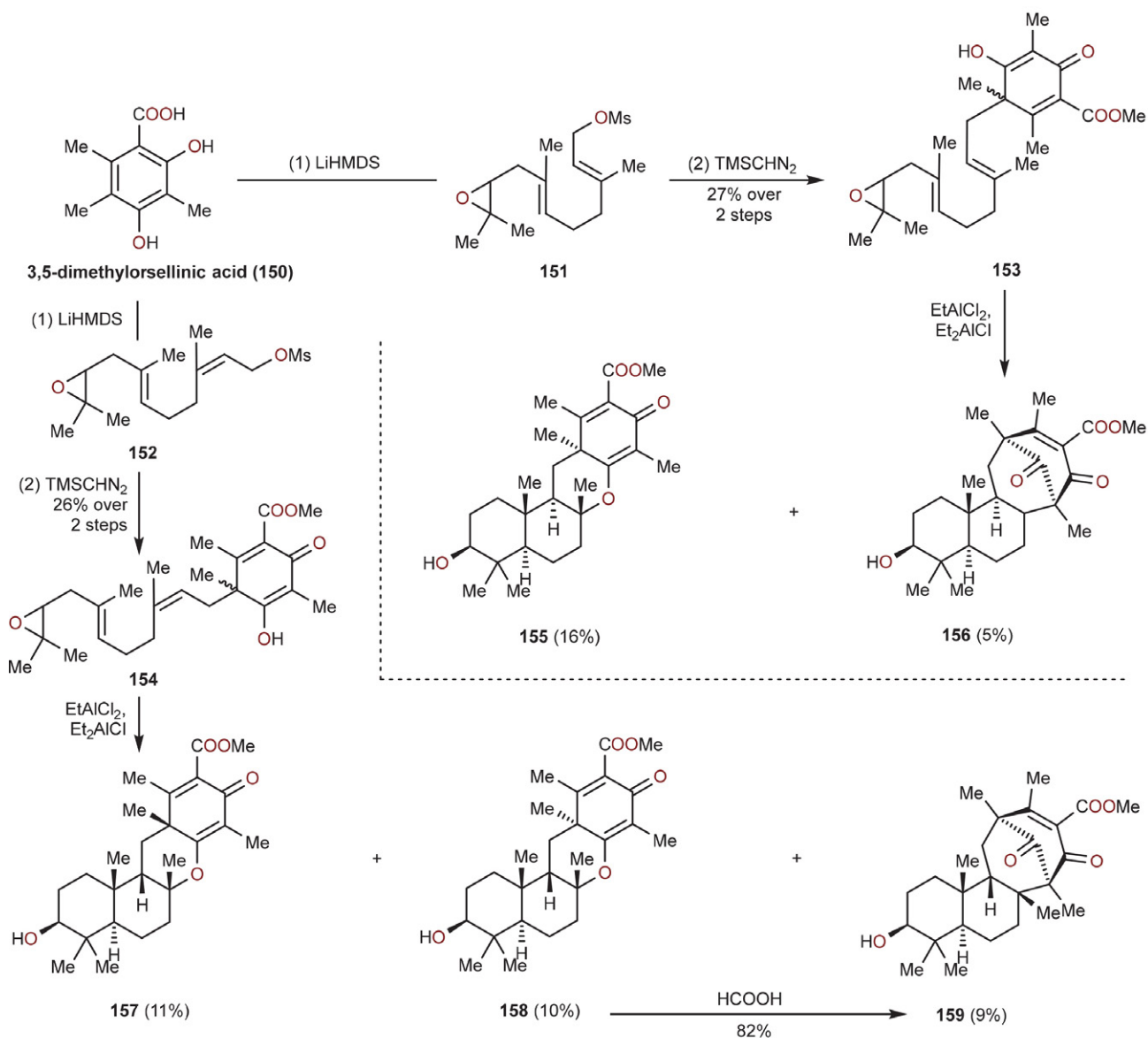
**Scheme 15:** Liu's and Porco's biomimetic total syntheses of meroterpenoids from *Rhodomyrtus tomentosa*. Ac = acetyl.

chemistry between *ortho*-quinone methides and  $\alpha$ -humulene (**12**).<sup>23</sup> Using this approach, they were able to access the aforementioned core starting from commercially available chiral pool material D-ribose (**127**). The protected acetonide form was treated with vinyl magnesium bromide to yield **128**, which subjected with NaIO<sub>4</sub> oxidatively cleaved the diol to the resulting aldehyde which spontaneously formed lactol **129**. Standard Wittig olefination installed the second vinyl handle in **130**, which was needed for ring-closing metathesis. Introduction of the first-generation Grubbs catalyst effectively forged a five-membered ring containing an allylic alcohol moiety (not shown) *via* RCM, which was successively oxidized with MnO<sub>2</sub> to provide enone **131**. Photochemical 1,4-addition of methanol and silyl protection yielded ketone **132**. The reactive exocyclic methylene group in **133** was appended using Es-

chenmoser methenylation. The key chemoselective hetero-Diels–Alder reaction with  $\alpha$ -humulene (**12**) gave a 2:1 mixture of products **134** and **135** after silyl deprotection. Enones **136** and **137** were formed *via* acid catalyzed rearrangements of the corresponding acetonides. The authors speculate that this transformation occurs through transient double bond isomerization and expulsion of acetone.

### 1. 11. Liu's and Porco's Total Syntheses of *Rhodomyrtus Tomentosa* Meroterpenoids (2019)

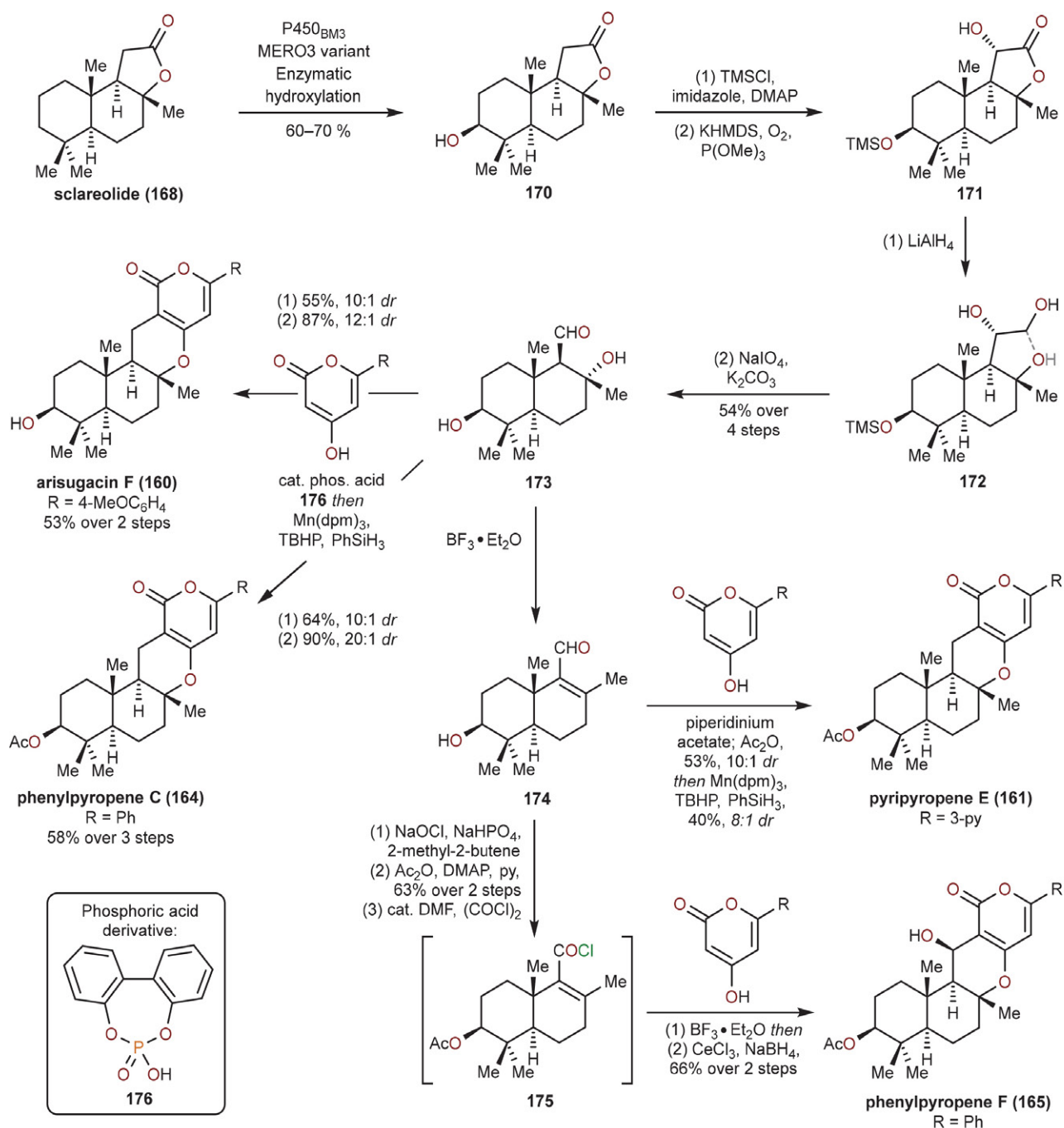
Collaborative efforts from Liu and Porco groups resulted in isolation of seven meroterpenoids from the leaves and stems of *Rhodomyrtus tomentosa*, evaluation of their AchE inhibitory activities, as well as their prepara-



**Scheme 16:** Porco's biomimetic synthesis of meroterpenoids **155**, **156**, **157** and **158**. HMDS = hexamethyldisilazane. TMS = trimethylsilyl.

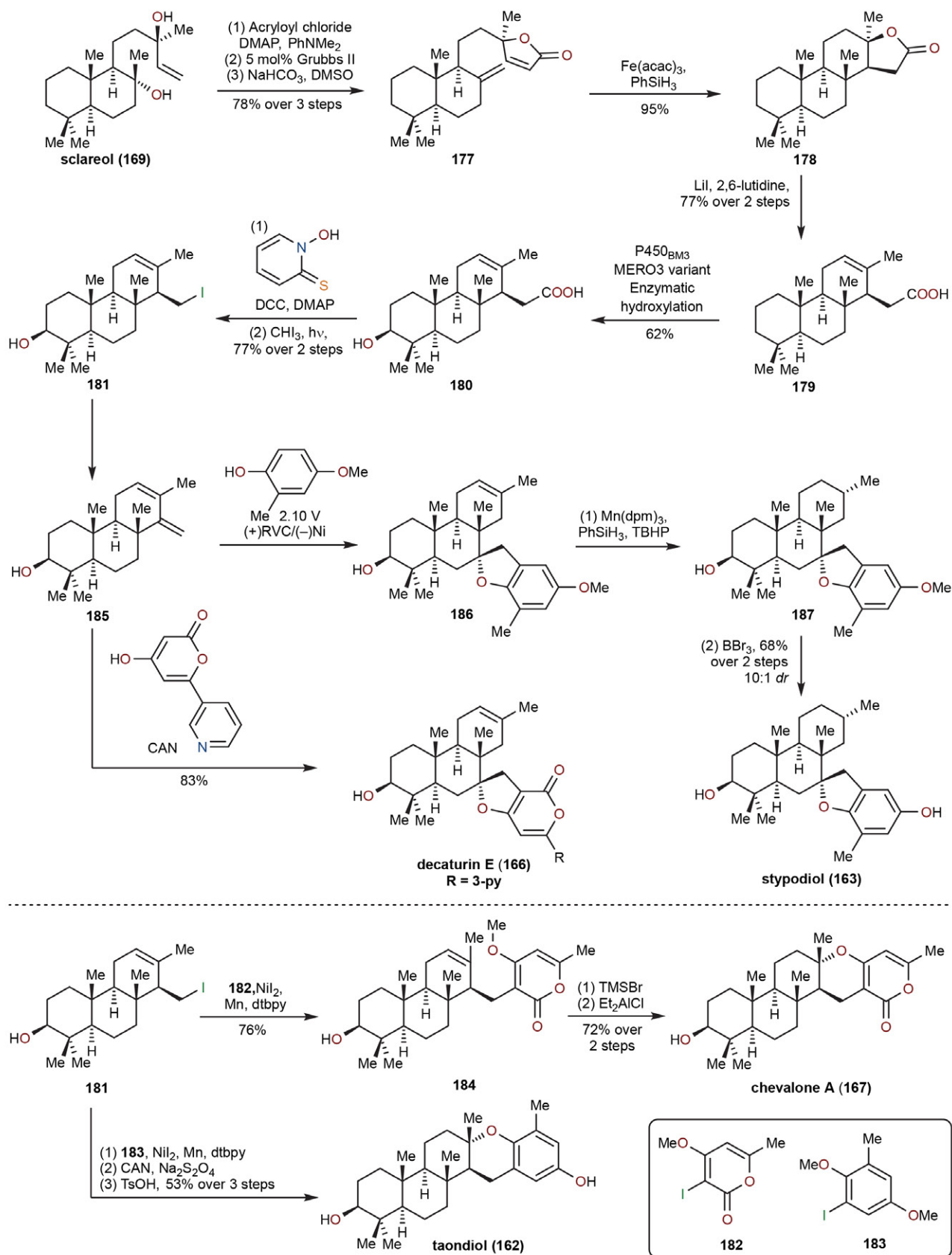
tion in six steps from commercially available starting materials. Their synthesis began with Friedel–Crafts acylation of phloroglucinol **8** (Scheme 15). Orcinol derivative **138** was dearomatized by exhaustive methylation with MeI / NaOMe. Acid catalyzed deacylation of **139** provided syncarpic acid **140**, which was then used in a proline catalyzed intermolecular aldol condensation with isovaleraldehyde. Afterwards, singlet oxygen [4+2]-cycloaddition with **141** gave a separable mixture of *syn*- (not shown) and *anti*-hydroxy-endoperoxide (**142**) in 52% and 20% yields respectively. It was found that *anti*-hydroxy-endoperoxide could be thermally equilibrated into a 1.5:1 mixture of *syn*- and *anti*-hydroxy-endoperoxides. Reactivity of both diastereoisomers with caryophyllene (**14**) was tested in the presence of molecular sieves. While the *syn*-diastereoisomer gave only a mixture of rhotomentodione B (**143**) and tomentodiones Q (**144**) and R (**145**) in the thermolysis reaction, the *anti*-diastereoisomer also provided rhotomento-

hydroxy-endoperoxide (**142**) in 52% and 20% yields respectively. It was found that *anti*-hydroxy-endoperoxide could be thermally equilibrated into a 1.5:1 mixture of *syn*- and *anti*-hydroxy-endoperoxides. Reactivity of both diastereoisomers with caryophyllene (**14**) was tested in the presence of molecular sieves. While the *syn*-diastereoisomer gave only a mixture of rhotomentodione B (**143**) and tomentodiones Q (**144**) and R (**145**) in the thermolysis reaction, the *anti*-diastereoisomer also provided rhotomento-



**Scheme 17:** Renata's chemoenzymatic total synthesis of arisugacin F (**160**), pyripropene E (**161**) and phenylpropenes C (**164**) and F (**165**). Ac = acetyl. DMAP = 4-dimethylaminopyridine. HMDS = hexamethyldisilazane. TBHP = *tert*-butyl hydroperoxide. TMS = trimethylsilyl.





**Scheme 18:** Renata's chemoenzymatic total synthesis of decaturin E (166), stypodiol (163), chevalone A (167) and taondiol (162). acac = acetylacetonate. CAN = cerium(IV) ammonium nitrate. DMAP = 4-dimethylaminopyridine. DMSO = dimethyl sulfoxide. RVC = reticulated vitreous carbon. dtbpy = 4,4'-di-*tert*-butyl-2,2'-dipyridine. TBHP = *tert*-butyl hydroperoxide. TMS = trimethylsilyl. Ts = tosyl.

dione A (**146**) as well as both rhodomyrtusals A (**147**) and C (**148**). The authors propose that both hydroxy-endoperoxides form the same reactive enetrione species (**149**) *in situ*, albeit, different mechanisms of formation could be operational. The chemistry of enetrione (**149**) was further explored as it displayed interesting modes of reactivity. Initial computational study indicated that asynchronous concerted hetero-Diels-Alder might be operational instead of the initially proposed stepwise Michael addition pathway. The latter mode resembles reactivity observed by the Cramer's group during their synthesis of psiguadial B (**16**) (Scheme 4).

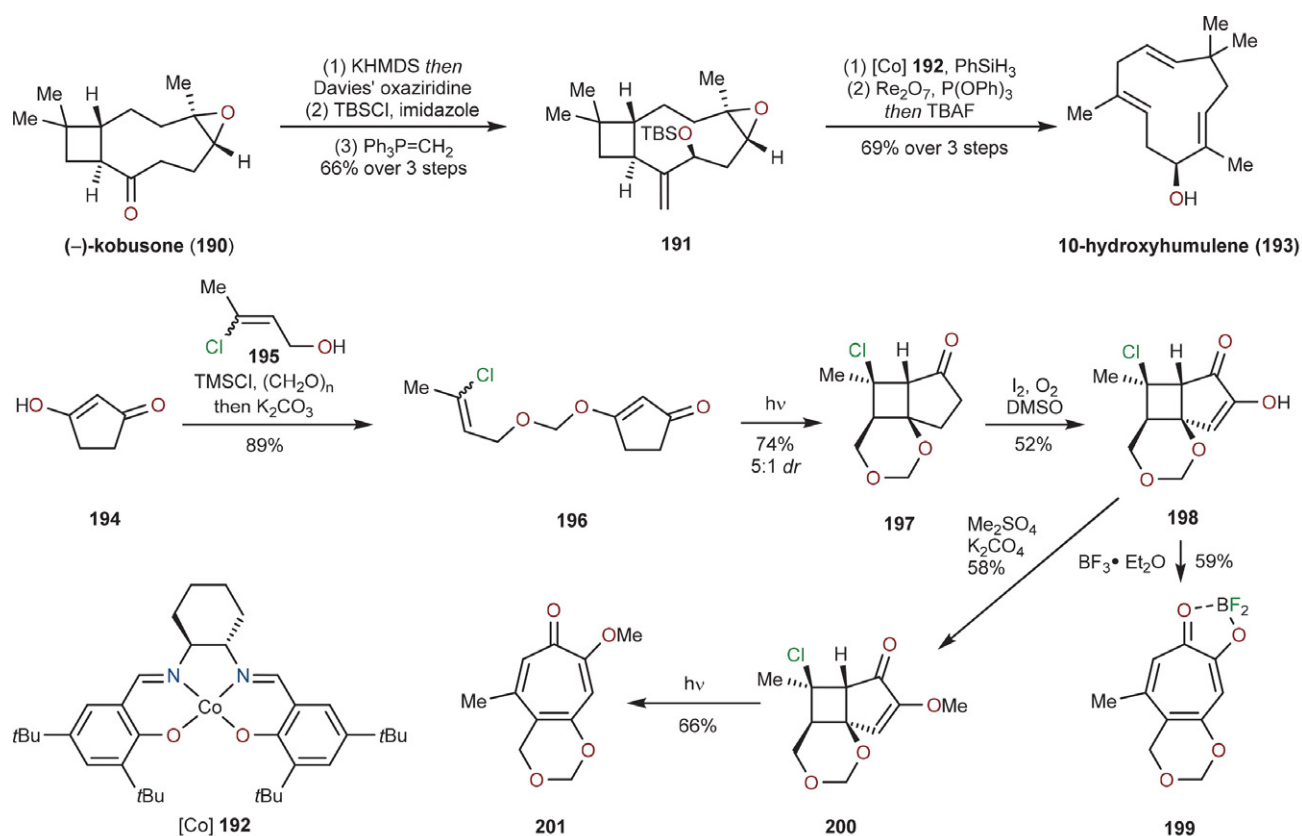
## 1. 12. Porco's Total Syntheses of DMOA-derived Meroterpenoids (2019)

As an addition to Maimone's and Newhouse's work on polyene cyclization derived meroterpenoids, the group of Porco devised their own syntheses of meroterpenoids using a biomimetic approach.<sup>24</sup> Their strategy features polyene cyclization with a dearomatized moiety acting as a terminating group. Development of selective alkylation procedure for 3,5-dimethylorsellinic acid (DMOA, **150**) was crucial for the preparation of suitable precursors for the aforementioned cyclization step (Scheme 16). The trianion of **150**, formed in the presence

of excess LiHMDS, was selectively alkylated with different electrophiles (such as **151** and **152**) at the C5 position (instead of the C3 position). Methylation employing trimethylsilyl diazomethane gave rise to precursors **153** and **154**, which would, upon treatment with Et<sub>2</sub>AlCl and EtAlCl<sub>2</sub>, furnish a mixture of tri- and tetracyclic meroterpenoids (**155**, **156**, **157**, **158** and **159**). They also demonstrated that formic acid would transform kinetic O-alkylated cyclization product **158** into thermodynamically more favored C-alkylated product **159** as suggested by relative energy levels of cyclized meroterpenoids based on computational studies.

## 1. 13. Renata's Total Syntheses of $\alpha$ -Pyrone and Diterpene Meroterpenoids (2020)

In early 2020, Renata's group accessed eight natural products from  $\alpha$ -pyrone and diterpene meroterpenoids subsets in a concise, high-yielding and modular fashion.<sup>25</sup> While some of them [arisugacin F (**160**)<sup>26</sup>, pyripyropene E (**161**)<sup>27</sup>, taondiol (**162**)<sup>28,29</sup>, and stypodiol (**163**)<sup>30</sup>] have been subjects of multiple synthetic studies, others [phenylpropenes C (**164**) and F (**165**), decaturin E (**166**) and chevalone A (**167**)] were synthesized for the first time. Instead of using more conventional Wieland-Mischer ketone, sclareolide (**168**) and sclareol (**169**) were



**Scheme 19:** Sarlah's syntheses of 10-hydroxyhumulene and two tropolone-derived ortho-quinone methide precursors. DMSO = dimethyl sulfoxide. TBAF = tetrabutylammonium fluoride. TBS = *tert*-butyldimethylsilyl. TMS = trimethylsilyl.

selected as commercially available, chiral pool starting materials. Traditional polar disconnections were replaced by a combination of radical chemistry and biocatalysis. **168** was successfully utilized for chemo-, regio- and diastereoselective C–H oxidation to install a hydroxyl group at the C3 position of the sclareolide drimane scaffold (Scheme 17). Silyl protection of the newly formed hydroxy group in **170** with trimethylsilyl chloride was followed by diastereoselective  $\alpha$ -oxygenation. Reduction of the lactone **171** with lithium aluminum hydride gave a mixture of a lactol and a triol **172** (unified structure shown). Convergent oxidative cleavage with NaIO<sub>4</sub> and concomitant silyl deprotection under the same reaction conditions resulted in the formation of  $\beta$ -hydroxyaldehyde **173**. This common precursor was transformed *via* enal **174** into an acyl chloride **175** through sequential Pinnick oxidation, acetate protection and nucleophilic substitution with oxalyl chloride/DMF. Intermediates **173** and **174** underwent formal [3+3] cycloadditions with 4-hydroxy-2*H*-pyran-2-one derivatives and promoters like piperidinium acetate or phosphoric acid derivative **176**. Chemo- and diastereoselective HAT reductions under Shenvi's conditions in the presence of labile pyrone moiety yielded natural products arisugacin F (**160**), phenylpropene C (**164**) and pyripropene E (**161**). Crude unsaturated acyl chloride **175** underwent Friedel–Crafts acylation in the presence of BF<sub>3</sub>·Et<sub>2</sub>O and after Luche reduction and concomitant cyclization yielded phenylpropene F (**165**).

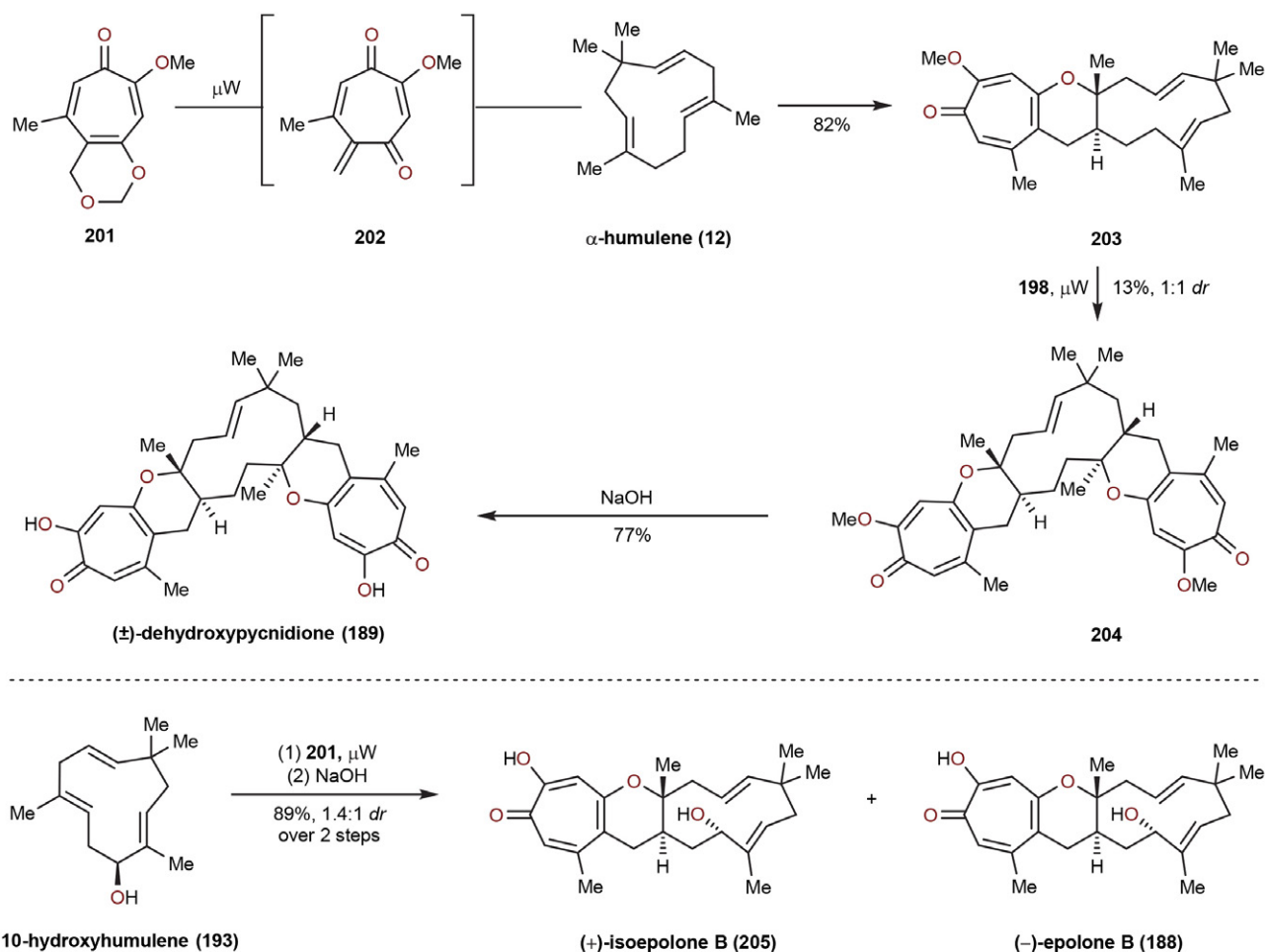
The remaining four diterpene meroterpenoids were constructed from butenolide **177**, which itself was forged from sclareol (**169**) *via* peracryloylation, ring-closing metathesis with Grubbs second-generation catalyst and NaHCO<sub>3</sub> mediated elimination (Scheme 18). Exocyclic double bond participated in a high-yielding and diastereoselective intramolecular Giese HAT coupling and thus formed lactone **178** was treated with LiI and 2,6-lutidine to arrive at carboxylic acid **179**. The acid was the optimal substrate in the synthetic sequence for the modified enzymatic hydroxylation conditions on a gram scale. The formation of a Barton ester from hydroxylated carboxylic acid **180** was followed by decarboxylation and the resulting primary radical was trapped with iodoform to give primary iodide **181**. On the one hand, primary iodide **181** was used in Weix nickel-catalyzed sp<sup>3</sup>–sp<sup>2</sup> cross electrophile coupling reactions with aryl iodides **182** and **183**. Subsequent manipulations provided taondiol (**162**) directly and chevalone A (**167**) *via* intermediate **184**. Alternatively, primary iodide **181** was taken forward and treated with KO*t*Bu to promote elimination; the conjugated diene **185** then reacted in either a CAN-mediated or electrochemical SET-based formal [3+2] coupling reactions. The former conditions gave decaturin E (**166**) directly. Synthesis of stypodiol (**163**) was completed with diastereoselective HAT reduction of **186** to give **187** and subsequent BBr<sub>3</sub> demethylation.

## 1. 14. Sarlah's Total Synthesis of (–)-Epolone B and (±)-Dehydroxypycnidione

The Sarlah group's interest in hetero-Diels–Alder reactions and meroterpenoids culminated in biomimetic and modular total syntheses of two naturally occurring tropolones; (–)-epolone B (**188**) and (±)-dehydroxypycnidione (**189**) (Scheme 20).<sup>31</sup> Both compounds share a common 11-membered core but differ in the number of attached tropolone moieties. It was envisioned that these two compounds could be prepared through the union of a tropolone-derived *ortho*-quinone methide and  $\alpha$ -humulene (**12**) (or its 10-hydroxy derivative **193**). The latter was prepared in an enantioselective fashion in five steps, starting from commercially available chiral pool (–)-kobusone (**190**) (Scheme 19). Diastereoselective  $\alpha$ -hydroxylation at the sterically more accessible position, followed by silyl protection and Wittig olefination provided an exocyclic olefin **191**. Shenvi's HAT conditions (cobalt catalyst **192** and phenylsilane) for catalytic olefin isomerization induced a retrocycloisomerization reaction, which opened up the four-membered ring in **191**.<sup>32</sup> Finally, stereospecific rhenium-catalyzed epoxide deoxygenation developed by Takai's group furnished 10-hydroxyhumulene (**193**).<sup>33</sup>

Next, synthesis of tropolone-derived *ortho*-quinone methide precursors was pursued. It commenced with O-alkylation of 1,3-cyclopentadione (**194**). This transformation was achieved with paraformaldehyde and a mixture of allylic alcohols (**195**) in the presence of TMSCl. Vinyl chloride **196** was converted into tricycle **197** *via* photochemical [2+2] cycloaddition under UV irradiation with 5:1 diastereoselectivity. Out of all tested oxidation conditions only a one pot  $\alpha$ -iodination/Kornblum oxidation protocol<sup>34</sup> allowed for a selective oxidation of the  $\alpha$ -position in the presence of a labile tertiary chloride moiety. While treatment of hydroxyenone **198** with boron trifluoride etherate yielded the expected de Mayo product **199**, fragmentation of methylated derivative **200** with Lewis acids proved to be more challenging. Ultimately, this challenge was solved with the discovery of a novel photochemical fragmentation, uniquely suited for this purpose, which resulted in formation of methylated tropolone **201**.

With all cycloaddition partners in hand, reactivity of both tropolone-derived *ortho*-quinone methide precursors **199** and **201** was tested in hetero-Diels–Alder reactions with humulenes. *Ortho*-quinone methide **202**, derived from the methyl protected precursor **201**, was found to efficiently react with  $\alpha$ -humulene (**12**) as a coupling partner, giving rise to monocycloadduct **203**. Due to the established superior biological activities of bicyclic adducts, a second cycloaddition was attempted. Resubjecting monocycloadduct **203** to the same reaction conditions gave penultimate bicyclic adduct **204**. Final deprotection with sodium hydroxide completed the first total synthesis of (±)-dehydroxypycnidione (**189**). Subsequently, the ability of 10-hydroxyhumulene (**193**) to react as a



Scheme 20: Sarlah's biomimetic total syntheses of **(±)-dehydroxypycnidione 189** and **(-)-epolone B (188)**

dienophile was explored. *Ortho*-quinone methide precursor **201** again proved to be superior. Under optimized conditions, a 1.4:1 mixture of diastereomeric adducts was formed. Quantitative NaOH deprotection of both diastereoisomers revealed **(+)-isoepolone B (205)** and **(-)-epolone B (188)** as major and minor diastereoisomer respectively. Notably, the second cycloaddition with both deprotected diastereoisomers was attempted, but gave exclusive diastereoselectivity to unnatural bistropolones; this selectivity was further supported with computational modeling. Ultimately, the culmination of these synthetic studies have suggested alternative biosynthetic routes for these compounds in addition to the stereochemical revision of several members.

## 2. Conclusion

Having reviewed some of the most elegant meroterpenoid syntheses from the past five years a few general observations are apparent. Polyene cyclizations and (formal) cycloadditions are still prevalent chemical tools for the

construction of meroterpenoid cores. The development of suitable reaction conditions and introduction of novel polyene cyclization terminating groups were crucial for the successful completion of several showcased syntheses. Reactivity of various *ortho*-quinone methides with naturally occurring dienophiles like  $\alpha$ -humulene and caryophyllene was thoroughly studied. One can observe a slow and subtle paradigm shift from more traditional polar disconnections to complementary radical-based disconnections. Certain admirable coupling name reactions (*e.g.* Suzuki coupling) were pushed to their limits as new types of coupling partners were explored. Progress was made on rather obscure asymmetric ketene trapping reactions as well as on highly sought-after C–H functionalization reactions. On a similar note, challenging undirected C–H oxidations were achieved with chemoenzymatic methods, which are finding their place among chemical methods by demonstrating high complementarity. To conclude, structural diversity and complexity of meroterpenoids will undoubtedly keep inspiring chemists to develop new chemical tools for future total syntheses.

### 3. References

- R. Geris, T. J. Simpson, *Nat. Prod. Rep.* **2009**, *26*, 1063–1094. DOI:10.1039/b820413f
- Y. Matsuda, I. Abe, *Nat. Prod. Rep.* **2016**, *33*, 26–53. DOI:10.1039/C5NP00090D
- A. El-Demerdash, D. Kumla, A. Kijjoa, *Mar. Drugs* **2020**, *18*, 317. DOI:10.3390/md18060317
- F. A. Macias, C. Carrera, J. C. G. Galindo, *Chem. Rev.* **2014**, *114*, 2717–2732. DOI:10.1021/cr300048m
- L. Murray, S. McKinnie, B. Moore, J. George, *Nat. Prod. Rep.* **2020**, *37*, 1334–1366. DOI:10.1039/D0NP00018C
- T. Sunazuka, S. Ōmura, *Chem. Rev.* **2005**, *105*, 4559–4580. DOI:10.1021/cr040628i
- M. Gordaliza, *Mar. Drugs* **2012**, *10*, 358–402. DOI:10.3390/md10020358
- J. A. Richard, *European J. Org. Chem.* **2014**, *2014*, 273–299. DOI:10.1002/ejoc.201300815
- H. C. Lam, J. T. J. Spence, J. H. George, *Angew. Chem. Int. Ed.* **2016**, *55*, 10368–10371. DOI:10.1002/anie.201606091
- L. M. Chapman, J. C. Beck, L. Wu, S. E. Reisman, *J. Am. Chem. Soc.* **2016**, *138*, 9803–9806. DOI:10.1021/jacs.6b07229
- C. G. Newton, D. N. Tran, M. D. Wodrich, N. Cramer, *Angew. Chem. Int. Ed.* **2017**, *56*, 13776–13780. DOI:10.1002/anie.201708333
- C. P. Ting, G. Xu, X. Zeng, T. J. Maimone, *J. Am. Chem. Soc.* **2016**, *138*, 14868–14871. DOI:10.1021/jacs.6b10397
- C. P. Ting, T. J. Maimone, *J. Am. Chem. Soc.* **2015**, *137*, 10516–10519. DOI:10.1021/jacs.5b06939
- M. Elkin, S. M. Szewczyk, A. C. Scrusse, T. R. Newhouse, *J. Am. Chem. Soc.* **2017**, *139*, 1790–1793. DOI:10.1021/jacs.6b12914
- G. Xu, M. Elkin, D. J. Tantillo, T. R. Newhouse, T. J. Maimone, *Angew. Chem. Int. Ed.* **2017**, *56*, 12498–12502. DOI:10.1002/anie.201705654
- H. Shigehisa, T. Aoki, S. Yamaguchi, N. Shimizu, K. Hiroya, *J. Am. Chem. Soc.* **2013**, *135*, 10306–10309. DOI:10.1021/ja405219f
- B. Gaspar, E. M. Carreira, *Angew. Chem. Int. Ed.* **2008**, *47*, 5758–5760. DOI:10.1002/anie.200801760
- R. Wildermuth, K. Speck, F. L. Haut, P. Mayer, B. Karge, M. Brönstrup, T. Magauer, *Nat. Commun.* **2017**, *8*, 1–9.
- K. Speck, R. Wildermuth, T. Magauer, *Angew. Chem. Int. Ed.* **2016**, *55*, 14131–14135. DOI:10.1002/anie.201608040
- W. Yu, P. Hjerrild, K. M. Jacobsen, H. N. Tobiesen, L. Clemmensen, T. B. Poulsen, *Angew. Chem. Int. Ed.* **2018**, *57*, 9805–9809. DOI:10.1002/anie.201805580
- W. Yu, P. Hjerrild, J. Overgaard, T. B. Poulsen, *Angew. Chem. Int. Ed.* **2016**, *55*, 8294–8298. DOI:10.1002/anie.201602476
- J. M. Winter, A. L. Jansma, T. M. Handel, B. S. Moore, *Angew. Chem. Int. Ed.* **2009**, *48*, 767–770. DOI:10.1002/anie.200805140
- P. J. Li, G. Dräger, A. Kirschning, *Org. Lett.* **2019**, *21*, 998–1001. DOI:10.1021/acs.orglett.8b04003
- Z. Powers, A. Scharf, A. Cheng, F. Yang, M. Himmelbauer, T. Mitsuhashi, L. Barra, Y. Taniguchi, T. Kikuchi, M. Fujita, I. Abe, J. A. Porco, *Angew. Chem. Int. Ed.* **2019**, *58*, 16141–16146. DOI:10.1002/anie.201910710
- J. Li, F. Li, E. King-Smith, H. Renata, *Nat. Chem.* **2020**, *12*, 173–179. DOI:10.1038/s41557-019-0407-6
- M. Handa, T. Sunazuka, A. Sugawara, Y. Harigaya, K. Otugro, S. Ōmura, *J. Antibiot. (Tokyo)*. **2003**, *56*, 730–733. DOI:10.7164/antibiotics.56.730
- A. B. Smith, T. Kinsho, T. Sunazuka, S. Ōmura, *Tetrahedron Lett.* **1996**, *37*, 6461–6464. DOI:10.1016/0040-4039(96)01439-6
- D. H. Dethe, S. Mahapatra, S. K. Sau, *Org. Lett.* **2018**, *20*, 2766–2769. DOI:10.1021/acs.orglett.8b00997
- A. S. Kumanireng, T. Kato, Y. Kitahara, *Chem. Lett.* **1973**, *2*, 1045–1047. DOI:10.1246/cl.1973.1045
- A. Abad, C. Agulló, M. Arnó, A. C. Cuñat, B. Meseguer, R. J. Zaragoza, *J. Org. Chem.* **1998**, *63*, 5100–5106. DOI:10.1021/jo980311g
- C. Y. Bemis, C. N. Ungarean, A. S. Shved, C. S. Jamieson, T. Hwang, K. S. Lee, K. N. Houk, D. Sarlah, *J. Am. Chem. Soc.* **2021**, *143*, 6006–6017. DOI:10.1021/jacs.1c02150
- S. W. M. Crossley, F. Barabé, R. A. Shenvi, *J. Am. Chem. Soc.* **2014**, *136*, 16788–16791. DOI:10.1021/ja5105602
- T. Nakagiri, M. Murai, K. Takai, *Org. Lett.* **2015**, *17*, 3346–3349. DOI:10.1021/acs.orglett.5b01583
- Y. F. Liang, X. Li, X. Wang, M. Zou, C. Tang, Y. Liang, S. Song, N. Jiao, *J. Am. Chem. Soc.* **2016**, *138*, 12271–12277. DOI:10.1021/jacs.6b07269

### Povzetek

Strukturna raznolikost meroterpenoidov, ki izvira iz kombinacije biosinteznih poti, buri domišljijo sinteznih kemikov in jih spodbuja, da konstanto izpopolnjujejo svojo retrosintezno logiko. Literaturni pregled nedavnih totalnih sintez meroterpenoidov razkriva izjemen napredek v razvoju kemijske metodologije. Namen tega preglednega članka je prikaz najbolj inovativnih sintez in sinteznih študij na področju kemije meroterpenoidov v zadnjih petih letih.



Except when otherwise noted, articles in this journal are published under the terms and conditions of the Creative Commons Attribution 4.0 International License

Review

# Sequencing of Nucleic Acids: from the First Human Genome to Next Generation Sequencing in COVID-19 Pandemic

Borut Furlani,<sup>1,§</sup> Katarina Kouter,<sup>2,§</sup> Damjana Rozman<sup>3,\*</sup>  
and Alja Videtič Paska<sup>2,\*</sup>

<sup>1</sup> University of Ljubljana, Faculty of Medicine, Vrazov trg 2, 1000 Ljubljana, Slovenia

<sup>2</sup> University of Ljubljana, Faculty of Medicine, Institute of Biochemistry and Molecular Genetics, Medical Centre for Molecular Biology, Vrazov trg 2, 1000 Ljubljana, Slovenia

<sup>3</sup> University of Ljubljana, Faculty of Medicine, Institute of Biochemistry and Molecular Genetics, Centre for Functional Genomics and Bio-Chips, Zaloška 4, 1000 Ljubljana, Slovenia

*§These two authors equally contributed to this work.*

*\* Corresponding author: E-mail: alja.videtic@mf.uni-lj.si; Tel. + 386 1 543 76 61; Fax. + 386 1 543 76 41, damjana.rozman@mf.uni-lj.si; Tel. + 386 1 543 75 91; Fax. + 386 1 543 76 41*

*Received: 01-26-2021*

## Abstract

Despite being around for more than 40 years, DNA sequencing is regarded as young technology in clinical medicine. As sequencing is becoming cheaper, faster and more accurate, it is rapidly being incorporated into clinical laboratories. In 2003, the completion of the first human genome opened the door to personalized medicine. Ever since it has been expected for genomics to widely impact clinical care and public health. However, many years can pass for genomic discoveries to reflect back and benefit the patients. DNA sequencing represents a less biased approach to diagnostics. It is not only a diagnostic tool, but can also influence clinical management and therapy. As new technologies rapidly emerge it is important for researchers and health professionals to have basic knowledge about the capabilities and drawbacks of the existing sequencing methods, and their use in clinical setting and research. This review provides an overview of nucleic acid sequencing technologies from historical perspective and later focuses on clinical utilization of sequencing. Some of the most promising areas are presented with selected examples from Slovenian researchers.

**Keywords:** Clinical sequencing; DNA; nucleic acid; genomics; next generation sequencing; precision medicine

## 1. Introduction

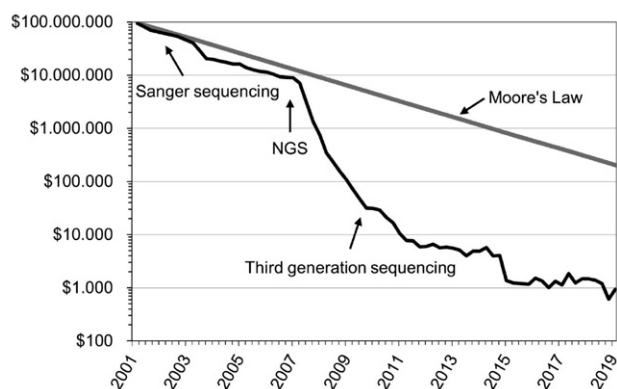
More than forty years ago, two papers described the first method for determining the sequence of nucleotide bases in DNA<sup>1,2</sup> and ever since, the development of new sequencing methods has been exponential. In 2003, the Human Genome Project (HGP) was finalized, presenting the complete version of the Human Genome.<sup>3</sup> Once the reference human genome was established, scientists tried to explain disease mechanisms or susceptibility for certain diseases through population resequencing and determination of disease-causing genomic variants. Recently, DNA sequencing has been moving into the clinical setting to be

implemented in diagnostics and clinical management. Due to the rapid development of novel technologies, sequencing of nucleic acids will contribute to the discovery of the genomic, transcriptomic and epigenomic basis of unsolved diseases, improved diagnostics, and personalized therapies.

Advances in sequencing technologies have contributed to a significant reduction of the sequencing costs in the last 15 years (Figure 1). In 2004, the National Human Genome Research Institute started an initiative to reduce the whole genome sequence cost to US\$1000<sup>4</sup> accelerating the development of cheaper and faster sequencing methods. A deviation of sequencing cost from 'Moore's law' oc-

curred around year 2008 which coincides with the transition from Sanger's sequencing of nucleic acids to the next generation sequencing technologies (NGS) resulting in a rapid fall of sequencing cost. Human genome sequencing for \$1000 was achieved a few years ago<sup>5</sup> and with novel technologies we are quickly approaching a \$100 human genome. With today's enormous sequencing outputs and lower cost per base the biggest challenge remains meaningful interpretation and informative reporting of sequencing results.

This review provides an overview of nucleic acid sequencing technologies and examples of clinical utilization of sequencing, also from Slovenian researchers.



**Figure 1:** Sequencing cost for the human genome. The departure of sequencing cost curve from Moore's law coincides with the emergence of next generation sequencing (NGS). Moore's law originates in the computer hardware industry that involves doubling of 'computing power' every two years. It is considered that technologies that follow the law are regarded as successful.<sup>6</sup> It thus represents a useful relationship to compare technology advances. Data shown in the figure was obtained from the National Human Genome Research Institute.<sup>6</sup>

## 2. Short Review of the Sequencing Technologies

In 1977, researchers developed two methods which enabled sequencing of nucleic acids of several hundred base pairs (bp), the Sanger's "dideoxy method" and the Maxam-Gilbert's method<sup>1,2</sup>, causing revolution in biology.

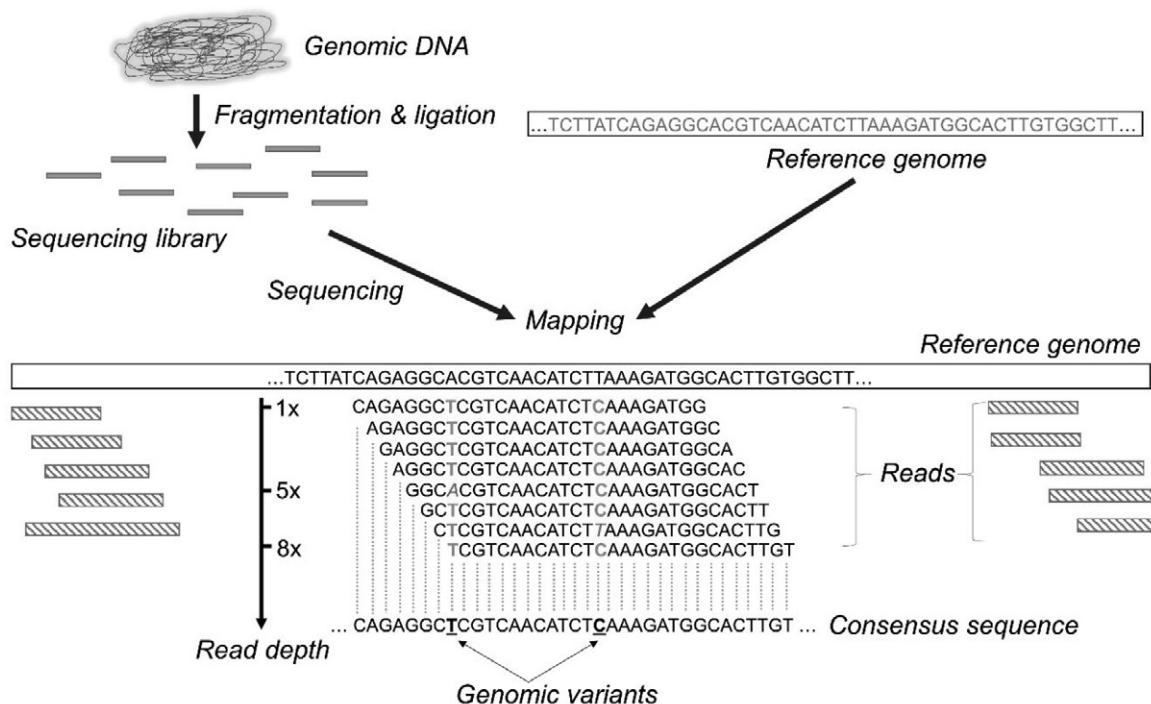
### 2. 1. First-Generation DNA Sequencing

The *Sanger sequencing* is known today as the first-generation DNA sequencing and was based on the use of polymerase chain reaction. DNA polymerase is an enzyme that can elongate an existing DNA molecule by adding deoxynucleotides (dNTPs; a nucleobase, deoxyribose, and phosphate groups) to the DNA 3'-end *via* a phosphodiester bond between the 3' carbon atom hydroxy group of the DNA incorporated deoxynucleotide and the

5' carbon atom phosphate group of a joining dNTP. What made the sequencing possible is the addition of labelled dideoxynucleotides (ddNTP); dNTPs lacking the deoxyribose 3' carbon atom hydroxy group needed to form the phosphodiester bond. After the incorporation of a ddNTP, DNA polymerase could no longer add new nucleotides as the phosphodiester bonds can no longer be formed. This results in the production of DNA fragments that vary in length; however, all fragments end with a labelled ddNTP. Initially, sequencing was performed using radioactively labelled ddNTPs. About a decade later Sanger sequencing was automated and commercialized using fluorescent-labelled ddNTPs<sup>7</sup> and capillary electrophoresis, providing a single base pair resolution.<sup>8</sup> Using automated Sanger sequencing, researchers were able to read up to 75,000 bp per day.<sup>9</sup> This method presented the foundation for the HGP, the biggest collaborative biological project that was officially completed in 2003 (it took 13 years and cost almost US\$3 billion to obtain the complete version of the human genome).<sup>3,6,10</sup> The next step was to identify genomic differences/variants among people to explain disease mechanisms and/or disease susceptibility. Such projects required genomes of many individuals to be sequenced, however, Sanger sequencing was far too time-consuming and expensive.

### 2. 2. Next (or Second) Generation Sequencing (NGS)

The "hunt" began for alternative DNA sequencing methods, ultimately resulting in the emergence of NGS *technologies*. NGS is based on massive parallel sequencing, meaning that billions of short DNA fragments are sequenced simultaneously producing short sequence "reads".<sup>11</sup> Reads are computationally aligned to the reference sequence to assemble the consensus DNA sequence (Figure 2). NGS technologies significantly increased sequencing throughput, decreased labour, and sequencing cost.<sup>12</sup> In 2004, the company 454 Life Sciences released the first commercially available NGS platform<sup>13</sup>, which is no longer used today. 454 Life Sciences technology was based on pyrosequencing; using detection of light to determine the DNA sequence. The basic principle of pyrosequencing consists of using enzymes to build the complementary DNA strand and detect the base order of DNA strands mobilized to beads located on a titer plate. Each addition of dNTPs to the growing DNA strand, catalysed by DNA polymerase, results in the release of a pyrophosphate. Pyrophosphate is then catalysed to adenosine triphosphate by sulfate adenyltransferase. Enzyme luciferase later utilizes the adenosine triphosphate to generate light by converting luciferin to oxyluciferin. Only one of the four dNTPs is added at a time, and unused dNTPs are degraded by the enzyme apyrase before the addition of new dNTP. Intensity of the light is detected by sensors, indicating if and how many dNTP were added to the complementary DNA strand.<sup>14</sup>



**Figure 2:** Schematic representation of NGS workflow. Steps common to different NGS platforms are DNA fragmentation (that is required or not depending on the library type), library preparation, massive parallel sequencing, bioinformatics analysis, and variant annotation and interpretation.<sup>27</sup> Sequencing generates billions of “reads” that are computationally aligned to the *reference genome* to assemble linear consensus sequence. The number of reads in which a particular base/variant appears is known as a read depth and determines the confidence with which a particular base/variant is called.<sup>12</sup> A particular single nucleotide variant should appear in more than 10 reads (meaning read depth to be at least 10 x) to be regarded as a genuine genomic variant.<sup>12</sup>

Illumina, Ion Torrent, and Beijing Genomics Institute (BGI) are currently the main NGS companies on the market.<sup>15</sup> Today, over 90% of all sequencing in the laboratories around the world is performed on Illumina’s platforms.<sup>16</sup> Illumina devices work on the principle of “sequencing by synthesis”. Sequencing takes place on the surface of the glass slide flow cell. The single-stranded DNA sequences of the DNA library to be sequenced bind by hybridization to oligonucleotides located at the surface of the flow cell. DNA polymerase completes the missing strand, resulting in a double-stranded DNA sequence, and then the source strand is removed. Only the newly formed DNA strand remains bound to the flow cell. Next, DNA strands are subjected to clonal amplification, denaturation and clustering. Antisense DNA sequences are removed from the surface of the flow cell. The next step is sequencing, which takes place simultaneously on all bound sequences. With each sequencing cycle, a single complementary dNTP is added to the bound sequence. A blocker is located at the 3’ of deoxyribose, thus allowing addition of only one dNTP per cycle. Various modes of use are available, with four channel chemistry, two channel chemistry and less often used but still available, one channel chemistry. For four channel chemistry based devices, each of the dNTPs in the mixture is labelled with a specific fluorescent dye (dATP with red, dGTP with blue, dTTP with green, and dCTP with yellow). After each multiplica-

tion cycle, the device determines the inserted dNTP using lasers and four filters to be able to distinguish all four possible bases. The number of multiplication cycles determines the length of the reading. Within an individual cluster, all sequences are identical; thus, in each multiplication cycle the whole cluster glows with the same colour. As for two channel chemistry, only two different fluorescent dyes are needed to label dNTPs; after laser excitation, the device detects dTTP as a green signal, dCTP as a red signal, dATP as a combination of the signal of both dyes, and dGTP is not marked and the device detects them as the absence of a signal. One channel chemistry, as the name suggests, uses a single dye to detect all four bases. Compared to glass slide flow cells, one channel chemistry uses CMOS (complementary metal-oxide semiconductor) chips. After each sequencing cycle, newly incorporated bases are detected using two chemistry steps and combination of two images. In the first chemistry steps, dATPs and dTTPs are labelled with the dye and the first image is taken. Next, during the second chemistry steps, added reagent removes the label from dATP (dATPs have a cleavable linker allowing the removal of the dye) and adds the dye to dCTPs (dCTPs have a linker group that allows dye binding). The second image is taken and the combination of both signals then determines, which of the four bases was incorporated at each sequencing cycle.<sup>17</sup> Additionally, Illumina offers also patterned flow cells. Their



surface area is organized in billions of evenly spaced nanowells with fixed locations, and in each nanowell a distinct cluster is generated. Therefore it offers more efficient use of the flow cell surface area, increased data output, reduced costs, and faster run times. Due to the structured organization patterned flowcells provide significant advantages over non-patterned cluster generation. It is more tolerant to a broader range of library densities, due to nanowell positioning there is no need to map cluster sites, thus saving sequencing running time. With higher cluster density also data per flow cell are better usable, affecting the reduction of the cost per gigabase (Gb).<sup>18</sup>

Illumina offers numerous sequencing platforms for different applications such as MiSeq FGx system that is the first validated benchtop sequencer designed specifically for forensic science or MiSeqDx and NextSeq550Dx which are both Food and Drug Administration-approved platform for *in vitro* diagnostic testing.<sup>19</sup> NGS has substantially increased sequencing output; the production-scale sequencing platform from Illumina NovaSeq 6000 System can read up to 6 tera-bases in 2 days and is ideal for ultra-deep sequencing of the entire genome.<sup>15</sup>

Compared to previously mentioned technologies, Ion Torrent detection of sequencing by synthesis is not based on optics and uses unlabelled dNTPs. As each new dNTP is being incorporated into a growing DNA strand, a pyrophosphate and a hydrogen ion are being released. Detection is therefore based on the change in pH by an ion-sensitive field-effect transistor sensor inside a CMOS layer.<sup>20</sup>

BGI sequencing platforms enable nanoball sequencing, a mechanism that bypasses the requirement for PCR amplification during the library preparation. DNA to be sequenced is first fragmented until a desired length is achieved. Next, fragments are end repaired and specific adaptor sequences and split oligo sequences are added. This enables the single stranded DNA fragments to then be circularized—forming a single stranded circular DNA shape—and replicated many times using a modified rolling circle amplification using Phi 29 polymerase, until a long single-stranded DNA is formed. DNA then forms into a nanoball of a few hundred nanometres in diameter. DNA nanoballs are adhered onto the patterned array flow cell. Similar to Illumina sequencing, one dNTP is incorporated per cycle and the sequence order is determined by laser excitation. BGI released the DNBSEQ-T7 machine that can produce 1–6 tera-bases of high-quality data per day for a wide range of applications. Interestingly, BGI also offers whole genome sequencing for only \$600, including sample processing, sequencing, and data analysis.<sup>21</sup> The high sequencing output and the rapid decrease of the sequencing cost made it possible for such platforms to be adopted by many clinical laboratories.<sup>22,23</sup> Exponential genomic data generation has accelerated translational research and development of new genomic tests.<sup>24</sup> However, NGS has also a few pitfalls. The read length is important for the accuracy of the generated sequence; technologies

that utilize longer reads generally produce longer and high-quality assemblies.<sup>9</sup> However, most of the NGS utilizes short reads (35–600 bp) due to the nature of sequencing chemistry.<sup>9,12</sup> Many genomic regions contain repetitive sequences<sup>9</sup> much longer than sequencing reads which may lead to misassemblies and sequencing gaps.<sup>16,25</sup> Moreover, short-read technologies less accurately detect larger structural variations that are frequently clinically relevant.<sup>26</sup> Another disadvantage is that most of the NGS platforms use PCR in the amplification step (to increase signal strength), which tends to be less accurate in genomic areas that are high in guanine-cytosine content, which can result in errors during DNA “photocopying”.<sup>9</sup>

### 2. 3. Third Generation Sequencing

The main characteristic of third generation sequencing is utilization of long (10,000–2 million bp) sequencing reads.<sup>15</sup> Long read lengths provide better resolution of repetitive genomic regions and structural variants<sup>28</sup> and allow the assembly of complex genomes.<sup>15</sup> Further, third generation technologies do not require library amplification to increase signal strength and enable real-time sequencing.<sup>9,29</sup> In 2011, Pacific Biosciences released technology named *Single-Molecule Real-Time (SMRT) sequencing*<sup>30</sup> and in 2014, *Nanopore sequencing* (Oxford Nanopore Technologies) was introduced.<sup>31</sup> Compared to Illumina, SMRT technology uses a differently labelled dNTPs; as there is no blocker bound to the deoxyribose and the label is located on the phosphate group, dNTPs can be added sequentially without the additional step of terminating blocker removal, hence measuring it in real-time. Nanopore sequencing is based on the tiny changes in current. During sequencing, DNA strands pass through protein nanopores of about 1.8 nanometres in diameter, which are embedded in a polymer membrane. As DNA strands enter the pore, current changes according to the DNA bases that are located inside the pore (about 6 DNA bases at a time). Nanopore sequencing platforms are distinguished by great portability (MinION is in the size of a USB key<sup>32</sup>), ultralong reads, and simple library preparation. Such devices can be used in virtually any environment; for example, to identify infectious disease outbreaks, as already demonstrated in several studies.<sup>33,34</sup> Most recently, Nanopore sequencing has been used for the accurate and comprehensive detection of SARS-Cov-2 during COVID-19 pandemic.<sup>35–37</sup> Third generation sequencing allows direct determination of epigenetic modifications<sup>38</sup> and base modifications in RNA sequencing.<sup>39</sup> The use of methylation profiling by Nanopore sequencing has already been reported by Euskirchen et al.<sup>40</sup> where the power of this technology for rapid tumour classification has been illustrated. However, one drawback of Nanopore sequencing is the higher error rate compared to short-read technologies.<sup>41</sup> Despite many intriguing possibilities of long-read technologies, lower output and accuracy limit their entry into the clinical environment for the time being.<sup>15</sup> Some shortcom-

ings of both second and third generation technologies can be compensated for by using them in combination – known as hybrid sequencing.<sup>42,43</sup> Recent Nanopore sequencing platforms already offer an improved sequencing throughput; PromethION 48 can run up to 48 flow cells at once, producing up to 7,6 tera-bp output yield.<sup>44</sup> Third generation technologies represent a new revolution in genomics as they enable identification of yet undetermined or poorly determined genomic regions.<sup>45,46</sup> For example, ultra-long-read nanopore sequencing enabled the complete resolution of human X-chromosome.<sup>47</sup> and SMRT enabled to resolve 2.25-kb-long stretches of short tandem repeats, implicated in Fragile X syndrome.<sup>48</sup> As the output and accuracy of third generation technologies further increase, they will likely play an important role in the clinical setting for the identification of important structural variants that are poorly determined by short-read technologies.

### 3. Genomic Sequencing in the Clinical Setting

The *precision medicine* is based on treating the patient as an individual, evolving current clinical practice to more individualized health care.<sup>49</sup> It seeks application of genomics as a major strategy in tailoring care to maximise health and minimize harm to patients. As the genome is the best source of information about what makes an individual unique (e.g. more/less susceptible to neurodegenerative diseases) the inclusion of genomic sequencing in the clinical practice accelerates the advancement of precision medicine.

#### 3. 1. Sequencing Approaches

Sequencing presents a less biased approach to diagnostics and has a great potential for ending the diagnostics odyssey for patients with rare diseases.<sup>50</sup> Clinicians choose between whole-genome sequencing (WGS), whole-exome sequencing (WES), transcriptome sequencing, and target-panel sequencing. The most comprehensive, but also the most expensive, is WGS as it interrogates the entire genome. On average, it detects 3 million genomic variants<sup>11,51</sup> most of which belong to non-coding regions of the genome making interpretation difficult.<sup>50</sup> An extensive bioinformatics analysis is thus required to narrow all genomic variants to only a few that might be related to the patient's phenotype. WGS poses problems of data interpretation and storing due to a large amounts of information.<sup>52</sup> Its use has been studied in neonatal intensive care units in critically ill new-borns<sup>53,54</sup> and oncology patients,<sup>55</sup> but is still mainly used in the scientific research. WES focuses on more manageable portion of the genome, known as exome that codes for proteins (only 1–2% of the genome). Variants from the exome are thus easier to interpret. It is also cheaper, faster and in most cases enough informative for

the clinical practice. One disadvantage, however, is lower accuracy in certain areas of genes that are relevant for some medical conditions; which can ultimately result in false-negative results.<sup>15,54,56</sup> Another disadvantage of the WES is also the limited detection of clinically relevant copy number variations (CNVs) and structural variations. Currently there are no accepted standard protocols or quality control measures for CNVs identification in NGS data, and in many cases microarrays are used over WES.<sup>57</sup> WES achieves the diagnostic rate in the range of 25–35%, compared to WGS, which is in the range of 40–60%.<sup>12,58</sup> Due to its better diagnostic yield, WGS is expected to become clinically more important as genomic variant interpretation improves and sequencing cost further decreases.<sup>58</sup> Today, most of the clinical sequencing utilizes target gene panels, which interrogate selected regions of the genome associated with a disease. Targeted sequencing is highly reliable in the identification of variants for disease-related genes, is cost effective, and sequencing results are easier to interpret compared to WES and WGS.<sup>15</sup> There are numerous predesigned targeted gene sequencing panels available from Illumina, for example, AmpliSeq or TrueSeq.<sup>19</sup> Based on numerous studies, small NGS panels focusing on a limited number of actionable genes are expected to become a standard diagnostic tool in oncology.<sup>59–61</sup> A comparison of different sequencing methods can be found in Table 1.

An illustrative example of how the genomic sequencing contributed to the development of minimally-invasive diagnostics (that stems from oncology) is use of *liquid biopsy*, in which circulating-free DNA (cfDNA) from non-solid biological tissues, primarily blood, is analysed.<sup>62</sup> Circulating tumor DNA (ctDNA) represents only a small fraction (<0.5%) of cfDNA<sup>63</sup> and is to some extent representative of the primary tumor DNA. Liquid biopsy is particularly suitable for tumors that are anatomically inaccessible to perform biopsy, in cases of metastatic and advanced stage cancers, and in minimize the number of recurrent biopsies (as a part of patient's follow up after diagnosis had already been made).<sup>5</sup> CfDNA sequencing was shown to be useful also to monitor response to targeted therapy and to detect new resistance mutations, for example in epidermal growth factor receptor (EGFR) gene.<sup>64</sup> Due to its short half life ctDNA is appropriate for the assessment of tumor dynamics especially in more advanced disease stages.<sup>62</sup> Liquid biopsy has also promising use in the population screening and early cancer diagnostics; high sensitivity and specificity were reported in early lung cancer diagnostics<sup>65</sup> and some mutations were detected 2 years before disease onset.<sup>66</sup> Besides, it also allows studying epigenetic modifications<sup>67,68</sup> and methylation pattern (methylome) which can aid to disease classification. Mutations combined with epigenomic, proteomic, and even demographic data, would present unique tumor molecular profile from individual patient and present an important step forward in personalized medicine.

**Table 1:** Comparison of next and third generation sequencing platforms.

Sequencing technology	Platform	Data type	Runtime	Read length	Accuracy	Output range	Applications
Illumina	NextSeq 550	Paired end	12–30h	2 × 150bp	>99.9%	120 Gb	Targeted sequencing (amplicon-based, gene panel). Transcriptome sequencing (total RNA-Seq, mRNA-Seq, gene expression profiling). Arrays.
Oxford Nanopore Technologies	NovaSeq 6000	Paired end	13–44h	2 × 250bp (maximum)	>99.9%	80–6000 Gb	Whole-genome sequencing, read length) exome sequencing, whole transcriptome sequencing, methylation sequencing.
	MinION	Long reads	72h	Longest > 4 Mbp	87–98%	Up to 50 Gb per Flow cell	Whole-genome sequencing, targeted sequencing, RNA sequencing, epigenetics.
PacBio	Sequel II	High fidelity reads	30h	10–25kb	>99%	15–30 Gb per Flow cell	Whole genome sequencing, RNA sequencing, targeted sequencing, population seq, epigenetics.
BGI	MGISEQ-T7	Paired end	24h	150bp	Q30 >80%	1.5–6Tb	Whole-genome sequencing, deep exome sequencing, transcriptome sequencing, targeted panel sequencing.

Q30 designates probability of an incorrect base call 1 in 1000 times.

Nevertheless, the cfDNA sequencing is becoming an important tool also as non-invasive prenatal diagnostics. It has been proven as effective and safe screening method for trisomies 21, 18, and 13, and sex chromosome aneuploidies compared with traditional prenatal screening. The tests also proved to be fast and financially sustainable.<sup>69</sup>

### 3. 2. Integration of Genomic Sequencing in the Clinical Practice

For a successful implementation in the clinical practice, sequencing must provide reliable results to the clinician. NGS requires end-to-end validation from DNA extraction to bioinformatic analysis to minimize the occurrence of false-positive and false-negative results.<sup>70</sup> Complete implementation also requires integration of genomic data into the *electronic health records* (EHRs), which can be quite challenging for smaller healthcare institutions.<sup>71</sup> Successful implementation of personalized medicine will increasingly rely on EHRs to store vast amounts of genomic data and to appropriately integrate relevant genomic information into clinical care.<sup>71</sup> One of the barriers for integrating sequencing results in EHRs is that they are frequently entered as a summary rather than raw data which limits data accession and reanalysis.<sup>72</sup> Although genomic data is static, its interpretation is not. As new knowledge arises, interpretation can yield additional diagnoses, and data reanalysis was found to be a cost-effective approach.<sup>73</sup> Routine reanalyses were shown to improve diagnostic rates<sup>74–76</sup> due to establishment of new

disease-gene associations, improved bioinformatics tools, and data sharing.<sup>77</sup> The integration of artificial intelligence (AI) is also promising, however, translating technical success in AI-driven analytics into meaningful clinical impact remains a challenge.<sup>78</sup> The proliferation of genomic sequencing also requires medical professionals who will be adept at understanding and returning genomic results to the patient. Thus, education for the next generation of health care providers is of great importance.<sup>79</sup> Another factor regarding implementation is the coverage of sequencing costs by health insurance companies, which unfortunately lags behind the advances in the sequencing technology.<sup>80</sup> The clinician must sometimes provide notes on how the genomic testing will affect the course of the disease or its management.<sup>81</sup> Increasing cost coverage by the health insurance companies will be catalysed by a further drop in sequencing cost and accumulating evidence in studies of clinical usefulness.<sup>81</sup> Several studies<sup>82–84</sup> demonstrated high diagnostic yield and cost-effectiveness of genomic sequencing which was maximized by its early application in the diagnostic pathway.<sup>81,82</sup>

### 3. 3. National Genomes Sequencing

To elucidate genetic background of a certain population, more and more countries are opting for studies of *national genomes*. The genomic data can be of great support to a healthcare system. If we are acquainted with common alleles in the healthy population, it is easier to identify disease related variants. National genome projects are

one of the fundamental elements in establishing effective identification and rapid diagnosis of rare diseases as they allow distinguishing between potentially causative genetic variants and rare, benign genetic variants that are unique for the original population. These rare genetic variants are the main source of false-positive results of genetic testing that can directly affect the clinical diagnosis and the course of treatment. Some projects are focused on rare diseases or cancer, whilst others have pursued population-based projects. In the UK, for example, the goal of 100,000 genomes was reached and served to establish the infrastructure needed for the integration of sequencing in the clinical setting.<sup>85</sup> The Chinese Academy of Sciences (CAS) launched the country's Precision Medicine Initiative with the goal of sequencing 1000 million human genomes by 2030.

In Europe, the 1+ Million European Genomes Project began in 2018, in which Slovenia also participates.<sup>86</sup> Slovenian Genome Project began at the end of 2019. This presents a pilot project which will outline the key directions of the future genomic projects, develop bioinformatic tools for data exchange, prepare the legal and ethical base, educate healthcare professionals and general public, and carry out a pilot genome sequencing project of Slovenian patients with rare diseases and healthy Slovenian population. In Slovenia, NGS methodology is already well established as its advances have been used in fields such as clinical neurology (dementia,<sup>87</sup> multiple sclerosis<sup>88</sup>) paediatrics (metabolism of new-borns,<sup>89</sup> hearing loss<sup>90</sup>), clinical oncology,<sup>91</sup> clinical microbiology (microbiota associated with preterm birth,<sup>92</sup> and age and gender<sup>93</sup>), pharmacogenomics<sup>94</sup> and forensic medicine.<sup>95</sup>

The use of genomic screening in preventive health is interesting, although it brings some concerns about its widespread implementation in routine clinical practice.<sup>96,97</sup> Current estimates predict that 3–5% of people present a medically actionable variant.<sup>98</sup> This assumption is based on the DiscovEHR project, which involved over 50,000 adult participants aimed at connecting high-performance sequencing to an integrated health system. Among ~ 4.2 million rare single nucleotide variants, including insertions and deletions, adverse variants in 76 clinically relevant genes were found in about 3.5% of individuals. This study set a basis of individual tailored medicine that is based on therapeutic discoveries guided by genomics.<sup>98</sup> In the cases of “medically actionable genes”, genomic screening of asymptomatic population could have a significant public health impact.<sup>99</sup> Finding new population specific actionable genes that may save lives and/or majorly impact the quality of lives remains among the goals of the national genome sequencing projects.

### 3. 4. Sequencing During the COVID-19 Pandemics

Sequencing technologies can be used to detect and identify pathogens, determine their resistance to antibiot-

ics, construct phylogenetic trees, or epidemiologically track disease outbreaks.<sup>100</sup> Genome sequencing can typify microbial strains with greater accuracy compared to classical microbiological methods.<sup>101</sup> As of April 2021, COVID-19 pandemic affected over 136 million people worldwide and resulted in death of almost 3 million people.<sup>102</sup> On January 5, 2020, next-generation meta-transcriptomic sequencing allowed researchers to obtain the first and complete viral genome of SARS-CoV-2 from a patient in Wuhan, China.<sup>103</sup> Soon, several hundred genomes became publicly available (<https://www.gisaid.org/>), allowing rapid development of diagnostic tests<sup>104</sup> vaccines and antivirals<sup>105</sup>, and disease tracking.<sup>106</sup> Few concepts of sequencing have been used for SARS-CoV-2.<sup>107</sup> Most studies have used the Illumina platform, however the Oxford Nanopore Technologies has been utilized for aforementioned shotgun metatranscriptomics<sup>108</sup> which enables de novo genome assembly without prior knowledge of the sequence.<sup>109</sup> Another method is amplicon-based sequencing, limited to specific parts of the viral genome. Such libraries can be sequenced on benchtop platforms with a mid-throughput (Illumina NexSeq, MiSeq, Ion torrent).<sup>107</sup> RNA sequencing using Oxford Nanopore Technologies and DNA nanoball sequencing was applied in a recent study<sup>36</sup> to reveal finished representation of SARS-CoV-2 transcriptome and epitranscriptome.

Comparative genomics revealed, that SARS-CoV-2 was a member of *Betacoronavirus* and fell into a subgenus *Sarbecovirus* that also includes Sars-Cov<sup>110</sup> and allowed the “hunt” for its zoonotic origins.<sup>103</sup> Sequencing is vital in aspects of finding novel viral hosts to block interspecies transmission. Bat coronavirus, RaTG13, sampled in Yunnan province, is at the nucleotide level approximately 96% similar to SARS-CoV-2; however, there were major differences in key genomic features important for infectivity of the virus.<sup>103,111</sup> Moreover, due to the ecological separation of humans and bats, it is probable that some other species acted as an intermediate host.<sup>103</sup> Recent research reports that viruses in Malayan pangolins are closely related to SARS-CoV-2<sup>112</sup> and these animals are of great interest because of involvement in illegal animal trafficking.<sup>103</sup> Pangolin-CoV was shown to be 91.02% identical to SARS-Cov-2 at the which makes him the second closest relative behind RaTG13.<sup>113</sup> It seems that betacoronaviruses exist in the number of mammalian species and it is thus imperative to perform a wider sampling of animals from wet markets and those who live close to human populations to block potential interspecies transmission.<sup>103</sup> Furthermore, NGS allows tracking of the viral strains. RNA viruses continuously accumulate mutations.<sup>114</sup> New mutations in SARS-CoV-2 genome will continuously arise over time and space and result in branching of the original “reference genome”. NGS allows us to observe evolutionary pattern of SARS-CoV-2, which is crucial for efficient disease prevention and control, for example, to reveal new routes of infection. Tracking mutations and variable regions of the viral is thus

imperative for development of effective therapy in the eyes of viral diversity and consequent drug resistance.<sup>115</sup> As of April 2021, more than 1 million coronavirus-related genome sequences have been uploaded to EpiFluTM (GISAID) world-wide and the number is rapidly increasing. NGS is used to trace interpersonal transmission of the virus.<sup>116</sup> High resolution genomic epidemiology is thereby becoming an effective tool for public health surveillance and disease control.<sup>117</sup> Knowing SARS-COV2 genome also helps to achieve a more effective disease strategy, to investigate cases with unclear sources of infection within a short turnaround time.<sup>110, 118</sup>

Furthermore, NGS technology was applied to investigate mechanisms of SARS-CoV-2 infection.<sup>116</sup> For example, RNA sequencing has been used to determine susceptible organs with higher expression of angiotensin-converting enzyme 2 (ACE2) receptor, which serves as a receptor for SARS-CoV-2.<sup>119</sup> NGS and single-cell RNA sequencing were used to determine expression of ACE2 receptor in numerous organs and cells after infection with SARS-CoV-2<sup>116</sup>, which will most definitely benefit diagnostic and therapeutic target identification.

#### 4. Future Outlook

Researches tend to sequence as many human genomes as possible, known as population-scale resequencing, capturing not just genomic but also epigenomic data. Genomics and epigenomics are frequently studied separately but to fully reach the potential of precision medicine it will be necessary to study them together. Only integrated data from various big “omics” will enable us to fully understand disease mechanisms and substantially increase the sensitivity of genomic sequencing. One of the obstacles, however, is the storage and processing of large amounts of data, which is why the parallel development of bioinformatic analysis is required. The question which obtained information is of importance requires the existence of large genomic databases. Integrated analysis of medical “big-data” will benefit from artificial intelligence technologies, such as machine learning and its subset, deep learning.<sup>120</sup> Novel long-read technologies will enable routine resequencing, allowing better determination of repetitive regions and structural variants. Epidemiologists will follow the outbreak of an infectious disease through microbial sequencing from various samples, such as wastewaters. Therefore, it will be possible to detect a disease outbreak at an early stage and possibly even prevent it. Small, portable devices will be useful in such situations. Oxford Nanopore has recently started developing device called SmidgION, which is even smaller than MinION.<sup>44</sup> It will be used with smartphones and other portable devices. The portability, high output, and simplicity of such machines have infinite on-site applications: in ecology, forensics, population screening, epidemiology, to name a few.

However, although the technology shows immense breakthrough, education of staff has to become the central concern of all countries employing next generation technologies. Well trained medical geneticists and consultants with narrow specializations on next generation sequencing will be the ones enabling meaningful interpretation of the results, thus providing use of the result in clinical setting.

#### Acknowledgments

The study was partially financed by Slovenian Research Agency programme grant No. P1-0390.

#### 5. References

1. A. M. Maxam, W. Gilbert, *PNAS* **1977**, *74*, 560–564. DOI:10.1073/pnas.74.2.560
2. F. Sanger, S. Nicklen, A. R. Coulson, *PNAS* **1977**, *74*, 5463–5467. DOI:10.1073/pnas.74.12.5463
3. J. C. Venter, M. D. Adams, E. W. Myers, P. W. Li, R. J. Mural, G. G. Sutton, et al., *Science* **2001**, *291*, 1304–1351.
4. J. A. Schloss, *Nat. Biotechnol.* **2008**, *26*, 1113–1115. DOI:10.1038/nbt1008-1113
5. E. L. Van Dijk, H. Auger, Y. Jaszczyszyn, C. Thermes, *Trends Genet.* **2014**, *30*, 418–426. DOI:10.1016/j.tig.2014.07.001
6. National Human Genome Research Institute, <https://www.genome.gov/>, (accessed: April 5, 2020)
7. J. M. Prober, G. L. Trainor, R. J. Dam, F. W. Hobbs, C. W. Robertson, R. J. Zagursky, et al., *Science* **1987**, *238*, 336–341. DOI:10.1126/science.2443975
8. H. Swerdlow, R. Gesteland, *Nucleic Acids Res.* **1990**, *18*, 1415–1419. DOI:10.1093/nar/18.6.1415
9. E. L. van Dijk, Y. Jaszczyszyn, D. Naquin, C. Thermes, *Trends in Genet.* **2018**, *34*, 666–681. DOI:10.1016/j.tig.2018.05.008
10. E. S. Lander, L. M. Linton, B. Birren, C. Nusbaum, M. C. Zody, J. Baldwin, et al., *Nature* **2001**, *409*, 860–921. DOI:10.1038/35057062
11. R. Drmanac, A. B. Sparks, M. J. Callow, A. L. Halpern, N. L. Burns, B. G. Kermani, et al., *Science* **2010**, *327*, 78–81.
12. K. R. Kumar, M. J. Cowley, R. L. Davis, *Semin. Thromb. Hemostasis* **2019**, *45*, 661–673. DOI:10.1055/s-0039-1688446
13. M. Margulies, M. Egholm, W. E. Altman, S. Attiya, J. S. Bader, L. A. Bemben, et al., *Nature* **2006**, *441*, 120–120. DOI:10.1038/nature04774
14. C. T. Harrington, E. I. Lin, M. T. Olson, J. R. Eshleman, *Arch. Pathol. Lab. Med.* **2013**, *137*, 1296–1303. DOI:10.5858/arpa.2012-0463-RA
15. G. Gao, D. I. Smith, *Clinical Chemistry* **2020**, *66*, 77–88. DOI:10.1373/clinchem.2019.303305
16. S. Goodwin, J. D. McPherson, W. R. McCombie, *Nat. Rev. Genet.* **2016**, *17*, 333. DOI:10.1038/nrg.2016.49
17. Illumina, CMOS Chip and One-Channel SBS Chemistry, <https://www.illumina.com/science/technology/next-genera->

- tion-sequencing/sequencing-technology/semiconductor-sequencing-cmos.html, (accessed: December 2, 2020)
18. Illumina, Patterned flow cells, <https://emea.illumina.com/science/technology/next-generation-sequencing/sequencing-technology/patterned-flow-cells.html>, (accessed: April 14, 2021)
  19. Illumina, <https://www.illumina.com/>, (accessed: March 20, 2020)
  20. J. M. Rothberg, W. Hinze, T. M. Rearick, J. Schultz, W. Mileski, M. Davey, et al., *Nature* **2011**, *475*, 348–352. DOI:10.1038/nature10242
  21. BGI Genomics, <https://www.bgi.com/global/>, (accessed: March 22, 2020)
  22. G. O. S. Coyne, N. Takebe, A. P. Chen, *Curr. Probl. Cancer* **2017**, *41*, 182–193. DOI:10.1016/j.currprobcancer.2017.02.001
  23. Y. O. Alekseyev, R. Fazeli, S. Yang, R. Basran, T. Maher, N. S. Miller, et al., *Academic Pathology* **2018**, *5*, 2374289518766521. DOI:10.1177/2374289518766521
  24. R. Luthra, K. P. Patel, M. J. Routbort, R. R. Broaddus, J. Yau, C. Simien, et al., *J. Mol. Diagn.* **2017**, *19*, 255–264. DOI:10.1016/j.jmoldx.2016.09.011
  25. S. L. Salzberg, J. A. Yorke, *Bioinformatics* **2005**, *21*, 4320–4321. DOI:10.1093/bioinformatics/bti769
  26. J. Weischenfeldt, O. Symmons, F. Spitz, J. O. Korbel, *Nat. Rev. Genet.* **2013**, *14*, 125–138. DOI:10.1038/nrg3373
  27. D. Qin, *Cancer Biol. Med.* **2019**, *16*, 4–10.
  28. A. Rhoads, K. F. Au, *Genomics Proteomics Bioinf.* **2015**, *13*, 278–289. DOI:10.1016/j.gpb.2015.08.002
  29. E. E. Schadt, S. Turner, A. Kasarskis, *Hum. Mol. Genet.* **2010**, *19*, 227–240. DOI:10.1093/hmg/ddq416
  30. M. A. Quail, M. Smith, P. Coupland, T. D. Otto, S. R. Harris, T. R. Connor, et al., *BMC Genomics* **2012**, *13*, 341. DOI:10.1186/1471-2164-13-341
  31. L. Steinbock, A. Radenovic, *Nanotechnology* **2015**, *26*, 074003. DOI:10.1088/0957-4484/26/7/074003
  32. T. Laver, J. Harrison, P. O'Neill, K. Moore, A. Farbos, K. Paszkiewicz, et al., *Biomol. Detect. Quantif.* **2015**, *3*, 1–8. DOI:10.1016/j.bdq.2015.02.001
  33. J. Quick, N. J. Loman, S. Duraffour, J. T. Simpson, E. Severi, L. Cowley, et al., *Nature* **2016**, *530*, 228–232.
  34. N. R. Faria, E. C. Sabino, M. R. Nunes, L. C. J. Alcantara, N. J. Loman, O. G. Pybus, *Genome Med.* **2016**, *8*, 97. DOI:10.1186/s13073-016-0356-2
  35. M. Wang, A. Fu, B. Hu, Y. Tong, R. Liu, Z. Liu, et al., *Small* **2020**, *16*, 2002169. DOI:10.1002/smll.202002169
  36. D. Kim, J.-Y. Lee, J.-S. Yang, J. W. Kim, V. N. Kim, H. Chang, *Cell* **2020**, *181*, 914–921.e10. DOI:10.1016/j.cell.2020.04.011
  37. S. Marquez, B. Prado-Vivar, J. J. Guadalupe, B. G. Granja, M. Jibaja, M. Tobar, et al., *medRxiv* **2020**.
  38. B. A. Flusberg, D. R. Webster, J. H. Lee, K. J. Travers, E. C. Olivares, T. A. Clark, et al., *Nat. Methods* **2010**, *7*, 461–465. DOI:10.1038/nmeth.1459
  39. D. R. Garalde, E. A. Snell, D. Jachimowicz, B. Sipos, J. H. Lloyd, M. Bruce, et al., *Nat. Methods* **2018**, *15*, 201–206. DOI:10.1038/nmeth.4577
  40. P. Euskirchen, F. Bielle, K. Labreche, W. P. Kloosterman, S. Rosenberg, M. Daniau, et al., *Acta Neuropathol.* **2017**, *134*, 691–703. DOI:10.1007/s00401-017-1743-5
  41. M. Jain, J. R. Tyson, M. Loose, C. L. Ip, D. A. Eccles, J. O'Grady, et al., *F1000Research* **2017**, *6*, 760. DOI:10.12688/f1000research.11354.1
  42. J. R. Miller, P. Zhou, J. Mudge, J. Gurtowski, H. Lee, T. Ramaraj, et al., *BMC Genomics* **2017**, *18*, 541. DOI:10.1186/s12864-017-3927-8
  43. R. Minei, R. Hoshina, A. Ogura, *BMC Genomics* **2018**, *19*, 700. DOI:10.1186/s12864-018-5067-1
  44. Oxford Nanopore Technologies, <https://nanoporetech.com/>, (accessed: April 5, 2020)
  45. M. J. Chaisson, J. Huddleston, M. Y. Dennis, P. H. Sudmant, M. Malig, F. Hormozdiari, et al., *Nature* **2015**, *517*, 608–611. DOI:10.1038/nature13907
  46. J. S. Seo, A. Rhie, J. Kim, S. Lee, M.-H. Sohn, C.-U. Kim, et al., *Nature* **2016**, *538*, 243–247. DOI:10.1038/nature20098
  47. K. H. Miga, S. Koren, A. Rhie, M. R. Vollger, A. Gershman, A. Bzikadze, et al., *Nature* **2020**, *585*, 79–84.
  48. M. H. Schmidt, C. E. Pearson, *DNA repair* **2016**, *38*, 117–126. DOI:10.1016/j.dnarep.2015.11.008
  49. F. S. Collins, H. Varmus, *N. Engl. J. Med.* **2015**, *372*, 793–795. DOI:10.1056/NEJMp1500523
  50. M. B. Neu, K. M. Bowling, G. M. Cooper, *Curr. Opin. Pediatr.* **2019**, *31*, 732–738. DOI:10.1097/MOP.0000000000000815
  51. E. A. Vidal, T. C. Moyano, B. I. Bustos, E. Pérez-Palma, C. Moraga, E. Riveras, et al., *Sci. Rep.* **2019**, *9*, 1–11. DOI:10.1038/s41598-019-39391-z
  52. A. Nekrutenko, J. Taylor, *Nat. Rev. Genet.* **2012**, *13*, 667–672. DOI:10.1038/nrg3305
  53. C. J. Saunders, N. A. Miller, S. E. Soden, D. L. Dinwiddie, A. Noll, N. A. Alnadi, et al., *Sci. Transl. Med.* **2012**, *4*, 135–154. DOI:10.1126/scitranslmed.3004041
  54. M. M. Clark, A. Hildreth, S. Batalov, Y. Ding, S. Chowdhury, K. Watkins, et al., *Sci. Transl. Med.* **2019**, *11*, eaat6177.
  55. H. Nakagawa, M. Fujita, *Cancer Sci.* **2018**, *109*, 513–522. DOI:10.1111/cas.13505
  56. S. W. Kong, I.-H. Lee, X. Liu, J. N. Hirschhorn, K. D. Mandl, *Genet. Med.* **2018**, *20*, 1617–1626. DOI:10.1038/gim.2018.51
  57. J. Y. Hehir-Kwa, R. Pfundt, J. A. Veltman, *Expert Rev. Mol. Diagn.* **2015**, *15*, 1023–32. DOI:10.1586/14737159.2015.1053467
  58. J. S. Mattick, M. Dinger, N. Schonrock, M. Cowley, *Med. J. Aust.* **2018**, *209*, 197–199. DOI:10.5694/mja17.01176
  59. J. F. Laes, P. Aftimos, P. Barthelemy, J. Bellmunt, G. Berchem, C. Camps, et al., *Oncotarget* **2018**, *9*, 20282–20293. DOI:10.18632/oncotarget.24757
  60. T. Giardina, C. Robinson, F. Grieco-Iacopetta, M. Millward, B. Iacopetta, D. Spagnolo, et al., *Pathology* **2018**, *50*, 389–401. DOI:10.1016/j.pathol.2018.01.005
  61. K. Sunami, H. Ichikawa, T. Kubo, M. Kato, Y. Fujiwara, A. Shimomura, et al., *Cancer Sci.* **2019**, *110*, 1480–1490. DOI:10.1111/cas.13969

62. E. Crowley, F. Di Nicolantonio, F. Loupakis, A. Bardelli, *Nat. Rev. Clin. Oncol.* **2013**, *10*, 472. DOI:10.1038/nrclinonc.2013.110
63. R. Mead, M. Duku, P. Bhandari, I. Cree, *BJC.* **2011**, *105*, 239–245. DOI:10.1038/bjc.2011.230
64. T. K. Sundaresan, L. V. Sequist, J. V. Heymach, G. J. Riely, P. A. Jänne, W. H. Koch, et al., *Clin. Cancer Res.* **2016**, *22*, 1103–1110. DOI:10.1158/1078-0432.CCR-15-1031
65. J. Phallen, M. Sausen, V. Adleff, A. Leal, C. Hruban, J. White, et al., *Sci. Transl. Med.* **2017**, *9*. DOI:10.1126/scitranslmed.aan2415
66. E. Gormally, P. Vineis, G. Matullo, F. Veglia, E. Caboux, E. Le Roux, et al., *Cancer Res.* **2006**, *66*, 6871–6876. DOI:10.1158/0008-5472.CAN-05-4556
67. W. Liang, Y. Zhao, W. Huang, Y. Gao, W. Xu, J. Tao, et al., *Theranostics* **2019**, *9*, 2056. DOI:10.7150/thno.28119
68. L. Giannopoulou, M. Zavridou, S. Kasimir-Bauer, E. S. Lianidou, *Transl. Res.* **2019**, *205*, 77–91. DOI:10.1016/j.trsl.2018.10.003
69. Ontario Health Technology, *Ontario health technology assessment series* **2019**, *19*, 1–166.
70. S. Yohe, B. Thyagarajan, *Arch. Pathol. Lab. Med.* **2017**, *141*, 1544–1557. DOI:10.5858/arpa.2016-0501-RA
71. N. S. Abul-Husn, E. E. Kenny, *Cell* **2019**, *177*, 58–69. DOI:10.1016/j.cell.2019.02.039
72. B. H. Shirts, J. S. Salama, S. J. Aronson, W. K. Chung, S. W. Gray, L. A. Hindorff, et al., *J. Am. Med. Assoc.* **2015**, *22*, 1231–1242. DOI:10.1093/jamia/ocv065
73. L. J. Ewans, D. Schofield, R. Shrestha, Y. Zhu, V. Gayevskiy, K. Ying, et al., *Genet. Med.* **2018**, *20*, 1564–1574. DOI:10.1038/gim.2018.39
74. S. M. Hiatt, M. D. Amaral, K. M. Bowling, C. R. Finnilla, M. L. Thompson, D. E. Gray, et al. *Clin. Genet.* **2018**, *94*, 174–178. DOI:10.1111/cge.13259
75. A. M. Wenger, H. Guturu, J. A. Bernstein, G. Bejerano, *Genet. Med.* **2017**, *19*, 209–214. DOI:10.1038/gim.2016.88
76. C. F. Wright, J. F. McRae, S. Clayton, G. Gallone, S. Aitken, T. W. FitzGerald, et al., *Genet. Med.* **2018**, *20*, 1216–1223. DOI:10.1038/gim.2017.246
77. A.-L. Bruel, A. Vitobello, F. T. Mau-Them, S. Nambot, Y. Duffourd, V. Quéré, et al., *Genet. Med.* **2019**, *21*, 1657–1661. DOI:10.1038/s41436-018-0383-z
78. Editorial, *Lancet* **2018**, *390*, 2739. DOI:10.1016/S0140-6736(17)31540-4
79. M. Champion, C. Goldgar, R. J. Hopkin, C. A. Prows, S. Dasgupta, *Genet. Med.* **2019**, *21*, 2422–2430. DOI:10.1038/s41436-019-0548-4
80. P. A. Deverka, D. Kaufman, A. L. McGuire, *JAMA* **2014**, *312*, 1857–1858. DOI:10.1001/jama.2014.14915
81. D. R. Adams, C. M. Eng, *N. Engl. J. Med.* **2018**, *379*, 1353–1362. DOI:10.1056/NEJMra1711801
82. T. Y. Tan, O. J. Dillon, Z. Stark, D. Schofield, K. Alam, R. Shrestha, et al., *JAMA Pediatrics* **2017**, *171*, 855–862. DOI:10.1001/jamapediatrics.2017.1755
83. L. Meng, M. Pammi, A. Saronwala, P. Magoulas, A. R. Ghazi, F. Vetrini, et al., *JAMA Pediatrics* **2017**, *171*, 173438–173438.
84. L. Farnaes, A. Hildreth, N. M. Sweeney, M. M. Clark, S. Chowdhury, S. Nahas, et al., *NPJ Genomic Med.* **2018**, *3*, 10. DOI:10.1038/s41525-018-0049-4
85. The 100,000 Genomes Project, <https://www.genomicsengland.co.uk/about-genomics-england/the-100000-genomes-project/>, (accessed: July 22, 2020)
86. European Commission, <https://ec.europa.eu/digital-single-market/en/european-1-million-genomes-initiative/>, (accessed: July 22, 2020)
87. B. Zalar, A. Maver, A. Kovanda, A. Peterlin, B. Peterlin, *Psychiatr. Danubina* **2018**, *30*, 216–219. DOI:10.24869/spsih.2018.216
88. L. Vidmar, A. Maver, J. Drušević, J. Sepčić, I. Novaković, S. Ristič, et al., *Sci. Rep.* **2019**, *9*, 1–10. DOI:10.1038/s41598-019-45598-x
89. A. Smon, B. R. Lampret, U. Groselj, M. Z. Tansek, J. Kovac, D. Perko, et al., *Clin. Biochem.* **2018**, *52*, 48–55. DOI:10.1016/j.clinbiochem.2017.10.016
90. J. Kovač, G. Klančar, K. Trebušak Podkrajšek, S. Battelino, *Front. Genet.* **2017**, *8*, 95. DOI:10.3389/fgene.2017.00095
91. D. Šekoranja, E. Boštjančič, V. Salapura, B. Mavčič, J. Pižem, *Cancer Genet.* **2018**, *228*, 12–16. DOI:10.1016/j.cancergen.2018.07.001
92. K. Hočevár, A. M. Maver, M. Vidmar Šimic, A. Hodžić, A. Haslberger, T. Premru-Sršen, et al., *Front. Med.* **2019**, *6*, 201. DOI:10.3389/fmed.2019.00201
93. A. Mahnic, M. Rupnik, *PLoS One* **2018**, *13*, e0209209. DOI:10.1371/journal.pone.0209209
94. K. Hočevár, A. Maver, B. Peterlin, *Front. Pharmacol.* **2019**, *10*, 240–240. DOI:10.3389/fphar.2019.00240
95. K. Kouter, T. Zupanc, A. Videtic Paska, *J. Affect. Disord.* **2019**, *253*, 419–425. DOI:10.1016/j.jad.2019.04.077
96. J. P. Evans, B. C. Powell, J. S. Berg, *JAMA* **2017**, *317*, 1904–1905. DOI:10.1001/jama.2017.0432
97. M. F. Murray, *Ann. Intern. Med.* **2018**, *169*, 407–408. DOI:10.7326/M18-1722
98. F. E. Dewey, M. F. Murray, J. D. Overton, L. Habegger, J. B. Leader, S. N. Fetterolf, et al., *Science* **2016**, *354*, aaf6814.
99. J. S. Berg, M. J. Khoury, J. P. Evans, *Genet. Med.* **2011**, *13*, 499–504. DOI:10.1097/GIM.0b013e318220aaba
100. A. Kozińska, P. Seweryn, I. Sitkiewicz, *J. Appl. Genet.* **2019**, *60*, 103–111. DOI:10.1007/s13353-019-00482-2
101. A. Schürch, S. Arredondo-Alonso, R. Willems, R. V. Goering, *Clin. Microbiol. Infect.* **2018**, *24*, 350–354. DOI:10.1016/j.cmi.2017.12.016
102. Coronavirus Update, <https://www.worldometers.info/coronavirus/>, (accessed: April 11, 2021)
103. Y.-Z. Zhang, E. C. Holmes, *Cell* **2020**, *181*, 223–227. DOI:10.1016/j.cell.2020.03.035
104. V. M. Corman, O. Landt, M. Kaiser, R. Molenkamp, A. Meijer, D. K. Chu, et al., *Eurosurveillance* **2020**, *25*, 2000045. DOI:10.2807/1560-7917.ES.2020.25.3.2000045
105. Y. Wang, F. Zhou, D. Zhang, J. Zhao, R. Du, Y. Hu, et al., *Trials* **2020**, *21*, 422.
106. N. D. Grubaugh, J. T. Ladner, P. Lemey, O. G. Pybus, A. Rambaut, E. C. Holmes, et al., *Nat. Microbiol.* **2019**, *4*,

- 10–19. DOI:10.1038/s41564-018-0296-2
107. M. Chiara, A. M. D'Erchia, C. Gissi, C. Manzari, A. Parisi, N. Resta, et al., *Brief. Bioinformatics* **2020**, *22*, 616–630. DOI:10.1093/bib/bbaa297
108. J. F.-W. Chan, S. Yuan, K.-H. Kok, K. K.-W. To, H. Chu, J. Yang, et al., *The Lancet* **2020**, *395*, 514–523. DOI:10.1016/S0140-6736(20)30154-9
109. J. Handelsman, *Microbiol. Mol. Biol. Rev.* **2004**, *68*, 669–85. DOI:10.1128/MMBR.68.4.669-685.2004
110. R. Lu, X. Zhao, J. Li, P. Niu, B. Yang, H. Wu, et al., *The Lancet* **2020**, *395*, 565–574. DOI:10.1016/S0140-6736(20)30251-8
111. B. Coutard, C. Valle, X. de Lamballerie, B. Canard, N. Seidah, E. Decroly, *Antiviral Res.* **2020**, *176*, 104742. DOI:10.1016/j.antiviral.2020.104742
112. T. T.-Y. Lam, N. Jia, Y.-W. Zhang, M. H.-H. Shum, J.-F. Jiang, H.-C. Zhu, et al., *Nature* **2020**, *583*, 282–285. DOI:10.1038/s41586-020-2169-0
113. T. Zhang, Q. Wu, Z. Zhang, *Curr. Biol.* **2020**, *30*, 1346–1351.e2.114. R. Sanjuan, M. R. Nebot, N. Chirico, L. M. Mansky, R. Belshaw, *J. Virol.* **2010**, *84*, 9733.
115. P. Ellis, F. Somogyvari, D. P. Virok, M. Nosedá, G. R. McLean, *Curr. Genet. Med. Rep.* **2021**, 1–12.
116. X. Chen, Y. Kang, J. Luo, K. Pang, X. Xu, J. Wu, et al., *Front. Cell. Infect. Microbiol.* **2021**, *11*. DOI:10.3389/fcimb.2021.632490
117. J. L. Gardy, N. J. Loman, *Nat. Rev. Gen.* **2018**, *19*, 9–20. DOI:10.1038/nrg.2017.88
118. X. Deng, W. Gu, S. Federman, L. du Plessis, O. G. Pybus, N. R. Faria, et al., *Science* **2020**, *369*, 582. DOI:10.1126/science.abb9263
119. M. M. Medina-Enriquez, S. Lopez-Leon, J. A. Carlos-Escalante, Z. Aponte-Torres, A. Cuapio, T. Wegman-Ostrosky, *Cell Biosci.* **2020**, *10*, 148. DOI:10.1186/s13578-020-00519-8
120. R. Hamamoto, M. Komatsu, K. Takasawa, K. Asada, S. Kaneko, *Biomolecules* **2020**, *10*, 62. DOI:10.3390/biom10010062

## Povzetek

Določanje nukleotidnega zaporedja – sekvenciranje je že več kot 40 let stara tehnologija, a kot orodje v klinični medicini velja za relativno mlado. Z napredkom in razvojem tehnologije sekvenciranje postaja občutno cenejše, hitrejše in natančnejše; prav zato ga je mogoče vključevati v klinične laboratorije za rutinsko uporabo. Leta 2003 je bilo prvič določeno zaporedje človeškega genoma, s tem pa postavljeni temelji za uporabo genomike v klinični praksi ter razvoj personalizirane medicine. Poznavanje nukleotidnega zaporedja predstavlja nepristranski pristop k diagnostiki ter ima lahko pomembno vlogo tudi pri spremljanju bolezni in zdravljenju, a prehod iz raziskovalne uporabe v klinično prakso lahko traja tudi veliko let. V zadnjem desetletju je bil porast novih tehnologij sekvenciranja skokovit, kar pa pomeni, da se mora strokovni kader relativno hitro izobraževati na področju osnovnega znanja o zmožnostih in pomanjkljivostih obstoječih metod ter njihovi uporabi v kliničnih okoljih in raziskavah. V preglednem članku predstavljamo pregled tehnologij sekvenciranja z zgodovinskega vidika in mu dodamo klinično uporabo sekvenciranja. Nekatera najbolj obetavna področja so predstavljena z izbranimi primeri slovenskih raziskovalcev.



Except when otherwise noted, articles in this journal are published under the terms and conditions of the Creative Commons Attribution 4.0 International License



Scientific paper

# Study of Electrical Discharge Machining Parameters on Stainless Steel Using Copper Tool Electrode and Its Effect on the Structure and Electrochemical Properties

Mozhgan Karimi, Sayyed Ahmad Nabavi-Amri\* and Ahmad Soleymanpour

School of Chemistry, Damghan University, Damghan 3671641167, Iran

\* Corresponding author: E-mail: nabavi@du.ac.ir

Tel/Fax: +982335220095

Received: 03-18-2020

## Abstract

In this work, the effect of the presence and the diffusion of the Copper from the tool electrode onto the EDMed stainless steel (SS) surface have been investigated by electrochemical impedance spectroscopy (EIS), X-ray diffraction (XRD), Quantometer analysis, and Optical microscopic observations. The Taguchi method was used to study the effects of Pulse-on time ( $t_{on}$ ), Pulse-off time ( $t_{off}$ ), discharge current ( $I$ ), and overall machining time ( $\tau$ ) on chemical composition, microstructures, micro-cracks, and electrochemical corrosion of EDMed stainless steel workpieces. The results show that the variation of machining parameters changes the chemical composition of the workpieces. By increasing the discharge current and decreasing the Pulse-on time, the copper and the carbon diffuse onto the surface of the workpiece. Consequently, the chemical composition of the workpiece surface changes, leading to an increment of the corrosion resistance. The XRD analysis shows the formation of  $Fe_2C$ ,  $Cr_3C_2$ , and  $CuNi$ . In addition, at higher values of discharge current and  $t_{on}/t_{off}$  ratio, the micro-cracks propagate on the surface of the workpiece.

**Keyword:** Electrical discharge machining; Stainless steel; Electrochemical impedance spectroscopy; Electrochemical corrosion; Copper diffusion

## 1. Introduction

Electrical discharge machining (EDM) is one of the most effective processes that can produce high-quality materials precisely with a wide range of strength, hardness, and shape.<sup>1,2</sup> In the EDM process by applying an electrical potential between the workpiece and the tool electrode immersed in a dielectric solution a discharge current is created. Then the discharge current overcomes the dielectric solution resistance and is discharged in the form of sparks on the workpiece surfaces. However, each of these sparks can act as a source of heat. So, the local temperature can increase to more than 10000 °C at the micro-second time intervals.<sup>3,4</sup> Hence, the temperature gradient developed on the surface of the workpiece leads to melting and changing material constituents,<sup>5</sup> as well as diffusion of very small particles to the surface of the tool electrode<sup>6</sup>, and Hence changing the mechanical,<sup>7,8</sup> structural<sup>9</sup> and electrochemical<sup>10</sup> properties of the workpiece. These alterations are related to machining parameters such as electrical discharge

current ( $I$ ), the type of modulation of applying voltage ( $V$ ), the time in which modulated voltage has been pulse-on time ( $t_{on}$ ) and pulse-off time ( $t_{off}$ ), machining time ( $\tau$ ), and the type of tool electrode and work-piece.<sup>11,12</sup> Whereas changes in the chemical composition of surface influences its corrosion behavior,<sup>13</sup> it is worthwhile to study the corrosion resistance of the workpiece made by EDM. Open circuit potential, potentiodynamic polarization, and electrochemical impedance spectrometry are the most common methods to study electrochemical corrosion.<sup>14,15</sup> Due to the formation of protective layer on the workpiece surface during the corrosion tests, the electrochemical impedance spectrometry method is used.

In this study, the EDM method was carried out on stainless steel with a copper electrode. The stainless steel was used as workpiece due to its excellent mechanical properties,<sup>16</sup> high corrosion resistance in the corrosive medium,<sup>17</sup> and the fact that it is the most applicable alloy<sup>18</sup> for use in different industries e.g. medicine,<sup>6</sup> military,<sup>19</sup> aerospace<sup>20</sup> and so on. A few studies have evaluated the

corrosion behavior of the workpieces made by EDM showing the tool electrodes significantly affect the amount of workpiece corrosion.<sup>6,10,15,21–24</sup>

Yan et al. using weight loss test have shown that Al–Zn–Mg alloy machined by a copper electrode has high corrosion resistance.<sup>21</sup> Tsai et al. have developed a sintered electrode tool made in Cu–Cr (80–20%) composite to improve the uniform corrosion resistance of the AISI 1045 EDM surfaces.<sup>22</sup> Sidoham et al. have determined the corrosion resistance of stainless steel using potentiometric test, which is machined by a graphite electrode in various EDM currents.<sup>23</sup> They have indicated that by increasing the discharge current, the amount of the diffused carbon into the surface of the stainless steel, and as result the corrosion rate increases. Saravanan et al. used open circuit potential (OCP) and linear polarization measurements to show that the corrosion has occurred in EDMed Al alloys by the brass electrode due to the localized transfer of copper from of brass on the workpiece surface.<sup>24</sup>

In this study, we investigate the presence and diffusion of Cu on the stainless steel workpiece by changing the EDM parameters such as  $I$ ,  $t_{on}$ ,  $t_{off}$  and  $\tau$ . Afterwards, the electrochemical corrosion rate of the workpiece is measured by the electrochemical impedance spectrometry (EIS) method. The Taguchi experimental design method is used in order to reduce the cost and time of the study. To keep the maintenance cost low and raising the efficiency of the industrial tools, we worked on the EDMed stainless steel using copper electrode and reporting the optimal values of the machining parameters.

## 2. Material and Methods

### 2.1. Material

- Stainless steel belt with a 5 mm thickness and copper rod with a 10 mm diameter, purchased from Tehran bazaar, Iran.

### 2.2. Equipments and Software

- Electric Discharge Machining, Model A6040L, Chmer Company, Taiwan.
- Quantometer, Model Foundry Master, Oxford Instruments GmbH, Germany.
- X-ray Diffractometer (XRD) System, Model D8 Advance, Bruker Company, Germany.
- Optical Microscope, Model Olympus BX51M, Japan.
- Autolab Instrument, Model PGSTAT 30, Eco-Chemie Utrecht Company, Netherlands.
- Minitab Software, Version 16.4.2, Minitab Company, USA.
- Highscore Plus Software, Version 3.0.5, PANalytical B.V. Almelo Company, Netherlands.
- FRA Software, Version 4.9, Eco Chemie B.V Company, Netherlands.

### 2.3. Material Preparation

The selected workpiece material was stainless steel (SS) with the dimensions  $30 \times 20 \times 5 \text{ mm}^3$  and the electrode tool used in this work was made of a copper rod with a 10 mm diameter. The chemical composition of stainless steel and copper performed by foundry master instrument is reported in Table 1 and Table 2 respectively. The EDM machining operations was carried out with Chmer A6040L on workpieces. The paraffin oil was used as dielectric fluid. The raw and EDMed workpiece and electrode tool are shown in Figure 1. Experiments were conducted by control parameters variations such as  $I$ ,  $t_{on}$ ,  $t_{off}$ ,  $\tau$ , and each one at five levels as shown in the Table 3. The design of experiments was performed by using L25 mixed levels of orthogonal arrays according to Taguchi method as listed in Table 4.

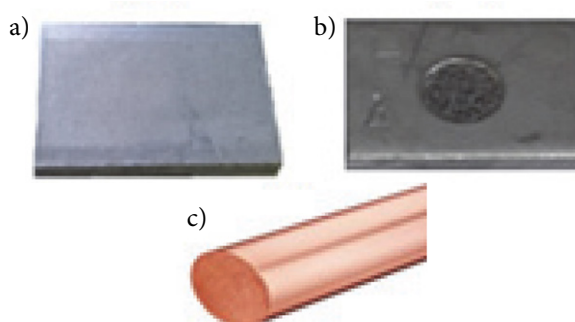


Figure 1. The image of (a) raw workpiece (b) EDMed workpiece (c) tool electrode.

Table 1. Chemical composition of raw workpiece (wt. %).

Fe	C	Si	Mn	P	S	Cr	Mo
70.2	0.0548	0.235	1.15	0.0325	0.005	19	0.22
Ni	Al	Co	Cu	Nb	Ti	V	W
8.36	0.001	0.122	0.432	0.0185	0.0078	0.0616	0.02

Table 2. Chemical composition of tool electrode (wt. %).

Cu	Zn	Pb	Sn	P	Mn	Fe	Ni
99.7	0.1	0.005	0.005	0.003	0.0054	0.05	0.005
Si	Al	Cr	Mg	S	As	Co	Ag
0.0183	0.0095	0.001	0.002	0.0113	0.0041	0.023	0.0082

Table 3. EDM design factors.

Design factor	Level				
	1	2	3	4	5
$I$ (A)	5	10	15	20	25
$t_{on}$ ( $\mu$ s)	50	75	100	125	150
$t_{off}$ ( $\mu$ s)	5	10	15	20	25
$\tau$ (min)	1	2	4	8	16

**Table 4.** The results of experimental design by using L25 orthogonal arrays.

Input parameters				
S. N.	<i>I</i> (A)	<i>t</i> <sub>on</sub> (μs)	<i>t</i> <sub>off</sub> (μs)	<i>τ</i> (min)
1	5	50	5	1
2	5	75	10	2
3	5	100	15	4
4	5	125	20	8
5	5	150	25	16
6	10	50	10	4
7	10	75	15	8
8	10	100	20	16
9	10	125	25	1
10	10	150	5	2
11	15	50	15	16
12	15	75	20	1
13	15	100	25	2
14	15	125	5	4
15	15	150	10	8
16	20	50	20	2
17	20	75	25	4
18	20	100	5	8
19	20	125	10	6
20	20	150	15	1
21	25	50	25	8
22	25	75	5	16
23	25	100	10	1
24	25	125	15	2
25	25	150	20	4

S. N. The number of EDMed workpieces.

## 2. 4. Methods

### 2. 4. 1. Quantometer Analysis

**Table 5.** Chemical composition (wt. %) of workpiece after EDM.

S.N.	Fe	C	Si	Mn	P	S	Cr	Mo	Ni	Al	Co	Cu	Nb	Ti	V	W
1	69.8	1.06	0.207	1.11	0.0204	0.005	18.3	0.198	8.51	0.001	0.130	0.489	0.0114	0.0063	0.0558	0.02
2	69.8	1.10	0.199	1.12	0.0067	0.005	18.2	0.206	8.60	0.001	0.118	0.474	0.0129	0.0064	0.0611	0.0278
3	69.7	1.23	0.195	1.10	0.0072	0.005	18.0	0.204	8.71	0.001	0.117	0.457	0.0134	0.0059	0.0612	0.0230
4	69.4	1.23	0.226	1.14	0.003	0.0050	18.4	0.191	8.47	0.0015	0.115	0.432	0.0088	0.0087	0.0611	0.124
5	69.1	1.49	0.191	1.16	0.003	0.005	18.2	0.185	8.74	0.001	0.123	0.448	0.0093	0.0074	0.0649	0.144
6	69.5	0.808	0.217	1.14	0.003	0.005	18.7	0.191	8.49	0.0013	0.12	0.561	0.0082	0.0079	0.0609	0.128
7	69.1	1.41	0.210	1.13	0.003	0.005	18.3	0.183	8.59	0.001	0.112	0.638	0.0075	0.0071	0.0596	0.120
9	69.5	0.983	0.184	1.16	0.0041	0.005	15.5	0.190	8.64	0.001	0.121	0.492	0.0099	0.0059	0.0646	0.0389
10	69.6	0.909	0.169	1.15	0.003	0.005	18.4	0.189	8.82	0.001	0.119	0.453	0.0107	0.0053	0.0651	0.0395
12	69.5	1.04	0.178	1.14	0.0035	0.005	18.2	0.190	8.61	0.001	0.126	0.72	0.0109	0.005	0.0645	0.0245
13	69.1	1.45	0.183	1.16	0.003	0.005	18.3	0.182	8.62	0.001	0.123	0.614	0.0087	0.006	0.0634	0.118
14	69.8	0.638	0.213	1.16	0.003	0.005	18.6	0.187	8.55	0.001	0.0988	0.486	0.0082	0.0072	0.0624	0.0933
15	69.4	1.28	0.190	1.119	0.003	0.005	18.1	0.183	8.58	0.001	0.124	0.528	0.0086	0.0073	0.0662	0.168
16	69.6	0.562	0.236	1.14	0.003	0.005	18.8	0.196	8.45	0.001	0.105	0.629	0.0098	0.0091	0.0611	0.125
17	69.2	1.44	0.225	1.11	0.003	0.005	18	0.196	8.61	0.0015	0.126	0.771	0.0125	0.0089	0.0601	0.143
18	67.2	2.6	0.212	1.10	0.003	0.005	17.1	0.190	8.52	0.0019	0.12	0.62	0.012	0.0088	0.0584	0.171
20	69.3	1.37	0.175	1.15	0.003	0.005	18.1	0.186	8.81	0.001	0.101	0.594	0.0112	0.0054	0.0646	0.0582
23	68.9	1.68	0.195	1.12	0.003	0.005	18.1	0.183	8.65	0.001	0.0997	0.757	0.0083	0.007	0.0597	0.111
24	67.7	2.6	0.165	1.11	0.003	0.005	17.3	0.192	8.87	0.001	0.117	0.833	0.0109	0.0059	0.0676	0.0913
25	67.1	2.6	0.201	1.11	0.003	0.005	17	0.179	8.72	0.0018	0.122	0.763	0.0094	0.008	0.0572	0.178

The EDM process induces changes in the chemical composition of the surface of the workpieces. Therefore, the chemical elements of these workpieces are performed by foundry master instrument (the quantometer analysis) and the results are presented in Table 5.

### 2. 4. 2. Optical Microscopy

The micrograph observation is performed by an Olympus BX51M optical microscope (OM) in a fixed magnification of 1000.

### 2. 4. 3. XRD Analysis

The phases on the workpiece's surface have been studied via XRD analysis. Analyses were performed by X-ray diffraction (XRD) (Bruker D8 advance) at a wavelength of 0.15406 nm using the copper  $\text{K}\alpha_1$  radiation. Diffraction patterns were recorded at 45 kV and 48 mA in 1°/s detectors movement speed, intensity was measured in  $2\theta = 0.02^\circ$ . Spectra were collected at  $2\theta$  values between  $20^\circ$ – $80^\circ$ . X'Pert High Score Plus, V3.0.5 software were used to analyze the obtained data.

### 2. 4. 4. Electrochemical Corrosion Test

The electrochemical behavior of EDMed workpieces was studied with the electrochemical impedance spectroscopy (EIS) using AUTOLAB model PGSTAT 30 equipped with a frequency response analyzer (FRA) software. The three electrode cell was used for the electrochemical measurements. We used workpiece with an exposed area of  $0.65 \text{ cm}^2$  as the working electrode. A saturated calomel

electrode (SCE) and platinum tip electrode were used as the reference and the counter, respectively. Every sample (S.N) from Table 4 was subject to measure three replication using fresh 3.5 wt. % NaCl solutions without aeration, at room temperature. The impedance studies were performed at a frequency range from 0.01 Hz to 1 MHz sine wave with 5 mV perturbation amplitude. All of the measurements were done in potentiostatic mode at room temperature. The EIS data are calculated by Nyquist plots. The boukamp equivalent circuit utility as a part of FRA program are the most reliable simulated electrical circuit based on the impedance data.

### 3. Results and Discussion

#### 3.1. Microstructural Changes

Thermal energy generated by EDM leads to changes in workpiece surface. The EDMed workpiece surface phases, identified by X-ray diffraction (see Figure 2), revealed several different phases such as copper ( $\text{Cu}_4$ ) with cubic crystal structure, carbon ( $\text{C}_{16}$ ) with cubic crystal structure, and carbides ( $\text{FeC}$  with hexagonal crystal structure,  $\text{Cr}_3\text{C}_2$  with orthorhombic crystal structure). Lattice parameters of these phases are calculated using X'Pert High Score Plus software and the results were reported in Table 6, and as an example the diffractograms of workpiece-16 is depicted in Figure 3.

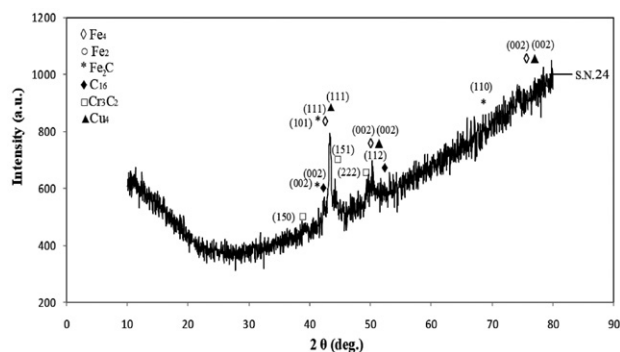


Figure 2. X-ray spectrum of the surface workpiece-24.

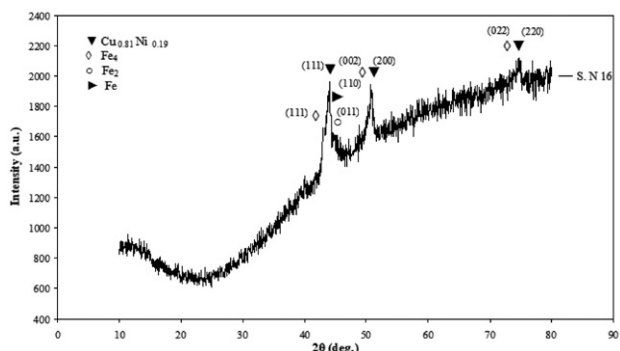


Figure 3. X-ray spectrum of the surface workpiece-16.

During the spark ignition in the EDM process, the copper is melted away from the tool electrode. Therefore, the copper particles diffuse into the workpiece surface and as a result of their combination with the Nickel particles,  $\text{Cu}_x\text{Ni}_y$  crystals were formed. It should be mentioned that copper and Nickel have the same lattice parameters. The lattice parameters of these phases were calculated using the X'Pert High Score Plus software and the results are reported in Table 7.

Table 6. Lattice parameters of workpiece surface phases, workpiece-24.

Chemical formula	Lattice parameters
$\text{Fe}_4$	Cubic $a = b = c = 0.362 \text{ nm}$ $\alpha = \beta = \gamma = 90^\circ$
$\text{Fe}_2$	Cubic $a = b = c = 0.362 \text{ nm}$ $\alpha = \beta = \gamma = 90^\circ$
$\text{Cu}_4$	Cubic $a = b = c = 0.362 \text{ nm}$ $\alpha = \beta = \gamma = 90^\circ$
$\text{Fe}_2\text{C}$	Hexagonal $a = b = c = 0.275 \text{ nm}$ $\alpha = \beta = 90, \gamma = 120^\circ$
$\text{Cr}_3\text{C}_2$	Orthorhombic $a = b = c = 0.701 \text{ nm}$ $\alpha = \beta = \gamma = 90^\circ$
$\text{C}_{16}$	Cubic $a = b = c = 0.429 \text{ nm}$ $\alpha = \beta = \gamma = 90^\circ$

Table 7. Lattice parameters of workpiece surface phases, workpiece-16.

Chemical formula	Lattice parameters
$\text{Fe}_4$	Cubic $a = b = c = 0.362 \text{ nm}$ $\alpha = \beta = \gamma = 90^\circ$
$\text{Fe}_2$	Cubic $a = b = c = 0.362 \text{ nm}$ $\alpha = \beta = \gamma = 90^\circ$
Fe	Cubic $a = b = c = 0.2853 \text{ nm}$ $\alpha = \beta = \gamma = 90^\circ$
$\text{Cu}_{0.8}\text{Ni}_{0.19}$	Cubic $a = b = c = 0.35934 \text{ nm}$ $\alpha = \beta = \gamma = 90^\circ$

As evident from Figures 2 and 3, the sources of carbon and copper particles penetrating on the workpiece surface are from the dielectric solution and copper elec-

trode, respectively. The diffused carbon particles are combined with the workpiece material to form a carbide zone. Our results are in line with Chundru,<sup>25</sup> Torres,<sup>26</sup> Sidhom,<sup>23</sup> and Cusanelli findings.<sup>27</sup> The mechanism of copper diffusion in the machining process is discussed below.

### 3. 2. Effect of Copper Diffusion on EDMed Surface

The schematic of the mechanism of copper diffusion in the machining process is shown in Figures 4.

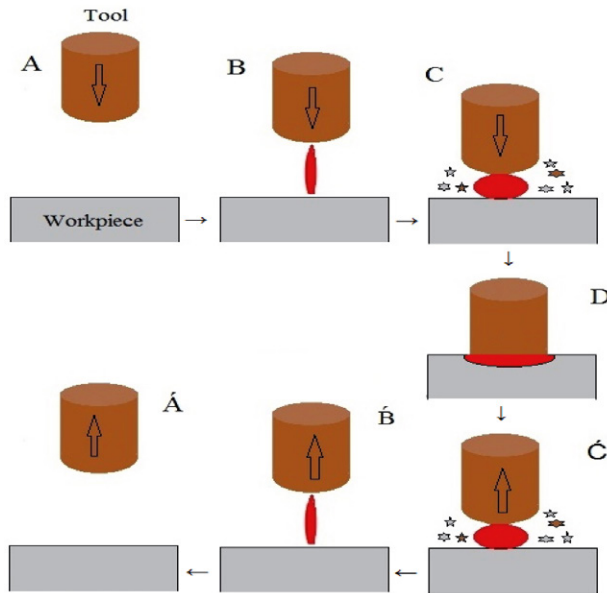


Figure 4. Schematic of the copper diffusion mechanism during EDM.

During step A, the tool electrode is coming close to the workpiece surface. Then, in step B, the discharge current is set between the tool electrode and workpiece by deionizing the dielectric fluid and the creation of the plasma channel. When the discharge current is increased, the thermal energy produced by sparks can warm up the electrodes. Therefore, it causes the debris melted materials to be sputtered into the dielectric liquid. Some of these particles do not exit the dielectric solution and, consequently, they fell on the workpiece (or tool electrode) surface (step C). Finally, as the tool electrode is getting closer to the workpiece its surface connects to the workpiece (step D). In this case, passing electric current produces heat due to joule effect. As a result, the tool electrode materials diffuse onto the surface of the substrate. During the next step the tool electrode is removed from the workpiece surface, and as a result of the distance the spark width and its impact are reduced. Flushing of dielectric liquid leads to a decrease in the temperature, such that there is no spark in step Á. Ultimately, the whole process would be repeated again. It is evident that step D can be introduced as the

main stage in which the Cu diffuses onto the workpiece. It should be noted that the copper diffusion also occurs in other stages of the EDM process; but the amount is not comparable with step D. The linear movement of the velocity of the tool electrode axle<sup>28</sup> will be constant during the whole steps from A to Á. Therefore, the amount of copper diffusion can be described as a function of pulse-on time.

### 3. 3. Effect of Discharge Current on Copper Diffusion

The results of the quantometer analysis show the different amounts of copper and carbon on the workpiece surface (Table 5). To investigate the overall effects of the copper and carbon amounts with different discharge currents, their mean values were calculated and are reported in Table 8.

Table 8. The mean values of copper and carbon of Stainless Steel.

Discharge Current (A)	Mean copper (wt. %)	Mean carbon (wt. %)
5	0.46	1.22
10	0.54	1.03
15	0.59	1.10
20	0.66	1.49
25	0.78	2.29

The effect of current on the mean values of the diffusion of Cu was already shown in Figure 5. The diffusion of Cu on stainless steel surface was increased by raising the current values. This can be attributed to the lower melting point of Cu rather than the stainless steel and the fact that EDM develops a high-temperature zone on the surface<sup>29</sup>. For this reason the incremental diffusion is slow.

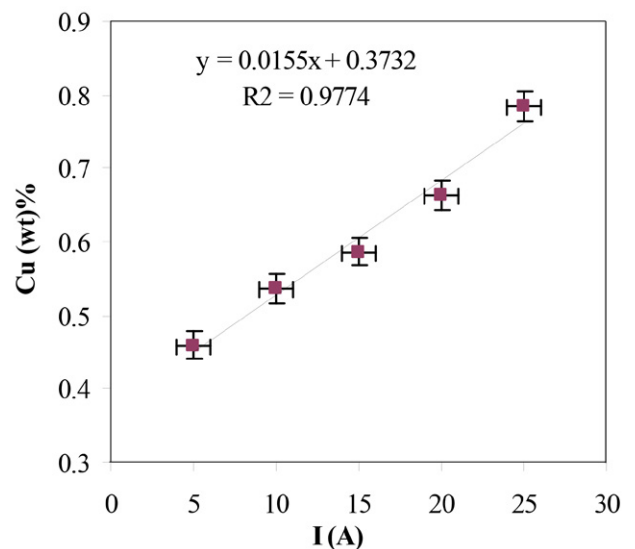


Figure 5. Effect of I on diffusion mean of copper in workpiece.

The change in the weight percent of other elements as well as for Cu can occur in the machining process. Table 8 shows that by increasing discharge current the weight percent (wt. %) of carbon increased from 0.0548% (without EDM) to 2.29% ( $I = 25$  A). This is related to the diffusion of the carbon from the dielectric solution into the workpiece surface when the flashing occurs. This result is in agreement with the Elaiyarsan,<sup>30</sup> Torres,<sup>26</sup> Kumar<sup>31</sup> and John<sup>32</sup>. The results from quantometer analysis agreed to ones obtained by XRD analysis.

### 3. 4. Effect of Pulse-on time and Pulse-off time on Copper Diffusion

The diffusion of Cu on the surface of workpiece in high (125, 150  $\mu$ s) and low (50, 70, 100  $\mu$ s) values of  $t_{on}$  vs. discharge current were sketched in Figure 6. The findings show that the amount of diffusion of copper on the surface of the workpiece was high when  $t_{on}$  was low. However, this phenomenon was amplified by increasing the discharge current.

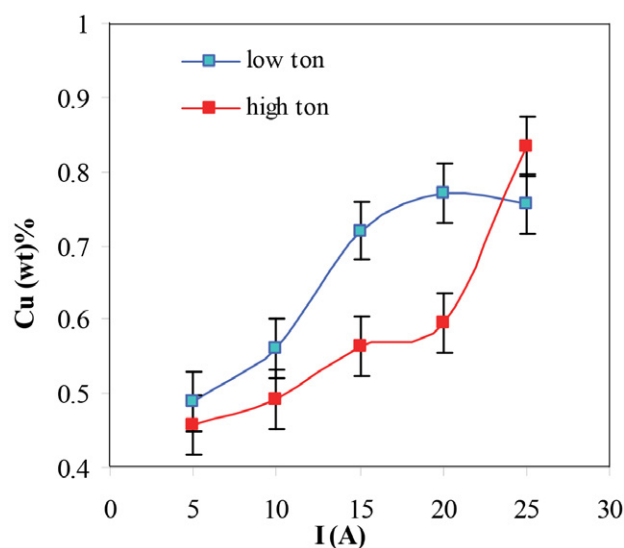


Figure 6. Diagram of diffused copper wt. % vs. discharge current at high and low  $t_{on}$ .

In the machining process, the greatest value of copper on the workpiece surface was observed at  $t_{off} = 15$  and 20  $\mu$ s. Figure 7 illustrates the copper values vs.  $t_{off}$ .

The results obtained from the optical microscopy show that the microscopic images of machined workpiece at the high discharge current, high  $t_{on}$  and low  $t_{off}$  have long and branched cracks on the surface. The presence of crack and micro-crack on the surface maybe attributed to the retention of the dielectric fluid during the cooling of the surface<sup>33,34</sup>. Ultimately, Stress Corrosion Cracking (SCC) in aggressive environments occurs in this case. Figure 8-a, shows the microscopic images of the workpiece-24 with high values of discharge current and  $t_{on}$ .

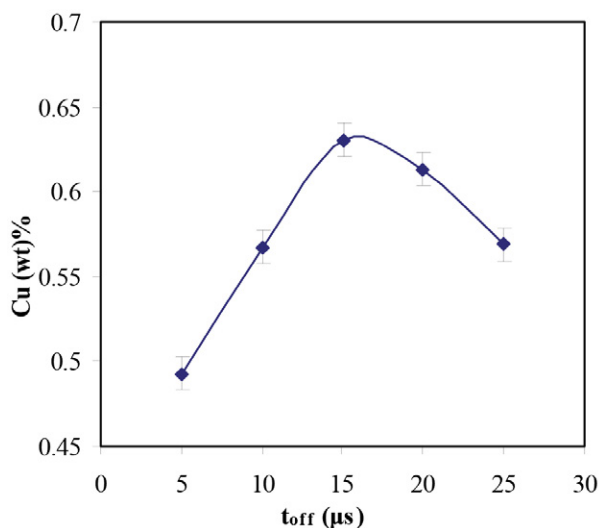


Figure 7. Diagram of diffused copper wt. % vs.  $t_{off}$ .

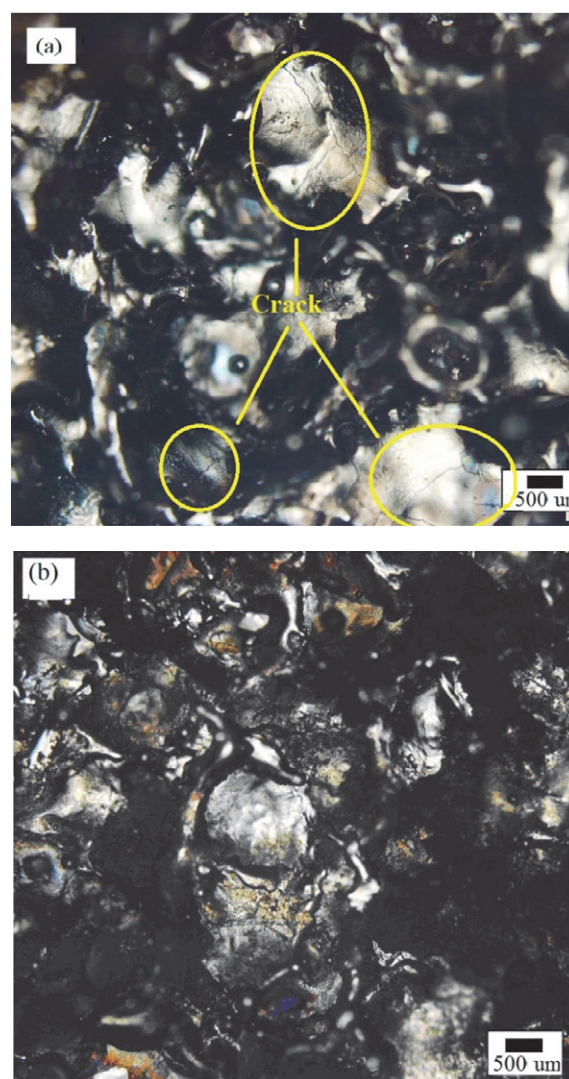


Figure 8. Optical micrograph of stainless steel EDMed through copper electrode at high discharge current and (a) high  $t_{on}$ , (b) low  $t_{on}$  by magnification of 1000.

As shown in workpiece-16, there is a suitable ratio of  $t_{on}/t_{off}$  (Figure 8-b). The highest amount of Cu diffusion and the surface without any cracks or micro-cracks are observed under the condition of higher amounts of discharge current, lower  $t_{on}$ , higher  $t_{off}$  with much shorter  $\tau$ . The value of diffused Cu is high (0.629 %) as reported in Table 5. These conditions prevent the workpiece from formation of any cracks, micro-cracks or branching.

### 3. 5. Electrochemical Corrosion

The electrochemical impedance spectroscopy diagram (Nyquist plot) for workpiece-16 is presented in Figure 9.

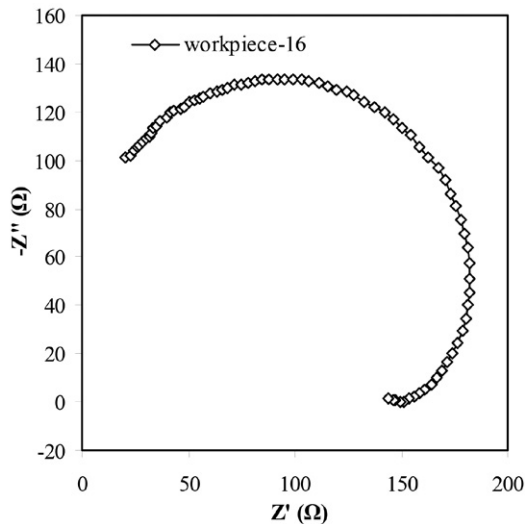


Figure 9. Nyquist plot of EIS results for workpiece 16.

To investigate the effect of copper on the corrosion resistance of Stainless Steel the mean values of the diffused copper (obtained by quantometer analysis) and the mean values of the corrosion resistance ( $R_{CT}$ ) as well as electrical double layer capacitance ( $C_{EDL}$ ) (obtained by EIS analysis) in various currents are presented in Table 9.

Table 9. The mean values of the diffused copper,  $R_{CT}$  and  $C_{EDL}$  in various discharge currents.

Discharge Current (A)	Mean copper (wt. %)	Mean $R_{CT}$ ( $\Omega$ )	Mean $C_{EDL}$ ( $\mu\text{F}$ )
5	0.46	385	7.6
10	0.536	453	12
15	0.587	495	14
20	0.66	590	21
25	0.78	456	18

The resulting effects of various discharge currents on the mean values of the diffused Cu and corrosion resistance (Table 9) of stainless steel are showed in Figure 10. It

shows that by increasing the discharge current ( $I = 20$  A) the corrosion resistance also rises ( $R_{CT} = 590 \Omega$ ). In this situation, the XRD analysis shows that the stable phase of  $\text{Cu}_{0.81}\text{Ni}_{0.19}$  is formed and also optical microscopy show no cracks or micro-cracks (Figure 8-b). However, when the discharge current is too high ( $I = 25$  A), the  $R_{CT}$  significantly is reduced ( $R_{CT} = 456 \Omega$ ) and the cracks are developed on the workpiece (Figure 8-a). These observations are consistent with the finding of Sidoham et al<sup>23</sup>.

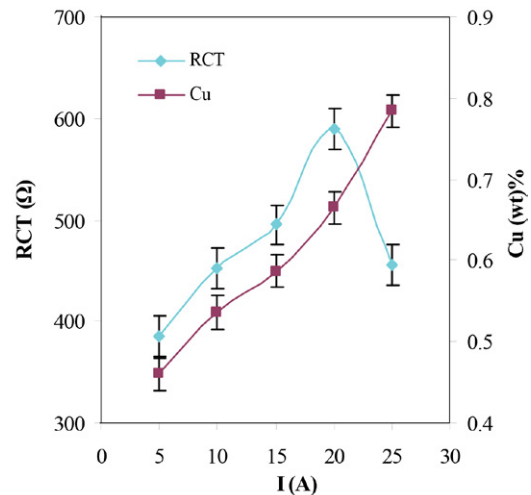


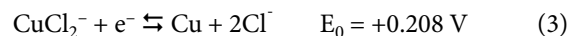
Figure 10. Effect of the discharge current on the mean value of  $R_{CT}$  and Cu (wt. %).

As Figure 10 shows, the Cu diffusion on the surface grows with the rising discharge current, and subsequently the corrosion rate is decreased. Many researchers<sup>35–39</sup> have reported that Cu diffusion plays an important role in corrosion resistance. Copper maybe stable either as metallic copper, soluble  $\text{CuCl}_2^-$  complex, insoluble  $\text{CuCl}$  salt film or as  $\text{Cu}^{2+}$  ions on the workpiece surface in corrosive environment by following mechanisms:

Ionization of Cu atom produces  $\text{Cu}^{2+}$  ions according to Eq. 1<sup>37,38</sup>.



The anodic reaction of Cu by the production of  $\text{CuCl}$  salt and  $\text{CuCl}_2^-$  complex occurs in chloride. The reaction is Eq. 2 and Eq. 3<sup>37,40</sup>.



The protective layer protects the stainless steel from corrosion. The corrosion resistance effect is related to the creation of an electrical double layer of metal/ electrolyte in this case. Whereas the protection of the copper chloride layer is severely unstable, during the EDM process the workpiece is corroded electrochemically by pitting corro-

sion mechanism. In contrast, in high  $t_{on}$ , workpiece doesn't have sufficient time for cooling; this situation provides the conditions for growing cracks on the surface (Figure 8-a). At high values of both discharge current and  $t_{on}$  (workpiece-24) the branched long cracks can be formed and the corrosion resistance of workpiece dramatically falls ( $R_{CT} = 456 \Omega$ ). The results of X-ray at very high discharge current and high  $t_{on}$  (Figure 2) indicate the presence of heterogeneous phases such as iron-phase with cubic structure, iron-carbide phase with hexagonal structure and chromium carbide with orthorhombic structure on the workpiece surface. Variation in workpiece lattice structure (cubic, hexagonal and orthorhombic) and different thermodynamic stability lead to the cracking of the workpiece and increase in the corrosion rates. The order of decreasing enthalpy formation of this workpiece is given in Table 10.

**Table 10.** Formation enthalpies of crystal observed in workpieces-16 and 24.

S.N	Component	$\Delta H_f$ KJ mol <sup>-1</sup>	Reference
24	Fe	13.79	41
	Fe <sub>2</sub> C	2.57	42
	Cr <sub>3</sub> C <sub>2</sub>	-111.95	43
16	Fe	13.79	41
	CuNi	3.7	44

The EDMed workpiece with a high discharge current and  $t_{off}$  and low  $t_{on}$  and  $\tau$  (workpiece-16) cools slowly enough to avoid cracks formation (Figure 8-b). XRD analysis (Figure 3) show that in this workpiece all the phases grow up in the same cubic crystal lattice (Table 7), which have the low formation enthalpy and subsequently are stable (Table 10). Under these conditions, the  $R_{CT}$  increases dramatically ( $R_{CT} = 590 \Omega$ ).

From the workpiece-16 results, it can be found that the corrosion rate is very low. In this workpiece, high discharge current and large amount of heat is developed on the surface. Also, it can be seen from Figure 8-b that the metal is allowed to cool sufficiently and therefore the cracks are not formed because the value of  $t_{on}$  is low. The quantometer analysis results (Table 4) show that during the machining process, the values of the diffused Cu and C on the workpiece's surface are 0.629 and 0.5072 respectively. In workpiece-16 the diffused Cu is higher and the diffused carbon is lower than the other workpieces. This leads to a good corrosion resistance properties. Note that the amount of  $C_{EDL}$  of workpiece-16 ( $C_{EDL} = 21 \mu F$ ) is the highest value among other workpieces as shown in Table 9.

## 4. Conclusions

The corrosion resistance of the stainless steel is an important issue because of its application in many indus-

tries. The EDM technique is one of the methods for production and manufacturing of industrial Stainless Steel. In EDM technique a locally rising temperature causes a change in the chemical composition and diffusion of the tool electrode onto the surface of workpiece. The electrochemical properties of the stainless steel are also changed due to the variation in EDM parameters. The results show that by increasing discharge current and  $t_{on}$ , the copper of tool electrode and carbon of dielectric liquid are diffused constituting some phases such as Fe<sub>2</sub>C, Cr<sub>3</sub>C<sub>2</sub>, and CuNi onto the surface of workpiece. Besides, at higher values of both discharge current and  $t_{on}/t_{off}$  ratio, the micro-cracks propagate. By increasing discharge current with an optimal level of  $t_{on}/t_{off}$  ratio, the amount of diffusion of Cu onto the surface rises and then the electrochemical corrosion is reduced. Workpiece under optimal conditions ( $I = 20A$ ,  $t_{on} = 50\mu s$ ,  $t_{off} = 20 \mu s$ ,  $\tau = 2$  min), shows high corrosion resistance due to the formation of the copper-nickel phase with no cracks or micro-cracks on its surface.

## 5. References

- R. P. Zeilmann, T. Vacaro, F. M. Zanotto and M. Czarnobay, *Matéria (Rio de Janeiro)* **2013**, *18*, 1541–1548. DOI:10.1590/S1517-70762013000400014
- T. Ni, Q. Liu, Y. Wang, Z. Chen and D. Jiang, *Coatings* **2021**, *11*, 322. DOI:10.3390/coatings11030322
- L. Tang and Y. Guo, *The international Journal of advanced manufacturing Technology* **2014**, *70*, 1369–1376. DOI:10.1007/s00170-013-5380-4
- D. N. Mishra, A. Bhatia and V. Rana, *The International Journal of Engineering and Science (IJES)* **2014**, *3*, 24–35.
- S. Arooj, M. Shah, S. Sadiq, S. H. I. Jaffery and S. Khushnood, *Arabian Journal for Science and Engineering* **2014**, *39*, 4187–4199. DOI:10.1016/j.dental.2010.08.001
- A. Ntasi, W. D. Mueller, G. Eliades and S. Zinelis, *dental materials* **2010**, *26*, e237–e245. DOI:10.1016/j.dental.2010.08.001
- Z. Karastojković, Z. Janjušević, in: J. Mickovski (ed.), *Hardness and structure changes at surface in electrical discharge machined steel C 3840: Proceedings of 3<sup>rd</sup> Balkan Conference on Metallurgy BMC-2003, Ohrid, Macedonia*, **2003**, Ohrid, Macedonia, pp. 129–133.
- S. Gopalakannan and T. Senthilvelan, *Journal of Minerals and Materials Characterization and Engineering* **2012**, *11*, 685. DOI:10.4236/jmmce.2012.117053
- A. K. Tiwari, *Int. Journal of Engineering Research and Applications* **2014**, *4*, 91–95.
- X. Yan, S. Zhang, J. Li and G. Wang: ASME 2015 International Manufacturing Science and Engineering Conference, American Society of Mechanical Engineers Digital Collection, **2015**. DOI:10.1115/MSEC2015-9261
- D. Thesiya, J. Dave and A. Rajurkar, *Advances in Manufacturing Science and Technology* **2014**, *38*. DOI:10.2478/amst-2014-0023
- M. Patel Gowdru Chandrashekarappa, S. Kumar, D. Y.



- Pimenov and K. Giasin, *Metals* **2021**, *11*, 419.  
DOI:10.3390/met11030419
13. A. Pardo, M. Merino, A. Coy, F. Viejo, R. Arrabal and E. Matykina, *Corrosion Science* **2008**, *50*, 1796–1806.  
DOI:10.1016/j.corsci.2008.04.005
  14. O. M. Ama, Book Nanostructured Metal-Oxide Electrode Materials for Water Purification: Fabrication, Electrochemistry and Applications, Springer Nature, **2020**.  
DOI:10.1016/j.teac.2014.07.001
  15. J. G. G. Manjunatha, *Journal of food and drug analysis* **2018**, *26*, 292–299. DOI:10.1016/j.jfda.2017.05.002
  16. Y. Guo, J. Hu, J. Li, L. Jiang, T. Liu and Y. Wu, *Materials* **2014**, *7*, 6604–6619. DOI:10.3390/ma7096604
  17. C. Loto, O. Fayomi and R. Loto, *International Journal of Electrochemical Science* **2012**, *7*, 3787–3797.  
DOI:10.1007/s00170-012-4156-6
  18. K. H. Lo, C. H. Shek and J. Lai, *Materials Science and Engineering: R: Reports* **2009**, *65*, 39–104.  
DOI:10.1016/j.msere.2009.03.001
  19. J. Tian, W. Wang, M. Babar Shahzad, W. Yan, Y. Shan, Z. Jiang and K. Yang, *Materials* **2017**, *10*, 1293.  
DOI:10.3390/ma10111293
  20. W. Garrison, *JOM* **1990**, *42*, 20–24.  
DOI:10.1007/BF03220942
  21. B. Yan, Y. Lin and F. Huang, *International Journal of Machine Tools and Manufacture* **2002**, *42*, 925–934.  
DOI:10.1016/S0890-6955(02)00026-3
  22. H. Tsai, B. Yan and F. Huang, *International Journal of Machine Tools and Manufacture* **2003**, *43*, 245–252.  
DOI:10.1016/S0890-6955(02)00238-9
  23. H. Sidhom, F. Ghanem, T. Amadou, G. Gonzalez and C. Braham, *The international journal of advanced manufacturing technology* **2013**, *65*, 141–153.  
DOI:10.1007/s00170-012-4156-6
  24. S. R. Arunachalam, S. E. G. Dorman, R. T. Buckley, N. A. Conrad and S. A. Fawaz, *International Journal of Fatigue* **2018**, *111*, 44–53. DOI:10.1016/j.ijfatigue.2018.02.005
  25. V. R. Chundru, R. Koonan and S. R. Pujari, *Arabian Journal for Science and Engineering* **2019**, *44*, 1425–1436.  
DOI:10.1007/s13369-018-3561-z
  26. A. Torres, C. Luis and I. Puertas, *Journal of Alloys and Compounds* **2017**, *690*, 337–347.  
DOI:10.1016/j.jallcom.2016.08.110
  27. G. Cusanelli, A. Hessler-Wyser, F. Bobard, R. Demellayer, R. Perez and R. Flükiger, *Journal of Materials Processing*  
DOI:10.1016/j.jmatprotec.2003.11.047
  28. K. Abrol, *Chemmer CNC EDM Opetation Manual*, **2018**, *3*, 118–164.
  29. S. Lee and X. Li, *Journal of materials processing Technology* **2001**, *115*, 344–358. DOI:10.1016/S0924-0136(01)00992-X
  30. U. Elaiyarsan, V. Satheeshkumar and C. Senthilkumar, *Journal of the Mechanical Behavior of Materials* **2020**, *29*, 69–76. DOI:10.1515/jmbm-2020-0007
  31. A. Kumar, V. Kumar and J. Kumar, *Machining Science and Technology* **2014**, *18*, 47–77.  
DOI:10.1080/10910344.2014.863632
  32. J. E. Fuller, EG and G Rocky Flats, Inc., Golden, CO (United States), **1991**.
  33. H. T. Lee and T. Y. Tai, *Journal of Materials Processing Technology* **2003**, *142*, 676–683.  
DOI:10.1016/S0924-0136(03)00688-5
  34. C. Li, X. Xu, Y. Li, H. Tong, S. Ding, Q. Kong, L. Zhao and J. Ding, *Journal of Alloys and Compounds* **2019**, *783*, 95–102.  
DOI:10.1016/j.jallcom.2018.12.283
  35. T. Xi, M. B. Shahzad, D. Xu, Z. Sun, J. Zhao, C. Yang, M. Qi and K. Yang, *Materials Science and Engineering: C* **2017**, *71*, 1079–1085. DOI:10.1016/j.msec.2016.11.022
  36. Y. Jiangnan, W. Lichang and S. Wenhao, *Corrosion science* **1992**, *33*, 851–859. DOI:10.1016/0010-938X(92)90049-9
  37. E. E. Oguzie, J. Li, Y. Liu, D. Chen, Y. Li, K. Yang and F. Wang, *Electrochimica Acta* **2010**, *55*, 5028–5035.  
DOI:10.1016/j.electacta.2010.04.015
  38. T. Ujiri, S. Satoh, R. W. Staehle and W. H. Smyrl, *Corrosion Science* **2001**, *43*, 2185–2200.  
DOI:10.1016/S0010-938X(01)00008-7
  39. E. E. Oguzie, J. Li, Y. Liu, D. Chen, Y. Li, K. Yang and F. Wang, *Journal of materials science* **2010**, *45*, 5902–5909.  
DOI:10.1007/s10853-010-4669-z
  40. T. Sourisseau, E. Chauveau and B. Baroux, *Corrosion Science* **2005**, *47*, 1097–1117. DOI:10.1016/j.corsci.2004.05.024
  41. G. Grimvall, Book Thermophysical properties of materials, Elsevier, **1999**. DOI:10.1016/j.heliyon.2017.e00408
  42. C. Fang and M. van Huis, *Heliyon* **2017**, *3*, e00408.  
DOI: 10.1016/j.heliyon.2017. e00408
  43. W. Dawson and F. Sale, *Metallurgical Transactions A* **1977**, *8*, 15–18. DOI:10.1007/BF02677258
  44. I. Nikolaenko and M. Turchanin, *Metallurgical and Materials Transactions B* **1997**, *28*, 1119–1130.  
DOI:10.1007/s11663-997-0068-5

## Povzetek

V tem delu je bil preučen vpliv prisotnosti in difuzije bakra z elektrode orodja na površino iz EDMed nerjavečega jekla (SS) z uporabo elektrokemične impedančne spektroskopije (EIS), rentgenske difrakcije (XRD), kvantometrične analize in optične mikroskopije. Metoda Taguchi je bila uporabljena za preučevanje učinkov časov pulzov (ton, toff), razelektritvenega toka (I) in celotnega časa obdelave ( $\tau$ ) na kemično sestavo, mikrostrukturo, mikrorazpoke in elektrokemijsko korozijo obdelovancev iz EDMed nerjavečega jekla. Rezultati kažejo, da spreminjanje obdelovalnih parametrov spremeni kemično sestavo obdelovancev. S povečanjem razelektritvenega toka in zmanjšanjem časa pulza ton, baker in ogljik difundirata na površino obdelovanca. Posledično se spremeni kemična sestava površine obdelovanca, kar vodi do povečanja korozijske odpornosti. XRD analiza je pokazala tvorbo  $\text{Fe}_2\text{C}$ ,  $\text{Cr}_3\text{C}_2$  in CuNi. Poleg tega se pri višjih vrednostih razelektritvenega toka in razmerja ton/toff mikro razpoke širijo po površini obdelovanca.



Except when otherwise noted, articles in this journal are published under the terms and conditions of the Creative Commons Attribution 4.0 International License

Scientific paper

# Combined 3D-QSAR and Molecular Docking Analysis of Thienopyrimidine Derivatives as *Staphylococcus aureus* Inhibitors

Mebarka Ouassaf,<sup>1</sup> Salah Belaidi,<sup>1,\*</sup> Saida Khamouli,<sup>1</sup> Houmam Belaidi<sup>1</sup> and Samir Chtita<sup>2</sup>

<sup>1</sup> University of Biskra, Group of Computational and Medicinal Chemistry, LMCE Laboratory, BP 145 Biskra 07000, Algeria

<sup>2</sup> Laboratory Physical Chemistry of Materials, Faculty of Sciences Ben M'Sik, Hassan II University of Casablanca, BP7955 Sidi Othmane, Casablanca, Morocco

\* Corresponding author: E-mail: prof.belaidi@gmail.com, s.belaidi@univ-biskra.dz.

Received: 03-18-2020

## Abstract

The discovery of antibacterials is considered one of the greatest medical achievements of all time. In this work, a combination of three computational analyzes: 3D-QSAR, molecular docking and ADME evaluation were applied in thienopyrimidine derivatives intended toward gram-positive bacterium *Staphylococcus aureus*.

The validity of 3D-QSAR model was tested with a set of data which is divided into a training and a test set. The two models constructed (CoMFA and CoMSIA) show good statistical reliability ( $q^2 = 0.758$ ;  $r^2 = 0.96$ ;  $r2pred = 0.783$ ) and ( $q^2 = 0.744$ ;  $r^2 = 0.97$ ;  $r2pred = 0.625$ ) respectively.

In addition, docking methods were applied to understand the structural features responsible for the affinity of the ligands in the binding of *S. aureus* DNA gyrase.

Drug likeness and ADME analysis applied in this series of new proposed compounds, have shown that the five lead molecules would have the potential to be effective drugs and could be used as a starting point for designing compounds against *Staphylococcus aureus*.

**Keywords:** 3D-QSAR; docking; *staphylococcus aureus*; thienopyrimidine; ADMET.

## 1. Introduction

The Gram-positive Bacterium *Staphylococcus aureus* is medically important pathogens in infection to deep-seated tissue infection and bacteremia,<sup>1</sup> due to the emergence of bacteria resistant to current therapeutic agents, the exploration of new antibiotics of a diversity of infections.<sup>2</sup>

The enzymes DNA gyrase B is present in bacteria and absent in humans thereby acting as a potential target in treating the *S. aureus* related diseases.<sup>3</sup>

Gyrase consists of two heterodimeric subunits, GyrA and GyrB. The inhibitors molecules induce cell death by trapping the gyrase DNA complex, inducing oxidative damage, and preventing DNA replication.<sup>4</sup>

Thienopyrimidines represent important chemical class in drug discovery due to vast range of pharmacological properties including antiallergic,<sup>5</sup> antiviral,<sup>6-7</sup> anti-in-

flammatory,<sup>8-12</sup> analgesic,<sup>13-14</sup> antispasmodic, antibacterial,<sup>14-15</sup> antifungal,<sup>16</sup> antimicrobial,<sup>17-21</sup> antidiabetic,<sup>22</sup> antioxidant,<sup>23</sup> antitumor,<sup>24-29</sup> antipsychotic<sup>30</sup> etc. This useful activity of thienopyrimidine generates our interest in developing a tool for screening novel thienopyrimidine analogs are promise antibacterial agent.<sup>31</sup>

The techniques of QSAR are the most prominent computational means to support chemistry within drug design projects where no three-dimensional structure of the macromolecular target is available, The primary aim of these techniques is to establish a correlation of biological activities of a series of structurally and biologically characterized compounds with the spatial fingerprints of numerous field properties of each molecule, such as steric demand, lipophilicity, and electrostatic interactions.<sup>32</sup>

For this study, the modern drug discovery aspects were applied such as 3D-QSAR (three-dimensional quan-

titative structure-activity relationship), Molecular Docking, ADMET (absorption, distribution, metabolism, excretion, toxicity), etc,

The combination of 3D-QSAR and docking analysis permit the direct visualization and interpretation of molecular modeling results within the active site of gyrase-DNA and some derivatives were consequently generated, and these compounds were evaluated for their drug likeness and (ADMET) properties.

We believe that the results of this work can offer insight into the structural requirements of *S. aureus* inhibitors, providing some reference to guide the design of novel antimicrobial potency against *staphylococcus aureus*.

## 2. Materials and Methods

### 2.1. Selection of Dataset

Analogues of thienopyrimidine derivatives reported to have potent and selective inhibitory activity against a gram positive (*S. aureus*), were taken from the literature.<sup>33</sup>

The structures of the compounds and corresponding pIC50 values ( $\text{pIC}_{50} = -\log \text{IC}_{50}$ ), where IC50 is the concentration of compound agreed for 50 that inhibited the visible growth of microorganism after overnight incubation for the whole set of ligands are presented in Table1.

For 3D-QSAR study, the 27inhibitors were randomly divided into a training set (20 molecules) and test set (7 molecules).

### 2.2. Computational Approaches

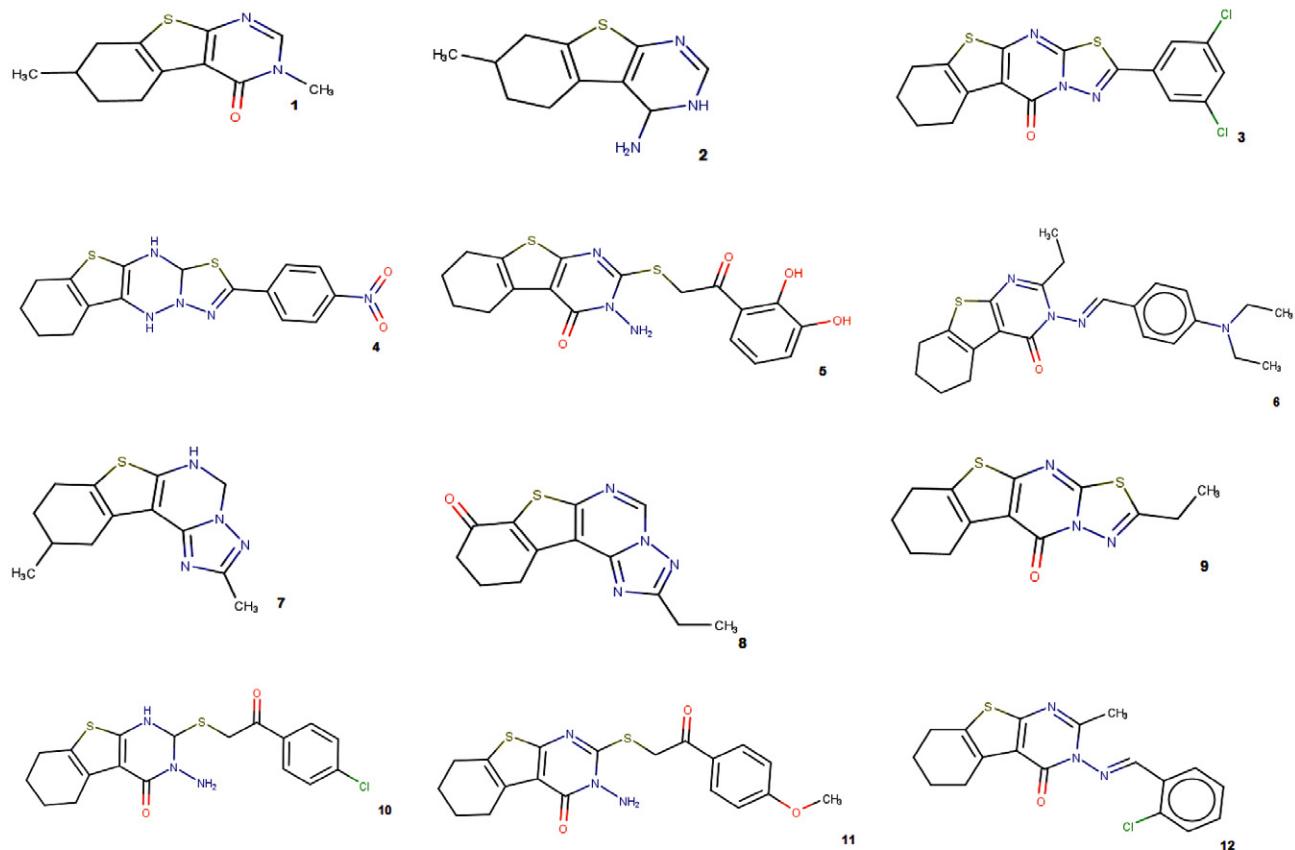
SYBYL-X2.0 package<sup>34</sup> running on windows 7, 64 bits workstation was used to perform 3D-QSAR modeling (CoMFA and CoMSIA).

The 2D structures of thienopyrimidine derivatives built using the SKETCH option in SYBYL, by utilizing molecular modeling software package SYBYL-X 2.0 with standard geometric parameters, The Tripos force field was employed to carry out energy minimization of each conformation of the molecule, The Gasteiger–Hückel atomic partial charges by the Powell method with a convergence criterion of 0.01 Kcal/mol Å were estimated during minimization, then subsequently converted into 3D structures.<sup>35</sup>

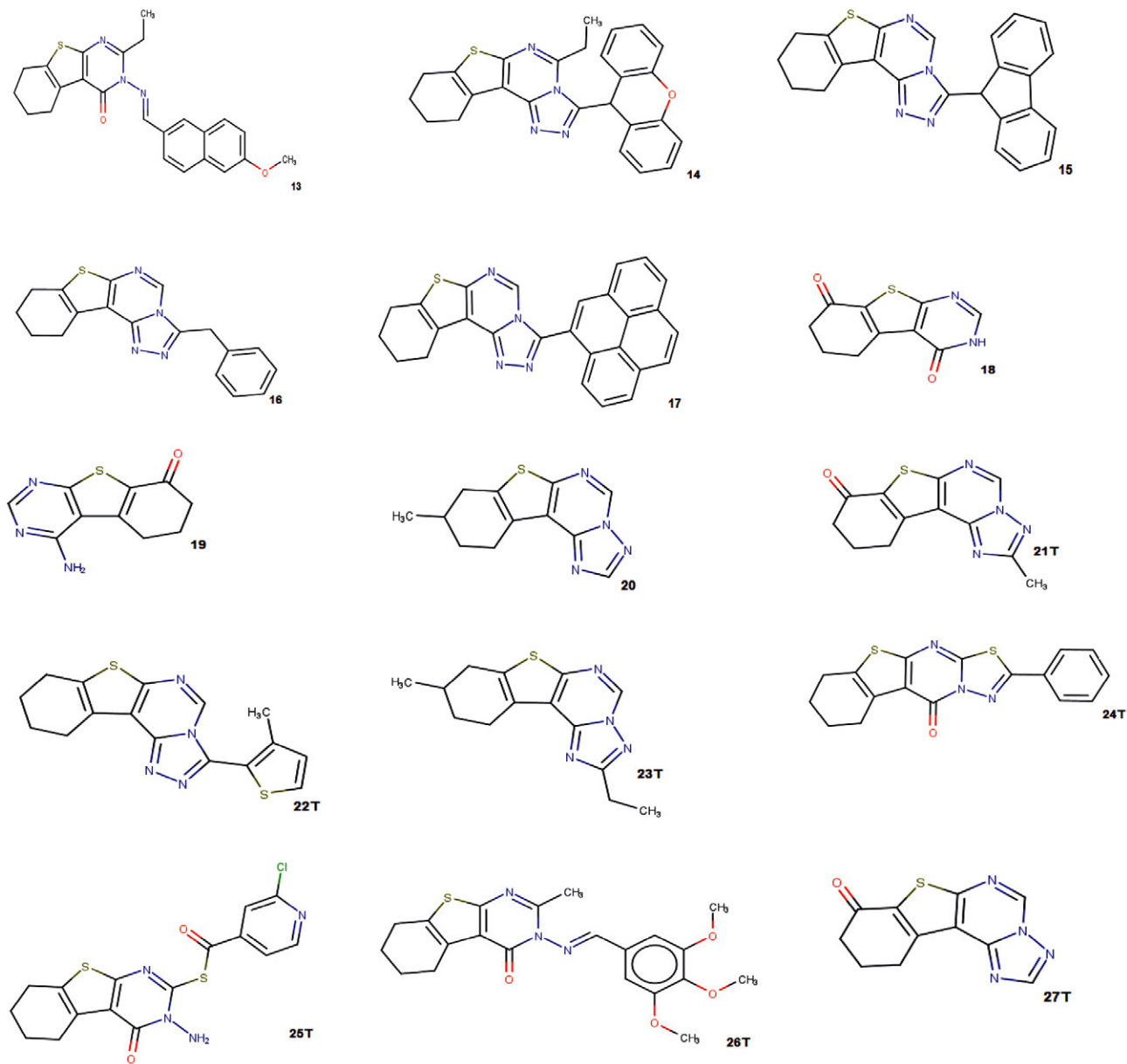
### 2.3. Molecular Alignment

Molecular alignment of compound is a capital step in the construction of 3D-QSAR models.<sup>36</sup>

In the present study ligand-based alignment technique has been chosen in which a template molecule is first isolated over which remaining molecules are aligned, the compound1 was selected as a template and all



## Continium



T = Test set molecule

Fig. 1: Structure of thienopyrimidine derivatives

other molecules were aligned based on the common structure.

During the process, all the dataset structures are aligned to the template common substructure using Distill module in SYBYL-X2.0. The superimposed structures of aligned data set are shown in Fig. 2.

## 2. 4. CoMFA and CoMSIA Analysis

The descriptor fields of both methods were calculated in a three-dimensional cubic with one angstrom grid

spacing, the frontier of the box extended extra 4 angstrom units from the order of aligned structures in each direction.

For CoMFA method, incorporating steric and electrostatic fields, the probe atom of a charged  $sp^3$  hybridized carbon atom was applied to compute electrostatic and steric fields; the cutoff value was  $30 \text{ kcal}\cdot\text{mol}^{-1}$ .<sup>37</sup>

In the case of CoMSIA analysis, five similarity index descriptors consisting of steric (Str), electrostatic (Ele), hydrophobic (Hyd), H-bond donor (HBD), and H-bond acceptor (HBA) fields, A Gaussian function was also applied

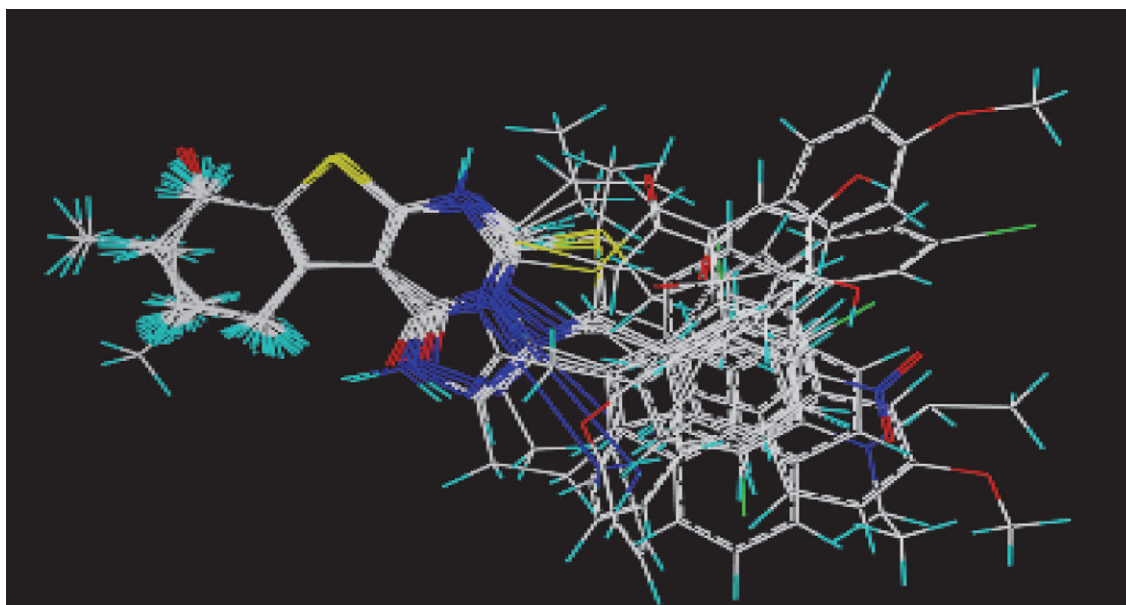


Fig. 2. 3D-QSAR structure superposition and alignment of training and test sets

in calculating the similarity indices, making it accounts for all grid points.<sup>38</sup>

## 2. 5. Partial Least Square (PLS) Analysis

The PLS statistical method implemented in SYBYL-X 2.0, was used to derive a linear relationship for the 3D-QSAR, and cross-validation was performed using the leave-one-out method.<sup>39</sup>

In PLS, the independent variables were the CoMFA and CoMSIA descriptors, and pIC50 values were used as dependent variables, The ONC was the number of components that led to the highest cross-validated correlated correlation coefficient  $q^2$  (or  $R^2_{cv}$ ).

## 2. 6. Model Validation

The predictive power of CoMFA and CoMSIA models was further validated by using an external test set (inhibitors marked with “T” in Table 2).

To avoid excessive extrapolation upon external prediction, Golbraikh and Tropsha’s Criteria followed in developing activity predictors, especially for continuous QSAR, are as follows: (i) correlation coefficient  $R$  between the predicted and observed activities; (ii) coefficients of determination predicted versus observed activities  $R^2_{pred}$  and  $R^2_{obs}$  and The inhibitors in the test set were given exactly the same pretreatment as the inhibitors in the corresponding training set. The correlation between the experimental and predicted activity for models was calculated as  $R^2_{pred}$  value observed versus predicted activities  $R^2_{obs}$  for regressions through the origin; and (iii) slopes  $k$  and  $k'$  of regression lines through the origin.<sup>40</sup>

## 2. 7. Molecular Docking

In order to check the reliability of the established 3D-QSAR models, were subjected to docking with DNA gyrase subunit b (PDB ID: 3G7B), 4 from the Protein Data Bank (RCSB) (<http://www.rcsb.org/pdb>).

Water and co-crystal ligand molecules were eliminated from the structures, molecular docking study was performed using Surflex-dock implemented in SYBYL-X2.0, The ligands and protein preparation steps for the docking protocol were carried out in SYBYL-X 2.0, then results were analyzed using Discovery Studio<sup>41</sup> and MOLCAD module implemented SYBYL-X 2.0.

The MOLCAD program (Molecular Computer Aided Design) was employed to visualize the binding mode between the protein and ligand. MOLCAD calculates and exhibits the surfaces of channels and cavities, as well as the separating surface between protein subunits.<sup>42</sup>

## 2. 8. Pharmacokinetic Profile

The chemical structure of the compound was submitted in the form of canonical simplified molecular input line entry system (SMILE), to estimate several in silico pharmacokinetic parameters using the Swiss ADME tool<sup>43</sup> the pharmacokinetic profile of the compound was evaluated. Gastrointestinal absorption, Blood-Brain Barrier penetration, Skin Permeation, synthetic associability and drug-likeness prediction like Lipinski,<sup>44</sup> and Veber rules,<sup>45</sup> interaction of molecules with cytochromes P450 (CYP) and bioavailability score. The toxicity of the hit Chemicals was predicted using pkCSM online server.<sup>46</sup>

### 3. Results and Discussion

#### 3. 1. 3D QSAR Studies

CoMFA and CoMSIA 3D-QSAR models were derived using DNA gyrase inhibitors.

The predicted and experimental activity values and their residual values for both the training and test sets of CoMFA and CoMSIA models are given in Table 1.

The results of CoMFA and CoMSIA SYBYL, studies are summarized in Table 2, The  $q^2$ ,  $R^2$ , F, and SEE values were computed as defined in PLS analysis showed a  $q^2$  value of 0,758 and  $R^2$  of 0,96 for CoMFA analysis, a non-cross-validated PLS analysis results in a conventional  $R^2$  of 0,944, F = 128, and a standard error of estimation (SEE) of 0,113 for CoMFA analysis.

The steric and electrostatic contributions were 0.576 and 0.246 respectively. These results indicate that steric field contributed highest to the binding affinity.

CoMSIA model was obtained by using the combination of steric, electrostatic, hydrophobic, H-bond donor and H-bond acceptor fields, the statistical results obtained from a combination of these five fields with the four components are ( $q^2 = 0,744$ ,  $R^2 = 0,97$ , F = 527, SEE = 0,097).

The corresponding field contributions are 0,116 (steric), 0,201 (electrostatic), 0,253 (hydrophobic), 0,211 (HBD) and 0,169 (HBA), this is suggesting that the hydrophobicity of the molecule influences their inhibitory potential.

The higher value of F, greater the probability that the QSAR equation is significant.<sup>47</sup> The F values for the

Table 1. Calculated data for the 3D-QSAR model

model	$R^2$	$q^2$	F	SEE	ONC	STR	Field contribution				$R^2_{pred}$
							Ele	Hyd	HBD	HBA	
CoMFA	0,96	0,758	128	0,113	3	0,574	0,426				0,783
CoMSIA	0,97	0,744	527	0,101	4	0,166	0,201	0,253	0,211	0,169	0,625

Table 2. Experimental and calculated activity (pIC50) for *staphylococcus aureus* inhibitors of set training and test set for the CoMFA and CoMSIA models.

Compounds	pIC50 exp. <sup>33</sup>	pIC50 pred.			
		CoMFA	residue	CoMSIA	residue
1	3,290	3,255	0,035	3,272	0,018
2	3,590	3,420	0,170	3,451	0,139
3	4,000	4,080	-0,080	4,131	-0,131
4	4,000	4,090	-0,090	4,033	-0,033
5	4,220	4,420	-0,200	4,240	-0,020
6	5,000	5,020	-0,020	5,018	-0,018
7	3,890	3,733	0,157	3,725	0,165
8	3,890	3,771	0,119	3,862	0,028
9	4,000	4,065	-0,065	4,012	-0,012
10	4,000	4,035	-0,035	4,005	-0,005
11	4,000	4,014	-0,014	4,029	-0,029
12	5,000	4,715	0,285	4,801	0,199
13	5,000	5,107	-0,107	5,125	-0,125
14	4,190	4,160	0,030	4,176	0,014
15	4,490	4,302	0,188	4,373	0,117
16	4,490	4,242	0,248	4,337	0,153
17	4,490	4,493	-0,003	4,530	-0,040
18	3,290	3,224	0,066	3,390	-0,100
19	3,590	3,515	0,075	3,584	0,006
20	3,590	3,459	0,131	3,608	-0,018
21 T	3,590	3,532	0,058	3,755	-0,165
22 T	4,190	3,964	0,226	4,079	0,111
23 T	3,890	3,685	0,205	3,772	0,118
24 T	4,220	4,331	-0,111	4,345	-0,125
25 T	4,090	4,320	-0,230	4,320	-0,230
26 T	5,000	4,884	-0,156	4,666	0,178
27 T	3,890	3,517	0,373	3,751	0,139

CoMFA and CoMSIA models were 128 and 527 respectively. The F value stands for the degree of statistical confidence.

Predicted versus experimental final pIC<sub>50</sub> values for CoMFA and CoMSIA models and their residues (for the training and test sets) are given in table 2.

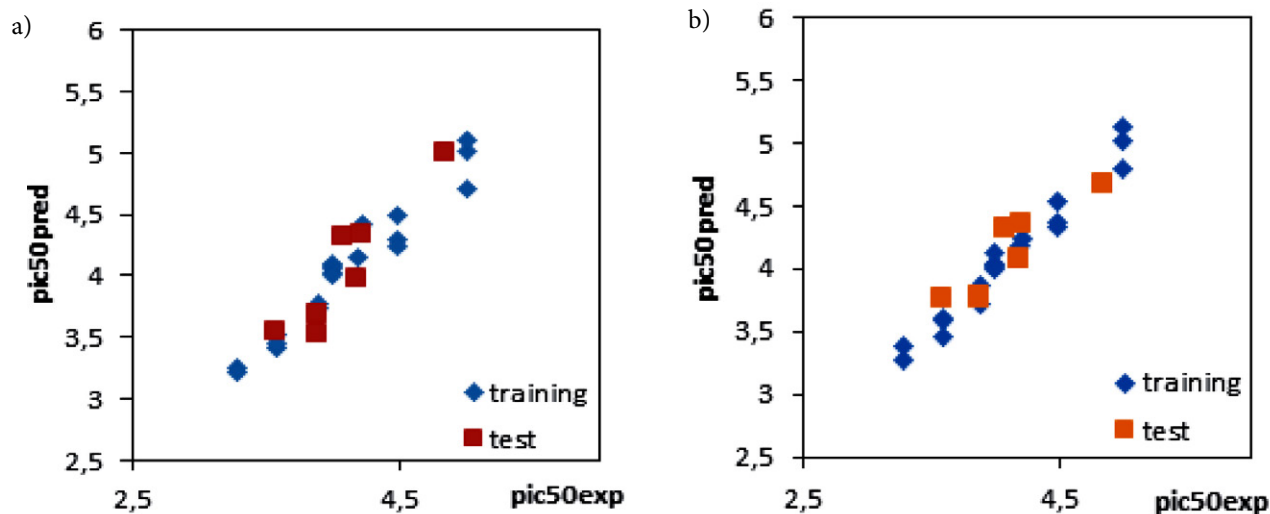


Fig. 3. Graph of *staphylococcus aureus* inhibitors predicted activity of training and test set from a) CoMFA and b) CoMSIA analysis.

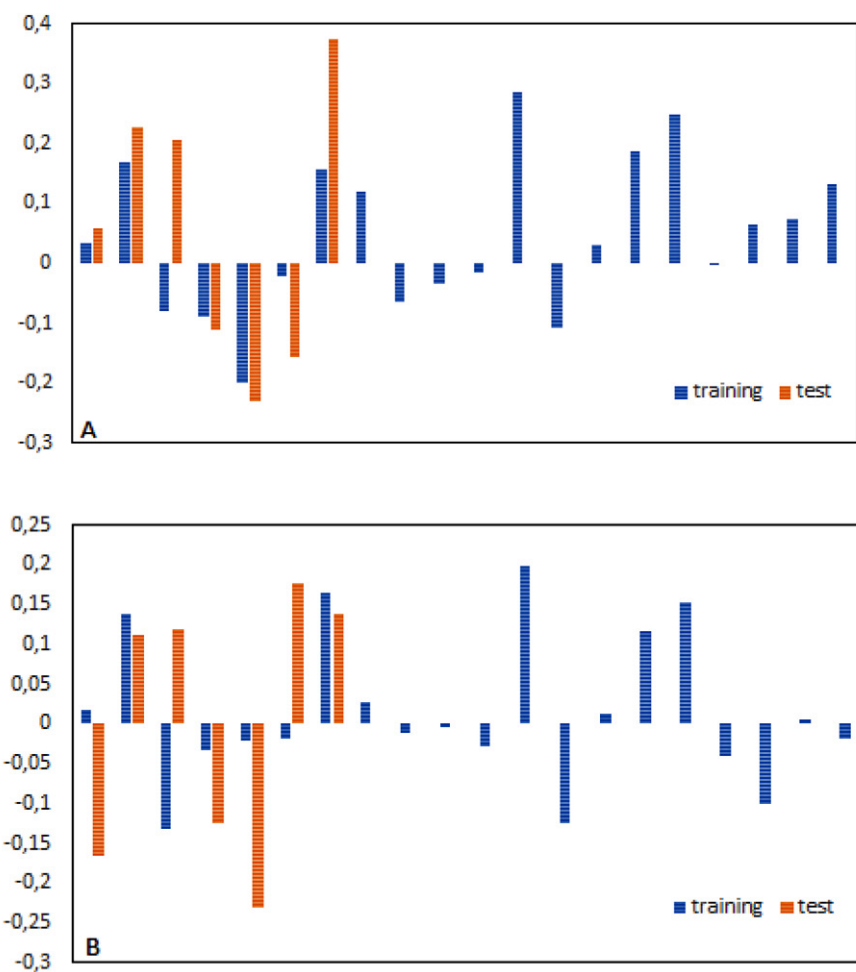


Fig. 4. Histogram of residual values from A) CoMFA analysis B) CoMSIA analysis



The correlation between the predicted and the experimental pIC50 of training and test sets is depicted in Figure 4 for CoMFA and CoMSIA analysis, illustrate the predicted activities using the CoMFA model are in good agreement with the experimental data, suggesting that the CoMFA model should have a satisfactory predictive ability. Results show that prediction by the CoMSIA model is reasonably accurate.

Finally, the predictability of the proposed models was confirmed using external verification and the  $R^2_{pred}$  values were 0,783 and 0,625 for CoMFA and CoMSIA models respectively, the results of these statistics indicated good stability and strong predictive power for the CoMFA and CoMSIA models.

Histogram of residual values obtained from CoMFA and CoMSIA analysis is depicted in Figure 4. They suggest the absence of any outlier compound in the training set whose residual activity is above one.

There is a slight statistical difference between CoMFA and CoMSIA models that indicate the five fields contribute almost as much to the relationship.

### 3. 2. Model Validation Results

The Table 3 shows statistical parameters associated with CoMFA and CoMSIA models. All the calculated pa-

rameters indicated that both models showed a good predictive power. It could be observed that all the Golbraikh–Tropsha criteria

$r^2_{pred}$   $0,85 < K < 1,15$ ,  $0,85 < K' < 1,1$ ,  $R^{o2}$  is close to 1,  $R'^{o2}$  is close to 1 and  $|R_0^2 - R'^2| < 0,3$  were fulfilled.

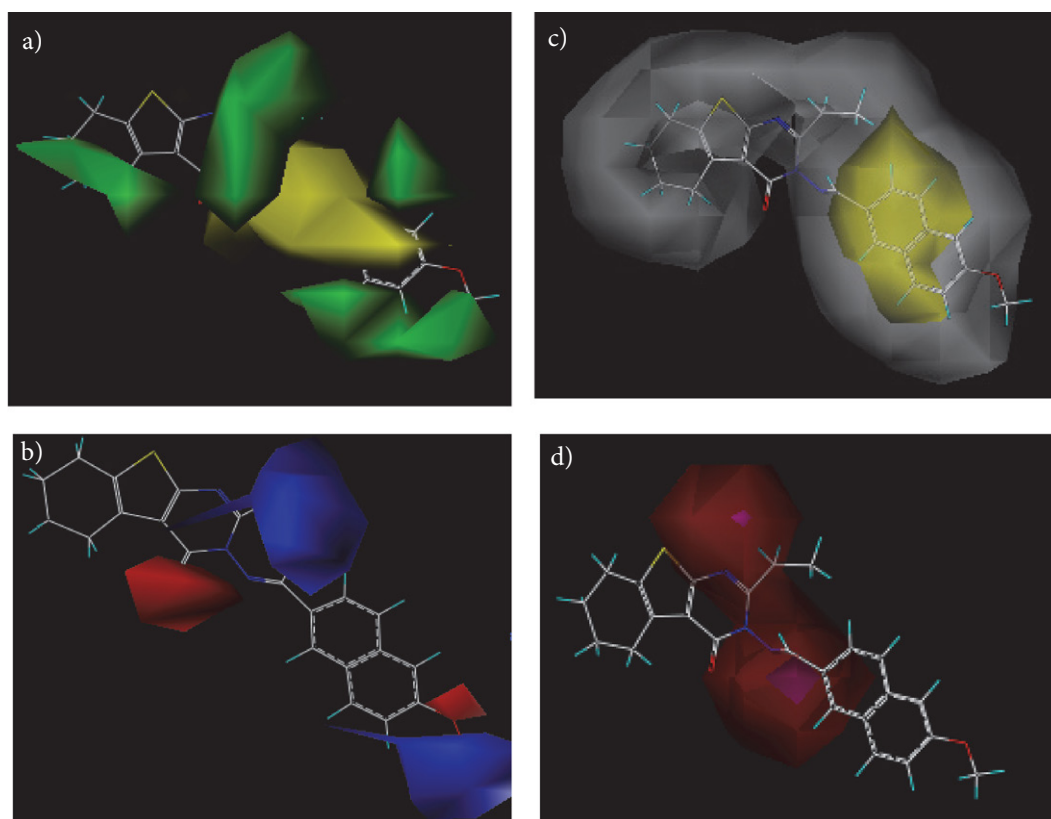
**Table 3.** Predictive power results for the external test set; Golbraikh and Tropsha criteria

MODEL	$r^2_{pred}$	K	K'	$R^{o2}$	$R'^{o2}$	$ R_0^2 - R'^2 $
CoMFA	0.783	0.976	1.021	0.941	0.965	0.02
CoMSIA	0.666	0.990	1.007	0.991	0.992	0.001

### 3. 3. CoMFA and CoMSIA Contour Maps

To visualize the information content of the derived 3D-QSAR model, CoMFA and CoMSIA contour maps were generated to rationalize the regions in 3D space around the molecules where changes in the steric, electrostatic, steric, hydrophobic, H-bond donor, and H-bond acceptor fields were predicted to increase or decrease the activity.

A thorough analysis of the contours obtained determines the vital physicochemical properties responsible in



**Fig. 5.** CoMFA and CoMSIA STDEV\*COEFF contour maps: a) steric, b) electrostatic, c) Hydrophobic, d) hydrogen-bond acceptor and hydrogen-bond donor fields; based on the most active compound 13.

determining the activity and explores the crucial importance of various substituents in their 3D orientation.

The visualization of the results of the CoMFA and CoMSIA models have been performed using the St-Dev\*Coeff mapping option contoured by contribution, the default level of contour with contribution, 80% for favored region and 20% for disfavored region was set during contour analysis.

The CoMFA and CoMSIA steric and electrostatic contour maps were shown in Fig. 5a, b using compound 13 the most active of the series as a reference structure explaining the key structural features required for inhibitory activity.

The steric contour maps of the CoMFA and CoMSIA models are shown in yellow and green colors, the green contours represent regions of high steric tolerance (80% contribution) while the yellow contours represent regions of low steric bulk tolerance (20% contribution).

In the contour map of steric field (Figure 5 a), a large green contour was observed near the naphthalene ring, suggesting the bulky substituent was favored at this region.

Therefore, it is reasonable for the activity order of those compounds, 17(pIC<sub>50</sub> = 4.49) > 16(pIC<sub>50</sub> = 4.46) > 14(pIC<sub>50</sub> = 4.19) > 2(pIC<sub>50</sub> = 2,59) > 1(pIC<sub>50</sub> = 2,5), with the corresponding R1 substituent pyrene, 9H-xanthene, Phenyl, Methyl and H respectively. (The figure 9 shows the location of the radicals R1 and R2).

It is clear that the N methyleneamino (the link between ring and thienopyrimidine) is surrounded by most of the yellow areas; the phenomenon demonstrates that bulky groups are unfavorable for increasing the activity.

The electrostatic field (Figure 5b) is indicated by Two blue regions were found near the R<sub>1</sub> and R<sub>2</sub> position, which can explain the fact that the activity of compounds 25 (R<sub>2</sub> = NH<sub>2</sub>) and 15 (R<sub>2</sub> = H) are less potent than the compound 14 (R<sub>2</sub> = C<sub>2</sub>H<sub>5</sub>), therefore, it is reasonable for the activity order of those compounds, 14 (R<sub>1</sub> = C<sub>2</sub>H<sub>5</sub>) > 12 (R<sub>1</sub> = CH<sub>3</sub>) > 11 (R<sub>1</sub> = NH<sub>2</sub>), because that substitution of electropositive groups at this position would increase the activity and emphasizes that the electronegative environment is undesirable at this position.

The red contour surrounding the oxygen atoms of the methoxy group sheds light on the fact that the activities of compound 13 (R<sub>2</sub> = O-CH<sub>3</sub>) is higher than that of the compound 16 (R<sub>2</sub> = H), and which can explain the fact that the activity of compound 30 which have three group methoxy around the naphthalene where any electronegative group at this region would increase the activity.

CoMSIA contribution maps denote those areas within the specified region where the presence of a group with a particular physicochemical property will be favored or disfavored for good inhibitory activity.

CoMSIA calculates both steric and electrostatic fields, as in CoMFA, but additionally uses hydrophobic, HBD and HBA fields, favored and disfavored levels fixed at 80% and 20%, respectively.

The CoMSIA hydrophobic contour map is shown in Fig 5c, represented by yellow (80% contribution) and gray (20% contribution) colored contours.

Yellow colored contours indicated the regions where hydrophobic groups on ligands are favored and gray colored contours represent those areas where hydrophobic groups are unfavored (or favorable for hydrophilic groups on ligands).

The calculated CoMSIA hydrophobic contours (Fig. 5c) display favorable hydrophobic substituents (yellow polyhedral) in proximity of the naphthalene ring, Unfavorable areas (white) are located around the thienopyrimidine and the substituent R1, and in proximity of the R2: methoxy group.

Presence of a big white contour near R1 substituents of thienopyrimidine ring shows the importance of hydrophilic groups on the antibacterial activity in this region.

As shown in Fig.5d, the magenta contours indicate hydrogen bond-accepting groups increase the inhibitory activity, whereas the red contours indicate hydrogen bond-accepting groups decrease the activity, a magenta contour located on the amino between thienopyrimidine and naphthalene around the N atom in the ring pyrimidone suggested that hydrogen bond-accepting groups were favored.

### 3. 4. Docking Analysis

Molecular docking is a computational approach that finds best binding orientation between two biomolecules the ligand and the protein.<sup>47</sup>

The Protein-Ligand interaction plays a vital role in structural based drug design.<sup>48</sup>

In our present study, docking of tested compounds with the primary drug pathway for *S. aureus* was per-

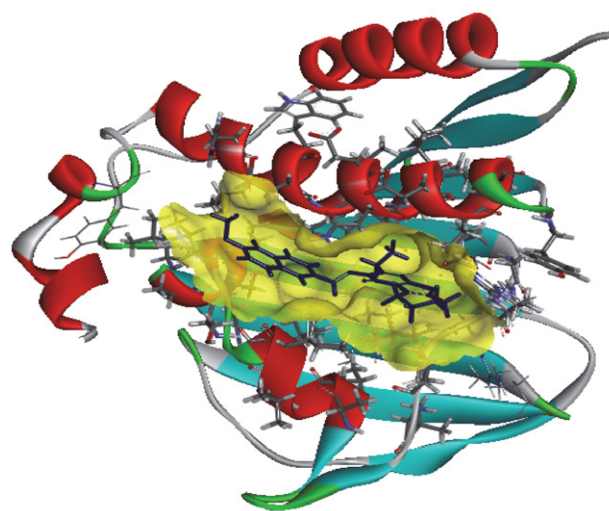


Fig. 6. Three-dimensional structure of the receptor proteins DNA gyrase Bin complex with the compound 13.

formed, subsequently, the active compound 13 and inactive compound 1 were docked into the ligand-binding pocket of DNA gyrase B protein (code PDB:3G7B), as described in Fig.6.

Docking interactions with two compounds (13 and 1) are shown in the Figs. 7a–c, respectively.

For the low active compound, the Docking results shows carbon-hydrogen bond with Gly85Asp81 and Arg84 residues, pi-alkyl interaction with Ile86 residue.

While compound 13 is stabilized by a number of hydrophobic contacts with the residues Ile 86, Pro87 and Ile 51 residues, as shown in Fig.7, the ligand 13 displayed three hydrogen bond interactions, one of the hydrogen bonds was observed between NH group val130 and O-atom of methoxy group at distance of 2,38Å.

Another hydrogen bond was observed between of Thr173 and one of the nitrogen atoms of the pyrimidinone ring at a distance of 2, 5 Å, the third bond was observed between Asn54 and NH- group.

The key amino acid residues within the docking complex model involved in the interaction between the two compounds (most active, and low active) were Gly 85 and Arg48 corroborating the studies of Berk et al. <sup>49</sup>

The type and the position of interactions were suggested by contour map analysis. This supports the validity of our results.

To further visualize the binding mode, the molecular computer aided design program (MOLCAD) was conducted, MOLCAD could calculate and display the cavity depth (CD), electrostatic potential (EP), lipophilic potential (LP), and hydrogen bond site (HB) of the binding pocket, which can be used to find the sites that act attractively on ligands by matching opposite colors.

In Figure 8(CD), the MOLCAD Multi-Channel cavity depth potential surfaces structure of the binding site within the compound 13 is displayed and the cavity depth color ramp ranged from blue (low depth values = outside of the pocket) to ORANG (high depth values = cavities deep inside the pocket), In Figure 8(CD), the R1 position naphthalene of compound 13 is observed in a blue area, revealing that this position was embedded deep inside the ATP pocket, It can be simply inferred that a bulky group at R1 position maybe favorable, Since the thienopyrimidine site was oriented to a light Yellow/Orange area, which illustrated a minor group was anchored into a favorable region, this suggests that minor groups may benefit the potency.

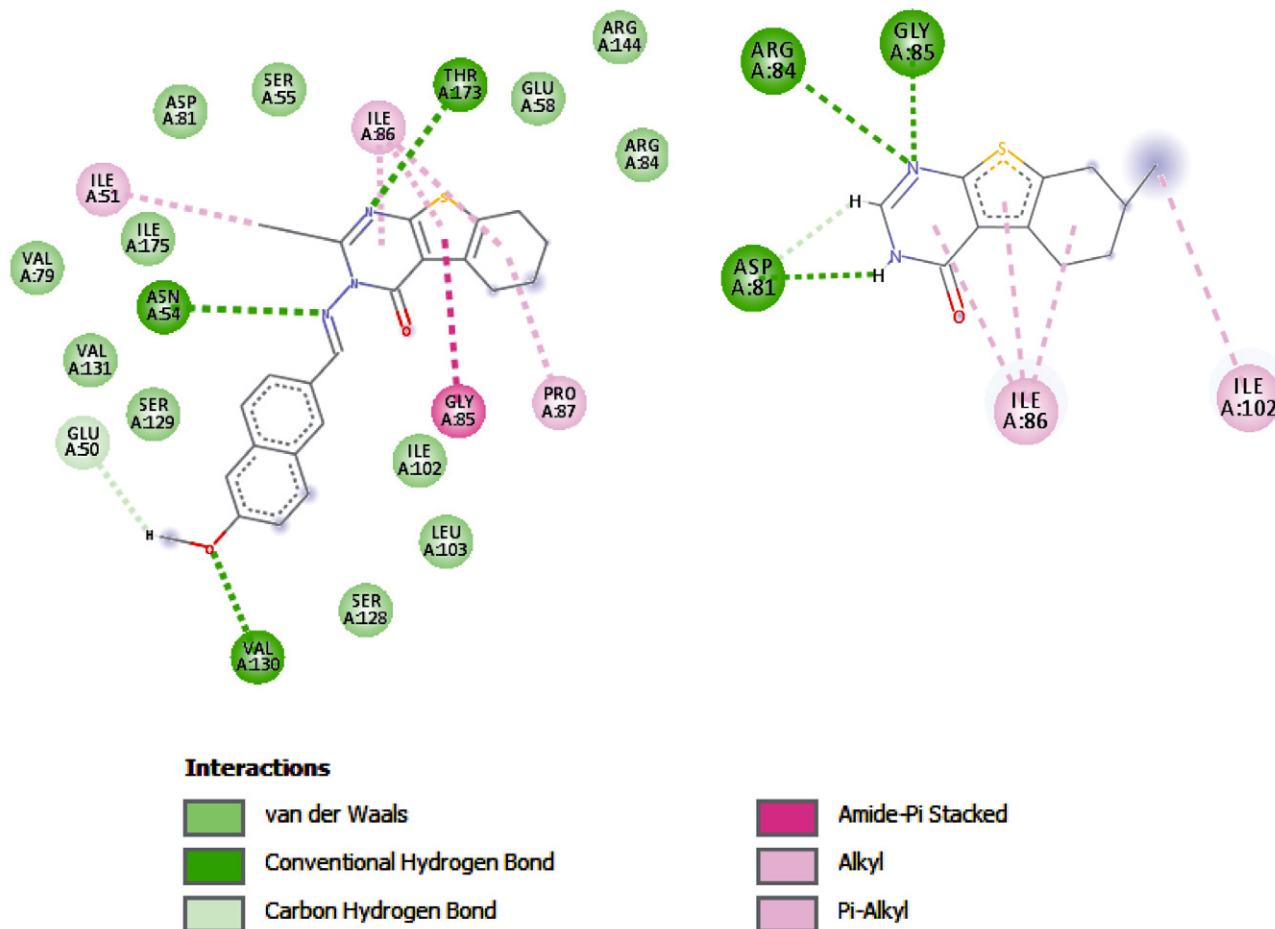


Fig. 7. Two-dimensional depiction of the docked conformations of Ligand 13 and ligand 1 with enzyme DNA gyrase protein

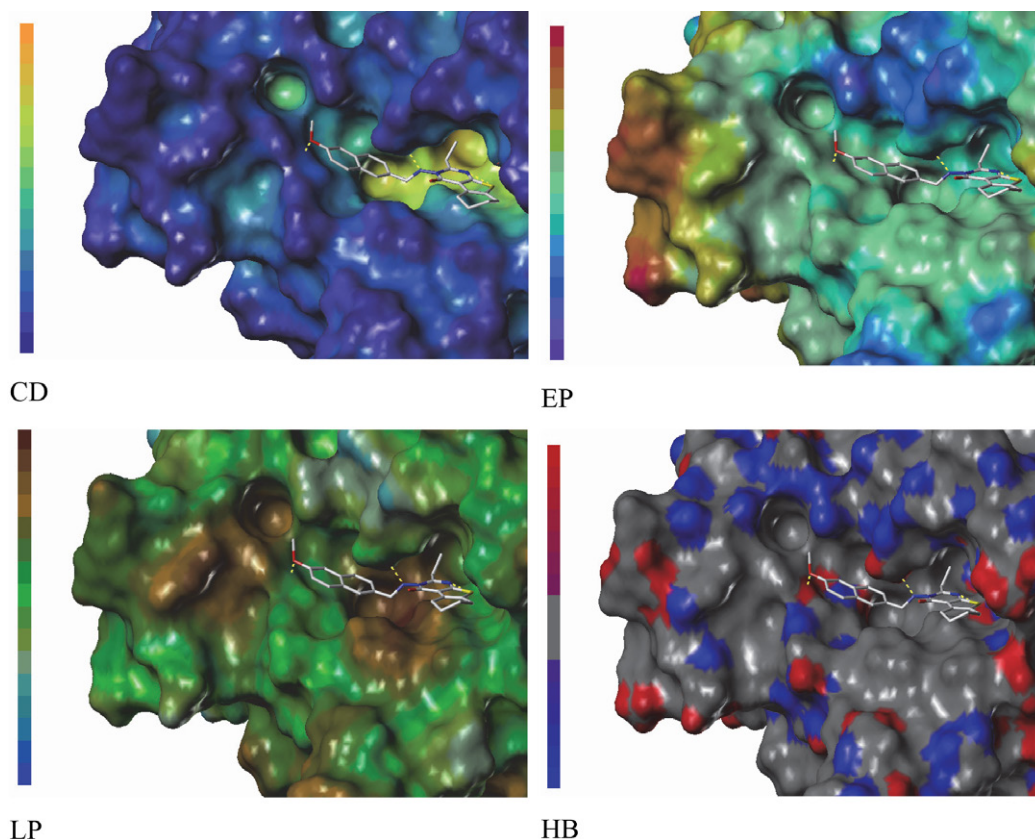


Fig. 8. MOLCAD surfaces of the binding site of DNA gyrase protein with molecule 13

In Fig. 8 (EP), the MOLCAD electrostatic potential surface of the binding region was demonstrated with the color ramp for EP ranging from red (most positive) to blue (most negative), the position R1 group was found in a blue area, which indicated that electron-donating properties at this site were essential for the potency; the sulfo group was in a yellow area, which suggested that electron-withdrawing properties would be favored; the  $-\text{CH}_2\text{CH}_3$  radical was anchored in a green area which suggested that an electron-donating substituent at this position would be essential for the potency.

These results were well compared with the corresponding CoMFA and CoMSIA electrostatic contour maps.

Figure 8 (HB) displayed the MOLCAD hydrogen bonding sites of the binding surfaces, ligands can be docked to proteins by matching the patterns displayed on the surface, the color ramp for HB ranges from red (hydrogen donors) to blue (hydrogen acceptors). The nitrogen of thienopyrimidine ring and N methyleneamino of compound 13 was found in the red surface, which suggested that the surface of this site are hydrogen bond donors, and a hydrogen bond acceptor substituent would be favorable; and the naphthalene ring of compound 13 was found in the blue surface, which indicated that the surface of this region are hydrogen bond acceptors, and a hydrogen bond donor substituent be favored.

The observations taken from this hydrogen bonding sites satisfactorily matched to the corresponding CoMSIA hydrogen bond donor contour maps.

Figure 8 (LP) showed the MOLCAD lipophilic potential surface of the binding area, the color ramp for LP ranges from brown (highest lipophilic area of the surface) to blue (highest hydrophilic area). The R1 position was oriented to a brown region, suggesting that a hydrophobic substituent may be favored; the methylene amino was oriented to a blue area, which indicated that a hydrophilic group would be favorable. The observations taken from Fig. 8 satisfactorily matched those of the CoMSIA hydrophobic contour map.

Combined 3D-QSAR and molecular docking analysis is corroborated and these results will help to better interpret the structure-activity relationship of these DNA gyrase inhibitors and provide valuable information into rational drug design.

### 3. 5. New Compounds Design and Activity Prediction

Based on the established two sets of 3D-QSAR models and related analysis results, the compound 13 was used as a template to modify its molecular structure, and five new compounds were designed. The structures of the new compounds are shown in Table 4.

We substituted R1 and R2 parts with proper groups according to the contour maps. The activities of these designed structures towards *Staphylococcus aureus* antagonist were almost better compared to that of reported thienopyrimidine derivatives.

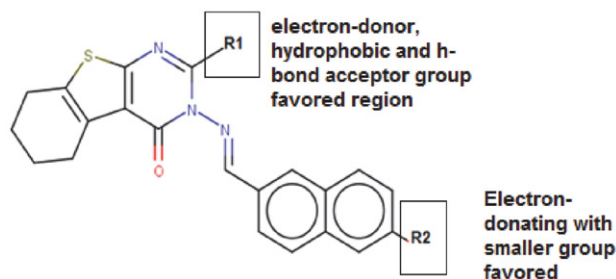


Fig. 9. Structure-activity relationship representation.

### 3. 6. Drug-likeness, Bioavailability, Synthetic Accessibility and Alerts for PAINS

Drug likeness may be defined as a complex balance of various molecular properties and structural features, which determine whether a particular molecule is drug or nondrug. Probably, the most widely used filter is Lipinski's Rule-of-five, which proposes that molecules with poor permeation and oral absorption have molecular weight > 500,  $\log P > 5$ , more than 5 hydrogen-bond donor and

more than 10 acceptor groups.<sup>44</sup> All the molecules exhibited drug likeness characteristics according to Lipinski rules. The other significant properties such as total polar surface area (TPSA) and the number of rotatable bonds and molar refractivity were also calculated. The results are depicted in Table 5. TPSA of a compound is less than 140 Å<sup>2</sup> and the number of rotatable bonds is less than 10, as the number of rotatable bonds increases, the molecule becomes more flexible and more adaptable for efficient interaction with a particular binding pocket<sup>50</sup>. Interestingly the compounds E, D and A have 6–7 rotatable bonds and flexible.

So, Lipinski and Veber rules are validated, therefore, theoretically, there would not have a problem with oral bioavailability for all proposed compounds.

Drug oral bioavailability is the fractional extent of the drug dosage that finally reaches the therapeutic site of action and is quantitatively symbolized as % F, acceptable probability score is 55%, which indicates that it passed the rule of five. The compounds showed a score of 55%, indicating good bioavailability.

For the discovery of oral administrative drugs, solubility is one of the major descriptors. Highly water solubility was useful for deliver active ingredient in sufficient quantity in small volume of such pharmaceutical dosage. These values are the decimal logarithm of the molar solubility in water ( $\log S$ ). From the results appear in the table 5, it can be said that the compounds tested has poorly wa-

Table 4. Structures of newly designed molecules and their predicted pIC<sub>50</sub> based on CoMFA and CoMSIA 3D-QSAR models.

	Smile	R1	R2	CoMFA	CoMSIA
13	<chem>CCc1nc2sc3c(c2c(=O)n1)/N=C/c1ccc2c(c1)ccc(c2)OC)CCCC3</chem>	CH <sub>2</sub> CH <sub>3</sub>	OCH <sub>3</sub>	5.107	5.125
A	<chem>CCCc1nc2sc3c(c2c(=O)n1)/N=C/Cc1ccc2cc(OC(C)C)ccc2c1)CCCC3</chem>	-(CH <sub>2</sub> ) <sub>2</sub> CH <sub>3</sub>	OCH(CH <sub>3</sub> ) <sub>2</sub>	5.129	5.125
B	<chem>CCOc1ccc2cc(C=Nn3c(CC(C)C)nc4sc5c(c4c3=O)CCCC5)ccc2c1</chem>	CH <sub>2</sub> CH(CH <sub>3</sub> ) <sub>2</sub>	OCH <sub>2</sub> CH <sub>3</sub>	5.181	5.135
C	<chem>NC1=CC2=CC=C(C1C=N3C(=O)C4=C(C5C=C4CCCC5)N=C3C3CCCC3)C=C2=C1</chem>	C <sub>6</sub> H <sub>11</sub>	NH <sub>2</sub>	5.124	5.126
D	<chem>CCCCC1=NC2=C(C3=C(C4CC3)S2)C(=O)N1N=CC1=CC=CC2=C1C=CC(=C2)N(C)C</chem>	(CH <sub>2</sub> ) <sub>3</sub> CH <sub>3</sub>	N(CH <sub>3</sub> ) <sub>2</sub>	5.218	5.154
E	<chem>CCCCC1nc2sc3c(c2c(=O)n1)/N=C/C/c1ccc2c(c1)cc(cc2)NC)CCCC3</chem>	(CH <sub>2</sub> ) <sub>4</sub> CH <sub>3</sub>	CH <sub>3</sub> NH	5.137	5.128

Table 5. Prediction of molecular properties descriptors of the new compounds design

Comp.	MW g/mol	logP	H-bond A	H-bond D	log S mol/L	n.rot	REF	TPSA (Å <sup>2</sup> )	S.A score	F %	Pains alert
13	417.52	4.30	4	0	-6.06	4	124.52	84.72	3.92	55	0
A	459.60	4.80	4	0	-6.88	6	138.94	84.70	4.30	55	0
B	458.62	4.93	3	0	-7.30	3	138.94	71.83	4.15	55	0
C	456.60	4.18	3	1	-6.93	3	139.54	101.5	4.32	55	0
D	458.62	4.74	3	0	-6.80	6	141.85	78.73	4.46	55	0
E	458.62	4.78	3	1	-6.99	7	141.75	87.52	4.38	55	0

ter solubility. Low water solubility translates to slow absorption and action.

Activity artifacts in assays present a major problem for biological screening and medicinal chemistry. Such artifacts are often caused by compounds that form aggregates or are reactive under assay conditions. Many pan assay interference compounds (PAINS) have been proposed to cause false-positive assay readouts.<sup>51</sup>

The PAINS violations of proposed compounds are given in table 5. Almost all the compounds showed zero PAINS alert and can be used as lead compounds.

One of the key aspects of CADD (Computer aided design and drafting) activities is help for the selection of most promising molecule which was synthesized and subjected for biological study is the synthetic accessibility (SA). For given molecule, SA score is the summation of the fragments and corrected by the terms describing size and complexity such as macrocycles, chiral centers, or spiro functions. The SA score ranges from 1 (very easy) to 10 (very difficult).<sup>52</sup> The obtained values were in the range of 3–5 revealed that the compounds here have easy synthesis route.

### 3. 7. ADME Evaluation of the New Candidates

The pharmacokinetic studies were performed using online SwissADME tool, the calculated absorption, distribution and metabolism parameters are presented in Table 6 and Table 7 respectively.

Transdermal delivery systems are attractive for both topical and systemic therapeutics. However, the skin barrier,

which protects the body from physical and chemical attacks, also hinders the delivery of the required drug dose through the skin to a target organ.<sup>53</sup>

The results in the table show that all the compounds found (table 6) to be poorly permeable to skin as all compounds have Kp negative values.

Moreover, other parameters used to measure the absorption and distribution of these drugs is through human intestinal absorption (HIA) or gastrointestinal (GI) adsorption data. These data show that all the compounds are predicted to be well absorbed, except for the compound C, whose absorption is weak. This result is also evident in the BOILED-Egg model. (FIG10)

The Blood–brain partitioning and brain distribution are critical properties for drugs targeting the central nervous system. The Compounds tested are predicted as non-brain penetrant thus, side effects at this level may be diminished.

Table 6. Predicted ADME properties for new inhibitors

Compound	GI Absorption	BBB Permeable	Log Kp (Cm/S)
13	High	Yes	–5.85
A	High	No	–4.42
B	High	No	–3.93
C	High	No	–4.54
D	High	No	–4.49
E	High	No	–4.20

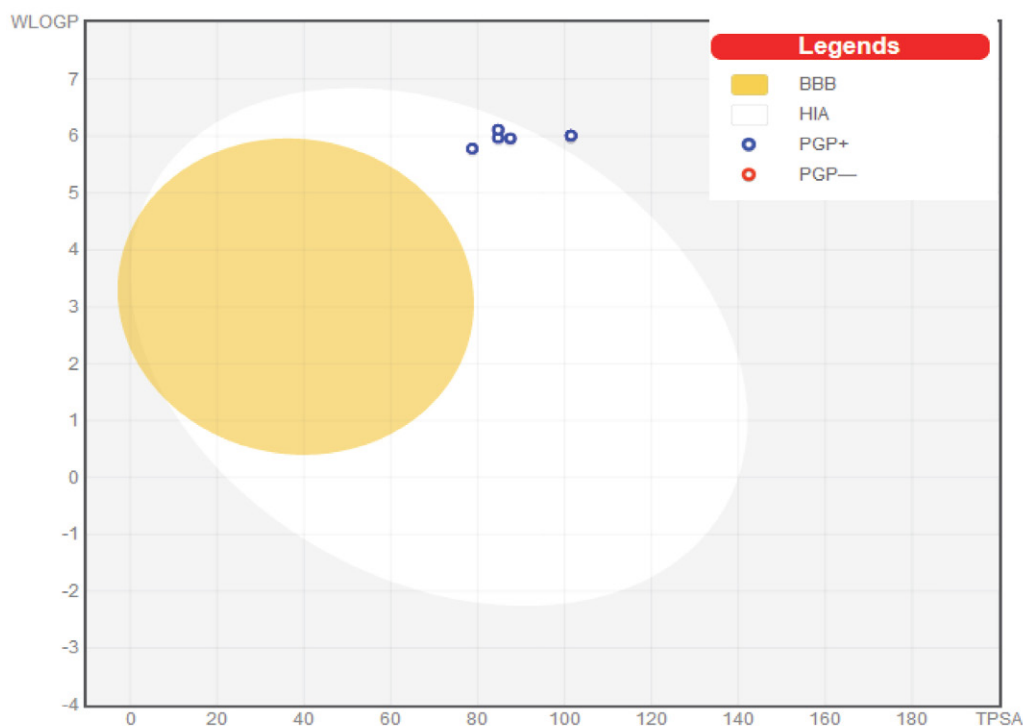


Fig. 10. BOILED-Egg model

The BOILED-Egg model is of great support for the users to apprehend the concepts of absorption and distribution, and to figure out what type of chemical modifications must be made to the small molecule to obtain the desired absorption and distribution, in an intuitive and iterative way.<sup>54</sup>

Inside circle [yellow] depicts BBB- blood brain barrier, none of the compounds are in this region. The white region that is outer to yellow depicts the human intestinal absorption. Almost all compound lies in this white area. Only molecule C is lying outside [grey area] which indicates poor intestinal absorption.

The study on the potential of compounds to inhibit the cytochrome P450 (CYP) enzymes is important in determining their possible drug interactions and toxicity.<sup>55</sup>

Approximately over 50% of therapeutic molecules are substrate of five major isoforms (CYP1A2, CYP2C19, CYP2C9, CYP2D6, and CYP3A4). These enzymes are involved in metabolism of drugs.<sup>56</sup>

Moreover, the compound design presented was found to be substrates of CYP1A2 and CYP2D6.

The compound D is predicted not to be inhibitors of three of CYP isoenzymes. This fact is very useful, because this compound is expected not to have CYP metabolism interactions with other drugs, and this compound could present a reduced Hepatic toxicity risk. All compounds are found to be substrates of P-Gp (table7), lipophilic substances of low molecular weight tend to be substrates for P-glycoprotein.<sup>57</sup>

The predictive results presented by pkCSM were presented in Table 8. The predicted results indicate that all compounds not inhibit the hERG channel and not have skin sensitization.

Ames mutagenicity was used for the evaluation of the potential teratogenicity and genotoxicity in the early stages of drug discovery, according to the results shown in Table 8 The suggested compounds A,B and D showed no toxicity to AMES.

Another toxicity test is the hepatotoxicity test. From Table 8 it can be seen that the compounds A and B are not hepatotoxic.

Also, from Table 8 it can be noted that the LD50 values are high (2.5 – 3.09), and this indicates that the compounds are fatal only at very high doses.

The predicted ADME-Tox descriptors for the compounds validated good pharmacokinetics properties better than the studied series, suggesting that these compounds could be used as hit for the development of the new active agents.

## 4. Conclusion

In this study, CoMFA and CoMSIA 3D-QSAR models were developed for a series of thienopyrimidine derivatives that has antimicrobial potency against *Staphylococcus aureus*; the two models have good statistical results in terms of  $q^2$  and  $R^2$  values.

The good predictive ability of CoMFA and CoMSIA observed for the test set of compounds indicates that these models could be successfully used for predicting the pIC50 values. Moreover, based on the contour's maps of the CoMFA/CoMSIA models, Steric, electrostatic and hydrophobic significant regions were identified to enhance bioactivity as well as H-bond interactions. Docking study was performed to analyze and identify the interactions of pos-

Table 7. Metabolism prediction for new inhibitors

Compound	P-Gp Substrata	CYP1A2 Inhibitor	CYP2C19 Iinhibitor	CYP2C9 Inhibitor	CYP2D6 Inhibitor	CYP3A4 Inhibitor
13	Yes	Yes	Yes	Yes	No	Yes
A	Yes	No	Yes	Yes	No	Yes
B	Yes	No	Yes	Yes	No	Yes
C	Yes	No	Yes	Yes	No	Yes
D	Yes	No	Yes	Yes	No	No
E	Yes	No	Yes	Yes	No	Yes

Table 8. Toxicity prediction for new inhibitors

Compound Number	Skin Sensitisation	Hepatotoxicity	AMES toxicity	hERG I inhibitor	Oral Rat Acute Toxicity (LD50)
33	No	Yes	Yes	No	2.112
A	No	No	No	No	2.568
B	No	No	No	No	2.950
C	No	Yes	Yes	No	2.285
D	No	Yes	No	No	3.049
E	No	Yes	Yes	No	2.289

sible antimicrobial compounds (The best effective compound being compound 13 and the weakest compound 1) in the active site of DNA gyrase. These results provided crucial clues for designing novel *Staphylococcus aureus* antagonists with high predicted potent activity. A set of 5 novel derivatives were designed by utilizing the structure-activity relationship taken from the present study. In silico analyzes of absorption, distribution, metabolism and excretion were carried out on these new molecules to investigate their activities in compliance with the standard. These five novel lead molecules have better pharmacological properties compared to the study series. The information obtained from this study can further be used for the design of potent inhibitors of *S. aureus* DNA gyrase enzyme.

## 5. References

1. D. Lowy. *N. Engl. J. Med.* **1998**, 339, 520–532. DOI:10.1056/NEJM199808203390806
2. G. Jagadeesan, V. Vijayakuma, M. Palayam, G. Suresh, G. Krishnaswamy, S. Aravindhan, G. H. Peters, *J. Proteomics Bioinform.* **2015**, 8, 1–7. DOI:10.4172/jpb.1000362
3. M. M. El-Enany, F.S. El-Shafie, *Orient. J. Chem.* **1989**, 5, 114–117. DOI:10.1016/j.ejmech.2010.08.044
4. S. M. Ronkin, M. Badia, S. Bellon, A. L. Grillot, C. H. Gross, T. H. Grossman, N. Mani, J. D. Parsons, D. Stamos, M. Trudeau, Y. Wei, P. S. Charifson, *Bioorg. Med. Chem. Lett.* **2010**, 20, 2828–2831. DOI:10.1016/0006-2952(75)90415-3
5. V. P. Litvinov, *Chem Inform.* **2006**, 92, 83–143. DOI:10.1016/S0065-2725(06)92003-0
6. Kharizomenova, A. N. Grinev, N. V. Samsonova, E. K. Panisheva, N. V. Kaplina, I. S. Nikolaeva, T. V. Punshkina, G. N. Pershin, *Pharm. Chem. J.* **1981**, 15, 645. DOI:10.1007/BF00760666
7. A. E. Rashad, A. H. Shamroukh, R. E. Abdel-Megeid, A. Mostafa, R. El-Shesheny, A. Kandeil, M. A. Ali, K. Banert, *Eur. J. Med. Chem.* **2010**, 45, 5251–5257. DOI:10.1016/j.ejmech.2010.08.044
8. V. Alagarsamy, S. Meena, K. V. Ramseshu, V. R. Solomon, K. Thirumurugan, K. Dhanabal, M. Murugan, *Eur. J. Med. Chem.* **2006**, 41, 1293–1300. DOI:10.1016/j.ejmech.2006.06.005
9. A. B. A. El-Gazzar, H. A. R. Hussein, H. N. Hafez, *Acta Pharm.* **2007**, 57, 395–406. DOI:10.2478/v10007-007-0032-6
10. N. S. Habib, R. Soliman, K. Ismail, A. M. Hassan, M. T. Sarg, *Bull. Chim. Farm.* **2003**, 142, 396–405. DOI:10.2478/v10007-007-0032-6
11. M. S. Tolba, M. Ahmed, A. M. Kamal El-Dean, R. Reda Hassanien, M. Farouk, J. J. Heterocycl. Chem. **2017**, 55, 408–418. DOI:10.1002/jhet.3056
12. M. S. El-Shoukrofy, H. A. Abd El Razik, O. M. Aboulwafa, A. E. Bayad, I. M. El-Ashmawy, *Bioorg Chem.* **2019**, 85, 541–557. DOI:10.1016/j.bioorg.2019.02.036
13. N. S. Shetty, R. S. Lamani, I. A. M. Khazi, *J. Chem. Sci.* **2009**, 121, 301–307. DOI:10.1007/s12039-009-0034-7
14. T. Horiuchi, J. Chiba, K. Uoto, T. Soga, *Bioorg. Med. Chem. Lett.* **2009**, 19, 305–308. DOI:10.1016/j.bmcl.2008.11.090
15. M. D. M. H. Bhuiyan, K. M. D. M. Rahman, M. D. K. Hossain, A. Rahim, M. I. Hossain, M. Abu Naser, *Acta Pharm.* **2006**, 56, 441–450.
16. C. Sharma, S. Yerande, R. Chavan, A. V. Bhosale, *J. Chem.* **2010**, 7, 655–664. DOI:10.1155/2010/369141
17. H. M. Aly, N. M. Saleh, A. Elhady, *Eur. J. Med. Chem.* **2011**, 46, 4566–4572. DOI:10.1016/j.ejmech.2011.07.035
18. N. Kerru, T. Settypalli, H. Nallapaneni, V.R. Chunduri, *Med. Chem.* **2014**, 4, 623–629. DOI:10.4172/2161-0444.1000204
19. M. R. Mahmoud, F. S. Abu El-Azm, A. T. Ali, Y. M. Ali, *Synth. Commun.* **2015**, 45, 982–992. DOI:10.1002/jhet.2824
20. T. A. Mohamed, M. K. Abou-Elregal, A. S. A.; Youssef, M. M. Hemdan, S. S. Samir, W. S. I. Abou-Elmagd, *Synth. Commun.* **2020**, 50, 399–411. DOI:10.1080/00397911.2019.1697822
21. S. Ramamurthy, E. H. Jayachandran, *J. D. Med.* **2015**, 7, 38–45.
22. J. Deng, Li Peng, G. Zhang, X. Lan, C. Li, F. Chen, Y. Zhou, Z. Lin, L. Chen, R. Dai, H. Xu, L. Yang, X. Zhang, W. Hu, *Eur. J. Med. Chem.* **2011**, 46, 71–76. DOI:10.1016/j.ejmech.2018.03.041
23. M. A. El-Sherbeny, M. B. El Ashmawy, H. I. El Subbagh, A. A. El Emam, F. A. Badria, *Eur. J. Med. Chem.* **1995**, 30, 445–449. DOI:10.1016/0223-5234(96)88255-9
24. Y. Guo, J. Li, J. L. Ma, Z. Yu, H. Wang, W. Zhu, X. Liao, Y. Zhao, *Chin. Chem. Lett.* **2015**, 26, 755–758. DOI:10.1007/s11164-015-2088-0
25. S. Kaizhen, M. Junjie, W. Xiao, G. Ping, Z. Yanfang, *Chem. Res. Chin. Univ.* **2014**, 30, 75–81. DOI:10.1016/j.ccl.2015.03.026
26. W. Zhu, C. Chen, C. Sun, S. Xu, C. Wu, F. Lei, H. Xia, Q. Tu, P. Zheng, *Eur. J. Med. Chem.* **2015**, 93, 64–73. DOI:10.1016/j.ejmech.2015.01.061
27. T. Becker, A. Sellmer, E. Eichhorn, H. Pongratz, C. Schächtele, F. Totzke, G. Kelter, R. Krumbach, H. Fiebig, F. Böhmer, S. Mhboobi, *Bioorg. Med. Chem. Lett.* **2012**, 20, 125–136. DOI:10.1016/j.bmc.2011.11.023
28. Y. Ni, A. Gopalsamy, D. Cole, Y. Hu, R. Denny, M. Lpek, J. Liu, J. Lee, J.P. Hall, M. Luong, J.B. Telliez, L. L. Lin, *Bioorg. Med. Chem. Lett.* **2011**, 21, 5952–5965. DOI:10.1016/j.bmcl.2011.07.069
29. M. M. Kandeil, H. M. Rafaat, A. E. Kassab, I. G. Shahin, T. M. Abdelghany, *Eur. J. Med. Chem.* **2015**, 90, 620–632. DOI:10.1016/j.ejmech.2014.12.009
30. S. I. Panchamukhi, A. K. Mohammed Iqbal, A. Y. Khan, M. B. Kalashetti, I. M. Khazi, *Pharm. Chem. J.* **2011**, 44, 694–696. DOI:10.1007/s11094-011-0545-7
31. S. G. Li, C. Vilchère, S. Chakraborty, X. Wang, H. Kim, M. Anisetti, S. Ekins, K. Y. Rhee, W. R. Jacobs, J. S. Freundlich, *Tetrahedron Lett.* **2015**, 56, 3246–3250. DOI:10.1016/j.cels.2015.12.005
32. M. A. Lill, *Drug Discov Today.* **2007**, 12, 1013–1017. DOI:10.1016/j.drudis.2007.08.004
33. M. B. Dewal, A. S. Wani, C. Vidailiac, D. Oupicky, M. J. Rybak, S. M. Firestine, *Eur J Med Chem.* **2012**, 51, 145–153. DOI:10.1016/j.ejmech.2012.02.035



34. SYBYL-X 2.0. St. Louis, MO, USA: Tripos Inc; Available from: <http://www.tripos.com>.
35. W. P. Purcell, J. A. Singer. *J. Chem. Eng. Data*. **1967**, *12*, 235–246. DOI:10.1021/je60033a020
36. J. G. Wilkes, I. B. Stoyanova-Slavova, D. A. Buzatu, J. Comput. Aid. Mol. Des. **2016**, *30*, 331–345. DOI:10.1007/s10822-016-9909-0
37. R. D. Cramer, D. E. Patterson, J. D. Bunce. *J. Am. Chem. Soc.* **1988**, *110*, 5959–5967. DOI:10.1021/ja00226a005
38. G. Klebe, U. Abraham, T. Mietzner, *J. Med. Chem.* **1994**, *37*, 4130–4146. DOI:10.1021/jm00050a010
39. P. Liu, W. Long. *Int. J. Mol. Sci.* **2009**, *10*, 1978–1998. DOI:10.3390/ijms10051978
40. A. Golbraikh, A. Tropsha, *J. Mol. Graph. Model.* **2002**, *16*, 357–369. DOI:10.1016/S1093-3263(01)00123-1
41. Discovery Studio Visualizer. San Diego: Dassault Systèmes BIOVIA; **2019**. Available from: <http://www.3dsbiovia.com/products/collaborative-science/biovia-discovery-studio/visualization-download.php>.
42. Y. Ai, S.-T. Wang, P.-H. Sun, F. J. Song. *Int. J. Mol. Sci.* **2010**, *11*, 3705–3724. DOI:10.3390/ijms11103705A
43. Daina, O. Michielin, V. Zoete. *Sci. Rep.* **2017**, *7*, 42717. DOI:10.1038/srep42717
44. C. A. Lipinski, F. Lombardo, B. W. Dominy, P. J. Feeney, *Adv. Drug Deliv. Rev.* **2001**, *46*, 3–26. DOI:10.1016/S0169-409X(00)00129-0
45. D. F. Veber, S. R. Johnson, H. Y. Cheng, B. R. Smith, K. W. Ward, K. D. Kopple, *J. Med. Chem.* **2002**, *45*, 2615–2623. DOI:10.1021/jm020017n
46. D. E. V. Pires, T. L. Blundell, D. B. Ascher, *J. Med. Chem.* **2015**, *58*, 4066–4072. DOI:10.1021/acs.jmedchem.5b00104
47. A. Cherkasov, E. N. Muratov, D. Fourches, A. Varnek, I. I. Baskin, M. Cronin, J. Dearden, P. Gramatica, Y. C. Martin, R. Todeschini, V. Consonni, V. E. Kuz'min, R. Cramer, R. Benigni, C. Yang, J. Rathman, L. Terfloth, J. Gasteiger, A. Richard, A. Tropsha, *J. Med. Chem.* **2014**, *57*, 4977–5010. DOI:10.1021/jm4004285
48. M. Ouassaf, S. Belaidi, K. Lotfy, I. Daoud, H. Belaidi, *J. Bionanosci.* **2018**, *12*, 1–11. DOI:10.1166/jbns.2018.1505
49. B. Berk, G. Kaynar, M. Ertaş, S. N. Biltekin. *Acta Pharm. Sci.* **2017**, *55*, 97–117. DOI:10.23893/1307-2080.APS.0551
50. M. Ouassaf, S. Belaidi, H. Belaidi, Z. Almi, *J. Fundam. Appl. Sci.* **2018**, *10*, 500–524. DOI: 10.4314/jfas.v10i3.33.
51. J. B. Baell, G. A. Holloway, *J. Med. Chem.* **2010**, *53*, 2719–2740. DOI:10.1021/jm901137j
52. P. Ertl, A. Schuffenhauer, *J. Cheminformatics.* **2019**, *82*, 1258–1263. DOI:10.1021/acs.jnatprod.8b01022
53. M. R. Prausnitz, R. Langer, *Nat. Biotechnol.* **2008**, *26*, 1261–1268. DOI:10.1038/nbt.1504
54. A. Daina, V. Zoete, *Chem. Med. Chem.* **2016**, *11*, 1117–1121. DOI:10.1002/cmdc.201600182
55. P. F. Hollenberg, *Drug Metab. Rev.* **2002**, *34*, 17–35. DOI:10.1081/DMR-120001387
56. L. Di. *Expert. Opin. Drug Metab. Toxicol.* **2014**, *10*, 379–393. DOI:10.1517/17425255.2014.876006
57. D. J. Begley, *Curr. Pharm. Des.* **2004**, *10*, 1295–1312. DOI:10.2174/1381612043384844

## Povzetek

Odkritje snovi z antibakteriocidnim učinkom predstavlja enega najpomembnejših medicinskih dosežkov vseh časov. V tem delu smo uporabili kombinacijo treh metode molekulskega modeliranja, 3D-QSAR, molekulske sidranje (ang. molecular docking) in ADME ovrednotenje, pri načrtovanju derivatov tienopirimidina proti gram pozitivni bakteriji *Staphylococcus aureus*.

Ustreznost 3D-QSAR modela smo preverili na množici podatkov, ki smo jo razdelili na podatke za učenje in testiranje. Dva konstruirana modela (CoMFA in CoMSIA) sta pokazala dobro ujemanje in napovedno moč ( $q^2 = 0.758$ ;  $r^2 = 0.96$ ;  $r^2_{pred} = 0.783$  in  $q^2 = 0.744$ ;  $r^2 = 0.97$ ;  $r^2_{pred} = 0.625$ ). Poleg tega smo uporabili metodo molekulskega sidranja za ugotavljanje strukturnih lastnosti, ki vplivajo na povečanje afinitete vezave s *S. aureus* DNA girazo. Na osnovi »drug-like« koncepta ter ADME analize smo pokazali, da pet preučenih struktur kaže ustrezen zdravilni potencial in bi jih lahko uporabili kot izhodišče za načrtovanje novih zdravil proti bakteriji *Staphylococcus aureus*.



Except when otherwise noted, articles in this journal are published under the terms and conditions of the Creative Commons Attribution 4.0 International License

Scientific paper

# Exergy Analysis of a Turbo Expander: Modeling and Simulation

Adel El-Husseiny,<sup>1</sup> Rania Farouq,<sup>2,\*</sup> Hassan A. Farag<sup>3</sup> and Yehia El Taweel<sup>3</sup>

<sup>1</sup> Chemical Engineer, Assistant General Manager of Process, Projects Division, Abu Qir Petroleum Co., Elmoltaka Bldg. Tutankhamoun St. Crossing To El ShahiedTayar Mahmoud Shaker Smouha - Sidi Gaber, Alexandria, Egypt.

<sup>2</sup> Petrochemical Department, Faculty of Engineering, Pharos University, Canal El Mahmoudeya St. Semouha, Alexandria, Egypt.

<sup>3</sup> Chemical Engineering Department, Faculty of Engineering, Alexandria University, P. O. Box 21544; Alexandria, Egypt.

\* Corresponding author: E-mail: rania.farouq@pua.edu.eg  
Tel: (+203) 01002706756

Received: 04-17-2020

## Abstract

Natural gas is a mixture that is widely used in the industries. Knowledge of its thermodynamic properties is essential for evaluating the process and equipment performance.

This paper quantifies the energy that can be extracted from natural gas using a turbo expander. Natural gases of wide-ranging compositions collected from 6 different gas fields in Egypt were investigated based on energy and exergy analysis. The study was conducted using MATLAB. Numerous simulation runs were made by taking various typical feed compositions classified as lean and rich.

The effects of increasing the amount of C<sub>1</sub>, C<sub>5</sub> in the feed stream on the efficiency of energy utilization are presented. A validation analysis was performed. The results show similar trends and good agreements. It was concluded from the results that when the concentration of methane in the gas mixture increase, the exergetic efficiency decreases. The results also show that the values of thermodynamic properties depend on the relative amount of heavy components in the feed stream.

**Keywords:** Exergy efficiency, turbo-expander; peng Robinson; feed composition effect; natural gas

## 1. Introduction

Natural gas (NG) has become the primary source of energy in many countries. When it is extracted from refinery it has a high pressure of about 7 MPa where it is consumed at the domestic and industrial sectors. In order to transport this high pressure gas to a distribution system where it is being consumed, its pressure should be reduced to a safe and usable level usually within 1.5–2 MPa. This is usually done in natural gas pressure reduction stations. Throttling valves are used to reduce the gas pressure where the physical exergy of high pressure gas is wasted.<sup>1–5</sup> Energy recovery from natural gas distribution network is a strategy for sustainable energy in the urban area.<sup>6</sup> For energy recovery purposes, the pressure drop can be exploited through dynamic or volumetric expanders by obtaining mechanical energy and thus electricity.<sup>7–8</sup> There are several studies on recovering physical exergy of high pressure natural gas during pressure reduction pro-

cess most of them focus on the pressure exergy recovering devices such as turboexpander.<sup>9–11</sup>

Researchers have developed case studies to estimate the amount of exergy recovery and the economics of turboexpander installations in NG pressure reduction stations. It was found that thermal efficiency of system increase about 8% in the optimum state<sup>12–14</sup> some researchers developed a mathematical model to predict the performance of a twin-screw expander as power generation unit.<sup>15–16</sup> Kuczynski et al presented formula that allows a quick and easy evaluation of the applicability of an expander on the selected gas regulation station.<sup>17</sup> Olfati et al.<sup>18</sup> presented the energy and exergy analyses of a pressure reduction station. They investigated various operating conditions for station inlet pressure and temperature and the modification on preheating natural gas was considered. It was found that the energy consumption is reduced to 33% and the exergy destruction is reduced to

15%. Osiadacz et al. investigate the factors influencing the efficiency of the gas expansion process application of turboexpanders at selected natural gas pressure regulator stations.<sup>9</sup>

The feed composition is an important factor that affects NGL recovery. The feed generally originates from upstream plants, so there may be a continuous variation in feed composition that causes plant instability. Feed composition has a seasonal variation, during cooler months the feed is a leaner gas and in the warmer months the feed is a richer gas.<sup>19–20</sup>

In this work, the effect of different feed characteristics on exergy efficiency was investigated; the process was simulated and analyzed to compare the differences in energy and thermodynamics properties (include exergy analysis). Different feed compositions were investigated and characterized under the basic classifications of lean and rich feed. A numerical method and a computer program were used to calculate the thermal properties of natural gas mixture such as enthalpy using Peng Robinson state equation. MATLAB has been utilized to model turbo-expander. The exergy analysis of a turbo-expander unit and the impact of various feed compositions has been investigated and validated according to the first and second laws of thermodynamics, and the performance of the TX is evaluated according to a different composition.

## 2. Mathematical Model Development

The NGL recovery for rich gas would require great power than lean gas, however; the more rich feed gas is, the more recovered condensate, the lower energy consumption per unit product consumed.<sup>19</sup> Aspen HYSYS V10 software and Peng-Robinson equation of state are selected for process simulation. A model of the proposed unit has been created to determine the performance using

real site data. Data for inlet pressure, temperature, flow rate, and required outlet pressure are key inputs.

The model will then calculate the rate of power and system efficiency. Numerical modeling of the exergy recovery is performed using MATLAB.

To study the different feed composition types; approximate composition and characteristics of the components of six typical feed natural gas samples were selected from six fields of six reservoirs shown in table 1 and the operating conditions are shown in table 2.

To simplify the proposed turbo-expander model, the following assumptions are made:

- There are no pressure losses in pipes and heat exchangers.
- The small difference between the intermediate pressure, the discharge pressure of the low-stage compressor and the suction pressure of the high-stage compressor is negligible.
- The NG is dry; no gas hydrates are formed.
- The gearbox and generator efficiencies are considered to be constant.

Using the data in Tables 1 and 2, we made an algorithm for thermodynamic calculation of a turbo-expander in order to form correct input data for model calculations:

1. Gas pressure at turboexpander inlet: The main input was the inlet temperature, which was used for the calculation of the inlet pressure by using a Peng Robinson equation. The equation of Peng Robinson is an empirical equation of state that is derived from the Van der Waals equation,<sup>22–25</sup> which is as follows:

$$P_{in} = \frac{R \cdot T_{in}}{V_m - b} - \frac{a}{V_m^2 + 2 \cdot b \cdot V_m - b^2} \quad (1)$$

Where

$$a = \frac{R^2 \cdot T_{pc}^2}{2.1870 \cdot P_{pc}} (1 + K \{1 - T_{re}^{1/2}\})^2$$

$$b = \frac{R \cdot T_{pc}}{12.8535 \cdot P_{pc}}$$

$$K = 0.37464 + 1.54226 \cdot \omega + 0.26922 \cdot \omega^2$$

Table 1. Typical feed selected to study

Composition (Mole %)		1 Borapetco El Salmiya-2	2 PS AES E2 (TAMMAM)	3 PS E6#1/1 AES-	4 Borapetco ZZ-4X	5 AQP W-A/Q A/Q (Sep. Gas)	6 AQP (Feed Gas)
N <sub>2</sub>	N <sub>2</sub>	0.95	0.905	0.617	0.059	0.1108	0.0864
CO <sub>2</sub>	CO <sub>2</sub>	3.914	0.426	0.518	1.771	0.8264	0.6117
H <sub>2</sub> S	H <sub>2</sub> S	0	0	0	0	0	0
C <sub>1</sub>	C <sub>1</sub>	<b>63.807</b>	<b>78.915</b>	<b>79.888</b>	<b>80.53</b>	<b>88.857</b>	<b>93.375</b>
C <sub>2</sub>	C <sub>2</sub>	13.129	8.97	9.151	8.825	4.9658	3.2473
C <sub>3</sub>	C <sub>3</sub>	8.656	5.483	4.898	4.135	2.3345	1.3393
iC <sub>4</sub>	C <sub>4</sub>	4.808	3.045	2.854	1.919	1.2878	0.7635
nC <sub>4</sub>	C <sub>4</sub>						
iC <sub>5</sub>	C <sub>5</sub>	1.924	1.308	1.318	1.026	0.3526	0.2715
nC <sub>5</sub>	C <sub>5</sub>						
C <sub>6+</sub>	C <sub>6+</sub>	2.812	0.948	0.756	1.735	1.2655	0.3051

Table 2. Feed operating conditions

Well # Company Well Name	1 Borapetco El Salmiya-2	2 PS AES E2 (TAMMAM)	3 PS AES-E6#1/1	4 Borapetco ZZ-4X	5 AQP W-A/Q (Sep. Gas)	6 AQP A/Q (Feed Gas)
Production Rate ( $m^3/hr$ )	17658	29429	23543	17658	58859	117717
Well Life in the Declining Production Regime (Years)	13 (2012–2025)	20 (2009–2029)	15 (2013–2033)	17 (2012–2029)	25 (2006–2031)	30 (2000–2030)
Feed Pretreatment for Transportation & its Conditions	Corrosion Inhibitor Injection	Corrosion Inhibitor Injection	Corrosion Inhibitor Injection	Corrosion Inhibitor Injection	Corrosion Inhibitor Injection	Corrosion Inhibitor Injection
The Design of a Turbo-Expander & its Operating Modes						
Max. F ( $m^3/hr$ )	58859	88288	88288	58859	141261	141261
Design P (KPa g)	7900	6000	6000	7900	11500	11500
Max. Design T ( $^{\circ}C$ )	80	80	80	80	58	58
Min Design T ( $^{\circ}C$ )	-35	-20	-20	-35	-70	-70
Operating Mode	Isentropic	Isentropic	Isentropic	Isentropic	Isentropic	Isentropic
Mechanical Efficiency	75 %	80 %	80 %	75 %	84 %	84%
Electrical Efficiency	70 %	75 %	75 %	70 %	80 %	80 %
The Target Substances of Petrochemical Synthesis & Engine Fuels Produced from the HC's.	N.G (fuel)	N.G (fuel)	N.G (fuel)	LPG (fuel)	LPG (fuel)	LPG (fuel)

2. Determination of the thermodynamic fluid properties: the correlations of Farazneh-Gord & Rahbari,<sup>26</sup> were used. The correlations are based on measurable real-time properties such as Temperature, Pressure, and specific gravity (molecular weight) of the natural gas for the non-measurable thermodynamic properties such as Entropy, Enthalpy, and Internal energy. 3.

$$h_i(T', P', Y') = A_1(T', Y') P'^4 + A_2(T', Y') P'^3 + A_3(T', Y') P'^2 + A_4(T', Y') P' + A_5(T', Y') \quad (2)$$

Where

$A_i(T', Y')$ ;  $i = 1, \dots, 5$  are defined as:

$$A_1(T', Y') = B_1(T') Y'^2 + B_2(T') Y' + B_3(T')$$

And  $B_j(T)$ ;  $j = 1, 2, 3$  for each  $A_i(T', Y')$  are defined as:

$$B_j(T) = C_1 T'^2 - C_2 T' - C_3$$

Where:  $T'$ ,  $P'$ , and  $Y'$  are functions of  $T$ ,  $P$ , and gas specific gravity respectively as follows:

$$T_i' = \frac{T_{in} - 300}{50}, \quad P_i' = \frac{P_{in} - 13}{7.3598}, \quad Y_i' = \frac{M_{wt}}{28.966}$$

$$Y_i' = \frac{Y_i - 0.62541}{0.07894}$$

3. Exergy analysis: Exergy analysis is based on the first and second laws of thermodynamics and is employed

to calculate the maximum useful power accessible by an assigned amount of input energy to a process. By neglecting the effects of kinetic, potential and nuclear energies (unchanged or insignificant), the total exergy can be divided into two parts, chemical, and physical exergy. Eqs. (3) – (5) express the exergy destruction, the total exergy, and the physical exergy, respectively

$$E'_{\text{destroyed}} = T_0 S' \quad (3)$$

$$E' = E'^{\text{ph}} + E'^{\text{chem}} \quad (4)$$

$$E'^{\text{ph}} = (H' - H'_o) - T_0(S' - S'_o) \quad (5)$$

4. Calculation of the turbo-expander efficiency: The outlet enthalpy is used in conjunction with the isentropic enthalpy and inlet enthalpy to determine isentropic expansion efficiency. The working fluid enters the turbo-expander and expands to the discharge pressure with the turbo-expander efficiency is defined as:

$$\eta_E = \frac{h_i - h_o}{h_i - h_{o,se}} \quad (6)$$

5. The electrical power obtained from the exergy recovery process can be expressed as:

$$W'_{\text{Gen}} = m'_{\text{N.G}} (h_i - h_o) \cdot \eta_{\text{GB}} \cdot \eta_{\text{Ge}} \quad (7)$$

6. The exergetic efficiency of the recovery can be obtained by comparing the reversible expansion work to the actual work produced by the electric generator. Therefore, by substituting in the following form:

$$\eta_{III,P} = \frac{w'_{Gen}}{w'_{Rev}} = \frac{(h_i - h_o) \cdot \eta_{GB} \cdot \eta_{Gen}}{\{h_i - h_{o,s,e} - T_o (S_i - S_{o,s,e})\}} \quad (8)$$

### 3. Results and Discussion

Because of the natural gas composition variation in the selected samples is the one who plays the main role in the study, and also methane content represents the huge fraction of that composition.<sup>19</sup> Therefore, the impact of the methane concentration variation on the selected samples of the thermodynamic properties was studied and validated using Aspen HYSYS V10. By entering the different feed compositions and operating condition; the HYSYS program calculates the thermodynamic properties of the different streams shown in table 3 & 4 from which expander and exergetic efficiency can be predicted.

#### 3. 1. Studying Gas Composition Variation Effect on Enthalpy

In this case, the selected feed samples are arranged in increasing order of hydrocarbon contents, from the C<sub>1</sub> content to heavier hydrocarbon.

Also, pentane content and its variations in the natural gas composition have been chosen as a basis to show its effect as a heavy component on the previous mentioned thermodynamic properties. In this case, the selected feed samples are re-arranged in decreasing order of hydrocarbon contents, from C<sub>5</sub> content to lighter hydrocarbon.

The first four feed samples (1–4) are classified as rich feed, while the remaining two feed samples (5&6) are taken as lean feed.

The classification for rich feed is merely based on the contents of C<sub>2</sub> and/or C<sub>3</sub>. If the C<sub>2</sub> content is less than 8% or the C<sub>3</sub> content less than 3% or the C<sub>2</sub> plus C<sub>3</sub> contents less than 10%, the feed is considered a lean feed; otherwise, it is taken as a rich feed.<sup>24</sup>

#### 3. 1. 1. Effect of Methane Concentration Variation on Inlet, Outlet and Isentropic Outlet Enthalpy

To sense their effects on each other, the inlet conditions (pressure and temperature) for all gas samples were kept the same as typical actual plant conditions at 6620 KPa and 21.9 °C respectively.

As shown from table 3; the difference in the feed enthalpy for the six feed types arises from the variation of the feed compositions. The relationship between the variation in methane concentration and the enthalpy of the gas mixture is a close linear relationship in an inverse proportion

Table 3. Effect of Methane concentration (C<sub>1</sub>%) variation on all properties

C <sub>1</sub> (mol. %)	Well # Units	1 <sup>st</sup> 63.807	2 <sup>nd</sup> 78.915	3 <sup>rd</sup> 79.888	4 <sup>th</sup> 80.53	5 <sup>th</sup> 88.8566	6 <sup>th</sup> 93.3752
<b>Property</b>							
<b>h<sub>in</sub></b>	<b>(kJ/kg)</b>	-37.144	-40.083	-40.269	-40.318	-41.669	-42.470
<b>h<sub>out</sub></b>	<b>(kJ/kg)</b>	-82.018	-83.302	-83.503	-90.300	-96.931	-97.746
<b>T<sub>out</sub></b>	<b>(°C)</b>	-17.560	-17.770	-17.880	-22.410	-26.280	-26.480
<b>h<sub>out,e,s</sub></b>	<b>(kJ/kg)</b>	-52.20	-55.64	-55.95	-55.86	-57.13	-57.80
<b>T<sub>out,e,s</sub></b>	<b>(°C)</b>	2.57	0.78	0.59	0.66	0.23	0.03
<b>S<sub>in</sub></b>	<b>(kJ/kg.k)</b>	-1.504	-1.539	-1.541	-1.542	-1.557	-1.565
<b>S<sub>out,e,s</sub></b>	<b>(kJ/kg.k)</b>	-1.388	-1.411	-1.413	-1.413	-1.426	-1.433

Table 4. Effect of Pentane concentration (C<sub>5</sub>%) variation on all properties

C <sub>5</sub> (mol. %)	Well # Units	1 <sup>st</sup> 1.924	2 <sup>nd</sup> 1.318	3 <sup>rd</sup> 1.308	4 <sup>th</sup> 1.026	5 <sup>th</sup> 0.3526	6 <sup>th</sup> 0.2715
<b>Property</b>							
<b>h<sub>in</sub></b>	<b>(kJ/kg)</b>	-37.144	-40.318	-40.082	-40.269	-41.669	-42.469
<b>h<sub>out</sub></b>	<b>(kJ/kg)</b>	-82.018	-83.503	-83.302	-90.300	-96.931	-97.746
<b>T<sub>out</sub></b>	<b>(°C)</b>	-17.560	-17.880	-17.770	-22.410	-26.280	-26.480
<b>h<sub>out,e,s</sub></b>	<b>(kJ/kg)</b>	-52.20	-55.95	-55.64	-55.86	-57.13	-57.80
<b>T<sub>out,e,s</sub></b>	<b>(°C)</b>	2.57	0.59	0.78	0.66	0.23	0.03
<b>S<sub>in</sub></b>	<b>(kJ/kg.k)</b>	-1.504	-1.541	-1.539	-1.542	-1.557	-1.565
<b>S<sub>out,e,s</sub></b>	<b>(kJ/kg.k)</b>	-1.433	-1.426	-1.413	-1.411	-1.413	-1.388

which means that by increasing methane concentration; the inlet and outlet enthalpy decreases while decreasing pentane concentration decreases the enthalpy. It is observed that the leaner feed generally give lower duty than those of rich feed. This is due to the presence of high heavier hydrocarbons ( $C_5^+$ ) components in the rich feed.

### a) Effect of methane concentration variation on outlet enthalpy: Using Constant Operating Conditions

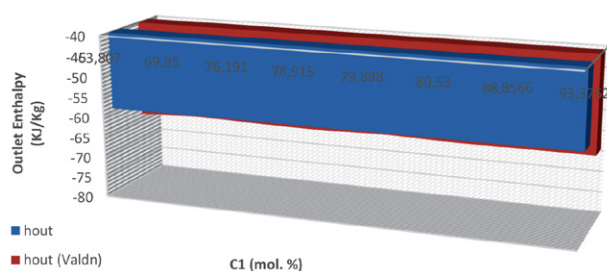


Fig. 1. Effect of methane concentration variation on outlet enthalpy (kJ/kg), Constant outlet conditions

Figure (1) shows the relation between the variation in methane concentration (mole %) and the outlet enthalpy (kJ/kg) in case of unification of the outlet conditions (pressure and temperature) at 2600 KPa g and  $-2.2\text{ }^{\circ}\text{C}$  as follows:

The methane rejection (The ratio of the molar flow of methane “residue” to the molar flow of methane “natural-gas feed”) is directly related to the feed-stream temperature on which the product temperature depends on. Rejection increases with decreasing temperature; however, in Konukman et.al (2005),<sup>27</sup> the methane rejection was found to be not very sensitive to the feed-stream temperature and in turn to the product temperature, and because outlet enthalpy depends on the temperature at a given pressure. So it is concluded that increasing methane % will not affect outlet enthalpy.

### b) Using Variable Operating Conditions

To study the effect of changing the operating conditions on the variation in the outlet enthalpy, the plant real

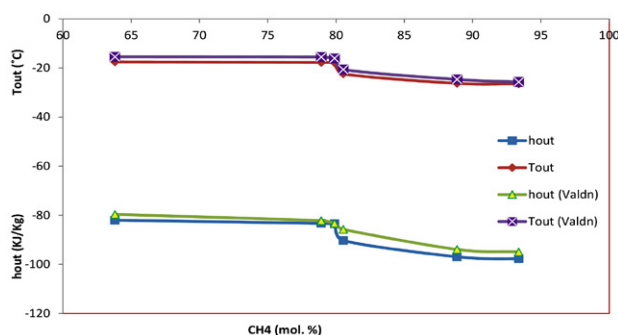


Fig. 2. Effect of methane concentration variation on outlet enthalpy (kJ/kg) and outlet temperature ( $^{\circ}\text{C}$ ), Variable outlet conditions

data were used for that by taking the required turbine duty to expand a certain gas sample from the utilized typical feed samples in this work, which corresponds to approximately 4000 KPa pressure drops and taking this value as a reference and set for all other samples.

Consequently, it has resulted in a change in outlet conditions (pressure and temperature). Therefore, the changes in the outlet enthalpy for all samples were obtained and recorded in figure (2).

The relatively high linearity deviation is almost due to some erratic points. Mainly these points of the rich samples, and for this reason, the enthalpy is raised.

### 3. 1. 2. Effect of Pentane Concentration Variation on Inlet; Outlet; Isentropic Outlet Enthalpy

Table 4 shows the relationship between the variation in pentane concentration, and the inlet enthalpy of the gas mixture is a non-linear direct proportional relationship. It is observed that the leaner feed generally give lower duty than those of rich feed. This is due to the presence of high heavier hydrocarbons ( $C_5^+$ ) components in the rich feed.

### 3. 2. Effect of Feed Composition on Entropy

#### 3. 2. 1. Effect of Methane Concentration Variation on Inlet and Outlet Entropy

Table 3 shows the relationship between the variation in methane concentration, and the inlet entropy of the gas mixture is a closely linear relationship in an inverse proportion. The results are consistent with the one observed in the discussion of the relation between methane concentration and the inlet enthalpy. As known, the value of enthalpy is proportional to the values of entropy.

#### 3. 2. 2. Effect of Pentane Concentration Variation on the Inlet and Outlet Entropy

From the illustrated table 4, the relationship between the variation in pentane concentration, and the inlet entropy of the gas mixture is nearly a non-linear direct proportional relationship. As mentioned before, it can be concluded that the leaner feed generally give lower entropy content than those of rich feed. This is also like enthalpy due to the presence of high heavier hydrocarbons ( $C_5^+$ ) components in the rich feed.

### 3. 3. Effect of Feed Composition on Expander Efficiency

#### 3. 3. 1. Effect of Methane Concentration Variation on Expander Efficiency

As shown in the figure (3); the relationship between the variation in methane concentration and the expander efficiency of the gas mixture is a close linear in an inverse

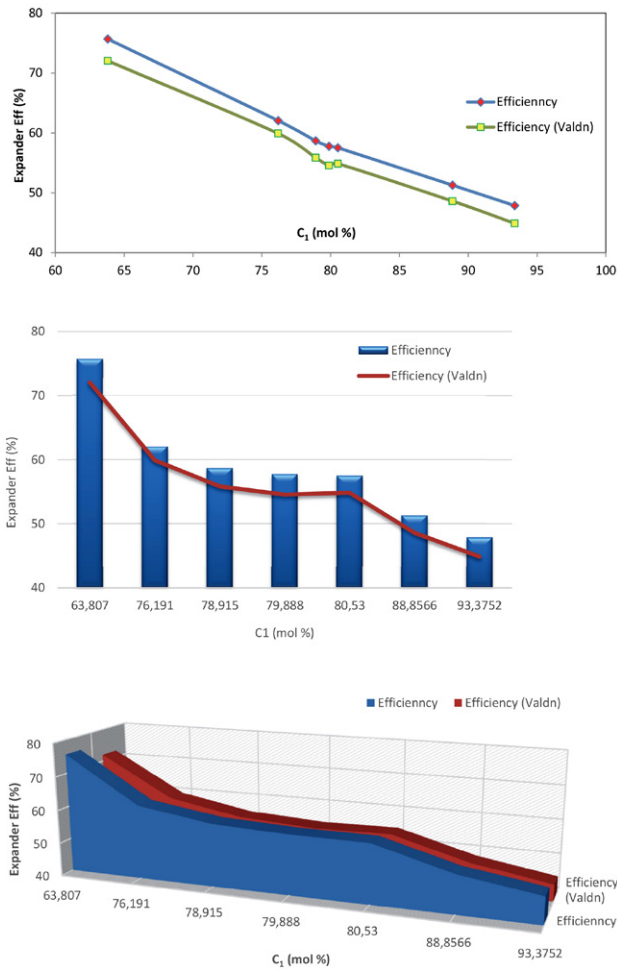


Fig. 3. Effect of methane concentration variation on expander Efficiency (%)

proportion. i.e., when the concentration of methane in the gas mixture increases, the expander efficiency decreases.

Since at standard condition the heat capacity at constant pressure ( $C_p$ ) of methane is higher than other hydrocarbons present in the natural gas mixture,  $C_p$  of the mixture will be increased in a higher concentration of methane. When  $C_p$  of the fluid increases, the required compression work to reach a certain pressure will be decreased. Also, by increasing the concentration of methane in the mixture the molecular weight and the specific heat ratio ( $k=C_p/C_v$ ) of the fluid will be decreased.

### 3. 3. 2. Effect of Pentane Concentration Variation on Expander Efficiency

From the illustrated figure (4); the relationship between the variation in pentane concentration and expander efficiency of the gas mixture is a quasi-linear direct proportional relationship.

It is observed also the leaner feed generally give higher efficiency than those of rich feed. This is due to the

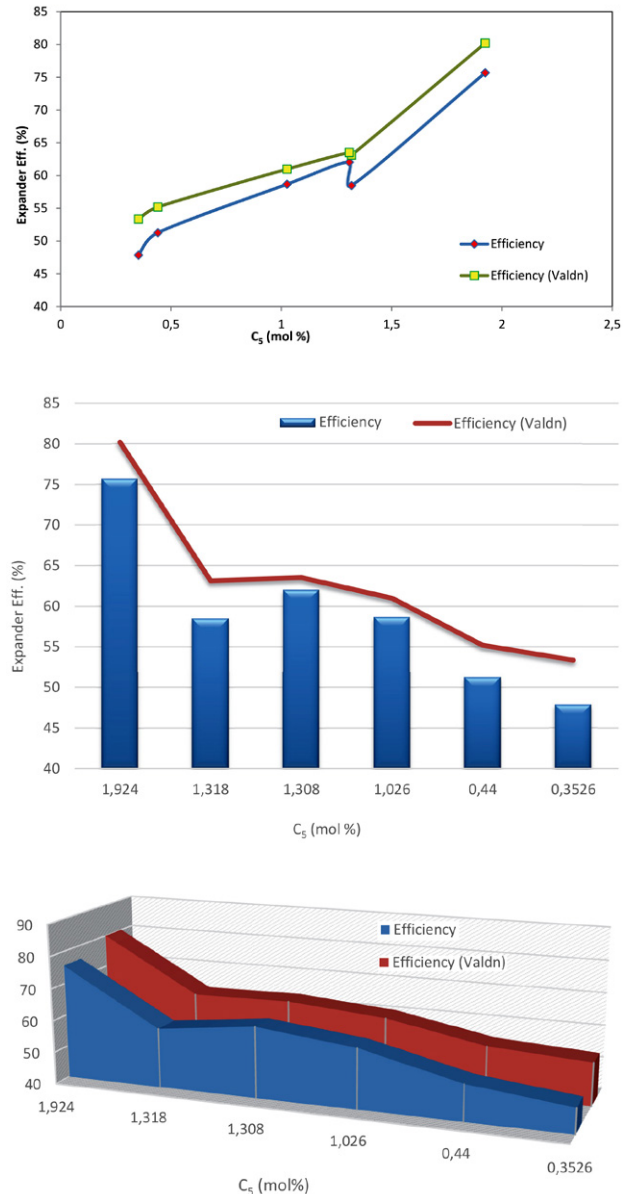


Fig. 4. Effect of Pentane Concentration Variation on Expander Efficiency (%)

presence of high heavier hydrocarbons ( $C_5^+$ ) components in the rich feed.

## 3. 4. Effect of Feed Composition on Exergetic Efficiency

### 3. 4. 1. Effect of Methane Concentration Variation on Exergetic Efficiency

As shown in the figure (5); the relationship between the variation in methane concentration and the exergetic efficiency of the gas mixture is a close linear in an inverse proportion. i.e., when the concentration of methane in the gas mixture increases, the exergetic efficiency decreases.

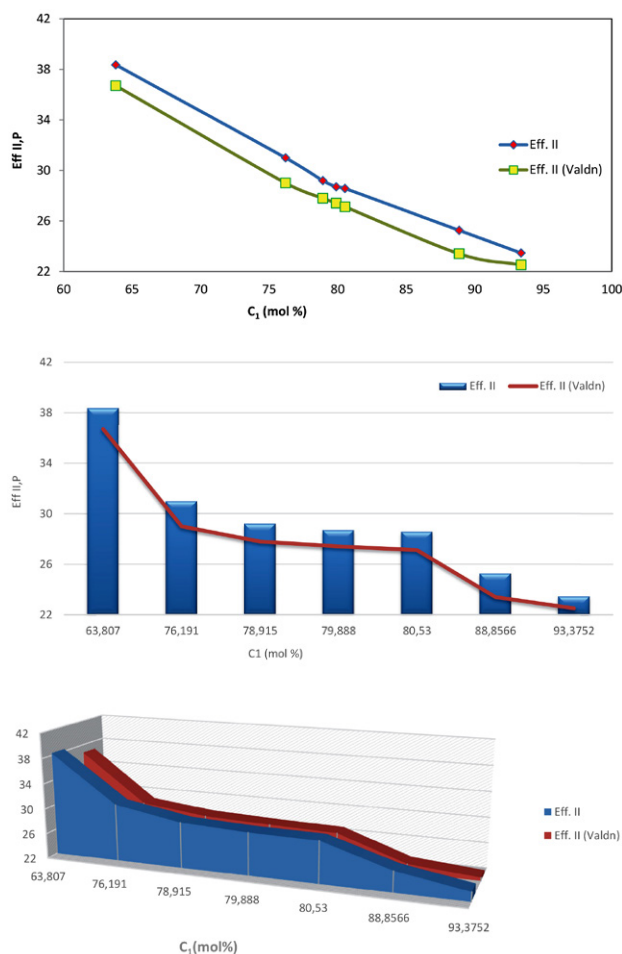


Fig. 5. Effect of methane concentration variation on exergetic efficiency (%)

### 3. 4. 2. Effect of Pentane Concentration Variation on Exergetic Efficiency

From the illustrated figure (6); the relationship between the variation in pentane concentration and the exergetic efficiency of the gas mixture is a quasi-linear direct proportional relationship. It is observed also the leaner feed generally give lower exergetic efficiency than those of rich feed. This is due to the presence of high heavier hydrocarbons ( $C_5^+$ ) components in the rich feed.

The linearity deviation is attributed to inaccurate points. Mainly such points are of the rich samples, and for this reason, the exergetic efficiency is raised.

## 3. Conclusions

Fifteen typical feed samples from ten gas reservoirs were obtained from four petroleum companies located at places that are spaced from each other between the Eastern & Western deserts of Egypt. Just six feeds from six gas reservoirs that have significant concentration differences were chosen as a study-base.

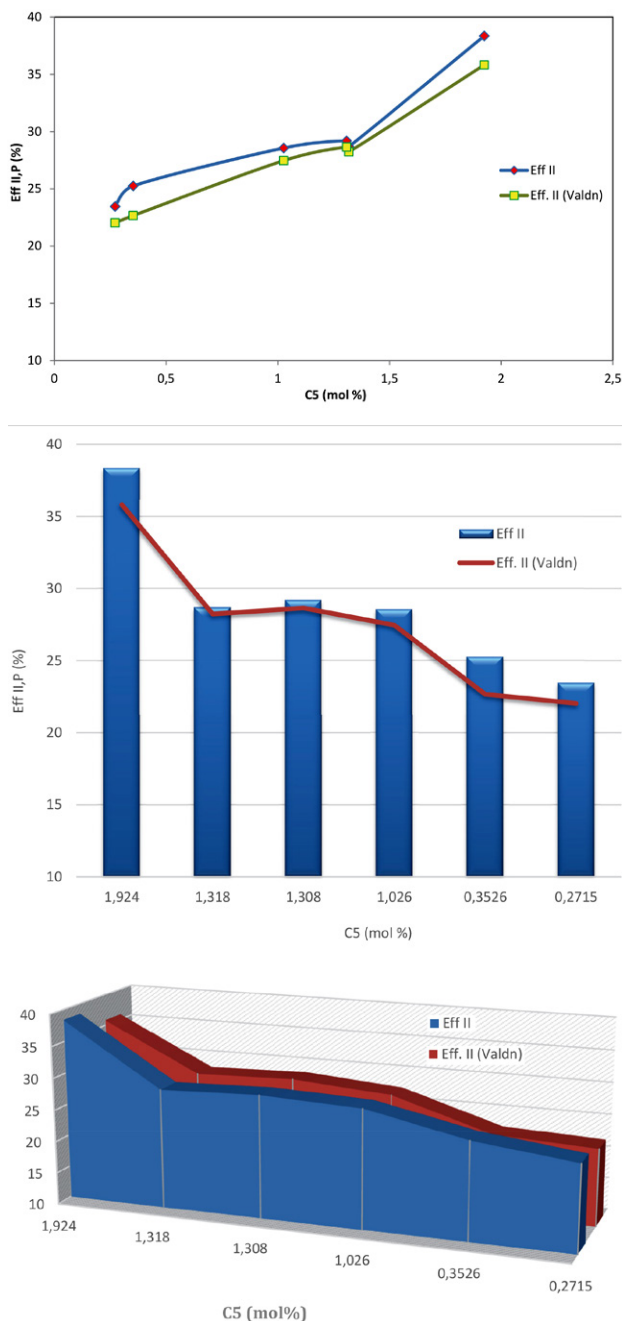


Fig. 6. Effect of Pentane Concentration Variation on Exergetic Efficiency (%)

Math models were developed based on Peng-Robinson correlation to predict the performance data of a turbo-expander handling N.G. The models were solved by MATLAB software, validated and analyzed to get the most asymptotic model of reality to be further developed.

The obtained data are near those obtained by other researchers;<sup>28</sup> which mean that the model was successful in predicting the thermodynamic properties of different gas composition such as inlet & outlet enthalpies, inlet & outlet entropies, expander & exergetic efficiencies and isentropic outlet enthalpy. Validation was performed for



verification of the results and shows good agreement with the calculated properties.

## Nomenclature

a	:	Measure of the Strength of Attraction between the Gas Molecules
b	:	Volume Occupied by gas molecules, which decreases the available open volume
H	:	Enthalpy, $kJ/kg$
$h_i$	:	Inlet Enthalpy, $kJ/kg$
$h_o$	:	Outlet Enthalpy, $kJ/kg$
$h_{o,s,e}$	:	Isentropic Outlet Enthalpy, $kJ/kg$
$m_{N,G}$	:	Natural Gas Mass Flow Rate
P	:	Pressure, $KPa$
$P_c$	:	Critical Pressure, $KPa$
$P_i^*$	:	Dimensionless Index in Novel Correlation
$P_{pc}$	:	Pseudo Critical Pressure for the mixture, $KPa$
Pr	:	Reduced Pressure, <i>dimensionless</i>
$P_{VP}$	:	Saturated Vapor Pressure of the gas at a temperature $T = 0.7 T_c$
Q	:	Inlet Volumetric Flowrate, $m^3/hr$
R	:	Universal Gas Constant, $(Pa \cdot m^3/mol \cdot K)$
$S_i$	:	Inlet Entropy, $kJ/kg \cdot K$
$S_{o,s,e}$	:	Isentropic Outlet Entropy, $kJ/kg \cdot K$
T	:	Temperature, $K$
$T_c$	:	Critical Temperature, $K$
$T_i^*$	:	Dimensionless Index in Novel Correlation
$T_{p_c}$	:	Pseudo Critical Temperature for the mixture, $K$
Tr	:	Reduced Temperature, <i>dimensionless</i>
V	:	Gas Volume, $m^3$
$V_m$	:	Molar Volume, $m^3/mol$
$W_{Gen}$	:	Electrical Power Obtained from the Exergy Recovery Process
$W_{Rev}^*$	:	Reversible Expansion Work
$Y_i$	:	Dimensionless Index in Novel Correlation
$Y_i^*$	:	Dimensionless Index in Novel Correlation
$\omega$	:	acentric factor

## 4. Reference

- Farzaneh-Gord, M., Ghezelbash, R., Sadi, M., & Moghadam, A. J. (2016). Integration of vertical ground-coupled heat pump into a conventional natural gas pressure drop station: Energy, economic and CO<sub>2</sub> emission assessment. *Energy*, 112, 998–1014. DOI:10.1016/j.energy.2016.06.100
- Jannatabadi, M., Farzaneh-Gord, M., Rahbari, H. R., & Nersi, A. (2018). Energy and exergy analysis of reciprocating natural gas expansion engine based on valve configurations. *Energy*, 158, 986–1000. DOI:10.1016/j.energy.2018.06.103
- Naderi, M., Ahmadi, G., Zarringhalam, M., Akbari, O., & Khalili, E. (2018). Application of water reheating system for waste heat recovery in NG pressure reduction stations, with experimental verification. *Energy*, 162, 1183–1192. DOI:10.1016/j.energy.2018.08.111
- Neseli, Mehmet Alparslan, Onder Ozgener, and Leyla Ozgener. "Energy and exergy analysis of electricity generation from natural gas pressure reducing stations." *Energy Conversion and Management* 2015, 93, 109–120. DOI:10.1016/j.enconman.2015.01.011
- Olfati, Mohammad, Mehdi Bahiraei, Setareh Heidari, and Farzad Veysi. "A comprehensive analysis of energy and exergy characteristics for a natural gas city gate station considering seasonal variations." *Energy* 2018, 155, 721–733. DOI:10.1016/j.energy.2018.05.069
- Golchoobian, H., Taheri, M. H., & Saedodin, S. (2019). Thermodynamic analysis of turboexpander and gas turbine hybrid system for gas pressure reduction station of a power plant. *Case Studies in Thermal Engineering*, 14, 100488. DOI:10.1016/j.csite.2019.100488
- Farzaneh-Gord, M., Izadi, S., Pishbin, S. I., Sheikhan, H., & Deymi-Dashtebayaz, M. (2015). Thermodynamic analysis of medium pressure reciprocating natural gas expansion engines. *Polish Journal of Chemical Technology*, 17(2), 119–125. DOI:10.1515/pjct-2015-0039
- Barone, G., Buonomano, A., Calise, F., & Palombo, A. (2018). Natural gas turbo-expander systems: A dynamic simulation model for energy and economic analyses. *Thermal Science*, 22(5), 2215–2233. DOI:10.2298/TSCI180109276B
- Osiadacz, A., Chaczykowski, M., & Kwestar, M. (2017). An evaluation of the possibilities of using turboexpanders at pressure regulator stations. *Journal of Power Technologies*, 97(4), 289–294.
- Sheikhnejad, Y., Simões, J., & Martins, N. (2020). Energy Harvesting by a Novel Substitution for Expansion Valves: Special Focus on City Gate Stations of High-Pressure Natural Gas Pipelines. *Energies*, 13(4), 956. DOI:10.3390/en13040956
- Morgese, G., Fornarelli, F., Oresta, P., Capurso, T., Stefanizzi, M., Camporeale, S. M., & Torresi, M. (2020). Fast Design Procedure for Turboexpanders in Pressure Energy Recovery Applications. *Energies*, 13(14), 3669. DOI:10.3390/en13143669
- Saadat-Targhi, M., & Khanmohammadi, S. (2019). Energy and exergy analysis and multi-criteria optimization of an integrated city gate station with organic Rankine flash cycle and thermoelectric generator. *Applied Thermal Engineering*, 149, 312–324. DOI:10.1016/j.applthermaleng.2018.12.079
- Ahmadi, G., Toghraie, D., & Akbari, O. (2019). Energy, exergy and environmental (3E) analysis of the existing CHP system in a petrochemical plant. *Renewable and Sustainable Energy Reviews*, 99, 234–242. DOI:10.1016/j.rser.2018.10.009
- Islam, S.U.; Ahmed, I.; Din, Z.U. Energy Recovery Opportunity at Natural Gas Regulating Station by replacing Pressure Control Valve with Turbo Expander using Aspen HYSYS: A case study of WAH SMS(Sale Metering Station ).Int. J. Innov. Sci. Eng. Technol.2016,3, 464–475
- Yao, S.; Zhang, Y.; Deng, N.; Yub, X.; Dong, S. Performance Research on a Power Generation System Using Twin-Screw

- Expanders for Energy Recovery at Natural Gas Pressure Reduction Stations under Off-Design Conditions. *Appl. Energy* **2019**, 236, 1218–1230. DOI:10.1016/j.apenergy.2018.12.039
16. Tian, Y.; Xing, Z.; He, Z.; Wu, H. Modeling and Performance Analysis of Twin-Screw Steam Expander under Fluctuating Operating Conditions in Steam Pipeline Pressure Energy Recovery Applications. *Energy* **2017**, 141, 692–701. DOI:10.1016/j.apenergy.2018.12.039
17. Kuczyński, S., Łaciak, M., Olijnyk, A., Szurlej, A., & Włodek, T. (2019). Techno-economic assessment of turboexpander application at natural gas regulation stations. *Energies*, 12(4), 755. DOI:10.3390/en12040755
18. Olfati, M., Bahiraei, M., & Veysi, F. (2019). A novel modification on preheating process of natural gas in pressure reduction stations to improve energy consumption, exergy destruction and CO<sub>2</sub> emission: Preheating based on real demand. *Energy*, 173, 598–609. DOI:10.1016/j.energy.2019.02.090
19. Jiang, H., Zhang, S., Jing, J., & Zhu, C. (2019). Thermodynamic and economic analysis of ethane recovery processes based on rich gas. *Applied Thermal Engineering*, 148, 105–119. DOI:10.1016/j.applthermaleng.2018.11.046
20. Jin, C., & Lim, Y. (2018). Economic evaluation of NGL recovery process schemes for lean feed compositions. *Chemical Engineering Research and Design*, 129, 297–305. DOI:10.1016/j.cherd.2017.11.027
21. Jalali, A., Lotfi, M., Zilabi, S., & Mohammadi, A. H. Recovery enhancement of liquid hydrocarbons in dew point control unit of natural gas processing plant. *Separation Science and Technology* **2019**, 1–8. DOI:10.1080/01496395.2019.1591450
22. Lopez-Echeverry, J. S., Reif-Acherman, S., & Araujo-Lopez, E. Peng-Robinson equation of state: 40 years through cubics. *Fluid Phase Equilibria* **2017**, 447, 39–71. DOI:10.1016/j.fluid.2017.05.007
23. Sodeifian, G., Ardestani, N. S., Sajadian, S. A., & Panah, H. S. Measurement, correlation and thermodynamic modeling of the solubility of Ketotifen fumarate (KTF) in supercritical carbon dioxide: evaluation of PCP-SAFT equation of state. *Fluid Phase Equilibria* **2018**, 458, 102–114. DOI:10.1016/j.fluid.2017.11.016
24. Guo, G., Wang, F., Liu, G. Q., Luo, S. J., & Guo, R. B. Calculation on the phase equilibrium and critical temperature of CH<sub>4</sub>/CO<sub>2</sub>. *Process Safety and Environmental Protection* **2018**, 113, 369–377. DOI:10.1016/j.psep.2017.11.007
25. Sodeifian, G., Ardestani, N. S., & Sajadian, S. A. Solubility measurement of a pigment (Phthalocyanine green) in supercritical carbon dioxide: Experimental correlations and thermodynamic modeling. *Fluid Phase Equilibria* **2019**, 494, 61–73. DOI:10.1016/j.fluid.2019.04.024
26. Farzaneh-Gord, M., & Rahbari, H. Developing novel correlations for calculating natural gas thermodynamic properties. *Chemical and Process Engineering* **2011**, 32(4), 435–452. DOI:10.2478/v10176-011-0035-1
27. Konukman, A. E. S., & Akman, U. Flexibility and operability analysis of a HEN-integrated natural gas expander plant. *Chemical Engineering Science* **2005**, 60(24), 7057–7074. DOI:10.1016/j.ces.2005.05.070
28. Jalali, A., Lotfi, M., Zilabi, S., & Mohammadi, A. H. Recovery enhancement of liquid hydrocarbons in dew point control unit of natural gas processing plant. *Separation Science and Technology* **2019**, 1–8. DOI:10.1080/01496395.2019.1591450

## Povzetek

Naravni plin predstavlja splošno uporabno plinsko mešanico. Poznavanje njegovih termodinamskih lastnosti je zato ključnega pomena za načrtovanje procesa in opreme. V tem delu smo določali energijo, ki jo lahko pridobimo iz naravnega plina z uporabo ekspanzijske turbine. Na osnovi energijske in eksergijske analize smo s pomočjo računalniškega programa MATLAB preučili naravne pline različnih sestav iz šestih plinskih polj v Egiptu. Izvedli smo numerične simulacije siromašnih in bogatih plinskih mešanic in preučili vpliv naraščajoče vsebnosti C1 in C5 na energijski izkoristek ter rezultate validirali. Rezultati so pokazali podobne trende in dobro ujemanje. Ugotovili smo, da eksergijska učinkovitost pada z naraščanjem koncentracije metana v plinski mešanici. Rezultati so tudi pokazali, da so termodinamske lastnosti plinske mešanice odvisne od relativnega deleža težjih komponent.



Except when otherwise noted, articles in this journal are published under the terms and conditions of the Creative Commons Attribution 4.0 International License

Scientific paper

# A New and Ecological Method to Quantify Vancomycin in Pharmaceutical Product by Infrared Spectrometry

Patrícia Aleixa do Nascimento,<sup>1</sup> Ana Carolina Kogawa<sup>1,2,\*</sup>  
and Hérica Regina Nunes Salgado<sup>1</sup>

<sup>1</sup> Department of Pharmaceutics, School of Pharmaceutical Sciences of Araraquara,  
Univ Estadual Paulista - UNESP, Araraquara, São Paulo, Brazil

<sup>2</sup> Laboratório de Controle de Qualidade, Faculdade de Farmácia, Universidade Federal de Goiás - UFG,  
Goiânia, Goiás, Brazil

\* Corresponding author: E-mail: ac\_kogawa@yahoo.com.br  
Phone: +55 62 3209-6470

Received: 07-10-2020

## Abstract

Vancomycin, an antimicrobial, does not present quantitative method by infrared spectrometry in the literature for the evaluation of a pharmaceutical product. This technique is considered a clean alternative because in the main, there is no solvent involved and the generation of waste is reduced. So, the aim of this study was to develop and validate a new, ecological, low cost and fast method by infrared spectrometry using KBr and band between 1450–1375  $\text{cm}^{-1}$ . It was linear in the range of 1.0–2.0 mg/150 mg, with a correlation coefficient of 0.9994. Selective when the spectra of vancomycin reference and sample were compared. Precise by repeatability (2.29%) and intermediate precision (3.12%). Accurate with average recovery of 99.37% and robust when strength and compression time of the pellets and KBr brand were varied. Considering all the methods found in literature, there is not one using infrared spectrometry for quantitative purpose, so the method developed and validated could be considered an innovation and clean alternative. This is due to the fact that it is fast, easy to handle, low cost, and non-toxic as well as generating minimal waste. The method can be applied in the routine analysis of vancomycin dosage form and is an important option for the current and sustainable pharmaceutical analysis.

**Keywords:** Vancomycin; infrared spectrometric method; green analytical chemistry; sustainable alternative; pharmaceutical analysis.

## 1. Introduction

Vancomycin is the first glycopeptide antibiotic discovered. It has a molecular formula  $\text{C}_{66}\text{H}_{75}\text{Cl}_2\text{N}_9\text{O}_{24}$  and molecular mass 1449.27  $\text{g mol}^{-1}$ . Its mechanism of action comprises the disruption of cell wall of Gram-positive bacteria, being the only antibiotic used nowadays for the treatment of infections caused by the methicillin-resistant *Staphylococcus aureus* (MRSA).<sup>1–3</sup> The main nucleus in glycopeptide antibiotics is an heptapeptide, which has a different substituent depending on the antibiotic.<sup>4–5</sup> Figure 1 shows the structure and the substituents of vancomycin.

Inhibition of the bacterial cell wall occurs when this drug binds to the final residues of D-Ala-D-Ala of peptidoglycan by van der Waals forces and five hydrogen bonds,

presenting strong binding, preventing the bind of peptidoglycan.<sup>5–7</sup>

In the context of the importance of vancomycin in the drug scenario, the development of analytical methods for its evaluation becomes extremely fundamental. Some analytical methods for this drug both physico-chemical<sup>8–14</sup> and microbiological were found in literature.<sup>15–18</sup> The spectrophotometry is a kind of very useful analytical method, which provides precise results and can be applied to quantify drugs. Only seven studies were found using this technique in literature for vancomycin and all of them in the UV region.<sup>19–25</sup> However, the spectrometry in the infrared region is also an alternative, mainly because it can also be applied in the quantitative analysis of drugs, and has already been done to other drugs.<sup>26–34</sup> No study relat-

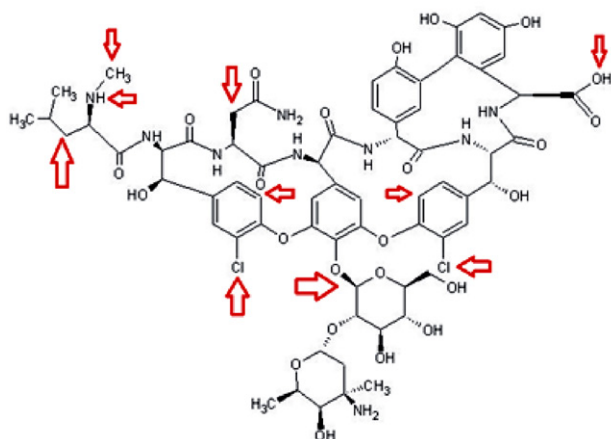


Figure 1. Structure of vancomycin with its substituents highlighted (CAS 1404-90-6).

ing this technique to vancomycin was found in literature, so the aim of this work was to develop and validate a spectrometric method in the infrared region for the quantification of vancomycin dosage form.

## 2. Experimental

### 2.1. Materials and Reagentes

Vancomycin reference (declared content 96.30%) and lyophilized powder for injection (sample) 500 mg (labeled content) were used in spectrometric analysis in the infrared region (IR) and they were kindly donated by the ABL Antibióticos do Brasil (Cosmópolis, São Paulo, Brazil). Potassium bromide (KBr, Neon<sup>TM</sup>, Suzano, São Paulo, Brazil), previously maintained in an oven for 24 h before the analysis was used as diluent for pellets preparation, each pellet contained 150 mg. A pool containing vancomycin reference or sample was prepared in the ratio of 1:10 and the pellets were obtained by weighing the appropriate amount from this pool.

### 2.2. Equipment

An analytical balance DV215CD (Discovery, Ohaus<sup>®</sup>, São Paulo, Brasil) was used. An agate mortar and pestle were used to prepare the pellets, which were transferred to a compression system. A spectrophotometer IR-Prestige-21 (Shimadzu<sup>®</sup>, Japan) was also used and the readings were performed using the software IR Solution<sup>®</sup>.

### 2.3. Method Development

#### 2.3.1. Pellets Preparation

Pellets of vancomycin reference and sample were prepared using KBr as a diluent. An amount of 20 mg of vancomycin reference and 180 mg of KBr were weighed and homogenized using the mortar and pestle. From this mixture an appropriate amount (16 mg) was taken and

added to 134 mg of KBr in order to obtain 1.60 mg/150 mg tablets. The same procedure was done to the vancomycin sample, considering the average weight from twenty vials of vancomycin (504.92 mg). An amount of 20.19 mg vancomycin sample and 179.81 mg of KBr were weighed and homogenized. Then an amount of 16 mg was weighed and added to 134 mg of KBr, obtaining a final concentration of 1.60 mg/150 mg. This powder was transferred to the compression system for 7 min at 90 kN. After this period, pellets were placed on the spectrophotometer and the readings were performed at 1450–1375 cm<sup>-1</sup>.

## 2.4. Method Validation

### 2.4.1. Validation Parameters

The validation procedure was performed according to the International Conference on Harmonization<sup>35</sup> specifications for linearity, selectivity, limits of detection and quantification, precision, robustness, and accuracy.

**Linearity:** An analytical curve was obtained in the range of 1.00 mg/150 mg to 2.00 mg/150 mg. For this, 99 mg of the vancomycin sample and 891 mg of KBr was weighed and transferred to the mortar and mixed. From this pool, an appropriate amount was weighed in order to obtain pellets of 1.00, 1.20, 1.40, 1.60, 1.80, and 2.00 mg/150 mg. The linearity assay was performed on three different days and in triplicate. The data obtained were evaluated by regression analysis. The equation of the line was determined by linear regression analysis using the method of the least squares. Analysis of Variance (ANOVA) was also performed using the absorbance values obtained for each concentration.

**Selectivity:** Selectivity of the method was determined by the absorbance obtained for the vancomycin reference and sample, as well as the evaluation of the overlap of their spectra.

**Limits of detection and quantification:** The limits of detection (LOD) and quantification (LOQ) were obtained from the three calibration curves, using the Equations 1 and 2, respectively:

$$\text{LOD} = 3x \frac{SD}{a} \quad (1)$$

$$\text{LOQ} = 10x \frac{SD}{a} \quad (2)$$

SD: standard deviation  
a: average slope

**Precision:** Precision was evaluated by repeatability and intermediate precision. Repeatability assay was performed using six replicates of the same concentration (1.60 mg/150 mg) on the same day, with the same analyst, under the same conditions of analysis. Intermediate precision assay was performed by another analyst on a different day, under the same conditions of analysis. The preci-

sion was evaluated by RSD (%) values. The method was considered precise when RSD (%) values were lower than 2.00%.

**Robustness:** The robustness assay of the method was performed using 1.60 mg/150 mg tablets and small variations in three fundamental parameters: time of compression (normal: 7 min, variation: 5 and 9 min), strength of compression (normal: 90 kN, variation: 88 and 92 kN) and KBr brand (normal: Neon<sup>®</sup>, variation: Dinâmica<sup>®</sup>). Each condition was analyzed in triplicate, on the same day and with the same analyst. The results were analyzed by F-test and *t*-test compared to normal conditions. The method was considered robust when  $t_{\text{calculated}}$  was smaller than  $t_{\text{critical}}$ .

**Accuracy:** The accuracy of the method was demonstrated by the recovery test, in triplicate and at three levels, 80, 100 and 120%, considering 1.60 mg/150 mg (100%). A standard pool was prepared with the vancomycin reference (30 mg + KBr: 270 mg). The sample pool was also prepared under the same conditions (sample: 30.29 mg + KBr: 272.60 mg). From the reference pool an amount of 10 mg was weighed and added to 140 mg of KBr, obtaining a pellet of 1.00 mg/150 mg. The same was done to the sample pool. The 3 levels, 80, 100 and 120%, were prepared using the same amount of the sample pool (10 mg) and a different amount of the reference pool, 28, 60 and 92 mg (equivalent to 2.80, 6.00 and 9.20 mg), respectively. Average recoveries, expressed in terms of percentage recovered from the standard and RSD (%), were determined. Method was considered accurate when recovery levels were 98 to 102% and RSD (%) values were lower than 2.00%.<sup>36</sup>

## 2. 5. Content Analysis

The preparation of the pellets was carried out according to section 2.3.1. Absorbance was measured at 1450–1375 cm<sup>-1</sup>. Pellet was submitted to the compression

system for 7 min under 90 kN. The values were compared using the Equation 3.

$$C_s = A_s \times \frac{C_r}{A_r} \quad (3)$$

C<sub>s</sub>: concentration of sample pellet;  
A<sub>s</sub>: absorbance of sample pellet;  
C<sub>r</sub>: concentration of reference pellet;  
A<sub>r</sub>: absorbance of reference pellet.

Content measurement was considered adequate when content was 90–115%.<sup>25</sup>

## 2. 6. Comparison of Methods

The results of the vancomycin final product content obtained using the proposed method were compared with the results obtained by a microbiological method using turbidimetry.<sup>37</sup>

## 3. Results and Discussion

### 3. 1. Method Development and Validation

An appropriate amount of standard vancomycin was weighed and added to KBr in order to obtain pellets of

Table 1. ANOVA results for linearity of the method

Parameters	1450–1375 cm <sup>-1</sup>
Linearity range (mg/150 mg)	1.0–2.0
Slope	0.38
Intercept	0.00
Correlation coefficient (r)	0.99
Regression	371.33 (4.75)
Lack of fit	(3.26)

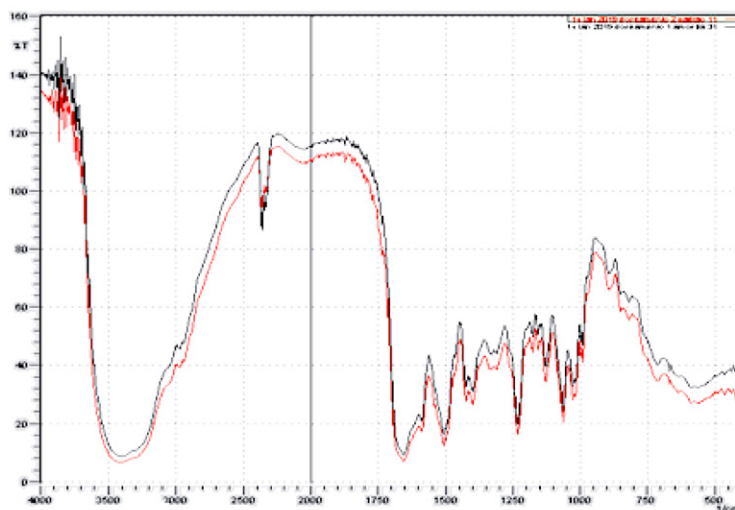


Figure 2. Overlapping spectra of vancomycin standard and sample.

**Table 2.** Precision results of the method by spectrometry in the infrared region for vancomycin

	Level	Absorbance*						RSD (%)
		1	2	3	4	5	6	
1450–1375 cm <sup>-1</sup>	Repeatability	0.58 <sup>a</sup>	0.60 <sup>a</sup>	0.60 <sup>a</sup>	0.62 <sup>a</sup>	0.60 <sup>a</sup>	0.59 <sup>a</sup>	2.29
	Intermediate	0.61 <sup>b</sup>	0.62 <sup>b</sup>	0.60 <sup>b</sup>	0.61 <sup>b</sup>	0.63 <sup>b</sup>	0.62 <sup>b</sup>	3.12
		0.63 <sup>c</sup>	0.63 <sup>c</sup>	0.62 <sup>c</sup>	0.61 <sup>c</sup>	0.66 <sup>c</sup>	0.65 <sup>c</sup>	

<sup>a</sup> Absorbance obtained by analyst 1 on day 1 <sup>b</sup> Absorbance obtained by analyst 1 on day 2 <sup>c</sup> Absorbance obtained by analyst 2 on day 2 \* Six replicates

**Table 3.** Robustness of the method by spectrometry in the infrared region for vancomycin

Normal condition	Parameters				KBr brand
	Strength of compression (kN)		Time of compression (min)		
90 (kN)	88*	92*	5*	9*	Dinâmica™*
7 (min)	$t_{\text{critical}} = 2.77$	$t_{\text{critical}} = 2.77$	$t_{\text{critical}} = 2.77$	$t_{\text{critical}} = 2.77$	$t_{\text{critical}} = 4.30$
Neon™	$t_{\text{critical}} = -2.46$	$t_{\text{critical}} = -1.27$	$t_{\text{critical}} = -5.04$	$t_{\text{critical}} = -0.75$	$t_{\text{critical}} = 3.98$

\* Three replicates

1.00–2.00 mg/150 mg. The data was validated by ANOVA (Table 1), which showed significant linear regression ( $F_{\text{calculated}} 371.33 > F_{\text{critical}} 4.75$ ,  $p = 0.05$ ), and no significant lack of fit ( $F_{\text{calculated}} 1.23 < F_{\text{critical}} 3.26$ ,  $p = 0.05$ ). In this way, the method can be considered linear.

The linearity was proven by the regression analysis using the least squares method, obtaining a correlation coefficient ( $r$ ) of 0.99. It was also proven by the Analysis of Variance (ANOVA), which showed significant linear regression and no significant lack of fit.

The selectivity of the method was analyzed by comparing the spectra of vancomycin reference (black) and sample (red) (Figure 2).

The selectivity assay of the method was performed by the overlapping spectra of vancomycin reference and sample, which identified the drug.

The LOD and LOQ obtained were, respectively, 0.01 and 0.03 mg/150 mg. The limits are low, which show the sensitivity of the method.

Precision was proven by repeatability (RSD 2.29%) and by intermediate precision (RSD 3.12%). Both showed adequate results of RSD (%) and the intermediate precision was also analyzed by F-test and  $t$ -test, showing values

of  $F_{\text{calculated}} < F_{\text{tabulated}}$  ( $3.74 < 5.05$ ) and  $t_{\text{calculated}} < t_{\text{tabulated}}$  ( $2.21 < 2.23$ ), respectively. So, the method can be considered precise. The results for repeatability and intermediate precision are shown in Table 2.

The robustness of the method was performed by small variations in three parameters. The method can be considered robust for these varied parameters when values of test  $t_{\text{calculated}}$  were smaller than the  $t_{\text{critical}}$ . The results are shown in Table 3.

The robustness of the method is an important parameter to be evaluated, which assures the results obtained. Variations performed in strength of compression,

**Table 5.** Content analysis for vancomycin reference and sample using spectrometry in the infrared region

Day	Average content (%) <sup>*</sup>	Final content (%)	RSD (%)
1	101.66		
2	101.75	102.35	1.09
3	103.63		

\* Three replicates

**Table 4.** Recovery results for vancomycin using the developed spectrometric method

	Vancomycin Standard added (mg/150 mg)*	Vancomycin Standard recovered (mg/150 mg)*	Recovery (%)	recovery (%)	RSD (%)
R1	0.28	0.28	99.65		
R2	0.60	0.60	99.48	99.37	0.32
R3	0.92	0.91	98.98		

\* Three replicates

Table 6. Comparison of methods

Method	Average content (%)*	Final content (%)	RSD (%)	Statistical evaluation
Proposed (physico-chemical)	101.66	102.35	1.09	0.32 (4.30)***
	101.75			
	103.63			
Turbidimetric** (microbiological)	108.20	103.32	4.97	
	103.81			
	97.96			

\*Average of 3 determinations \*\*<sup>37</sup> \*\*\**t*-test

time of compression and KBr brand showed that the method remains robust and the quality of the results are reliable. This parameter is also useful in the development of other conditions for other drugs and samples, serving as a start for the conditions to be tested.

The accuracy of the developed method was determined by the standard recovery test. Recovery values are shown in Table 4, as well as the RSD (%). The method can be considered accurate, considering the average recovery in three days of analysis, in accordance to 98–102% specified by AOAC<sup>36</sup> and RSD (%) values below 2%.

### 3. 2. Content Analysis

The content of vancomycin in the final product was analyzed and is shown in Table 5.

Content analysis is not a parameter required for validation but it is also important to perform because it assures the content of the drug in the marketed sample. The analysis showed that the content of vancomycin is within the limits stipulated by Japanese Pharmacopoeia (90–115%).<sup>25</sup>

### 3. 3. Comparison of Methods

The result of the comparison between the proposed method (physico-chemical) and the turbidimetric method (microbiological) was made by the vancomycin content values in the final product and is shown in Table 6.

An antimicrobial must always be analyzed using 2 methods, 1 physico-chemical and 1 microbiological, as many times physico-chemical methods are unable to assess the real potency of the antimicrobial.

In this case, the proposed method was directly compared with the microbiological method and was statistically equivalent, which allows its reliable use in the evaluation of the vancomycin final product.

Spectrometric method in infrared region is an important technique that can be used to quantify drugs, mainly because of its ecological characteristics and simplicity to perform. It also protects the environment, due to the less generation of waste, and the analyst, who does not need to get in touch with solvents.

## 4. Conclusions

In the present work a spectrometric method in infrared region was developed for the evaluation of vancomycin in lyophilized powder. This method is by itself greener when compared to a chromatographic method or a spectrophotometric method in the UV region, because there is no use of solvents, which generates less waste, for example. It is sensitive and proven to be precise to quantify the drug, being a great alternative to the routine quality control process of vancomycin in chemical and pharmaceutical laboratories. The method is also linear in the range of 1.00 to 2.00 mg/150 mg, selective, precise, robust, and accurate. It is worth remembering that each drug has specific characteristics and specific analysis rigidities. Many times, the method of analysis of one drug is not necessarily useful for another, so this work is important, which shows the ideal and eco-friendly conditions for the analysis of vancomycin in final product by spectrometry in infrared region. It generates less waste, does not use solvents, is fast and very simple to perform the test. Furthermore, it is advantageous because the sample can be analyzed in solid state, does not require the use of diluents or solvents, does not expose analysts to vapors that can be toxic and it can be used in production line control.

### Acknowledgements

The authors acknowledge CNPq (Conselho Nacional de Desenvolvimento Científico e Tecnológico, Brasília, Brazil), FAPESP (Fundação de Amparo à Pesquisa do Estado de São Paulo, São Paulo, Brasil), CAPES (Coordenação de Aperfeiçoamento de Pessoal de Nível Superior, São Paulo, Brasil), PADC/FCF/UNESP (Programa de Apoio ao Desenvolvimento Científico/Faculdade de Ciências Farmacêuticas/Universidade Estadual Paulista, Araraquara, Brazil) and ABL Antibióticos do Brasil.

### Declaration of interest

The authors have no financial or other potential conflicts of interest.

## 5. References

1. T. L. Smith, M. L. Pearson, K. R. Wilcox, C. Cruz, M. V. Lancaster, B. Robinson-Dunn, F. C. Tenover, M. J. Zervos, J. D. Band, E. White, W. R. Jarvis, *The New England Journal of Medicine* **1999**, *340*, 493–501. DOI:10.1056/NEJM199902183400701
2. D. Kahne, C. Leimkuhler, W. Lu, C. Walsh, *Chemical Reviews* **2005**, *105*, 425–448. DOI:10.1021/cr030103a
3. P. M. Wright, I. B. Seiple, A. G. Myers, *Angewandte Chemie International Edition England* **2015**, *53*, 8840–8869. DOI:10.1002/anie.201310843
4. R. Nagarajan, *The Journal of Antibiotics* **1993**, *46*, 1181–1195. DOI:10.7164/antibiotics.46.1181
5. H. K. Kang, P. Yoonkyung, *Journal of Bacteriology and Virology* **2015**, *45*, 67–78. DOI:10.4167/jbv.2015.45.2.67
6. K. Lazar, S. Walker, *Current Opinion in Chemical Biology* **2002**, *6*, 786–793. DOI:10.1016/S1367-5931(02)00355-1
7. D. H. Williams, B. Bardsley, *Angewandte Chemie International Edition* **1999**, *38*, 1172–1193. DOI:10.1002/(SICI)1521-3773(19990503)38:9<1172::AID-ANIE1172>3.0.CO;2-C
8. T. M. Lima, K. S. Seba, J. C. S. Gonçalves, F. L. L. Cardoso, C. E. Estrela, *Journal of Chromatographic Science* **2018**, *56*, 115–121. DOI:10.1093/chromsci/bmx089
9. X. Song, J. Xie, M. Zhang, Y. Zhang, J. Li, Q. Huang, *Journal of Chromatography B* **2018**, *1076*, 103–109. DOI:10.1016/j.jchromb.2018.01.020
10. A. Serri, H. R. Moghimi, A. Mahboubi, A. Zarghi, *Acta Polonica Pharmaceutica – Drug Research* **2017**, *74*, 73–79.
11. L. Kirk, P. Lewis, Y. Luu, S. Brown, *International Journal of Pharmaceutical Compounding* **2016**, *20*, 159–163.
12. A. D. Berti, P. R. Hutson, L. T. Schulz, A. P. Webb, W. E. Rose, *American Journal of Health-System Pharmacy* **2015**, *72*, 390–395. DOI:10.2146/ajhp140369
13. C. Anderson, S. Boehme, J. Ouellette, C. Stidham, M. Mackay, *Hospital Pharmacy* **2014**, *49*, 42–47. DOI:10.1310/hpj4901-42
14. P. A. Whaley, M. A. Voudrie Ii, *International Journal of Pharmaceutical Compounding* **2013**, *16*, 167–169.
15. J. J. Aguilera-Correa, A. L. Doadrio, A. Conde, M. A. Arenas, J. J. Damborenea, M. Vallet-Regí, J. Esteban, *Journal of Materials Science: Materials in Medicine* **2018**, *29*, 2–10. DOI:10.1007/s10856-018-6119-4
16. F. L. Francisco, A. M. Saviano, T. S. B. Almeida, F. R. Lourenço, *Journal of Microbiology Methods* **2016**, *124*, 28–34. DOI:10.1016/j.mimet.2016.03.005
17. J. A. Montes, D. Johnson, J. Jorgensen, L. Mcelmeel, L. C. Fulcher, J. W. Kiel, *Cornea* **2016**, *35*, 122–126.
18. R. Gálvez-López, A. Peña-Monje, R. Antelo-Lorenzo, J. Guardia-Olmedo, J. Moliz, J. Hernández-Quero, J. Parra-Ruiz, *Diagnostic Microbiology and Infectious Disease* **2014**, *78*, 70–74. DOI:10.1097/ICO.0000000000000676
19. T. H. Hoang Thi, F. Chai, S. Leprêtre, N. Blanchemain, B. Martel, F. Siepmann, H. F. Hildebrand, J. Siepmann, M. P. Flament, *International Journal of Pharmaceutics* **2010**, *400*, 74–85. DOI:10.1016/j.diagmicrobio.2013.09.014
20. S. Bakhshandeh, Z. G. Karaji, K. Lietaert, A. C. Fluit, C. H. E. Boel, H. C. Vogely, T. Vermonden, W. E. Hennink, H. Weinsans, A. A. Zadpoor, S. A. Yavari, *ACS Applied Materials and Interfaces* **2017**, *9*, 25691–25699. DOI:10.1016/j.jipharm.2010.08.035
21. N. Sarkar, G. Sahoo, R. Das, G. Prusty, S. K. Swain, *European Journal of Pharmaceutical Sciences* **2017**, *109*, 359–371. DOI:10.1021/acsami.7b04950
22. A. Esmaeili, S. Ghobadianpour, *International Journal of Pharmaceutics* **2016**, *501*, 326–330. DOI:10.1016/j.ejps.2017.08.015
23. G. Sayet, M. Sinegre, M. Ben Reguiga, *Annales Pharmaceutiques Françaises* **2014**, *72*, 41–50. DOI:10.1016/j.jipharm.2016.02.013
24. L. Yongxin, J. Genlong, S. Guodong, Z. Lili, W. Shilong, L. Hanchao, L. Zhizhong, *Luminescence* **2014**, *29*, 109–117. DOI:10.1016/j.pharma.2013.10.002
25. Japanese Pharmacopoeia. 16th E d. Tokyo Society of Japanese Pharmacopoeia, 2011.
25. P. A. Nascimento, A. C. Kogawa, H. R. N. Salgado, *Austin Journal of Analytical and Pharmaceutical Chemistry* **2019**, *6*, 1–5.
27. E. G. Tótolí, H. R. N. Salgado, *Journal of AOAC International* **2017**, *100*, 1569–1576.
28. A. H. Moreno, H. R. N. Salgado, *Physical Chemistry* **2012**, *2*, 6–11. DOI:10.5740/jaoacint.17-0067
29. B. S. Rechelo, A. C. Kogawa, H. R. N. Salgado, *Spectrochimica Acta Part A: Molecular and Biomolecular Spectroscopy* **2019**, *208*, 157–161. DOI:10.5923/j.pc.20120201.02
30. C. T. Rebouças, A. C. Kogawa, H. R. N. Salgado, *Journal of AOAC International* **2018**, *101*, 2001–2005. DOI:10.1016/j.saa.2018.09.058
31. A. C. Kogawa, H. R. N. Salgado, *Current Pharmaceutical Analysis* **2018**, *14*, 108–115. DOI:10.5740/jaoacint.17-0431
32. A. C. Kogawa, N. P. Mello, H. R. N. Salgado, *Pharmaceutica Analytica Acta* **2016**, *7*, 463–466.
33. A. C. Kogawa, H. R. N. Salgado, *Physical Chemistry* **2013**, *3*, 1–6.
34. M. T. Trindade, H. R. N. Salgado, *Physical Chemistry* **2017**, *7*, 55–62.
35. ICH, International Conference on Harmonization of technical requirements for registration of pharmaceuticals for human use. Validation of analytical procedures: Text and Methodology Q2(R1), [https://www.ema.europa.eu/en/documents/scientific-guideline/ich-q-2-r1-validation-analytical-procedures-text-methodology-step-5\\_en.pdf](https://www.ema.europa.eu/en/documents/scientific-guideline/ich-q-2-r1-validation-analytical-procedures-text-methodology-step-5_en.pdf) (assessed: April 28, 2020)
36. AOAC, Association of Official Analytical Chemists. Official Methods of Analysis, [http://members.aoac.org/aoac\\_prod\\_imis/AOAC\\_Docs/StandardsDevelopment/SLV\\_Guidelines\\_Dietary\\_Supplements.pdf](http://members.aoac.org/aoac_prod_imis/AOAC_Docs/StandardsDevelopment/SLV_Guidelines_Dietary_Supplements.pdf) (assessed: April 28, 2020)
37. P. A. Nascimento, A. C. Kogawa, H. R. N. Salgado, *Journal of AOAC International* **2020**, *103*, 1582–1587. DOI:10.1093/jaoacint/qsaa068



## Povzetek

Za določanje protimikrobne učinkovine vankomicina v farmacevtskih proizvodih v literaturi ni najti kvantitativne metode z infrardečo spektrometrijo. Ta tehnika se smatra za *čistejšo* alternativo, saj v splošnem ne uporablja nobenih topil in je tudi količina odpadkov zmanjšana. Cilj te raziskave je bil razviti in validirati novo ekološko, poceni in hitro metodo z infrardečo spectrometrijo z uporabo KBr in traka 1450–1375 cm<sup>-1</sup>. Metoda je bila linearna v območju 1,0–2,0 mg/150 mg s korelacijskim koeficientom 0,9994. Selektivna ob primerjavi spektra referenčnega vankomicina in vzorca. Natančna s ponovljivostjo 2,29% in vmesno ponovljivostjo 3,12%. Točna s povprečnim izkoristkom 99,37% ter robustna, če smo spreminjali moč in čas kompresije peletov ter znamko KBr. Ob primerjavi z metodami v literaturi ni nobene, ki bi uporabljala infrardečo spektrometrijo za kvantitativne namene, zato predstavljeno validirano metodo lahko smatramo za inovacijo in *čistejšo* alternativo. Razlog je, da je hitra, enostavna za uporabo, poceni, nestrupena ter proizvaja minimalno odpadkov. Metodo se lahko uporabi za rutinsko analizo vankomicina v farmacevtskem prašku in predstavlja pomembno možnost za sodobno in trajnostno farmacevtsko analitiko.



Except when otherwise noted, articles in this journal are published under the terms and conditions of the Creative Commons Attribution 4.0 International License

Scientific paper

# Theoretical B3LYP Study on Electronic Structure of Contrast Agent Iopamidol

Fatma Genç,<sup>1,\*</sup> Sedat Giray Kandemirli<sup>2</sup> and Fatma Kandemirli<sup>3</sup><sup>1</sup> Department of General Chemistry, Faculty of Pharmacy, University of İstanbul Yeni Yuzyil, Maltepe Mh., Yilanli Ayazma Cd., İstanbul, Turkey<sup>2</sup> Department of Radiology, Roy Carver College of Medicine, University of Iowa, Iowa City, United States<sup>3</sup> Department of Biomedical Engineering, Faculty of Engineering and Architecture, University of Kastamonu, Kuzeykent 37150, Kastamonu, Turkey

\* Corresponding author: E-mail: ftmgenc@yahoo.com

Received: 07-01-2020

## Abstract

Nonionic low-osmolar contrast agents are thought about safe for intravenous or intra-arterial administration. Iopamidol is one of the contrast agents used for diagnostic clinical computed tomography (CT) protocols last four decades years. The molecular structure of Iopamidol was calculated by the B3LYP density functional model with the LANL2DZ basis set by the Gaussian program. The natural bond orbital analysis in terms of the hybridization of atoms and the electronic structure of the title molecule have been analyzed by using the data obtained from the quantum chemical results. First-order hyperpolarizability ( $\beta_{tot}$ ), the dipole moment ( $\mu$ ) and polarizability ( $\alpha$ ) and anisotropic polarizability ( $\Delta\alpha$ ) of the molecule have been reported. HOMO and LUMO energies and parameters related to energies, and dipole moment, polarizability and hyperpolarizability show minor dependences on the solvent polarity. The hardness of Iopamidol decreases with increasing solvent polarity. The stability of the Iopamidol contrast agent with the hyper conjugative interactions, charge delocalization has been analyzed using natural bond orbital analysis. In addition, thermodynamic properties were obtained in the range of 200–1000 K.

**Keywords:** Quantum chemical calculations; DFT; B3LYP; Iopamidol; gaussian program; electronic structure.

## 1. Introduction

Iodinated X-ray contrast agents (ICM) are often used to enable the medical imaging of soft tissues like organs and blood vessels.<sup>1</sup> The nonionic, water-soluble, low-osmolar contrast agents such as Iopamidol with the 1-N,3-N-bis(1,3-dihydroxypropan-2-yl)-5-[[[(2S)-2-hydroxypropanoyl]amino]-2,4,6-triiodobenzene-1,3-dicarboxamide IUPAC name is widely used for intravascular administration.<sup>2,3</sup> It has very wide diagnostic applications, including the central nervous system, the cardiovascular apparatus, and the urinary tract.<sup>4</sup> Iopamidol, a clinically approved X-Ray contrast agent, exhibits high water solubility and low toxicity.<sup>4,5</sup> For this reason, it can be safely administered intravenously at very high doses like 400 mg/ml.<sup>4</sup> This contrast agent was eliminated through the kidneys with a half-life of 2 hours.<sup>2</sup>

The molecule of Iopamidol contains a high number of mobile protons on amide and alcohol moiety exchang-

ing with water. This contributes to a reduction in the MR signal density of the water proton. So, Iopamidol commonly used for CT, may be also considered as a contrast agent for Magnetic resonance imaging (MRI) applications.<sup>4</sup>

The geometry, dipole moment, polarizability, hyperpolarizability, and other molecular properties can be affected by the polarity of the solvent due to variable interactions with the highest occupied and lowest unoccupied molecular orbitals (HOMO-LUMO)<sup>6,7</sup> and so the polarity of the solvent can influence the stability and reactivity of the molecule.<sup>8</sup> They can be obtained by quantum chemical calculation without laboratory measurements, thus saving time and equipment, reducing safety and disposal concerns. So, investigation of the theoretical properties of the molecules has recently attracted the attention of scientists and quantum chemical calculation has been widely used to study reaction mechanisms.<sup>9</sup>

Bellich et al. discussed the structure of Iopamidol for three different crystalline phases. In the anhydrous and monohydrate crystal forms, they reported that Iopamidol molecules are shown conformation of the long branches emerging from the triiodobenzene ring, while the pentahydrate phase had anti-conformation. IR and Raman spectroscopic studies, conducted in conjunction with quantum chemical calculations on three crystal forms, revealed that distinctly different spectral properties can be attributed, in particular, to different molecular structures.<sup>10</sup>

The Density Functional Theory (DFT) calculations eventually lead to a good understanding of molecular properties and a detail of the molecular characteristics and interactions.<sup>8</sup> Thermodynamic properties such as enthalpy, entropy, and Gibbs free energy are important to understand the stability of molecules at different temperatures and pressures, which can be easily explained using DFT with the Gaussian 03 program.<sup>11,12</sup>

DFT has recently gained popularity as a cost-effective general procedure for studying the physical properties of molecules. Unlike the Hartree-Fock theory, DFT gives a good electron correlation through electron density functions in the self-consistent Kohn-Sham procedure and complex operations. Descriptions for systems requiring electron correlation in the traditional *ab initio* approach is, therefore, a cost-effective and reliable method.<sup>13,14,15</sup>

Descriptors such as Chemical hardness, chemical potential, polarizability, and softness known as global reactivity descriptors based on density functional theory have found great utility in field selectivity as well as in predicting the reactivity of atoms and molecules, therefore this work presents the quantum chemical studies of the effects of solvents on molecular properties of Iopamidol such as the highest occupied molecular orbital energy ( $E_{\text{HOMO}}$ ), the lowest unoccupied molecular orbital energy ( $E_{\text{LUMO}}$ ), energy gap ( $\Delta E$ ), electronegativity ( $\chi$ ), electron affinity ( $A$ ), global hardness ( $\mu$ ), softness ( $S$ ), ionization potential ( $I$ ), the fraction of electrons transferred and the total energy ( $\Delta N_{\text{max}}$ ), nucleofugality ( $\Delta E_{\text{n}}$ ) electrofugality ( $\Delta E_{\text{e}}$ ). These molecular properties of Iopamidol were computed by the B3LYP density functional model with the LANL2DZ basis set by the Gaussian program in the gas phase and in solvents (chloroform, acetic acid, ethanol, DMF, DMSO and water). This study was conducted to report the media effect of Iopamidol on dipole moment, polarizability, first-order hyperpolarizability and chemical reactivity, the stability of Iopamidol in different solvent systems and the development of new pharmaceutical and (bio) chemical products derived from Iopamidol.

## 2. Theory and Computational Details

DFT (density functional theory) methods have become very popular in recent years were used in this study. The fundamental base of DFT is the use of electronic den-

sity instead of the wave function for calculating the energy constitutes. All calculations were done by GAUSSIAN 09W software package,<sup>16</sup> using the B3LYP functional<sup>9</sup> and the LANL2DZ basis set.<sup>17</sup> The B3LYP, a version of the DFT method, uses Becke's three-parameter functional (B3) and includes a mixture of HF with DFT exchange terms associated with the gradient corrected correlation function of Lee, Yang, and Parr (LYP)<sup>9</sup>. The geometry of the Iopamidol contrast agent under investigation was determined by optimizing all the geometrical variables without any symmetry constraints. In solvents with different dielectric constants such as water, DMSO, DMF, ethanol, acetic acid and chloroform, the Solubility on Density Model applied in Gaussian 09 was used for all calculations. The SMD model is highly parameterized, uses the original polarizable continuity model (PCM), and the charge density of the dissolved molecule interacts with the dielectric environment of the solvent via the surface tension at the solvent-solvent boundary.

## 3. Results and Discussion

In the case of electronic response, the main effects caused by the solvent medium<sup>18</sup> (i) change of wave function due to change in structure perturbing environment, (ii) change of geometric structure (iii) change of response properties, and (iv) altering the dynamics of the excitation processes.

Optimized structure, the highest occupied molecular orbital (HOMO), the lowest unoccupied molecular orbital (LUMO) and electron density of Iopamidol in the gas phase calculated at the DFT/B3LYP level with the LANL2DZ basis set was given in Figure 1. As seen from Figure 1, HOMO and LUMO are formed from mainly benzene ring and iodine group attached to benzene ring.

A large  $E_{\text{HOMO}} - E_{\text{LUMO}}$  gap means high kinetic stability and low chemical reactivity due to energetically unfavorable to add electrons to a high-lying LUMO. Meanwhile, a molecule with a small  $E_{\text{HOMO}} - E_{\text{LUMO}}$  gap is more polarizable, is generally associated with a high chemical reactivity-low kinetic stability and is termed as a soft molecule.<sup>19</sup> The solvent medium changes the properties of solvated molecules and sometimes significantly affects the dynamics of the processes. Ten molecular orbital energy near  $E_{\text{HOMO}}$  and  $E_{\text{LUMO}}$  to study the photo-physics and kinetic stability of Iopamidol compounds were shown in Figure 2 in different phases such as gas, chloroform, acetic acid, ethanol, DMF, DMSO and water.  $E_{\text{HOMO}}$  and five molecular orbital energy near HOMO of Iopamidol for -6.80, -6.85, -6.95, -6.98, -7.10, -7.16 eV.  $E_{\text{LUMO}}$  and five molecular orbital energy near LUMO of Iopamidol for gas phase are -2.19, -1.51, -1.46, -1.12, -0.95, -0.41 eV.

The highest occupied molecular orbital (HOMO) which is the outermost orbital filled by electrons and the lowest unoccupied molecular orbital (LUMO) represent-

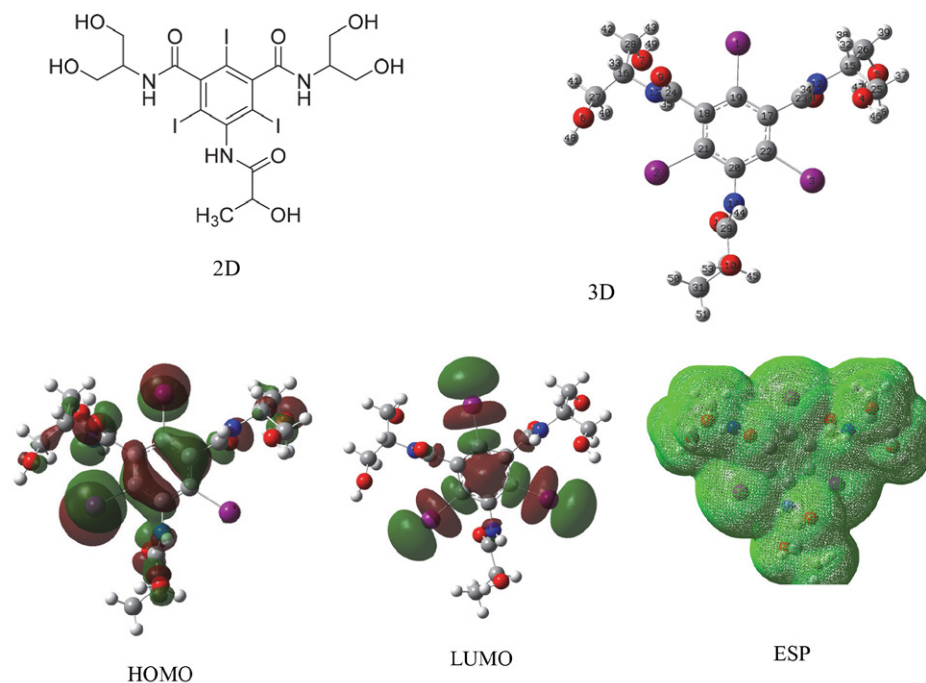


Figure 1. Optimized Structure, HOMO, LUMO and electron density of Iopamidol

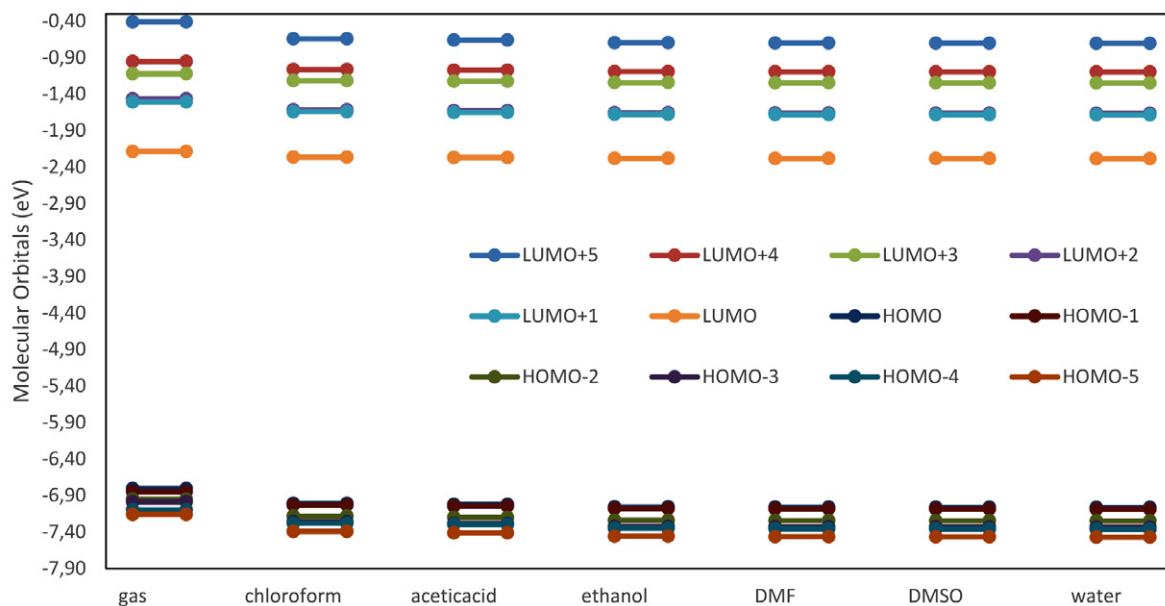


Figure 2. Frontier orbital energies for Iopamido

ing the first empty inner most orbital unfilled by electrons called frontier orbitals are the main orbitals taking part in a chemical reaction.<sup>20</sup>

The HOMO-LUMO energy band gap is a very important parameter for the determination of molecular electrical properties and an indication of molecular chemical stability. The quantum molecular descriptors such as ionization potential, electron affinity, chemical reactivity, kinetic stability, polarizability, chemical hardness and softness, and electro-

negativity, electrofugality, nucleofugality can be calculated by using the gap between  $E_{\text{HOMO}}$  and  $E_{\text{LUMO}}$ .

$E_{\text{HOMO}}$  and  $E_{\text{LUMO}}$  values and  $E_{\text{HOMO}}$  and  $E_{\text{LUMO}}$  band gap values, computed with the B3LYP / LANL2DZ level, and additionally, chemical potential, electron affinity, electronegativity chemical hardness, softness and electrophilicity, electrofugality, nucleofugality index parameters, found using the computed HOMO and LUMO energy values, were summarized in Table 1.

**Table 1.** Parameters related with  $E_{\text{HOMO}}$  and  $E_{\text{LUMO}}$ .

	$E_{\text{HOMO}}$	$E_{\text{LUMO}}$	$\Delta E$	$\eta$	S	$\chi$	$\mu$	$\Omega$	$\Delta N_{\text{max}}$	$\Delta E_n$	$\Delta E_e$
Gas	-6.80	-2.19	4.62	2.31	0.22	4.50	-4.50	4.38	1.95	1.04	10.03
Chloroform	-7.01	-2.26	4.75	2.37	0.21	4.64	-4.64	4.53	1.95	1.08	10.35
Acetic acid	-7.02	-2.27	4.75	2.38	0.21	4.65	-4.65	4.54	1.95	1.08	10.37
Ethanol	-7.06	-2.28	4.77	2.39	0.21	4.67	-4.67	4.57	1.96	1.09	10.43
DMF	-7.06	-2.28	4.78	2.39	0.21	4.67	-4.67	4.57	1.96	1.09	10.43
DMSO	-7.06	-2.28	4.78	2.39	0.21	4.67	-4.67	4.57	1.96	1.09	10.44
Water	-7.06	-2.29	4.78	2.39	0.21	4.67	-4.67	4.57	1.96	1.09	10.44

The highest occupied molecular orbitals (HOMO) and the lowest empty molecular orbitals (LUMO), called boundary molecule orbitals (FMOs), are the main orbitals involved in the chemical reaction. The energy gap formed between HOMO and LUMO indicates the chemical stability of the molecules and is a critical parameter for determining the molecular electrical transport properties as well as the properties of the molecules. The highest HOMO value of -6.80 eV was found in the gas phase followed by -7.01, -7.02, -7.06, -7.06, -7.06 in chloroform, acetic acid, ethanol, DMF, DMSO and water phases indicate that the molecule will be best electron donor in the gas phase. So, it was observed that the negative value of the HOMO increased with the increase of dielectric constants of the solvents. They reported that the inclusion of solvents for Iopamidol causes the HOMO values to become more negative.<sup>21</sup>

The lowest LUMO energy of -2.29 eV was found to be in water indicating that the molecule will be the best accept electron in water compare to the gas phase and other solvents. The energy gap is used in determining molecular electrical transport properties. The largest HOMO-LUMO gap of 4.78 eV was found in water solvent which implies higher kinetic stability and less chemical reactivity<sup>22</sup> followed by 4.78 eV and the other studied solvents and found 4.62 eV in the gas phase.

The electronic chemical potential as seen in Equation 1 is defined as the energy changes of the system with respect to the electron number  $N$  at a fixed external potential  $v(r)$ , i.e., the potential created by the nuclei.<sup>23, 24</sup> The electronic chemical potential is associated with the feasibility of a system to exchange electron density with the environment at the ground state.

$$\mu = \left( \frac{\partial E}{\partial N} \right)_{v(r)} \quad (1)$$

When the finite difference approximation is used the following simple expression is obtained:

$$\mu \approx -\frac{(I+A)}{2} \quad (2)$$

Where,  $I$  is the ionization potential and  $A$  is the electron affinity of an atom or molecule. The ionization poten-

tial and the electron affinity can be approached by the frontier HOMO and LUMO energies as by  $E_{\text{HOMO}}$  and as by  $E_{\text{LUMO}}$  according to Koopmans theorem<sup>25</sup> and Kohn-Sham formalism<sup>26</sup> within the DFT, as a result, the electronic chemical potential can be expressed as:

$$\mu \cong \left( \frac{E_{\text{HOMO}} + E_{\text{LUMO}}}{2} \right) \quad (3)$$

Accordingly, the electronic chemical potential allows the establishment of the flux direction of the Global Electron Density Transfer<sup>27</sup> along in a polar reaction. Likewise, in a polar reaction having two molecules, such as A and B, with  $u_A < u_B$ , the electron density flux will occur from molecule B, which has the higher, towards molecule A, which has the lower. So, in such a reaction A will act as the electron-acceptor, whereas, B will act as the electron-donor, i.e., the nucleophile. The larger electronic chemical potential difference means global Electron Density Transfer presents a low polar character. Iopamidol molecule in solvent acts as a more electron acceptor molecule than in the gas phase. The chemical potential of the molecule was found to be increased as the dielectric constants of the solvents increased from the gas phase. The chemical potentials of the Iopamidol in chloroform, acetic acid, ethanol, DMF, DMSO, water are -4.64, -4.65, -4.67, -4.67, -4.67, -4.67 eV, respectively.

Pearson proposed the hard and soft acids and bases (HSAB) principle in an acid/base reaction.

In 1963, Pearson established a classification of Lewis acids and bases into hard and soft.<sup>28–30</sup> Within the conceptual DFT, Parr defined, in 1983, a quantitative expression for the chemical hardness, which can be expressed as the changes of the electronic chemical potential of the system with respect to the electron number  $N$  at a fixed external potential  $v(r)$ .<sup>18</sup>

$$\eta = \left( \frac{\partial \mu}{\partial^2 N} \right)_{v(r)} = \left( \frac{\partial^2 E}{\partial^2 N} \right)_{v(r)} \quad (4)$$

The resistance of a molecule to exchange electron density with the environment is defined as the chemical hardness and when the finite difference approximation is applied, the following simple expression is obtained:

$$\eta \approx -\frac{(I-A)}{2} \quad (5)$$

With the substitution of I by  $E_{\text{HOMO}}$  and A by  $E_{\text{LUMO}}$  can be expressed as:

$$\eta \cong \left( \frac{E_{\text{LUMO}} + E_{\text{HOMO}}}{2} \right) \quad (6)$$

Also the chemical hardness, chemical potential of the molecule was found to be increased, the chemical softness of the molecule was found to be decreased as the dielectric constants of the solvents increased from gas phase to water and was confirmed to decrease as the dielectric constant of the solvents increased from ethanol to water.

According to Parr and co-workers, global molecular electrophilicity ( $\omega_{\text{mol}}$ ) and global molecular nucleophilicity ( $\epsilon_{\text{mol}}$ ) index were defined and they were calculated based on molecular hardness and molecular electronegativity of the studied compounds with the help of the following equations, respectively.

$$\omega = \frac{\mu^2}{2\eta} \quad (7)$$

The electrophilicity index measures the property of a molecule to accept electrons. Nucleophile molecule is characterized by a lower value of  $\mu$ ,  $\omega$ ; and conversely electrophile molecule is characterized by a high value of  $\mu$ ,  $\omega$ . Organic molecules having a value of more than 1.5 is classified as strong electrophiles, the value between 0.8 and 1.5 eV is classified as moderate electrophiles, smaller than 0.8 eV is said as marginal electrophiles.<sup>31</sup> Terrier classified high reactivity of the species that he studied as super electrophiles.<sup>32</sup> So, the electrophilicity index of Iopamidol in the gas phase and different solvents of more than 1.5 eV is classified as super electrophilic. The electrophilicity index of Iopamidol increases with the increase of the dielectric constant of the solvent.

The maximum number of electrons that an electrophile can obtain is given by the following formula.<sup>33</sup>

$$\Delta N_{\text{max}} = -\frac{\mu}{\eta} \quad (8)$$

The maximum charge transfer that is completely determined by the electronic chemical potential of the molecule measures the stabilization in energy when the system acquires an additional electronic charge ( $\Delta N$ ) from the environment.<sup>34–36</sup> The maximum charge transfer  $\Delta N_{\text{max}}$  to the electrophile means the ability of the system to obtain additional electronic charge from the medium defining the charge capacity of the molecule.

The maximum amount of electronic charge ( $\Delta N_{\text{max}}$ ) can define the donor and acceptor electron charge of molecules. The  $\Delta N_{\text{max}} < 0$  indicates the molecule acts as an

electron donor.<sup>37</sup> In gas and solvent phase, Iopamidol are electron acceptors and can have significant power of electron affinity. The  $\Delta N_{\text{max}}$  index of Iopamidol increases as follow: gas < chloroform < acetic acid < ethanol = DMF = DMSO < water at the B3LYP/ LANL2DZ basis set. According to these results, it can be easily predicted that Iopamidol has the biggest  $\Delta N_{\text{max}}$  in water for the studied solvents.

Ayers and co-workers<sup>38,39</sup> have proposed nucleophilic and electrophilic capabilities of a leaving group as nucleofugality ( $\Delta E_n$ ) and electrofugality ( $\Delta E_e$ ) and defined as follows:

$$\Delta E_n = EA + \omega = \frac{(\mu + \eta)^2}{2\eta} \quad (9)$$

$$\Delta E_e = IP + \omega = \frac{(\mu - \eta)^2}{2\eta} \quad (10)$$

Electrofugality values of Iopamidol in gas chloroform, acetic acid, ethanol, DMF, DMSO and water are 10.03, 10.35, 10.37, 10.43, 10.43, 10.44, 10.44, respectively. As seen from the result electrophilic capabilities of a leaving group for Iopamidol are the highest in the water phase.

The electronic transitions of Iopamidol were calculated by time-dependent DFT in the gas phase Theoretical results were used for the interpretation of experimental absorption bands. The experimental ( $\lambda_{\text{max}}$ ) and calculated ( $\lambda_{\text{DFT}}$ ) wavelengths of maximum absorption are 241nm<sup>40</sup> and 242.11 nm which was marked as HOMO-15→LUMO, HOMO-11→LUMO+1, HOMO-10→LUMO+1, HOMO-7→LUMO+1, HOMO-6→LUMO+1, HOMO-6→LUMO+2, HOMO-5→LUMO+1, HOMO-2→LUMO+2, HOMO-2→LUMO+4, HOMO-1→LUMO+5, HOMO→LUMO+1, HOMO-1→LUMO+4 transitions which contributions are -0.20018, 0.17061, 0.14008, -0.12374, 0.19838, 0.25823, 0.21063, -0.11627, 0.18419, -0.17126, -0.12012, 0.12035.

Electric dipole polarizability which is a measure of the linear response of an infinitesimal electric field (F) and represents second-order variation energy is an important property used in determining the polarizability of a molecule or compound.<sup>41</sup>

$$\alpha = -\frac{\partial^2 E}{\partial F_a \partial F_b} \quad (11)$$

Where, the  $\alpha_{xx}$ ,  $\alpha_{yy}$  and  $\alpha_{zz}$  quantities are the principal values of polarizability tensor. Polarizability ( $\alpha$ ) which is the measure of distortion of a molecule in an electric field, the anisotropy of the polarizability  $\langle \Delta \alpha \rangle$  and Kappa were calculated using the following equation, respectively:

$$\alpha = \frac{1}{3}(\alpha_{xx} + \alpha_{yy} + \alpha_{zz}) \quad (12)$$

$$\Delta\alpha = \left[ \frac{(\alpha_{xx} - \alpha_{yy})^2 + (\alpha_{yy} - \alpha_{zz})^2 + (\alpha_{zz} - \alpha_{xx})^2 + 6(\alpha_{xz}^2 + \alpha_{xy}^2 + \alpha_{yz}^2)}{2} \right]^{1/2} \quad (13)$$

$$\kappa = \frac{\alpha_{xx}^2 + \alpha_{yy}^2 + \alpha_{zz}^2}{6\langle\alpha\rangle^2} \quad (14)$$

In unsubstituted aromatic molecules, the  $\pi$  electrons in a direction perpendicular to the plane do not contribute to the polarizability in a direction perpendicular to the plane, only sigma bonds in the vertical direction contribute to the polarization of the molecules. Since the anisotropy  $j$  becomes zero for the spherical symmetric charge distribution, it gives a measure of the spherical symmetry deviations. The calculated polarizability  $\langle\alpha\rangle$ , the anisotropy of the polarizability  $\langle\Delta\alpha\rangle$  and Kappa for Iopamidol molecules are listed in Table 2.

The variation of  $\langle\alpha\rangle$  is in the atomic units and  $\langle\Delta\alpha\rangle$  in esu ( $\times 10^{-24}$ ) for Iopamidol molecule are given. The result shows that the lowest polarizability and anisotropic polarizability values obtained were 296 au and  $21.77 \times 10^{-24}$  esu in the gas phase. It was observed that polarizability and anisotropic polarizability increases with an increase in the polarity of the solvents while the kappa decreases as the polarity of the solvents increases.

$$\begin{aligned} \beta_{tot} &= (\beta_x^2 + \beta_y^2 + \beta_z^2)^{1/2} \\ \beta_x &= \beta_{xxx} + \beta_{xyy} + \beta_{xzz} \\ \beta_y &= \beta_{yyy} + \beta_{xxy} + \beta_{yzz} \\ \beta_z &= \beta_{zzz} + \beta_{xxz} + \beta_{yyz} \end{aligned} \quad (15)$$

The  $\beta_x$ ,  $\beta_y$ , and  $\beta_z$  refer to the components of hyperpolarizability along  $x$ ,  $y$  and  $z$  components of molecular dipole moment.

It can be seen from Table 3, the calculated  $\beta$  values of Iopamidol using B3LYP/ LANL2DZ level (the  $\beta$  of Iopamidol for gas, chloroform, acetic acid, ethanol, DMF,

DMSO, water) are  $1.48 \times 10^{-30}$  esu.,  $2.55 \times 10^{-30}$  esu.,  $2.69 \times 10^{-30}$  esu.,  $1.87 \times 10^{-30}$  esu.,  $3.04 \times 10^{-30}$  esu.,  $3.06 \times 10^{-30}$  esu.,  $2.94 \times 10^{-30}$  esu., respectively. The first polarizability values obtained using B3LYP/LANL2DZ level for Iopamidol are the largest value in DMSO and the lowest value in gas phase.

## 4. Thermodynamic Properties

The total contribution of the electronic, translational, rotational and vibrational energies to the entropy (S) and heat capacity (Cv), as well as the rotational constants and zero-point vibrational energies (ZPVE) of Iopamidol in the gas phase and different solvents were presented in Table 4.

It can be observed in Table 4 that the specific heat capacity of Iopamidol was found to increase with an increase in the polarity of the solvent except in acetic acid solution. The highest entropy value of 240.311 cal/mol was found in the gas phase followed by 235.989, 235.189, 234.749 cal/mol in chloroform, acetic acid, ethanol solution. It was observed that as the dielectric constant of the solvents was increased from chloroform to water the entropy was found to be slightly decreased, while, entropy was found to increase slightly in DMF, DMSO, water. The zero-point vibrational energy (ZPVE) decreases except in acetic acid solution with the increase of dielectric constant.

Based on vibrational analysis at B3LYP/LANL2DZ level, the standard statistical thermodynamic functions: heat capacity ( $C^0_{P,m}$ ), entropy ( $S^0_m$ ), and enthalpy changes ( $H^0_m$ ),

for the Iopamidol, are obtained from the theoretical harmonic frequencies in gas and solvent phases and presented in Figure 3. It can be observed that these thermodynamic functions are increasing with temperature ranging from 200 to 1000 K because molecular vibrational intensities increase with temperature.<sup>42</sup>

Table 5, demonstrates the correlation of heat capacity at constant pressure, entropy, enthalpy respectively, for

**Table 2.** Polarizability ( $\langle\alpha\rangle$ ), anisotropic polarizability ( $\Delta\alpha$ ), Kappa ( $\kappa$ ) of the optimized Iopamidol molecule in the gas phase and different solvents.

Polarisibility	Gas	Chloroform	Acetic acid	Ethanol	DMF	DMSO	Water
$\langle\alpha\rangle$ (au)	296	365	371	386	387	388	389
$\langle\Delta\alpha\rangle$ (esu) $10^{-24}$	21.77	25.64	25.95	26.69	26.78	26.82	26.88
$\kappa$	0.02646	0.02341	0.02315	0.02254	0.02247	0.02244	0.0224

**Table 3.**  $\beta \times 10^{-30}$  (esu),  $\beta_x$ ,  $\beta_y$ ,  $\beta_z$ , in (a.u.) components and values calculated using DFT levels of theory for Iopamidol.

	Gas	Chloroform	Acetic Acid	Ethanol	DMF	DMSO	Water
$\beta_x$	76.7636	173.4901	177.5463	184.9257	185.4881	185.5127	83.0876
$\beta_y$	-87.2752	-224.2531	-240.4815	71.3396	-286.2781	-288.0864	273.9023
$\beta_z$	57.6274	83.6470	85.2293	88.1287	88.4319	88.5943	184.1473
$\beta_{total}^2$	1.48	2.55	2.69	1.87	3.04	3.06	2.94

**Table 4.** Thermodynamic properties of the optimized Iopamidol molecule in the gas phase and different solvents.

Positions	Vibrational Cv	Total	Rotational S	Vibrational	Total
Gas	117.731	123.692	38.531	155.952	240.311
Chloroform	117.758	123.720	38.536	151.624	235.989
Acetic acid	117.751	123.713	38.536	150.823	235.189
Ethanol	117.760	123.722	38.536	150.384	234.749
DMF	117.764	123.726	38.536	150.414	234.779
DMSO	117.766	123.728	38.536	150.426	234.791
Water	117.769	123.731	38.536	150.453	234.818
	Rotational Constants (GHz)			ZPVE (Kcal/Mol)	
Gas	0.08199	0.06561	0.04052	249.87778	
Chloroform	0.08118	0.06626	0.04031	249.85006	
Acetic acid	0.08114	0.06629	0.04030	249.86599	
Ethanol	0.08109	0.06635	0.04029	249.84713	
DMF	0.08109	0.06636	0.04029	249.84051	
DMSO	0.08109	0.06636	0.04029	249.83742	
Water	0.08108	0.06637	0.04029	249.83212	

For Cv Electronic: 0.000, Translational: 2.981, Rotational: 2.981 For S Electronic: 0.000, Translational: 45.829

**Table 5.** Correlation of heat capacity, entropy and enthalpy with temperature for Iopamidol molecule

Iopamidol			
Gas	$C = -0.0002T^2 + 0.3841T + 28.257$ $R^2 = 0.9996$	$S = -0.0001T^2 + 0.5054T + 106.3$ $R^2 = 0.9997$	$H = 9E-05T^2 + 0.0865T - 9.6639$ $R^2 = 0.9998$
Chloroform	$C = -0.0002T^2 + 0.3846T + 28.184$ $R^2 = 0.9996$	$S = -0.0001T^2 + 0.5085T + 101.17$ $R^2 = 0.9999$	$H = 9E-05T^2 + 0.0866T - 9.7776$ $R^2 = 0.9998$
Acetic acid	$C = -0.0001T^2 + 0.3412T + 41.995$ $R^2 = 0.996$	$S = -9E-05T^2 + 0.44T + 122.2$ $R^2 = 0.9977$	$H = 0.0001T^2 + 0.0712T - 4.8992$ $R^2 = 0.999$
Ethanol	$C = -0.0002T^2 + 0.362T + 31.162$ $R^2 = 0.9997$	$S = -0.0001T^2 + 0.4743T + 105.21$ $R^2 = 0.9999$	$H = 6E-05T^2 + 0.1283T - 14.295$ $R^2 = 0.999$
DMF	$C = -0.0002T^2 + 0.3847T + 28.152$ $R^2 = 0.9996$	$S = -0.0001T^2 + 0.5086T + 99.937$ $R^2 = 0.9999$	$H = 9E-05T^2 + 0.0867T - 9.8173$ $R^2 = 0.9998$
DMSO	$C = -0.0002T^2 + 0.4077T + 19.679$ $R^2 = 0.9988$	$S = -0.0001T^2 + 0.5129T + 98.095$ $R^2 = 0.9999$	$H = 8E-05T^2 + 0.1063T - 14.192$ $R^2 = 0.9997$
Water	$C = -0.0002T^2 + 0.3917T + 26.68$ $R^2 = 0.9997$	$S = -0.0001 T^2 + 0.5086 T + 99.973$ $R^2 = 0.9999$	$H = 9E-05T^2 + 0.0828T - 9.2518$ $R^2 = 0.9998$

the methods of DFT/LANL2DZ level. The correlation equations between heat capacities, entropies, enthalpy changes and temperatures were fitted by quadratic formulas, and the corresponding fitting factors ( $R^2$ ) for these thermodynamic properties are 0.9996, 0.9997, and 0.9998 respectively for gas-phase; 0.9996, 0.9999, 0.9998 respectively for chloroform. All the thermodynamic data supply helpful information for further study on the Iopamidol. All thermodynamic calculations were done in the gas phase in solution such as chloroform, acetic acid, ethanol, DMF, DMSO, water.

The net atomic charges of the Iopamidol contrast agent in various solvents using the Mulliken Population Analysis (MPA) method were given in Table 6. MPA values in different solvents were evidence of charge transfer and polarization.<sup>43</sup> The significant influences of the sol-

vents on the atomic charges are observed from the calculation. As seen from Table 6, the atomic charges increase with the increase of solvent polarity from acetone to water.

All carbon atoms making a bond with iodine atom in the benzene ring have a negative charge and the negative charge of the carbon atom bonded iodine atom increase with the increase of polarity of the solvent. The charge of C<sub>19</sub> atom of Iopamidol in gas, chloroform, acetic acid, ethanol, DMF, DMSO, and water phases is  $-0.7531$ ,  $-0.7667$ ,  $-0.7680$ ,  $-0.7711$ ,  $-0.7715$ ,  $-0.7717$ ,  $-0.7719$  e<sup>-</sup>. The rest of the carbon atoms in the benzene ring have positive excess charges accumulation and the positive charge of the carbon atom in the benzene ring increase with the increase of polarity of the solvent. The charges of nitrogen atoms are the negative and negative value of the charge decreases with the increase of polarity of the solvent. The charge of



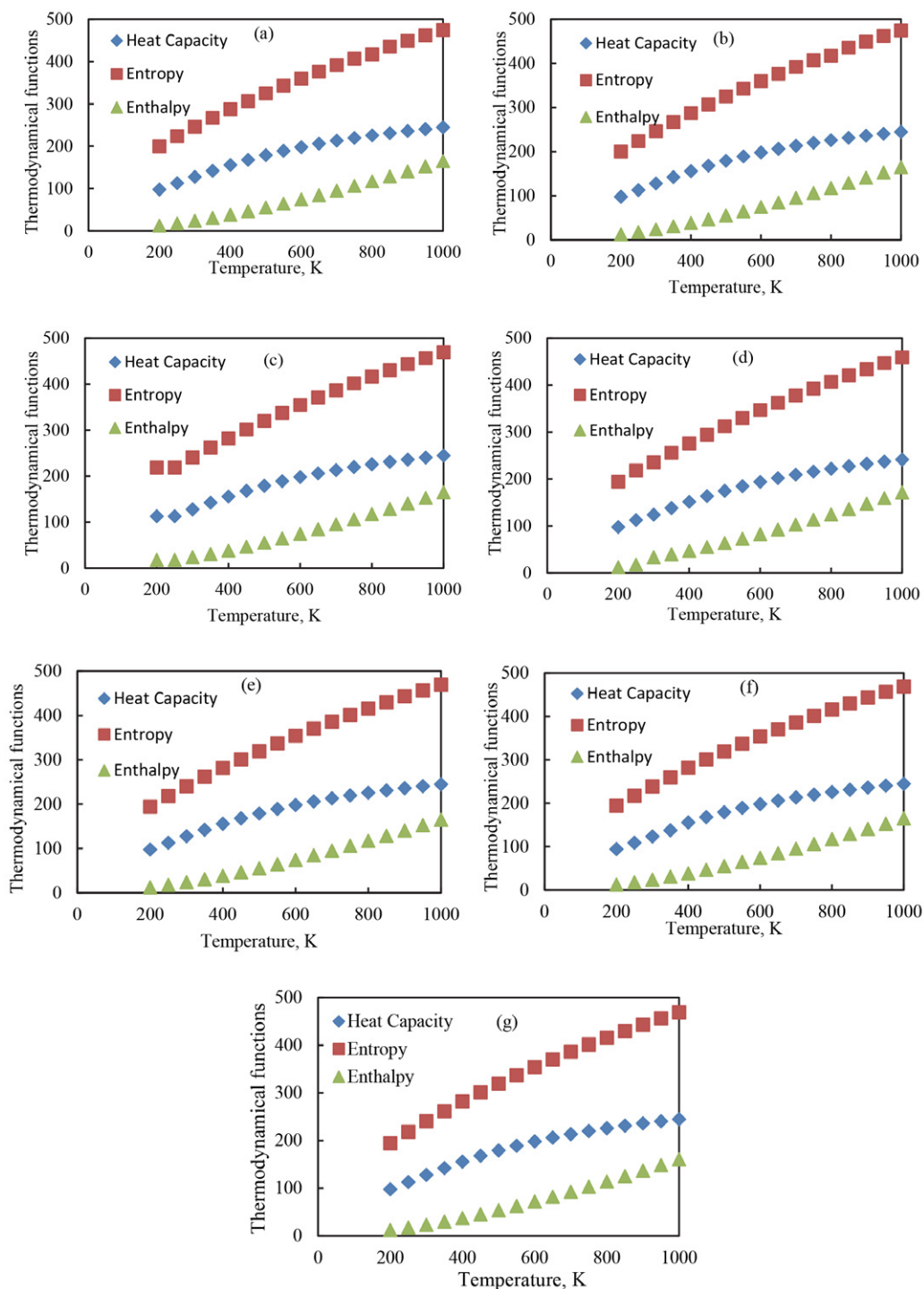


Figure 3. Correlation graph of heat capacity, entropy and enthalpy with temperature for Iopamidol molecule

$N_{12}$  atom of Iopamidol in gas, chloroform, acetic acid, ethanol, DMF, DMSO, and the water phase is  $-0.3366$ ,  $-0.3298$ ,  $-0.3293$ ,  $-0.3280$ ,  $-0.3278$ ,  $-0.3278$ ,  $-0.3277$   $\bar{e}$ . The charge of  $N_{13}$  atom is  $-0.3473$ ,  $-0.3406$ ,  $-0.3397$ ,  $-0.3376$ ,  $-0.3373$ ,  $-0.3372$ ,  $-0.3371$   $\bar{e}$ . All oxygen atoms belonging to the hydroxyl group and carbonyl group for Iopamidol have negative charge, and the negative charge

of both oxygen atoms increases with the increase of polarity of the solvent.

Selected second-order perturbation energies ( $E(2)$  kcal/mol) with values greater than 5 kcal/mol

for Iopamidol in gas phase were presented in Table 7, and Table 8 includes only energies for the other studied solvents and gas phase. The energies for the interaction

Table 6. Some Mulliken Atomic charges (e) of Iopamidol in various solvents.

	Gas	Chloroform	Acetic acid	Ethanol	DMF	DMSO	Water
I <sub>1</sub>	0.1672	0.1899	0.1919	0.1970	0.1976	0.1978	0.1982
I <sub>2</sub>	0.1792	0.1868	0.1878	0.1904	0.1907	0.1909	0.1911
I <sub>3</sub>	0.1704	0.1910	0.1927	0.1967	0.1972	0.1974	0.1977
O <sub>4</sub>	-0.5147	-0.5337	-0.5353	-0.5390	-0.5394	-0.5396	-0.5398
O <sub>5</sub>	-0.4972	-0.5264	-0.5290	-0.5352	-0.5359	-0.5363	-0.5367
O <sub>6</sub>	-0.4761	-0.5177	-0.5210	-0.5290	-0.5299	-0.5303	-0.5309
O <sub>7</sub>	-0.5135	-0.5409	-0.5428	-0.5473	-0.5479	-0.5481	-0.5484
O <sub>8</sub>	-0.3082	-0.3494	-0.3529	-0.3616	-0.3626	-0.3630	-0.3636
O <sub>9</sub>	-0.2577	-0.3129	-0.3176	-0.3290	-0.3303	-0.3309	-0.3317
O <sub>10</sub>	-0.5047	-0.5291	-0.5307	-0.5343	-0.5347	-0.5348	-0.5351
O <sub>11</sub>	-0.2612	-0.3174	-0.3220	-0.3330	-0.3343	-0.3349	-0.3357
N <sub>12</sub>	-0.3366	-0.3298	-0.3293	-0.3280	-0.3278	-0.3278	-0.3277
N <sub>13</sub>	-0.3473	-0.3406	-0.3397	-0.3376	-0.3373	-0.3372	-0.3371
N <sub>14</sub>	-0.5198	-0.5101	-0.5092	-0.5068	-0.5065	-0.5064	-0.5062
C <sub>17</sub>	0.5775	0.5957	0.5971	0.6001	0.6004	0.6005	0.6007
C <sub>18</sub>	0.5511	0.5666	0.5679	0.5710	0.5714	0.5715	0.5718
C <sub>19</sub>	-0.7531	-0.7667	-0.7680	-0.7711	-0.7715	-0.7717	-0.7719
C <sub>20</sub>	0.8067	0.8134	0.8139	0.8153	0.8155	0.8155	0.8156
C <sub>21</sub>	-0.7098	-0.7287	-0.7303	-0.7343	-0.7348	-0.7350	-0.7353
C <sub>22</sub>	-0.7149	-0.7283	-0.7296	-0.7325	-0.7328	-0.7330	-0.7332

Table 7. Selected second-order perturbation energy (E(2) kcal/mol) with values greater than 10 kcal/mol (except for iodine interaction) for Iopamidol in gas phase.

Donor (i)	Type	Occupancy	ED(j)	Acceptor	Type	Occupancy	ED(j)	E(2) kcal/mol	E(j)-E(i) a.u.	F(i,j) a.u.
C <sub>17</sub> -C <sub>22</sub>	π	1.67185	-0.74673	C <sub>18</sub> -C <sub>19</sub>	π*	0.39117	-0.00725	18.95	0.29	0.067
C <sub>17</sub> -C <sub>22</sub>	π	1.67185	-0.74673	C <sub>20</sub> -C <sub>21</sub>	π*	0.39095	-0.00959	22.39	0.29	0.073
C <sub>18</sub> -C <sub>19</sub>	π	1.67060	-0.29565	C <sub>17</sub> -C <sub>22</sub>	π*	0.39611	-0.00844	23.39	0.29	0.074
C <sub>18</sub> -C <sub>19</sub>	π	1.67060	-0.29565	C <sub>20</sub> -C <sub>21</sub>	π*	0.39095	-0.00959	19.16	0.29	0.067
C <sub>20</sub> -C <sub>21</sub>	π	1.65835	-0.29446	C <sub>17</sub> -C <sub>22</sub>	π*	0.39611	-0.00844	19.73	0.29	0.068
C <sub>20</sub> -C <sub>21</sub>	π	1.65835	-0.29446	C <sub>18</sub> -C <sub>19</sub>	π*	0.39117	-0.00725	23.60	0.29	0.074
I <sub>1</sub>	LP3	1.94231	-0.27742	C <sub>18</sub> -C <sub>19</sub>	π*	0.39117	-0.00725	7.31	0.27	0.043
I <sub>2</sub>	LP3	1.93293	-0.26730	C <sub>20</sub> -C <sub>21</sub>	π*	0.39095	-0.00959	7.83	0.26	0.044
I <sub>3</sub>	LP3	1.93545	-0.27219	C <sub>17</sub> -C <sub>22</sub>	π*	0.39611	-0.00844	7.81	0.26	0.044
O <sub>8</sub>	LP2	1.86415	-0.29057	N <sub>12</sub> -C <sub>23</sub>	σ*	0.06954	0.42301	16.06	0.71	0.097
O <sub>8</sub>	LP2	1.86415	-0.29057	C <sub>17</sub> -C <sub>23</sub>	σ*	0.06831	0.35615	18.75	0.65	0.100
O <sub>9</sub>	LP2	1.86542	-0.25360	N <sub>13</sub> -C <sub>24</sub>	σ*	0.07259	0.42608	21.11	0.68	0.109
O <sub>9</sub>	LP2	1.86542	-0.25360	C <sub>18</sub> -C <sub>24</sub>	σ*	0.07486	0.35976	19.38	0.61	0.099
O <sub>11</sub>	LP2	1.87731	-0.25037	N <sub>14</sub> -C <sub>29</sub>	σ*	0.07966	0.41160	23.83	0.66	0.113
O <sub>11</sub>	LP2	1.87731	-0.25037	C <sub>29</sub> -C <sub>30</sub>	σ*	0.08219	0.33581	19.06	0.59	0.095
N <sub>12</sub>	LP1	1.65078	-0.27471	O <sub>8</sub> -C <sub>23</sub>	σ*	0.20853	0.18886	24.37	0.46	0.098
N <sub>12</sub>	LP1	1.65078	-0.27471	O <sub>8</sub> -C <sub>23</sub>	π*	0.17216	0.23265	12.69	0.51	0.075
N <sub>13</sub>	LP1	1.66817	-0.26134	O <sub>9</sub> -C <sub>24</sub>	σ*	0.25871	0.09976	39.60	0.36	0.109
N <sub>14</sub>	LP1	1.66817	-0.26134	O <sub>11</sub> -C <sub>29</sub>	π*	0.21432	0.10625	33.67	0.38	0.103

LP3(I<sub>1</sub>) → π\*(C<sub>18</sub>-C<sub>19</sub>), LP3(I<sub>2</sub>) → π\*(C<sub>20</sub>-C<sub>21</sub>) and LP3(I<sub>3</sub>) → π\*(C<sub>17</sub>-C<sub>22</sub>) 7.31, 7.83 and 7.81 kcal mol<sup>-1</sup>, respectively demonstrate the intramolecular hyperconjugative interaction between the iodine atoms and benzene ring in the ground state for Iopamidol in gas phase.

The interaction energy from the I<sub>1</sub> electron pairs corresponds to conjugation with the antibonding molecular orbitals of the neighboring C<sub>20</sub>-C<sub>21</sub> whereas, these interac-

tion energies correspond to conjugation with the antibonding molecular orbitals of the neighboring LP3(I<sub>1</sub>) → π\*(C<sub>17</sub>-C<sub>19</sub>) with the stabilization energy 7.41, 7.42, 7.43 kcal/mol in chloroform, acetic acid, and ethanol, respectively, and 7.44 kcal/mol in DMF, DMSO, water. The interaction LP3(I<sub>2</sub>) → π\*(C<sub>20</sub>-C<sub>21</sub>) in gas phase shifted to LP3(I<sub>2</sub>) → π\*(C<sub>18</sub>-C<sub>21</sub>) in studied solvents and LP3(I<sub>3</sub>) → π\*(C<sub>17</sub>-C<sub>22</sub>) was shifted to LP3(I<sub>3</sub>) → π\*(C<sub>20</sub>-C<sub>22</sub>) in studied solvents.

Table 8. Interaction energies of Iopamidol in gas phase and in different solvents.

Donor	Type	Acceptor	Type	Gas E(2) kcal/mol	Chloroform	Acetic Acid	Ethanol	DMF	DMSO	Water
I <sub>1</sub> -C <sub>19</sub>	σ	C <sub>17</sub> -C <sub>22</sub>	σ*	7.06	7.10	7.11	7.12	7.12	7.12	7.12
I <sub>1</sub> -C <sub>19</sub>	σ	C <sub>18</sub> -C <sub>21</sub>	σ*	7.07	7.05	7.05	7.06	7.06	7.06	7.06
I <sub>2</sub> -C <sub>21</sub>	σ	C <sub>18</sub> -C <sub>19</sub>	σ*	7.15	7.16	7.16	7.16	7.17	7.17	7.17
I <sub>2</sub> -C <sub>21</sub>	σ	C <sub>20</sub> -C <sub>22</sub>	σ*	7.12	7.19	7.19	7.21	7.21	7.21	7.21
I <sub>3</sub> -C <sub>22</sub>	σ	C <sub>17</sub> -C <sub>19</sub>	σ*	7.11	7.17	7.39	7.19	7.19	7.19	7.19
I <sub>3</sub> -C <sub>22</sub>	σ	C <sub>20</sub> -C <sub>21</sub>	σ*	7.13	7.21	7.22	7.23	7.24	7.24	7.24
C <sub>17</sub> -C <sub>19</sub>	π	C <sub>18</sub> -C <sub>21</sub>	π*		22.60	22.58	22.53	22.53	22.53	22.52
C <sub>17</sub> -C <sub>19</sub>	π	C <sub>20</sub> -C <sub>22</sub>	π*		19.17	19.17	19.17	19.17	19.17	19.17
C <sub>17</sub> -C <sub>22</sub>	π	C <sub>18</sub> -C <sub>19</sub>	π*	18.95						
C <sub>17</sub> -C <sub>22</sub>	π	C <sub>20</sub> -C <sub>21</sub>	π*	22.39						
C <sub>18</sub> -C <sub>19</sub>	π	C <sub>17</sub> -C <sub>22</sub>	π*	23.39						
C <sub>18</sub> -C <sub>19</sub>	π	C <sub>20</sub> -C <sub>21</sub>	π*	19.16						
C <sub>18</sub> -C <sub>21</sub>	π	C <sub>17</sub> -C <sub>19</sub>	π*		19.64	19.64	19.63	19.63	19.63	19.63
C <sub>18</sub> -C <sub>21</sub>	π	C <sub>20</sub> -C <sub>22</sub>	π*		22.71	22.67	22.60	22.59	22.59	22.58
C <sub>18</sub> -C <sub>24</sub>	σ	N <sub>13</sub> -C <sub>16</sub>	σ*		6.25	6.26	6.29	6.30	6.30	6.30
C <sub>20</sub> -C <sub>21</sub>	π	C <sub>17</sub> -C <sub>22</sub>	π*	19.73						
C <sub>20</sub> -C <sub>21</sub>	π	C <sub>17</sub> -C <sub>19</sub>	π*	23.60		23.53	23.53	23.53	23.53	23.53
C <sub>20</sub> -C <sub>22</sub>	π	C <sub>18</sub> -C <sub>21</sub>	π*		23.53	19.52	19.61	19.62	19.62	19.63
C <sub>20</sub> -C <sub>22</sub>	π	C <sub>18</sub> -C <sub>19</sub>	π*		19.48					
I <sub>1</sub>	LP3	C <sub>17</sub> -C <sub>19</sub>	π*		7.41	7.42	7.43	7.44	7.44	7.44
I <sub>1</sub>	LP3	C <sub>18</sub> -C <sub>19</sub>	π*	7.31						
I <sub>2</sub>	LP3	C <sub>18</sub> -C <sub>21</sub>	π*		7.90	7.90	7.90	7.90	7.90	7.90
I <sub>2</sub>	LP3	C <sub>20</sub> -C <sub>21</sub>	π*	7.83						
I <sub>3</sub>	LP3	C <sub>17</sub> -C <sub>22</sub>	π*	7.81						
I <sub>3</sub>	LP3	C <sub>20</sub> -C <sub>22</sub>	π*		7.65	7.66	7.69	7.69	7.69	7.69
O <sub>8</sub>	LP2	O <sub>5</sub> -H <sub>47</sub>	σ*	9.35	14.20	14.52	15.38	15.48	15.52	15.59
O <sub>8</sub>	LP2	N <sub>12</sub> -C <sub>23</sub>	σ*	16.06	13.76	13.59	13.17	13.12	13.10	13.06
O <sub>8</sub>	LP2	C <sub>17</sub> -C <sub>23</sub>	σ*	18.75	18.21	18.14	17.97	17.95	17.94	17.93
O <sub>9</sub>	LP2	N <sub>13</sub> -C <sub>24</sub>	σ*	21.11	20.05	19.96	19.74	19.72	19.71	19.69
O <sub>9</sub>	LP2	C <sub>18</sub> -C <sub>24</sub>	σ*	19.38	18.35	18.26	18.05	18.03	18.02	18.00
O <sub>11</sub>	LP2	N <sub>14</sub> -C <sub>29</sub>	σ*	23.83	22.61	22.51	22.27	22.24	22.23	22.21
O <sub>11</sub>	LP2	C <sub>29</sub> -C <sub>30</sub>	σ*	19.06	18.02	17.93	17.72	17.70	17.69	17.67
N <sub>12</sub>	LP1	O <sub>8</sub> -C <sub>23</sub>	σ*	24.37	72.52	75.67	82.43	83.14	83.44	83.90
N <sub>12</sub>	LP1	O <sub>8</sub> -C <sub>23</sub>	π*	12.69						
N <sub>13</sub>	LP1	O <sub>9</sub> -C <sub>24</sub>	σ*	39.60	81.88	83.09	85.07	85.29	85.37	85.50
N <sub>14</sub>	LP1	O <sub>11</sub> -C <sub>29</sub>	σ*		15.95	17.47	21.64	22.15	22.37	22.73
N <sub>14</sub>	LP1	O <sub>11</sub> -C <sub>29</sub>	π*	33.67	16.10	14.84	12.02	11.73	11.61	11.41

The stabilization energy for the interaction LP1(O<sub>8</sub>) → σ\*(N<sub>12</sub>-C<sub>23</sub>) and LP2(O<sub>8</sub>) → σ\*(O<sub>5</sub>-H<sub>47</sub>) increases with the increase of the dielectric constant of the solvent whereas the stabilization energy for the interaction LP2(O<sub>8</sub>) → σ\*(N<sub>12</sub>-C<sub>23</sub>) and LP2(O<sub>8</sub>) → σ\*(C<sub>17</sub>-C<sub>23</sub>) decreases with the increase of the dielectric constant of the solvent.

## 5. Conclusions

The ground state molecular geometries, polarizability, anisotropic polarizability, hyperpolarizability, and frontier orbital energies of Iopamidol were theoretically investigated in gas, chloroform, acetic acid, ethanol, DMF, DMSO, and water phase to understand the structure–property relationship of the molecular structure of Iopamidol in terms of solvent effects.

From the obtained results by using the DFT calculations, it was obtained that the dipole moment, electrophilicity index, polarizability and first-order hyperpolarizability of Iopamidol was gradually increased with the increase of dielectric constant of the solvent.

Likewise, the largest HOMO-LUMO gap was found in water solvent and this means higher kinetic stability and less chemical reactivity with increasing polarity of solvents. Therefore, quantum chemical calculations aid the understanding of the structure–property relationship of molecules.

Solvent effects on thermodynamic properties of the optimized geometry of the molecule were investigated and reported. The variation of solvent influences the structural, electronic, and molecular properties of the Iopamidol and will be useful in the design and development of Iopamidol as a contrast agent.

The NBO analysis has provided a detailed in-sight into the type of hybridization and the nature of bonding in loperamide. The stabilization energy for the interaction  $LP1(O_8) \rightarrow \sigma^*(N_{12}-C_{23})$  increases with the increase of the dielectric constant of the solvent whereas the stabilization energy for the interaction  $LP2(O_8) \rightarrow \sigma^*(N_{12}-C_{23})$  decreases with the increase of the dielectric constant of the solvent. The negative charge of carbon atoms attached to the iodine atom in the benzene ring increase with the increase of polarity of the solvent. The rest of the carbon atoms in the benzene ring have positive and positive charge density with the increase of polarity of the solvent.

## 6. References

1. F. M. Wendel, C. L. Eversloh, E. J. Machek, S. E. Duirk, M. J. Plewa, S.D. Richardson, T.A. Ternes, *Environ. Sci. Technol.*, **2014**, *48*, 12689–12697. DOI:10.1021/es503609s
2. M. R. Karim, L. Balsam and S. Rubinstein, *Am. J. Kidney Dis.*, **2010**, *55*(4), 712–716. DOI:10.1053/j.ajkd.2009.08.016
3. H. Dib, K. Agan, I. Midi, C. A. Bingöl, *The Internet J. Neurol.*, **2008**, *11*(1), 1–3. DOI:10.5580/1a64
4. S. Aime, L. Calabi, L. Biondi, M. De Miranda, S. Ghelli, L. Paleari, C. Rebaudengo, E. Terreno, *Magn. Reson. Med.*, **2005**, *53*, 830–834. DOI:10.1002/mrm.20441
5. D. L. Longo, W. Dastru, G. Digilio, J. Keupp, S. Langereis, S. Lanzardo, S. Prestigio, O. Steinbach, E. Terreno, F. Uggeri, S. Aime, *Magn. Reson. Med.*, **2011**, *65*, 202–211. DOI:10.1002/mrm.22608
6. P. L. Praveen, D. P. Ojha, *Cryst. Res. Technol.*, **2012**, *47*, 91–100. DOI:10.1002/crat.201100481
7. M. F. Khan, R. B. Rashid, S. M. Islam, M. A. Rashid, *SQU. J. Sci.*, **2016**, *21*, 89–101. DOI:10.24200/squjs.vol21iss2pp89-101
8. M. Targema, N. O. Obi-Egbedi, M. D. Adeoye, *Comput. Theor. Chem.*, **2013**, *1012*, 47–53. DOI:10.1016/j.comptc.2013.02.020
9. S. G. Zhang, W. Lei, M. Z. Xia, F. Y. Wang, *J. Mol. Struct. (THEOCHEM)*, **2005**, *732*, 173–182. DOI:10.1016/j.theochem.2005.02.091
10. B. Bellich, S. Di Fonzo, L. Tavagnacco, M. Paolantoni, C. Masciovecchio, F. Bertolotti, G. Giannini, R. De Zorzi, S. Geremia, A. Maiocchi, F. Uggeri, N. Masciocchi, A. Cesàro, *Mol. Pharmaceutics*, **2017**, *14*(2), 468–477. DOI:10.1021/acs.molpharmaceut.6b00902
11. P. Sun, G. Y. Yang, H. X. Liu, Z. Y. Wang, *J. Chem. Eng. Data*, **2009**, *54*, 2404–2410. DOI:10.1021/jc8008304
12. Y. Wang, X. L. Zeng, H. J. Chen, H. J. Wang, *J. Chem. Eng. Data*, **2007**, *52*, 1442–1448. DOI:10.1021/jc700127w
13. B. G. Johnson, P. M. W. Gill, J. A. Pople, *J. Chem. Phys.* **1993**, *98*(7), 5612–5626. DOI:10.1063/1.464906
14. N. C. Handy, C. W. Murray, R. D. Amos, *J. Phys. Chem.*, **1993**, *97*(17), 4392–4396. DOI:10.1021/j100119a023
15. X. F. Zhou, J. A. Krauser, D. R. Tate, A. S. Vanburen, *J. Phys. Chem.*, **1996**, *100*(42), 16822–16827. DOI:10.1021/jp960170r
16. M. J. Frisch, G. W. Trucks, H. B. Schlegel, G. E. Scuseria, M. A. Robb, J. R. Cheeseman, G. Scalmani, V. Barone, B. Mennucci, G. A. Petersson, H. Nakatsuji, M. Caricato, X. Li, H. P. Hratchian, A. F. Izmaylov, J. Bloino, G. Zheng, J. L. Sonnenberg, M. Hada, M. Ehara, K. Toyota, R. Fukuda, J. Hasegawa, M. Ishida, T. Nakajima, Y. Honda, O. Kitao, H. Nakai, T. Vreven, J. A. Montgomery, Jr. J. E. Peralta, F. Ogliaro, M. Bearpark, J. J. Heyd, E. Brothers, K. N. Kudin, V. N. Staroverov, R. Kobayashi, J. Normand, K. Raghavachari, A. Rendell, J. C. Burant, S. S. Iyengar, J. Tomasi, M. Cossi, N. Rega, J. M. Millam, M. Klene, J. E. Knox, J. B. Cross, V. Bakken, C. Adamo, J. Jaramillo, R. Gomperts, R. E. Stratmann, O. Yazyev, A. J. Austin, R. Cammi, C. Pomelli, J. W. Ochterski, R. L. Martin, K. Morokuma, V. G. Zakrzewski, G. A. Voth, P. Salvador, J. J. Dannenberg, S. Dapprich, A. D. Daniels, Ö. Farkas, J. B. Foresman, J. V. Ortiz, J. Cioslowski, D. J. Fox, *Gaussian Inc.*, Wallingford CT, **2009**.
17. T. H. Dunning Jr., P. J. Hay, in *Modern Theoretical Chemistry*, (Ed.): H. F. Schaefer III, Plenum, New York, **1977**, *3*, 1–28.
18. P. Macak, Solvent and vibrational effects on nonlinear optical properties; Ph.D. thesis, Royal Institute of Technology: Stockholm, **2002**.
19. I. Fleming, *Frontier orbitals and organic chemical reaction*. New York, NY: John Wiley and Sons, **1976**.
20. K. Fukui, *Science*, **1982**, *218*, 747–754. DOI:10.1126/science.218.4574.747
21. S. G. Kandemirli, F. Genç, F. Kandemirli, M. Evecen, *EJOSAT*, **2020**, *20*, 351–359. DOI:10.31590/ejosat.732239
22. T. Abbaz, A. Benjeddou, D. Villemin, *Pharm. Biol. Eval.*, **2018**, *5*(2), 27–39. DOI:10.26510/2394-0859.pbe.2018.04
23. R. G. Parr, R.G. Pearson, *J. Am. Chem. Soc.*, **1983**, *105*, 7512–7516. DOI:10.1021/ja00364a005
24. R. G. Parr, W. Yang, *Density functional theory of atoms and molecules*, Oxford University Press: New York, NY, USA, **1989**.
25. T. Koopmans, *Physica*, **1934**, *1*, 104–113. DOI:10.1016/S0031-8914(34)90011-2
26. W. Kohn, L.J. Sham, *Phys. Rev.*, **1965**, *140*, A1133–A1138. DOI:10.1103/PhysRev.140.A1133
27. L. R. Domingo, *RSC Adv.*, **2014**, *4*, 32415–32428. DOI:10.1039/C4RA04280H
28. R. G. Pearson, *J. Am. Chem. Soc.*, **1963**, *85*, 3533–3539. DOI:10.1021/ja00905a001
29. R. G. Pearson, *Science*, **1966**, *151*, 172–177. DOI:10.1126/science.151.3707.172
30. R. G. Pearson, J. Songstad, *J. Am. Chem. Soc.*, **1967**, *89*, 1827–1836. DOI:10.1021/ja00984a014
31. L. R. Domingo, M. J. Aurell, P. Pérez, R. Contreras, *Tetrahedron*, **2002**, *58*, 4417–4423. DOI:10.1016/S0040-4020(02)00410-6
32. Y. P. Semenyuk, P.G. Morozov, O.N. Burov, M. K. Kletskii, A. V. Lisovin, S. V. Kurbatov, F. Terrier, *Tetrahedron*, **2016**, *72*, 2254–2264. DOI:10.1016/j.tet.2016.03.024
33. R. G. Parr, L. von Szentpaly, S. Liu, *J. Am. Chem. Soc.*, **1999**, *121*, 1922–1924. DOI:10.1021/ja983494x

34. J. Padmanabhan, R. Parthasarathi, V. Subramaniaan, P. K. Chattaraj, *J. Phys. Chem.*, **2007**, *111*, 1358–1361. DOI:10.1021/jp0649549
35. R. G. Pearson, *J. Org. Chem.* **1989**, *54*, 1423–1430. DOI:10.1021/jo00267a034
36. R. G. Parr, W. Yang, *J. Am. Chem. Soc.*, **1984**, *106*, 404. DOI:10.1021/ja00326a036
37. R. Ahmadi, M. Pirahan-Foroush, *Ann. Mil. Health. Sci. Res. (AMHSR)*, **2014a**, *12(2)*, 86–90.
38. P. W. Ayers, J. S. M. Anderson, L. J. Bartolotti, *Int. J. Quantum Chem.*, **2005**, *101*, 520–534. DOI:10.1002/qua.20307
39. G. Roos, S. Loverix, E. Brosens, K. Van Belle, L. Wyns, P. Geerlings, J. Messens, *ChemBioChem.*, **2006**, *7*, 981–989. DOI:10.1002/cbic.200500507
40. M. Grandi, D. Pitre, *Biomed. Mass Spectrom.*, **1983**, *10(1)*, 17–23. DOI:10.1002/bms.1200100105
41. H. Abdulaziz, A. S. Gidado, A. Musa, A. Lawal, *J. Mater. Sci. Rev.*, **2019**, *2(3)*, 1–13. DOI: 10.9734/JMSRR/2019/45683.
42. M. Govindarajan, M. Karabacak, *Spectrochimica Acta Part A*, **2012**, *85*, 251–260. DOI:10.1016/j.saa.2011.10.002
43. R. S. J. Mulliken, *J. Chem. Phys.*, **1962**, *36*, 3428. termodinamske lastnosti v območju 200–1000.

## Povzetek

Neionske kontrastne snovi z nizko osmolalnostjo veljajo za varne pri intravenozni in intraarterialni aplikaciji. Iopamidol je eno od kontrastnih sredstev ki se uporablja za diagnostično računalniško tomografijo (CT) že štiri desetletja. Molekulsko strukturo Iopamidola smo izračunali s funkcionalnim modelom B3LYP in baznim setom LANL2DZ določenim z Gaussovimi programom. Analizo veznih orbital, hibridizacijo atomov in elektronsko strukturo molekule smo izvedli s podatki dobljenimi iz kvantno kemijskih izračunov. V članku podajamo vrednosti za hiperpolarizabilnost prvega reda ( $\beta_{tot}$ ), dipolni moment ( $\mu$ ), polarizabilnost ( $\alpha$ ) in anizotropno polarizabilnost ( $\Delta\alpha$ ) molekule. Energije HOMO in LUMO in parametri povezani z energijami, dipolnim momentom, polarizabilnostjo in hiperpolarizabilnostjo so le malo odvisni od polarnosti topila. Trdota Iopamidola se zmanjšuje z naraščanjem polarnosti topila. Analizirali smo stabilnost kontrastnega sredstva Iopamidol s hiperkonjugativnimi interakcijami in izračunali K.



Scientific paper

# Efficient and Facile Synthesis of Chromenopyrano[2,3-*b*]pyridine Derivatives Catalyzed by Sodium Carbonate

Raziyeh Keshavarz, Mahnaz Farahi\* and Bahador Karami

Department of Chemistry, Yasouj University, P. O. Box 353, Yasouj 75918-74831, Iran

\* Corresponding author: E-mail: farahimb@yu.ac.ir

Received: 07-09-2020

## Abstract

In this research, a number of new and known chromenopyrano[2,3-*b*]pyridine derivatives have been prepared. Initially, according to the reported procedure, pyrano[2,3-*c*]chromene derivatives were synthesized by the reaction between 4-hydroxycoumarin, aromatic aldehydes and malononitrile using silica sodium carbonate (SSC) as the catalyst. Next, the prepared pyrano[2,3-*c*]chromenes were reacted by dimethyl acetylenedicarboxylate (DMAD) or cyclohexanone in the presence of sodium carbonate to produce chromenopyrano[2,3-*b*]pyridine derivatives. The presented protocol avoids the use of expensive catalysts and gives useful potentially bioactive heterocycles in excellent to high yields.

**Keywords:** Chromenopyrano[2,3-*b*]pyridine; pyrano[2,3-*c*]chromene, dimethyl acetylenedicarboxylate, cyclohexanone

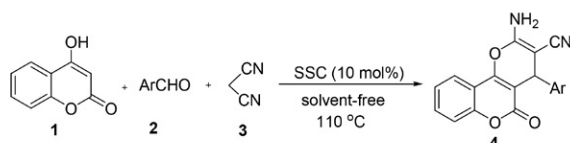
## 1. Introduction

Heterocycles as the most prevalent organic compounds are present in various drugs, natural products, vitamins and bioactive compounds.<sup>1–3</sup> They have been found to be useful as anti-HIV,<sup>4</sup> anti-tumor,<sup>5,6</sup> anti-inflammatory,<sup>7–9</sup> anti-malarial,<sup>10,11</sup> anti-depressant, anti-microbial, anti-bacterial and anti-fungal agents.<sup>12</sup> Most heterocycles are used in materials science such as fluorescent sensors, dyes, data storage, plastics, illuminators and analytical reagents.<sup>3,13</sup> Also, they are applied as important intermediates for the synthesis of medicinal compounds.<sup>14</sup> Nitrogen-containing six-membered heterocycles, due to their high biological activity are of interest to both medicinal chemists and biochemists.<sup>15,16</sup> Among them, pyridine and its derivatives play the most fundamental structural role in many natural compounds and medicinally beneficial molecules.<sup>17,18</sup> Owing to the great variety of biologically active pyridines, it is not surprising that the pyridine ring system has become a vital basic component in many pharmaceutical agents. Some of the pyridine-derived drugs are trademarks of Reyataz and Gleevec drugs that are prescribed for HIV and chronic anemia, respectively. Some natural alkaloid products based on pyridine are nicotine and niacin derivatives.<sup>19</sup> In particular, condensed pyridines are known for their several biological activities. For example, pyranopyridines have been proven to be the most active anti-tumor heterocyclic systems with activity

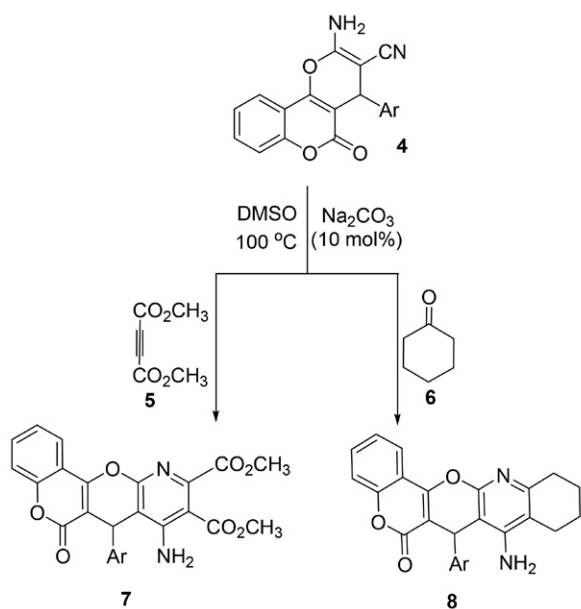
against various filamentous tumors and specific activity against lung and ovarian cancer cells and antimicrobial action.<sup>20,21</sup> Moreover, pyrazolo-[3,4-*b*]pyridine derivatives are an important class of fused pyridines with a broad spectrum of biological activities that find widespread use in the pharmaceutical industries.<sup>22</sup> Another class of fused pyridine derivatives is thiazolo[4,5-*b*]pyridin, which have anti-inflammatory and antimicrobial activity against human and veterinary pathogens. Also, some of these compounds have antifungal and anti-tumor activity.<sup>23,24</sup>

Coumarin-thiazole scaffolds are used as fluorescence probes for staining and imaging of DNA and to study the biological function of cell membranes.<sup>25,26</sup> Other compounds fused to the coumarin ring, such as pyranochromenes as the most imperative fused polycyclic heterocycles have gained attention for their extensive occurrence in important pharmaceutical drugs.<sup>27</sup> Many of pyranochromene derivatives exhibit significant biological activity, such as excellent antimicrobial potency, spasmolytic, anticoagulant, diuretic, cytotoxic, antituberculosis, anticancer, and antianaphylactic activities.<sup>28–30</sup> Some of these compounds have found the use for the treatment of neurodegenerative diseases, including Parkinson's disease, Down's syndrome, Alzheimer's disease and AIDS associated dementia.<sup>31</sup> Furthermore, pyranochromene derivatives have been applied as the key intermediates for the preparation of thioxo-imidazolidinedione, dithioxodiazetidone and Schiff's bases.<sup>32</sup>

Considering the above reports and in connection with our program on the synthesis of polycyclic compounds,<sup>33–40</sup> we present in this paper an efficient and environmentally benign strategy for the synthesis of pyranochromene fused with pyridine derivatives. For this purpose, initially, pyrano[2,3-*c*]chromenes were prepared *via* the reaction between 4-hydroxycumarin (1), aromatic aldehydes 2 and malononitrile (3) using silica sodium carbonate (SSC) (Scheme 1).<sup>28</sup> Subsequently, the synthesized pyrano[2,3-*c*]chromenes were reacted by dimethyl acetylenedicarboxylate (DMAD, 5) or cyclohexanone (6) to yield chromenopyrano[2,3-*b*]pyridine derivatives 7 and 8 (Scheme 2).



Scheme 1. SSC-catalyzed synthesis of pyranochromenes 4.

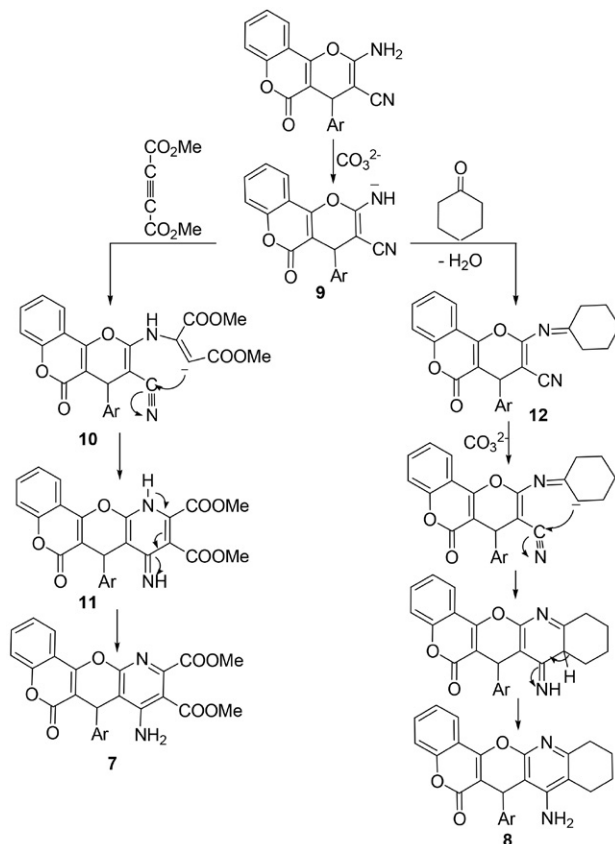


Scheme 2. Synthesis of chromenopyrano[2,3-*b*]pyridine derivatives 7 and 8 in the presence of Na<sub>2</sub>CO<sub>3</sub> as the catalyst.

## 2. Results and Discussion

First, pyrano[2,3-*c*]chromenes 4 were prepared and identified according to the mentioned method (Table 1). In the following, in order to optimize the conditions, the reaction between pyranochromene 4a and DMAD was selected as a model system. The reaction was not completed in the absence of a catalyst at room temperature. Next, the model reaction was performed in the presence of 5 mol% of Na<sub>2</sub>CO<sub>3</sub> in various solvents such as acetone, CH<sub>2</sub>Cl<sub>2</sub>, EtOAc, DMF and DMSO. As can be seen in Table 2, the best result

was obtained by performing the reaction mixture in DMSO (100 °C) to yield product 7a. Next, we evaluated the required amount of the catalyst for this transformation. When 10 mol% of Na<sub>2</sub>CO<sub>3</sub> was used, the reaction efficiently proceeded and was complete in shorter reaction time. By further increasing the catalyst amount no appreciable improvement in the product yield and reaction time was observed. Various bases were screened for their efficiency in this reaction. We obtained the best yield of 7a when the reaction was performed by Na<sub>2</sub>CO<sub>3</sub>. Also, low temperatures led to the reaction product in a very low yield. In short, according to the obtained results, the best yield was achieved in DMSO at 100 °C in the presence of 10 mol% of Na<sub>2</sub>CO<sub>3</sub> (Table 2, Entry 8). In view of the success of the above reaction and having established the optimal conditions, we then investigated the scope and general applicability of this methodology by using different pyranochromenes and the results are given in Table 3. The structures of the synthesized compounds 7 were deduced from their elemental analysis, IR, <sup>1</sup>H and <sup>13</sup>C NMR spectroscopy. Subsequently, by employing this method, a number of chromenopyrano[2,3-*b*]pyridines 8 were produced *via* the reaction between pyrano[2,3-*c*]chromenes 4 and cyclohexanone (6) under the optimized reaction conditions. In the majority of cases, the reactions performed cleanly and the desirable products 8 were formed in high



Scheme 3. Proposed mechanism for the synthesis of chromenopyrano[2,3-*b*]pyridines 7 and 8 using sodium carbonate.

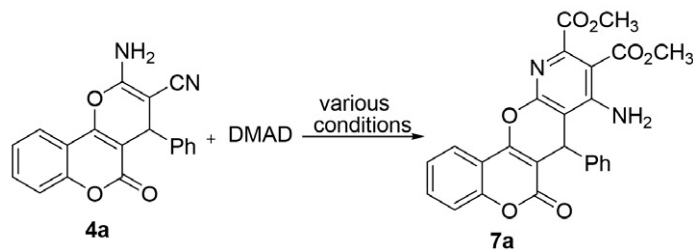
**Table 1.** Synthesis of pyrano[2,3-*c*]chromenes **4** using SSC catalyst.

**4a-k**

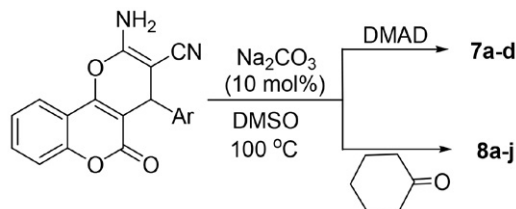
Entry	Ar	Product	Yield <sup>a</sup> (%)	Mp [Ref.] (°C)
4a	C <sub>6</sub> H <sub>5</sub>		83	260–262 [261–263] <sup>28</sup>
4b	4-Cl-C <sub>6</sub> H <sub>4</sub>		85	262–264 [262–264] <sup>28</sup>
4c	4-Br-C <sub>6</sub> H <sub>4</sub>		80	245–247 [247–249] <sup>41</sup>
4d	3-NO <sub>2</sub> -C <sub>6</sub> H <sub>4</sub>		85	264–265 [263–265] <sup>28</sup>
4e	4-NO <sub>2</sub> -C <sub>6</sub> H <sub>4</sub>		90	259–261 [260–262] <sup>28</sup>
4f	3-CH <sub>3</sub> -C <sub>6</sub> H <sub>4</sub>		90	255–257 <sup>b</sup>
4g	4-F-C <sub>6</sub> H <sub>4</sub>		93	258–260 [260–262] <sup>41</sup>
4h	3-CH <sub>3</sub> -C <sub>6</sub> H <sub>4</sub>		87	250–252 [255–257] <sup>28</sup>
4i	2-Cl-C <sub>6</sub> H <sub>4</sub>		85	271–272 [269–271] <sup>28</sup>
4j	4-OCH <sub>3</sub> -C <sub>6</sub> H <sub>4</sub>		80	243–245 [246–248] <sup>28</sup>
4k	2,4-Cl <sub>2</sub> -C <sub>6</sub> H <sub>3</sub>		83	259–260 [259–260] <sup>28</sup>

<sup>a</sup> Isolated yield.

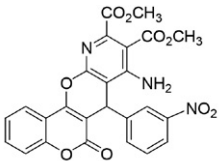
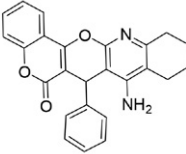
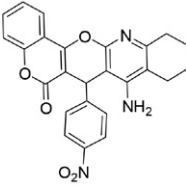
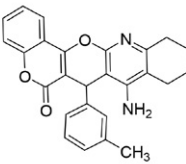
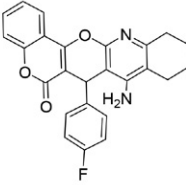
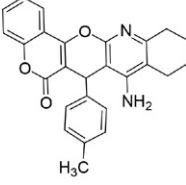
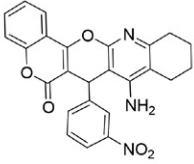
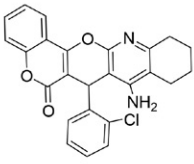
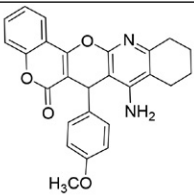


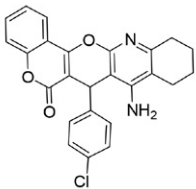
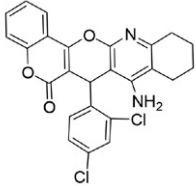
**Table 2.** Synthetic results of **7a** under different reaction conditions.

Entry	Catalyst (mol %)	Solvent/Temp. (°C)	Time (h)	Yield <sup>a</sup> (%)
1	None	None/25	24	5
2	Na <sub>2</sub> CO <sub>3</sub> (5)	EtOAc/reflux	5	40
3	Na <sub>2</sub> CO <sub>3</sub> (5)	DMSO/100	5	50
4	Na <sub>2</sub> CO <sub>3</sub> (5)	CH <sub>2</sub> Cl <sub>2</sub> /reflux	5	30
5	Na <sub>2</sub> CO <sub>3</sub> (5)	Acetone/reflux	5	40
6	Na <sub>2</sub> CO <sub>3</sub> (5)	DMF/100	5	30
7	Na <sub>2</sub> CO <sub>3</sub> (1)	DMSO/100	5	30
8	Na <sub>2</sub> CO <sub>3</sub> (10)	DMSO/100	4	80
9	Na <sub>2</sub> CO <sub>3</sub> (15)	DMSO/100	4	75
10	Piperidine (10)	DMSO/100	5	35
11	NaOH (10)	DMSO/100	5	42
12	KOH (10)	DMSO/100	5	45
13	Na <sub>2</sub> CO <sub>3</sub> (10)	DMSO/50	4	37
14	Na <sub>2</sub> CO <sub>3</sub> (10)	DMSO/70	4	50

<sup>a</sup> Isolated yield.**Table 3.** Synthesis of chromenopyrano[2,3-*b*]pyridine derivatives **7** and **8** in the presence of Na<sub>2</sub>CO<sub>3</sub> catalyst.

Entry	Ar	Product	Time (h)	Yield <sup>a</sup> (%)	Mp [Ref.] (°C)
7a	C <sub>6</sub> H <sub>5</sub>		4	80	decomp. >300 <sup>b</sup>
7b	4-Cl-C <sub>6</sub> H <sub>4</sub>		3	75	decomp. >300 <sup>b</sup>
7c	4-Br-C <sub>6</sub> H <sub>4</sub>		3	73	290–291 <sup>b</sup>

<b>7d</b>	3-NO <sub>2</sub> -C <sub>6</sub> H <sub>4</sub>		3.5	80	decomp. >300 <sup>b</sup>
<b>8a</b>	C <sub>6</sub> H <sub>5</sub>		7	85	267–269 [>260] <sup>42</sup>
<b>8b</b>	4-NO <sub>2</sub> -C <sub>6</sub> H <sub>4</sub>		6	82	270–272 <sup>b</sup>
<b>8c</b>	3-CH <sub>3</sub> -C <sub>6</sub> H <sub>4</sub>		7	75	269–271 <sup>b</sup>
<b>8d</b>	4-F-C <sub>6</sub> H <sub>4</sub>		8	70	decomp. >260 [>260] <sup>42</sup>
<b>8e</b>	4-CH <sub>3</sub> -C <sub>6</sub> H <sub>4</sub>		6	90	265–268 [>260] <sup>42</sup>
<b>8f</b>	3-NO <sub>2</sub> -C <sub>6</sub> H <sub>4</sub>		5	90	decomp. >260 [>260] <sup>42</sup>
<b>8g</b>	2-Cl-C <sub>6</sub> H <sub>4</sub>		5.5	80	259–261 [>260] <sup>42</sup>
<b>8h</b>	4-OCH <sub>3</sub> -C <sub>6</sub> H <sub>4</sub>		8	95	263–265 [>260] <sup>42</sup>

Entry	Ar	Product	Time (h)	Yield <sup>a</sup> (%)	Mp [Ref.] (°C)
8i	4-Cl-C <sub>6</sub> H <sub>4</sub>		4.5	93	261–263 [248–250] <sup>42</sup>
8j	2,4-Cl <sub>2</sub> -C <sub>6</sub> H <sub>3</sub>		8.5	70	decomp. >300 [>300] <sup>42</sup>

<sup>a</sup> Isolated yield. <sup>b</sup> Novel compound.

yields and the nature of the Ar group appeared to have no notable effect on the reaction rate (Table 3).

We propose a mechanism for the Na<sub>2</sub>CO<sub>3</sub>-catalyzed synthesis of chromenopyrano[2,3-*b*]pyridine derivatives **7** (Scheme 3). Firstly, intermediate **9** is produced by the deprotonation of NH<sub>2</sub> of pyranochromene in the presence of Na<sub>2</sub>CO<sub>3</sub>. Next, a Michael-type addition of NH<sup>-</sup> to dimethyl acetylenedicarboxylate creates adduct **10**. The intramolecular cyclization of **10** gives adduct **11** which rearranges into the product **7**. The synthesis of product **8** also can be visualized as proceeding through a condensation of intermediate **9** with cyclohexanone to produce **12**. Subsequently, cyclization and then tautomerization of **12** gives the desired product **8** (Scheme 3).

### 3. Experimental

All chemicals and reagents were purchased from Fluka and Merck companies. The reaction progress was monitored by using TLC on silica gel polygram SIL G/UV254 plates. Reported melting points were determined by an electrothermal KSB1N apparatus. <sup>1</sup>H NMR spectra were recorded in DMSO-*d*<sub>6</sub> on a Bruker Avance Ultra Shield 400 MHz instrument spectrometer and <sup>13</sup>C NMR spectra were recorded at 100 MHz. A Vario-El CHN instrument at the Isfahan Industrial University was used for the elemental analyses. IR spectra were obtained with a JASCO FT-IR/680 instrument spectrometer using KBr pellets.

#### Procedure for the Preparation of the SSC Catalyst

Silica sodium carbonate (SSC) was synthesized as a low-cost, recyclable and green catalyst in two steps according to the literature procedure.<sup>43</sup> Initially, by adding thionyl chloride gradually to the silica gel, the silica chloride was prepared. Then, silica chloride and sodium bicarbonate were refluxed in hexane solvent for 24 hours. The solid product obtained, after washing and drying was used as a silica sodium carbonate catalyst.

#### General Procedure for the Synthesis of Pyranochromenes **4**

SSC (0.1 mmol, 0.2 g) was added to a mixture of malononitrile, aryl aldehyde, and 4-hydroxycoumarin at 110 °C under solvent-free conditions. The reaction progress was monitored by TLC. After completion of the reaction, boiling EtOAc (10 mL) was added, and the catalyst was separated by filtration. To further purify the product, obtained powder was recrystallized from EtOH.<sup>28</sup>

#### Preparation of Chromenopyrano[2,3-*b*]pyridines **7**

A solution of DMAD (1 mmol), compound **4** (1 mmol) and Na<sub>2</sub>CO<sub>3</sub> (10 mol%) in DMSO (5 mL) was stirred at 100 °C for the appropriate time. The progress of the reaction was monitored by TLC (EtOAc/*n*-hexan). After completion of the reaction, the catalyst was separated by filtration and the solvent was evaporated under reduced pressure. The obtained products were purified by column chromatography.

#### Preparation of Chromenopyrano[2,3-*b*]pyridines **8**

A mixture of compound **4** (1 mmol), cyclohexanone (**5**) (2 mmol) and Na<sub>2</sub>CO<sub>3</sub> (10 mol%) in DMSO (5 mL) was stirred and heated at 100 °C in a preheated oil bath for a required time. After termination of the reaction as demonstrated by TLC (EtOAc/*n*-hexan), the catalyst was separated by filtration. The solvent was removed and the crude powder **8** was purified by crystallization from EtOAc.

**Dimethyl 8-Amino-6-oxo-7-phenyl-6*H*,7*H*-chromeno[3',4':5,6]pyrano[2,3-*b*]pyridine-9,10-dicarboxylate (7a).** Yield: 80% (0.35 g), IR (KBr) ( $\nu_{\max}$ , cm<sup>-1</sup>) 3446, 2918, 1650, 1640, 1420, 1321. <sup>1</sup>H NMR (400 MHz, DMSO-*d*<sub>6</sub>)  $\delta$  8.15 (s, 2H), 7.52–8.13 (m, 3H), 7.42–7.50 (m, 3H), 7.24–7.34 (m, 3H), 5.21 (s, 1H), 2.35 (s, 3H), 2.24 (s, 3H). <sup>13</sup>CNMR (100 MHz, DMSO-*d*<sub>6</sub>)  $\delta$  160.16, 152.78, 151.24, 142.01, 132.81, 128.59, 124.63, 122.37, 117.23, 113.48, 100.22, 100.16, 77.35, 77.24, 77.04, 76.72, 53.22, 34.95, 30.98. Anal. Calcd for C<sub>25</sub>H<sub>18</sub>N<sub>2</sub>O<sub>7</sub> C, 65.50; H, 3.96; N, 6.11. Found C, 65.53; H, 3.90; N, 6.18.

**Dimethyl 8-Amino-7-(4-chlorophenyl)-6-oxo-6H,7H-chromeno[3',4':5,6]pyrano[2,3-b]pyridine-9,10-dicarboxylate (7b).** Yield: 75% (0.37 g), IR (KBr) ( $\nu_{\max}$ ,  $\text{cm}^{-1}$ ) 3417, 2946, 1648, 1636, 1490, 1321, 777.  $^1\text{H}$  NMR (400 MHz, DMSO- $d_6$ )  $\delta$  7.84 (s, 2H), 7.71 (s, 2H), 7.11–7.52 (m, 5H), 7.09 (s, 1H), 5.45 (s, 1H), 3.35 (s, 3H), 2.51–2.53 (m, 3H).  $^{13}\text{C}$  NMR (100 MHz, DMSO- $d_6$ )  $\delta$  169.90, 168.01, 165.61, 154.02, 153.91, 145.04, 142.75, 140.74, 138.25, 137.42, 131.91, 125.07, 122.51, 119.51, 112.17, 97.94, 79.88, 49.07, 31.15. Anal. Calcd for  $\text{C}_{25}\text{H}_{17}\text{ClN}_2\text{O}_7$  C, 60.92; H, 3.48; N, 5.68. Found C, 60.91; H, 3.51; N, 5.65.

**Dimethyl 8-Amino-7-(4-bromophenyl)-6-oxo-6H,7H-chromeno[3',4':5,6]pyrano[2,3-b]pyridine-9,10-dicarboxylate (7c).** Yield: 73% (0.39 g), IR (KBr) ( $\nu_{\max}$ ,  $\text{cm}^{-1}$ ) 3450, 2923, 1667, 1563, 1488, 1348, 764.  $^1\text{H}$  NMR (400 MHz, DMSO- $d_6$ )  $\delta$  7.941 (s, 2H), 7.588–7.918 (m, 3H), 7.314–7.438 (m, 2H), 7.147 (d,  $J = 8.1$  Hz, 3H), 6.332 (s, 1H), 2.762 (s, 3H), 2.523 (s, 3H).  $^{13}\text{C}$  NMR (100 MHz, DMSO- $d_6$ )  $\delta$  168.24, 166.04, 165.14, 161.19, 152.74, 150.21, 144.47, 140.36, 132.38, 131.31, 129.61, 124.42, 124.17, 118.99, 118.51, 116.42, 104.27, 97.91, 94.51, 52.12, 36.24. Anal. Calcd for  $\text{C}_{25}\text{H}_{17}\text{BrN}_2\text{O}_7$  C, 55.88; H, 3.19; N, 5.21. Found C, 55.90; H, 3.15; N, 5.27.

**Dimethyl 8-Amino-7-(3-nitrophenyl)-6-oxo-6H,7H-chromeno[3',4':5,6]pyrano[2,3-b]pyridine-9,10-dicarboxylate (7d).** Yield: 80% (0.40 g), IR (KBr) ( $\nu_{\max}$ ,  $\text{cm}^{-1}$ ) 3415, 2953, 1634, 1554, 1530, 1437, 1349.  $^1\text{H}$  NMR (400 MHz, DMSO- $d_6$ )  $\delta$  8.033 (d,  $J = 7.8$  Hz, 2H), 7.937 (s, 1H), 7.875 (d,  $J = 7.5$  Hz, 1H), 7.503–7.645 (m, 4H), 7.267–7.352 (m, 2H), 6.404 (s, 1H), 3.581 (s, 3H), 2.564 (s, 3H).  $^{13}\text{C}$  NMR (100 MHz, DMSO- $d_6$ )  $\delta$  49.07, 50.46, 82.67, 102.51, 106.85, 110.73, 112.09, 126.68, 128.51, 129.39, 132.14, 138.14, 139.24, 144.53, 154.53, 157.15, 160.46, 161.82, 167.32, 167.86. Anal. Calcd for  $\text{C}_{25}\text{H}_{17}\text{N}_3\text{O}_9$  C, 59.65; H, 3.40; N, 8.35. Found C, 59.66; H, 3.43; N, 8.32.

**8-Amino-7-phenyl-9,10,11,12-tetrahydro-7H-5,14-dioxo-13-azabenz[*a*]naphthacen-6-one (8a).** Yield: 85% (0.34 g), IR (KBr) ( $\nu_{\max}$ ,  $\text{cm}^{-1}$ ) 3419, 2933, 1727, 1670, 1641, 1602, 1492, 1454, 1382, 1307, 1201, 1039, 754, 700, 543, 460.  $^1\text{H}$  NMR (400 MHz, DMSO- $d_6$ )  $\delta$  8.05 (d,  $J = 8.0$  Hz, 1H), 8.01 (t,  $J = 7.8$  Hz, 1H), 7.77 (d,  $J = 8.0$  Hz, 1H), 7.55 (t,  $J = 8.0$  Hz, 1H), 7.52 (d,  $J = 7.8$  Hz, 1H), 7.31 (s, 2H), 7.26 (d,  $J = 8.0$  Hz, 3H), 7.24 (d,  $J = 8.0$  Hz, 1H), 5.39 (s, 1H), 2.81–2.90 (m, 2H), 1.77–1.95 (m, 6H).  $^{13}\text{C}$  NMR (100 MHz, DMSO- $d_6$ )  $\delta$  160.1, 156.1, 153.9, 152.5, 149.9, 141.3, 133.7, 129.1, 128.8, 127.9, 125.4, 122.9, 117.1, 114.5, 113.4, 106.1, 98.8, 40.6, 40.2, 39.3, 33.7, 21.3, 21.1. Anal. Calcd for  $\text{C}_{25}\text{H}_{20}\text{N}_2\text{O}_3$  C, 75.74; H, 5.08; N, 7.07. Found C, 75.72; H, 5.10; N, 7.05.

**8-Amino-7-(4-nitrophenyl)-9,10,11,12-tetrahydro-7H-5,14-dioxo-13-azabenz[*a*]naphthacen-6-one (8b).** Yield: 82% (0.36 g), IR (KBr) ( $\nu_{\max}$ ,  $\text{cm}^{-1}$ ) 3338, 3230, 2935, 2861, 1722, 1668, 1604, 1517, 1454, 1382, 1346,

1276, 1201, 1106, 1043, 906, 763, 543.  $^1\text{H}$  NMR (400 MHz, DMSO- $d_6$ )  $\delta$  8.16 (d,  $J = 8.0$  Hz, 2H), 8.04 (d,  $J = 8.0$  Hz, 1H), 7.79 (d,  $J = 8.0$  Hz, 2H), 7.55 (s, 2H), 7.52 (t,  $J = 8.0$  Hz, 3H), 5.54 (s, 1H), 2.78–2.93 (m, 2H), 1.77–1.88 (m, 6H).  $^{13}\text{C}$  NMR (100 MHz, DMSO- $d_6$ )  $\delta$  160.0, 156.2, 153.8, 149.7, 141.1, 137.9, 133.7, 129.6, 128.6, 126.2, 122.9, 117.1, 114.5, 106.1, 98.9, 40.6, 40.4, 40.2, 40.0, 33.7, 22.8, 21.5, 21.3. Anal. Calcd for  $\text{C}_{25}\text{H}_{19}\text{N}_3\text{O}_5$  C, 68.02; H, 4.34; N, 9.52. Found C, 68.06; H, 4.37; N, 9.50.

**8-Amino-7-(3-methylphenyl)-9,10,11,12-tetrahydro-7H-5,14-dioxo-13-azabenz[*a*]naphthacen-6-one (8c).** Yield: 75% (0.31 g), IR (KBr) ( $\nu_{\max}$ ,  $\text{cm}^{-1}$ ) 3334, 3232, 2937, 1727, 1668, 1641, 1604, 1490, 1454, 1382, 1307, 1274, 1201, 1043, 902, 763, 586.  $^1\text{H}$  NMR (400 MHz, DMSO- $d_6$ )  $\delta$  8.01 (d,  $J = 8.0$  Hz, 1H), 7.74 (t,  $J = 8.0$  Hz, 2H), 7.53 (t,  $J = 8.0$  Hz, 2H), 7.47 (d,  $J = 8$  Hz, 1H), 7.35 (s, 2H), 7.17 (t,  $J = 8.0$  Hz, 1H), 7.03 (d,  $J = 8.0$  Hz, 1H), 5.34 (s, 1H), 2.83–2.98 (m, 2H), 2.52 (s, 3H), 1.77–1.90 (m, 6H).  $^{13}\text{C}$  NMR (100 MHz, DMSO- $d_6$ )  $\delta$  159.9, 156.5, 153.6, 152.5, 149.4, 146.8, 141.0, 137.9, 133.7, 129.6, 128.7, 126.3, 125.4, 122.9, 117.1, 114.5, 113.2, 106.1, 98.9, 40.1, 39.3, 33.6, 22.8, 21.5, 21.2, 21.0. Anal. Calcd for  $\text{C}_{26}\text{H}_{22}\text{N}_2\text{O}_3$  C, 76.08; H, 5.40; N, 6.82. Found C, 76.05; H, 5.36; N, 6.78.

## 4. Conclusions

In summary, we have demonstrated that the reaction between pyrano[2,3-*c*]chromenes and dimethyl acetylenedicarboxylate or cyclohexanone in the presence of sodium carbonate provides a simple method for the preparation of chromenopyrano[2,3-*b*]pyridine derivatives. One of the important benefits of this protocol is the use of sodium carbonate as a commercially available and inexpensive catalyst. This study has helped to find an effective production of biologically useful compounds belonging to the family of pyranopyridines.

## Acknowledgements

The authors gratefully acknowledge the partial support of this work by Yasouj University, Iran.

## 5. References

1. H. M. Elwahy, M. R. Shaaban, *RSC Adv.* **2015**, *5*, 75659–75710.
2. X. F. Wu, H. Neumann, M. Beller, *Chem. Rev.* **2013**, *113*, 1–35. DOI:10.1039/C5RA11421G
3. B. Jiang, T. Rajale, W. Wever, S. J. Tu, G. Li, *Chem. Asian J.* **2010**, *5*, 2318–2335. DOI:10.1002/asia.201000310
4. E. G. Hammam, N. A. A. El-hafeza, W. H. Midurab, M. Z. Mikolajczyk, *Naturforsch. B: Chem. Sci.* **2000**, *55*, 417–423. DOI:10.1515/znb-2000-0511

5. K. Ishiguro, K. Takahashi, K. Yazawa, S. Sakiyama, T. Arai, *J. Biol. Chem.* **1981**, 256, 2162–2167.
6. R. M. Mohareb, N. N. E. El-Sayed, M. E. Abdelaziz *Molecules* **2012**, 17, 8449–8463. DOI:10.3390/molecules17078449
7. G. E. Amr, M. M. Abdulla, *Bioorg. Med. Chem.* **2006**, 14, 4341–4352. DOI:10.1016/j.bmc.2006.02.045
8. M. Ghate, R. A. Kusanur, M. V. Kulkarni, *Eur. J. Med. Chem.* **2005**, 40, 882–887. DOI:10.1016/j.ejmech.2005.03.025
9. S. Shafi, M. M. Alam, N. Mulakayala, C. Mulakayala, G. Vanaja, A. M. Kalle, R. Pallu, M. S. Alam, *Eur. J. Med. Chem.* **2012**, 49, 324–333. DOI:10.1016/j.ejmech.2012.01.032
10. M. V. B. Reddy, C. R. Su, W. F. Chiou, Y. N. Liu, R. Y. H. Chen, K. F. Bastow, K. H. Lee, T. S. Wu, *Bioorg. Med. Chem.* **2008**, 16, 7358–7370. DOI:10.1016/j.bmc.2008.06.018
11. V. V. Shinde, M. V. Reddy, Y. H. Kim, B. K. Cho, Y. T. Jeong, *Monatsh. Chem.* **2015**, 146, 673–682. DOI:10.1007/s00706-014-1380-9
12. M. Yusuf, P. Jain, *Arab. J. Chem.* **2011**, 5, 553–596.
13. M. A. P. Martins, C. P. Frizzo, D. N. Moreira, L. Buriol, P. Machado, *Chem. Rev.* **2009**, 109, 4140–4182. DOI:10.1021/cr9001098
14. M. A. P. Martins, C. P. Frizzo, D. N. Moreira, N. Zanatta, H. G. Bonaccorso, *Chem. Rev.* **2008**, 108, 2015–2050. DOI:10.1021/cr078399y
15. L. Zheng, J. Ju, Y. Bin, R. Hua, *J. Org. Chem.* **2012**, 77, 5794–5800. DOI:10.1021/jo3010414
16. S. A. Raw, C. D. Wilfred, R. J. K. Taylor, *Org. Biomol. Chem.* **2004**, 2, 788–796. DOI:10.1039/b315689c
17. M. Movassaghi, M. D. Hill, O. K. Ahmad, *J. Am. Chem. Soc.* **2007**, 129, 10096–10097. DOI:10.1021/ja073912a
18. A. Antonyraj, S. Kannan, *Appl. Catal. A* **2008**, 338, 121–129. DOI:10.1016/j.apcata.2007.12.028
19. M. D. Hill, *Chem. Eur. J.* **2010**, 16, 12052–12062. DOI:10.1002/chem.201001100
20. A. F. S. Rostom, G. S. Hassan, H. I. El-Subbagh, *Arch. Pharm. Chem. Life Sci.* **2009**, 342, 584–586. DOI:10.1002/ardp.200900062
21. M. M. Ghorabaa, I. Y. Hassan, *Phosph. Sulfur Silicon Relat. Elem.* **1998**, 141, 251–261. DOI:10.1080/10426509808033737
22. Z. Huang, Y. Hu, Y. Zhou, D. Shi, *ACS Comb. Sci.* **2011**, 12, 45–49. DOI:10.1021/co1000162
23. T. I. Chaban, V. V. Ogurtsov, V. S. Matiychuk, I. G. Chaban, I. L. Demchuk, I. A. Nektageyev, *Acta Chim. Slov.* **2019**, 66, 103–111. DOI:10.17344/acsi.2018.4570
24. T. I. Chaban, R. R. Panchuk, O. V. Klenina, N. R. Skorokhyd, V. V. Ogurtsov, I. G. Chaban, *Biopolym. Cell.* **2012**, 28, 389–396. DOI:10.7124/bc.000075
25. S. Pajk, M. Garvas, J. Štrancar, *Acta Chim. Slov.* **2019**, 66, 668–674. DOI:10.17344/acsi.2019.5089
26. N. Narayanaswamy, M. Kumar, S. Das, R. Sharma, P. K. Samanta, S. K. Pati, S. K. Dhar, T. K. Kundu, T. Govindaraju, *Sci. Rep.* **2014**, 25, 6476–6483.
27. H. Mohamadi Tanuraghaj, M. Farahi, *Tetrahedron Lett.* **2019**, 60, 557–559. DOI:10.1016/j.tetlet.2019.01.030
28. M. Farahi, M. Abdipour, *Org. Chem. Res.* **2018**, 4, 182–193.
29. C. Mungra, M. P. Patel, D. P. Rajani, R. G. Patel, *Eur. J. Med. Chem.* **2011**, 46, 4192–4200. DOI:10.1016/j.ejmech.2011.06.022
30. B. D. Parmar, T. R. Sutariya, G. C. Brahmabhatt, N. J. Parmar, R. Kant, V. K. Gupta, *J. Org. Chem.* **2016**, 81, 4955–4964. DOI:10.1021/acs.joc.6b00107
31. B. Sameem, M. Saeedi, M. Mahdavi, H. Nadri, F. Homayouni Moghadam, N. Edraki, M. I. Khan, M. Amini, *Bioorg. Med. Chem.* **2017**, 25, 3980–3988. DOI:10.1016/j.bmc.2017.05.043
32. Z. M. Nofal, H. H. Fahmy, M. M. Kamel, A. I. Sarhan, A. S. Maghraby, *Egypt. J. Chem.* **2004**, 47, 345–368.
33. H. Mohamadi Tanuraghaj, M. Farahi, *Tetrahedron Lett.* **2019**, 60, 557–559. DOI:10.1016/j.tetlet.2019.01.030
34. M. Farahi, B. Karami, H. Mohamadi Tanuraghaj, Z. Bazrafshan, *J. Heterocycl. Chem.* **2018**, 55, 125–131. DOI:10.1002/jhet.3014
35. M. Farahi, B. Karami, H. Mohamadi Tanuraghaj, *Tetrahedron Lett.* **2015**, 56, 1833–1836. DOI:10.1016/j.tetlet.2015.02.087
36. M. Farahi, B. Karami, Z. Banaki, F. Rastgoo, K. Eskandari, *Monatsh. Chem.* **2017**, 148, 1469–1475. DOI:10.1007/s00706-017-1932-x
37. M. Farahi, B. Karami, A. Jokar, K. Eskandari, *Org. Prep. Proc. Int.* **2017**, 49, 514–524. DOI:10.1080/00304948.2017.1380495
38. M. Farahi, M. Davoodi, M. Tahmasebi, *Tetrahedron Lett.* **2016**, 57, 1582–1584. DOI:10.1016/j.tetlet.2016.02.101
39. M. Farahi, F. Tamaddon, B. Karami, S. Pasdar, *Tetrahedron Lett.* **2015**, 56, 1887–1890. DOI:10.1016/j.tetlet.2015.02.105
40. H. Mohamadi Tanuraghaj, M. Farahi, *RSC Adv.* **2018**, 8, 27818–27824. DOI:10.1039/C8RA05501G
41. H. Mehrabi, H. Abusaidi, *J. Iran. Chem. Soc.* **2010**, 7, 890–894. DOI:10.1007/BF03246084
42. M. Khoobi, M. Alipour, A. Moradi, A. Sakhteman, H. Nadri, S. F. Razavi, M. Ghandi, A. Foroumadi, A. Shafiee, *Eur. J. Med. Chem.* **2013**, 68, 291–300. DOI:10.1016/j.ejmech.2013.07.045
43. K. Eskandari, B. Karami, S. Khodabakhshi, *Catal. Commun.* **2014**, 54, 124–130. DOI:10.1016/j.catcom.2014.05.029

## Povzetek

V okviru te raziskave smo pripravili serijo novih in nekaj že znanih kromenopirano[2,3-*b*]piridinskih derivatov. Skladno z že objavljenimi postopki smo najprej z reakcijo med 4-hidroksikumarinom, aromatskimi aldehidi in malononitrilom ob prisotnosti silika natrijevega karbonata (SSC) kot katalizatorja pripravili pirano[2,3-*c*]kromenske derivate, ki smo jih v naslednji stopnji reagirali z dimetil acetilendikarboksilatom (DMAD) ali cikloheksanonom v prisotnosti natrijevega karbonata. Tako smo pripravili serijo kromenopirano[2,3-*b*]piridinskih derivatov. Za izvedbo našega protokola ne potrebujemo dragih katalizatorjev in vendar lahko potencialno bioaktivne heterociklične spojine pripravimo z odličnimi do visokimi izkoristki.



Except when otherwise noted, articles in this journal are published under the terms and conditions of the Creative Commons Attribution 4.0 International License

Scientific paper

# Application of Chemically Modified Industrial Slag to As(III) Adsorption from Wastewater: Kinetics and Mass Transfer Analysis

Arijit Dutta Gupta,<sup>1</sup> Vivek Jaiswal,<sup>2</sup> Vivek Bhadauria<sup>3</sup> and Harinder Singh<sup>1,\*</sup><sup>1</sup> Department of Chemical Engineering, Motilal Nehru National Institute of Technology Allahabad, Prayagraj – 211004, India<sup>2</sup> Department of Chemical Engineering & Technology, Indian Institute of Technology (BHU), Varanasi – 221005, India<sup>3</sup> Department of Chemistry, Ewing Christian College, Prayagraj – 211003, India

\* Corresponding author: E-mail: harinderpdfb@gmail.com

Mob. No.: +91-9936393111

Received: 07-25-2020

## Abstract

In the present study, brick kiln slag (BKS) has been utilized for low concentration As(III) adsorption in batch mode. BKS was modified with H<sub>2</sub>SO<sub>4</sub> (SA) and NaOH (SB) for enhancing As(III) uptake capacity. Maximum adsorption capacity (13.7 mg/g) was observed for SA at 298 K, pH = 7.0, adsorbent dose = 0.3 g and time = 70 min which was 1.4 times higher than that of SB. Adsorption data modelled into Freundlich isotherm and pseudo-second-order kinetics. Mass transfer coefficients decreased with increase in As(III) concentration. Film diffusion significantly dominated the adsorption of As(III) ions irrespective of the initial concentration. Dimensionless Sherwood number (*Sh*) interrelated As(III) concentration (*C<sub>o</sub>*) as:  $Sh = 2.97(C_o)^{-0.376}$ ,  $Sh = 4.12(C_o)^{-0.215}$ ,  $Sh = 4.83(C_o)^{-0.588}$  for H<sub>2</sub>SO<sub>4</sub> modified, NaOH modified and native slag respectively. Low temperature (298 K) favoured As(III) adsorption (based on  $\Delta G^\circ$  value). Therefore, the modified slag can be used as an effective adsorbent for As(III) remediation from groundwater.

**Keywords:** As(III) adsorption; industrial slag; mass Transfer; film diffusion; sherwood number

## 1. Introduction

In the recent years, rapid industrialization has led to an alarming increase in the contamination of heavy metals in soil and water bodies due to accumulation of various pollutants discharged from the industrial waste water. Imprudent use of such metalloids and heavy metals causes to concentrate in aquatic flora and fauna via discharge in the water bodies. Arsenic is a metalloid with atomic number 33. The earth's crust comprises of about 0.00005% of arsenic. Rocks and other minerals contain about 0.5–2.5 mg/kg and usually occur in combination with other metals or non-metals, sulphur and phosphorites.<sup>1–3</sup> Mobilization of arsenic takes place either in the form of natural phenomena such as weathering, volcanic eruptions, mining of gold, combustion of fossil fuels, smelting processes, agricultural pesticides or leaching of synthetic arsenic pollutants via soil.<sup>4</sup> Long term exposure to arsenic in drinking water causes lung, kidney and skin cancer, disordering of bone

marrow and cartilages, neurological disorders, cardiovascular diseases, abdominal pain and gastrointestinal diseases. Due to its high toxicity on human health, WHO and USEPA have fixed a global maximum permissible limit of 10 ppb or 0.01 ppm for arsenic in drinking water.<sup>1</sup>

Adsorption is a time dependent separation process. The transport of As(III) from the adsorbate (liquid phase) to the adsorbent (solid phase) is typically carried out by mass transfer operation due to the presence of concentration gradient between the adsorbate and the adsorbent. The slowest of these steps is the rate-determining step and is said to control the overall adsorption process. Moreover, in a well agitated batch adsorber, liquid mixing is quite rapid. Therefore, a uniform concentration is assumed between the adsorbate concentration and the solute particles within the system. This step is also referred as the equilibrium step, because the equilibrium between the solute in the bulk adsorbate and the solute on the film of the adsorbent is achieved instantaneously. Therefore, adsorption

process mainly constitutes two types of mass transfer resistances i.e. external and internal diffusion resistances. The rate limiting step depends on various physical factors such as size of the adsorbent particle, solute affinity for the particular adsorbent and the degree of mixing.<sup>5,6</sup>

Difference in chemical potential acts as the driving force for any mass transfer operation which is well defined through their thermodynamic gradients. For any mass transfer operation or any separation processes, theoretical extent of a given separation depends on the position of thermodynamic equilibrium, while the actual rate of separation depends on the rate of mass transfer which is manifested by additional parameters such as flow patterns and diffusivities of the given species in a particular phase.<sup>6</sup> The actual rate of mass transfer is quantified through the application of various mass transfer coefficients. Such mass transfer coefficients are generally represented in terms of dimensionless numbers such as Sherwood numbers, Transport numbers etc.<sup>7</sup>

Various chemically modified adsorbents for As(III) adsorption have been reported in literature. As(III) adsorption using chemically modified activated carbon was reported to show an adsorption capacity of around 8.7 mg/g.<sup>8</sup> Chemical modification of water melon rind showed a maximum arsenic removal percentage of around 94%.<sup>9</sup> Arsenic removal using stainless steel slag was found to show an adsorption capacity of 13.7 mg/g.<sup>10</sup> Chemical modification of pine wood biochar by Wang et al., 2015 was found to exhibit maximum arsenic capacity of 5.0 mg/g.<sup>11</sup> Iron ore scrap exhibited an As(III) adsorption capacity of 0.74 mg/g.<sup>12</sup> However, these studies dealt with high initial concentration of As(III) ions which required a large mass transfer driving force and was easily separable.

The objective of the present study is to determine the applicability of brick kiln slag, as an industrial waste as an adsorbent for low concentration As(III) ions from water. Chemical modification of the slag has been done in order to increase the the affinity for As(III) adsorption. Mass transfer coefficients have been evaluated through the use of various mass transfer models to determine the rate controlling step for adsorption of As(III) using native and chemically modified brick kiln slag. Since the study of mass transfer analysis for adsorption of As(III) adsorption is limited in the literature, this work is being reported for the first time in literature wherein the rate-limiting steps have been determined through various mass transfer models and dimensionless numbers for batch adsorption of As(III) ions.

## 2. Materials and Methods

All chemicals were of AR grade without further purification. Sulphuric acid (H<sub>2</sub>SO<sub>4</sub>), hydrogen peroxide (H<sub>2</sub>O<sub>2</sub>), sodium arsenite (NaAsO<sub>2</sub>) and sodium hydroxide (NaOH) were purchased from Merck. The glass wares

were cleaned with 1% potassium dichromate and HNO<sub>3</sub> solution and rinsed several times with distilled water before use.

### 2. 1. Preparation of Adsorbents

The brick kiln slag (BKS) was collected from a local brick kiln from Prayagraj District, India. Prior to chemical modification, the brick kiln slag was washed several times with double distilled water to remove the suspended impurities thereafter chemical activation was done using 10% (v/v) hydrogen peroxide (H<sub>2</sub>O<sub>2</sub>) and subsequently dried in a hot air oven at 100 °C for 24 h. The obtained kiln slag was modified with 0.5 M solution of H<sub>2</sub>SO<sub>4</sub> and NaOH at room temperature followed by stirring for another 6 h. The obtained adsorbents were the sonicated for another 30 min at 30 °C to prevent agglomeration of flocs. The mixture was then centrifuged and washed several times with distilled water and ethanol till the pH of the supernatant was neutral. The adsorbent samples were then dried in a hot air oven at 120 °C overnight and stored in desiccators for further use. The synthesised adsorbents were labelled as SN, SA and SB respectively, for native, acid modified and alkali modified slag.

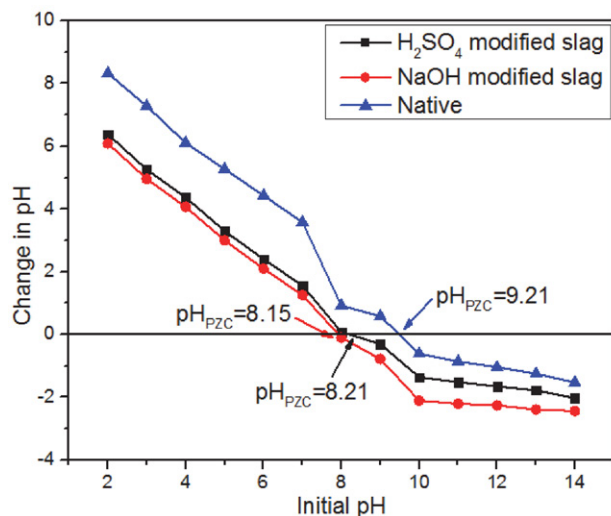
### 2. 2. Physical Properties of the Native and Modified Brick Kiln Slag

Volume of the adsorbent particles was measured by taking 100 g of adsorbent in a 250 mL measuring cylinder which was compacted by tapping up to 20–25 times to ensure absence of any voids. Bulk density was determined by dividing the mass of the adsorbent with the volume. Particle size of the adsorbents was determined by using standard test sieve. The adsorbent samples were placed on the sieve covered with a lid and a pan at the bottom and shaken at 350 rpm for 30 min. The particles with specific size were collected on the pan. Point of zero charge (pH<sub>PZC</sub>) was determined by NaCl method. Briefly, 0.01 M NaCl was prepared and its pH was adjusted between 1.0–13.0 using 1 M HCl and NaOH. 50 mL of NaCl at different pH was taken and 0.2 g of the adsorbent was added to the flasks and shaken for 24 h at 350 rpm. Final pH was measured after 24 h and pH<sub>PZC</sub> was determined from the graph between pH change against initial pH (Figure 1). Porosity was determined from the SEM analysis. Surface area per unit volume was determined from the relation in Eq. (1):

$$A = \frac{6M}{V d_p \rho (1-\varepsilon)} \quad (1)$$

where  $V$  is the adsorbate volume in  $L$ ,  $M$  is the mass of the adsorbent in  $g$ ,  $d_p$  is the particle diameter in  $m$ ,  $\varepsilon$  is the particle porosity and  $\rho$  is the bulk density of the adsorbent in  $g/cm^3$ . The physical properties of the native and the chemically modified slag have been summarised in Table 1.





**Figure 1.** Point of zero charge ( $\text{pH}_{\text{PZC}}$ ) of the synthesised adsorbents

**Table 1.** Physical properties of the native and chemically modified brick kiln slag (BKS)

Properties	Native BKS	H <sub>2</sub> SO <sub>4</sub> modified BKS	NaOH modified BKS
Bulk density ( $\text{g}/\text{cm}^3$ )	1.78	1.82	1.84
Particle size ( $\mu\text{m}$ )	10.05	9.34	9.45
Porosity	0.231	0.265	0.248
Point of zero charge ( $\text{pH}_{\text{PZC}}$ )	9.12	8.21	8.15
Surface area per unit volume of the particle ( $\text{m}^{-1}$ )	12685.6	12795.5	12845.7

### 2.3. Batch Adsorption Experiment

In a batch adsorption experiment, influence of various adsorption parameters (time, adsorbent dose and pH) on the removal percentage of As(III) was studied. Stock solution of 1000  $\text{mg}/\text{L}$  As(III) was prepared by dissolving 0.1734 g NaAsO<sub>2</sub> in 100 mL of distilled water. Adsorption experiments were carried out by dilution of the stock by varying the initial adsorbate concentration from 1 to 5  $\text{mg}/\text{L}$  at  $\text{pH} = 7.0$ . pH adjustment was done using 0.1 M HCl and NaOH solution. 100 mL of known concentration of As(III) solution was taken in a 250 mL Erlenmeyer flask. After pH adjustment, known amount of adsorbent was added and was magnetically stirred (200 rpm) at room temperature ( $25 \pm 2$  °C) until the attainment of equilibrium. Presence of As(III) in solution was determined by variamine oxidation method.<sup>13</sup> Briefly, aliquot of arsenic containing water was taken in 10 mL calibrated flasks. Following this, 1 mL each of 2% KIO<sub>3</sub> and 0.4 M HCl were added and the mixture was shaken gently for 10 min. Then, 1 mL of 0.05% variamine blue and 2 mL of 2 M CH<sub>3</sub>COONa were added. The resultant solution was left undisturbed

for 5 min and made up to the mark with distilled water. Reagent blank was prepared simultaneously with distilled water following the same procedure. The absorbance was measured using UV spectrophotometer at 556 nm against the corresponding reagent blank. The As(III) ions capacity at equilibrium was determined from the Eq. (2):

$$q_e = \frac{(C_i - C_e)}{m} \times V \quad (2)$$

The removal percentage was calculated from the Eq. (3):

$$\% \text{ Removal} = \frac{(C_i - C_e)}{C_i} \times 100 \quad (3)$$

where  $q_e$  is the adsorption capacity at equilibrium ( $\text{mg}/\text{g}$ ),  $C_i$  and  $C_e$  are the initial and equilibrium adsorbate concentration ( $\text{mg}/\text{L}$ ),  $m$  is the adsorbate mass (g),  $V$  is the volume of the solution (L).

### 2.4. Adsorbent Characterizations

The adsorbent samples were washed with acetone, dried in hot air oven, pulverised and then subjected to gold coating in a vacuum sputtering unit for 15 min to increase the conductivity of the samples. SEM analysis of the adsorbent samples was done using Zeiss Evo MA-15 scanning electron microscope. The adsorbent samples were dried in an oven to remove any residual moisture and FTIR analysis was performed using PerkinElmer Spectrum Version 10.03.06. X-Ray Diffraction analysis was carried out using Rigaku Smart Lab 3KW X-Ray diffractometer at  $2\theta = 5^\circ - 70^\circ$  with a step size of  $0.02^\circ$  using Cu-K $\alpha$  radiation at 50 kV voltage and 40 mA current.

### 2.5. Theoretical Mass Transfer Models

In any adsorption process, the transfer of adsorbate from the bulk solution to the solid adsorbent takes place either due to film diffusion or internal pore diffusion. The rate limiting step is determined from the slowest of these steps. Therefore, in order to determine the rate controlling step, various theoretical mass transfer models and dimensionless numbers have been studied in the present research.

#### 2.5.1. External Diffusion Model

Liquid film diffusion or external diffusion model plays an important role in adsorption, when there is transfer of molecules from the bulk adsorbate solution to the solid phase adsorbent boundary. This model assumes the fact that the adsorbate concentration at the solid adsorbent's surface tends to zero or intraparticle diffusion resistance is negligible and thus can be neglected at the initial stages of adsorption. This model is derived based on Fick's

first law of diffusion expressing difference in solute concentrations in the bulk adsorbate and that at the adsorbent's interface as a function of time.<sup>14</sup> The change in the solute concentration as a function of time can be written as in Eq. (4):

$$\frac{dC}{dt} = -k_f A(C - C_o) \quad (4)$$

The above equation may be simplified as:

$$\left[ \frac{d\left(\frac{C}{C_o}\right)}{dt} \right]_{t \rightarrow 0} = -k_f A \quad (5)$$

where  $C$  is the bulk adsorbate concentration in  $mg/L$  at any time  $t$ ,  $C_o$  is the initial adsorbate concentration in  $mg/L$ ,  $k_f$  is the external mass transfer coefficient in  $m/s$  and  $A$  is the surface area per unit volume ( $m^{-1}$ ) calculated from Eq. (1). External mass transfer coefficient  $k_f$  can be determined from the slope of the dimensionless curve of  $C/C_o$  against time ( $t$ ).

## 2. 5. 2. Boyd Model

An exact mechanism of As(III) adsorption is easier to predict by examining the differences between the intraparticle and external diffusion model. The equation for Boyd mass transfer model is represented in Eq. (6):

$$F = 1 - \frac{6}{\pi^2} \exp(-Bt) \quad (6)$$

$$F(t) = \frac{qt}{q_e} \quad (7)$$

where  $F(t)$  is the fraction of As(III) ions adsorbed at any time  $t$  and  $Bt$  is a mathematical function of  $F$ . The above equation may be simplified as shown in Eq. (8):

$$Bt = [-0.4977 - \ln(1 - F)] \quad (8)$$

For the adsorption process to be controlled by film diffusion, the plot of  $[-0.4977 - \ln(1 - F)]$  against  $t$  should not pass through origin.

## 2. 5. 3. McKay et al. Model

This model is used to analyse the effect of mass transfer resistance on the rate of adsorption. The mass transfer coefficient  $\beta_L$  in  $m/s$  of As(III) at the adsorbate-adsorbent interface can be determined by Eq. (9):

$$\ln\left(\frac{C}{C_o} - \frac{1}{1+mK}\right) = \ln\left(\frac{mK}{1+mK}\right) - \left(\frac{1+mK}{mK}\right) \beta_L A t \quad (9)$$

$$K = q_m \times k_L \quad (10)$$

where  $q_m$  is the maximum adsorption capacity in  $mg/g$  and  $k_L$  is the Langmuir constant in  $L/mg$ .  $\beta_L$  is calculated from the slope of the linear plot of  $\ln((C/C_o) - 1/(1+mK))$  vs time ( $t$ ).

## 2. 5. 4. Dimensionless Numbers

### 2. 5. 4. 1. Sherwood Number

Sherwood Number ( $Sh$ ) relates the rate of adsorption as a function of adsorbate concentration in terms of external and internal mass transfer resistances. It is the ratio of rate of solute transfer across the adsorbate (liquid) surface to the rate of intraparticle mass transport. It is expressed in the form of Eq. (11):

$$Sh = \left(\frac{k_f}{D_e}\right) \left(\frac{d}{\rho}\right) \left(\frac{C_o}{q_m}\right) \quad (11)$$

where  $\rho$  is the particle density in  $g/cm^3$  and  $q_m$  is the maximum adsorption capacity in  $mg/g$  (calculated from Langmuir isotherm model). The conventional form of Sherwood Number is expressed in the form of Eq. (12):

$$Sh = \frac{k_f d}{D_e} \quad (12)$$

The process is film diffusion controlled if  $Sh < 1.0$ , while  $Sh > 1.0$  infers intraparticle diffusion as the rate-limiting step.

### 2. 5. 4. 2. Transport Number

Transport Number ( $n$ ) is used to determine the mode of diffusion. It is shown in Eq. (13):

$$\frac{qt}{q_e} = K_m t^n \quad (13)$$

where  $K_m$  is the adsorbent-adsorbate interaction constant and  $n$  is the transport number. A plot of  $\log(q_t/q_e)$  vs.  $\log t$  yields a straight line from which  $K_m$  and  $n$  can be determined from the y-intercept and slope respectively. If  $n = 1$ , non-Fickian mechanism is inferred while  $n = 0.5$ , represents Fickian (surface) mechanism.

## 3. Results and Discussion

### 3. 1. Adsorbent Characterizations

#### 3. 1. 1. Fourier Transform Infrared Spectroscopy (FTIR)

The FTIR spectra of the native and modified adsorbents before and after adsorption is shown in Figure 2. The sharp peak around  $3500\text{ cm}^{-1}$  represents H-O-H stretching was due to the presence of moisture in the samples. The major peak corresponding to  $1050\text{ cm}^{-1}$  was attributed to asymmetric stretching of Si-O-T bonds (T = Si or Al). The peak intensity was found to be relatively less in SA adsor-

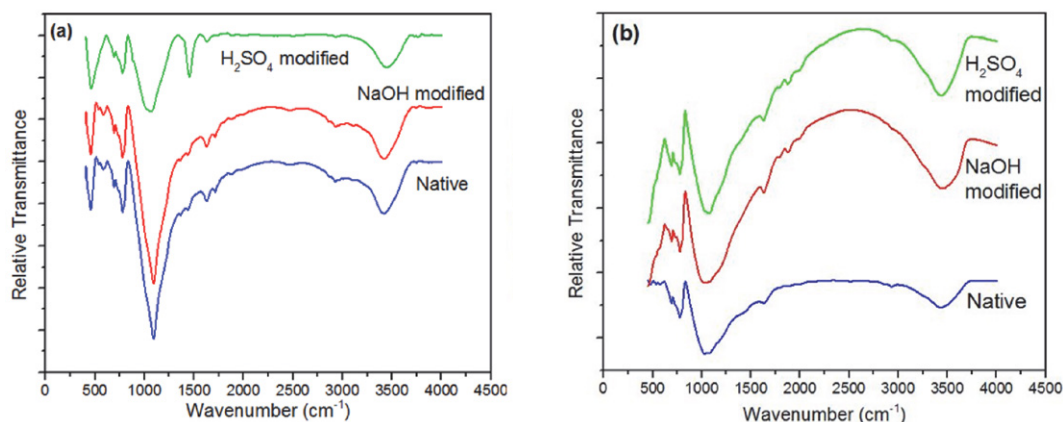


Figure 2. FTIR spectra of the synthesised adsorbents (a) before and (b) after adsorption of As(III)

bent as compared to SN and SB. This may be due to the reaction between silicon (II) oxide and sulphuric acid resulting in the formation of sulphur dioxide and water.<sup>15</sup> Another sharp peak was observed at  $1490\text{ cm}^{-1}$  in the FTIR spectra of acid modified slag (SA) which indicated the presence of stretched vibrations of O-C-O bonds of  $\text{CO}_3^{2-}$ . The peak corresponding to  $870\text{ cm}^{-1}$  which was present in all adsorbent samples was attributed to the asymmetric stretched vibrations of tetrahedral aluminium ions which confirmed the presence of  $\text{AlO}_4$  and  $\text{SiO}_4$  in different configurations.<sup>16</sup> The absorption bands of slag consisting of clay showed stretching and bending of Si-O as well as bending of O-H groups from  $1300\text{--}1450\text{ cm}^{-1}$  in all the adsorbent samples. A peak around  $750\text{--}780\text{ cm}^{-1}$  may be attributed to the presence of vibrational Si-O-Al bonds indicating the presence of feldspar in all the samples. The bands around  $500\text{--}550\text{ cm}^{-1}$  were assigned to octahedral Si-O-Al and Si-O-Si respectively. A small peak at  $790\text{ cm}^{-1}$  which was present in all adsorbents was attributed to the presence of quartz.<sup>17</sup>

### 3. 1. 2. X-Ray Diffraction Analysis (XRD)

Figure 3 shows the XRD diffraction patterns of the native and modified slag. The presence of sharp peak around  $2\theta = 25^\circ$  in the acid and alkali modified slag indicated greater crystallinity as compared to the native slag. The small peak around  $2\theta = 20^\circ$  was attributed to the pres-

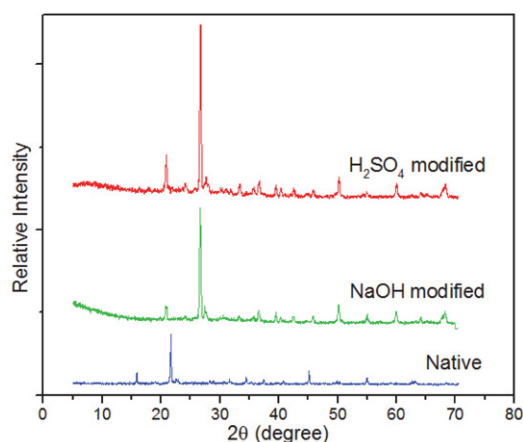


Figure 3. XRD of the native and chemically modified brick kiln slag

ence of feldspars in the adsorbent samples.<sup>18</sup> However, the intensity of these peaks in the modified adsorbents has been reduced as compared to the native adsorbent. Reaction between acid in SA and alkali in SB adsorbents and sodium silicate in slag resulting in the formation of insoluble precipitated silica may be attributed as one of the reason for this decrease in peak intensity. Presence of cristobalite in all adsorbent samples is confirmed by the presence of minute peaks occurring in  $2\theta = 30\text{--}60^\circ$ . Cristobalite is found in many clays such as bentonite, diatomite and has been reported to show adsorption characteristics.<sup>19</sup>

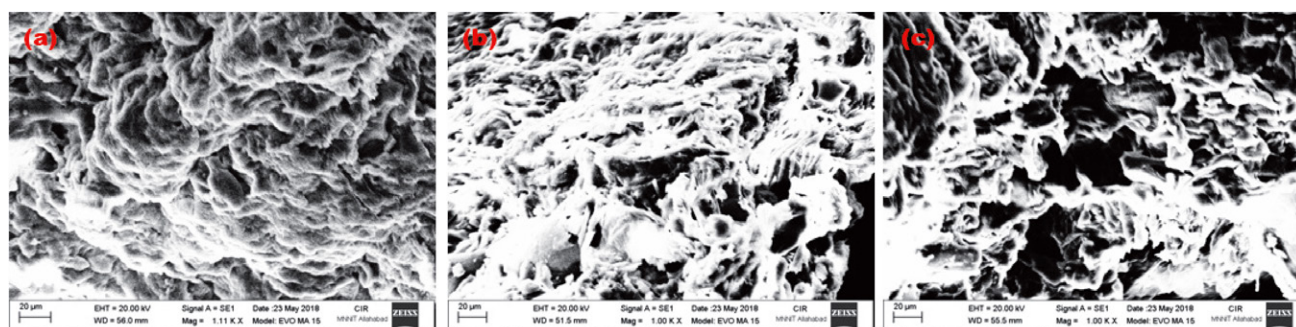


Figure 4. SEM micrographs of (a)  $\text{H}_2\text{SO}_4$  modified slag; (b) NaOH modified slag; (c) native slag

### 3. 1. 3. Scanning Electron Microscopy (SEM)

The SEM micrographs of the native and modified adsorbents have been shown in Figure 4. Relatively thick and homogeneous morphology resulting from processing of bricks at high temperature was seen in all the adsorbent samples. The modified adsorbent samples represented relatively high porosity as compared to the native. The acid modified adsorbent sample was observed to have porous surface morphology with minute cracks generation. These cracks may have been created due to elevated oxidizing property of  $H_2SO_4$  that breaks down the crystal lattice of the calcined clay. However, in the case of alkali modified slag, insoluble sodium silicate was formed when the adsorbent was treated with NaOH which was washed with water thus resulting in equal and lesser porosity of the NaOH modified adsorbent as compared to the native.<sup>20</sup>

## 3. 2. Adsorption Study

### 3. 2. 1. Effect of Contact Time

In order to investigate the effect of time on the adsorption, batch adsorption was performed using 100 mL of 1 mg/L of As(III) ions solution using 0.25 g of each adsorbent. It was observed that the relative removal percentage of As(III) ions increased with contact time with saturation occurring after 75 and 120 min respectively, for acid and alkali modified and native slag (Figure 5(a)). Presence of the concentration gradient between those of the adsorbed and the unadsorbed As(III) ions and the availability of vacant sites provided the necessary driving force for increase in adsorption capacity as a function of time.<sup>21</sup> Greater number of As(III) ions were adsorbed at the onset of adsorption due to greater number of available active sites. It was also observed that the SB adsorbent exhibited the lesser adsorption capacity than the acid modified slag with the same saturation time. This was probably due to oxidising tendency and greater porosity of the SA adsorbent than that of native. Saturation of the active sites may be ascribed to the presence of repulsive forces between the adsorbed As(III) ions and the bulk adsorbate concentration.

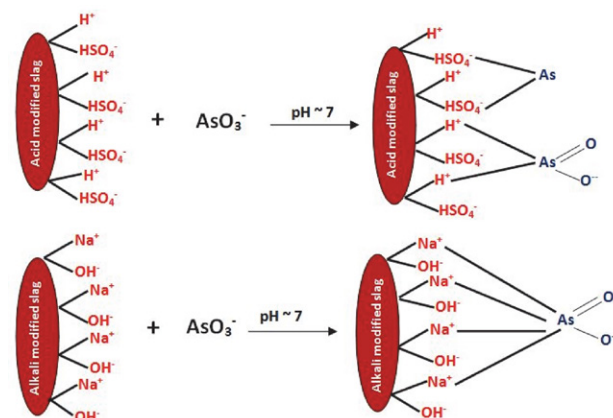
### 3. 2. 2. Effect of Adsorbent Dose

The effect of adsorbent dose on removal percentage of As(III) ions has been shown in Figure 5(b). Adsorbent dose was varied from 0.1 to 0.9 g/100 mL at pH = 7.0 in order to study its effect on removal percentage of As(III). Initially the removal percentage of As(III) ions was found to increase with adsorbent dose with saturation reaching at 0.3 and 0.6 g/100 mL respectively for acid and alkali modified and native slag respectively. Decrease in removal capacity of As(III) ions beyond the equilibrium may be probably due to increase in mass transfer resistance which decreased the relative uptake capacity of As(III) ions from its aqueous solution.<sup>22</sup> It can also be inferred from Figure 5(b) that the acid modified slag showed greater adsorption

capacity than the alkali modified slag with the same adsorbent dose due to the oxidising tendency of acid than that of alkali. Another reason may be attributed to the presence of surface charge resulting in increase of binding tendency of As(III) ions on the surface of the acid modified adsorbent. Lower removal percentage for alkali modified slag than that of acid modified with same adsorbent dose may also be due to the reaction of alkali and silica in slag resulting in the formation of insoluble precipitates of silicates which hindered the adsorption capacity of As(III) ions.<sup>20</sup>

### 3. 2. 3. Effect of pH

The pH of the adsorbate was varied from 2.0 to 10.0 at a fixed adsorbate concentration in order to study its effect on the adsorption capacity of the synthesised adsorbents. It was observed from Figure 5(c) that the adsorption capacity was observed to be quite low at both acidic and alkaline pH. The maximum adsorption took place at pH = 7.0 irrespective of the nature of the adsorbent. This was probably due to speciation of As(III) ions. As(III) ions are predominantly available as  $H_3AsO_3$  at pH < 8.0 and  $H_2AsO_3^-$ ,  $HAsO_3^{2-}$  and  $AsO_3^{3-}$  at pH > 8.0. From Table 1, it can be observed that the values of  $pH_{PZC}$  are 8.2, 8.1 and 9.1 respectively, for  $H_2SO_4$  modified slag, NaOH modified slag and native. Consequently, As(III) ions can be adsorbed by the electrostatic force of attraction between the neutral species from the positively charged surface of the adsorbent at a pH <  $pH_{PZC}$ . The maximum removal percentage at pH = 7.0 was probably due to the Van-der-waals forces of attraction between  $H_3AsO_3$  (neutral) and the adsorbent's surface. This may result in the binding of these neutral species to the positively charged surface of the adsorbent. At alkaline pH, the dominating negatively charged species are formed resulting in electrostatic repulsion between the negatively charged surface of the adsorbent and the negatively charged As(III) ions thereby reducing the relative uptake capacity of As(III) ions at alkaline pH.<sup>23</sup> Under optimised condition of pH (~7.0), As(III) ions are capable of binding with the sulphate ions on



**Scheme 1.** Schematic representation of the proposed mechanism for As(III) ions adsorption using acid and alkali modified industrial slag at pH = 7.0 and temperature = 298 K

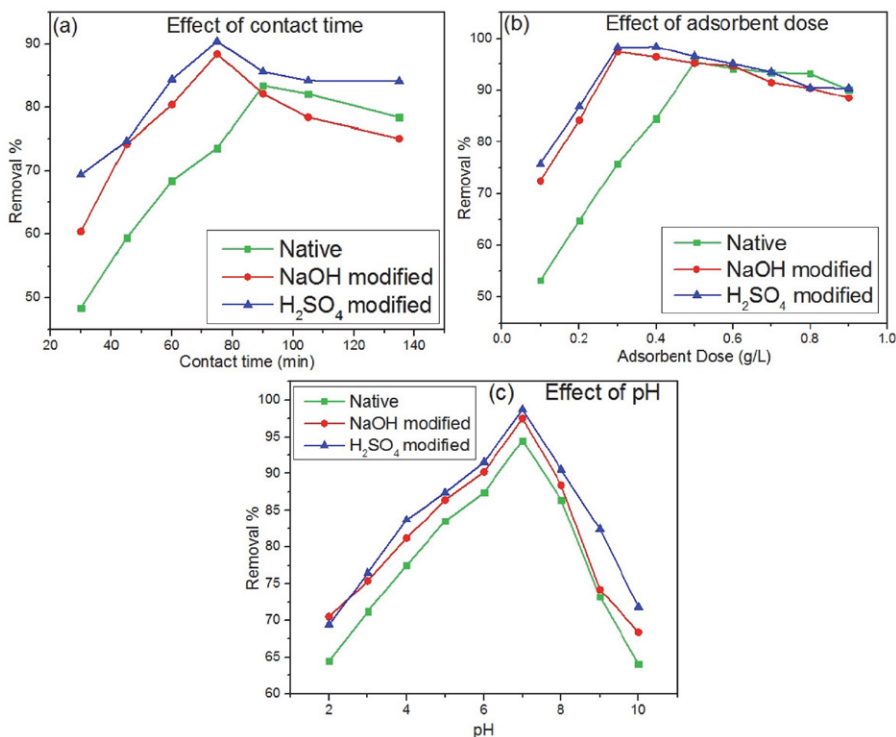


Figure 5. Influence of (a) Contact time; (b) Adsorbent dose; (c) pH on the adsorption of As(III) using native and modified brick kiln slag at 298 K

the surface of the acid modified slag releasing a water molecule as a by-product while arsenate ions can bind with the hydrogen ions forming weak arsenious acid. In the case of alkali modified slag, arsenic (III) oxides have the tendency to bind with the sodium ions forming sodium arsenite.<sup>24</sup> The probable mechanism has been illustrated in Scheme 1.

### 3. 3. Adsorption Kinetics

Kinetics of adsorption dictates the dependence of adsorption capacity with time. Adsorption experiments were performed using 0.3 g each of SA and SB and 0.6 g of SN at pH = 7.0 and temperature = 298 K. Acid and alkali modified slag exhibited a rapid uptake time for the first 75 min and then the rate of adsorption decreased and equilibrium was attained in 100 min. In the present study, three kinetic models (pseudo first order kinetic, pseudo second order kinetic and intraparticle diffusion models) have been studied to describe the behaviour of experimental adsorption capacity with time.

Pseudo first order kinetic model is represented in Eq. (14):

$$\ln(q_e - q_t) = \ln q_e - k_1 t \quad (14)$$

Pseudo second order kinetic model can be represented in Eq. (15):

$$\frac{t}{q_t} = \frac{1}{k_2 q_e^2} + \frac{t}{q_e} \quad (15)$$

where  $q_e$  and  $q_t$  represents the equilibrium and instantaneous adsorption capacities in  $mg/g$ ,  $k_1$  and  $k_2$  are the first and second order rate constants respectively. Intraparticle diffusion model is represented in Eq. (16):

$$q_t = K_{id} t^{1/2} + C \quad (16)$$

where  $K_{id}$  is the intraparticle rate constant in  $mg/g \cdot min^{1/2}$  and  $C$  is the y-intercept.

The kinetic plots for As(III) adsorption using native and modified slag have been presented in Figure 6 and the parameters are tabulated in Table 2. It can be seen from the table that the  $R^2$  values obtained from the pseudo first order kinetic model were less than 0.9 irrespective of the nature of the adsorbent. The obtained values of the first order rate constants ( $k_1$ ) were 0.033, 0.028 and 0.035  $min^{-1}$  respectively, for  $H_2SO_4$  modified, NaOH modified and native. The theoretically obtained values of  $q_e$  were 8.2, 3.2 and 1.2  $mg/g$ , respectively, for  $H_2SO_4$  modified slag, NaOH modified slag and native which were observed to be much lower than the values obtained from the experiments (14.2  $mg/g$  for  $H_2SO_4$  modified slag, 12.05  $mg/g$  for NaOH modified slag and 7.32  $mg/g$  for native slag). Thus, it can be inferred that pseudo first order kinetic model did not give a good correlation with the experimental values irrespective of the type of modification.

The second order rate constant values ( $k_2$ ) obtained from the pseudo second order kinetic plots were  $6.6 \times 10^{-5}$ ,  $3.1 \times 10^{-4}$  and  $2.6 \times 10^{-3}$   $g(mg \cdot min)^{-1}$ , respectively, for  $H_2SO_4$  modified slag, NaOH modified slag and native. The

Table 2. Estimated kinetic parameters for As(III) adsorption using native and chemically modified slag

Adsorbents	Pseudo First order kinetics			Pseudo Second order kinetics			Intraparticle Diffusion model		
	$q_e$ (mg/g)	$k_1$ ( $\text{min}^{-1}$ )	$R^2$	$q_e$ (mg/g)	$k_2$ ( $\text{g}(\text{mg} \cdot \text{min})^{-1}$ )	$R^2$	$K_{id}$ ( $\text{mg}/\text{g} \cdot \text{min}^{1/2}$ )	C	$R^2$
Acid modified BKS	8.21	0.033	0.832	10.64	$6.61 \times 10^{-5}$	0.985	0.033	0.241	0.842
Alkali modified BKS	3.24	0.028	0.715	5.72	$3.11 \times 10^{-4}$	0.988	0.034	0.145	0.854
Native	1.12	0.036	0.851	2.25	$2.41 \times 10^{-3}$	0.974	0.024	0.041	0.889

values of the initial rate constant ( $h = k_2 \cdot q_e^2$ ) were  $7.4 \times 10^{-3}$ , 0.012 and 0.031  $\text{mg}/\text{g}\cdot\text{min}$ , respectively, for  $\text{H}_2\text{SO}_4$  modified slag, NaOH modified slag and native and were observed to be significantly higher than the rate  $k_2$  values. This showed that As(III) adsorption over the native and modified slag was quite rapid at the onset of adsorption.<sup>24,25</sup> Moreover, the  $R^2$  values ( $> 0.95$ ) obtained from pseudo second order kinetic model showed its goodness of fit with the adsorption data. From the intraparticle diffusion plots (Figure 6(c)), it can be ascertained that the plots does not passes through origin indicating that intraparticle diffusion was not solely the rate controlling mechanism and some degree of film diffusion was expected to occur for As(III) adsorption. In order to have a clear picture of the rate controlling mechanism, mass transfer models have been studied.

The values of  $q_e$  shown in the above table represent the theoretical values of the equilibrium adsorption capacity calculated from the respective kinetic model equations.

### 3. 4. Mass Transfer Models

#### 3. 4. 1. External Diffusion Model

It was observed from Table 3 that the mass transfer coefficients decreased with increase in the concentration of As(III) ions. Driving force for adsorption is directly proportional to the adsorbate concentration. As the number of active sites on the adsorbent's surface was fixed, the mass transfer coefficients decreased with increase in As(III) concentration. Another reason for this behaviour may be attributed from the adsorption equilibrium theory. Since the external mass transfer coefficient is inversely proportional to the slope of operating lines at equilibrium, the values of external mass transfer coefficient decreased with increase in initial As(III) ions concentration in the bulk solution. The external mass transfer is also said to be the controlling variable when the model is linear. Increase in contact time decreased the strength of boundary layer resistance which significantly increased the mobility of

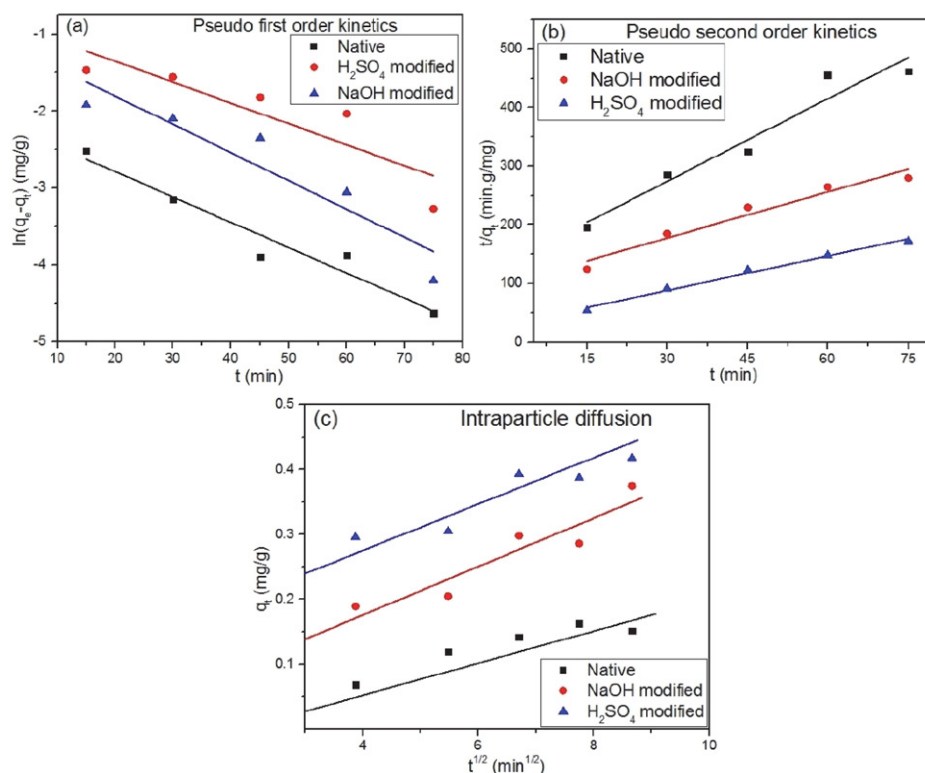


Figure 6. Kinetic plots for As(III) adsorption using native and chemically modified brick kiln slag at 298 K and pH = 7.0

**Table 3.** External Diffusion Model Mass Transfer Coefficients for As(III) adsorption

$C_o$ (mg/L)	Native		$H_2SO_4$ modified		NaOH modified	
	$k_f$ (m/s)	$R^2$	$k_f$ (m/s)	$R^2$	$k_f$ (m/s)	$R^2$
1	$1.15 \times 10^{-10}$	0.982	$1.49 \times 10^{-10}$	0.972	$1.30 \times 10^{-10}$	0.964
2	$0.85 \times 10^{-10}$	0.964	$1.38 \times 10^{-10}$	0.982	$1.21 \times 10^{-10}$	0.976
3	$0.65 \times 10^{-10}$	0.971	$1.25 \times 10^{-10}$	0.958	$1.12 \times 10^{-10}$	0.963
4	$0.51 \times 10^{-10}$	0.975	$1.07 \times 10^{-10}$	0.964	$1.02 \times 10^{-10}$	0.975
5	$0.39 \times 10^{-10}$	0.961	$0.95 \times 10^{-10}$	0.955	$0.85 \times 10^{-10}$	0.985

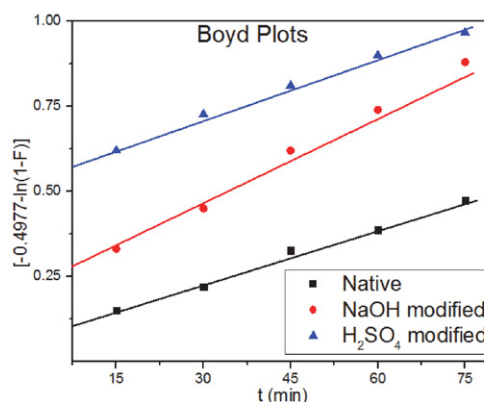
As(III) ions during the initial stages of adsorption. Thus external mass transfer coefficient cannot be neglected even during the initial stages of adsorption.<sup>26</sup>

### 3. 4. 2. Boyd Model

A clear difference between the intraparticle and film diffusion helps to understand the exact rate determining step for As(III) adsorption using native and modified slag. The linear plot of  $[-0.4977 - \ln(1-F)]$  versus time is shown in Figure 7. The plots does not passes through origin which in an indicative of the film diffusion as the rate determining step in As(III) adsorption using native and modified brick kiln slag. Moreover, the  $R^2$  values obtained from intraparticle diffusion ( $R^2 = 0.85$ ) was significantly lower than those obtained from the Boyd plots ( $R^2 = 0.96$ ). This further confirmed the possibility of film diffusion at the onset of adsorption and thereafter intraparticle diffusion. The obtained  $B$  values from the linear plots shown in Figure 7 have been used to estimate the effective diffusivity values ( $D_i$ ) in  $m/s$ . It is shown in Eq. (17):

$$B = \frac{D_i \pi^2}{r^2} \quad (17)$$

where  $r$  is the radius of the adsorbent particle in  $m$ . The estimated  $D_i$  values were:  $0.18 \times 10^{-10}$ ,  $0.25 \times 10^{-10}$  and  $0.27 \times 10^{-10} m/s$  respectively, for native, NaOH and  $H_2SO_4$  modified slag. These values almost show a similar trend irrespective of the nature of the adsorbent. However, the  $D_i$  value of  $H_2SO_4$  modified slag was slightly higher than NaOH modified slag. This further confirmed the ease of mobility of As(III) ions from the bulk solution to the  $H_2SO_4$  modified slag. These findings clearly show that the

**Figure 7.** Boyd Mass plots for As(III) adsorption using native and chemically modified brick kiln slag

adsorption of As(III) ions using native,  $H_2SO_4$  and NaOH modified slag was controlled by film diffusion or surface diffusion at the initial stages followed by intraparticle diffusion.

### 3. 4. 3. McKay et al Model

The plots of the experimental adsorption data for As(III) adsorption using native and modified slag at different initial concentrations have been shown in Figure 8 and the estimated mass transfer coefficients ( $\beta_L$ ) from this model have been summarised in Table 4. It can be clearly observed that  $\beta_L$  decreased with increase in initial As(III) concentration irrespective of the type of adsorbent. The values for  $\beta_L$  showed that the velocity of the As(III) ions to migrate from the bulk liquid phase to the solid adsorbent's surface.<sup>27</sup> The obtained values of mass transfer coefficients ( $\beta_L$ ) from this model were observed to be much higher

**Table 4.** Estimated values of mass transfer coefficients ( $\beta_L$ ) from McKay et al model

$C_o$ (mg/L)	Native		$H_2SO_4$ modified		NaOH modified	
	$\beta_L$ (m/s)	R2	$\beta_L$ (m/s)	R2	$\beta_L$ (m/s)	R2
1	$2.12 \times 10^{-7}$	0.705	$5.26 \times 10^{-7}$	0.605	$4.21 \times 10^{-7}$	0.634
2	$2.05 \times 10^{-7}$	0.635	$4.15 \times 10^{-7}$	0.648	$3.15 \times 10^{-7}$	0.607
3	$1.25 \times 10^{-7}$	0.715	$3.02 \times 10^{-7}$	0.705	$2.02 \times 10^{-7}$	0.615
4	$0.82 \times 10^{-7}$	0.698	$2.12 \times 10^{-7}$	0.687	$1.11 \times 10^{-7}$	0.708
5	$0.65 \times 10^{-7}$	0.714	$1.08 \times 10^{-7}$	0.713	$0.93 \times 10^{-7}$	0.652

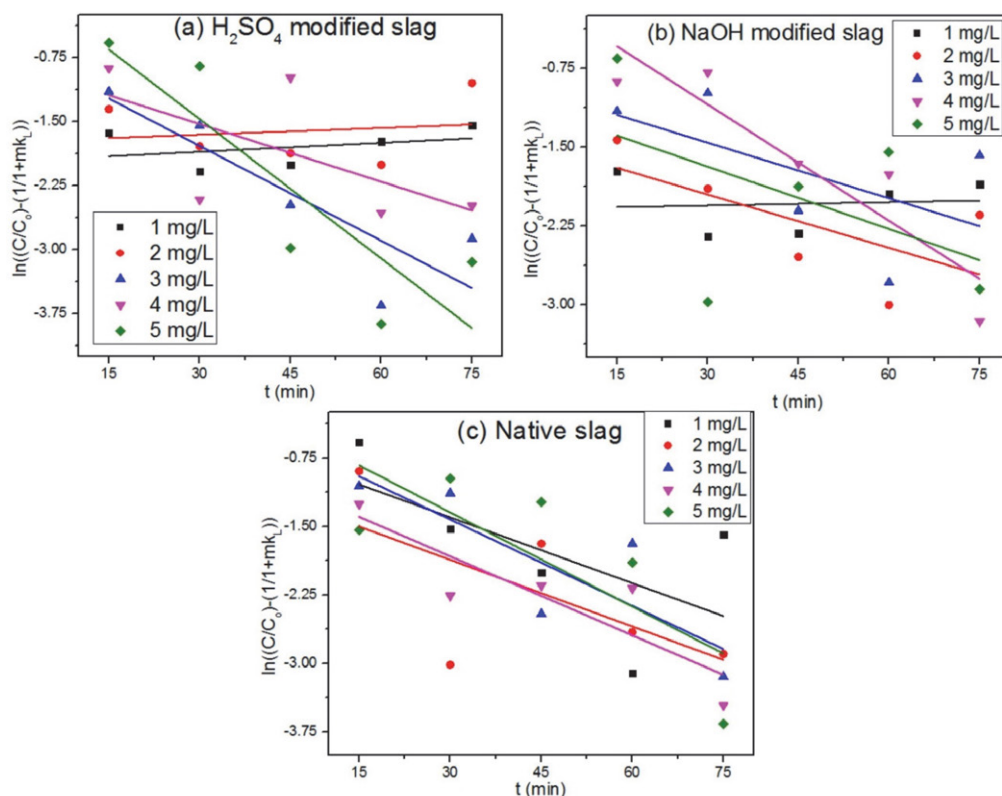


Figure 8. McKay et al mass transfer plots for native and modified slag at different initial As(III) concentrations

than those calculated from the external diffusion model. The linear regression values calculated from this model ( $R^2 < 0.9$ ) indicated that the ease of migration of As(III) ions from the bulk solution was quite high and thus cannot be inferred as the rate controlling mechanism.

### 3. 4. 4. Dimensionless Numbers

#### 3. 4. 4. 1. Sherwood Number

The influence of initial concentration of As(III) ions on the Sherwood number is shown in Figure 9. The values of the dimensionless number were less than 1.0 indicating the rate of adsorption of As(III) ions on to the native and modified adsorbents was controlled by film mass transfer or surface diffusion. Based on the linearity of the plots, Eqs. (18)–(20) have been obtained for the adsorbent samples modified with  $H_2SO_4$ , NaOH and native respectively. It was observed that Sherwood number decreased with the increase in initial concentration of As(III) ions in the bulk adsorbate phase. Thus, it can be inferred that the rate of mass transfer for adsorption of As(III) ions increased with decrease in the bulk adsorbate concentration.

$$Sh = 2.97(C_0)^{-0.376} \quad (18)$$

$$Sh = 4.12(C_0)^{-0.215} \quad (19)$$

$$Sh = 4.83(C_0)^{-0.588} \quad (20)$$

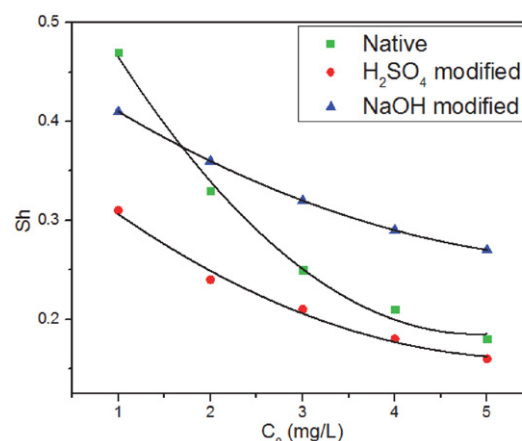


Figure 9. Influence of Sherwood number on initial As(III) concentration using native and chemically modified brick kiln slag

#### 3. 4. 4. 2. Transport Number

The variation of Transport number with respect to initial As(III) ions concentration has been shown in Table 5. It was observed that the values of Transport number ( $n$ ) was almost equal to 0.5 thus showing Fickian diffusion or surface diffusion. This was probably due to interaction of As(III) ions with the surface of the adsorbent through the external film of adsorbate or boundary layer surrounding the adsorbent particle.<sup>28</sup> Thus, in the present research, it can be inferred that external mass transfer had a dominating effect than intraparticle diffusion. This may be attributed to



**Table 5.** Estimated Transport number at various initial concentration of As(III) ions

$C_0$ (mg/L)	Native		$H_2SO_4$ modified		NaOH modified	
	$n$	$k_m$	$n$	$k_m$	$n$	$k_m$
1	0.524	0.758	0.547	0.775	0.522	0.755
2	0.498	0.697	0.559	0.749	0.517	0.849
3	0.517	0.847	0.568	0.687	0.567	0.825
4	0.589	0.719	0.497	0.682	0.529	0.715
5	0.510	0.729	0.518	0.798	0.579	0.709

the rate of adsorptive mass transfer taking place through the stagnant film of the adsorbate which was caused by laminar motion (as the fluid transport takes place without the aid of any external agent) of the bulk liquid phase during the batch adsorption experiments. It was also observed that the value of transport number remained constant irrespective of the bulk adsorbate concentration showing that the initial As(III) concentration has no effect on transport number.

### 3. 5. Adsorption Isotherms

Adsorption isotherms are used to describe the metal uptake capacity at fixed temperature. Adsorption of As(III) ions was performed at 298 K and 7.0 pH at different adsorbent doses (0.2–1.0 g). In the present study, three isotherms (Langmuir, Freundlich and Temkin isotherms) have been used to study the As(III) adsorption behaviour with native and modified slag. The linearized model for Langmuir isotherm is represented in Eq. (21):

$$\frac{C_e}{q_e} = \frac{C_e}{q_m} + \frac{1}{k_L q_m} \quad (21)$$

where  $q_m$  is the maximum adsorption capacity (mg/g),  $k_L$  is the Langmuir constant (L/g). Separation factor ( $R_L$ ) is used to determine the feasibility of the process and is given by Eq. (22):

$$R_L = \frac{1}{k_L C_{i+1}} \quad (22)$$

The isotherm is considered to be favourable if  $0 < R_L < 1$ . The Freundlich isotherm is represented in Eq. (23):

$$\log q_e = \left(\frac{1}{n}\right) \log C_e + \log k_f \quad (23)$$

where  $k_f$  and  $n$  are Freundlich constants. The extent of feasibility of the adsorption of As(III) ions can be determined from the value of  $n$ . For a favourable process,  $(1/n) < 1$ . Temkin isotherm is shown in Eq. (24):

$$q_e = B \ln C_e + B \ln A_T \quad (24)$$

$$B = \frac{RT}{b} \quad (25)$$

where  $b$  is the Temkin constant (J/mol),  $A_T$  is the equilibrium binding constant (L/g),  $R$  is universal gas constant (8.314 J/mol.K),  $T$  is the absolute temperature (K).

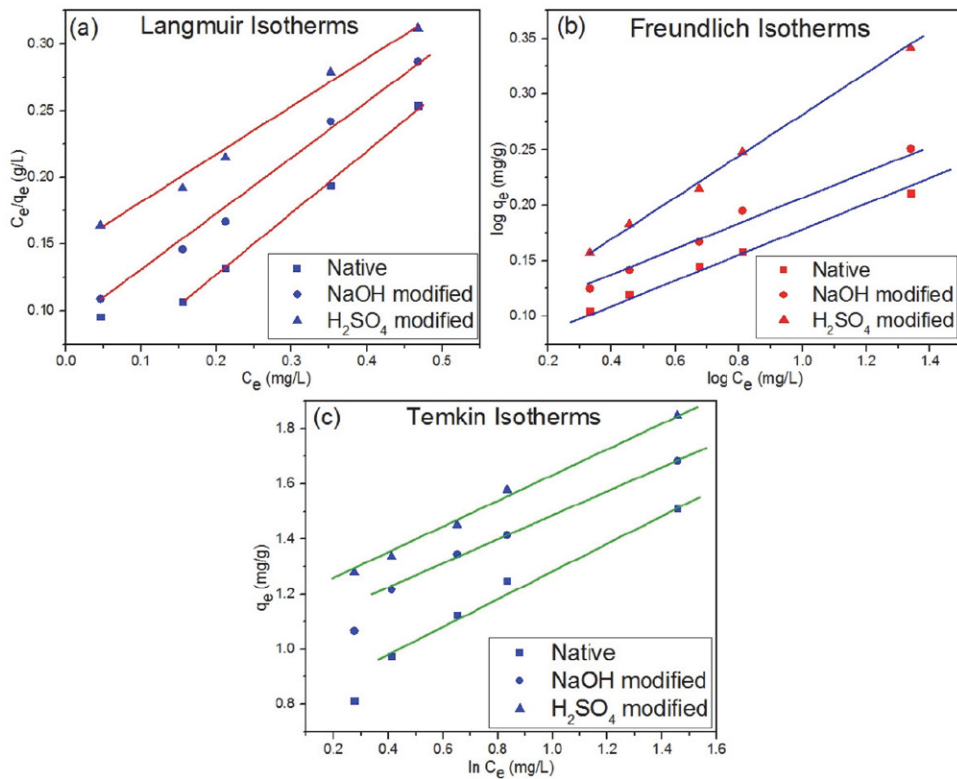
The adsorption isotherm plots are shown in Figure 10 and the calculated parameters are shown in Table 6. Based on the value of linear regression coefficient ( $R^2$ ), it was observed that adsorption of As(III) ions on native and modified brick kiln slag followed Freundlich isotherm indicating multilayer adsorption and heterogeneous nature of the adsorbent. The acid modified slag (SA) was observed to show a maximum As(III) uptake capacity of 13.6 mg/g which was observed to be 1.4 times that of SB and 2.1 times that of BKS. The  $n$  values from Freundlich isotherm indicated a good adsorption affinity towards As(III) ions. The obtained  $A_T$  values (from the Temkin isotherm) was found to be maximum (8.86 L/g) for  $H_2SO_4$  modified slag (SA) indicating its maximum adsorption affinity towards As(III). The relative affinity for As(III) adsorption follows the order of: SA > SB > Native. The  $b_T$  values were almost same irrespective of the type of adsorbent which showed less variation in heat of adsorption.<sup>29</sup>  $HNO_3$  modified activated carbon fibres showed a maximum uptake capacity of 8.65 mg/g where Langmuir isotherm was observed to show the best correlation coefficient.<sup>8</sup> Iron scrap slag was found to show adsorption capacity of 13.7 mg/g.<sup>10</sup> Thus, the adsorbent used in the present study can be used to remove As(III) from groundwater without any energy expense.

### 3. 6. Adsorption Thermodynamics

Adsorption thermodynamics expresses the removal capacity as a function of its temperature. Thermodynamic parameters were evaluated at pH = 7.0 using 0.3 g each of SA and SB and 0.6 g of BKS at different temperatures (298 – 313 K). This is generally expressed in the form of change in Gibbs Free energy ( $\Delta G^\circ$ ) which is shown in Eq. (26):

**Table 6.** Isotherm Parameters for As(III) ions adsorption using native and chemically modified slag

Adsorbents	Langmuir Isotherm parameters				Freundlich Isotherm parameters			Temkin Isotherm parameters		
	$q_m$ (mg/g)	$k_L$ (L/mg)	$R_L$	$R^2$	$k_f$ (mg/g)	$(1/n)$	$R^2$	$A_T$ (L/g)	$b$ (J/mol)	$R^2$
Acid modified BKS	13.57	3.58	0.252	0.875	8.57	0.18	0.974	8.86	94.08	0.954
Alkali modified BKS	10.34	2.79	0.207	0.864	6.48	0.21	0.965	7.38	93.08	0.951
Native	6.48	2.08	0.184	0.887	3.27	0.11	0.979	5.89	92.19	0.937



**Figure 10.** (a) Langmuir; (b) Freundlich; (c) Temkin isotherms at 298 K and 7.0 pH for As(III) adsorption using native and chemically modified brick kiln slag

$$\Delta G^\circ = -RT \ln K_c \quad (26)$$

For a favourable and spontaneous process,  $\Delta G^\circ < 0$ . Distribution coefficient ( $K_c$ ) is represented in Eq. (27):

$$K_c = \frac{q_e}{C_e} \quad (27)$$

$$\ln K_c = \frac{\Delta S}{R} + \frac{\Delta H}{RT} \quad (28)$$

Entropy ( $\Delta S$ ) and enthalpy ( $\Delta H$ ) was calculated from the linear plot of  $\ln K_c$  versus ( $1/T$ ). The evaluated thermodynamic parameters are shown in Table 7. From the Table 7, it can be observed that the values of Gibbs's free energy change ( $\Delta G^\circ$ ) were negative in nature thus indicating the feasibility of the adsorption of As(III) ions over the native and modified slag. Gibbs's free energy change is said to be an important thermodynamic parameter reflecting the spontaneity of the adsorption process. A higher value of

$\Delta G^\circ$  is an indicative of more energetically favoured adsorption. The adsorption is said to occur favourably and spontaneously if the value of  $\Delta G^\circ$  is negative. Thus from Table 7, it can be inferred that the adsorption of As(III) ions over native and modified slag was favourable and spontaneous at all temperatures. However, maximum negative values of  $\Delta G^\circ$  was observed at 298 K which is an indicative of maximum As(III) adsorption capacity at this temperature.

Negative values of enthalpy ( $\Delta H$ ) show the liberation of energy during the adsorption of As(III) ions i.e. the process is exothermic. Moreover, the calculated values of enthalpy change suggested that the adsorption of As(III) ions on the native and modified slag correspond to physical adsorption since the obtained values were below 40 kJ/mol.<sup>24</sup> Positive values of entropy showed the increase in the disorderness of the adsorbate-adsorbent interface due to adsorption of As(III) ions which was supposed to be less ordered than that in the bulk solution and thus reflected

**Table 7.** Estimated Thermodynamic Parameters for As(III) ions adsorption

Adsorbents	$\Delta G^\circ$ (kJ/mol)				$\Delta H$ (kJ/mol)	$\Delta S$ (J/molK)
	298 K	303 K	308 K	313 K		
Acid modified BKS	-6.52	-4.74	-1.85	-0.85	-20.17	41.28
Alkali modified BKS	-6.15	-3.75	-1.43	-0.73	-17.58	35.76
Native	-4.52	-2.15	-0.87	-0.64	-10.49	21.28

the affinity of the adsorbent towards As(III) ions in the bulk solution.<sup>30</sup>

## 4. Conclusions

Acid modified brick kiln slag (SA) showed the maximum rate of adsorption followed by alkali modified (SB) and native slag (SN). Mass transfer coefficients calculated were in the order of  $10^{-10}$  m/s for all the adsorbents which decreased with increasing concentration of As(III) ions in the bulk solution indicating that the driving force for mass transfer was inversely proportional to the As(III) concentration. Maximum value of mass transfer coefficients was obtained for the slag modified with  $H_2SO_4$  thus showing its fairly good adsorption capacity over a particular temperature range.

Maximum adsorption occurred at pH = 7.0 due to electrostatic attraction phenomena. Freundlich adsorption described the adsorption process indicating multilayer formation. Sherwood number interrelated initial concentration of As(III) ions according to Power Law model and were less than 1.0 for all the adsorbents showing that the mass transfer was limited by film diffusion. Thermodynamic evaluation showed that the adsorption was feasible at all temperatures with maximum adsorption taking place at 25 °C (298 K). Transport numbers obtained were independent of initial concentration of As(III) ions and the values were almost equal to 0.5 indicating Fickian mechanism or surface diffusion. This mass transfer study can be extensively used for the design of batch adsorbers to find the effect of various mass transfer parameters on the adsorption capacity and to determine the rate controlling mechanism.

## Conflict of Interests

The authors declare no conflict of interests regarding the publication of this paper.

## Acknowledgement

The authors are thankful to Technical Education Quality Improvement Programme (TEQIP-III) for providing the required funding to carry out the experiments and Centre for Interdisciplinary Research (CIR) of MNNIT Allahabad for allowing us to carry out sample characterizations.

## 5. References

1. D. Mohan, C. U. Pittman, Arsenic removal from water/wastewater using adsorbents-A critical review, *J. Hazard. Mater.* **2007**, *142*, 1–53. DOI:10.1016/j.jhazmat.2007.01.006
2. S. Verma, P. K. Verma, D. Chakrabarty, Arsenic Bio-volatilization by Engineered Yeast Promotes Rice Growth and Reduces Arsenic Accumulation in Grains, *Int. J. Environ. Res.* **2019**, *13*, 475–485. DOI:10.1007/s41742-019-00188-7
3. S. Shevade, R. G. Ford, Use of synthetic zeolites for arsenate removal from pollutant water, *Water Res.* **2004**, *38*, 3197–3204. DOI:10.1016/j.watres.2004.04.026
4. T. S. Y. Choong, T. G. Chuah, Y. Robiah, F. L. Gregory Koay, I. Azni, Arsenic toxicity, health hazards and removal techniques from water: an overview, *Desalination.* **2007**, *217*, 139–166. DOI:10.1016/j.desal.2007.01.015
5. V. P. Mulgundmath, R. A. Jones, F. H. Tezel, J. Thibault, Fixed bed adsorption for the removal of carbon dioxide from nitrogen: Breakthrough behaviour and modelling for heat and mass transfer, *Sep. Purif. Technol.* **2012**, *85*, 17–27. DOI:10.1016/j.seppur.2011.07.038
6. E. Torrik, M. Soleimani, M. T. Ravanchi, Application of Kinetic Models for Heavy Metal Adsorption in the Single and Multicomponent Adsorption System, *Int. J. Environ. Res.* **2019**, *13*, 813–828. DOI:10.1007/s41742-019-00219-3
7. C. J. Geankoplis, Transport Processes and Separation Process Principles: Includes Unit Operations, Transp. Process. Sep. Process Princ. (Includes Unit Oper. (2003).
8. J. Shi, Z. Zhao, J. Zhou, T. Sun, Z. Liang, Enhanced adsorption of As(III) on chemically modified activated carbon fibers, *Appl. Water Sci.* **2019**, *9*, 41. DOI:10.1007/s13201-019-0919-7
9. M. B. Shakoor, N. K. Niazi, I. Bibi, M. Shahid, F. Sharif, S. Bashir, S. M. Shaheen, H. Wang, D. C. W. Tsang, Y. S. Ok, J. Rinklebe, Arsenic removal by natural and chemically modified water melon rind in aqueous solutions and groundwater, *Sci. Total Environ.* **2018**, *645*, 1444–1455. DOI:10.1016/j.scitotenv.2018.07.218
10. V. Liem-Nguyen, V. Sjöberg, N. P. Dinh, D. H. Huy, S. Karlsson, Removal mechanism of arsenic (V) by stainless steel slags obtained from scrap metal recycling, *J. Environ. Chem. Eng.* **2020**, *8*, 103833. DOI:10.1016/j.jece.2020.103833
11. S. Wang, B. Gao, Y. Li, A. Mosa, A. R. Zimmerman, L.Q. Ma, W. G. Harris, K. W. Migliaccio, Manganese oxide-modified biochars: Preparation, characterization, and sorption of arsenate and lead, *Bioresour. Technol.* **2015**, *181*, 13–17. DOI:10.1016/j.biortech.2015.01.044
12. T. V. Nguyen, T. V. T. Nguyen, T. L. Pham, S. Vigneswaran, H. H. Ngo, J. Kandasamy, H. K. Nguyen, D. T. Nguyen, Adsorption and removal of arsenic from water by iron ore mining waste, *Water Sci. Technol.* **2009**, *60*, 2301–2308. DOI:10.2166/wst.2009.667
13. B. Narayana, T. Cherian, M. Mathew, C. Pasha, Spectrophotometric determination of arsenic in environmental and biological samples, *Indian J. Chem. Technol.* **2006**, *13*, 36–40. DOI: http://hdl.handle.net/123456789/6993.
14. M. Jansson-Charrier, E. Guibal, J. Roussy, B. Delanghe, P. Le Cloirec, Vanadium (IV) sorption by chitosan: Kinetics and equilibrium, *Water Res.* **1996**, *30*, 465–475. DOI:10.1016/0043-1354(95)00154-9
15. F. Matalkah, M. Mahmoud, A.G.N.D. Darsanasiri, N. Abdol, P. Soroushian, A. M. Balachandra, High-recycled-content hy-

- draulic cements of alternative chemistry for concrete production, *Int. J. Sustain. Eng.* **2018**, *11*, 282–291. DOI:10.1080/19397038.2018.1431973
16. M. L. Granizo, M. T. Blanco-Varela, S. Martínez-Ramírez, Alkali activation of metakaolins: Parameters affecting mechanical, structural and microstructural properties, *J. Mater. Sci.* **2007**, *42*, 2934–2943. DOI:10.1007/s10853-006-0565-y
17. J. Ojima, Determining of crystalline silica in respirable dust samples by Infrared Spectrophotometry in the presence of interferences, *J. Occup. Health.* **2003**, *45*, 94–103. DOI:10.1539/joh.45.94
18. A. Soultana, A. Valouma, G. Bartzas, K. Komnitsas, Properties of inorganic polymers produced from brick waste and metallurgical slag, *Minerals.* **2019**, *9*, 551. DOI:10.3390/min9090551
19. B. R. Berger, P. M. Bethke, The Behavior of Silica in Hydrothermal Solutions, in: Geol. Geochemistry Ep. Syst., **2020**. DOI:10.5382/Rev.02.03
20. L. Shrestha, M. Thapa, R. Shrestha, S. Maji, R. Pradhananga, K. Ariga, Rice Husk-Derived High Surface Area Nanoporous Carbon Materials with Excellent Iodine and Methylene Blue Adsorption Properties, *Carbon.* **2019**, *5*, 10. DOI:10.3390/c5010010
21. A. D. Gupta, S. Pandey, V. K. Jaiswal, V. Bhadauria, H. Singh, Simultaneous oxidation and esterification of cellulose for use in treatment of water containing Cu(II) ions, *Carbohydr. Polym.* **2019**, *222*, 114964. DOI:10.1016/j.carbpol.2019.06.003
22. S. Rahdar, M. Taghavi, R. Khaksefidi, S. Ahmadi, Adsorption of arsenic (V) from aqueous solution using modified saxaul ash: isotherm and thermodynamic study, *Appl. Water Sci.* **2019**, *9*, 87. DOI:10.1007/s13201-019-0974-0
23. K. Yang, W. Qin, W. Liu, Extraction of metal arsenic from waste sodium arsenate by roasting with charcoal powder, *Metals.* **2018**, *8*, 542. DOI:10.3390/met8070542
24. S. Ghosh, R. Prabhakar, S. R. Samadder, Performance of  $\gamma$ -aluminium oxide nanoparticles for arsenic removal from groundwater, *Clean Technol. Environ. Policy.* **2019**, 121–138. DOI:10.1007/s10098-018-1622-3
25. Z. Peng, X. Liu, H. Chen, Q. Liu, J. Tang, Characterization of ultraviolet-modified biochar from different feedstocks for enhanced removal of hexavalent chromium from water, *Water Sci. Technol.* **2019**, 1705–1716. DOI:10.2166/wst.2019.170
26. Z. Aksu, I.A. Isoglu, Use of agricultural waste sugar beet pulp for the removal of Gemazol turquoise blue-G reactive dye from aqueous solution, *J. Hazard. Mater.* **2006**, *137*, 418–430. DOI:10.1016/j.jhazmat.2006.02.019
27. D. Fu, Y. Zhang, F. Lv, P. K. Chu, J. Shang, Removal of organic materials from TNT red water by Bamboo Charcoal adsorption, *Chem. Eng. J.* **2012**, *193*, 39–49. DOI:10.1016/j.cej.2012.03.039
28. C. R. Girish, V. R. Murthy, Mass Transfer studies on Adsorption of Phenol from Wastewater using Lantana Camara, Forest Waste, *Int. J. Chem. Eng.* **2016**, *2016*, 5809505. DOI:10.1155/2016/5809505
29. İ. Şentürk, M. Alzein, Adsorption of Acid Violet 7 onto Acid-Activated Pistachio Shell: Isotherm, Kinetic and Thermodynamic Studies, *Acta Chim. Slov.* **2020**, *67*, 55–69. DOI:10.17344/acsi.2019.5195
30. P. M. Carijo, G. S. dos Reis, É. C. Lima, M. L. S. Oliveira, G.L. Dotto, Functionalization of corn stover with 3-aminopropyltriethoxysilane to uptake Reactive Red 141 from aqueous solutions, *Environ. Sci. Pollut. Res.* **2019**, *26*, 32198–32208. DOI:10.1007/s11356-019-06386-2

## Povzetek

Žlindro iz procesa žganja opeke (ang. brick kiln slag – BKS) smo uporabili za adsorpcijo nizkih koncentracij As(III) v šaržnem načinu. BKS smo modificirali s  $\text{H}_2\text{SO}_4$  (SA) in NaOH (SB) s ciljem povečanja adsorpcije. Maksimalno kapaciteto adsorpcije ( $13.7 \text{ mg/g}$ ) smo opazili pri SA in temperaturi 298 K, pH = 7.0, količini adsorbenta 0.3 g in času 70 min in je bila 1.4-krat višja od SB. Podatke adsorpcije smo modelirali s Freundlichovo adsorpcijsko izotermo in kinetiko psevdodrugega reda. Koeficient masnega transporta je padal z naraščajočo koncentracijo As(III), prevladujoči upor pa je bila difuzija skozi mejni sloj, ne glede na začetno koncentracijo As(III) ionov. Brezdimenzijsko Sherwoodovo število ( $Sh$ ) je bilo odvisno od As(III) koncentracije ( $C_0$ ) in sicer  $Sh = 2.97(C_0)^{-0.376}$  za SA,  $Sh = 4.12(C_0)^{-0.215}$  za SB in  $Sh = 4.83(C_0)^{-0.588}$  za BKS. Adsorpcije je bila favorizirana pri 298 K temperature (glede na vrednost  $\Delta G^\circ$ ). Obdelano žlindro lahko torej uporabimo za učinkovito odstranjevanje As(III) ionov iz površinskih voda.



Except when otherwise noted, articles in this journal are published under the terms and conditions of the Creative Commons Attribution 4.0 International License

Scientific paper

# Effect of the Exchanged Cation in an Algerian Montmorillonite Used as a Heterogeneous Catalyst for Biginelli Reaction

Fatiha Belferdi,<sup>1,\*</sup> Farida Bouremmad,<sup>2</sup> Shalima Shawuti<sup>3</sup>  
and Mehmet Ali Gulgun<sup>3</sup>

<sup>1</sup> Laboratoire de Pharmacologie et de Phytochimie, Université Mohamed Seddik Ben Yahia, Jijel, Algeria.

<sup>2</sup> Laboratoire de l'Interaction des Matériaux et de l'Environnement (LIME) Université Mohamed Seddik Ben Yahia, Jijel, Algeria.

<sup>3</sup> Sabanci University, FENS, Orhanli Tuzla, Istanbul 34956, Turkey.

\* Corresponding author: E-mail: fbelferdi@gmail.com

Received: 07-26-2020

## Abstract

In this work, an Algerian montmorillonite (Mt) is exchanged by different cations from the transition metals family, namely: Cu<sup>2+</sup>, Ni<sup>2+</sup>, Cr<sup>3+</sup>, Co<sup>2+</sup>, Fe<sup>2+</sup> and Fe<sup>3+</sup>, it is used as a heterogeneous catalyst for Biginelli reaction. The exchanged cations are known for their catalytic properties in homogeneous catalysis. The main purpose is to study the effect of the exchanged cations on the yield and the kinetics of the reaction. The characterization of montmorillonite was carried out by XRD, which allows us to follow the evolution of the basal spacing  $d_{001}$  as a function of the exchanged cation and to show that the exchange operation has not altered the montmorillonite structure. The cation exchange capacity (CEC) is determined by the titration of the exchanged cation by atomic absorption. The product of the reaction is characterized by NMR, IR and by the determination of the melting point. In addition, the importance of the introduction order of the reagents into the reaction medium has been demonstrated on the yield and the kinetics. Finally, the obtained results show that the exchanged montmorillonite is competitive with other costly heterogeneous and homogeneous catalysts.

**Keywords:** Montmorillonite; heterogeneous catalyst; Biginelli reaction; multi-component reactions (MCRs).

## 1. Introduction

Currently, the chemical industry and in particular the fields of organic and pharmaceutical chemistry are confronted with certain constraints of environmental interests. This requires the adoption of new procedures which respect the environmental and ecological balance while improving the cost and efficiency of the reactions. In this sought-after environmental framework, heterogeneous catalysis greatly contributes to the development of the chemical industry and offers many advantages compared to homogeneous catalysis, because the solid catalyst is easy to recover from the reaction medium and to regenerate and it can also be used in small amounts.<sup>1–3</sup> Scientific research continues to progress in this area and mainly aims to find new solid catalysts that better meet economic and environmental requirements. In this field common-

ly known as green chemistry, montmorillonite which is a material of natural origin, has gained interest for contact and surface phenomena applications such as adsorption for elimination of pollutants and heterogeneous catalysis; this is justified by its abundance and low cost, its effectiveness in developing important specific surfaces area, the presence of electrical charges on its surface and its cation exchange capacity.<sup>4–7</sup>

Montmorillonite is a natural 2/1 type aluminosilicate, consisting of a superposition of sheets each containing an octahedral AlO<sub>6</sub> layer sandwiched between two tetrahedral SiO<sub>4</sub> layers. The vertices of AlO<sub>6</sub> layer are occupied by oxygen or by hydroxides and the center by aluminum, while the vertices of SiO<sub>4</sub> layer are occupied by oxygen and the center by silicon.<sup>8</sup> Each sheet has a negative charge due to the substitution of the central atoms of these layers by atoms of lower charges; the negative charge

thus generated is balanced by the so-called compensating cation, occupying the interfoliar space.<sup>9</sup>

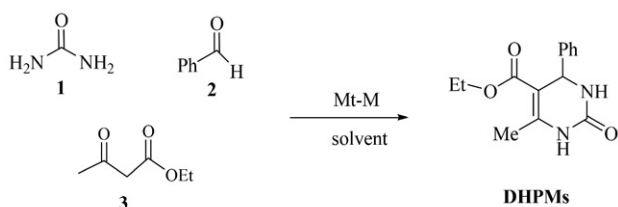
Generally, montmorillonites can be subjected to different treatments which lead to many structural modifications having a direct effect on their properties and thus on their applications in various fields. The cation exchange property, representing the quantity of cations which equilibrates the negative charge of the sheets, expressed in meq/100 g of clay, is very interesting as long as the interfoliar cations (generally Na<sup>+</sup> and Ca<sup>2+</sup>) can be replaced by cations from the transition metal series having the ability to catalyze reactions in a homogeneous medium.

Among the reactions of organic chemistry catalyzed by cations, we have the multicomponent reaction of Biginelli<sup>10</sup> where reagents ethyl acetoacetate and benzaldehyde react to give the dihydropyrimidinones (DHPMs). These latter are well known to have important therapeutic and pharmaceutical properties; indeed they work as tension regulators and calcium blockers,<sup>11–13</sup> moreover they show anti-HIV,<sup>14</sup> anti-malarial,<sup>15</sup> anti-epileptics,<sup>16</sup> antitumors,<sup>17–20</sup> anti-microbials,<sup>21</sup> anti-inflammatories,<sup>22</sup> anti-tubercular,<sup>23–24</sup> anti-bacterials,<sup>25–26</sup> and analgesic activities.<sup>27</sup>

Given its importance, the Biginelli reaction has been the subject of several researches and was carried out in the presence of various catalysts such as Brønsted acids in homogeneous medium as HCl,<sup>28–32</sup> H<sub>2</sub>SO<sub>4</sub>,<sup>33–34</sup> *para*-toluenesulfonic acid,<sup>35</sup> methanesulfonic acid,<sup>36</sup> HBF<sub>4</sub>,<sup>37</sup> boric acid,<sup>38</sup> phenylboronic acid,<sup>39</sup> formylphenylboronic acid,<sup>40</sup> carboxylic acid,<sup>41</sup> molybdophosphoric acid,<sup>42</sup> trifluoroacetic acid,<sup>43</sup> Lewis acids in homogeneous medium<sup>44–47</sup> as FeCl<sub>2</sub>, FeCl<sub>3</sub>, NiCl<sub>2</sub>, CoCl<sub>2</sub>, Ce(NO<sub>3</sub>)<sub>3</sub>, and heterogeneous catalysts as Fe<sub>2</sub>O<sub>3</sub> nanoparticles,<sup>48</sup> Nafion-Ga, Al<sub>2</sub>O<sub>3</sub>, TiO<sub>2</sub>, SiO<sub>2</sub> oxides.<sup>49–50</sup>

The Biginelli reaction was also carried out in the presence of montmorillonite of different origins, which has undergone various modifications and treatments. In the works of Singh, ZrO<sub>2</sub>-pillared clay was prepared and used in the Biginelli reaction under thermal and microwave heating.<sup>51</sup> A commercial montmorillonite KSF (Aldrich Chemical Co., USA) was used under microwave conditions by Mitra.<sup>52</sup> An acid treatment using HCl was applied to a montmorillonite from India to prepare a mesoporous catalyst<sup>53</sup> applied for the synthesis of DHPMs. Montmorillonite was also used as a composite catalyst material for the Biginelli reaction using the montmorillonite-graphene oxide<sup>54</sup> and bentonite/PS-SO<sub>3</sub>H composites.<sup>55</sup>

In the present work, an Algerian montmorillonite is used as a heterogeneous catalyst for the preparation of DHPMs by Biginelli reaction (Scheme 1). The main purpose is specifically to study the effect of the exchangeable cation on the yield and the kinetics of the reaction; a range of transition metal cations known for their catalytic activity in the homogeneous medium was selected, namely: Cu<sup>2+</sup>, Ni<sup>2+</sup>, Cr<sup>3+</sup>, Co<sup>2+</sup>, Fe<sup>2+</sup> and Fe<sup>3+</sup>.



Mt: Montmorillonite

M: (Cu<sup>2+</sup>, Ni<sup>2+</sup>, Cr<sup>3+</sup>, Co<sup>2+</sup>, Fe<sup>2+</sup> or Fe<sup>3+</sup>)

**Scheme 1.** Biginelli reaction catalyzed by exchanged montmorillonite.

## 2. Materials and Methods

### 2.1. Chemicals and Apparatus

The Algerian Na-montmorillonite (naturally, the exchangeable cation is Na<sup>+</sup>) comes from the deposit of Hammam Boughrara in Maghnia, located in western Algeria (hence the name Maghnite). It is supplied by ENOF Company (National company of useful substances and non-ferrous materials). Its chemical composition is: 69.4% SiO<sub>2</sub>, 1.1% MgO, 14.7% Al<sub>2</sub>O<sub>3</sub>, 0.8% K<sub>2</sub>O, 0.3% CaO, 1.2% Fe<sub>2</sub>O<sub>3</sub>, 0.5% Na<sub>2</sub>O, 0.2% TiO<sub>2</sub>, 0.05% As and 11% loss of ignition.<sup>56</sup>

X-ray diffraction (XRD) experiments were performed with a D8 Advance Bruker AXS diffractometer with CuK $\alpha$  radiation equipped with a curved graphite monochromator. The data were collected in the 2 $\theta$  range of 10–80° with a step size of 0.03° and a count time of 2 s per step. The cation exchange capacity CEC was determined by the titration of the exchanged cation in solution by using atomic absorption on a Perkin-Elmer Analyst 400 device, before and after the exchange operation. Then, the amount of exchanged cation was expressed relatively to the mass of clay used in the exchange operation.

All reactions were monitored by analytical thin-layer chromatography (TLC) and visualized by UV light (254–264 nm). Melting points were determined with a Kofler bench. Infrared (IR) spectra were recorded on a Shimadzu Fourier transform infrared spectrometer. Nuclear Magnetic Resonance (NMR) spectroscopy was registered on an Advance Bruker apparatus (600 MHz). Chemical shifts are reported in parts per million (ppm,  $\delta$ ) downfield from tetramethylsilane. Proton coupling patterns are described as singlet (s), doublet (d), triplet (t), quartet (q) and multiplet (m).

### 2.2. Preparation of the Exchanged Montmorillonite

For the exchange operation, 20 g of the natural Na-montmorillonite is stirred in 1 L of cation chloride solution (1 M) for 10 hours at 60 °C. This operation is

repeated three times. The exchanged montmorillonite is then washed several times with distilled water to remove chlorides which are controlled by measuring the conductivity of the washing water and its pH. Finally the final montmorillonite is oven-dried at 105 °C.

### 2. 3. Synthesis of 3,4-Dihydropyrimidin-2(1H)-one (DHPM)

A mixture of benzaldehyde (6.5 mmol), ethyl acetate (9.5 mmol), urea (6.25 mmol) and catalyst (20 % of benzaldehyde amount) was refluxed in solvent under magnetic stirring for an appropriate time. The progress of the reaction was monitored by TLC. The combined organic phases were washed with methanol to remove the impurities. The mixture was then filtered and the filtrate was collected. Thereafter, the methanol was evaporated to obtain a white solid. The crude products were purified by recrystallization from ethanol to get the desired product as a white solid.

## 3. Results and Discussion

### 3. 1. Characterization of the Exchanged Montmorillonite

#### 3. 1. 1. XRD Characterization

Figure 1 shows the diffractograms of montmorillonite exchanged with various cations and compared to the

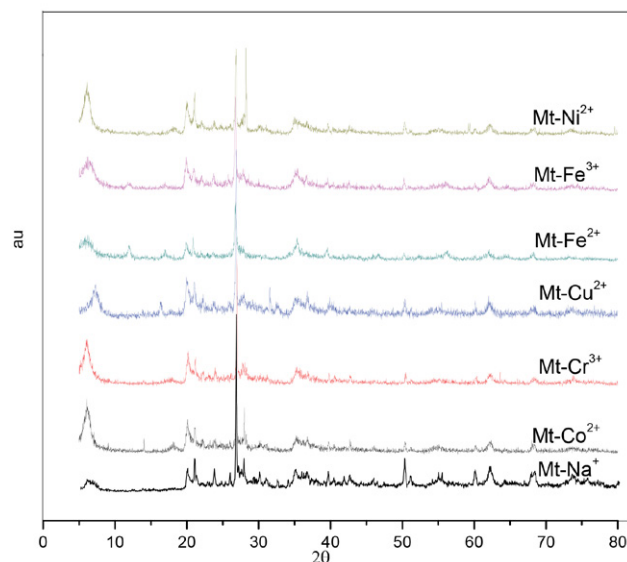


Figure 1. XRD diffractograms of montmorillonite exchanged with different cations.

Table 1. Basal spacing  $d_{001}$  and  $2\theta$  angle for each cation.

Mt-M	Mt-Na <sup>+</sup>	Mt-Fe <sup>3+</sup>	Mt-Fe <sup>2+</sup>	Mt-Co <sup>2+</sup>	Mt-Cr <sup>3+</sup>	Mt-Cu <sup>2+</sup>	Mt-Ni <sup>2+</sup>
$2\theta$ (°)	5.84	6.24	6.18	6.27	6.1	7.19	6.1
$d_{001}$ (Å)	15.12	14.15	14.28	14.08	14.48	12.28	14.48

base montmorillonite exchanged with Na<sup>+</sup> characterized by the peaks ( $2\theta = 6.22^\circ, 26^\circ, 35^\circ$  and  $50^\circ$ ).

Overall, we note that the cationic exchange did not alter the structure, only the angle  $2\theta$  shifts at the characteristic value of each cation; this leads to a change of the basal spacing  $d_{001}$  characterizing the interfoliar space, which can be calculated from the following Bragg equation:

$$d_{001} = \frac{\lambda}{2 \cdot \sin(\theta)} \quad (1)$$

Note that the value of  $d_{001}$  is a function of cation solvation degree, *i.e.* the number of water layers surrounding each cation. Table 1 shows the values of the distance  $d_{001}$  and the angle  $2\theta$  corresponding to each cation.

#### 3. 1. 2. Cation Exchange Capacity

For the cation exchange capacity (CEC), the obtained results are summarized in Table 2.

Table 2. Values of the cation exchange capacity.

Mt-M	CEC (meq/100 g)
Mt-Cu <sup>2+</sup>	47.40
Mt-Co <sup>2+</sup>	111.60
Mt-Ni <sup>2+</sup>	50.60
Mt-Fe <sup>2+</sup>	112.60
Mt-Fe <sup>3+</sup>	108.10
Mt-Cr <sup>3+</sup>	45.10

In Table 2, we note that the highest CEC values are obtained for montmorillonite exchanged with iron(II) (Fe<sup>2+</sup>), cobalt(II) (Co<sup>2+</sup>) and iron(III) (Fe<sup>3+</sup>); the CEC increases in this order: Fe<sup>2+</sup> > Co<sup>2+</sup> > Fe<sup>3+</sup> > Ni<sup>2+</sup> > Cu<sup>2+</sup> > Cr<sup>3+</sup>. Eberl<sup>57</sup> explained this behavior by the fact that the cation selectivity and cation fixation in clay depend on two competing forces: the first one is the attraction force of the cation for its hydration shell and the second is the attraction force of the cation for clay surfaces, thus the selectivity varies as these forces are different for each cation and the fixation occurs when the second force is greater than the first one.

### 3. 2. Characteristics of 3,4-Dihydropyrimidin-2(1H)-one (DHPM)

The analytical and spectroscopic data of the final product DHPM are: m.p. 205–207 °C (lit<sup>58</sup>: 206 °C). IR (KBr)  $\nu$ : 3235, 3103, 2942, 1718, 1695, 1593, 1216 cm<sup>-1</sup>.

$^1\text{H}$  NMR (300 MHz,  $\text{CDCl}_3$ )  $\delta$  1.24 (t, 3H), 2.35 (s, 3H), 4.09 (q, 2H), 5.30 (s, 1H), 5.89 (s, 1H), 7.09–7.26 (m, 5H), 8.28 (s, 1H).

### 3. 3. Effect of the Exchanged Cation on Biginelli Reaction

The Biginelli reaction was carried out in the presence of the montmorillonite used as a heterogeneous catalyst while being exchanged with different cations, a comparison with the conventional homogeneous catalyst in the presence of HCl was also performed. The results are shown in Table 3 in terms of the reaction time and yield; they clearly show that the highest yield was obtained by the Mt-Fe<sup>3+</sup> (60%), followed by the Mt-Co<sup>2+</sup> (57%), the Mt-Fe<sup>2+</sup> is in the third position, then the other three exchanged montmorillonites with chromium, nickel and copper give very similar yields. These results are primarily related to the high cation exchange capacity with Fe<sup>3+</sup> and Co<sup>2+</sup> and to the electronegativity of the cations (Co<sup>2+</sup> and Fe<sup>3+</sup> are more electronegative than Fe<sup>2+</sup>), which directly influences the acidity of the metal cations. Note that the use of Mt-Na<sup>+</sup> leads to a very low yield (13%) with a very long reaction time (32 h).

As can be seen, the use of montmorillonite exchanged with Fe<sup>3+</sup> and Co<sup>2+</sup> as a heterogeneous catalysts produces higher yields (60% and 57%, respectively) than the classical Biginelli method in homogeneous medium (56%) (catalysis in the presence of HCl). This is a very interesting result; it shows that the proposed heterogeneous catalysts (Mt-Fe<sup>3+</sup> and Mt-Co<sup>2+</sup>) are as efficient if not better than the homogeneous HCl catalyst considering their other advantages as well (easy to recover from the reaction medium and to regenerate, they can also be used in small amounts, low cost and eco-friendly).

Table 3. Effect of the exchanged cation on Biginelli reaction.

Catalyst	Time (h)	Yield (%)
Mt-Na <sup>+</sup> (raw material)	32	13
Mt-Cu <sup>2+</sup>	7	20
Mt-Co <sup>2+</sup>	9	57
Mt-Ni <sup>2+</sup>	9	20
Mt-Fe <sup>2+</sup>	7	34
Mt-Fe <sup>3+</sup>	8	60
Mt-Cr <sup>3+</sup>	10	24
HCl	7	56
Without catalyst	11	16

### 3. 4. Parameters Influencing the Reaction

In order to establish the optimal conditions for the reaction, we carried out a series of experiments by varying the parameters influencing the reaction such as the catalyst amount, the solvents and the introduction order of the reagents.

### 3. 4. 1. Effect of the Catalyst Amount

To improve the yields, we changed in this part the quantity of the catalyst, while limiting our study to the two catalysts that gave the highest yields, namely Mt-Fe<sup>3+</sup> and Mt-Co<sup>2+</sup>. The obtained results are summarized in Table 4. It is clear that the increase in the catalyst amount leads to an increase in yield; this can be explained by the increase of the active sites on the catalyst surface, which can fix more reagent molecules. The highest yield is obtained with the highest catalyst amount (60% of catalyst). We note that beyond 60% of the catalyst, we have obtained a pasty mixture, difficult to stir and the reaction becomes impossible.

Table 4. Effect of the catalyst amount on the yield of the reaction.

Catalyst	Catalyst amount (%)	Time (h)	Yield (%)
Mt-Fe <sup>3+</sup>	20	8	60
Mt-Fe <sup>3+</sup>	40	7	68
Mt-Fe <sup>3+</sup>	50	7	76
Mt-Fe <sup>3+</sup>	60	7	86
Mt-Co <sup>2+</sup>	20	9	57
Mt-Co <sup>2+</sup>	40	8	62
Mt-Co <sup>2+</sup>	50	8	69
Mt-Co <sup>2+</sup>	60	8	73

### 3. 4. 2. Effect of the Solvent

Various solvents were used: ethanol, water, toluene and glacial acetic acid with 50% of catalyst. The results are summarized in the Table 5.

Table 5. Effect of the solvent on the yield of the reaction.

Solvent	Mt-Fe <sup>3+</sup>		Mt-Co <sup>2+</sup>	
	Time (h)	Yield (%)	Time (h)	Yield (%)
Ethanol	7	76	8	69
Water	7	44	8	36
Toluene	5	62	7	65
Glacial acetic acid	5	82	6	77

The effect of the solvent is significant on both the kinetics and the yield of the reaction. In the presence of water as the solvent qualified as “clean solvent”, we have unfortunately noticed a considerable drop in yield compared to the other solvents (Table 5), whatever the catalyst used. The glacial acetic acid is the best solvent in terms of yield than all other tested solvents as shown in Table 5 (82% for Mt-Fe<sup>3+</sup> and 77% for Mt-Co<sup>2+</sup>), this can be explained by the fact that the acid can play the dual role of solvent and catalyst. We note that the reaction in the presence of acetic acid without catalyst has given a yield of 40% for a reaction time of 10 h.



### 3. 4. 3. Effect of the Introduction Order of the Reagents

In heterogeneous catalysis, it is well known that the adsorption of the reactants on the surface of the catalyst is an important and limiting step of the chemical reaction. Thus the introduction order of the reagents into the reaction medium becomes important. We therefore proceeded in three different processes with Mt-Fe<sup>3+</sup> (50%) each consisting of two steps: in the first step, one of the three reagents was stirred with Mt-Fe<sup>3+</sup> in the presence of the solvent for 2 hours to allow sufficient time for the adsorption phenomenon, in the second step, the other two reagents were added under refluxing conditions (Table 6). **Note:** As the acetic acid has a double role of catalyst and solvent, we use in this part ethanol as solvent in order to show only the catalytic effect of montmorillonite.

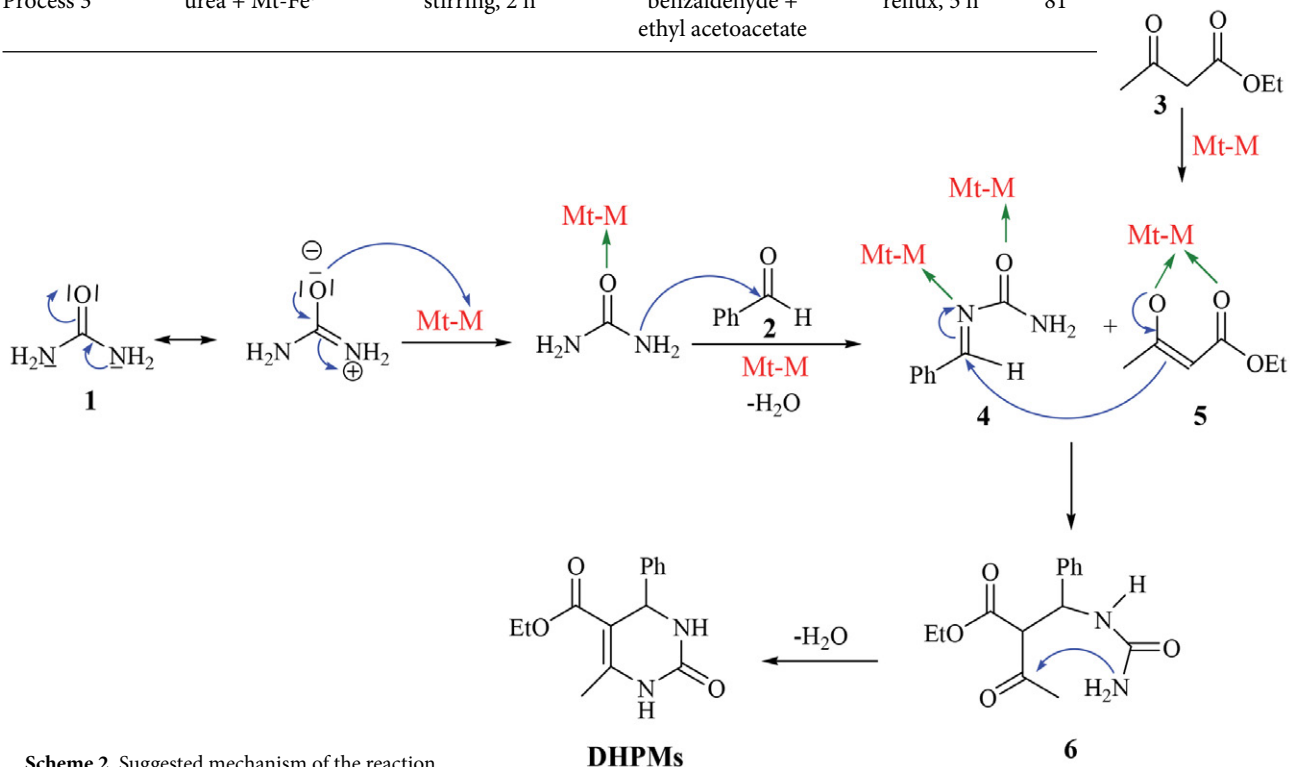
The obtained results show the importance of the introduction order of the reagents (Table 6): the yields and the kinetics obtained with the 3<sup>rd</sup> and the 2<sup>nd</sup> processes are the best (81% in 5 h and 81% in 6 h, respectively) compared to the 1<sup>st</sup> process (68% in 7 h) and to that where all reagents are introduced at the same time (76% in 7 h) (Table 4).

The obtained results are linked to the adsorption phenomenon of the molecules on the surface of the catalyst, indeed when all reagents are introduced simultaneously (Table 4, entry 3), there can be a competition of their adsorption on the catalyst, which can decrease their reactivity towards each other. According to the results in Table 6, we propose the following mechanism of the reaction (Scheme 2).

Urea (1) is a molecule with a carbonyl group and two nitrogen atoms related to this carbonyl. The δ<sup>+</sup> character of the carbonyl carbon atom is also accentuated by the presence of the two more electronegative nitrogen atoms. Consequently, the oxygen atom has a very high electron density which allows it to attack the electropositive site (M) of montmorillonite; this step corresponds to the adsorption of urea on montmorillonite. According to Kappe,<sup>59</sup> the reaction of urea and benzaldehyde (2) affords the intermediate acyl imine 4 which is catalyzed and stabilized by Mt-M. The adsorption of ethyl acetoacetate (3) on montmorillonite leads to ethyl acetoacetate enolate (5). The addition of the latter 5 to the acyl imine provides 6. Finally, cyclisation and dehydration of 6 give the corresponding dihydropyrimidine (DHPM).

Table 6. Effect of introduction order of reagents.

	First step		Second step		Yield (%)
	Reagents	Operating condition	Reagents	Operating condition	
Process 1	benzaldehyde + Mt-Fe <sup>3+</sup>	stirring, 2 h	ethyl acetoacetate + urea	reflux, 7 h	68
Process 2	ethyl acetoacetate + Mt-Fe <sup>3+</sup>	stirring, 2 h	benzaldehyde + urea	reflux, 6 h	81
Process 3	urea + Mt-Fe <sup>3+</sup>	stirring, 2 h	benzaldehyde + ethyl acetoacetate	reflux, 5 h	81



Scheme 2. Suggested mechanism of the reaction.

Overall, the obtained yields in ethanol as the solvent are very attractive and show that the exchanged montmorillonite which is a low cost, natural, eco-friendly and abundant material, competes favourably with other costly heterogeneous catalysts such as polystyrene–poly(ethylene glycol) resin-supported sulfonic acid,<sup>60</sup> sulfonic acid-functionalized polypropylene fibers,<sup>61</sup> Nafion-Ga,<sup>62</sup> ZnO nanoparticles on SBA-15<sup>63</sup> and even with some homogeneous catalysts such as Co phthalocyanines,<sup>64</sup> copper complexes,<sup>65</sup> and Hf(OTf)<sub>4</sub><sup>66</sup> (Table 7).

**Table 7.** Comparison between Mt-Fe<sup>3+</sup> and other catalysts reported in the literature.

Catalyst	Time	Yield (%) in ethanol
Mt-Fe <sup>3+</sup> (our study)	5 h	81
PS-PEG-SO <sub>3</sub> H <sup>60</sup>	10 h	80
PPF-SO <sub>3</sub> H <sup>61</sup>	8 h	81
Nafion-Ga <sup>62</sup>	1 h	84
ZnO@SBA-15 <sup>63</sup>	150 min	96
Co phthalocyanines <sup>64</sup>	16 h	10
NHC copper complexes <sup>65</sup>	24 h	39
Hf(OTf) <sub>4</sub> <sup>66</sup>	9 h	88

## 4. Conclusion

Montmorillonite is a natural heterogeneous catalyst, abundant, inexpensive and conforms to the concept of the green chemistry. In this work, the Biginelli reaction which consists of the preparation of dihydropyrimidinone from ethyl acetoacetate, benzaldehyde and urea, is carried out in the presence of an Algerian montmorillonite exchanged with different cations, as heterogeneous catalyst. Our study focuses mainly on the effect of the cation exchanged. Various cations were used (Cu<sup>2+</sup>, Ni<sup>2+</sup>, Cr<sup>3+</sup>, Co<sup>2+</sup>, Fe<sup>2+</sup> and Fe<sup>3+</sup>) and the montmorillonite exchanged with the Fe<sup>3+</sup> and Co<sup>2+</sup> showed high and satisfactory catalytic properties as they give pure final products with high yields, thus competing with the homogeneous acid catalysts which are dangerous, toxic and corrosive. The effect of the introduction order of the reagents into the reaction medium on the performance of the reaction is studied for the first time for montmorillonite in this work and we have shown that this order plays an important role and allows improving the yield and the kinetics of the reaction.

## 5. References

1. Y. Nishina, *J. Syn. Org. Chem. Jpn.* **2013**, *71*, 1307–1308. DOI:10.5059/yukigoseikyokaishi.71.1307
2. Y. Liu, G. Zhao, D. Wang, Y. Li, *Natl. Sci. Rev.* **2015**, *2*, 150–166. DOI:10.1093/nsr/nwv014

3. H. Göksu, Y. Yıldız, B. Çelik, M. Yazıcı, B. Kılbaş, F. Şen, *ChemistrySelect* **2016**, *1*, 953–958. DOI:10.1002/slct.201600207
4. N. Kaur, D. Kishore, *Chem. Pharm. Res.* **2012**, *4*, 991–1015.
5. C. Liu, P. Wu, Y. Zhu, L. Tran, *Chemosphere* **2016**, *144*, 1026–1032. DOI:10.1016/j.chemosphere.2015.09.063
6. S. Yang, Z. Huang, P. Wu, Y. Li, X. Dong, C. Li, N. Zhu, X. Duan, *Appl. Catal. B-Environ.* **2020**, *260*, 118129. DOI:10.1016/j.apcatb.2019.118129
7. S. Zhu, M. Xia, Y. Chu, M. A. Khan, W. Lei, F. Wang, *Structure. Appl. Clay Sci.* **2019**, *169*, 40–47. DOI:10.1016/j.clay.2018.12.017
8. E. G. Ralph, *Clay Mineralogy*, 2nd Ed., McGraw-Hill, New York, 1968.
9. F. Effenberger, M. Schweizer, W. S. Mohamed, *J. Appl. Polym. Sci.* **2009**, *112*, 1572–1578. DOI:10.1002/app.29605
10. P. Biginelli, *Gazz. Chim. Ital.* **1893**, *23*, 360–416.
11. C. A. Sehon, G. Z. Wang, A. Q. Viet, K. B. Goodman, S. E. Dowdell, P. A. Elkins, S. F. Semus, L. J. Jolivet, S. Kirkpatrick, T. Yi, L. Wright, G. K. Smith, D. J. Behm, R. Bentley, C. P. Doe, E. Hu, D. Lee, *J. Med. Chem.* **2008**, *51*, 6631–6634. DOI:10.1021/jm8005096
12. R. V. Chikhale, R. P. Bhole, P. B. Khedekar, *Eur. J. Med. Chem.* **2009**, *44*, 3645–3653. DOI:10.1016/j.ejmech.2009.02.021
13. O. Alam, S. A. Khan, N. Siddiqui, W. Ahsan, S. P. Verma, S. J. Gilani, *Eur. J. Med. Chem.* **2010**, *45*, 5113–5119. DOI:10.1016/j.ejmech.2010.08.022
14. A. D. Patil, N. V. Kumar, W. C. Kokke, F. Mark, M. F. Bean, A. J. Freyer, S. Mai, A. Truneh, B. Carte, *J. Org. Chem.* **1995**, *60*, 1182–1188. DOI:10.1021/jo00110a021
15. A. N. Chiang, J. C. Valderramos, R. Balachandran, R. J. Chovatiya, B. P. Mead, C. Schneider, S. L. Bell, M. G. Klein, D. M. Huryn, X. S. Chen, B. W. Day, D. A. Fidock, P. Wipf, J. L. Brodsky, *Bioorg. Med. Chem.* **2009**, *17*, 1527–1530. DOI:10.1016/j.bmc.2009.01.024
16. R. W. Lewis, J. Mabry, J. G. Polisar, K. P. Eagen, B. Ganem, G. P. Hess, *Biochemistry* **2010**, *49*, 4841–4851. DOI:10.1021/bi100119t
17. B. R. Kumar, G. Sankar, R. Nasir Baig, S. Chandrashekar, *Eur. J. Med. Chem.* **2009**, *44*, 4192–4198. DOI:10.1016/j.ejmech.2009.05.014
18. D. A. Ibrahim, A. M. El-Metwally, *Eur. J. Med. Chem.* **2010**, *45*, 1158–1166. DOI:10.1016/j.ejmech.2009.12.026
19. H. Y. Kaan, V. Ulaganathan, O. Rath, H. Prokopcová, D. Dallinger, C. O. Kappe, F. Kozielski, *J. Med. Chem.* **2010**, *53*, 5676–5683. DOI:10.1021/jm100421n
20. O. C. Agbaje, O. O. Fadeyi, S. A. Fadeyi, *Bioorg. Med. Chem. Lett.* **2011**, *21*, 989–992. DOI:10.1016/j.bmcl.2010.12.022
21. E. Rajanarendar, M. N. Reddy, K. R. Murthy, K. G. Reddy, S. Raju, M. Srinivas, B. Praveen, M. S. Rao, *Bioorg. Med. Chem. Lett.* **2010**, *20*, 6052–6055.
22. S. N. Mokale, S. S. Shinde, R. D. Elgire, *Bioorg. Med. Chem. Lett.* **2010**, *20*, 4424–4446.
23. V. Virsodia, R. R. Pissurlenkar, D. Manvar, C. Dholakia, P. Adlakha, A. Shah, E. C. Coutinho, *Eur. J. Med. Chem.* **2008**, *43*, 2103–2115. DOI:10.1016/j.ejmech.2007.08.004

24. A. Trivedi, V. R. Bhuvu, B. H. Dholariya, D. K. Dodiya, V. B. Kataria, V. H. Shah, *Bioorg. Med. Chem. Lett.* **2010**, *20*, 6100–6102. DOI:10.1016/j.bmcl.2010.08.046
25. M. B. Deshmukh, S. M. Salunkhe, D. R. Patil, P. V. Anbhule, *Eur. J. Med. Chem.* **2009**, *44*, 2651–2654. DOI:10.1016/j.ejmech.2008.10.018
26. S. Chitra, D. Devanathan, K. Pandiarajan, *Eur. J. Med. Chem.* **2010**, *45*, 367–371. DOI:10.1016/j.ejmech.2009.09.018
27. Y. S. Sadanadam, M. M. Shetty, P. V. Diwan, *Eur. J. Med. Chem.* **1992**, *27*, 87–92. DOI:10.1016/0223-5234(92)90066-A
28. F. Aslanoglu, E. Akbas, M. Sönmez, B. Anil, *Phosphorus Sulfur Silicon Relat. Elem.* **2007**, *182*, 1589–1597. DOI:10.1080/10426500701263554
29. I. O. Lebedyeva, M. V. Povstyanoy, V. M. Povstyanoy, O. G. Panasyuk, E. S. Guban, A. B. Ryabitskii, *Monatsh. Chem.* **2010**, *141*, 997–1000. DOI:10.1007/s00706-010-0354-9
30. L. F. Valverde, F. D. Cedillo, A. C. Luis, *Monatsh. Chem.* **2010**, *141*, 75–78. DOI:10.1007/s00706-009-0223-6
31. J. Svetlik, V. Kettmann, *Tetrahedron Lett.* **2011**, *52*, 1062–1066. DOI:10.1016/j.tetlet.2010.12.051
32. H. Cho, Y. Nishimura, Y. Yasui, *Tetrahedron* **2011**, *67*, 2661–2669. DOI:10.1016/j.tet.2011.01.092
33. Z. Hassani, M. R. Islami, M. Kalantari, *Bioorg. Med. Chem. Lett.* **2006**, *16*, 4479–4482. DOI:10.1016/j.bmcl.2006.06.038
34. K. A. Dilmaghan, B. Zeynizadeh, M. Yari, *Phosphorus Sulfur Silicon Relat. Elem.* **2009**, *184*, 1722. DOI:10.1080/10426500802293153
35. J. Tongshou, Z. Suling, L. Tongshuang, *Synth. Commun.* **2002**, *32*, 1847–1851.
36. T. S. Jin, H. X. Wang, C. Y. Chun-Yong Xing, X. L. Li, *Synth. Commun.* **2004**, *34*, 3009–3016. DOI:10.1081/SCC-200026660
37. W. Y. Chen, S. D. Quin, J. R. Jin, *Catal. Commun.* **2007**, *8*, 123–126. DOI:10.1016/j.catcom.2006.05.026
38. S. Tu, F. Fang, C. Miao, H. Jiang, Y. Feng, *Tetrahedron Lett.* **2003**, *44*, 6153–6155. DOI:10.1016/S0040-4039(03)01466-7
39. A. Debache, B. Boumoud, M. Amimour, *Tetrahedron Lett.* **2006**, *47*, 5697–5699. DOI:10.1016/j.tetlet.2006.06.015
40. J. Martínez, S. Romero-Vega, R. Abeja-Cruz, *Int J Mol Sci.* **2013**, *14*, 2903–2915. DOI:10.3390/ijms14022903
41. S. Noreen, S. Perveen, M. N. Khan, A. Nazeer, M. A. Khan, M. A. Munawar, R. Babar, F. Suhail, M. Azad, A. M. Bernardino, M. S. Dos Santos, *Asian J. Chem.* **2013**, *25*, 4770–4772. DOI:10.14233/ajchem.2013.14094
42. M. M. Heravi, K. Bakhtiari, F. Bamoharram, *Catal. Commun.* **2006**, *7*, 373–376. DOI:10.1016/j.catcom.2005.12.007
43. M. R. Mohammadzadeh, N. Firoozi, *e-J. Chem.* **2011**, *8*, S266–S270. DOI:10.1155/2011/751282
44. J. Lu, Y. Bai, *Synthesis* **2002**, *4*, 466–447. DOI:10.1055/s-2002-20956
45. M. Adib, K. Ghanbary, M. Mostofi, M. Ganjali, *Molecules* **2006**, *11*, 649–654. DOI:10.3390/11080649
46. M. Majd, K. Saidi, H. Khabazzadeh, *Phosphorus Sulfur Silicon Relat. Elem.* **2010**, *185*, 325. DOI:10.1080/10426500902796931
47. L. M. Ramos, A. Y. Ponce de Leon y Tobio, M. R. dos Santos, H. C. B. de Oliveira, A. F. Gomes, F. C. Gozzo, A. L. de Olivei-  
ra, B. A. D. Neto, *J. Org. Chem.* **2012**, *77*, 10184–10193. DOI:10.1021/jo301806n
48. N. E. Masoud, S. J. Hoseini, F. Mohammadi, *Chin. J. Catal.* **2011**, *32*, 1484–1489.
49. G. K. S. Prakash, H. Lau, C. Panja, I. Bychinskaya, S. K. Ganesh, B. Zaro, T. Mathew, G. A. Olah, *Catal. Lett.* **2014**, *144*, 2012–2020. DOI:10.1007/s10562-014-1364-8
50. O. V. Fedorova, Y. A. Titova, A. Y. Vigorov, M. S. Toporova, O. A. Alisienok, A. N. Murashkevich, V. P. Krasnov, G. L. Rusinov, V. N. Charushin, *Catal. Lett.* **2016**, *146*, 493–498. DOI:10.1007/s10562-015-1666-5
51. V. Singh, V. Sapehiyia, V. Srivastava, S. Kaur, *Catal. Commun.* **2006**, *7*, 571–578. DOI:10.1016/j.catcom.2005.12.021
52. A. K. Mitra, K. Banerjee, *Synth. Lett.* **2003**, *10*, 1509–1511. DOI:10.1055/s-2003-40828
53. A. Phukan, S. J. Borah, P. Bordoloi, K. SharmaBorah, *Adv. Powder Technol.* **2017**, *28*(6), 1585–1592. DOI:10.1016/j.appt.2017.03.030
54. D. P. Narayanan, A. Gopalakrishnan, Z. Yaakob, S. Sugunan, B. N. Narayanan, *Arab. J. Chem.* **2017**, *10*, 1–17.
55. R. J. Kalbasi, A. R. Massah, B. Daneshvarnejad, *Appl. Clay Sci.* **2012**, *55*, 1–9. DOI:10.1016/j.clay.2011.05.015
56. H. Khalaf, O. Bouras, V. Perrichon, *Microporous Mater.* **1997**, *8*, 141–150. DOI:10.1016/S0927-6513(96)00079-X
57. D. D. Eberl, *Clays and Clay Minerals.* **1980**, *146*, 493–498.
58. P. Salehi, M. Dabiri, M. A. Zolfigo, *Tetrahedron Lett.* **2003**, *44*, 2889–2891. DOI:10.1016/S0040-4039(03)00436-2
59. C. O. Kappe, *J. Org. Chem.* **1997**, *62*, 7201–7204. DOI:10.1021/jo971010u
60. Z. J. Quan, Y. X. Da, Z. Zhang, X. C. Wang, *Catal. Commun.* **2009**, *10*, 1146–1148. DOI:10.1016/j.catcom.2008.12.017
61. X. L. Shi, H. Yang, M. Tao, W. Zhang, *RSC Adv.* **2013**, *3*, 3939–3945. DOI:10.1039/c3ra23187a
62. G. K. S. Prakash, H. Lau, C. Panja, I. Bychinskaya, S. K. Ganesh, *Catal. Lett.* **2014**, *144*, 2012–2020. DOI:10.1007/s10562-014-1364-8
63. D. Bhuyan, M. Saikia, *Microporous Mesoporous Mater.* **2018**, *256*, 39–48. DOI:10.1016/j.micromeso.2017.06.052
64. R. Medyouni, W. Elgabsi, O. Naouali, A. Romerosa, S. A. Al-Ayed, L. Baklouti, N. Hamdi, *Spectrochim. Acta Mol. Biomol. Spectrosc.* **2016**, *167*, 165–174. DOI:10.1016/j.saa.2016.04.045
65. R. Pawlowski, E. Zaorska, S. Staszko, A. Szadkowska, *Appl. Organomet. Chem.* **2018**, *32*, 4256–4266. DOI:10.1002/aoc.4256
66. R. Kong, S. B. Han, J. Y. Wei, X. C. Peng, Z. B. Xie, S. S. Gong, Q. Sun, *Molecules* **2019**, *24*, 364–377. DOI:10.3390/molecules24020364

**Povzetek:**

## Povzetek

V tem prispevku opisujemo kako smo v alžirskem montmorillonitu (Mt) izvedli izmenjavo kationa z različnimi drugimi kationi iz družine prehodnih kovin, t.j.  $\text{Cu}^{2+}$ ,  $\text{Ni}^{2+}$ ,  $\text{Cr}^{3+}$ ,  $\text{Co}^{2+}$ ,  $\text{Fe}^{2+}$  and  $\text{Fe}^{3+}$ ; tako pripravljene heterogene katalizatorje smo uporabili pri Biginellijevi reakciji. Kationi, izbrani za izmenjavo, so znani po svojih katalitskih lastnostih v primerih homogene katalize. Glavni namen našega dela je bil študirati vpliv izmenjave kationa na izkoristek in kinetiko reakcije. Karakterizacijo montmorillonita smo izvedli z rentgensko praškovno difrakcijo, ki omogoča spremljanje spreminjanja razdalj  $d_{001}$  v odvisnosti od izmenjanega kationa in hkrati tudi pokaže, če je med izmenjavo prišlo do spremembe strukture montmorillonita. Kationsko izmenjevalno kapaciteto (CEC) smo določili s titracijo izmenjenih kationov z atomsko absorpcijo. Produkt Biginellijeve reakcije smo karakterizirali z NMR, IR in z določitvijo tališča. Dodatno smo tudi raziskali vpliv vrstnega reda dodajanja reaktantov na izkoristek in kinetiko. Tako smo pokazali, da se lahko izmenjani montmorillonit ugodno kosa z ostalimi dražjimi hetero- in homogenimi katalizatorji.



Except when otherwise noted, articles in this journal are published under the terms and conditions of the Creative Commons Attribution 4.0 International License

Scientific paper

# Methylene Blue Dye Removal from Aqueous Media Using Activated Carbon Prepared by Lotus Leaves: Kinetic, Equilibrium and Thermodynamic Study

Roya Salahshour,<sup>1</sup> Mehdi Shanbedi<sup>1</sup> and Hossein Esmaeili<sup>2,\*</sup><sup>1</sup> Department of Chemical Engineering, School of Chemical Engineering, Kherad Institute of Higher Education, Bushehr, Iran<sup>2</sup> Department of Chemical Engineering, Bushehr Branch, Islamic Azad University, Bushehr, Iran\* Corresponding author: E-mail: [esmaeili.hossein@gmail.com](mailto:esmaeili.hossein@gmail.com) [esmaeili.hossein@iaubushehr.ac.ir](mailto:esmaeili.hossein@iaubushehr.ac.ir)

Received: 08-01-2020

## Abstract

In the present work, methylene blue was eliminated from aqueous solution using activated carbon prepared by lotus leaves. To perform the experiments, batch method was applied. Also, several analyses such as SEM, FTIR, EDAX and BET were done to determine the surface properties of the activated carbon. The results showed that the maximum sorption efficiency of 97.59% was obtained in initial dye concentration of 10 mg/L, pH of 9, adsorbent dosage of 4 g/L, temperature of 25 °C, contact time of 60 min and mixture speed of 400 rpm. Furthermore, the maximum adsorption capacity was determined 80 mg/g, which was a significant value. The experimental data was analyzed using pseudo-first order, pseudo-second order and intra-particle diffusion kinetic models, which the results showed that the pseudo-second order kinetic model could better describe the kinetic behavior of the sorption process. Also, the constant rate of the pseudo-second order kinetic model was obtained in the range of 0.0218–0.0345 g/mg.min. Moreover, the adsorption equilibrium was well described using Freundlich isotherm model. Furthermore, the thermodynamic studies indicated that the sorption process of methylene blue dye using the activated carbon was spontaneous and exothermic.

**Keyword:** Activated carbon; lotus leaves; methylene blue dye; removal; synthetic wastewater.

## 1. Introduction

Environmental pollution is currently a global problem.<sup>1</sup> Because of the population growth, the expansion of industry and agriculture and shortage of fresh water in the world, the need for treatment and recovery of wastewater has become critical in recent years.<sup>2,3</sup> Among the various industries, the textile industry has expanded rapidly both in the world and our country, and dyeing units in the textile industry are the main environmental pollutants due to the consumption of thousands types of dye chemicals. Textile effluents usually contain a wide range of different chemical compounds. The biggest problem with these effluents is the presence of dyes and biodegradable chemicals. The most obvious characteristic of textile industry effluents is that it is colored and the two main stages of dyeing and finishing in the textile industry produce a large volume of effluent with high dye concentration.<sup>4</sup>

These dyes not only give unfavorable colors to water, but in some cases are themselves harmful compounds and

can produce other toxic products by oxidation, hydrolysis, or other chemical reactions that take place in water. Dyes are one of the most dangerous groups of chemical compounds found in industrial effluents that are of considerable importance due to the reduction of light permeability and thus disrupting the process of photosynthesis in water sources.<sup>5–7</sup>

These compounds also have an aesthetic negative effect on water quality for drinking and other uses<sup>4</sup> and at the same time, they cause allergies, dermatitis, irritation,<sup>8</sup> cancer<sup>9</sup> as well as genetic mutations in humans.<sup>10</sup> Methylene blue is the most common dye compound used for cotton, wool and silk coloring. Inhalation of this compound can cause respiratory disorders and direct exposure to it can cause permanent damage to the eyes of humans and animals, local burns, nausea and vomiting, increased sweating, mental disorders and methemoglobinemia.<sup>9,11,12</sup>

Improper treatment and disposal of synthetic wastewater from the textile, dyeing, printing, and related industries has caused many environmental problems around the

world.<sup>13</sup> Dye removal from wastewater is usually done by physical, physicochemical, biological or chemical methods.<sup>14–16</sup> The most efficient way to remove synthetic dyes from industrial effluents is the adsorption process, because the dye compounds in the effluent are easily transferred to the solid phase.<sup>17</sup> Besides, the adsorbent used can be regenerated and used in the adsorption process or stored after use in a dry place without direct contact with the environment.<sup>10</sup> Also, it has been proven that the adsorption process is a safe treatment solution due to its minimal investment cost, ease of design and operation, and insensitivity to toxic compounds. But at the same time, the use of adsorbents can be a limiting factor, because some adsorbents are expensive. To reduce the cost of preparation, the use of inexpensive materials (such as agricultural and industrial residues) for the production of activated carbon is a good option.<sup>17,18</sup> In addition to reducing costs, converting agricultural waste into low-cost adsorbents and solving the problem of biomass disposal has increased the value of agricultural waste even more. Carbon from agricultural wastes has advantages such as low ash content, reasonable hardness, high cross section, and a porous structure.<sup>4,18</sup>

The aim of this study was to eliminate methylene blue dye from synthetic effluent using activated carbon. To this end, the impact of various parameters on the methylene blue dye removal efficiency was investigated. The structural properties of activated carbon prepared from the lotus leaves were analyzed using BET, SEM, FTIR, and EDAX analyses. Also, the kinetic, equilibrium, and thermodynamic behavior of the adsorption process were thoroughly investigated.

## 2. Materials and Methods

### 2.1. Materials

In this study, sodium hydroxide and Hydrochloric acid (Merck, Germany) were used to adjust the pH of the solutions. Also, methylene blue dye (Merck, Germany) was used to prepare stock solutions.

### 2.2. Preparation of Methylene Blue Stock Solution

To prepare the stock solution, one gram of methylene blue was dissolved in 1000 mL of water to prepare a solution of methylene blue dye at a concentration of 1000 ppm. To prepare solutions with lower concentrations, distillation of the initial stock solution was diluted twice using water.

### 2.3. Preparation of Activated Carbon from Lotus Leaves

To prepare activated carbon, we first collected the lotus leaves and washed it several times with water to remove

the dust. After washing, the leaves are placed in an oven (dryer) at 105 °C for 2 hours to dry completely. The dried lotus leaves are placed in a furnace at 700 °C for 2 hours to produce carbon. The activated carbon is then pulverized using a grinder and granulated by sieve No. 25 (ASTM 11) and stored in plastic bottles at room temperature. They can be used as adsorbents to recover and remove methylene blue dye.

### 2.4. Adsorption Tests

The methylene blue dye adsorption test was performed discontinuously in 200 mL Erlenmeyer flasks containing 100 mL of methylene blue dye solution. To adjust the initial pH of the solutions, sodium hydroxide and hydrochloric acid solutions with a concentration of 0.1 M were used. To investigate the effect of pH on the adsorption of methylene blue dye, experiments were performed in the pH range of 3–11. Other conditions including initial concentration of 10 ppm, contact time of 40 min, temperature of 25 °C, adsorbent dose of 1.5 g/L and mixing speed of 400 rpm were considered constant. To mix, the sample was placed on a heater. Then the mixing temperature and speed were adjusted and the samples were mixed for a contact time of 40 min. At the end of this time, the sample was filtered using a funnel equipped with Whatman 42 filter paper, and the residual methylene blue dye in the solution was measured by a UV-vis spectrophotometer. The removal efficiency and adsorption capacity were then calculated. To evaluate the effect of other parameters such as temperature (25–50 °C), adsorbent dose (0.5–1 g/L), contact time (5–200 minutes) and dye concentration (10–100 mg/L), one of the parameters was changed and the rest of the parameters were considered constant. Also, the optimized values of the parameters in the previous step were used to investigate the effect of another parameter.

The adsorption capacity and removal efficiency of methylene blue dye were determined after determining the secondary concentration and having the primary concentration. Adsorption efficiency (R%) and adsorption capacity ( $q_e$ ) of activated carbon adsorbent are obtained by the following equations:

$$R(\%) = \left( \frac{C_i - C_o}{C_i} \right) \times 100 \quad (1)$$

$$q_e = \left( \frac{C_i - C_o}{M} \right) \times v \quad (2)$$

### 2.5. Equilibrium Behavior

The adsorption isotherm is important for describing the adsorption of molecular or ionic contaminants to the active sites of the adsorbent surface.<sup>20–23</sup> In this study, three isotherm models such as Langmuir, Freundlich and Dubinin-Radishkevich models were used.

The Langmuir isotherm is based on the assumption that all adsorption sites are the same and the adsorption of contaminants on the adsorbent surface is monolayer. The linear form of the Langmuir isotherm is shown in Equation (3):<sup>24</sup>

$$\frac{C_e}{q_e} = \frac{1}{q_{\max} K_L} + \frac{C_e}{q_{\max}} \quad (3)$$

Where,  $K_L$  is the Langmuir isotherm constant. Also,  $q_{\max}$  determines the maximum adsorption capacity of the activated carbon.<sup>23</sup>

To know the feasibility of the adsorption process, the separation parameter  $R_L$  is used, which is obtained from the following relation:

$$R_L = \frac{1}{1 + K_L C_0} \quad (4)$$

If the value of  $R_L$  is greater than one, equal to one, between zero and one, and less than one, it indicates that the adsorption process is unfavorable, linear, favorable, and irreversible.<sup>23</sup>

On the other, the Langmuir constant parameter ( $K_L$ ) is related to the Gibbs free energy change of the adsorption process ( $\Delta G^\circ$  (kJ/mol)), which is determined from the following equation:

$$\Delta G^\circ = -RT \ln(K_L) \quad (5)$$

where  $R$  and  $T$  are the universal gas constant (8.314 J/mol K) and temperature (K), respectively.<sup>25</sup>

Also, the Freundlich isotherm is an experimental model that expresses adsorption on heterogeneous surfaces. The linear form of the Freundlich isotherm is expressed as follows:<sup>23,24</sup>

$$\ln q_e = \ln K_F + \left(\frac{1}{n}\right) \ln C_e \quad (6)$$

Here,  $K_F$  ( $\text{mg/g (L/mg)}^{1/n}$ ) is indicator of constant relative adsorption capacity of the bond energy, and  $n$  is related to the adsorption capacity and heterogeneity of the adsorbent surface sites. A value of  $\frac{1}{n}$  indicates the desirability of adsorption. Values of  $n > 1$  indicate that the adsorption process is favorable.

Moreover, the Dubinin-Radishkevich isotherm is generally used to express the adsorption mechanism by distributing Gaussian energy on a heterogeneous surface. This isotherm is determined by Equations 7 and 8:<sup>26</sup>

$$q_e = q_D \exp(-\beta_D \varepsilon_D^2) \quad (7)$$

$$\varepsilon_D = -RT \ln \left(1 + \frac{1}{C_i}\right) \quad (8)$$

Here,  $q_D$  is the saturation capacity of the Dubinin-Radishkevich model (mg/g),  $q_e$  is the equilibrium of the adsorbed pollutants on the adsorbent (mg/g),  $\beta_D$  is Dubinin-Radishkevich isotherm model constant ( $\text{mol}^2/\text{KJ}^2$ ), and  $\varepsilon_D$  is the Polanyi potential.  $E$  is the absorption energy, which is calculated as follows:

$$E = \frac{1}{\sqrt{2\beta_D}} \quad (9)$$

If  $E < 8$  KJ/mol and  $8 < E < 16$  KJ/mol, the adsorption process is physical and chemical, respectively. Also, for  $E > 16$  KJ/mol, the adsorption mechanism is intraparticle diffusion.<sup>26</sup>

## 2. 6. Kinetics of Adsorption

Kinetic models are used to investigate the control rate of the adsorption process. To determine the adsorption kinetics of methylene blue dye using activated carbon, three models namely pseudo-first order (PFO), pseudo-second order (PSO), and intraparticle diffusion were used.

The linear and non-linear forms of the PFO kinetic model is described by Equations 10 and 11:<sup>23,24, 27</sup>

$$\ln(q_e - q_t) = \ln q_e - k_1 t \quad (10)$$

$$q_t = q_e (1 - e^{-k_1 t}) \quad (11)$$

Here,  $q_e$  and  $q_t$  are the amount of adsorption capacity of adsorbed pollutants per unit weight of adsorbent at equilibrium time (mg/g), the adsorption capacity of adsorbed pollutants at time  $t$  (mg/g), respectively. Also,  $k_1$  is the pseudo-first order kinetic rate constant ( $\text{min}^{-1}$ ).<sup>23,24</sup>

The linear and non-linear forms of the PSO kinetic model is also expressed as follows:<sup>27</sup>

$$\frac{t}{q_t} = \frac{1}{k_2 q_e^2} + \frac{t}{q_e} \quad (12)$$

$$q_t = \frac{k_2 q_e^2 t}{1 + k_2 q_e t} \quad (13)$$

Where,  $k_2$  is the pseudo-second order kinetic constant ( $\text{mg mol}^{-1} \text{min}^{-1}$ ).

Another kinetic model is the intraparticle diffusion model. The adsorption process on a porous adsorbent is generally described by four steps. These steps are described as mass diffusion, film diffusion, intraparticle diffusion, and finally adsorption of contaminants on the adsorbent surface. The intraparticle diffusion model can be expressed as follows:

$$q_t = K_{id} t^{1/2} + I \quad (14)$$

Here,  $K_{id}$  ( $\text{mg g}^{-1} \text{min}^{-1/2}$ ) is the intraparticle diffusion rate constant. Also,  $I$  ( $\text{mg/g}$ ) is a constant, which is determined by the intercept of the plot of  $q_t$  against  $t^{1/2}$ .<sup>28</sup>

## 2. 7. Adsorption Thermodynamics

Changes in the rate of adsorption with respect to temperature are explained based on thermodynamic parameters such as change in enthalpy ( $\Delta H^\circ$ ), change in entropy ( $\Delta S^\circ$ ) and Gibbs free energy change ( $\Delta G^\circ$ ), which are obtained by using equations 15 and 16:<sup>29,30</sup>

$$\Delta G^\circ = -RT \ln K_c \quad (15)$$

$$\ln K_c = \frac{\Delta S^\circ}{R} - \frac{\Delta H^\circ}{RT} \quad (16)$$

The change in Gibbs free energy in the process depends on the quantity of equilibrium constant  $K_c$ , which is expressed as follow:

$$K_c = \frac{C_{Ae}}{C_e} \quad (17)$$

In Equation (14),  $K_c$  is the equilibrium constant and  $C_{Ae}$  is the equilibrium concentration in the solid phase

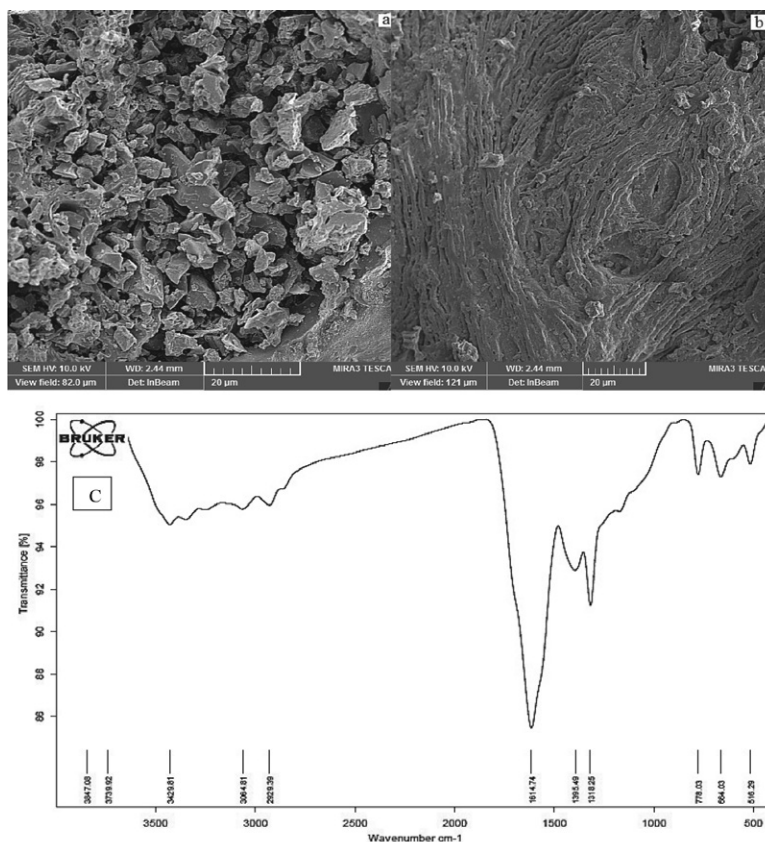
( $\text{mg/L}$ ). The amount of changes in enthalpy ( $\Delta H^\circ$ ) and entropy ( $\Delta S^\circ$ ) are obtained by plotting  $\ln K_c$  versus  $1/T$ .

## 3. Results and Discussion

### 3. 1. Determining the Properties of Activated Carbon

Various analyses including SEM, FTIR, EDAX, and BET were used to determine the physical properties of activated carbon adsorbent obtained from the lotus leaves. Figure 1 shows the SEM analysis of the activated carbon surface prepared from the lotus leaves, before and after the adsorption of methylene blue dye. Figure 1(a) shows that the activated carbon prepared from the lotus leaves before absorbing the methylene blue dye has uneven structure and a large number of adsorption channels. Then, Figure 1(b) shows the activated carbon prepared from the lotus leaves after adsorption of methylene blue dye. The adsorbent surface is uniform and the adsorption channels have disappeared.<sup>31,32</sup> This uniformity and disappearance of adsorption channels in Figure 1(b) indicates the adsorption of methylene blue dye on the activated carbon adsorbent.

To evaluate the functional groups on the surface of activated carbon adsorbent, FTIR analysis was used, which

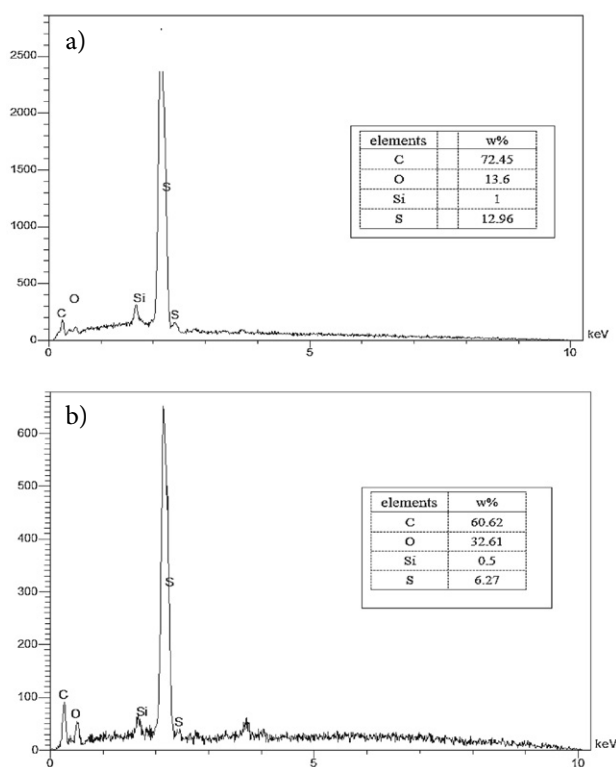


**Figure 1.** SEM image for activated carbon (a), activated carbon after adsorption of methylene blue dye (b), and FTIR analysis for activated carbon prepared from lotus leaves (c).



is shown in Figure 1. FTIR analysis has identified groups in different ranges. There are several peaks at 3847.08, 3739.92, 3429.81, 3064.81, 2929.39, 1614.74, 1395.49, 1318.25, 778.03, 664.03, and 516.29, which are attributed to the functional groups of O-H, O-H, O-H, C-H, C-H, C=C, C-O, C-O, C-H, O-H, and O-H, respectively.<sup>33–36</sup>

Also, the EDAX analysis of activated carbon prepared from the lotus leaves before and after the methylene blue dye adsorption process is shown in Figure 2. According to Figure 3(b), before the adsorption process, activated carbon contains elements such as carbon (72.45%), oxygen (13.6%), silicon (1%) and sulfur (12.96%). After the methylene blue dye adsorption process, the amount of these elements changed, which includes carbon (60.62%), oxygen (32.61%), silicon (0.5%), and sulfur (6.27%). Changes in the amounts of activated carbon constituents before and after the methylene blue dye adsorption process can be due to the adsorption of the dye by activated carbon.<sup>37</sup>



**Figure 2.** EDAX analysis (a) Activated carbon produced from lotus leaves before the adsorption process and (b) Activated carbon after the sorption of methylene blue dye

Properties such as specific surface area, average pore volume, and pore diameter are determined using BET analysis and the results are presented in Table 1. According to the results, the specific surface area of activated carbon, the average pore volume and the pore diameter obtained from BET analysis were determined 64.415 g/m<sup>2</sup>, 0.056948 g/cm<sup>3</sup> and 35.3633 °A, respectively. These values indicate that the activated carbon prepared from the lotus leaves

**Table 1.** Surface properties of activated carbon prepared from the lotus leaves using BET analysis.

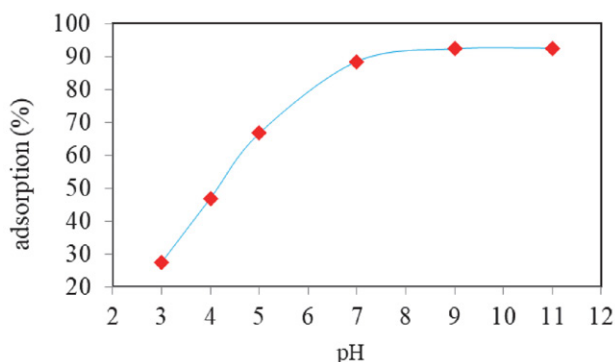
Properties	Values
Analyzed activated carbon mass	0.5588 g
Specific surface area	64.4152 g/m <sup>2</sup>
Average pore volume	0.056948 g/cm <sup>3</sup>
Average pore diameter	35.3633 °A

has a good specific surface area and pore volume. Also, the average pore diameter indicates that the activated carbon has a mesoporous structure, because the pore diameter is in the range of 20 to 500 °A.

## 3. 2. The Effect of Different Parameters on the Adsorption Process

### 3. 2. 1. pH Effect

Solution pH is one of the most important and effective parameters in controlling the adsorption process. Also, it gives the valuable information regarding the mechanism of adsorption. The effect of pH on the adsorption efficiency of methylene blue dye by using activated carbon prepared from the lotus leaves is shown in Figure 3. The results show that by increasing the initial pH, the methylene blue dye adsorption efficiency is increased and the maximum yield is obtained approximately at the initial pH of 9. This result can be described according to the cationic properties of methylene blue dye. At low initial pHs (pH < 5), the adsorption efficiency of methylene blue dye using a prepared adsorbent is low, indicating that acidic pHs are not suitable for adsorption of methylene blue dye. This is because at acidic pHs the adsorbent surface is positively charged and, as a result, the methylene blue cationic dye is repelled by the positively charged adsorbent surface. Also, by increasing the initial pH, the percentage of methylene blue dye adsorption using the adsorbent increases, because by in-

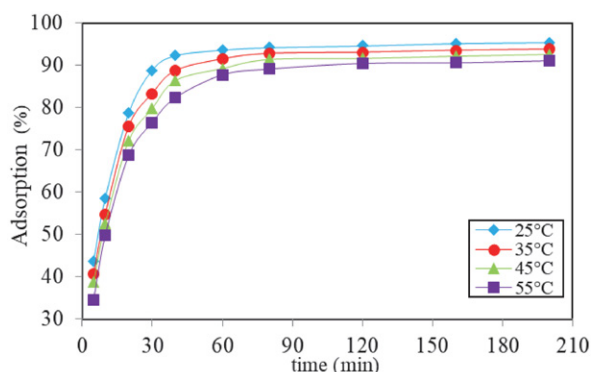


**Figure 3.** Effect of pH on methylene blue dye removal efficiency (adsorbent dose of 1.5 g/L, contact time of 40 min, initial dye concentration of 10 ppm, temperature of 25 °C and mixing speed of 400 rpm).

creasing pH, negative charges on the adsorbent surface increases and an attractive force is created between the adsorbent surface and the cationic dye.<sup>38</sup> Therefore, the optimal pH for the sorption of methylene blue dye from aqueous solution using activated carbon was obtained as 9.

### 3. 2. 2. Effect of Temperature and Contact Time

The effect of different contact times (5–200 min) at 25, 35, 45 and 55 °C on the removal efficiency of methylene blue dye by activated carbon is shown in Figure 4. The results show that during the initial contact time (5 min), the adsorption of methylene blue dye was high at 25 °C, which is equal to 43.63%. By increasing the temperature up to 55 °C, the removal efficiency decreases and reaches 34.64%. Thus, by increasing the temperature, the adsorption efficiency decreased, which indicates that the adsorption process is exothermic. The decrease in removal efficiency with increasing temperature is due to the weakening of the adsorption forces between the active sites of the activated carbon adsorbent and the methylene blue dye. In this case, methylene blue dye is released in the solution phase. Thus, the removal efficiency decreases. However, by increasing the contact time, the removal efficiency increased and reached equilibrium after 60 min reaction time. Methylene blue dye adsorption efficiency remained uniform after 60 min. Because in this case, the adsorption sites on the adsorbent surface are saturated and it is observed that the removal efficiency has not changed much. Therefore, the maximum methylene blue dye removal efficiency was obtained at a contact time of 60 min and a temperature of 25 °C. Under these conditions, the adsorption efficiency of methylene blue dye was 93.67%.



**Figure 4.** Effect of temperature and contact time on the removal efficiency of methylene blue dye by activated carbon (conditions: pH of 9, adsorbent dose of 1.5 g/L, initial dye concentration of 10 ppm, and mixing speed of 400 rpm).

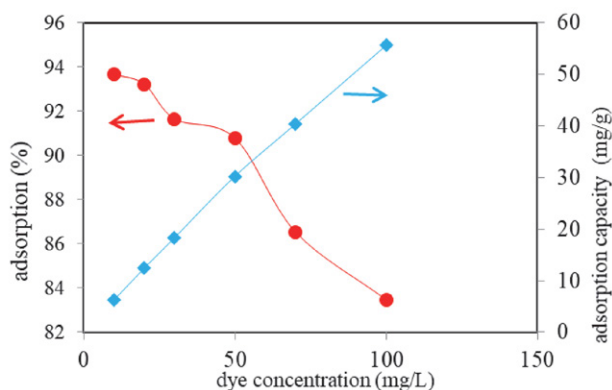
### 3. 2. 3. Effect of Initial Concentration of Methylene Blue Dye

The effect of methylene blue dye concentration on removal efficiency and adsorption capacity at constant pH

of 9, adsorbent dose 1.5 g/L, contact time of 60 min, temperature 25 °C, and mixing speed 400 rpm are shown in Figure 5. The effect of methylene blue dye concentration in the range of 10–100 ppm has been selected.

As shown in the figure, by increasing the concentration from 10 to 100 ppm, the removal efficiency decreases. To check the initial concentration parameter, the amount of concentrations is different and the amount of adsorbent dose is constant. In this case, by increasing dye concentration, the amount of methylene blue dye in the aqueous solution increases relative to the adsorbent dose and there are fewer adsorption sites for methylene blue dyes to be placed on the adsorbent surface, and as a result, the removal efficiency is decreased.

On the other hand, in Figure 5, by increasing the concentration from 10 to 100 ppm, the adsorption capacity is increasing. As the concentration of methylene blue dye in aqueous solution increases, the desired amount of contaminant increases. As a result, the contact of methylene blue dyes increases, which causes the methylene blue dye to be adsorbed more on the activated carbon sites, thus increasing the adsorption capacity.



**Figure 5.** Effect of initial methylene blue dye concentration on removal efficiency and adsorption capacity of methylene blue dye (pH equal to 9, adsorbent dose 1.5 g/L, contact time 60 min, temperature 25 °C and mixing speed 400 rpm).

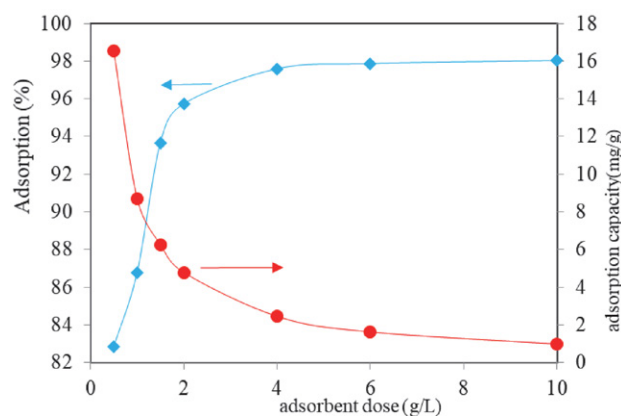
### 3. 2. 4. Effect of Activated Carbon Adsorbent Dose

The values of adsorption capacity and methylene blue dye removal efficiency at different doses of activated carbon are shown in Figure 6. By increasing the dose of activated carbon adsorbent from 0.5 to 10 g/L, the removal efficiency has increased from 82.84% to 98.032%, while adsorption capacity ( $q_e$ ) presents an inverse trend. Increasing the removal efficiency is due to the increase in surface area and the increase in adsorption sites available for methylene blue dye.

The decrease of adsorption capacity ( $q_e$ ) from 16.568 to 0.98032 mg/g is observed with increasing the adsorbent dose from 0.5 to 10 g/L, which is due to the competition

between contaminants and adsorbents.<sup>39</sup> By increasing the adsorbent dose, the adsorbent surface becomes saturated and reduces the adsorption capacity ( $q_e$ ).

When the dose of activated carbon adsorbent from the lotus leaves was 4 g/L, the removal efficiency and adsorption capacity ( $q_e$ ) were 97.59% and 2.439 mg/g, respectively. At adsorbent dose of above 4 g/L, there was no significant increase in methylene blue removal efficiency and the diagram is almost constant and the adsorption capacity ( $q_e$ ) is also reduced. Therefore, according to the adsorption capacity ( $q_e$ ) and removal efficiency, the adsorbent dose of 4 g/L was determined as the optimal value.

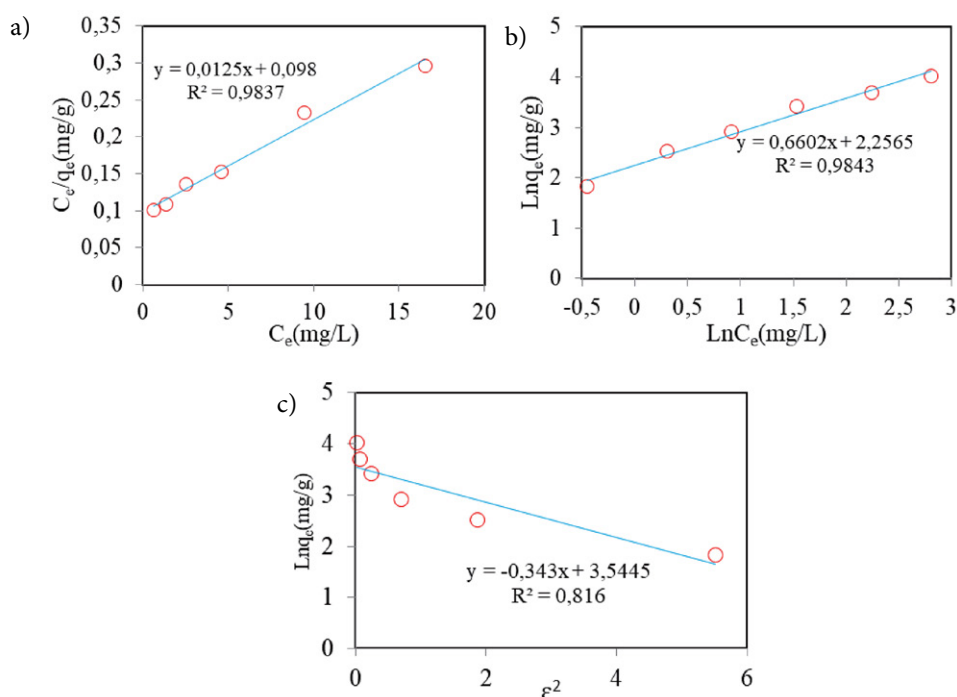


**Figure 6.** Effect of activated carbon adsorbent dose on removal efficiency and adsorption capacity of methylene blue dye (pH equal to 9, initial concentration 10 ppm, contact time 60 min, temperature 25 °C and mixing speed 400 rpm).

### 3. 3. Equilibrium Study of Adsorption Process

Three isotherm models such as Langmuir, Freundlich, and Dubinin Radushkevitch (D-R) were used to remove methylene blue dye using the activated carbon adsorbent prepared from lotus leaves. Isotherm models were investigated at different concentrations (10–100 ppm) of methylene blue, and other conditions were kept constant, including pH of 9, contact time of 60 min, temperature of 25 °C, adsorbent dose of 1.5 g/L, and mixing speed of 400 rpm.

The Langmuir, Freundlich, and Dubinin-Radushkevitch (D-R) isotherm models are plotted in Figure 7, and their constant values are given in Table 2. According to the Langmuir isotherm model, the  $R_L$  value was in the range of 0.729–0.44, which indicates that the adsorption process of methylene blue dye with activated carbon adsorbent is favorable. Also, the maximum adsorption capacity of the activated carbon was obtained 80 mg/g. In addition, according to the values of the coefficient of determination obtained for all three models, the Freundlich isotherm model could better describe the equilibrium behavior of the methylene blue dye adsorption process than other isotherm models. Also, the value of parameter  $n$  using the Freundlich isotherm was equal to 1.514, which indicates that the adsorption process is favorable because its value is greater than one. Moreover, the value of parameter  $K_f$  was determined 9.55 mg/g(L/mg)<sup>1/n</sup>. Furthermore, according to the amount of energy  $E$  obtained using the D-R isotherm model (1.207 KJ/mol), the adsorption mechanism of methylene blue dye with the adsorbent is physical. Be-



**Figure 7.** Langmuir (a), Freundlich (b) and D-R (c) isotherms for the uptake of methylene blue dye using the activated carbon

**Table 2.** Values and constants of adsorption isotherms.

Isothermal models	Quantities	Methyl violet dye
Langmuir	$q_{\max}$ (mg/g)	80
	$K_L$ (L/mg)	0.127
	$\Delta G^\circ$ (kJ/mol)	-5.112
	$R^2$	0.9837
	$R_L$	0.729 – 0.44
Freundlich	$n$	1.514
	$K_f$ (mg/g(L/mg) <sup>1/n</sup> )	9.5496
	$R^2$	0.9843
Dubinin Radushkevitch (D-R)	$E$ (KJ/mol)	1.207
	$q_D$ (mg/g)	34.622
	$B \times 10^{-6}$ (mol <sup>2</sup> /J <sup>2</sup> )	0.343
	$R^2$	0.816

**Table 3.** Comparing the maximum sorption capacity of different adsorbents in the removal of methylene blue from aqueous media

Adsorbent	Maximum sorption capacity (mg/g)	Ref.
Palm tree sawdust	54	4
Sour lemon sawdust	52.4	4
Eucalyptus sawdust	53.5	4
Kaolin/CuFe <sub>2</sub> O <sub>4</sub> nanocomposite	120.48	17
activated carbon prepared by Ficus caricabast	47.62	42
magnetic cellulose/graphene oxide composite	70.03	43
Activated carbon	1.23	44
Activated carbon prepared by lotus leaves	80	Present study

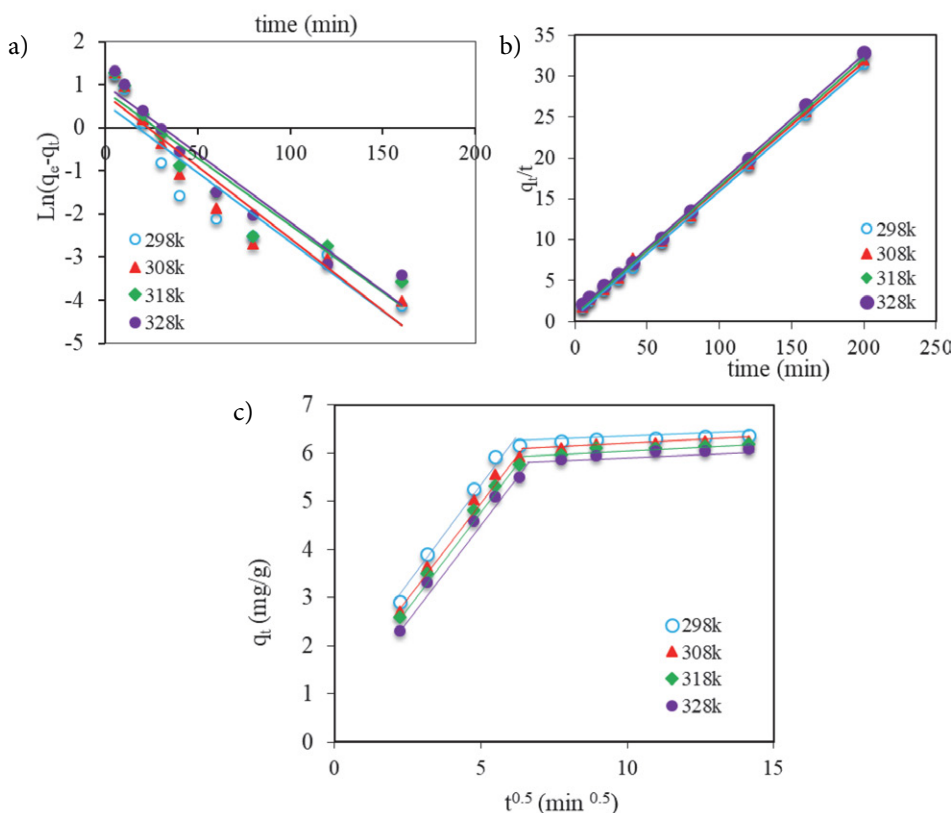
sides, the maximum adsorption capacity using the D-R isotherm was obtained 34.62 mg/g.<sup>40,41</sup> In addition, the Gibbs free energy ( $\Delta G^\circ$ ) using the Langmuir model was determined -5.112 KJ/mol, which indicates the spontaneity degree of the sorption process. Also, negative value of  $\Delta G^\circ$  shows a favorable sorption process.<sup>25</sup>

The maximum sorption capacity obtained in this research for the sorption of methylene blue was compared to previous studies and the results are presented in Table 3. According to this table, the maximum sorption capacity of the activated carbon used in this study was

obtained 80 mg/g, which was comparable with other adsorbents in removing methylene blue from aqueous media.

### 3. 4. Kinetic Study of Adsorption

Figure 8 illustrates pseudo-first order, pseudo-second order, and intraparticle diffusion kinetic models. The graphs drawn include the linear equation and the coefficient of determination ( $R^2$ ). The amounts of models were calculated from the obtained linear equations and the re-

**Figure 8.** The linear forms of PFO (a), PSO (b) and intraparticle diffusion (c) kinetic models at different temperatures and times.

sults are reported in Table 4. The constant rate of pseudo-first order kinetics ( $k_1$ ), the constant rate of pseudo-second order kinetics ( $k_2$ ), the constant rate of intraparticle diffusion kinetics ( $K_{id,1}$ ), and the equilibrium adsorption capacity ( $q_{e,theoretical}$ ) were calculated for all temperatures.<sup>45, 46</sup>

The calculated adsorption capacity values ( $q_{e,theoretical}$ ) using the pseudo-first order kinetic model are very different from the laboratory adsorption capacity values ( $q_{e,exp}$ ). Whereas, the calculated adsorption capacity values ( $q_{e,theoretical}$ ) are very close to the laboratory adsorption capacity values ( $q_{e,exp}$ ) of the pseudo-second order kinetic model. In addition,  $R^2$  values of the pseudo-first order kinetic models and intraparticle diffusion are lower than the pseudo-second order kinetic model. Also, the constant rate of pseudo-first order kinetics ( $k_1$ ) at all temperatures are less than the constant rate of pseudo-first order kinetics ( $k_2$ ). Moreover, a comparison between the PFO and PSO kinetic models and the experimental data

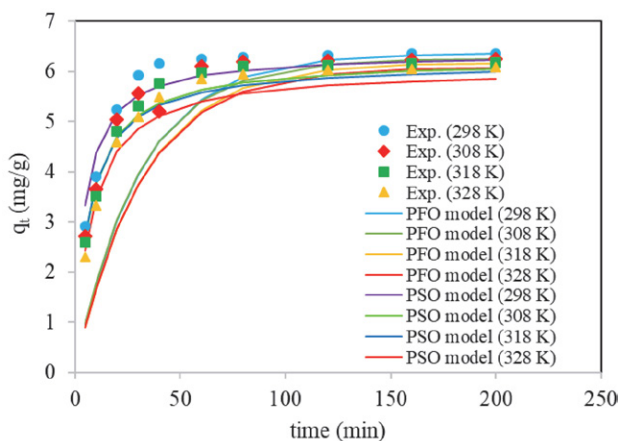


Figure 9. Fitting non-linear forms of kinetic models to experimental data

Table 4. Values of kinetic models at different temperatures and times.

kinetic models	Parameter	Temperature (55 °C)	Temperature (45 °C)	Temperature (35 °C)	Temperature (25 °C)
pseudo-first order	$R^2$	0.9348	0.9116	0.9129	0.8784
	$k_1$ ( $\text{min}^{-1}$ )	0.0319	0.0311	0.0334	0.0322
	$q_{e,theoretical}$ (mg/g)	2.6564	2.3094	2.1593	1.7550
	$q_{e,exp}$ (mg/g)	6.078	6.178	6.256	6.364
pseudo-second order	$R^2$	0.9995	0.9996	0.9992	0.9995
	$k_2$ (g/mg.min)	0.0218	0.0254	0.0242	0.0345
	$q_{e,theoretical}$ (mg/g)	6.3451	6.4061	6.4977	6.5402
intraparticle diffusion	$q_{e,exp}$ (mg/g)	6.078	6.178	6.256	6.364
	$R^2$	0.8863	0.8366	0.8514	0.9776
	$K_{id,1}$ (mg/gmin <sup>1/2</sup> )	0.0328	0.0263	0.0213	0.0184
	$I_1$	5.6348	5.8178	5.9667	6.1099
	$R^2$	0.9712	0.977	0.8596	0.9672
$K_{id,2}$ (mg/gmin <sup>1/2</sup> )	0.7823	0.7844	0.6711	0.8195	
$I_2$	0.7711	0.9976	1.5196	1.2754	

is shown in Figure 9. As shown, the PSO kinetic model is well fitted with the experimental data compared to the PFO model. Therefore, it can be concluded that the pseudo-second order kinetic model is more suitable for the mechanism of adsorption of methylene blue dye with activated carbon adsorbent prepared from lotus leaves.<sup>47</sup> Besides, the intraparticle diffusion kinetic model describes that the sorption process of methylene blue is nonlinear and shows that more than one mechanism contributes to the dye sorption on the surface of activated carbon. The initial linear part of the figure has a higher slope and is attributed to the film diffusion in which methylene blue dye is transported to the adsorbent surface. This step is performed at a high rate. The second linear part has a lower slope, which demonstrates dye diffusion into the activated carbon.<sup>48</sup>

### 3. 5. Study of Thermodynamics of Adsorption Process

Table 5 lists the values of  $\Delta G^\circ$ ,  $\Delta H^\circ$  and  $\Delta S^\circ$  at different temperatures. Figure 9 also shows  $\text{Ln}K_D$  versus  $1/T$  for the sorption of methylene blue dye using activated carbon at different temperatures.

$\Delta G^\circ$  value at 25 °C was  $-5.673$  KJ/mol, and enthalpy change in the range of 25–55 °C was  $-19.671$  KJ/mol, which indicates that the methylene blue dye removal process was spontaneous and exothermic. Also, the  $\Delta G^\circ$  value using the thermodynamic study was comparable to the value obtained by the Langmuir model ( $-5.112$  KJ/mol). Moreover, the value of  $\Delta S^\circ$  in the temperature range of 25–55 °C was equal to  $-47.207$  KJ/mol, which shows the irregularity and randomness of the methylene blue dye adsorption process and shows the physical nature of the methylene blue dye removal process with activated carbon adsorbent.

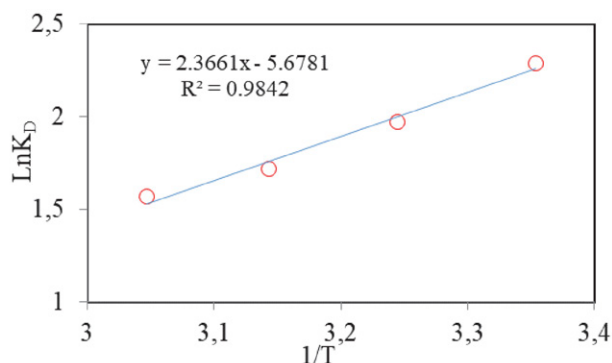


Figure 10.  $\text{Ln}K_D$  versus  $1/T$  diagram for the sorption of methylene blue dye with activated carbon at different temperatures

Table 5. Values of thermodynamic parameters of methylene blue dye adsorption by activated carbon at different temperatures.

Temperature	$K_D$	$\Delta G^\circ$ (KJ/mol)	$\Delta H^\circ$ (KJ/mol)	$\Delta S^\circ$ (KJ/mol)
25 °C	9.864	-5.673		
35 °C	7.194	-5.055		
45 °C	5.575	-4.545	-19.671	-47.207
55 °C	4.802	-4.28		

## 4. Conclusion

In this study, the adsorption process of methylene blue dye using activated carbon prepared from the lotus leaves was performed discontinuously. To prepare activated carbon adsorbent, lotus leaves were used and SEM, FTIR, EDAX, and BET analyses were done before and after removal of methylene blue dye with activated carbon adsorbent. BET analysis showed that the specific surface area of activated carbon adsorbent was high. The adsorption results showed that the highest adsorption efficiency was obtained at pH 9, 10 ppm dye concentration, 60 min, and 25 °C, in which the adsorption efficiency was 97.59%. Among the pseudo-first order, pseudo-second order, and intraparticle diffusion models, the pseudo-second order kinetic model better described the mechanism of the adsorption process. Also, three isotherm models including Langmuir, Freundlich, and Dubinin Radushkevitch (D-R) isotherms were investigated. Among these models, the Freundlich isotherm with a higher  $R^2$  value was able to better express the equilibrium behavior of the adsorption process. Moreover, the highest adsorption capacity of methylene blue dye was obtained 80 mg/g. Furthermore, the thermodynamic study showed that the adsorption process of methylene blue dye by activated carbon is exothermic and spontaneous.

## Conflict of Interests Statement

The authors declare that there is no conflict of interests.

## 5. References

- J. Paul, K. P. Rawat, K. S. S. Sarma, S. Sabharwal, *Appl. Radiat. Isot.* **2011**, *69*, 982–987. DOI:10.1016/j.apradiso.2011.03.009
- S. Tamjidi, H. Esmaeili, B. K. Moghadas, *Mater. Res. Express.* 2019, *6*, 102004. DOI:10.1088/2053-1591/ab3ffb
- I. Khoshkerdar, H. Esmaeili, *Acta Chim. Slov.* **2019**, *66*, 208–216. DOI:10.17344/acsi.2018.4795
- H. Esmaeili, R. Foroutan, *J. Dispers. Sci. Technol.* **2019**, *40*, 990–999. DOI:10.1080/01932691.2018.1489828
- L. Liu, J. Li, F. Yue, X. Yan, F. Wang, S. Bloszies, Y. Wang, *Chemosphere.* **2018**, *194*, 495–503. DOI:10.1016/j.chemosphere.2017.12.025
- L. He, F. Shao, L. Ren, *Environ. Dev. Sustain.* **2020**. DOI:10.1007/s10668-020-00650-z
- Z. Wei, W. Chen, Z. Wang, N. Li, P. Zhang, M. Zhang, L. Zhao, Q. Qiang, *J. Am. Ceram. Soc.* **2020**. DOI:10.1111/jace.17579
- B. Andre, D. Santos, J. Francisco, B. Jules, V. Lier, *Bioresour. Technol.* **2007**, *98*, 2369–2385. DOI:10.1016/j.biortech.2006.11.013
- B. Royer, N. F. Cardoso, E. C. Lima, J. C. P. Vaghetti, N. M. Simon, T. Calvete, R. C. Veses, *J. Hazard. Mater.* **2009**, *164*, 1213–1222. DOI:10.1016/j.jhazmat.2008.09.028
- E. C. Lima, B. Royer, J. C. P. Vaghetti, N. M. Simon, B. M. Cunha, F. A. Pavan, E. V. Benvenuti, R. CatalunaVeses, C. Airoidi, *J. Hazard. Mater.* **2008**, *155*, 536–550. DOI:10.1016/j.jhazmat.2007.11.101
- D. S. Brookstein, *Dermatol. Clin.* **2009**, *27*, 309–322. DOI:10.1016/j.det.2009.05.001
- X. Li, R. Zhang, X. Zhang, P. Zhu, T. Yao, *Chem. Asian J.* **2020**, *15*, 1175–1179. DOI:10.1002/asia.202000059
- R. O. A. de Lima, A. P. Bazo, D. M. F. Salvadori, C. M. Rech, D. de Palma Oliveira, G. de Aragão Umbuzeiro, *Mutat. Res.* **2007**, *626*, 53–60. DOI:10.1016/j.mrgentox.2006.08.002
- C. Namasivayam, D. Kavitha, *Dyes Pigm.* **2002**, *54*, 47–58. DOI:10.1016/S0143-7208(02)00025-6
- K. Vijayaraghavan, Y. S. Yun, *Dyes Pigm.* **2008**, *76*, 726–732. DOI:10.1016/j.dyepig.2007.01.013
- H. Liu, X. Liu, F. Zhao, Y. Liu, L. Liu, L. Wang, C. Geng, P. Huang, *J. Colloid Interface Sci.* **2020**, *562*, 182–192. DOI:10.1016/j.jcis.2019.12.017
- L. Bulgariu, L. B. Escudero, O. S. Bello, M. Iqbal, J. Nisar, K. A. Adegoke, F. Alakhras, M. Kornaros, I. Anastopoulos, *J. Mol. Liq.* **2019**, *276*, 728–747. DOI:10.1016/j.molliq.2018.12.001
- A. Bhatnagar, M. Sillanpää, *Chem. Eng. J.* **2010**, *157*, 277–296. DOI:10.1016/j.cej.2010.01.007
- S. Abbasi, R. Foroutan, H. Esmaeili, F. Esmaeilzadeh, *Desalin. Water Treat.* **2019**, *141*, 269–278. DOI:10.5004/dwt.2019.23569
- K. S. Tong, M. Jain Kassim, A. Azraa, *Chem. Eng. J.* **2011**, *170*, 145–153. DOI:10.1016/j.cej.2011.03.044
- M. M. Boushehrian, H. Esmaeili, R. Foroutan, *J. Environ. Chem. Eng.* **2020**, *8*, 103869. DOI:10.1016/j.jece.2020.103869

22. Y. Deng, T. Zhang, B. K. Sharma, H. Nie, *Sci. Total Environ.* **2019**, 646, 1140–1154. DOI:10.1016/j.scitotenv.2018.07.369
23. T. Zhang, X. Wu, X. Fan, D. C. Tsang, G. Li, Y. Shen, *J. Environ. Manage.* **2019**, 236, 108–117. DOI:10.1016/j.jenvman.2019.01.018
24. S. M. Mousavi, S. A. Hashemi, A. M. Amani, H. Esmaeili, Y. Ghasemi, A. Babapoor, F. Mojoudi, O. Arjomand, *Phys. Chem. Res.* **2018**, 6, 759–771. DOI: 0.22036/PCR.2018.133392.1490
25. M. S. Karmacharya, V. K. Gupta, I. Tyagi, S. Agarwal, V. K. Jha, *J. Mol. Liq.* **2016**, 216, 836–844. DOI:10.1016/j.molliq.2016.02.025
26. K. Vijayaraghavan, T. V. N. Padmesh, K. Palanivelu, M. Velan, *J. Hazard. Mater.* **2006**, 133, 304–308. DOI:10.1016/j.jhazmat.2005.10.016
27. P. K. Jha, V. K. Jha, 2020. *Mong. J. Chem.* 21, 1–11. DOI:10.5564/mjc.v21i47.1249
28. N. Ünlü, M. Ersoz, *J. Hazard. Mater.* **2006**, 136, 272–280. DOI:10.1016/j.jhazmat.2005.12.013
29. F. Takmil, H. Esmaeili, S. M. Mousavi, S. A. Hashemi, *Adv. Powder Technol.* **2020**. DOI:10.1016/j.apt.2020.06.015
30. H. Esmaeili, S. Tamjidi, *Environ. Sci. Pollut. Res.* **2020**. DOI:10.1007/s11356-020-09448-y
31. T. Zhang, X. He, Y. Deng, D. C. Tsang, H. Yuan, J. Shen, S. Zhang, *Sci. Total Environ.* **2020**, 729, 138999. DOI:10.1016/j.scitotenv.2020.138999
32. H. Li, T. Zhang, D. C. Tsang, G. Li, *Chemosphere.* **2020**, 248, 125927. DOI:10.1016/j.chemosphere.2020.125927
33. F. Ahmadi, H. Esmaeili, *Desalin. Water Treat.* **2018**, 110, 154–167. DOI:10.5004/dwt.2018.22228
34. Y. Abshirini, R. Foroutan, H. Esmaeili, *Mater. Res. Express.* **2019**, 6, 045607. DOI:10.1088/2053-1591/aaf45
35. W. Yang, D. Pudasainee, R. Gupta, W. Li, B. Wang, L. Sun, *Fuel Process. Technol.* **2020**, 106657. DOI:10.1016/j.fuproc.2020.106657
36. Y. Liu, B. Hu, S. Wu, M. Wang, Z. Zhang, B. Cui, L. He, M. Du, *Appl. Catal. B.* **2019**, 258, 117970. DOI:10.1016/j.apcatb.2019.117970
37. D. Cui, J. Li, X. Zhang, L. Zhang, H. Chang, Q. Wang, *J. Anal. Appl. Pyrolysis.* **2021**, 153, 104980. DOI:10.1016/j.jaap.2020.104980
38. H. S. Jamwal, S. Kumari, G. S. Chauhan, N. S. Reddy, J. H. Ahn, *J. Environ. Chem. Eng.* **2017**, 5, 103–113. DOI:10.1016/j.jece.2016.11.029
39. H. Esmaeili, R. Foroutan, D. Jafari, M. Aghil Rezaei, *Korean J. Chem. Eng.* **2020**, 37, 804–814. DOI:10.1007/s11814-020-0493-6
40. P. Wang, X. Zhang, W. Duan, W. Teng, Y. Liu, Q. Xie, *Chin. J. Chem.* DOI:10.1002/cjoc.202000543
41. B. Wang, Z. Song, L. Sun, *Chem. Eng. J.* **2020**, 128136. DOI:10.1016/j.cej.2020.128136
42. L. He, J. Shen, Y. Zhang, *J. Environ. Manage.* **2018**, 206, 1115–1125. DOI:10.1016/j.jenvman.2017.11.059
43. S. Chen, M. K. Hassanzadeh-Aghdam, R. Ansari, *J. Alloys Compd.* **2018**, 767, 632–641. DOI:10.1016/j.jallcom.2018.07.102
44. C. O. Ijagbemi, J. I. Chun, D. H. Han, H. Y. Cho, S. J. O, D. S. Kim, *J. Environ. Sci. Heal. A.* **2010**, 45, 958–967. DOI:10.1080/10934521003772378
45. Y. Song, M. Xu, Z. Li, L. He, M. Hu, L. He, Z. Zhang, M. Du, *Sens. Actuators B Chem.* **2020**, 321, 128527. DOI:10.1016/j.snb.2020.128527
46. X. Li, Y. Feng, B. Liu, D. Yi, X. Yang, W. Zhang, G. Chen, Y. Liu, P. Bai, *J. Alloys Compd.* **2019**, 788, 485–494. DOI:10.1016/j.jallcom.2019.02.223
47. Q. Jia, S. Huang, M. Hu, Y. Song, M. Wang, Z. Zhang, L. He, *Sens. Actuators B Chem.* **2020**, 323, 128647. DOI:10.1016/j.snb.2020.128527
48. A. Ahmadi, R. Foroutan, H. Esmaeili, S. Tamjidi, *Environ. Sci. Pollut. Res.* **2020**, 27, 14044–14057. DOI:10.1007/s11356-020-07756-x

## Povzetek

Preučili smo odstranjevanje barvila metilensko modro iz vodnih raztopin z uporabo aktivnega oglja pripravljenega iz lotusovih listov. Eksperimenti so bili izvedeni šaržno. Površinske lastnosti aktivnega oglja smo analizirali s pomočjo SEM, FTIR, EDAX in BET. Maksimalno adsorpcijsko učinkovitost 97.59 % smo dosegli pri koncentraciji barvila 10 mg/L, pH vrednosti 9, koncentraciji adsorbenta 4 g/L, temperaturi 25 °C, kontaktnem času 60 min in mešanju pri 400 rpm. Maksimalna adsorpcijska kapaciteta je znašala 80 mg/g. Eksperimentalne podatke smo analizirali s kinetičnimi modeli psevdoprvega in psevdodrugega reda ter modelom znotraj delčne difuzije. Rezultati so pokazali najboljše ujemanje s kinetičnim modelom psevdodrugega reda s kinetično konstanto v območju 0.0218–0.0345 g/mg.min. Ravnotežje smo dobro opisali z Freundlichovo adsorpcijsko izotermo. Proces adsorpcije barvila metilensko modro na aktivno oglje je spontan in eksotermni proces.



Except when otherwise noted, articles in this journal are published under the terms and conditions of the Creative Commons Attribution 4.0 International License

# Chitosan-silica Sulfate Nano Hybrid: An Efficient Biopolymer Based-heterogeneous Nano Catalyst for Solvent-free Synthesis of 3,4-Dihydropyrimidine-2(1*H*)-one/thiones

Somayeh Behrouz,<sup>1,\*</sup> Masoome Nazar Abi<sup>1</sup> and Mohammad Amin Piltan<sup>1</sup>

<sup>1</sup> Medicinal Chemistry Research Laboratory, Department of Chemistry, Shiraz University of Technology, Shiraz 71555-313, Iran

\* Corresponding author: E-mail: behrouz@sutech.ac.ir  
phone: +98-713-7354520; fax: +98-713-7354523

Received: 08-20-2020

## Abstract

A green and highly efficient approach for the synthesis of 3,4-dihydropyrimidine-2(1*H*)-one/thione derivatives is described. In this approach, the three-component Biginelli reaction between (thio)urea, methyl acetoacetate and aldehydes under solvent-free condition in the presence of chitosan-silica sulfate nano hybrid (CSSNH) as a green and heterogeneous nano catalyst affords the corresponding products in good to excellent yields and in short reaction times. CSSNH is a cheap, eco-friendly, and non-toxic nano catalyst that could be easily prepared, handled, and reused for many reaction runs without significant loss of its activity.

**Keywords:** Chitosan-silica sulfate nano hybrid; 3,4-Dihydropyrimidines; green chemistry; heterogeneous catalysis; multicomponent reaction

## 1. Introduction

In recent decades, the status of environmental issues has dramatically directed the main goal of science and technology towards environmentally benign processes. Among different tasks to achieve this target, replacing the harmful solvents/catalysts with the green solvents/cata-

lysts and even performing the reactions in the absence of solvent are of high significance.<sup>1,2</sup> Meanwhile, multi-component reactions (MCRs) have gained tremendous attention in comparison with established stepwise synthesis since MCRs exhibit various significant advantages which are in accordance with the green chemistry guidelines and protocols.<sup>2,3</sup> MCRs afford desirable benefits such as at-

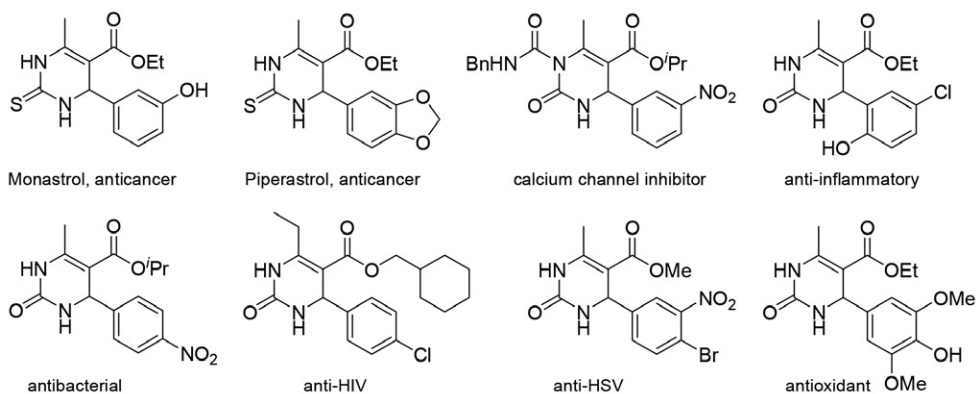


Figure 1. Structure and activity of some DHPMs.



om-efficiency, minimizing the waste and pollution, low-cost and green transformations, simple operation, and high yields.<sup>2,3</sup> MCRs prove to be an ideal strategy for easy and quick access to numerous heterocyclic compounds among which 3,4-dihydropyrimidine-2(1*H*)-ones (DHPMs) derivatives have gained noticeable attention due to their unique and promising biological profiles.<sup>4,5</sup> DHPMs display a wide spectrum of biological activities such as anti-diabetic, anti-inflammatory, anticancer, antimalarial, antiviral, antiproliferative, antileishmanial, antihypertensive, calcium channel modulators and antibacterial in particular antitubercular.<sup>4,6</sup> In addition, DHPMs have been widely used in polymer industries, fabric dyes, and adhesives.<sup>4</sup> They are also found as natural alkaloids in marine creatures.<sup>7,8</sup> The structure and the activity of several bioactive DHPMs are shown in Figure 1.<sup>4,6</sup>

The rapid and straightforward method to access 3,4-dihydropyrimidine-2(1*H*)-ones/thiones involves the three-component cyclocondensation of aldehyde,  $\beta$ -ketoester, and (thio)urea under acidic condition namely known as Biginelli reaction.<sup>4,9</sup> Due to the problems associated with the classical Biginelli reaction such as harsh reaction conditions, low yields, and long reaction times and also regarding to the significance of DHPMs, hence the numerous reaction conditions using various Lewis and Brønsted acid catalysts have been developed so far.<sup>5</sup> To date, a plenty of homogeneous and heterogeneous catalysts such as nano  $\text{BF}_3 \cdot \text{SiO}_2$ ,<sup>10</sup> Bi(III) supported on silica-coated  $\text{Fe}_3\text{O}_4$  nanoparticles,<sup>11</sup>  $\text{TiCl}_3\text{OTf} \cdot [\text{bmim}]\text{Cl}$ ,<sup>12</sup>  $[\text{TEAPS}]\text{H}_2\text{PMo}_{12}\text{O}_{40}$ ,<sup>13</sup>  $\text{CuCl}_2/\text{HCl}$ ,<sup>14</sup> sulfated silica tungstic acid,<sup>15</sup>  $\text{ErCl}_3 \cdot 6\text{H}_2\text{O}$ ,<sup>16</sup>  $\text{SnCl}_2/\text{nano SiO}_2$ ,<sup>17</sup> L-proline nitrate,<sup>18</sup> D-xylonic acid,<sup>19</sup>  $\text{Fe}(\text{OTs})_3 \cdot 6\text{H}_2\text{O}$ ,<sup>20</sup>  $\text{NiCl}_2 \cdot 6\text{H}_2\text{O}/\text{HCl}$ ,<sup>21</sup>  $\text{Co@imine-Na}^+$ -montmorillonite,<sup>22</sup> dendrimer-attached phosphotungstic acid nanoparticles immobilized on nanosilica,<sup>23</sup>  $\text{Ce}(\text{LS})_3$ ,<sup>24</sup> bentonite/ $\text{PS-SO}_3\text{H}$ ,<sup>25</sup> silica sulfuric acid,<sup>26</sup>  $\text{HClO}_4 \cdot \text{SiO}_2$ ,<sup>27</sup> and the exchanged cations in an Algerian montmorillonite<sup>28</sup> under conventional heating, ultrasound and microwave irradiations as well as solvent-free conditions have been reported to achieve DHPMs synthesis.<sup>5</sup> Although these protocols are accompa-

nied with several advantages; however, they suffer from several defects such as the use of metal-based, corrosive, toxic, expensive, non-reusable, and moisture sensitive catalysts, tedious work-up and purification processes, environmental contaminations, the use of harmful organic solvents, inadequate yields, and also long reaction times. Hence, their exploitation causes both economic and environmental concerns. In addition, the use of strongly acidic conditions has no compatibility with acid-sensitive moieties. Consequently, developing an alternative, mild and green protocol for synthesis of DHPMs which overcomes those limitations is still a challenging issue in organic chemistry.

Undoubtedly, catalysts play a crucial role in countless chemical processes. Taking the numerous advantages of heterogeneous catalysts from both environmental and economic points of view, the use of heterogeneous catalysts has attracted a massive attention in comparison with homogeneous catalysts from both academic and industrial aspects. Currently, the application of natural biopolymers is growing tremendously in different research areas especially for preparation of green heterogeneous catalysts owing to their biodegradable, biocompatible, non-toxic, and cheap materials. To this end, polysaccharides have found increasing applications since these biomolecules exhibit unique chelating power and ease of chemical modifications and also due to their abundance in the nature.<sup>29</sup> Along this line, utilizing the natural biopolymer-based catalysts for synthesis of DHPMs is an attractive strategy. In this context, the use of acidic heterogeneous catalysts including cellulose sulfuric acid<sup>30</sup> and starch sulfuric acid<sup>31</sup> has been reported in refluxing water and EtOH, respectively. Lal *et al.* reported the synthesis of DHPM derivatives of curcumin using chitosan/ $\text{AcOH}/\text{H}_2\text{O}$ .<sup>32</sup> From both economic and ecological perspectives, utilizing the green nano heterogeneous catalysts under solvent-free condition is in demand. To the best of our knowledge, only one solvent-free synthesis of DHPMs using chitosan/graphene oxide nanocomposite has been established.<sup>33</sup> Hence, developing an efficient solvent-free protocol for

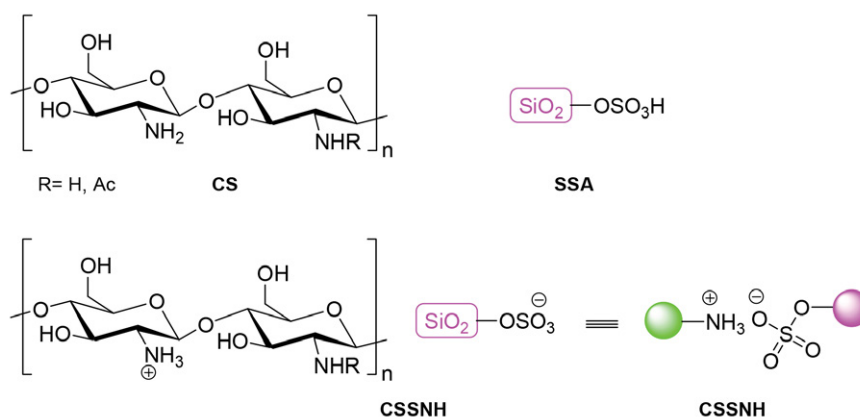
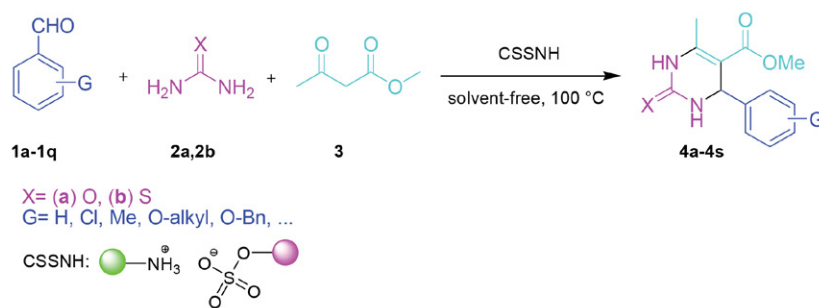


Figure 2. The structure of chitosan (CS), silica sulfuric acid (SSA) and CSSNH.



Scheme 1. Synthesis of DHPMs using CSSNH.

synthesis of DHPMs in the presence of biopolymer-based nano heterogeneous catalysts is still quite appealing.

Chitosan is a biodegradable, non-toxic, and cheap natural biopolymer which can easily undergo chemical modifications through its amine and hydroxyl functional groups.<sup>34</sup> Accordingly, chitosan has found considerable research interest in numerous fields of science and industry.<sup>35–38</sup> Recently, we have reported the synthesis, characterization, and application of chitosan-silica sulfate nano hybrid (CSSNH) as a new, green, highly proficient, and cheap heterogeneous nano-catalyst (Figure 2). The high efficacy and potency of CSSNH was confirmed by its successful applications in many organic transformations.<sup>39–41</sup> Inspired by the unique biological profile of DHPMs and our interest in multi-component reactions<sup>42–46</sup> as well as discovering another new application for CSSNH, hereby we report a facile and efficient protocol for synthesis of 3,4-dihydropyrimidine-2(1H)-one/thione derivatives *via* three-component reaction (3CR) of commercial and synthetic aldehydes, (thio)urea, and methyl acetoacetate in the presence of CSSNH as an eco-friendly and heterogeneous nano catalyst at 100 °C under the solvent-free condition (Scheme 1).

## 2. Experimental

All chemicals were purchased from Merck or Sigma-Aldrich. CSSNH was prepared according to the reported procedure.<sup>40</sup> Solvents were purified by standard procedures, and stored over 3 Å molecular sieves. Reactions were followed by TLC using SILG/UV 254 silica-gel plates. Column chromatography was performed on silica gel 60 (0.063–0.200 mm, 70–230 mesh; ASTM). <sup>1</sup>H and <sup>13</sup>C NMR spectra were recorded on Bruker Avance-DPX-300 spectrometer operating at 300 MHz or 75 MHz, respectively. Chemical shifts are given in  $\delta$  (on ppm scale) relative to tetramethylsilane (TMS) as an internal standard, coupling constants *J* are given in Hz. HRMS and IR spectra were obtained using a Bruker micrOTOF-Q 134 apparatus and a Shimadzu FT-IR-8300 spectrophotometer, respectively. Melting points were measured using Electrothermal IA 9000 melting point apparatus in open capillary tubes and are uncorrected.

### Preparation of 3,4-Dihydropyrimidine-2(1H)-(thio)ones 4a–s

In a round bottom flask (25 mL), a mixture of thio(urea) (6 mmol), methyl acetoacetate (5 mmol), appropriate aldehyde (5 mmol), and CSSNH (0.04 g) under solvent free condition was heated at 100 °C in a paraffin bath. When no further improvement was observed on the reaction progress (TLC monitoring, Table 4), the reaction mixture was diluted with EtOH (10 mL). Subsequently, the crude mixture was filtered off to separate the catalyst. The catalyst was then washed with EtOH (2 × 5 mL) to remove any substrate from CSSNH. The pure DHPM derivatives were obtained *via* recrystallization from the ethanolic solution of the reaction mixture.

### Recovery of CSSNH

After accomplishment of the reaction and separation of CSSNH, the catalyst was washed with EtOH (2 × 5 mL). CSSNH was then dried in a vacuum oven at 50 °C for 2 h and kept in a closed vessel in the refrigerator.

### Methyl 6-Methyl-2-oxo-4-phenyl-1,2,3,4-tetrahydropyrimidine-5-carboxylate (4a) C<sub>13</sub>H<sub>14</sub>N<sub>2</sub>O<sub>3</sub>

Recrystallization from ethanol afforded 1.18 g (96%) **4a** as a white solid. Mp 208–210 °C (Lit.<sup>26</sup> 210–212 °C); <sup>1</sup>H NMR (300 MHz, DMSO-*d*<sub>6</sub>):  $\delta$  2.24 (s, 3H, CH<sub>3</sub>), 3.51 (s, 3H, OCH<sub>3</sub>), 5.12 (s, 1H, PhCH), 7.21–7.33 (m, 5H, ArH), 7.76 (s, 1H, NH), 9.23 (s, 1H, NH); <sup>13</sup>C NMR (75 MHz, DMSO-*d*<sub>6</sub>):  $\delta$  17.89, 50.87, 53.85, 99.03, 126.04, 127.22, 128.42, 144.67, 148.58, 152.14, 165.88; IR (KBr):  $\nu_{\text{max}}$  3350, 3180, 2950, 1700, 1640, 1470, 1250, 1172 cm<sup>-1</sup>; HRMS: *m/z* (M + H)<sup>+</sup> calculated for C<sub>13</sub>H<sub>14</sub>N<sub>2</sub>O<sub>3</sub>: 247.1083, found: 247.1097.

### Methyl 6-Methyl-2-oxo-4-*para*-tolyl-1,2,3,4-tetrahydropyrimidine-5-carboxylate (4b) C<sub>14</sub>H<sub>16</sub>N<sub>2</sub>O<sub>3</sub>

Recrystallization from ethanol afforded 1.22 g (94%) **4b** as a white solid. Mp 199–201 °C (Lit.<sup>49</sup> 198–200 °C); <sup>1</sup>H NMR (300 MHz, DMSO-*d*<sub>6</sub>):  $\delta$  2.23–2.24 (Complex, 6H, CH<sub>3</sub>, PhCH<sub>3</sub>), 3.50 (s, 3H, OCH<sub>3</sub>), 5.08 (s, 1H, PhCH), 7.10 (br s, 4H, ArH), 7.71 (s, 1H, NH), 9.19 (s, 1H, NH); <sup>13</sup>C NMR (75 MHz, DMSO-*d*<sub>6</sub>):  $\delta$  17.84, 20.62, 50.74, 53.45, 99.05, 126.02, 128.86, 136.41, 144.63, 148.45, 152.05, 165.79; IR (KBr):  $\nu_{\text{max}}$  3250, 3125, 2964, 1698, 1629, 1438,

1257, 1172  $\text{cm}^{-1}$ ; HRMS:  $m/z$  ( $M + H$ )<sup>+</sup> calculated for  $\text{C}_{14}\text{H}_{16}\text{N}_2\text{O}_3$ : 261.1239, found: 261.1252.

**Methyl 4-(2-Chlorophenyl)-6-methyl-2-oxo-1,2,3,4-tetrahydropyrimidine-5-carboxylate (4c)**  $\text{C}_{13}\text{H}_{13}\text{ClN}_2\text{O}_3$

Recrystallization from ethanol afforded 1.23 g (88%) **4c** as a white solid. Mp 257–259 °C (Lit.<sup>49</sup> 256–259 °C); <sup>1</sup>H NMR (300 MHz, DMSO- $d_6$ ):  $\delta$  2.28 (s, 3H, CH<sub>3</sub>), 3.43 (s, 3H, OCH<sub>3</sub>), 5.43 (s, 1H, PhCH), 7.26–7.40 (m, 4H, ArH), 7.72 (s, 1H, NH), 9.32 (s, 1H, NH); <sup>13</sup>C NMR (75 MHz, DMSO- $d_6$ ):  $\delta$  17.86, 51.97, 59.58, 98.40, 128.16, 129.09, 129.23, 129.87, 132.14, 142.25, 149.83, 151.79, 165.55; IR (KBr):  $\nu_{\text{max}}$  3240, 3163, 2975, 1696, 1620, 1468, 1225, 1145, 748  $\text{cm}^{-1}$ ; HRMS:  $m/z$  ( $M + H$ )<sup>+</sup> calculated for  $\text{C}_{13}\text{H}_{13}\text{ClN}_2\text{O}_3$ : 281.0693, found: 281.0715.

**Methyl 4-(2,4-Dichlorophenyl)-6-methyl-2-thioxo-1,2,3,4-tetrahydropyrimidine-5-carboxylate (4d)**  $\text{C}_{13}\text{H}_{12}\text{Cl}_2\text{N}_2\text{O}_2\text{S}$

Recrystallization from ethanol afforded 1.42 g (86%) **4d** as a white solid. Mp 252–254 °C; <sup>1</sup>H NMR (300 MHz, DMSO- $d_6$ ):  $\delta$  2.49 (s, 3H, CH<sub>3</sub>), 3.35 (s, 3H, OCH<sub>3</sub>), 5.43 (s, 1H, PhCH), 6.99 (br s, 2H, ArH), 7.17 (s, 1H, ArH), 7.29 (s, 1H, NH), 9.00 (s, 1H, NH); <sup>13</sup>C NMR (75 MHz, DMSO- $d_6$ ):  $\delta$  17.78, 50.77, 51.52, 97.36, 128.09, 128.86, 130.02, 132.46, 132.62, 140.90, 149.63, 151.25, 165.30; IR (KBr):  $\nu_{\text{max}}$  3340, 3150, 2961, 1680, 1459, 1225, 1190, 1145, 752  $\text{cm}^{-1}$ ; HRMS:  $m/z$  ( $M + H$ )<sup>+</sup> calculated for  $\text{C}_{13}\text{H}_{12}\text{Cl}_2\text{N}_2\text{O}_2\text{S}$ : 329.9997, found: 330.0018.

**Methyl 4-(4-Methoxyphenyl)-6-methyl-2-oxo-1,2,3,4-tetrahydropyrimidine-5-carboxylate (4e)**  $\text{C}_{14}\text{H}_{16}\text{N}_2\text{O}_4$

Recrystallization from ethanol afforded 1.28 g (93%) **4e** as a white solid. Mp 186–188 °C (Lit.<sup>49</sup> 187–190 °C); <sup>1</sup>H NMR (300 MHz, DMSO- $d_6$ ):  $\delta$  2.21 (s, 3H, CH<sub>3</sub>), 3.50 (s, 3H, OCH<sub>3</sub>), 3.69 (s, 3H, OCH<sub>3</sub>), 5.05 (s, 1H, PhCH), 6.85 (br s, 2H, ArH), 7.11 (br s, 2H, ArH), 7.68 (s, 1H, NH), 9.17 (s, 1H, NH); <sup>13</sup>C NMR (75 MHz, DMSO- $d_6$ ):  $\delta$  17.86, 50.64, 53.13, 54.99, 99.33, 113.73, 127.26, 136.83, 148.39, 152.19, 158.48, 165.84; IR (KBr):  $\nu_{\text{max}}$  3300, 3170, 2981, 1693, 1618, 1455, 1237, 1148  $\text{cm}^{-1}$ ; HRMS:  $m/z$  ( $M + H$ )<sup>+</sup> calculated for  $\text{C}_{14}\text{H}_{16}\text{N}_2\text{O}_4$ : 277.1188, found: 277.1213.

**Methyl 4-(4-Methoxyphenyl)-6-methyl-2-thioxo-1,2,3,4-tetrahydropyrimidine-5-carboxylate (4f)**  $\text{C}_{14}\text{H}_{16}\text{N}_2\text{O}_3\text{S}$

Recrystallization from ethanol afforded 1.33 g (91%) **4f** as a yellow solid. Mp 178–180 °C (Lit.<sup>18</sup> 181–183 °C); <sup>1</sup>H NMR (300 MHz, DMSO- $d_6$ ):  $\delta$  2.27 (s, 3H, CH<sub>3</sub>), 3.53 (s, 3H, OCH<sub>3</sub>), 3.71 (s, 3H, OCH<sub>3</sub>), 5.09 (s, 1H, PhCH), 6.87 (d, 2H,  $J = 6.0$  Hz, ArH), 7.10 (d, 2H,  $J = 6.0$  Hz, ArH), 9.63 (s, 1H, NH), 10.33 (s, 1H, NH); <sup>13</sup>C NMR (75 MHz, DMSO- $d_6$ ):  $\delta$  17.13, 51.15, 53.32, 55.16, 100.69, 114.03, 127.66, 135.51, 145.01, 158.79, 165.69, 174.12; IR (KBr):  $\nu_{\text{max}}$  3310, 3175, 2943, 1682, 1439, 1225, 1190, 1153  $\text{cm}^{-1}$ ; HRMS:  $m/z$  ( $M + H$ )<sup>+</sup> calculated for  $\text{C}_{14}\text{H}_{16}\text{N}_2\text{O}_3\text{S}$ : 293.0960, found: 293.0974.

**Methyl 4-(3,5-Dimethoxyphenyl)-6-methyl-2-thioxo-1,2,3,4-tetrahydropyrimidine-5-carboxylate (4g)**  $\text{C}_{15}\text{H}_{18}\text{N}_2\text{O}_4\text{S}$

Recrystallization from ethanol afforded 1.43 g (89%) **4g** as a yellow solid. Mp 195–197 °C; <sup>1</sup>H NMR (300 MHz, DMSO- $d_6$ ):  $\delta$  2.30 (s, 3H, CH<sub>3</sub>), 3.57 (s, 3H, OCH<sub>3</sub>), 3.73 (s, 6H, 2 OCH<sub>3</sub>), 5.14 (s, 1H, PhCH), 6.69–6.72 (m, 1H, ArH), 6.86–6.92 (m, 1H, ArH), 9.63 (s, 1H, NH), 10.34 (s, 1H, NH); <sup>13</sup>C NMR (75 MHz, DMSO- $d_6$ ):  $\delta$  17.26, 51.15, 53.45, 55.34, 100.11, 101.11, 113.96, 136.21, 145.63, 159.08, 165.83, 173.99; IR (KBr):  $\nu_{\text{max}}$  3300, 3193, 2971, 1685, 1467, 1229, 1182, 1138  $\text{cm}^{-1}$ ; HRMS:  $m/z$  ( $M + H$ )<sup>+</sup> calculated for  $\text{C}_{15}\text{H}_{18}\text{N}_2\text{O}_4\text{S}$ : 323.1066, found: 323.1085.

**Methyl 4-(4-(5-(Methoxycarbonyl)-6-methyl-2-oxo-1,2,3,4-tetrahydropyrimidin-4-yl)phenyl)-6-methyl-2-oxo-1,2,3,4-tetrahydropyrimidine-5-carboxylate (4h)**  $\text{C}_{20}\text{H}_{22}\text{N}_4\text{O}_6$

Recrystallization from ethanol afforded 1.80 g (87%) **4h** as a white solid. Mp >245 °C (dec.); <sup>1</sup>H NMR (300 MHz, DMSO- $d_6$ ):  $\delta$  2.51 (s, 6H, 2 CH<sub>3</sub>), 3.36 (s, 6H, 2 OCH<sub>3</sub>), 5.65 (s, 2H, 2 PhCH), 7.18 (br s, 4H, ArH), 7.71 (s, 2H, 2 NH), 9.24 (s, 2H, 2 NH); <sup>13</sup>C NMR (75 MHz, DMSO- $d_6$ ):  $\delta$  18.01, 51.04, 54.08, 99.29, 127.70, 144.53, 148.50, 152.12, 165.92; IR (KBr):  $\nu_{\text{max}}$  3350, 3240, 3056, 1700, 1645, 1472, 1250, 1140  $\text{cm}^{-1}$ ; HRMS:  $m/z$  ( $M + H$ )<sup>+</sup> calculated for  $\text{C}_{20}\text{H}_{22}\text{N}_4\text{O}_6$ : 415.1618, found: 415.1641.

**Methyl 4-(4-Butoxyphenyl)-6-methyl-2-oxo-1,2,3,4-tetrahydropyrimidine-5-carboxylate (4i)**  $\text{C}_{17}\text{H}_{22}\text{N}_2\text{O}_4$

Recrystallization from ethanol afforded 1.46 g (92%) **4i** as a white solid. Mp 173–175 °C; <sup>1</sup>H NMR (300 MHz, DMSO- $d_6$ ):  $\delta$  0.88 (t, 3H,  $J = 6.0$  Hz, CH<sub>2</sub>CH<sub>3</sub>), 1.39–1.41 (m, 2H, CH<sub>2</sub>CH<sub>3</sub>), 1.65 (br s, 2H, OCH<sub>2</sub>CH<sub>2</sub>), 2.22 (s, 3H, CH<sub>3</sub>), 3.51 (s, 3H, OCH<sub>3</sub>), 3.91 (s, 2H, OCH<sub>2</sub>), 5.06 (s, 1H, PhCH), 6.84 (d, 2H,  $J = 3.0$  Hz, ArH), 7.09 (d, 2H,  $J = 6.0$  Hz, ArH), 7.68 (s, 1H, NH), 9.18 (s, 1H, NH); <sup>13</sup>C NMR (75 MHz, DMSO- $d_6$ ):  $\delta$  13.93, 17.73, 19.89, 31.79, 50.71, 53.12, 66.35, 99.32, 113.64, 127.43, 136.88, 148.22, 152.00, 158.49, 165.78; IR (KBr):  $\nu_{\text{max}}$  3342, 3225, 3080, 1694, 1627, 1459, 1241, 1126  $\text{cm}^{-1}$ ; HRMS:  $m/z$  ( $M + H$ )<sup>+</sup> calculated for  $\text{C}_{17}\text{H}_{22}\text{N}_2\text{O}_4$ : 319.1658, found: 319.1679.

**Methyl 4-(4-(Isopentyloxy)phenyl)-6-methyl-2-oxo-1,2,3,4-tetrahydropyrimidine-5-carboxylate (4j)**  $\text{C}_{18}\text{H}_{24}\text{N}_2\text{O}_4$

Recrystallization from ethanol afforded 1.49 g (90%) **4j** as a white solid. Mp 171–173 °C; <sup>1</sup>H NMR (300 MHz, DMSO- $d_6$ ):  $\delta$  0.94 (d, 6H,  $J = 6.0$  Hz, CH(CH<sub>3</sub>)<sub>2</sub>), 1.62–1.68 (m, 2H OCH<sub>2</sub>CH<sub>2</sub>), 1.78–1.87 (m, 1H, CH<sub>2</sub>CH), 2.32 (s, 3H, CH<sub>3</sub>), 3.62 (s, 3H, OCH<sub>3</sub>), 3.62 (t, 2H,  $J = 6.0$  Hz, OCH<sub>2</sub>), 5.35 (s, 1H, PhCH), 6.22 (s, 1H, NH), 6.77–6.88 (m, 3H, ArH), 7.18–7.26 (m, 1H, ArH), 8.82 (s, 1H, NH); <sup>13</sup>C NMR (75 MHz, DMSO- $d_6$ ):  $\delta$  17.48, 23.79, 24.91, 40.09, 50.60, 53.96, 66.41, 100.17, 113.41, 127.46, 136.51, 148.77, 152.16, 158.29, 165.73; IR (KBr):  $\nu_{\text{max}}$  340, 3231, 3076, 1699, 1620, 1455, 1228, 1139  $\text{cm}^{-1}$ ; HRMS:

$m/z$  (M + H)<sup>+</sup> calculated for C<sub>18</sub>H<sub>24</sub>N<sub>2</sub>O<sub>4</sub>: 333.1814, found: 333.1823.

**Methyl 6-Methyl-4-(4-((4-methylbenzyl)oxy)phenyl)-2-oxo-1,2,3,4-tetrahydropyrimidine-5-carboxylate (4k)** C<sub>21</sub>H<sub>22</sub>N<sub>2</sub>O<sub>4</sub>

Recrystallization from ethanol afforded 1.66 g (91%) **4k** as a white solid. Mp 250–252 °C; <sup>1</sup>H NMR (300 MHz, DMSO-*d*<sub>6</sub>): δ 2.25 (s, 3H, CH<sub>3</sub>), 2.30 (s, 3H, PhCH<sub>3</sub>), 3.53 (s, 3H, OCH<sub>3</sub>), 5.01 (s, 2H, OCH<sub>2</sub>), 5.12 (s, 1H, PhCH), 6.80–6.90 (m, 4H, ArH), 7.18–7.31 (m, 4H, ArH), 7.76 (s, 1H, NH), 9.24 (s, 1H, NH); <sup>13</sup>C NMR (75 MHz, DMSO-*d*<sub>6</sub>): δ 17.29, 20.37, 50.67, 53.72, 70.29, 100.09, 115.26, 127.70, 128.70, 129.71, 134.81, 135.94, 136.78, 148.92, 152.50, 158.28, 165.49; IR (KBr): ν<sub>max</sub> 3337, 3250, 3041, 1693, 1617, 1469, 1240, 1125 cm<sup>-1</sup>; HRMS:  $m/z$  (M + H)<sup>+</sup> calculated for C<sub>21</sub>H<sub>22</sub>N<sub>2</sub>O<sub>4</sub>: 367.1658, found: 367.1679.

**Methyl 4-(3-(Benzyloxy)phenyl)-6-methyl-2-oxo-1,2,3,4-tetrahydropyrimidine-5-carboxylate (4l)** C<sub>20</sub>H<sub>20</sub>N<sub>2</sub>O<sub>4</sub>

Recrystallization from ethanol afforded 1.56 g (89%) **4l** as a white solid. Mp 196–198 °C; <sup>1</sup>H NMR (300 MHz, DMSO-*d*<sub>6</sub>): δ 2.26 (s, 3H, CH<sub>3</sub>), 3.52 (s, 3H, OCH<sub>3</sub>), 5.07 (s, 2H, OCH<sub>2</sub>), 5.10 (s, 1H, PhCH), 6.95 (d, 2H, *J* = 6.0 Hz, ArH), 7.14 (d, 2H, *J* = 9.0 Hz, ArH), 7.32–7.42 (m, 5H, ArH), 7.73 (s, 1H, NH), 9.23 (s, 1H, NH); <sup>13</sup>C NMR (75 MHz, DMSO-*d*<sub>6</sub>): δ 17.20, 50.41, 53.67, 69.87, 100.66, 111.47, 112.57, 118.49, 127.16, 127.70, 128.76, 129.57, 136.58, 147.13, 149.32, 152.56, 159.31, 165.25; IR (KBr): ν<sub>max</sub> 3300, 3227, 3065, 1700, 1626, 1453, 1250, 1129 cm<sup>-1</sup>; HRMS:  $m/z$  (M + H)<sup>+</sup> calculated for C<sub>20</sub>H<sub>20</sub>N<sub>2</sub>O<sub>4</sub>: 353.1501, found: 353.1512.

**Methyl 4-(2-Methoxy-4-phenethoxyphenyl)-6-methyl-2-oxo-1,2,3,4-tetrahydropyrimidine-5-carboxylate (4m)** C<sub>22</sub>H<sub>24</sub>N<sub>2</sub>O<sub>5</sub>

Recrystallization from ethanol afforded 1.68 g (85%) **4m** as a white solid. Mp 193–195 °C; <sup>1</sup>H NMR (300 MHz, DMSO-*d*<sub>6</sub>): δ 2.24 (s, 3H, CH<sub>3</sub>), 3.03 (t, 2H, *J* = 6.0 Hz, PhCH<sub>2</sub>), 3.54 (s, 3H, OCH<sub>3</sub>), 3.74 (s, 3H, PhOCH<sub>3</sub>), 4.07 (t, 2H, *J* = 6.0 Hz, OCH<sub>2</sub>), 5.26 (s, 1H, PhCH), 5.99 (s, 1H, NH), 6.68–6.75 (m, 3H, ArH), 7.13–7.28 (m, 5H, ArH), 8.52 (s, 1H, NH); <sup>13</sup>C NMR (75 MHz, DMSO-*d*<sub>6</sub>): δ 17.45, 34.98, 50.25, 53.30, 54.07, 69.96, 100.56, 101.25, 115.20, 126.56, 127.66, 128.51, 128.62, 135.47, 137.174, 148.96, 152.88, 157.07, 158.08, 164.93; IR (KBr): ν<sub>max</sub> 3350, 3215, 3027, 1698, 1635, 1477, 1241, 1117 cm<sup>-1</sup>; HRMS:  $m/z$  (M + H)<sup>+</sup> calculated for C<sub>22</sub>H<sub>24</sub>N<sub>2</sub>O<sub>5</sub>: 397.1763, found: 397.1775.

**Methyl 4-(4-(4-(1,3-Dioxoisindolin-2-yl)butoxy)phenyl)-6-methyl-2-oxo-1,2,3,4-tetrahydropyrimidine-5-carboxylate (4n)** C<sub>25</sub>H<sub>25</sub>N<sub>3</sub>O<sub>6</sub>

Recrystallization from ethanol afforded 2.17 g (94%) **4n** as a white solid. Mp 134–136 °C; <sup>1</sup>H NMR (300 MHz, DMSO-*d*<sub>6</sub>): δ 1.82 (br s, 4H, OCH<sub>2</sub>CH<sub>2</sub>CH<sub>2</sub>), 2.31 (s, 3H, CH<sub>3</sub>), 3.64 (s, 3H, OCH<sub>3</sub>), 3.73–3.75 (m, 2H, NCH<sub>2</sub>),

3.93–3.95 (m, 2H, OCH<sub>2</sub>), 4.94 (s, 1H, PhCH), 6.34 (s, 1H, NH), 6.71 (d, 2H, *J* = 9.0 Hz, ArH), 7.15 (d, 2H, *J* = 9.0 Hz, ArH), 7.70–7.83 (m, 4H, ArH), 8.70 (s, 1H, NH); <sup>13</sup>C NMR (75 MHz, DMSO-*d*<sub>6</sub>): δ 17.63, 29.41, 32.46, 37.77, 50.37, 52.95, 67.00, 100.05, 113.32, 123.13, 127.30, 132.33, 133.92, 135.05, 148.76, 152.37, 158.44, 165.72, 168.15; IR (KBr): ν<sub>max</sub> 3346, 3229, 3050, 1700, 1642, 1466, 1240, 1124 cm<sup>-1</sup>; HRMS:  $m/z$  (M + H)<sup>+</sup> calculated for C<sub>25</sub>H<sub>25</sub>N<sub>3</sub>O<sub>6</sub>: 464.1822, found: 464.1850.

**Methyl 4-(4-(4-(1,3-Dioxoisindolin-2-yl)butoxy)phenyl)-6-methyl-2-thioxo-1,2,3,4-tetrahydropyrimidine-5-carboxylate (4o)** C<sub>25</sub>H<sub>25</sub>N<sub>3</sub>O<sub>5</sub>S

Recrystallization from ethanol afforded 2.20 g (92%) **4o** as a white solid. Mp 130–132 °C; <sup>1</sup>H NMR (300 MHz, DMSO-*d*<sub>6</sub>): δ 1.89–1.96 (m, 2H, NCH<sub>2</sub>CH<sub>2</sub>), 2.22 (s, 3H, CH<sub>3</sub>), 2.40–2.44 (m, 2H, OCH<sub>2</sub>CH<sub>2</sub>), 3.50 (s, 3H, OCH<sub>3</sub>), 3.91–3.94 (m, 2H, NCH<sub>2</sub>), 4.01–4.07 (m, 2H, OCH<sub>2</sub>), 5.06 (s, 1H, PhCH), 6.56 (d, 2H, *J* = 6.0 Hz, ArH), 6.83 (d, 2H, *J* = 6.0 Hz, ArH), 7.10 (d, 2H, *J* = 6.0 Hz, ArH), 7.33 (d, 2H, *J* = 6.0 Hz, ArH), 7.69 (s, 1H, NH), 9.18 (s, 1H, NH); <sup>13</sup>C NMR (75 MHz, DMSO-*d*<sub>6</sub>): δ 17.88, 30.23, 32.89, 37.93, 50.54, 53.21, 67.25, 100.34, 113.80, 123.36, 127.41, 132.62, 134.02, 135.12, 147.88, 158.54, 156.69, 168.24, 174.10; IR (KBr): ν<sub>max</sub> 3380, 3260, 3029, 1647, 1452, 1185, 1137 cm<sup>-1</sup>; HRMS:  $m/z$  (M + H)<sup>+</sup> calculated for C<sub>25</sub>H<sub>25</sub>N<sub>3</sub>O<sub>5</sub>S: 480.1593, found: 480.1620.

**Methyl 4-(4-(4-(4-Allyl-2-methoxyphenoxy)butoxy)phenyl)-6-methyl-2-oxo-1,2,3,4-tetrahydropyrimidine-5-carboxylate (4p)** C<sub>27</sub>H<sub>32</sub>N<sub>2</sub>O<sub>6</sub>

Recrystallization from ethanol afforded 2.18 g (91%) **4p** as a white solid. Mp 145–147 °C; <sup>1</sup>H NMR (300 MHz, DMSO-*d*<sub>6</sub>): δ 1.91 (br s, 4H, OCH<sub>2</sub>CH<sub>2</sub>CH<sub>2</sub>), 2.27 (s, 3H, CH<sub>3</sub>), 3.25 (d, 2H, *J* = 6.0 Hz, PhCH<sub>2</sub>), 3.55 (s, 3H, OCH<sub>3</sub>), 3.76 (s, 3H, OCH<sub>3</sub>), 3.92–4.01 (m, 4H, 2 OCH<sub>2</sub>), 4.97–5.04 (m, 2H, =CH<sub>2</sub>), 5.27 (s, 1H, PhCH), 5.82–5.95 (m, 1H, =CH), 6.62 (d, 2H, *J* = 6.0 Hz, ArH), 6.73–6.76 (m, 3H, ArH), 7.13–7.19 (m, 3H, NH, ArH), 8.11 (s, 1H, NH); <sup>13</sup>C NMR (75 MHz, DMSO-*d*<sub>6</sub>): δ 17.83, 30.01, 32.56, 39.91, 50.72, 53.28, 55.83, 67.09, 68.83, 100.08, 111.97, 112.58, 113.78, 115.57, 120.68, 127.25, 132.67, 136.89, 137.92, 148.00, 148.31, 149.64, 152.06, 158.50, 165.85; IR (KBr): ν<sub>max</sub> 3350, 3200, 3046, 1694, 1625, 1448, 1223, 1165 cm<sup>-1</sup>; HRMS:  $m/z$  (M + H)<sup>+</sup> calculated for C<sub>27</sub>H<sub>32</sub>N<sub>2</sub>O<sub>6</sub>: 481.2339, found: 481.2365.

**Methyl 4-(3-(4-(4-Allyl-2-methoxyphenoxy)butoxy)phenyl)-6-methyl-2-oxo-1,2,3,4-tetrahydropyrimidine-5-carboxylate (4q)** C<sub>27</sub>H<sub>32</sub>N<sub>2</sub>O<sub>6</sub>

Recrystallization from ethanol afforded 2.09 g (87%) **4q** as a white solid. Mp 141–143 °C; <sup>1</sup>H NMR (300 MHz, DMSO-*d*<sub>6</sub>): δ 1.84 (br s, 4H, OCH<sub>2</sub>CH<sub>2</sub>CH<sub>2</sub>), 2.24 (s, 3H, CH<sub>3</sub>), 3.29 (m, 2H, PhCH<sub>2</sub>), 3.53 (s, 3H, OCH<sub>3</sub>), 3.72 (s, 3H, OCH<sub>3</sub>), 3.96–3.99 (m, 4H, 2 OCH<sub>2</sub>), 5.00–5.11 (Complex, 3H, PhCH, = CH<sub>2</sub>), 5.90–5.96 (m, 1H, =CH),

6.67–6.87 (m, 6H, ArH), 7.22 (s, 1H, ArH), 7.74 (s, 1H, NH), 9.22 (s, 1H, NH);  $^{13}\text{C}$  NMR (75 MHz, DMSO- $d_6$ ):  $\delta$  17.78, 30.06, 32.51, 39.87, 50.73, 53.37, 55.82, 67.04, 68.79, 100.16, 111.75, 111.80, 112.44, 112.61, 115.59, 118.77, 120.67, 129.71, 132.62, 138.03, 146.91, 148.03, 148.35, 149.61, 152.05, 159.40, 165.72; IR (KBr):  $\nu_{\text{max}}$  3347, 3215, 3081, 1697, 1613, 1463, 1228, 1170  $\text{cm}^{-1}$ ; HRMS:  $m/z$  ( $M + H$ ) $^+$  calculated for  $\text{C}_{27}\text{H}_{32}\text{N}_2\text{O}_6$ : 481.2339, found: 481.2370.

**Methyl 4-(3-(4-(4-Chlorophenoxy)butoxy)phenyl)-6-methyl-2-oxo-1,2,3,4-tetrahydropyrimidine-5-carboxylate (4r)**  $\text{C}_{23}\text{H}_{25}\text{ClN}_2\text{O}_5$

Recrystallization from ethanol afforded 1.97 g (89%) **4r** as a white solid. Mp 162–164  $^{\circ}\text{C}$ ;  $^1\text{H}$  NMR (300 MHz, DMSO- $d_6$ ):  $\delta$  1.83 (br s, 4H,  $\text{OCH}_2\text{CH}_2\text{CH}_2$ ), 2.22 (s, 3H,  $\text{CH}_3$ ), 3.51 (s, 3H,  $\text{OCH}_3$ ), 3.99 (m, 4H, 2  $\text{OCH}_2$ ), 5.08 (s, 1H, PhCH), 6.75–6.81 (m, 3H, ArH), 6.93 (d, 2H,  $J = 6.0$  Hz, ArH), 7.20 (d, 1H,  $J = 5.4$  Hz, ArH), 7.28 (d, 2H,  $J = 6.0$  Hz, ArH), 7.73 (s, 1H, NH), 9.21 (s, 1H, NH);  $^{13}\text{C}$  NMR (75 MHz, DMSO- $d_6$ ):  $\delta$  17.85, 28.54, 29.64, 50.60, 53.20, 65.50, 66.86, 100.13, 111.65, 112.43, 116.10, 118.46, 125.52, 129.38, 129.72, 147.06, 148.36, 152.28, 157.98, 159.37, 165.72; IR (KBr):  $\nu_{\text{max}}$  3360, 3200, 3044, 1700, 1625, 1450, 1231, 1164, 758  $\text{cm}^{-1}$ ; HRMS:  $m/z$  ( $M + H$ ) $^+$  calculated for  $\text{C}_{23}\text{H}_{25}\text{ClN}_2\text{O}_5$ : 445.1530, found: 445.1549.

**Methyl 4-(3-(4-(4-Chloro-3-methylphenoxy)butoxy)phenyl)-6-methyl-2-oxo-1,2,3,4-tetrahydropyrimidine-5-carboxylate (4s)**  $\text{C}_{24}\text{H}_{27}\text{ClN}_2\text{O}_5$

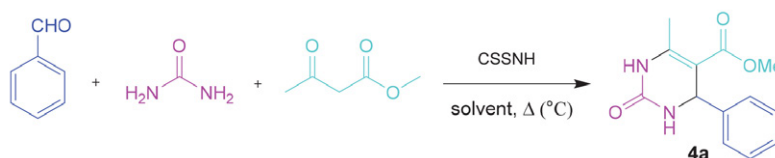
Recrystallization from ethanol afforded 1.99 g (87%) **4s** as a white solid. Mp 170–172  $^{\circ}\text{C}$ ;  $^1\text{H}$  NMR (300 MHz, DMSO- $d_6$ ):  $\delta$  1.84 (br s, 4H,  $\text{OCH}_2\text{CH}_2\text{CH}_2$ ), 2.24 (s, 3H,

$\text{CH}_3$ ), 2.27 (s, 3H,  $\text{PhCH}_3$ ), 3.52 (s, 3H,  $\text{OCH}_3$ ), 3.99 (m, 4H, 2  $\text{OCH}_2$ ), 5.10 (s, 1H, PhCH), 6.77–6.82 (m, 4H, ArH), 6.94 (s, 1H, ArH), 7.20–7.28 (m, 2H, ArH), 7.75 (s, 1H, NH), 9.23 (s, 1H, NH);  $^{13}\text{C}$  NMR (75 MHz, DMSO- $d_6$ ):  $\delta$  17.88, 19.87, 28.48, 30.00, 50.74, 53.39, 65.51, 67.20, 100.00, 111.40, 112.57, 114.32, 114.47, 118.69, 129.23, 129.70, 130.68, 133.32, 147.06, 148.38, 152.30, 155.52, 159.19, 165.61; IR (KBr):  $\nu_{\text{max}}$  3400, 3250, 3083, 1697, 1618, 1472, 1230, 1169, 750  $\text{cm}^{-1}$ ; HRMS:  $m/z$  ( $M + H$ ) $^+$  calculated for  $\text{C}_{24}\text{H}_{27}\text{ClN}_2\text{O}_5$ : 459.1687, found: 459.1708.

### 3. Results and Discussion

To perform the efficient synthesis of DHPMs, our initial effort was focused on finding the optimized reaction conditions. Thus, the three-component reaction of urea, methyl acetoacetate and benzaldehyde in the presence of CSSNH was selected as the sample reaction to afford methyl 6-methyl-2-oxo-4-phenyl-1,2,3,4-tetrahydropyrimidine-5-carboxylate (**4a**). Then, the effects of diverse parameters like type of solvent and temperature were studied on the reaction progress (Table 1). Performing the reaction in the absence of solvent is one of the significant aspects of green chemistry. In this regard, the synthesis of DHPM **4a** was studied under solvent-free condition. As shown in Table 1, when the reaction was carried out at room temperature, only 57% of **4a** was obtained after prolonging the reaction time up to 12 h (entry 1). Regarding to imperative role of the temperature on the reaction progress, we examined the solvent-free synthesis of **4a** at different temperatures (Table 1, entries 1–7). Remarkably, raising the reaction tem-

**Table 1.** The effect of solvents and temperature for synthesis of **4a**.<sup>a</sup>



Entry	Solvent	Temperature ( $^{\circ}\text{C}$ )	Time (h)	Yield <sup>b</sup> (%)
1	solvent-free	r.t.	12	57
2	solvent-free	70	7	83
3	solvent-free	80	4.5	86
4	solvent-free	90	3	91
5	solvent-free	100	2	96
6	solvent-free	110	2	96
7	solvent-free	120	2	94
8	MeCN	reflux	8	50
9	DMF	100	8	45
10	toluene	reflux	10	36
11	$\text{H}_2\text{O}$	reflux	5	82
12	PEG 400	100	5	84
13	EtOH	reflux	5	87

<sup>a</sup> Reaction condition: benzaldehyde (5 mmol), methyl acetoacetate (5 mmol), urea (6 mmol), CSSNH (0.04 g). <sup>b</sup> Isolated yield.

perature resulted in higher yields of **4a** in shorter reaction times. The best result was gained when the synthesis of **4a** was achieved at 100 °C (entry 5). Practically, further increment of the reaction temperature up to 120 °C afforded no more considerable improvement in reaction efficacy (entries 6, 7). To demonstrate the efficiency of CSSNH under solvent-free condition, the synthesis of **4a** was also achieved using different solvents (Table 1, entries 8–13). Using MeCN, DMF, and toluene as the solvent affords low to moderate yields of **4a** (entries 8–10). As the results in Table 1 indicate, H<sub>2</sub>O, PEG 400, and EtOH led to the synthesis of **4a** in 82–87% yields in longer reaction times (entries 11–13). These results confirm the remarkable efficiency of CSSNH for green and solvent-free synthesis of DHPMs.

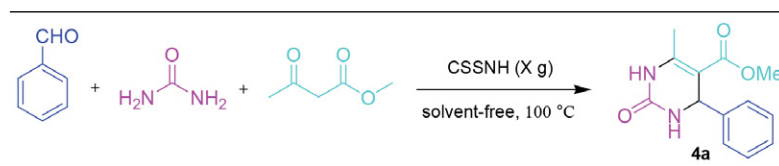
The catalyst has undeniable role for progress of 3CR synthesis of DHPMs. Accordingly, the effect of different loaded amounts of CSSNH was evaluated on the progress of the sample reaction (Table 2). As shown in Table 2, in the absence of CSSNH, only 15% of **4a** was produced even after prolonging the reaction time up to 24 h (Table 2, entry 1). However, increasing the amount of CSSNH considerably affects the reaction progress (entries 2 and 3). The desired DHPM **4a** was efficiently obtained when the reac-

tion was carried out using 0.04 g of the catalyst (entry 4). No distinguishable improvement was observed when the amount of CSSNH was enhanced from 0.04 g up to 0.06 g (entries 5 and 6). Hence, 0.04 g of the catalyst was successfully used for synthesis of various DHPMs using CSSNH.

To realize the efficiency and limitations of the present protocol, we compared our obtained data with some previously reported results for synthesis of DHPM **4a** (Table 3). As the results in Table 3 demonstrate, the reactions were performed in the presence or absence of solvent at different temperatures. In most methods, the lower yields of **4a** were obtained except entry 7 which uses acidic catalyst in refluxing EtOH. In general, the present method proved to be a smart choice for synthesis of DHPM derivatives. The activity of SSA, and chitosan alone was also compared with that of CSSNH using optimized reaction conditions (Table 3, entries 8–10). Practically neither parental SSA nor chitosan are as efficient as CSSNH for solvent-free 3CR synthesis of DHPMs.

After optimizing the reaction conditions, we explored the versatility and generality of the present method for synthesis of structurally diverse 3,4-dihydropyrimidine-2(1*H*)-one/thione derivatives. Accordingly, 3CRs be-

Table 2. The effect of catalyst amount for synthesis of **4a**.<sup>a</sup>



Entry	CSSNH (X g)	Time (h)	Yield <sup>b</sup> (%)
1	-	24	15
2	0.02	7	61
3	0.03	4	83
4	0.04	2	96
5	0.05	2	96
6	0.06	1.8	93

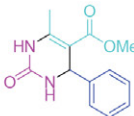
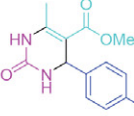
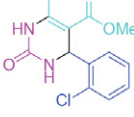
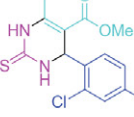
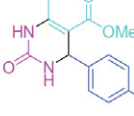
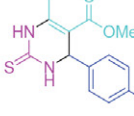
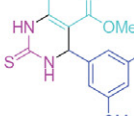
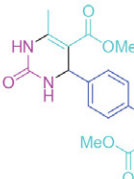
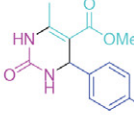
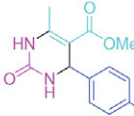
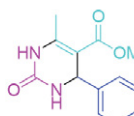
<sup>a</sup> Reaction conditions: benzaldehyde (5 mmol), methyl acetoacetate (5 mmol), urea (6 mmol), CSSNH (X g). <sup>b</sup> Isolated yield.

Table 3. Synthesis of **4a** under various conditions.

Entry <sup>Ref.</sup>	Catalyst and conditions	Time (min)	Yield <sup>a</sup> (%)
1 <sup>33</sup>	GO-Chitosan, solvent-free, 110 °C	10	86
2 <sup>47</sup>	[Btto][ <i>p</i> -TSA], solvent-free, 90 °C	30	89
3 <sup>24</sup>	Dendrimer-PWA <sup>n</sup> , solvent-free, 80 °C	40	91
4 <sup>24</sup>	Dendrimer-PWA <sup>n</sup> , EtOH, 50 °C, ultrasound irradiation	10	90
5 <sup>48</sup>	Isopolyoxomolybdate, solvent-free, 110 °C	19	92
6 <sup>13</sup>	[TEAPS]H <sub>2</sub> PMo <sub>12</sub> O <sub>40</sub> , solvent-free, 105 °C	15	91
7 <sup>26</sup>	SSA, EtOH, reflux	360	96
8 <sup>-</sup>	SSA, solvent-free, 100 °C	120	83
9 <sup>-</sup>	Chitosan, solvent-free, 100 °C	120	79
10 <sup>This work</sup>	CSSNH, solvent-free, 100 °C	120	96

<sup>a</sup> Isolated yield.

Table 4. Synthesis of 4a–s using CSSNH.<sup>a</sup> Continued on next page

Entry <sup>Ref.</sup>	Product <sup>b</sup>	Product Number	Time (h)	Yield <sup>c</sup> (%)
1 <sup>26</sup>		4a	2	96
2 <sup>49</sup>		4b	2	94
3 <sup>49</sup>		4c	2.5	88
4		4d	2.5	86
5 <sup>49</sup>		4e	2	93
6 <sup>18</sup>		4f	2	91
7		4g	2	89
8		4h	2.5	87
9		4i	2	92
10		4j	2	90
11		4k	2.5	91

## Continued

Entry <sup>Ref.</sup>	Product <sup>b</sup>	Product Number	Time (h)	Yield <sup>c</sup> (%)
12		4l	2.5	89
13		4m	2.5	85
14		4n	2.5	94
15		4o	2.5	92
16		4p	2.5	91
17		4q	2.5	87
18		4r	2.5	89
19		4s	2.5	87

<sup>a</sup> Reaction condition: benzaldehyde (5 mmol), methyl acetoacetate (5 mmol), urea (6 mmol), CSSNH (0.04 g), 100 °C. <sup>b</sup> All products were characterized by different techniques. <sup>c</sup> Isolated yield. <sup>d</sup> Two equivalents of urea and methyl acetoacetate were used.

tween (thio)urea, methyl acetoacetate and different aldehydes were carried out in the presence of CSSNH under the solvent-free condition at 100 °C to produce the desired products **4a–s** in good to excellent yields and also in short reaction times (Table 4).

Obviously, CSSNH proved to be a suitable, green, and heterogeneous nano catalyst that effectively catalyzes the synthesis of dihydropyrimidine derivatives **4**. As shown in Table 4, current protocol also works well with different functional groups present in the structure of al-

dehydes. In addition, the sterically hindered *ortho*-substituted aldehydes were successfully converted to the corresponding dihydropyrimidine derivatives in short reaction times and with satisfactory yields (Table 4, entries 3, 4, and 13). The reaction of terephthalaldehyde with 2 equivalents of urea and methyl acetoacetate afforded the desired product **4h** in 87% yield (Table 4, entry 8). In addition to commercially available aldehydes, several synthetic aldehydes were also employed to synthesize functionalized DHPMs as potential chemotherapeutic agents. These aldehydes



were pre-synthesized via  $S_N2$ -type reaction of the appropriate hydroxybenzaldehydes with proper alkyl halides. The biological activities of the synthesized compounds are currently under investigation and will be reported in due course.

The recyclability and reusability of the catalyst is another important feature of a green and environmentally friendly method for organic transformations. Thus, the reusability of CSSNH was investigated by its application in five consecutive reactions of model substrates under optimized conditions. To this end, after achieving the first run of **4a** synthesis, CSSNH was separated from the reaction mixture using a sintered glass funnel, washed continuously with EtOH ( $2 \times 5$  mL), and dried in a vacuum oven at 50 °C for 2 h. The recycled and recovered catalyst was then applied for the next run while no fresh CSSNH was added to the reaction flask. The result of this study is presented in Figure 3.

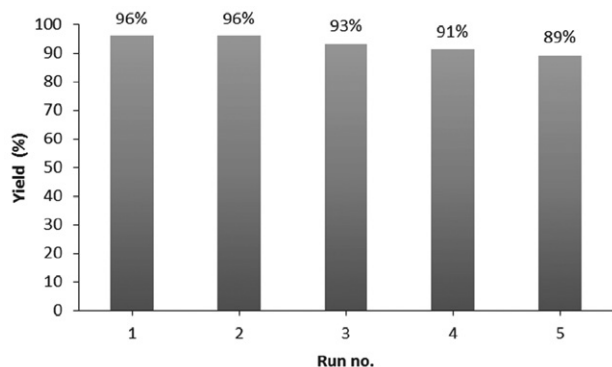


Figure 3. The reusability of CSSNH for synthesis of **4a**.

Practically, the ease of recovery and stability of CSSNH enable its adequate reusability potential. Thus,

CSSNH effectively catalyzes at least five sequential reaction runs while no substantial decline of its catalytic was observed. Moreover, the IR spectrum of reused catalyst after five successive reaction runs is very similar to that of the fresh CSSNH (Figure 4). Apparently, the functionality and nature of CSSNH remain intact which in turn proves the stability of this sustainable and eco-friendly catalyst.

Eventually after elucidating the optimized condition, we were interested to investigate the applicability of this green protocol on a large scale. Consequently, the 3CR of model substrates was conducted on a 70 mmol scale under the optimized conditions which furnished the corresponding DHPM **4a** in 90% yield.

A plausible mechanism for synthesis of DHPMs using CSSNH as catalyst is outlined in Scheme 2. Hence, the treatment of CSSNH with aldehyde **1** affords the activated intermediate **I** which undergoes the nucleophilic addition of (thio)urea to form intermediate **II**, followed by dehydration and formation of the acyl imine intermediate **III**.<sup>50</sup> Simultaneously, activation of  $\beta$ -ketoester **3** using CSSNH affords the enol tautomer **3'** as the nucleophilic species to attack the acyl imine intermediate **III** which results in the ureide intermediate **IV**. Subsequent intramolecular cyclization of intermediate **IV** followed by dehydration of intermediate **V** in the presence of CSSNH affords the corresponding DHPM **4**. It is worth mentioning that, beside the presence of numerous active ammonium residues in the structure of catalyst, there are plenty of other distributed functional groups such as amine and hydroxyl on the surface of CSSNH that can activate the substrates and intermediates through the hydrogen bonding interactions. This unique property makes CSSNH as a good candidate for achieving various organic reactions in the presence of a green and efficient heterogeneous nano catalyst.

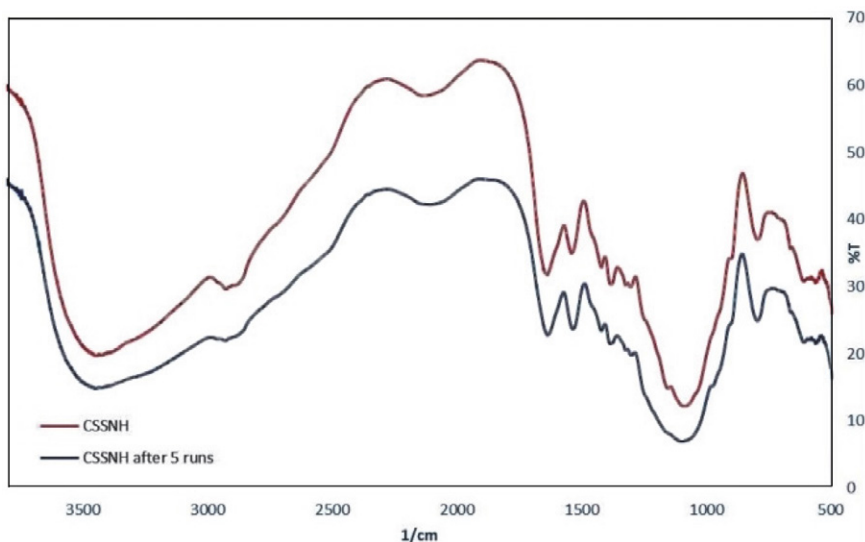
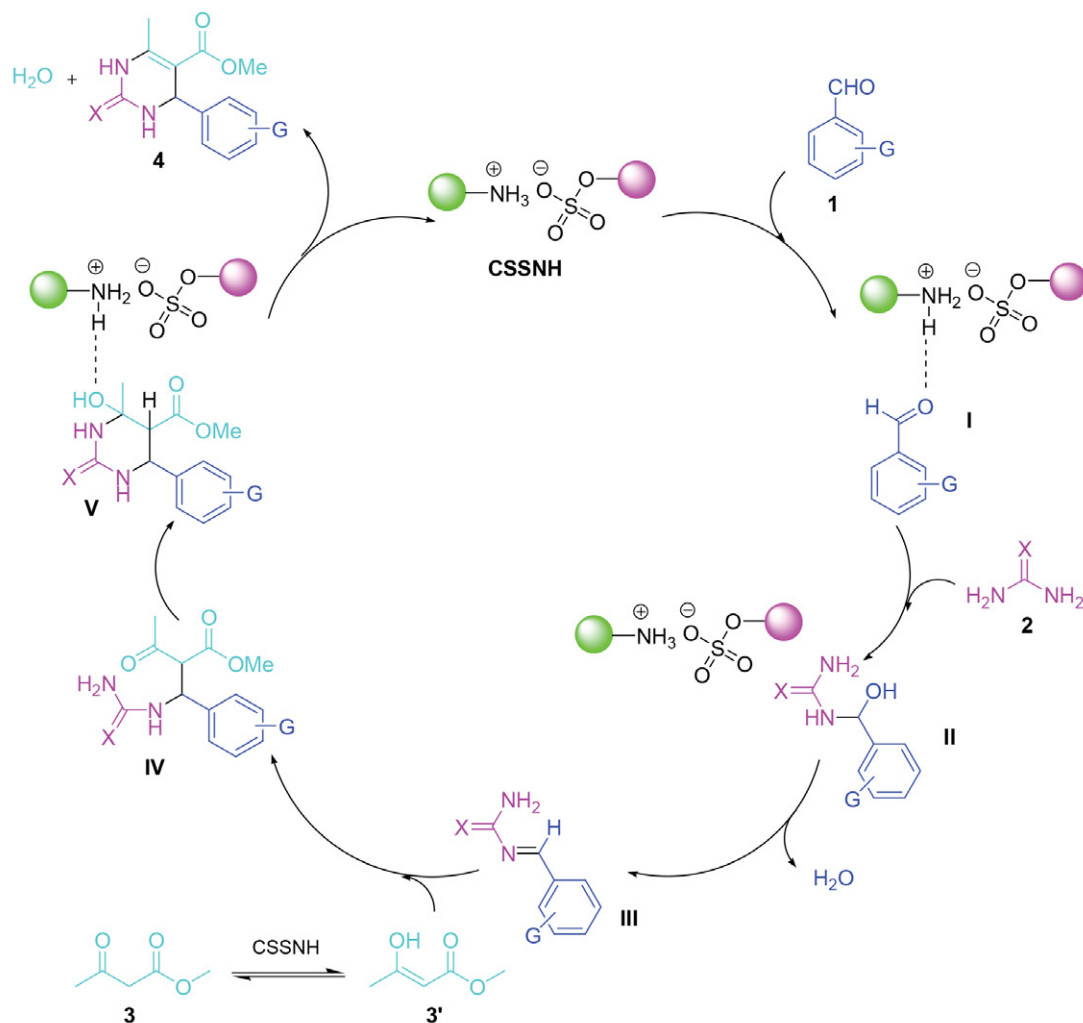


Figure 4. FTIR spectra of fresh CSSNH and recycled CSSNH after five consecutive runs.



Scheme 2. A plausible mechanism for synthesis of DHPMs using CSSNH.

## 4. Conclusion

In summary, we have described a green and facile protocol based on Biginelli reaction for synthesis of 3,4-dihydropyrimidine-2(1*H*)-one/thione derivatives. In this protocol, three-component reaction of commercial and synthetic aldehydes with (thio)urea and methyl acetoacetate under the solvent-free condition in the presence of CSSNH affords the corresponding dihydropyrimidine derivatives in good to excellent yields. The use of a green and heterogeneous nano catalyst, simple operation, cheapness, feasibility on large scale synthesis, elimination of organic solvents and avoidance of strong acidic conditions as well as no need to use toxic transition metals make this method attractive to develop structurally divers DHPMs which are important building blocks in medicinal chemistry and industry.

## Acknowledgements

The authors are grateful to Shiraz University of Technology Research Councils for partial support of this work.

## 5. References

1. K. Tanaka, F. Toda, *Chem. Rev.* **2000**, *100*, 1025–1074. DOI:10.1021/cr940089p
2. M. S. Singh, S. Chowdhury, *RSC Advances* **2012**, *2*, 4547–4592. DOI:10.1039/c2ra01056a
3. A. Dömling, W. Wang, K. Wang, *Chem. Rev.* **2012**, *112*, 3083–3135. DOI:10.1021/cr100233r
4. H. Nagarajaiah, A. Mukhopadhyay, J. N. Moorthy, *Tetrahedron Lett.* **2016**, *57*, 5135–5149. DOI:10.1016/j.tetlet.2016.09.047
5. B. Mohammadi, F. K. Behbahani, *Mol. Divers.* **2018**, *22*, 405–446. DOI:10.1007/s11030-017-9806-z
6. A. de Fátima, T.C. Braga, L. da S. Neto, B. S. Terra, B. G. F. Oliveira, D. L. da Silva, L. V. Modolo, *J. Adv. Res.* **2015**, *6*, 363–373. DOI:10.1016/j.jare.2014.10.006
7. M. A. Arnold, K. A. Day, S. G. Duron, D. Y. Gin, *J. Am. Chem. Soc.* **2006**, *128*, 13255–13260. DOI:10.1021/ja063860+
8. Z. D. Aron, L. E. Overman, *J. Am. Chem. Soc.* **2005**, *127*, 3380–3390. DOI:10.1021/ja042875+
9. P. Biginelli, *Gazz. Chim. Ital.* **1893**, *23*, 360–413.

10. B. F. Mirjalili, A. Bamoniri, A. Akbari, *J. Iran Chem. Soc.* **2011**, *8*, S135–S140. DOI:10.1007/BF03254290
11. A. Mobinikhaledi, N. Foroughifar, A. Khajeh-Amiri, *React. Kinet. Mech. Cat.*, **2016**, *117*, 59–75. DOI:10.1007/s11144-015-0931-3
12. A. Farhadi, J. Noei, R. Haji Aliyari, M. Albakhtiyari, M. A. Takassi, *Res. Chem. Intermed.* **2016**, *42*, 1401–1406. DOI:10.1007/s11164-015-2092-4
13. H. Peng, Y. Hu, R. Xing, D. Fang, *Monatsh. Chem.* **2015**, *146*, 2053–2058. DOI:10.1007/s00706-015-1505-9
14. V. Ramachandran, K. Arumugasamy, S. K. Singh, N. Edayadulla, P. Ramesh, S. K. Kamaraj, *J. Chem. Biol.* **2016**, *9*, 31–40. DOI:10.1007/s12154-015-0142-4
15. N. Ahmed, Z. N. Siddiqui, *J. Mol. Catal. A Chem.* **2014**, *387*, 45–56. DOI:10.1016/j.molcata.2014.02.019
16. M. Oliverio, P. Costanzo, M. Nardi, I. Rivalta, A. Procopio, *ACS Sustainable Chem. Eng.* **2014**, *2*, 1228–1233. DOI:10.1021/sc5000682
17. J. Safaei Ghomi, R. Teymuri, A. Ziarati, *Monatsh. Chem.* **2013**, *144*, 1865–1870. DOI:10.1007/s00706-013-1068-6
18. S. P. Bahekar, P. B. Sarode, M. P. Wadekar, H. S. Chandak, *J. Saudi Chem. Soc.* **2017**, *21*, 415–419. DOI:10.1016/j.jscs.2015.09.004
19. J. Ma, L. Zhong, X. Peng, R. Sun, *Green Chem.* **2016**, *18*, 1738–1750. DOI:10.1039/C5GC01727K
20. J. T. Starcevic, T. J. Laughlin, R. S. Mohan, *Tetrahedron Lett.* **2013**, *54*, 983–985. DOI:10.1016/j.tetlet.2012.12.032
21. Ş. Gülten, *J. Heterocyclic Chem.* **2017**, *54*, 1252–1260. DOI:10.1002/jhet.2700
22. A. Khorshidi, K. Tabatabaeian, H. Azizi, M. Aghaei-Hashjin, E. Abbaspour-Gilandeh, *RSC Adv.* **2017**, *7*, 17732–17740. DOI:10.1039/C7RA00794A
23. J. Safaei-Ghomi, M. Tavazo, G. H. Mahdavinia, *Ultrason. Sonochem.* **2018**, *40*, 230–237. DOI:10.1016/j.ultsonch.2017.07.015
24. Y. Qiu, H. Sun, Z. Ma, W. Xia, *J. Mol. Catal. A Chem.* **2014**, *392*, 76–82. DOI:10.1016/j.molcata.2014.04.031
25. R. Javad-Kalbasi, A. R. Massah, B. Daneshvarnejad, *Appl. Clay Sci.* **2012**, *55*, 1–9. DOI:10.1016/j.clay.2011.05.015
26. P. Salehi, M. Dabiri, M. A. Zolfigol, M. A. Bodaghi Fard, *Tetrahedron Lett.* **2003**, *44*, 2889–2891. DOI:10.1016/S0040-4039(03)00436-2
27. M. Maheswara, S. H. Oh, K. T. Kim, J. Y. Do, *Bull. Korean Chem. Soc.* **2008**, *29*, 1752–1754.
28. F. Belferdi, F. Bouremmad, S. Shawuti, M. A. Gulgun, *Acta Chim. Slov.* **2021**, *in press*, <http://dx.doi.org/10.17344/acsi.2020.6300>
29. R. H. Vekariya, H. D. Patel, *Arkivoc* **2015**, *1*, 136–159. DOI:10.3998/ark.5550190.p008.975
30. A. Rajack, K. Yuvaraju, Ch. Praveen, Y. L. N. Murthy, *J. Mol. Catal. A Chem.* **2013**, *370*, 197–204. DOI:10.1016/j.molcata.2013.01.003
31. R. Rezaei, S. Malek, M. R. Sheikhi, M. K. Mohammadi, *Chem. J. Moldova* **2013**, *8*, 101–106. DOI:10.19261/cjm.2013.08(2).13
32. J. Lal, S.K. Gupta, D. D. Agarwal, *Catal. Commun.* **2012**, *27*, 38–43. DOI:10.1016/j.catcom.2012.06.017
33. A. Maleki, R. Paydar, *React. Funct. Polym.* **2016**, *109*, 120–124. DOI:10.1016/j.reactfunctpolym.2016.10.013
34. F. Quignard, A. Choplin, A. Domard, *Langmuir* **2000**, *16*, 9106–9108. DOI:10.1021/la000937d
35. H. Honarkar, M. Barikani, *Monatsh. Chem.* **2009**, *140*, 1403–1420. DOI:10.1007/s00706-009-0197-4
36. O. Arjmand, M. Ardjmand, A. M. Amani, M. H. Eikani, *Acta Chim. Slov.* **2020**, *67*, 496–506. DOI:10.17344/acsi.2019.5513
37. G. Kravanja, M. Globočnik, M. Primožič, Ž. Knez, M. Leitgeb, *Acta Chim. Slov.* **2019**, *66*, 337–343. DOI:10.17344/acsi.2018.4822
38. Ozyilmaz, A. T. Ozyilmaz, E. I. Bayram, R. H. Akyüreköglü, *Acta Chim. Slov.* **2019**, *66*, 950–957. DOI:10.17344/acsi.2019.5171
39. S. Behrouz, M. N. Soltani Rad, M. A. Piltan, M. M. Doroodmand, *Helv. Chim. Acta* **2017**, *100*, e1700144. DOI:10.1002/hlca.201700144
40. S. Behrouz, M. N. Soltani Rad, M. A. Piltan, *Ultrason. Sonochem.* **2018**, *40*, 517–526. DOI:10.1016/j.ultsonch.2017.07.046
41. S. Behrouz, M. N. Soltani Rad, M. A. Piltan, *Chem. Pap.* **2020**, *74*, 113–124. DOI:10.1007/s11696-019-00863-1
42. S. Behrouz, M. N. Soltani Rad, M. Abdollahzadeh, M. A. Piltan, *ChemistrySelect* **2020**, *5*, 7467–7473. DOI:10.1002/slct.202001722
43. S. Behrouz, *J. Saudi Chem. Soc.* **2018**, *22*, 261–268. DOI:10.1016/j.jscs.2016.07.003
44. S. Behrouz, *J. Heterocyclic Chem.* **2017**, *54*, 1863–1871. DOI:10.1002/jhet.2777
45. S. Behrouz, *J. Saudi Chem. Soc.* **2017**, *21*, 220–228. DOI:10.1016/j.jscs.2016.08.003
46. S. Behrouz, *J. Chem. Res.* **2016**, *40*, 540–544. DOI:10.3184/174751916X14709292404728
47. Y. Zhang, B. Wang, X. Zhang, J. Huang, C. Liu, *Molecules* **2015**, *20*, 3811–3820. DOI:10.3390/molecules20033811
48. A. Nakhaei, A. Davoodnia, S. Yadegarian, *Russ. J. Gen. Chem.* **2016**, *86*, 2870–2876. DOI:10.1134/S1070363216120537
49. M. G. Dekamin, F. Mehdipoor, A. Yaghoubi, *New J. Chem.* **2017**, *41*, 6893–6901. DOI:10.1039/C7NJ00632B
50. C. O. Kappe, *J. Org. Chem.* **1997**, *62*, 7201–7204.

## Povzetek

V prispevku opisujemo zelen in visoko učinkovit pristop k sintezi 3,4-dihidropirimidin-2(1*H*)-onskih oz. -tionskih derivatov. Naša strategija vključuje trokomponentno Biginellijevo reakcijo med (tio)sečnino, metil acetoacetatom in aldehidi pod pogoji brez prisotnosti topil ob dodatku hitosan-silikatno sulfatnega nano hibrida (CSSNH) kot zelenega, heterogenega nano katalizatorja. Optimizirani pogoji omogočajo tvorbo ustreznih produktov v kratkih reakcijskih časih z dobrimi do odličnimi izkoristki. CSSNH je cenen, okolju prijazen in nestrupen nano katalizator, ki ga lahko enostavno pripravimo in z njim rokujemo, možna pa je tudi ponovna uporaba brez bistvene izgube aktivnosti.



Except when otherwise noted, articles in this journal are published under the terms and conditions of the Creative Commons Attribution 4.0 International License

Scientific paper

# Catalysis, Kinetic and Mechanistical Studies for the Transformation of Ethylene Glycol by Alumina and Silica Gel under Autogenous Pressure and Solvent-free Conditions

Taoufik Rohand<sup>1,\*</sup> and Kiyoshi Tanemura<sup>2</sup>

<sup>1</sup> Laboratory of Analytical and Molecular Chemistry, Faculty Polydisciplinaire of Safi, Route Sidi Bouzid BP 4162, 46000 Safi, University Cadi Ayyad Marrakech, Morocco

<sup>2</sup> Chemical Laboratory, School of Life Dentistry at Niigata, Nippon Dental University, Hamaura-cho, Niigata 951-8580, Japan

\* Corresponding author: E-mail: Taoufik.Rohand@uca.ac.ma

Received: 09-26-2020

## Abstract

A kinetic and mechanistical studies of the new pathway for competitive transformation of ethylene glycol by alumina and silica gel have been described. Commercial alumina (Al com), synthetic alumina (Al syn), commercial silica gel (Si com) and synthetic silica gel (Si syn) were used for the transformation of ethylene glycol to a mixture of diethylene glycol, 1,4-dioxane and 2-methyl-1,3-dioxolane *via* acetaldehyde by heating at 150 °C under autogenous pressure without solvent. The results show that the yield of these three products strongly depends on the nature of the used catalyst and the reaction time.

**Keywords:** Dioxolanes; ethylene glycol; dimerization; acetalization; environmental effects; kinetic studies

## 1. Introduction

In recent years, the use of silica gel as a catalyst in environmentally friendly conditions became an interesting topic for investigations in organic chemistry reactions. In the same way, the use of pollutant and harmful organic solvents has been replaced by solvent-free reactions which became very advantageous alternatives.<sup>1–3</sup> However, protic acids are well-known to suffer from a number of shortcomings, including their corrosive and noxious nature.<sup>4,5</sup> The recent move towards green chemistry has seen silica gel and alumina gradually replacing mineral acids in the synthesis of organic compounds. Indeed, these non-polluting heterogeneous catalysts possess numerous advantages such as ready availability, efficient recycling, low cost and ease of separation from crude reaction mixtures by simple filtration.<sup>6–8</sup> For example, the condensation of epoxystyrene with benzylmethylamine, the cyclization of enones, the vinylogous Michael double additions, the transformation of 1-amino-2-ke-toesters and of 4-amino-3,4-dihydro-2H-1,4-thiazines have all been carried out in the presence of silica gel.<sup>9–11</sup> Alumina also catalyses the oxidation of alcohols to ketones by trichlo-

roacetic acid, the dehydration of alcohols to alkenes, the synthesis of isoxazolines and of 1,2-aminoalcohols.<sup>12–17</sup> Ethylene glycol is frequently used in organic synthesis to protect aldehydes and ketones, enabling other functional groups in the molecule to undergo chemoselective transformations. These acetalization and ketalization reactions are typically carried out in ecologically harmful organic solvent, in the presence of noxious protic acids at various temperatures, and typically, at atmospheric pressure.<sup>18–20</sup>

In this work, we have continued our investigation on the use of silica gel in chemical reactions,<sup>12–14</sup> so we have been led to advance a new method of the synthesis of 2-methyl-1,3-dioxolane (5) by the conversion of ethylene glycol on solid catalysts such as silica gel and alumina while meeting the requirements of green chemistry.

## 2. Experimental

### 2.1. General

NMR spectra were recorded on a Bruker AC spectrometer (<sup>1</sup>H at 300 MHz and <sup>13</sup>C at 75 MHz) in CDCl<sub>3</sub>

solution. The chemical shift ( $\delta$ ) of the signals described is expressed in ppm relative to TMS taken as the internal reference. The following abbreviations are used: s: singlet, d: doublet, t: triplet, m: multiplet, l: large. The coupling constants ( $J$ ) are expressed in Hz. The reagents were from Aldrich. The silica gel was commercial type Merck 60 (70–230 mesh) and alumina was an Aldrich commercial product. In all experiments, ethylene glycol (1) present in the crude reaction product was removed by adding water to the crude reaction mixture. After the treatment, the mixture of carbonyl compounds 4 and 2-methyl-1,3-dioxolane (5) was recovered. The yields of products 5 were estimated from the  $^1\text{H}$  and  $^{13}\text{C}$  NMR spectra of the crude reaction mixtures using an internal reference in order to avoid their decomposition during chromatographic purification, as reported in the other work.<sup>21</sup> Compounds 2, 3 and 5 were identified by comparing their  $^1\text{H}$  and  $^{13}\text{C}$  NMR spectra with authentic samples marketed by Aldrich. We used the following abbreviations in the text: Si syn: synthetic silica gel, Si com: commercially available silica gel, Al syn: synthetic alumina, Al com: commercially available alumina.

## 2. 2. Synthesis of 2-Methyl-1,3-dioxolane (5) Using Sulfuric Acid

**Procedure at atmospheric pressure.** Ethylene glycol (1) (7.67 g, 124 mmol) and  $\text{H}_2\text{SO}_4$  (4% by mass) were placed in a flask (50 mL) equipped with a reflux condenser and then heated at 196 °C for 3 h. After cooling, 20 mL of water was added to the crude mixture to remove residual ethylene glycol. The aqueous solution was extracted with diethyl ether (3 × 50 mL). The organic phases were combined and then dried over  $\text{MgSO}_4$ . After filtration and evaporation of the ether *in vacuo*, the mixture of 2 and 3 was recovered. The yields of products 2 and 3 are displayed in Table 1.

**Procedure under pressure.** Ethylene glycol (1) (7.67 g, 124 mmol) and  $\text{H}_2\text{SO}_4$  (4% by mass) were placed in an autoclave (100 mL). The sealed reactor was heated at 150 °C for 3 h or for 24 h. After cooling, the residue was treated in the same manner as described above. The yields of products 2 and 3 are listed in Table 1.

## 2. 3. Synthesis of 1,3-Dioxolanes by Silica Gel

**Procedure at atmospheric pressure.** Ethylene glycol (1) (7.67 g, 124 mmol) and 0.1 g of silica gel were placed in a flask (50 mL) equipped with a reflux condenser and the whole was heated at 196 °C for 120 h. After cooling and separating the silica gel by filtration, the residue was treated in the same manner as described above. Diethylene glycol (2) was obtained in a yield of 1% (Table 1).

**Procedure under pressure.** Ethylene glycol (1) (7.67 g, 124 mmol) and 0.1 g of silica gel were placed in an autoclave (100 mL). The sealed reactor was heated to 150 °C for various amounts of time. After cooling and separating the

silica gel by filtration, the residue was treated in the same manner as described above. The yields of products 2 and 5 are listed in Table 1.

## 2. 4. Reaction Under Atmospheric Pressure

In a ground-glass flask equipped with a refrigerator and a magnetic stirrer, ethylene glycol (1) (6.9 mL, 7.68 g, 0.124 mmol) was introduced to which 0.307 g (1.3% by mass) of concentrated sulfuric acid was added. The mixture was heated under reflux for 1 h and 3 h and under atmospheric pressure. After cooling to room temperature, 20 mL of water was added to the reaction crude to remove ethylene glycol (1). The aqueous phase was extracted by diethyl ether (3 × 20 mL) and then the organic phase was dried over  $\text{MgSO}_4$ . After filtration and evaporation of the solvent under vacuum, the mixture of diethylene glycol (2) and 1,4-dioxane (3) was recovered.

## 2. 5. Autogenous Pressure Reaction

Ethylene glycol (1) (6.9 mL, 7.68 g, 0.124 mmol) and concentrated sulfuric acid (0.307 g, 1.3% by weight) were placed in a sealed autoclave and the mixture was heated to 150 °C (oil bath temperature) under autogenous pressure for varying times. After cooling the reactor to room temperature, 20 mL of water was added to the filtrate to remove the remaining ethylene glycol (1) in the reaction mixture. The aqueous phase was extracted by diethyl ether (3 × 20 mL) and then the organic phase was dried over  $\text{MgSO}_4$ . After filtration and evaporation of the solvent under vacuum, the mixture of diethylene glycol (2) and 1,4-dioxane (3) was recovered.

## 2. 6. Preparation of Synthetic Silica

Synthetic silica (Si syn) was obtained by precipitating the silica from a sodium silicate solution of concentration  $[\text{Si}] = 1.667 \text{ mol} \cdot \text{L}^{-1}$  by adding, drop by drop and with agitation, 2M HCl until a pH of 4 was reached. Si syn silica was recovered after successive washing to remove sodium chloride and drying at a temperature of 100 °C for a few hours. Sodium silicate was obtained by alkaline fusion of extra-silica sand, originating from the Safi region in Morocco, with sodium carbonate with a  $\text{SiO}_2/\text{Na}_2\text{O}$  ratio of 1.

## 2. 7. Preparation of Synthetic Silica

The procedure followed is similar to the method described by Noor Abdulateef Ghulam.<sup>22</sup>

## 2. 8. Reaction of Catalysts on Ethylene Glycol (1)

Ethylene glycol (1) (7.68 g, 124 mmol) and the catalyst (0.1 g, 1.3% by weight) were placed in a sealed auto-

clave and heated to 150 °C (oil bath temperature) under autogenous pressure for varying times. After cooling the reactor to room temperature, the catalyst was separated by filtration. 20 mL of water was added to the filtrate to remove the remaining ethylene glycol (1) in the reaction mixture. The aqueous phase was extracted by diethyl ether (3 × 20 mL) and then the organic phase was dried over MgSO<sub>4</sub>. After filtration and evaporation of the solvent under vacuum, a mixture of diethylene glycol (2), 1,4-dioxane (3) and 2-methyl-1,3-dioxolane (5) was recovered.

### 3. Results and Discussion

It is known that distillation of ethylene glycol (1) in the presence of sulfuric acid in small proportions (4% by mass) leads to three products.<sup>23–25</sup> 1,4-Dioxane (3) is the majority product of this reaction while diethylene glycol (2), acetaldehyde (4) and 2-methyl-1,3-dioxolane (5) are obtained in low yields (Scheme 1).

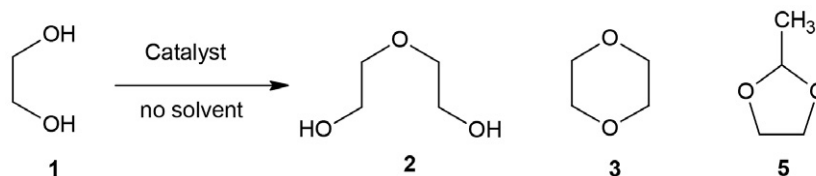
From our part, we have shown in this work that the heating of this same mixture at high temperatures for 2 h and under different pressures and with three different acids, *i.e.* formic acid, acetic acid and sulfuric acid, allows the formation of diethylene glycol (2) as the majority product (Table 1, entries 1, 3 and 5). It is noted that the prolonga-

tion of the duration of the heating of this reaction mixture from 2 h to 2 days considerably increased the yield of dimer 2 while keeping 1,4-dioxane (3) as a minor product of this reaction, whereas acetaldehyde (4) and 2-methyl-1,3-dioxolane (5) were not obtained (Table 1, entries 2, 4 and 6). However, the best results were obtained using sulfuric acid as the catalyst.

These unexpected results then motivated us to generalize this type of conversion by using imported and commercial solid catalysts, such as commercial silica gel (Si com) (Aldrich) and a local catalyst such as inexpensive synthetic Moroccan silica (Si syn) and easy to prepare from sand originating from the sea side of Safi in Morocco,<sup>4</sup> while the alumina is commercial (Al com) (Aldrich) (Table 2), also alumina (Al syn) was synthesised following the standard procedure published by Ghulam.<sup>22</sup> It is interesting to note that these three heterogeneous solid catalysts exhibit Brønsted and Lewis acidic sites at their active surfaces.

The cation exchange capacities (CEC) then make it possible to classify in decreasing order of reactivity with respect to ethylene glycol (1): Si syn > Si com > Al com > Al syn (Si syn: synthetic silica gel, Si com: commercially available silica gel, Al syn: synthetic alumina, Al com: commercially available alumina).

Thus, heating the ethylene glycol (1) in an autoclave at a constant temperature of 150 °C (oil bath temperature)



Scheme 1.

Table 1. Conversion of ethylene glycol (1) in homogenous acid medium.

Entry	Catalyst	T (°C)	Time (h)	1 (%)	2 (%)	3 (%)	4 (%)
1	H <sub>2</sub> SO <sub>4</sub> (4% wt.)	196 <sup>a</sup>	3	95	4	1	–
2	H <sub>2</sub> SO <sub>4</sub> (4% wt.)	150 <sup>b</sup>	3	75	16	9	–
3	H <sub>2</sub> SO <sub>4</sub> (4% wt.)	150 <sup>b</sup>	24	26	65	9	–
4	Silica gel	196	120	99	1	–	–
5	Silica gel	150	3	100	–	–	–
6	Silica gel	150	7	81	–	–	19

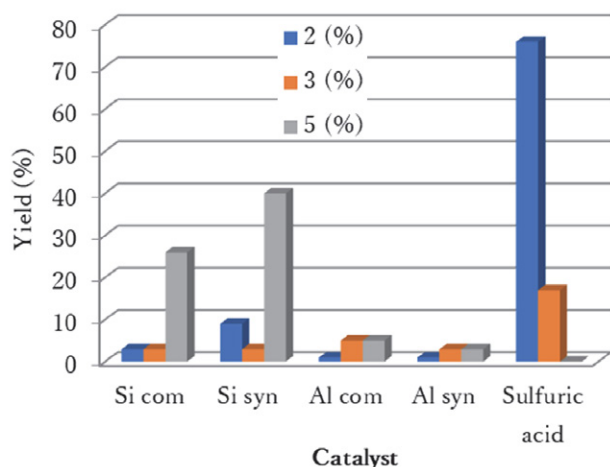
<sup>a</sup> P atm: atmospheric pressure (110 kPa). Reactor: 50 mL flask.

<sup>b</sup> P auto: autogenous pressure (P at 150 °C = 153 kPa).

Entry	Pressure	T (°C)	Catalyst	Time	Global Yield <sup>a</sup> (%)
1	P atm	150	HCOOH	2 h	5
2	P atg	150	HCOOH	2 days	12
3	P atm	150	CH <sub>3</sub> COOH	5 h	9
4	P atg	150	CH <sub>3</sub> COOH	2 days	28
5	P atm	150	H <sub>2</sub> SO <sub>4</sub>	5 h	41
6	P atg	150	H <sub>2</sub> SO <sub>4</sub>	24 h	93

<sup>a</sup> The conversion of the ethylene glycol (1) using each catalyst separately.

for 24 h under autogenous pressure and in the presence of these solid catalysts promotes the formation of the three products; 2-methyl-1,3-dioxolane (5) is the major product of this reaction while diethylene glycol (2) and 1,4-dioxane (3) are obtained in low yields (Table 2). The difference in the results reported in Tables 1 and 2 shows that the conversion of ethylene glycol (1) proceeds in a different way from the homogeneous to the heterogeneous medium. It is interesting to note that sulfuric acid (4% wt.) promotes the selective formation of dimer 2 while silica and alumina catalysts (1.3% wt.) selectively transform ethylene glycol (1) into 2-methyl-1,3-dioxolane (5) (Fig. 1).



**Figure 1.** Evaluation of the yield of products 2, 3 and 5 in the presence of  $\text{H}_2\text{SO}_4$  (4% wt.) and of catalysts based on silica gel and alumina (1.3% wt.).

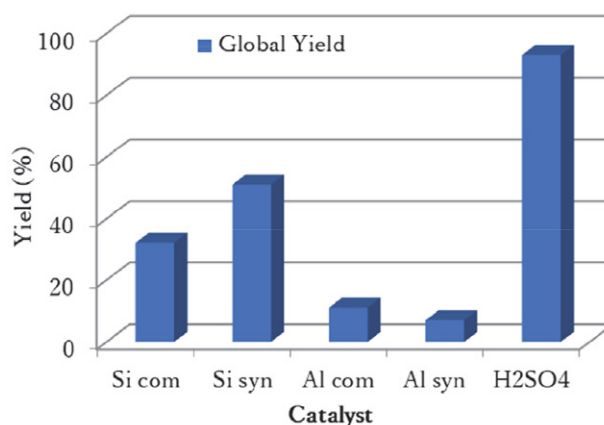
We can then conclude that the homogeneous medium accelerates the dimerization of ethylene glycol (1) to diol 2, which cyclising to 1,4-dioxane (3) while the heterogeneous medium promotes the dehydration of diol 1 to

acetaldehyde (4), which in turn will be trapped by a second molecule of ethylene glycol (1) in excess to lead to 2-methyl-1,3-dioxolane (5) (Scheme 2).

From the results recorded above, we have found that commercial catalysts such as Si com silica gel and Al com alumina are not very active against ethylene glycol (1) (Table 2, entries 1 and 3), while synthetic Si syn silica being the catalyst promotes the formation of 2-methyl-1,3-dioxolane (5) in 40% yield (Table 2, entry 2). In addition, Si syn synthetic silica proved to be the best catalyst in this series with an overall reaction efficiency of 51% (Fig. 2).

### 3. 1. Kinetic Study

In order to better understand the transformation of ethylene glycol (1) in a heterogeneous environment, we conducted a kinetic study by means of catalysts Al com, Si com and Si syn, except Al syn due to the low efficiency at 150 °C under autogenous pressure and for variable times. Analysis of the appearance of the curves shown in Figures



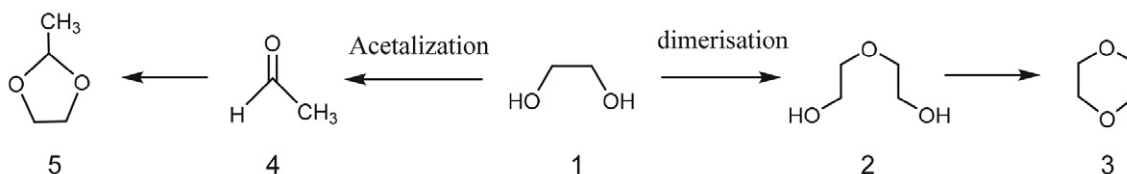
**Figure 2.** Evaluation of the overall yield in the presence of  $\text{H}_2\text{SO}_4$  (4% wt.) and catalysts based on silica gel and alumina (1.3% wt.).

**Table 2.** Transformation of ethylene glycol (1) by silica gel and alumina catalysts<sup>a</sup>

Entry	Catalyst	CEC <sup>b</sup>	Global Yield <sup>c</sup> (%)	2 (%)	3 (%)	4 (%)
1	Si com	16	32	3	3	26
2	Si syn	25	51	9	3	40
3	Al com	10	11	1	5	5
4	Al syn	21	7	1	3	3

<sup>a</sup> Reaction conditions: temperature 150 °C, time 24 h <sup>b</sup> Cationic exchange capacity (meq/100 g).

<sup>c</sup> The conversion of the ethylene glycol (1) using each catalyst separately.



**Scheme 2.**



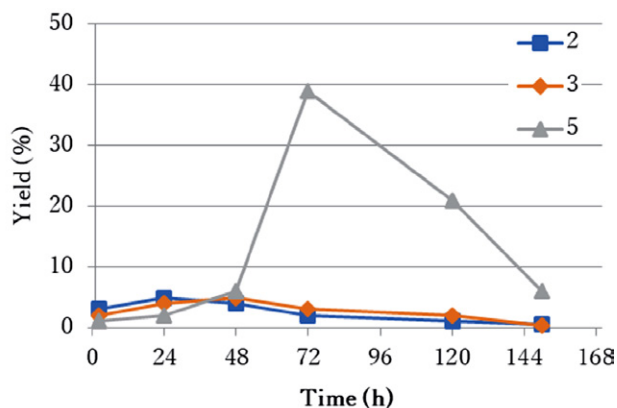


Figure 3. Evaluation of products 2, 3 and 5 formed in the presence of commercial alumina Al com.

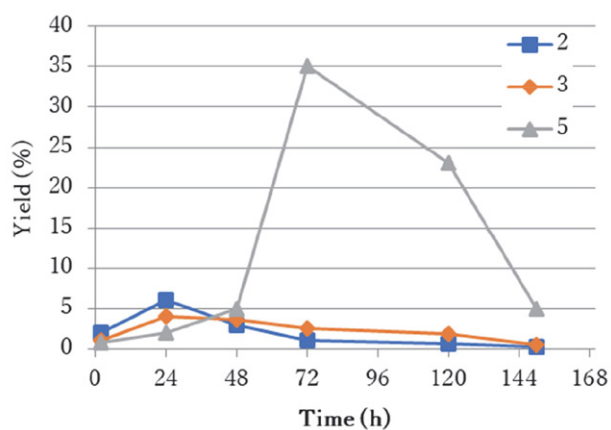


Figure 4. Evaluation of products 2, 3 and 5 formed in the presence of synthetic alumina Al syn.

3–6 indicates that the conversion of ethylene glycol (1) to diethylene glycol (2), 1,4-dioxane (3) and 2-methyl-1,3-dioxolane (5) depends closely on the nature of the used catalyst and the duration of the reaction. The formation of secondary products by the action of these three catalysts is a perceptible result.

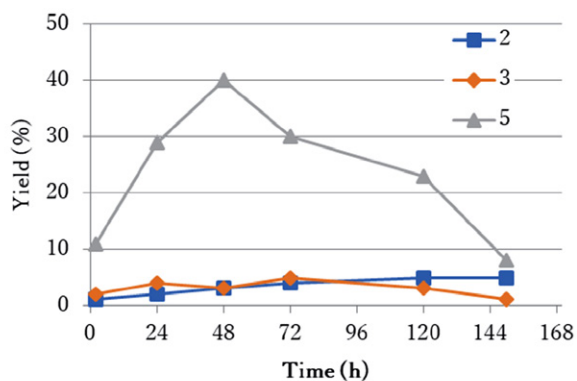


Figure 5. Evaluation of products 2, 3 and 5 formed in the presence of commercial silica Si com.

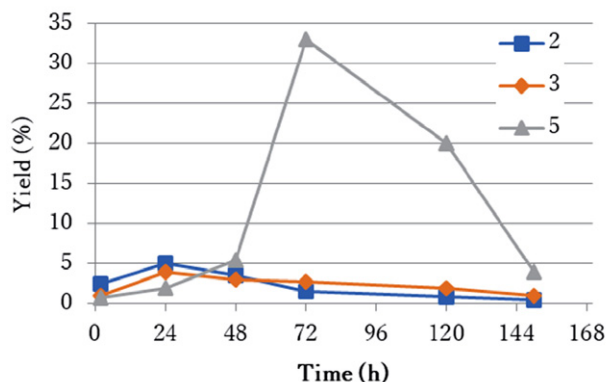


Figure 6. Evaluation of products 2, 3 and 5 formed in the presence of synthetic silica Si syn.

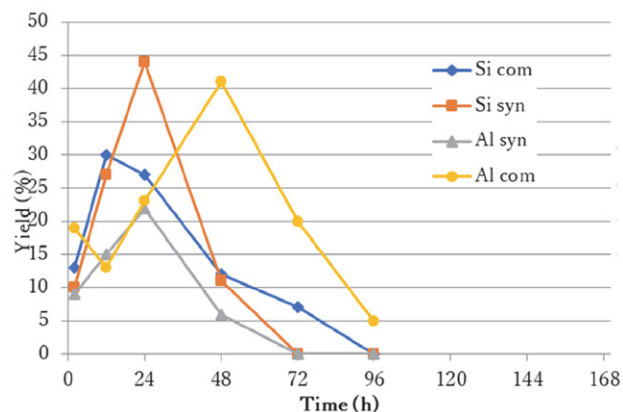


Figure 7. Evaluation of 2-methyl-1,3-dioxolane (5) according to the nature of the catalyst and the reaction time.

Indeed, we have noticed that dimerization products 2 and 3 are obtained in low yields not exceeding 7% regardless of the nature of the used catalyst and the reaction time.

We have also noticed that compound 5 is the main product of these reactions; it is obtained with a yield of 38% in the presence of alumina Al com after 48 h of the reaction, 29% in the presence of silica gel Si com after 24 h of the reaction and 40% when using synthetic silica Si syn after 48 h of the reaction (Fig. 7). The decrease in the yields of 5 is due to a decomposition.

We also found that the overall efficiency of the transformation of ethylene glycol (1) into products 2, 3 and 5 reached a maximum of 34% in the presence of alumina Al com after 72 h of the reaction, 22% in the presence of silica gel Si com after 24 h of the reaction and 44% in the presence of synthetic silica Si syn after 48 h of the reaction (Fig. 8).

It is interesting to note that the speed of the dimerization reaction is less important than that of the acetalization reaction (Figs. 3–6). Synthetic Moroccan silica Si syn therefore represents the promising catalyst because it promotes the yield of dimerization (11%) and acetalization (40%) products after 48 h of reaction (Fig. 6). We can thus conclude that Moroccan synthetic silica Si syn represents

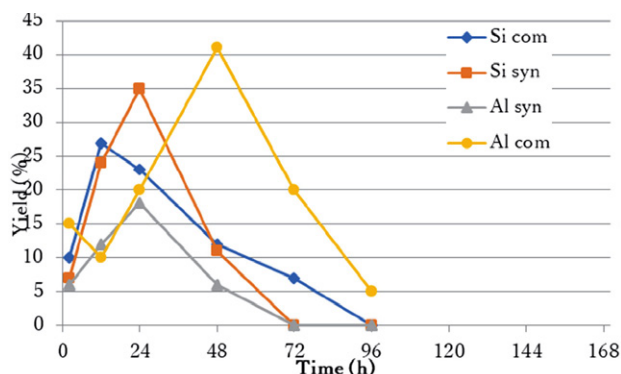


Figure 8. Evaluation of the overall efficiency according to the nature of the catalyst used.

the promising catalyst because it favours the highest yield for a relatively long reaction time.

### 3. 2. Spectroscopic Study

Indeed, we noted that in the case of ethylene glycol (1) and 1,4-dioxane (3), the C1 and C2 carbon atoms have the same atomic charges and the same for the oxygen atoms O1 and O2 (Table 3).

In the cases of diethylene glycol (2), acetaldehyde (4) and 2-methyl-1,3-dioxolane (5) carbon atoms, C1, C2

and C3 do not have the same atomic charge values, identical for oxygen atoms O1 and O2 (Table 3). In addition, the lengths of the C–C, C–O and C–H bonds are closely related to the structure of the molecule under study (Table 3).

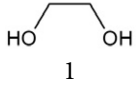
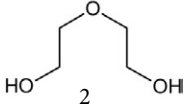
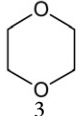
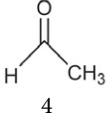
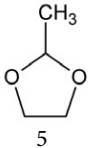
Finally, the nature of the atoms and the structure of the molecules have a significant effect on the dihedral angles of compounds 1–5 (Table 3).

Similarly, during the heating of ethylene glycol (1), two major intermediates were formed *in situ*, 1,4-oxirane (3) and acetaldehyde (4), which evolved differently to lead to products 2–5. The theoretical calculation of the NBO loads of these intermediates shows that the reaction evolves in the directions of formation of 2-methyl-1,3-dioxolane (5) from acetaldehyde (4), since the atomic carbon load of the C=O group of acetaldehyde (4) (0.452) is higher than that of the carbons (–0.080) of oxirane.

The addition of ethylene glycol (1) introduced in excess is then more favoured on the most electrophilic carbon of acetaldehyde (4) despite two oxirane carbons (Scheme 3).

On the other hand, the comparative spectroscopic study of  $^1\text{H}$  NMR (Table 3) and  $^{13}\text{C}$  NMR reveals that the differences in the chemical shifts of  $^1\text{H}$  and  $^{13}\text{C}$  NMR spectra of compounds 1–5 are closely dependent on their electronic effects.

Table 3. Some physical characteristics of ethylene glycol (1) and its derivatives 2–5

Products	Atomic charge	Dihedral angle	Bond length	$^1\text{H}$ NMR
 1	C1 = 0.025 C2 = 0.025 O1 = 0.416 O2 = 0.416	O1C1C2O2 = 179.86	C1-O1 = 1.462 C2-O2 = 1.462 C1-C2 = 1.512 C1-H = 1.091 C2-H = 1.091	CH <sub>2</sub> OH 3.06 ppm CH <sub>2</sub> OH 3.70 ppm
 2	C1 = 0.022 C2 = 0.022 O1 = 0.414 O2 = –0.414	O1C1C2O2 = 0.10	C1-O1 = 1.420 C2-O2 = 1.420 C1-C2 = 1.542 C1,2-H = 1.090	CH <sub>2</sub> OH 3.66 ppm CH <sub>2</sub> O 4.20 ppm
 3	C1 = 0.022 C2 = 0.022 O1 = –0.414 O2 = –0.414	O1C1C2O2 = 0.10	C1-O1 = 1.420 C2-O2 = 1.420 C1-C2 = 1.542 C1-H = 1.090	CH <sub>2</sub> O 3.67 ppm
 4	C1 = –0.676 C2 = 0.452 O1 = –0.533		C1-O1 = 1.203 C2-H = 1.107	CH <sub>3</sub> 2.22 ppm
 5	C1 = 0.023 C2 = 0.024 C3 = 0.450 O1 = –0.375 O2 = –0.425	O1C1C2O2 = –17.95 C3O2C2C1 = 34.16 C3O1C1C2 = –4.91	C1-O1 = 1.430 C2-O2 = 1.422 C1-C2 = 1.538 C3-O1 = 1.413 C3-O2 = 1.423 C1,2,3-H = 1.090;1.092;1.101	CH <sub>2</sub> O 3.83-4.30 ppm CH <sub>3</sub> 1.40 ppm

### 3. 3. Plausible Mechanism

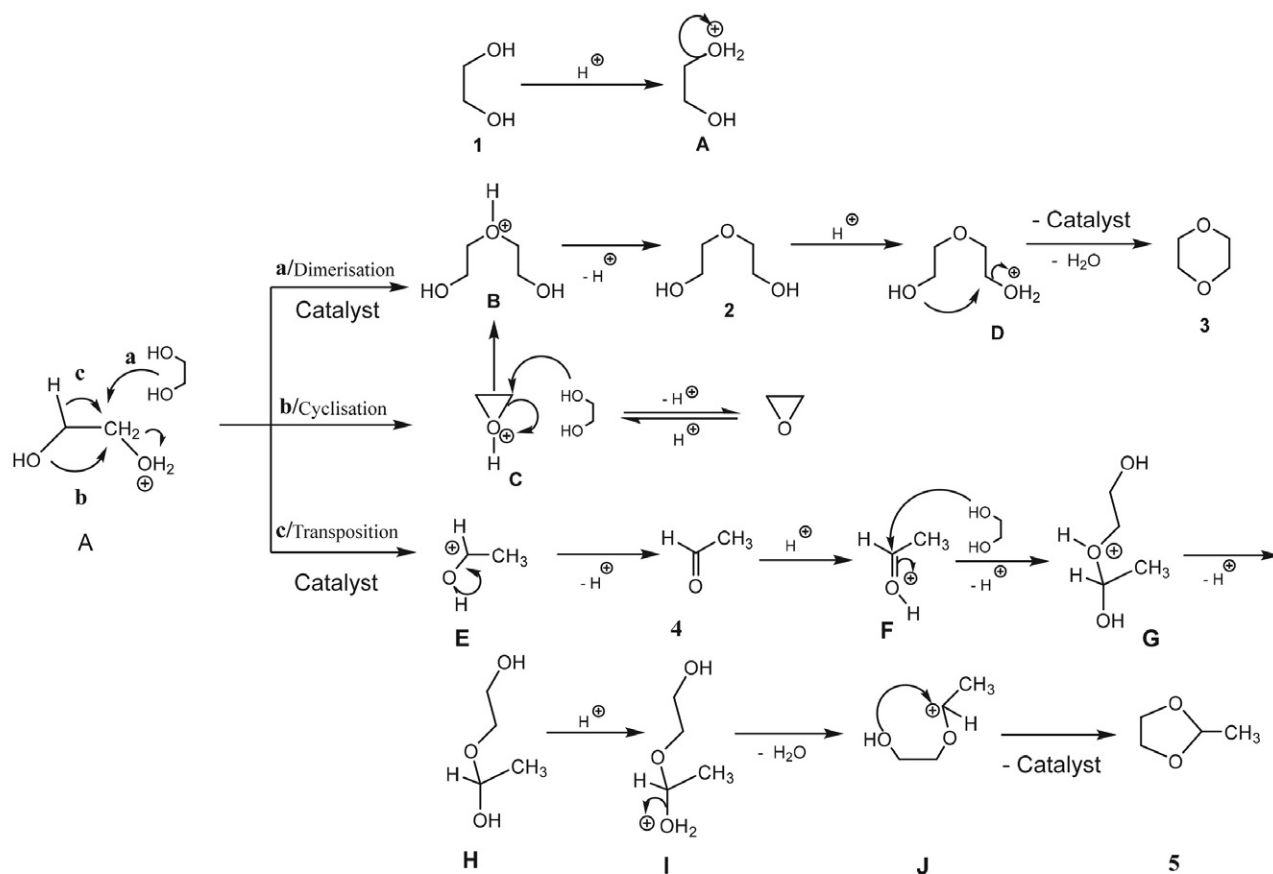
These interesting results then led us to propose an ionic mechanism to explain the formation of the mixture of three products **2**, **3** and **5** from ethylene glycol (**1**) (Scheme 3). The first step in the conversion of ethylene glycol (**1**) to 2-methyl-1,3-dioxolane (**5**) is the reaction of 1,2-diol **1** with the Brønsted sites located on the active surface of the three catalysts Al com, Si com and Si syn to lead first, after the removal of water from the oxonium ion **A**. In this case, there are three possibilities: the first one where this oxonium ion **A** undergoes directly the nucleophilic attack of ethylene glycol (**1**) in excess to lead to diethylene glycol (**2**) *via* oxonium ion **B**. The dehydration of this dimer **2** initiated by heating in an acidic medium leads to oxonium ion **D**. The intramolecular cyclisation of intermediate **D** gives 1,4-dioxane (**3**) (Scheme 3, route a). The second possibility is that oxonium ion **A** cyclises into protonated oxirane **C** which undergoes the nucleophilic addition of reagent **1** on methylenic carbon to lead to diethylene glycol (**2**) *via* oxonium ion **B** (Scheme 3, route b). Finally, the third way shows that this oxonium ion **A** undergoes a Wagner–Meerwein rearrangement, transforming it into a more stable secondary carbocation **E**. The acetaldehyde (**4**) formed *in situ* will in turn be trapped by

diol **1** to lead to the oxonium ion **F** which is converted into oxonium ions **G** and **I**. Dehydration of the latter **I** leads to a tertiary carbocation which is cyclised by an intramolecular *O*-alkylation to 2-methyl-1,3-dioxolane (**5**) (Scheme 3, route c).

We can then conclude that the spectral analysis confirms the experimental results well and that compound **5** is the main product of the conversion of ethylene glycol (**1**) and also the most thermodynamically stable product, which confirms its proportions in the obtained mixture. It should be noted that the other two products **2** and **3** are less stable and therefore have low proportions in the same mixture. In addition, we can note that *in situ* intermediates such as oxirane and acetaldehyde (**4**) are indeed the kinetic products in the conversion reaction of ethylene glycol (**1**) (Table 3).

## 4. Conclusions

In this work, we presented a new way of synthesising 2-methyl-1,3-dioxolane (**5**) using solid catalysts that meet the demands of environmental and green chemistry. From the obtained results, we have showed that the yields of diethylene glycol (**2**), 1,4-dioxane (**3**) and 2-methyl-1,3-di-



Scheme 3.

oxolane (5) depends on the cation exchange capacity of alumina, silica gel and especially synthetic Moroccan silica. The rate of the acetalization reaction of acetaldehyde (4) formed *in situ* is more important than that of the dimerization reaction of ethylene glycol (1). In addition, synthetic silica is very effective in transforming ethylene glycol (1) to 2-methyl-1,3-dioxolane (5).

## Acknowledgments

Prof. Dr. Taoufik Rohand thanks the University Cadi Ayyad and specially the Faculty Polydisciplinaire of Safi for the financial support to the LACM laboratory. Dr. Kiyoshi Tanemura thanks Nippon Dental University for the financial support to the Chemical Laboratory.

## Supporting Materials

There is no supplementary information associated with this paper.

## 5. References

- B. Hatano, S. Toyota, F. Toda, *Green Chem.*, **2001**, 3, 140–142. DOI:10.1039/b102447g
- A. Sakakura, Y. Koshikari, K. Ishihara, *Tetrahedron Lett.*, **2008**, 49, 5017–5020. DOI:10.1016/j.tetlet.2008.06.058
- F. Toda, T. Suzuki, S. Higa, *J. Chem. Soc. - Perkin Trans. 1*, **1998**, 3521–3522. DOI:10.1039/a805884i
- K. R. Prasad, P. Anbarasan, *Tetrahedron Asymmetry*, **2007**, 18, 1419–1427. DOI:10.1016/j.tetasy.2007.05.014
- H. K. Patney, *Tetrahedron Lett.*, **1991**, 32, 2259–2260. DOI:10.1016/S0040-4039(00)79696-1
- K. Wilson, J. H. Clark, *Pure Appl. Chem.*, **2000**, 72, 1313–1319. DOI:10.1351/pac200072071313
- B. Péro, M. J. Dozias, P. Jacquault, J. Hamelin, *Tetrahedron Lett.*, **1997**, 38, 7867–7870. DOI:10.1016/S0040-4039(97)10149-6
- J. F. Knifton, *Appl. Catal. A, Gen.*, **1995**, 130, 79–88. DOI:10.1016/0926-860X(95)00090-9
- M. Onaka, M. Kawai, Y. Izumi, *Chem. Lett.*, **1985**, 14, 779–782. DOI:10.1246/cl.1985.779
- D. Schinzer, M. Kalesse, *Synlett*, **1989**, 1, 34–35. DOI:10.1055/s-1989-34704
- S. Manfredini, D. Simoni, V. Zanirato, A. Casolari, *Tetrahedron Lett.*, **1988**, 29, 3997–4000. DOI:10.1016/S0040-4039(00)80403-7
- T. Rohand, J. Savary, I. E. Markó, *Monatsh. Chem.*, **2018**, 149, 1429–1436. DOI:10.1007/s00706-018-2198-7
- K. Tanemura, *Tetrahedron Lett.*, **2018**, 59, 4293–4298. DOI:10.1016/j.tetlet.2018.10.043
- K. Tanemura, T. Rohand, *Tetrahedron Lett.*, **2020**, 61, 152142. DOI:10.1016/j.tetlet.2020.152142
- A. Costa, *J. Chem. Educ.*, **1982**, 59, 1066. DOI:10.1021/ed059p1066
- K. Bougrin, A. Loupy, M. Soufiaoui, *Tetrahedron*, **1998**, 54, 8055–8064. DOI:10.1016/S0040-4020(98)00431-1
- B. Syassi, K. Bougrin, M. Soufiaoui, *Tetrahedron Lett.*, **1997**, 38, 8855–8858. DOI:10.1016/S0040-4039(97)10392-6
- K. P. C. Vollhardt, N. E. Schore: *Traité de Chimie Organique*, 4<sup>ème</sup> Edit, De Boeck & Larcier, Bruxelles, Bruxelles, **2004**, p 760.
- M. B. Smith: *Organic Synthesis*, McGraw-Hill, New York, **1994**, p. 652.
- T. W. Green, P. G. M. Wuts: *Protective Groups in Organic Synthesis*, Wiley Intersciences, New York, **1999**, p. 308. DOI:10.1002/0471220574
- B. Joy, S. Ghosh, P. Padmaja, M. Lalithambika, *Catal. Commun.*, **2005**, 6, 573–577. DOI:10.1016/j.catcom.2005.04.021
- N. A. Ghulam, M. N. Abbas, D. E. Sachit, *Indian Chem. Eng.*, **2020**, 62, 301–313. DOI:10.1080/00194506.2019.1677512
- S. D. Barton, W. D. Ollis: *Comprehensive Organic Chemistry, The Synthesis and Reactions of Organic Compounds*, Pergamon Press, Paris, **1979**, p. 881.
- R. C. Elderfield: *Heterocyclic Compounds, Six Membered Heterocycles Containing Two Heteroatoms and Their Benzo Derivatives*, John Wiley & Sons, New York, London, Chapman & Hall, **1957**, p. 3.
- R. Grignard, J. Colonge: *Précis de Chimie Organique*, 4<sup>ème</sup> Edit, Masson et Cie, **1958**, p. 344.

## Povzetek

Opisujemo kinetične in mehanistične študije nove poti kompetitivne pretvorbe etilen glikola ob prisotnosti aluminijskega ali silicijskega oksida. Za pretvorbo etilen glikola v zmes dietilen glikola, 1,4-dioksana in 2-metil-1,3-dioksolana, z acetaldehidom kot vmesnim produktom, pri 150 °C in pod avtogenim tlakom brez prisotnega topila smo uporabili komercialno dostopnen aluminijev oksid (Al com), sintetični aluminijev oksid (Al syn), komercialno dostopni silikagel (Si com) in sintetični silikagel (Si syn). Rezultati kažejo, da so izkoristki vseh treh produktov močno odvisni od narave uporabljenega katalizatorja in reakcijskega časa.



Except when otherwise noted, articles in this journal are published under the terms and conditions of the Creative Commons Attribution 4.0 International License

Scientific paper

# Quinazoline-containing Hydrazides of Dicarboxylic Acids and Products of Their Structural Modification: A Novel Class of Anti-inflammatory Agents

Nataliia Krasovska,<sup>1</sup> Viktor Stavytskyi,<sup>1</sup> Inna Nosulenko,<sup>2</sup>  
Oleksandr Karpenko,<sup>3</sup> Oleksii Voskoboinik,<sup>1</sup> and Serhii Kovalenko<sup>1,\*</sup>

<sup>1</sup> Department of Organic and Bioorganic Chemistry, Zaporizhzhia State Medical University, 26 Maiakovski av., Zaporizhzhia, 69035, Ukraine

<sup>2</sup> Department of Pharmacognosy, Pharmacology and Botany, Zaporizhzhia State Medical University, 26 Maiakovski ave., Zaporizhzhia, 69035, Ukraine

<sup>3</sup> Enamine Ltd., Chervonotkatska Street 78, Kyiv 02094, Ukraine

\* Corresponding author: E-mail: kovalenko.si@zsmu.zp.ua

Received: 10-09-2020

## Abstract

The synthesis of hydrazides formed by quinazolin-4(3*H*)-ylidenehydrazine and dicarboxylic acids, as well as their further modification are described in the present manuscript. It was shown that above-mentioned hydrazides may be obtained *via* acylation of initial quinazolin-4(3*H*)-ylidenehydrazine by corresponding acylhalides, cyclic anhydrides and imidazolides of dicarboxylic acids monoesters. Obtained hydrazides were converted into [1,2,4]triazolo[1,5-*c*]quinazolines that were used as initial compounds for chemical modification aimed to the introduction of amide fragment to the molecule. The IR, <sup>1</sup>H NMR and chromat-mass spectral data of obtained compounds were studied and discussed. Obtained substances were studied for anti-inflammatory activity using carrageenan-induced paw inflammation model. Amides of ([1,2,4]triazolo[1,5-*c*]quinazolin-2-yl)alkyl carboxylic acids were detected as promising class of anti-inflammatory agents for further purposeful synthesis and profound study of anti-inflammatory activity.

**Keywords:** [1,2,4]triazolo[1,5-*c*]quinazolines, quinazolines; anti-inflammatory activity

## 1. Introduction

The search for new biologically active compounds and the further development of drugs based on them is one of the most important tasks of medicinal and organic chemistry. It should be noted that elaboration of the new biologically active agents is a multistep process and choice of the research strategy and objects of investigation are quite important stages. Hydrazides formed by quinazolin-4(3*H*)-ylidenehydrazine are one of the promising objects for studies aimed to the development of novel pharmacologically active substances. Such high potential of above-mentioned compounds caused by the possibility of chemical modification aimed to the introduction of diverse pharmacophore fragments.<sup>1-7</sup> Moreover, cyclisation of above-mentioned hydrazides yielded substituted triazolo[*c*]quinazolines that show a wide range of biological

activity including anticonvulsant, antitumor, hypoglycemic, antibacterial and other activities.<sup>8-21</sup> Despite the numerous publications devoted to the chemistry and biology of hydrazides formed by quinazolin-4(3*H*)-ylidenehydrazine, some features of their formation, reactivity, physicochemical and biological properties have been insufficiently studied. One of the promising directions of studies is the synthesis and further cyclization of hydrazides formed by quinazolin-4(3*H*)-ylidenehydrazine and dicarboxylic acids or their monoesters. These transformations would allow to combine heterocyclic fragments with quinazoline or [1,2,4]triazolo[1,5-*c*]quinazoline heterocyclic fragment, what is reasonable in scope of elaboration of novel anti-inflammatory agents.

Therefore, the aim of the present study is to develop procedures for the synthesis of hydrazides formed by quinazolin-4(3*H*)-ylidenehydrazine and derivatives of di-

carboxylic acids. Also the purpose was to study their cyclization, further modification of obtained tricyclic derivatives, as well as to study physicochemical properties and anti-inflammatory activity of obtained products.

## 2. Experimental Section

Melting points were determined in open capillary tubes in a «Stuart SMP30» apparatus and are uncorrected. The elemental analyses (C, H, N) were performed using the «ELEMENTAR vario EL cube» analyzer. IR spectra (4000–600  $\text{cm}^{-1}$ ) were recorded on a Bruker ALPHA FT-IR spectrometer using a module ATR eco ZnSe.  $^1\text{H}$  NMR spectra (400 MHz) were recorded on a Varian-Mercury 400 (Varian Inc., Palo Alto, CA, USA) spectrometer with TMS as internal standard in  $\text{DMSO}-d_6$  solution. LC-MS were recorded using chromatography/mass spectrometric system which consists of high performance liquid chromatograph «Agilent 1100 Series» (Agilent, Palo Alto, CA, USA) equipped with diode-matrix and mass-selective detector «Agilent LC/MSD SL» (atmospheric pressure chemical ionization – APCI). The purity of all obtained compounds was checked by  $^1\text{H}$  NMR and LC-MS.

Compound **1a** was synthesized according to the reported procedures.<sup>1–3</sup> Other starting materials and solvents were obtained from commercially available sources and were used without additional purification.

### 2.1. General Method for the Synthesis of 2-(4(3H)-Quinazolinylidene)hydrazides of Dicarboxylic Acids and Their Monoesters (2a–f)

**Method A.** 1.11 g (11 mmol) of triethylamine was added to the suspension of 1.6 g (10 mmol) of 4-hydrazinoquinazoline (**1a**) in 10 mL of dioxane. The formed mixture was cooled to 0–5 °C and 11 mmol of ethyl 2-chloro-2-oxoacetate or ethyl 3-chloro-3-oxopropanoate was added under stirring. The formed mixture was stirred for 1.5 h at 0–5 °C, then poured in saturated solution of sodium acetate. The formed mixture was filtered off and dried. For additional purification compounds **2a** and **2b** may be crystallized from methanol.

**Method B.** 1.78 g (11 mmol) of  $N,N'$ -carbonyldiimidazole (CDI) was added to the solution of corresponding monoethyl ester of dicarboxylic acid in 20 mL of anhydrous dioxane. The formed mixture was heated at 80 °C for 1 h (until the carbon dioxide was completely released). Then 1.6 g (10 mmol) of 4-hydrazinoquinazoline (**1a**) was added and stirred for 1.5–3 h. The formed mixture was cooled and poured into water and acidified to pH 5–6. The formed mixture was filtered off and dried. For additional purification compounds **2a** and **2b** may be crystallized from methanol.

Compounds **2a** and **2b** that were synthesized by methods A and B have identical physicochemical properties.

**Method C.** 11 mmol of corresponding anhydride of dicarboxylic acid under stirring was added to the suspension of 1.6 g (10 mmol) of 4-hydrazinoquinazoline (**1a**) in 10 mL of dioxane. Formed mixture was stirred at ambient temperature for 24 h or at 80 °C for 1–1.5 h. Then, reaction mixture was cooled, and the formed mixture was filtered off, washed by ethanol and dried. For additional purification obtained compounds may be crystallized from methanol.

**Ethyl 2-oxo-2-(2-(quinazolin-4(3H)-ylidene)hydrazin-eyl)acetate (2a).** Yield: 1.83 g (70%) (method A), 2.25 g (86%) (method B). Mp 199–202 °C; IR 3007 ( $\nu_{\text{NH}}$ ), 1741 ( $\nu_{\text{CO}}$ ), 1689 ( $\nu_{\text{CO}}$ ), 1616 ( $\delta_{\text{NH}}$ ), 1546, 1444, 1110 ( $\nu_{\text{COC}}$ ), 760, 688  $\text{cm}^{-1}$ .  $^1\text{H}$  NMR (400 MHz,  $\text{DMSO}-d_6$ )  $\delta$  1.36 (t,  $J = 7.1$  Hz, 3H,  $-\text{CH}_3$ ), 4.28 (q,  $J = 7.1$  Hz, 2H,  $-\text{CH}_2-$ ), 7.17 (d,  $J = 7.8$  Hz, 1H, H-8), 7.26 (t,  $J = 7.9$  Hz, 1H, H-6), 7.42 (t,  $J = 7.9$  Hz, 1H, H-7), 7.91 (s, 1H, H-2), 8.02 (d,  $J = 7.8$  Hz, 1H, H-5), 11.11 (br. s, 1H,  $-\text{NH}-$ ), 11.79 (br. s, 1H,  $-\text{NH}$ ). LC-MS  $m/z = 261$  [M+1]; Anal. Calcd. for  $\text{C}_{12}\text{H}_{12}\text{N}_4\text{O}_3$ : C, 55.38; H, 4.65; N, 21.53; Found: C, 55.46; H, 4.71; N, 21.58.

**Ethyl 3-oxo-3-(2-(quinazolin-4(3H)-ylidene)hydrazin-eyl)propanoate (2b).** Yield: 1.93 g (70%) (method A), 2.42 g (88.3%) (method B). Mp 165–167 °C; IR 3250 ( $\nu_{\text{NH}}$ ), 3198 ( $\nu_{\text{NH}}$ ), 2986 ( $\nu_{\text{CH}_2}$ ), 1723 ( $\nu_{\text{CO}}$ ), 1656 ( $\nu_{\text{CO}}$ ), 1519 ( $\delta_{\text{NH}}$ ), 1435, 1309, 1158 ( $\nu_{\text{COC}}$ ), 1023, 987, 759, 640  $\text{cm}^{-1}$ .  $^1\text{H}$  NMR (400 MHz,  $\text{DMSO}-d_6$ )  $\delta$  1.24 (t,  $J = 7.1$  Hz, 3H,  $-\text{CH}_2\text{CH}_3$ ), 3.46 (s, 2H,  $-\text{CH}_2-$ ), 4.16 (q,  $J = 7.1$  Hz, 2H,  $-\text{CH}_2\text{CH}_3$ ), 7.17 (d,  $J = 7.8$  Hz, 1H, H-8), 7.26 (t,  $J = 7.9$  Hz, 1H, H-6), 7.42 (t,  $J = 7.9$  Hz, 1H, H-7), 7.91 (s, 1H, H-2), 8.02 (d,  $J = 7.8$  Hz, 1H, H-5), 10.66 (br. s, 1H,  $-\text{NH}-$ ), 11.10 (br. s, 1H,  $-\text{NH}$ ). LC-MS  $m/z = 275$  [M+1]; Anal. Calcd. for  $\text{C}_{13}\text{H}_{14}\text{N}_4\text{O}_3$ : C, 56.93; H, 5.15; N, 20.43; Found: C, 57.02; H, 5.19; N, 20.48.

**4-Oxo-4-(2-(quinazolin-4(3H)-ylidene)hydrazin-eyl)butanoic acid (2c).** Yield: 2.43 g (93%) (method C). Mp 177–179 °C; IR 3270 ( $\nu_{\text{OH}}$ ), 3258 ( $\nu_{\text{NH}}$ ), 1703 ( $\nu_{\text{CO}}$ ), 1602 ( $\nu_{\text{CO}}$ ), 1555 ( $\delta_{\text{NH}}$ ), 1527, 1442, 1212, 929 ( $\delta_{\text{OH}}$ ), 740, 687  $\text{cm}^{-1}$ .  $^1\text{H}$  NMR (400 MHz,  $\text{DMSO}-d_6$ )  $\delta$  2.91 (m, 2H,  $-\text{CH}_2\text{CH}_2-$ ), 3.58 (m, 2H,  $-\text{CH}_2\text{CH}_2-$ ), 7.10 (d,  $J = 7.7$  Hz, 1H, H-8), 7.59 and 7.20 (2xt,  $J = 7.6$  Hz, 1H, H-6), 7.52 and 7.36 (2xt,  $J = 7.6$  Hz, 1H, H-7), 8.25 and 7.74 (2xs, 1H, H-2), 8.04 and 7.88 (2xd,  $J = 7.5$  Hz, 1H, H-5), 10.01 and 9.52 (2xs, 1H,  $-\text{NH}-$ ), 11.37 and 10.88 (2xs, 1H,  $-\text{NH}$ ). LC-MS  $m/z = 261$  [M+1]; Anal. Calcd. for  $\text{C}_{12}\text{H}_{12}\text{N}_4\text{O}_3$ : C, 55.38; H, 4.65; N, 21.53; O, 18.44; Found: C, 55.46; H, 4.69; N, 21.66.

**5-Oxo-5-(2-(quinazolin-4(3H)-ylidene)hydrazin-eyl)pentanoic acid (2d).** Yield: 2.73 g (99%) (method C). Mp 133–135 °C; IR 3356 ( $\nu_{\text{OH}}$ ), 3204 ( $\nu_{\text{NH}}$ ), 2935 ( $\nu_{\text{CH}_2}$ ), 1705 ( $\nu_{\text{CO}}$ ), 1635 ( $\nu_{\text{CO}}$ ), 1566 ( $\delta_{\text{NH}}$ ), 1537, 1369, 1257, 792, 763, 684  $\text{cm}^{-1}$ .  $^1\text{H}$  NMR (400 MHz,  $\text{DMSO}-d_6$ )  $\delta$  1.87 (m, 2H,  $-\text{CH}_2\text{CH}_2\text{CH}_2-$ ), 2.30 (m, 2H,  $-\text{CH}_2\text{CH}_2\text{CH}_2-$ ), 2.68 (m, 2H,  $-\text{CH}_2\text{CH}_2\text{CH}_2-$ ), 7.08 (d,  $J = 7.7$  Hz, 1H, H-8), 7.50 and

7.19 (2x,  $J = 7.8$  Hz, 1H, H-6), 7.52 and 7.36 (2x,  $J = 7.7$  Hz, 1H, H-7), 7.73 (s, 1H, H-2), 8.11 and 7.87 (2x,  $J = 7.6$  Hz, 1H, H-5), 9.93 and 9.48 (2xs, 1H, -NH-), 11.80 and 11.35 (2xs, 1H, -NH-). LC-MS  $m/z = 275$  [M+1]; Anal. Calcd. for  $C_{13}H_{14}N_4O_3$ : C, 56.93; H, 5.15; N, 20.43; Found: C, 56.99; H, 5.21; N, 20.50.

**3-Methyl-5-oxo-5-(2-(quinazolin-4(3H)-ylidene)hydrazineyl)pentanoic acid (2e).** Yield: 2.86 g (99%) (method C). Mp 170–173 °C; IR 3724 ( $\nu_{OH}$ ), 3256 ( $\nu_{NH}$ ), 2928 ( $\nu_{CH_2}$ ), 1720 ( $\nu_{CO}$ ), 1600 ( $\nu_{CO}$ ), 1530 ( $\delta_{NH}$ ), 1371, 871, 760, 688  $cm^{-1}$ .  $^1H$  NMR (400 MHz, DMSO- $d_6$ )  $\delta$  1.03–1.01 (m, 3H, -CH<sub>2</sub>CH(CH<sub>3</sub>)CH<sub>2</sub>-), CH<sub>3</sub>), 2.66–2.07 (m, 5H, -CH<sub>2</sub>CH(CH<sub>3</sub>)CH<sub>2</sub>-), 7.09 (d,  $J = 7.5$  Hz, 1H, H-8), 7.19 (t,  $J = 6.6$  Hz, 1H, H-6), 7.45–7.25 (m, 1H, H-7), 7.73 (s, 1H, H-2), 7.87 (d,  $J = 7.5$  Hz, 1H, H-5), 9.93 and 9.50 (2xs, 1H, -NH-), 11.80 and 11.35 (2xs, 1H, -NH-). LC-MS  $m/z = 289$  [M+1]; Anal. Calcd. for  $C_{14}H_{16}N_4O_3$ : C, 58.32; H, 5.59; N, 19.43; Found: C, 58.37; H, 5.63; N, 19.49.

**2-(1-(2-Oxo-2-(2-(quinazolin-4(3H)-ylidene)hydrazineyl)ethyl)cyclopentyl)acetic acid (2f).** Yield: 2.63 g (80%) (method C). Mp 189–191 °C; IR 3694 ( $\nu_{OH}$ ), 3256 ( $\nu_{NH}$ ), 2988 ( $\nu_{CH_2}$ ), 1703 ( $\nu_{CO}$ ), 1692 ( $\nu_{CO}$ ), 1580 ( $\delta_{NH}$ ), 1524, 1329, 938 ( $\delta_{OH}$ ), 796, 668  $cm^{-1}$ .  $^1H$  NMR (400 MHz, DMSO- $d_6$ )  $\delta$  1.88–1.38 (m, 8H, -CH<sub>2</sub>(cyclopentyl)CH<sub>2</sub>-), 2.90 and 2.45 (2xm, 4H, -CH<sub>2</sub>(cyclopentyl)CH<sub>2</sub>-), 7.10 (d,  $J = 7.0$  Hz, 1H, H-8), 7.24–7.14 (m, 1H, H-6), 7.45–7.29 (m, 1H, H-7), 7.75 (s, 1H, H-2), 7.85 (d,  $J = 7.4$  Hz, 1H, H-5), 10.01 and 9.59 (2xs, 1H, -NH-), 11.90 and 11.40 (2xs, 1H, -NH-). LC-MS  $m/z = 329$  [M+1]; Anal. Calcd. for  $C_{17}H_{20}N_4O_3$ : C, 62.18; H, 6.14; N, 17.06; Found: C, 62.23; H, 6.19; N, 17.12.

## 2. 2. General Method for the Synthesis of ([1,2,4]Triazolo[1,5-c]quinazolin-2-yl)carboxylic Acids and Their Esters (3a–b)

*Method A.* The solution of 5 mmol of corresponding quinazoline-containing hydrazide of dicarboxylic acid (2c–f) or ester (2a, 2b) in 20 mL of acetic acid was refluxed for 3–4 h with removing of formed water. After completing of reaction, the solvent was evaporated under vacuum. 30 mL of methanol was added to the residue and mixture was shaken. The formed precipitate was filtered, washed by 10 mL of ether and dried. For additional purification, compounds 3a–f may be crystallized from ethanol (3a, 3b) or dioxane (3c–f).

*Method B.* 5.5 mmol of sodium acetate was added to the suspension of 0.8 g (5 mmol) of 4-hydrazinoquinazoline (1a) in 10 mL of glacial acetic acid. The formed mixture was cooled to 0–5 °C and 5.5 mmol of ethyl 2-chloro-2-oxoacetate or ethyl 3-chloro-3-oxopropanoate was added dropwise under stirring. The formed mixture was stirred for 1.5 h and then refluxed for 3 h. The formed precipitate of sodium chloride was filtered off, the solvent was evaporated under vacuum, 10 mL of methanol was

added and formed mixture was shaken. The formed precipitate was filtered, washed by 10 mL of ether and dried. For additional purification compounds 3a–f may be crystallized from ethanol.

*Method C.* 5.5 mmol of corresponding dicarboxylic acid anhydride was added to the solution of 0.8 g (5 mmol) 4-hydrazinoquinazoline (1a) in 20 mL of glacial acetic acid. The formed mixture was refluxed for 3–4 h with water removal. After completing of the reaction, the solvent was evaporated under vacuum, 10 mL of methanol was added and formed mixture was shaken. The formed precipitate was filtered off, washed by diethyl ether and dried. Compounds 3a–f may be additionally purified by crystallization from dioxane.

Compounds 3a, 3b that were synthesized by methods A and B have identical physicochemical properties.

**Ethyl [1,2,4]triazolo[1,5-c]quinazoline-2-carboxylate (3a).** Yield: 1.03 g (85%) (method A), 0.87 g (72%) (method B). Mp 172–175 °C; IR 2920 ( $\nu_{CH_2}$ ), 2851 ( $\nu_{CH}$ ), 1730 ( $\nu_{CO}$ ), 1625, 1517, 1458, 1363, 1201 ( $\nu_{COC}$ ), 1019, 862, 780, 708, 654  $cm^{-1}$ .  $^1H$  NMR (400 MHz, DMSO- $d_6$ )  $\delta$  1.44 (t,  $J = 7.2$  Hz, 3H, CH<sub>3</sub>), 4.46 (q,  $J = 7.1$  Hz, 2H, CH<sub>2</sub>), 7.83 (t,  $J = 7.7$  Hz, 1H, H-9), 7.92 (t,  $J = 7.7$  Hz, 1H, H-8), 8.05 (d,  $J = 7.7$  Hz, 1H, H-7), 8.54 (d,  $J = 7.7$  Hz, 1H, H-10), 9.52 (s, 1H, H-5). LC-MS  $m/z = 243$  [M+1]; Anal. Calcd. for  $C_{12}H_{10}N_4O_2$ : C, 59.50; H, 4.16; N, 23.13; Found: C, 59.58; H, 4.21; N, 23.19.

**Ethyl 2-([1,2,4]triazolo[1,5-c]quinazolin-2-yl)acetate (3b).** Yield: 1.02 g (79%) (method A), 0.73 g (57%) (method B). Mp 125–127 °C; IR 2944 ( $\nu_{CH_2}$ ), 1722 ( $\nu_{CO}$ ), 1621, 1524, 1370, 1219 ( $\nu_{COC}$ ), 1026, 897, 774, 710, 668  $cm^{-1}$ .  $^1H$  NMR (400 MHz, DMSO- $d_6$ )  $\delta$  1.28 (t,  $J = 7.1$  Hz, 3H, -CH<sub>3</sub>), 3.96 (s, 2H, -CH<sub>2</sub>-), 4.17 (q,  $J = 7.1$  Hz, 2H, -CH<sub>2</sub>CH<sub>3</sub>), 7.77 (t,  $J = 7.5$  Hz, 1H, H-9), 7.87 (t,  $J = 7.6$  Hz, 1H, H-8), 8.02 (d,  $J = 8.2$  Hz, 1H, H-7), 8.44 (d,  $J = 7.8$  Hz, 1H, H-10), 9.40 (s, 1H, H-5). LC-MS  $m/z = 257$  [M+1]; Anal. Calcd. for  $C_{13}H_{12}N_4O_2$ : C, 60.93; H, 4.72; N, 21.86; Found: C, 61.02; H, 4.80; N, 21.94.

**3-([1,2,4]Triazolo[1,5-c]quinazolin-2-yl)propanoic acid (3c).** Yield: 1.20 g (99%) (method C). Mp 200–203 °C; IR 2900 ( $\nu_{CH_2}$ ), 1723 ( $\nu_{CO}$ ), 1625, 1502, 1362, 1338, 1259, 907 ( $\delta_{OH}$ ), 782, 710, 668  $cm^{-1}$ .  $^1H$  NMR (400 MHz, DMSO- $d_6$ )  $\delta$  2.82 (t,  $J = 7.3$  Hz, 2H, -CH<sub>2</sub>CH<sub>2</sub>COOH), 3.18 (t,  $J = 7.2$  Hz, 2H, -CH<sub>2</sub>CH<sub>2</sub>COOH), 7.71 (t,  $J = 7.6$  Hz, 1H, H-9), 7.82 (t,  $J = 7.6$  Hz, 1H, H-8), 7.98 (d,  $J = 7.7$  Hz, 1H, H-7), 8.42 (d,  $J = 7.7$  Hz, 1H, H-10), 9.26 (s, 1H, H-5), 11.90 (br. s, 1H, -COOH). LC-MS  $m/z = 243$  [M+1]; Anal. Calcd. for  $C_{12}H_{10}N_4O_2$ : C, 59.50; H, 4.16; N, 23.13; Found: C, 59.56; H, 4.20; N, 23.21.

**4-([1,2,4]Triazolo[1,5-c]quinazolin-2-yl)butanoic acid (3d).** Yield: 1.16 g (91%) (method C). Mp 184–186 °C; IR 2928 ( $\nu_{CH_2}$ ), 1714 ( $\nu_{CO}$ ), 1625, 1521, 1404, 1366, 1329,

1241, 1181, 909 ( $\delta_{\text{OH}}$ ), 792, 756, 711, 669  $\text{cm}^{-1}$ .  $^1\text{H NMR}$  (400 MHz, DMSO- $d_6$ )  $\delta$  2.10 (m, 2H,  $-\text{CH}_2\text{CH}_2\text{CH}_2\text{COOH}$ ), 2.41 (t,  $J = 7.2$  Hz, 2H,  $-\text{CH}_2-(\text{CH}_2)_2\text{COOH}$ ), 3.00 (t,  $J = 7.2$  Hz, 2H,  $-(\text{CH}_2)_2\text{CH}_2\text{COOH}$ ), 7.73 (t,  $J = 7.7$  Hz, 1H, H-9), 7.82 (t,  $J = 7.7$  Hz, 1H, H-8), 8.00 (d,  $J = 7.7$  Hz, 1H, H-7), 8.44 (d,  $J = 7.7$  Hz, 1H, H-10), 9.27 (s, 1H, H-5), 11.82 (br. s, 1H,  $-\text{COOH}$ ). LC-MS  $m/z = 257$  [M+1]; Anal. Calcd. for  $\text{C}_{13}\text{H}_{12}\text{N}_4\text{O}_2$ : C, 60.93; H, 4.72; N, 21.86; Found: C, 60.99; H, 4.78; N, 21.94.

**4-([1,2,4]Triazolo[1,5-c]quinazolin-2-yl)-3-methylbutanoic acid (3e).** Yield: 0.70 g (52%) (method C). Mp 168–170 °C; IR 2958 ( $\nu_{\text{CH}_2}$ ), 1714 ( $\nu_{\text{CO}}$ ), 1628, 1528, 1470, 1370, 1316, 1258, 911 ( $\delta_{\text{OH}}$ ), 771, 704, 653  $\text{cm}^{-1}$ .  $^1\text{H NMR}$  (400 MHz, DMSO- $d_6$ )  $\delta$  1.05 (d,  $J = 6.2$  Hz, 3H,  $-\text{CH}_2\text{CH}(\text{CH}_3)\text{CH}_2-$ ), 2.17 (dd,  $J^2 = 15.5$  Hz,  $J^3 = 8.1$  Hz, 1H,  $-\text{CH}_2\text{CH}(\text{CH}_3)\text{CH}_2-$ ), 2.41 (dd,  $J^2 = 15.5$  Hz,  $J^3 = 5.0$  Hz, 1H,  $-\text{CH}_2\text{CH}(\text{CH}_3)\text{CH}_2-$ ), 2.66–2.52 (m, 1H,  $-\text{CH}_2\text{CH}(\text{CH}_3)\text{CH}_2-$ ), 2.83 (dd,  $J^2 = 14.0$  Hz,  $J^3 = 7.5$  Hz, 1H,  $-\text{CH}_2\text{CH}(\text{CH}_3)\text{CH}_2-$ ), 2.96 (dd,  $J^2 = 14.0$  Hz,  $J^3 = 6.0$  Hz, 1H,  $-\text{CH}_2\text{CH}(\text{CH}_3)\text{CH}_2-$ ), 7.76 (t,  $J = 7.5$  Hz, 1H, H-9), 7.86 (t,  $J = 7.6$  Hz, 1H, H-8), 8.01 (d,  $J = 8.1$  Hz, 1H, H-7), 8.44 (d,  $J = 7.9$  Hz, 1H, H-10), 9.37 (s, 1H, H-5), 11.83 (s, 1H,  $-\text{COOH}$ ). LC-MS  $m/z = 271$  [M+1]; Anal. Calcd. for  $\text{C}_{14}\text{H}_{14}\text{N}_4\text{O}_2$ : C, 62.21; H, 5.22; N, 20.73; Found: C, 62.29; H, 5.31; N, 20.81.

**2-(1-([1,2,4]Triazolo[1,5-c]quinazolin-2-ylmethyl)cyclopentyl)acetic acid (3f).** Yield: 0.79 g (51%) (method C). Mp 147–149 °C; IR 2952 ( $\nu_{\text{CH}_2}$ ), 2310, 1706 ( $\nu_{\text{CO}}$ ), 1620, 1553, 1515, 1486, 1353, 1313, 1237, 931 ( $\delta_{\text{OH}}$ ), 899, 774, 728, 698  $\text{cm}^{-1}$ .  $^1\text{H NMR}$  (400 MHz, DMSO- $d_6$ )  $\delta$  1.86–1.42 (m, 8H,  $-\text{CH}_2(\text{cyclopentyl})\text{CH}_2-$ ), 2.47–2.31 (m, 2H,  $-\text{CH}_2(\text{cyclopentyl})\text{CH}_2-$ ), 3.17–3.05 (m, 2H,  $-\text{CH}_2(\text{cyclopentyl})\text{CH}_2-$ ), 7.76 (t,  $J = 7.1$  Hz, 1H, H-9), 7.86 (t,  $J = 7.0$  Hz, 1H, H-8), 8.02 (d,  $J = 8.0$  Hz, 1H, H-7), 8.45 (d,  $J = 7.7$  Hz, 1H, H-10), 9.39 (s, 1H, H-5), 11.75 (s, 1H,  $-\text{COOH}$ ). LC-MS  $m/z = 311$  [M+1]; Anal. Calcd. for  $\text{C}_{14}\text{H}_{14}\text{N}_4\text{O}_2$ : C, 65.79; H, 5.85; N, 18.05; Found: C, 65.84; H, 5.91; N, 18.11.

### 2.3 General Method for the Synthesis of Amides of ([1,2,4]Triazolo[1,5-c]quinazolin-2-yl)alkylcarboxylic Acids (4a–j)

*Method A.* 5.5 of mmol of *para*-methoxybenzylamine and 1–2 mL of DMF was added to the 5 mmol of corresponding ester (**3a**, **3b**). The formed mixture was treated at 140–150 °C for 3–4 h. The 5 mL of methanol and 5 mL of water were added to the mixture after completing of the reaction. The formed precipitate was filtered off and dried. Obtained compounds may be additionally purified by crystallization from ethanol.

*Method B.* 0.89 g (5.5 mmol) of *N,N'*-carbonyldiimidazole (CDI) was added to the solution of 5 mmol of corresponding carboxylic acid (**3a–f**) in 20 mL of anhydrous dioxane. The formed mixture was heated at 80 °C for 1 h

(until the carbon dioxide was completely released). Then 5 mmol of corresponding amine was added and stirred (or refluxed) for 1.5–3 h. The formed mixture was cooled and poured into water and acidified by hydrochloric acid to pH 5–6. The formed mixture was filtered off and dried.

**N-(4-Methoxybenzyl)-[1,2,4]triazolo[1,5-c]quinazolin-2-carboxamide (4a).** Yield: 0.97 g (58%). Mp 183–185 °C; IR 3857 ( $\nu_{\text{NH}}$ ), 3753 ( $\nu_{\text{NH}}$ ), 2928 ( $\nu_{\text{CH}_2}$ ), 2510, 1656 ( $\nu_{\text{CO}}$ ), 1553 ( $\delta_{\text{NH}}$ ), 1516, 1465, 1319, 1236, 741, 689  $\text{cm}^{-1}$ .  $^1\text{H NMR}$  (400 MHz, DMSO- $d_6$ )  $\delta$  3.74 (s, 3H,  $-\text{OCH}_3$ ), 4.47 (d,  $J = 5.7$  Hz, 2H,  $-\text{NHCH}_2-$ ), 6.81 (d,  $J = 7.6$  Hz, 2H, H-3,5 Bn), 7.29 (d,  $J = 7.9$  Hz, 2H, H-2,6 Bn), 7.81 (t,  $J = 7.6$  Hz, 1H, H-9), 7.92 (t,  $J = 7.8$  Hz, 1H, H-8), 8.07 (d,  $J = 7.9$  Hz, 1H, H-7), 8.49 (d,  $J = 8.0$  Hz, 1H, H-10), 9.06 (t,  $J = 5.4$  Hz, 1H,  $-\text{NHCH}_2-$ ), 9.56 (s, 1H, H-5). LC-MS  $m/z = 334$  [M+1]; Anal. Calcd. for  $\text{C}_{18}\text{H}_{15}\text{N}_5\text{O}_2$ : C, 64.86; H, 4.54; N, 21.01; Found: C, 64.93; H, 4.60; N, 21.09.

**2-([1,2,4]Triazolo[1,5-c]quinazolin-2-yl)-N-(4-methoxybenzyl)acetamide (4b).** Yield: 1.20 g (69%). Mp 172–175 °C; IR 3697 ( $\nu_{\text{NH}}$ ), 2920 ( $\nu_{\text{CH}_2}$ ), 2851 ( $\nu_{\text{CH}}$ ), 1669 ( $\nu_{\text{CO}}$ ), 1547 ( $\delta_{\text{NH}}$ ), 1458, 1363, 1201, 1019, 862, 780, 708, 654  $\text{cm}^{-1}$ .  $^1\text{H NMR}$  (400 MHz, DMSO- $d_6$ )  $\delta$  3.77 (s, 3H,  $-\text{OCH}_3$ ), 4.45 (d,  $J = 5.7$  Hz, 2H,  $-\text{NHCH}_2-$ ), 6.87 (d,  $J = 7.6$  Hz, 2H, H-3,5 Bn), 7.22 (d,  $J = 7.9$  Hz, 2H, H-2,6 Bn), 7.63 (t,  $J = 7.6$  Hz, 1H, H-9), 7.78 (t,  $J = 7.8$  Hz, 1H, H-8), 8.00 (d,  $J = 7.9$  Hz, 1H, H-7), 8.43 (d,  $J = 8.1$  Hz, 1H, H-10), 9.08 (t,  $J = 5.4$  Hz, 1H,  $-\text{NHCH}_2-$ ), 9.38 (s, 1H, H-5). LC-MS  $m/z = 348$  [M+1]; Anal. Calcd. for  $\text{C}_{19}\text{H}_{17}\text{N}_5\text{O}_2$ : C, 65.69; H, 4.93; N, 20.16; Found: C, 65.74; H, 4.98; N, 20.21.

**3-([1,2,4]Triazolo[1,5-c]quinazolin-2-yl)-N-(4-fluorophenyl)propanamide (4c).** Yield: 1.07 g (64%). Mp 206–208 °C; IR 3297 ( $\nu_{\text{NH}}$ ), 1665 ( $\nu_{\text{CO}}$ ), 1530 ( $\delta_{\text{NH}}$ ), 1493, 1371, 1214, 901, 834, 767, 710  $\text{cm}^{-1}$ .  $^1\text{H NMR}$  (400 MHz, DMSO- $d_6$ )  $\delta$  2.90 (t,  $J = 7.6$  Hz, 2H,  $-\text{CH}_2\text{CH}_2-$ ), 3.54–3.07 (t,  $J = 7.6$  Hz, 2H,  $-\text{CH}_2\text{CH}_2-$ ), 6.95 (t,  $J = 8.6$  Hz, 2H, H-3,5 Ph), 7.60 (dd,  $J^2 = 8.5$  Hz,  $J^3 = 4.9$  Hz, 2H, H-2,6 Ph), 7.74 (t,  $J = 7.5$  Hz, 1H, H-9), 7.84 (t,  $J = 7.7$  Hz, 1H, H-8), 7.99 (d,  $J = 8.1$  Hz, 1H, H-7), 8.40 (d,  $J = 8.3$  Hz, 1H, H-10), 9.95 (s, 1H,  $-\text{NH}$ ). LC-MS  $m/z = 336$  [M+1]; Anal. Calcd. for  $\text{C}_{18}\text{H}_{14}\text{FN}_5\text{O}$ : C, 64.47; H, 4.21; N, 20.88; Found: C, 64.54; H, 4.26; N, 20.93.

**3-([1,2,4]Triazolo[1,5-c]quinazolin-2-yl)-N-(4-bromophenyl)propanamide (4d).** Yield: 0.93 g (47%). Mp 210–212 °C; IR 3840 ( $\nu_{\text{NH}}$ ), 3727 ( $\nu_{\text{NH}}$ ), 3286 ( $\nu_{\text{NH}}$ ), 1662 ( $\nu_{\text{CO}}$ ), 1529 ( $\delta_{\text{NH}}$ ), 1488, 1394, 1245, 900, 767, 711, 660  $\text{cm}^{-1}$ .  $^1\text{H NMR}$  (400 MHz, DMSO- $d_6$ )  $\delta$  2.91 (t,  $J = 7.6$  Hz, 2H,  $-\text{CH}_2\text{CH}_2-$ ), 3.24 (t,  $J = 7.6$  Hz, 2H,  $-\text{CH}_2\text{CH}_2-$ ), 7.32 (d,  $J = 8.7$  Hz, 2H, H-2,6 Ph), 7.56 (d,  $J = 8.6$  Hz, 2H, H-3,5 Ph), 7.74 (t,  $J = 7.6$  Hz, 1H, H-9), 7.84 (t,  $J = 7.7$  Hz, 1H, H-8), 8.00 (d,  $J = 8.2$  Hz, 1H, H-7), 8.41 (d,  $J = 8.0$  Hz, 1H, H-10), 9.36 (s, 1H, H-5), 10.03 (s, 1H,  $-\text{NH}$ ). LC-MS  $m/z = 396$  [M+1]; Anal. Calcd. for  $\text{C}_{18}\text{H}_{14}\text{BrN}_5\text{O}$ : C, 54.56; H, 3.56; N, 17.67; Found: C, 54.63; H, 3.62; N, 17.73.



**Ethyl 4-(3-([1,2,4]triazolo[1,5-*c*]quinazolin-2-yl)propa-*n*-amido)benzoate (4e).** Yield: 1.18 g (61%). Mp 214–216 °C; IR 3857 ( $\nu_{\text{NH}}$ ), 3725 ( $\nu_{\text{NH}}$ ), 2901 ( $\nu_{\text{CH}_2}$ ), 1711 ( $\nu_{\text{CO}}$ ), 1667 ( $\nu_{\text{CO}}$ ), 1599 ( $\delta_{\text{NH}}$ ), 1493, 1408, 1311, 1274, 899, 854, 766, 694  $\text{cm}^{-1}$ .  $^1\text{H NMR}$  (400 MHz, DMSO- $d_6$ )  $\delta$  1.35 (t,  $J = 7.1$  Hz, 3H,  $-\text{CH}_2\text{CH}_3$ ), 2.96 (t,  $J = 7.6$  Hz, 2H,  $-\text{CH}_2\text{CH}_2-$ ), 3.25 (dd,  $J^2 = 8.6$  Hz,  $J^3 = 6.7$  Hz, 2H,  $-\text{CH}_2\text{CH}_2-$ ), 4.26 (q,  $J = 7.1$  Hz, 2H,  $-\text{CH}_2\text{CH}_3$ ), 7.69 (d,  $J = 8.4$  Hz, 2H, H-2,6 Ph), 7.73 (t,  $J = 7.6$  Hz, 1H, H-9), 7.88–7.80 (m, 3H, H-8, H-3,5 Ph), 7.99 (d,  $J = 8.2$  Hz, 1H, H-7), 8.40 (d,  $J = 7.5$  Hz, 1H, H-10), 9.36 (s, 1H, H-5), 10.21 (s, 1H,  $-\text{NH}-$ ). LC-MS  $m/z = 390$  [M+1]; Anal. Calcd. for  $\text{C}_{21}\text{H}_{19}\text{N}_5\text{O}_3$ : C, 64.77; H, 4.92; N, 17.98; Found: C, 64.74; H, 4.99; N, 18.03.

**4-([1,2,4]Triazolo[1,5-*c*]quinazolin-2-yl)-*N*-(4-fluorophenyl)butanamide (4f).** Yield: 0.78 g (45%). Mp 173–175 °C; IR 3295 ( $\nu_{\text{NH}}$ ), 1658 ( $\nu_{\text{CO}}$ ), 1528 ( $\delta_{\text{NH}}$ ), 1504, 1432, 1404, 1336, 1207, 904, 835, 722, 697  $\text{cm}^{-1}$ .  $^1\text{H NMR}$  (400 MHz, DMSO- $d_6$ )  $\delta$  2.18 (p,  $J = 7.3$  Hz, 2H,  $-\text{CH}_2\text{CH}_2\text{CH}_2-$ ), 2.41 (t,  $J = 7.4$  Hz, 2H,  $-(\text{CH}_2)_2\text{CH}_2-$ ), 2.97 (t,  $J = 7.7$  Hz, 2H,  $-\text{CH}_2(\text{CH}_2)_2-$ ), 6.93 (t,  $J = 8.7$  Hz, 2H, H-3,5 Ph), 7.56 (dd,  $J^2 = 8.8$  Hz,  $J^3 = 5.0$  Hz, 2H, H-2,6 Ph), 7.75 (t,  $J = 7.4$  Hz, 1H, H-9), 7.85 (t,  $J = 7.7$  Hz, 1H, H-7), 8.01 (d,  $J = 8.2$  Hz, 1H, H-8), 8.43 (d,  $J = 7.8$  Hz, 1H, H-10), 9.36 (s, 1H, H-5), 9.70 (s, 1H,  $-\text{NH}-$ ). LC-MS  $m/z = 350$  [M+1]; Anal. Calcd. for  $\text{C}_{19}\text{H}_{16}\text{FN}_5\text{O}$ : C, 65.32; H, 4.62; N, 20.05; Found: C, 65.39; H, 4.69; N, 20.13.

**4-([1,2,4]Triazolo[1,5-*c*]quinazolin-2-yl)-*N*-(4-chlorophenyl)butanamide (4g).** Yield: 0.96 g (52%). Mp 199–201 °C; IR 3904 ( $\nu_{\text{NH}}$ ), 3725 ( $\nu_{\text{NH}}$ ), 3249 ( $\nu_{\text{NH}}$ ), 1656 ( $\nu_{\text{CO}}$ ), 1520 ( $\delta_{\text{NH}}$ ), 1491, 1396, 1333, 1251, 903, 817, 771, 721, 702, 668  $\text{cm}^{-1}$ .  $^1\text{H NMR}$  (400 MHz, DMSO- $d_6$ )  $\delta$  2.25–2.07 (m, 2H,  $-\text{CH}_2\text{CH}_2\text{CH}_2-$ ), 2.43 (t,  $J = 7.2$  Hz, 2H,  $-(\text{CH}_2)_2\text{CH}_2-$ ), 2.98 (t,  $J = 7.3$  Hz, 2H,  $-\text{CH}_2(\text{CH}_2)_2-$ ), 7.17 (d,  $J = 8.8$  Hz, 2H, H-2,6 Ph), 7.57 (d,  $J = 8.8$  Hz, 2H, H-3,5 Ph), 7.74 (t,  $J = 7.5$  Hz, 1H, H-9), 7.84 (t,  $J = 8.4$  Hz, 1H, H-8), 8.00 (d,  $J = 7.7$  Hz, 1H, H-7), 8.41 (d,  $J = 9.1$  Hz, 1H, H-10), 9.35 (s, 1H, H-5), 9.80 (s, 1H,  $-\text{NH}-$ ). LC-MS  $m/z = 366$  [M+1]; Anal. Calcd. for  $\text{C}_{19}\text{H}_{16}\text{ClN}_5\text{O}$ : C, 62.38; H, 4.41; N, 19.14; Found: C, 62.46; H, 4.47; N, 19.19.

**4-([1,2,4]Triazolo[1,5-*c*]quinazolin-2-yl)-*N*-(4-bromophenyl)butanamide (4h).** Yield: 1.41 g (69%). Mp 200–202 °C; IR 3250 ( $\nu_{\text{NH}}$ ), 1651 ( $\nu_{\text{CO}}$ ), 1522 ( $\delta_{\text{NH}}$ ), 1489, 1334, 1283, 1244, 904, 814, 773, 703, 659  $\text{cm}^{-1}$ .  $^1\text{H NMR}$  (400 MHz, DMSO- $d_6$ )  $\delta$  2.18 (p,  $J = 7.4$  Hz, 2H,  $-\text{CH}_2\text{CH}_2\text{CH}_2-$ ), 2.42 (t,  $J = 7.3$  Hz, 2H,  $-(\text{CH}_2)_2\text{CH}_2-$ ), 2.97 (t,  $J = 7.5$  Hz, 2H,  $-\text{CH}_2(\text{CH}_2)_2-$ ), 7.31 (d,  $J = 8.8$  Hz, 2H, H-2,6 Ph), 7.52 (d,  $J = 8.7$  Hz, 2H, H-3,5 Ph), 7.75 (t,  $J = 7.5$  Hz, 1H, H-9), 7.85 (t,  $J = 8.3$  Hz, 1H, H-8), 8.00 (d,  $J = 8.2$  Hz, 1H, H-7), 8.42 (d,  $J = 7.9$  Hz, 1H, H-10), 9.36 (s, 1H, H-5), 9.79 (s, 1H,  $-\text{NH}-$ ). LC-MS  $m/z = 411$  [M+1]; Anal. Calcd. for  $\text{C}_{19}\text{H}_{16}\text{BrN}_5\text{O}$ : C, 55.62; H, 3.93; N, 17.07; Found: C, 55.68; H, 4.01; N, 17.12.

**Ethyl 4-(4-([1,2,4]triazolo[1,5-*c*]quinazolin-2-yl)butan-amido)benzoate (4i).** Yield: 0.77 g (38%). Mp 92–94 °C; IR 3340 ( $\nu_{\text{NH}}$ ), 1692 ( $\nu_{\text{CO}}$ ), 1625 ( $\nu_{\text{CO}}$ ), 1524 ( $\delta_{\text{NH}}$ ), 1367, 1308, 1275, 1017, 960, 901, 854, 767, 697  $\text{cm}^{-1}$ .  $^1\text{H NMR}$  (400 MHz, DMSO- $d_6$ )  $\delta$  1.35 (t,  $J = 7.1$  Hz, 3H,  $-\text{CH}_2\text{CH}_3$ ), 2.19 (p,  $J = 7.3$  Hz, 2H,  $-\text{CH}_2\text{CH}_2\text{CH}_2-$ ), 2.45 (t,  $J = 6.9$  Hz, 2H,  $-(\text{CH}_2)_2\text{CH}_2-$ ), 2.99 (t,  $J = 7.3$  Hz, 2H,  $-\text{CH}_2(\text{CH}_2)_2-$ ), 4.26 (q,  $J = 7.0$  Hz, 2H,  $-\text{CH}_2\text{CH}_3$ ), 7.66 (d,  $J = 8.3$  Hz, 2H, H-3,5 Ph), 7.74 (t,  $J = 7.5$  Hz, 1H, H-9), 7.90–7.79 (m, 3H, H-8, H-2,6 Ph), 8.00 (d,  $J = 8.3$  Hz, 1H, H-7), 8.42 (d,  $J = 7.9$  Hz, 1H, H-10), 9.35 (s, 1H, H-5), 10.01 (s, 1H,  $-\text{NH}-$ ). LC-MS  $m/z = 404$  [M+1]; Anal. Calcd. for  $\text{C}_{22}\text{H}_{21}\text{N}_5\text{O}_3$ : C, 65.50; H, 5.25; N, 17.36; Found: C, 65.57; H, 5.31; N, 17.41.

**4-([1,2,4]Triazolo[1,5-*c*]quinazolin-2-yl)-*N*-(4-chlorophenyl)-3-methylbutanamide (4j).** Yield: 0.59 g (31%). Mp 196–198 °C; IR 3348 ( $\nu_{\text{NH}}$ ), 1657 ( $\nu_{\text{CO}}$ ), 1527 ( $\delta_{\text{NH}}$ ), 1491, 1465, 1338, 1283, 1250, 903, 821, 773, 703, 658  $\text{cm}^{-1}$ .  $^1\text{H NMR}$  (400 MHz, DMSO- $d_6$ )  $\delta$  1.05 (d,  $J = 6.6$  Hz, 3H,  $-\text{CH}_2\text{CH}(\text{CH}_3)\text{CH}_2-$ ), 2.26 (dd,  $J^2 = 14.2$  Hz,  $J^3 = 8.2$  Hz, 1H,  $-\text{CH}_2\text{CH}(\text{CH}_3)\text{CH}_2-$ ), 2.44 (dd, 1H,  $J^2 = 14.2$  Hz,  $J^3 = 8.2$  Hz,  $-\text{CH}_2\text{CH}(\text{CH}_3)\text{CH}_2-$ ), 2.65 (dq,  $J^2 = 13.8$  Hz,  $J^3 = 6.6$  Hz, 1H,  $-\text{CH}_2\text{CH}(\text{CH}_3)\text{CH}_2-$ ), 2.84 (dd,  $J^2 = 14.2$  Hz,  $J^3 = 7.8$  Hz, 1H,  $-\text{CH}_2\text{CH}(\text{CH}_3)\text{CH}_2-$ ), 2.98 (dd,  $J^2 = 14.2$  Hz,  $J^3 = 6.2$  Hz, 1H,  $-\text{CH}_2\text{CH}(\text{CH}_3)\text{CH}_2-$ ), 7.16 (d,  $J = 8.7$  Hz, 2H, H-3,5 Ph), 7.58 (d,  $J = 8.7$  Hz, 2H, H-2,6 Ph), 7.74 (t,  $J = 7.6$  Hz, 1H, H-9), 7.85 (t,  $J = 7.7$  Hz, 1H, H-8), 8.00 (d,  $J = 8.1$  Hz, 1H, H-7), 8.43 (d,  $J = 7.9$  Hz, 1H, H-10), 9.35 (s, 1H, H-5), 9.84 (s, 1H,  $-\text{NH}-$ ). LC-MS  $m/z = 380$  [M+1]; Anal. Calcd. for  $\text{C}_{20}\text{H}_{18}\text{ClN}_5\text{O}$ : C, 63.24; H, 4.78; N, 18.44; Found: C, 63.31; H, 4.83; N, 18.48.

## 2. 2. Anti-inflammatory Activity

Evaluation of anti-inflammatory activity of the synthesized compounds was conducted on 144 Wistar white rats (weight 150–160 g), obtained from the nursery «Institute of Pharmacology and Toxicology of Ukraine» (Kyiv). All experimental procedures and treatment were carried out according to the European Convention and «Regulations on the use of animals in biomedical research».<sup>22</sup> Screening of the synthesized compounds with estimated anti-inflammatory activity began with the study of their effect on exudative phase of acute aseptic inflammation («carrageenan» test).<sup>23</sup> Phlogogen (1% aqueous solution of  $\lambda$ -carrageenan) was subplantally injected in a dose of 0.1 mL in the rats' back right paw. The left one was used as a control. Intra-gastric administration of the studied compounds was conducted using atraumatic probe as water solution or finely dispersed suspension stabilized by Tween-80 in a dose of 10 mg/kg 1 h before the injection of phlogogen. The reference drug diclofenac sodium was administered intra-gastrically in a recommended dose of 8 mg/kg for pre-clinical studies. Measurement of paws volume was conducted before the experiment and in 4 h («carrageenan» test) after injection of phlogogen using the

described methods. The activity of these substances was determined by their ability to reduce the swelling compared with control group and was expressed in percentage. It showed how the substance inhibited phlogogen swelling in relation to control swelling where the value was taken as 100%. The activity of the studied compounds was calculated as following:

$$AA, \% = 100\% - \left( \frac{V_{pe} - V_{he}}{V_{pc} - V_{hc}} * 100\% \right) \quad (1)$$

where AA – antiexudative activity, %;  $V_{pe}$  – the volume of paw edema in the experiment;  $V_{he}$  – the volume of healthy paw in the experiment;  $V_{pc}$  – the volume of paw edema in control;  $V_{hc}$  – the volume of healthy paw in control.

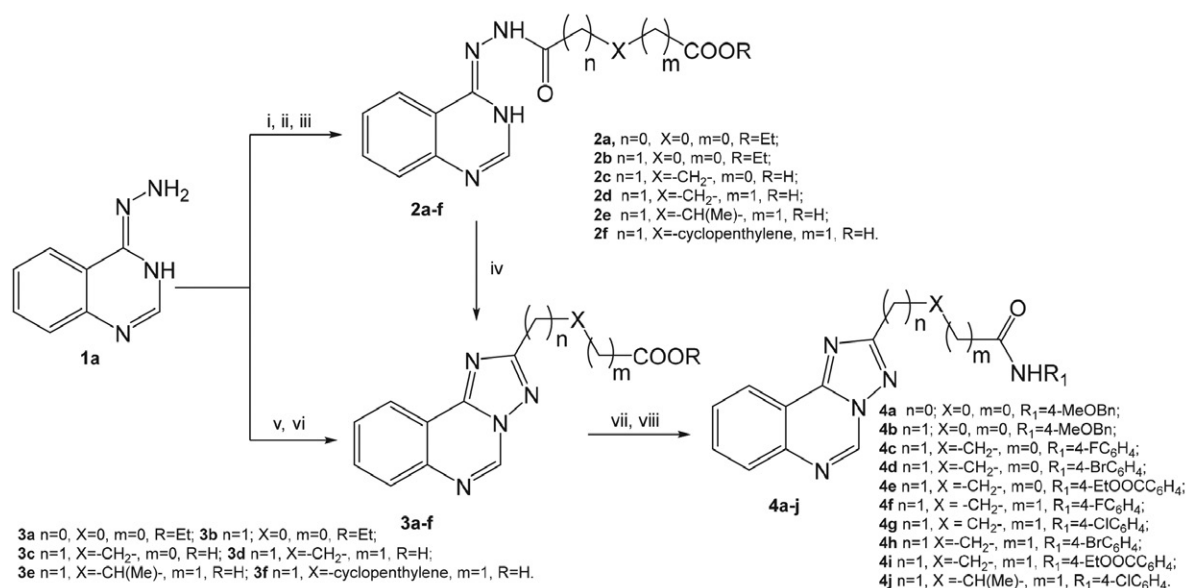
Statistical data processing was performed using a license program «STATISTICA® for Windows 10.0» (Stat-Soft Inc., № AXXR712D833214FAN5) and «SPSS 16.0», «Microsoft Office Excel 360». The results are presented as mean  $\pm$  standard error of the mean. Arithmetic mean and standard error of the mean were calculated for each of the studied parameters. During verification of statistical hypothesis, null hypothesis was declined if statistical criterion was  $p < 0.05$ .<sup>24</sup>

### 3. Results and Discussion

Previously heterocyclization of corresponding (3*H*-quinazoline-4-ylidene)hydrazides was described as the most efficient and convenient method for 2-*R*-[1,2,4]triazolo[1,5-*c*]quinazolines synthesis.<sup>1–8</sup> The preparation

of the above-mentioned hydrazides is based on the acylation of 4-hydrazinoquinazoline by anhydrides, acyl halides, *N*-acyl imidazolides and other highly reactive derivatives of carboxylic acids.<sup>1–3</sup> Namely, above-mentioned approaches were used for the synthesis of target compounds. It was found that initial compound **1a** may be easily acylated in dioxane medium by ethyl 2-chloro-2-oxoacetate or ethyl 3-chloro-3-oxopropanoate (Method B) as well as by imidazolides of monoethyl esters of oxalic or malonic acids. Above-mentioned reaction yielded corresponding hydrazides (**2a**, **2b**, Scheme 1). It should be noted that acylation by acyl halides required the presence of an organic base (triethylamine) and cooling of reaction medium to 0–5 °C. At the same time the reaction between **1a** and corresponding imidazolides may be conducted under heating (80 °C). Hydrazides **2c–f**, that contain prolonged alkyl moiety, were synthesized by interaction between initial compound **1a** and cyclic anhydrides. Reaction was conducted in dioxane medium at ambient temperature or under heating (Method C, Scheme 1). The significant differences in yield values depending on the synthetic protocols used were not observed.

The following cyclization of hydrazides **2a–f** yielded corresponding 2-([1,2,4]triazolo[1,5-*c*]quinazoline-2-yl)carboxylic acids and their esters (**3a–f**, Scheme 1). Besides, for compounds **3a–f** one-pot synthesis method was elaborated. Thus compounds **3a** and **3b** were obtained *via* interaction of 4-hydrazinoquinazoline (**1a**) with above-mentioned acylhalides in acetic acid medium and the presence of sodium acetate at 0–5 °C followed by refluxing of reaction mixture for 3 h (Scheme 1). Compounds **3d–f** were synthesized by reaction of compound **1a** with cyclic anhy-



i:  $ClC(O)(CH_2)_nCOOEt$ , dioxane,  $N(Et)_3$ , 0–5 °C, 1.5 h; ii)  $HCOO(CH_2)_nCOOEt$ , CDI, dioxane, 80°C, 1.5–3 h; iii) anhydrides, dioxane, reflux, 80°C, 1–1.5 h or r.t., 24 h; iv:  $AcOH$ , reflux, 3–4 h; v: 1)  $ClC(O)(CH_2)_nCOOEt$ ,  $AcOH$ ,  $AcONa$ , 0–5°C, 1.5 h; 2) reflux, 3 h; vi: anhydrides,  $AcOH$ , reflux, 3–4 h; vii: 4- $MeOBnNH_2$ , 1–2 drop,  $DMF$ , 130–140°C, 3–4 h; viii: 1) dioxane, CDI, 80°C; 2)  $ArNH_2$  reflux, 1.5 h.

Scheme 1.

drives in acetic acid. It should be noted that [1,2,4]triazolo[4,3-*c*]quinazolines played a role of intermediate products of condensation process. Above-mentioned intermediates underwent acid catalyzed Dimroth-type rearrangement that yielded isomeric [1,5-*c*]-series.<sup>1-3</sup>

Considering the presence of carboxylic or ester group in the structure of compounds **3** it was decided to conduct the chemical modification of above-mentioned fragment to obtain agents with higher anti-inflammatory activity. The synthesis of amides **4** was conducted by known methods, namely *via* aminolysis of esters **3a**, **3b** or imidazolides of acids **3c-f**. Compounds **4a** and **4b** were obtained by fusing of initial esters **3a** and **3b** with 4-methoxybenzylamine at 130–140 °C. At the same time aminolysis of imidazolides of acids **3c-f** occurred easily in anhydrous dioxane (Scheme 1).

Obtained compounds **2a-f**, **3a-f**, **4a-j** are white, pale yellow crystalline powders that are not soluble in water, soluble in saturated aqueous solution of sodium (potassium) hydrocarbonates (**3a-f**), alcohols, dioxane and DMF.

Elemental analysis, <sup>1</sup>H NMR and LS-MS data proved purity and structure of synthesized substances. The LC-MS using positive-ion atmospheric pressure chemical ionization (APCI) showed the appropriate molecular ions [M+1], which corresponded to the expected molecular weights of **2**, **3** and **4**.

In <sup>1</sup>H NMR spectra of hydrazides **2a-f** the signals of endocyclic NH-protons and protons of hydrazide moiety were observed as broad or doubled singlets at the 11.80–10.88 ppm and 11.11–9.48 ppm, correspondingly. The signals of protons in heterocyclic fragments were registered as a singlet at the 7.91–7.73 ppm (proton at the second position), doublets at the 8.02–7.73 ppm and 7.52–7.36 ppm (protons at the position 5 and positions 7, correspondingly), triplets at the 7.26–7.19 ppm and 7.17–7.08 ppm (protons at the position 6 and position 8, correspondingly). It should be mentioned that in some cases above-mentioned signals were broadened due to the hydrazide-hydrazonol tautomerism.

<sup>1</sup>H NMR spectra of compounds **3a-f** and **4a-j** were characterized by the paramagnetic shift (relative to the <sup>1</sup>H NMR spectra of compounds **2a-f**) of the signals of the protons in heterocyclic moiety. Above-mentioned phenomenon may be explained by formation of electron-deficient heterocyclic system. The signal of proton at the position 5 of triazoloquinazoline system was characteristic for <sup>1</sup>H NMR spectra of compounds **3a-f** and was registered as a singlet at the 9.56–9.26 ppm.<sup>1-3</sup> The other protons of tricyclic fragment formed ABCD system which consisted of sequentially located doublets and triplets with corresponding splitting constants.

The signal of carboxylic group protons was not observed in <sup>1</sup>H NMR spectra of compounds **2c-f** due to the deuterium exchanging processes. At the same time the signal of above-mentioned group protons was registered in low field as singlets at the 11.90–11.75 ppm in <sup>1</sup>H NMR

spectra of compounds **3c-f**. In <sup>1</sup>H NMR spectra of compounds **4a-j** the chemical shifts of the signals of amide group proton depended on its chemical surrounding and were registered as triplets at the 9.08–9.06 ppm (compounds **4a**, **4b**) or singlets at the 10.21–9.70 ppm (**4c-j**). Besides, the signals of aromatic protons of benzylamide or anilide fragments were characteristic for <sup>1</sup>H NMR spectra of compounds **4**.<sup>25</sup> In <sup>1</sup>H NMR spectra of compounds **2**, **3** and **4** the signals of aliphatic moieties protons were observed with corresponding chemical shifts and multiplicity.<sup>25</sup> It should be noted that additional splitting of signals caused by diastereotopic methylene group protons of 3-methylbutyl fragment was observed in <sup>1</sup>H NMR spectra of compounds **3e** and **4j**.

The characteristic bands of stretching vibrations of NH group at the 3256–3007 cm<sup>-1</sup>, CO group at the 1741–1703 cm<sup>-1</sup>, CONH group (“amide I” band) at the 1689–1600 cm<sup>-1</sup>, “amide II” band at the 1616–1519 cm<sup>-1</sup> were present in IR spectra of compounds **2**. IR spectra of compounds **3** were characterized by the absence of absorption bands caused by the stretching vibrations of amide group at the 3256–3007 cm<sup>-1</sup> and the presence of intensive bands of CO group stretching vibrations at the 1730–1706 cm<sup>-1</sup>. IR spectra of compounds **4** were characterized by wide bands of NH group stretching vibrations at the 1669–1651 cm<sup>-1</sup>, stretching vibrations bands of NH group at the 3857–3249 cm<sup>-1</sup>, vibrations bands of CO group («amide I») at the 1669–1651 cm<sup>-1</sup> and combined stretching-deformation vibrations of NH and CN group («amide II» band) at the 1599–1520 cm<sup>-1</sup>. IR spectra of halogen-containing compounds were additionally characterized by absorption bands caused by stretching vibrations of C-halogen bond:  $\nu_{C-F}$  at the 1110–1102 cm<sup>-1</sup> (**4c**, **4f**),  $\nu_{C-Br}$  at the 660–650 cm<sup>-1</sup> (**4d**, **4h**),  $\nu_{C-Cl}$  at the 750–700 cm<sup>-1</sup> (**4g**, **4j**). It should be noted that in IR spectra of compounds **2**, **3** and **4** low intensity bands  $\nu_{C=C}$  bond at the 1486–1424 cm<sup>-1</sup>,  $\gamma_{(=C-H)}$  at the 850–666 cm<sup>-1</sup>,  $\nu_{CH_2}$  and  $\delta_{CH_2}$ -group at the 2988–2928 and 1491–1404 cm<sup>-1</sup> were observed.

Screening of obtained compounds for anti-exudative activity was conducted in continuation of our studies aimed to the purposeful search of anti-inflammatory agents among compounds that contain heterocyclic fragment and carboxylic group. The studies were carried out using carrageenan-induced inflammation model.<sup>23</sup> According to the obtained results (Table 1) in most of the cases obtained compounds were characterized by moderate anti-inflammatory activity. It should be noted that pharmacological effects of some compounds were comparable with activity of reference compound – sodium diclofenac. Thus, compounds **4a**, **2b**, **4e**, **4g**, **4h**, **2e** and **4j** revealed anti-inflammatory activity on the level of 40.28–54.86%.

The conducted SAR-analysis showed that anti-exudative activity of hydrazides **2** depends on the length of alkyl moiety between heterocyclic fragment and carboxylic group. Compounds with propyl (**2b**), 3-methylpentyl (**2e**) and (cyclopentyl)ethyl (**2f**) fragments were the most

Table 1. Anti-inflammatory activity of the synthesized compounds ( $M \pm m$ ,  $n = 6$ )<sup>\*</sup>

№	Compd.	The healthy paw volume, mL <sup>*</sup>	Edema paw volume on 4 <sup>th</sup> h of exp., mL <sup>*</sup>	AA, %
	Control	1.410 ± 0.021	2.370 ± 0.042	–
	Diclofenac sodium	1.553 ± 0.041	1.843 ± 0.046	69.79
1.	<b>2a</b>	1.390 ± 0.037	2.186 ± 0.133	17.01
2.	<b>3a</b>	1.336 ± 0.039	2.330 ± 0.066	-3.47
3.	<b>4a</b>	1.64 ± 0.031	2.073 ± 0.027	54.86
4.	<b>2b</b>	1.723 ± 0.046	2.273 ± 0.059	42.71
5.	<b>3b</b>	1.460 ± 0.080	2.073 ± 0.099	36.11
6.	<b>4b</b>	1.623 ± 0.044	2.226 ± 0.075	37.15
7.	<b>2c</b>	1.370 ± 0.060	2.100 ± 0.058	23.96
8.	<b>3c</b>	1.280 ± 0.047	2.126 ± 0.108	11.81
9.	<b>4c</b>	1.370 ± 0.026	2.110 ± 0.114	22.92
10.	<b>4d</b>	1.640 ± 0.024	2.140 ± 0.075	47.92
11.	<b>4e</b>	1.460 ± 0.046	2.156 ± 0.076	27.43
12.	<b>2d</b>	1.306 ± 0.053	2.076 ± 0.097	19.79
13.	<b>3d</b>	1.400 ± 0.066	2.333 ± 0.095	2.78
14.	<b>4f</b>	1.870 ± 0.030	2.556 ± 0.075	28.47
15.	<b>4g</b>	1.573 ± 0.048	2.110 ± 0.074	44.10
16.	<b>4h</b>	1.403 ± 0.020	1.956 ± 0.053	42.36
17.	<b>4i</b>	1.740 ± 0.037	2.430 ± 0.055	28.13
18.	<b>2e</b>	1.463 ± 0.081	1.943 ± 0.110	50.00
19.	<b>3e</b>	1.386 ± 0.045	2.206 ± 0.098	14.58
20.	<b>4j</b>	1.563 ± 0.066	2.136 ± 0.058	40.28
21.	<b>2f</b>	1.386 ± 0.049	1.983 ± 0.122	37.85
22.	<b>3f</b>	1.370 ± 0.05	2.096 ± 0.072	24.31

<sup>\*</sup>Note: significant changes in control ( $p < 0.05$ );  $n$  is the number of animals in the group

active among the compounds **2**. Compounds **3** were less active comparing to hydrazides **2**. Thus, cyclization of compounds **2** resulted in significant decrease of anti-inflammatory activity. At the same time amides **4** revealed high pharmacological effect. It was shown that level of anti-inflammatory activity depend on the nature of amide fragment. Amides that contain 4-chloro(bromo)phenyl moieties (**4d**, **4g**, **4h**, **4j**) showed higher activity comparing to compounds **4e** and **4i** with “pharmacophore” 4-ethyl-carboxyphenyl fragment. The presence of 4-methoxybenzylamide moiety (compounds **4a** and **4b**) also had positive effect on the level of anti-inflammatory activity.

The conducted studies showed that amides of ([1,2,4]triazolo[1,5-*c*]quinazoline-2-yl)alkyl carboxylic acids are promising group of anti-inflammatory agents. The further study of their chemical modification and profound study of their pharmacological effects are reasonable in scope of purposeful search of novel effective anti-inflammatory drugs.

#### 4. Conclusion

It was found that acylation of quinazolin-4(3*H*)-ylidenehydrazine by cyclic anhydrides of dicarboxylic acids, acylhalides or imidazolides of dicarboxylic acids monoesters is an efficient approach for the synthesis

of corresponding hydrazides. The cyclization of obtained hydrazides yielded products that combine [1,2,4]triazolo[1,5-*c*]quinazoline fragment and carboxylic or ester groups in their structures. Above-mentioned compounds were used for the synthesis of corresponding amides. Screening of the synthesized compounds for anti-exudative activity revealed the potential of ([1,2,4]triazolo[1,5-*c*]quinazoline-2-yl)alkyl carboxylic acids amides as promising anti-inflammatory agents.

#### 5. References

- O. V. Karpenko, S. I. Kovalenko, *J. Org. Pharm. Chem.* **2005**, *2*, 47–54.
- O. V. Karpenko, S. I. Kovalenko, *J. Org. Pharm. Chem.* **2005**, *4*, 61–69.
- O. V. Karpenko, S. I. Kovalenko, *J. Org. Pharm. Chem.* **2006**, *2*, 65–70.
- Yu. V. Martynenko, M. S. Kazunin, E. A. Selivanova, S. I. Kovalenko, *Zaporozhye Med. J.* **2016**, *4*, 89–96.
- Yu. V. Martynenko, M. S. Kazunin, I. S. Nosulenko, G. G. Berest, S. I. Kovalenko, O. M. Kamyshnyi, N. M. Polishchuk, *Zaporozhye Med. J.* **2018**, *3*, 413–420.
- Yu. V. Martynenko, O. M. Antypenko, I. S. Nosulenko, G. G. Berest, S. S. Kovalenko, *Anti-Inflammatory & Anti-Allergy Agents in Med. Chem.* **2019**, *19*, 60–71.

7. Yu. V. Martynenko, O. M. Antypenko, O. A. Brazhko, I. B. Labenska, S. I. Kovalenko, *Acta Chim. Slov.* **2019**, *66*, 145–154. DOI:10.17344/acsi.2018.4731
8. L. N. Antypenko, A. V. Karpenko, S. I. Kovalenko, A. M. Katsev, E. Z. Komarovska-Porokhnyavets, V. P. Novikov, *Arch. Pharm. Chem. Life Sci.* **2009**, *342*, 651–662. DOI:10.1002/ardp.200900077
9. S. K. Pandey, A. Singh, A. Singh, A. Nizamuddin, *Eur. J. Med. Chem.* **2009**, *44*, 1188–119.
10. J. Kehler, A. Ritzén, M. Langgård, S. L. Petersen, M. M. Farah, C. Bundgaard, J. P. Kilburn, *Bioorg. Med. Chem. Lett.* **2011**, *21*, 3738–3742. DOI:10.1016/j.bmcl.2011.04.067
11. S. I. Kovalenko, L. M. Antypenko, A. K. Bilyi, S. V. Kholodnyak, O. V. Karpenko, O. M. Antypenko, N. S. Mykhaylova, T. I. Los, O. S. Kolomoets, *Sci. Pharm.* **2013**, *81*, 359–391.
12. V. G. Ugale, S. B. Bari, *Eur. J. Med. Chem.* **2014**, *80*, 447–501. DOI:10.1016/j.ejmech.2014.04.072
13. D. Wang, F. Gao, *Chem. Centr. J.* **2013**, *7*, 95.
14. A. K. Bilyi, L. M. Antypenko, V. V. Ivchuk, O. M. Kamyshnyi, N. M. Polishchuk, S. I. Kovalenko, *ChemPlusChem* **2015**, *80*, 980–989. DOI:10.1002/cplu.201500051
15. L. M. Antypenko, S. I. Kovalenko, A. M. Katsev, E. Z. Komarovska-Porokhnyavets, V. P. Novikov, N. S. Fedyunina, *Curr. Comput. Aided Drug Des.* **2015**, *12*, 29–41. DOI:10.2174/1573409912666160126142236
16. O. M. Antypenko, L. M. Antypenko, S. I. Kovalenko, A. M. Katsev, O. M. Achkasova, *Arab. J. Chem.* **2016**, *9*, 792–805. DOI:10.1016/j.arabjc.2014.09.009
17. Y. A.-M. El-Badry, E. Nassar, M. A.-A. El-Hashash, *Eur. J. Chem.* **2016**, *7*, 128–134. DOI:10.5155/eurjchem.7.1.128-134.1370
18. O. M. Antypenko, S. I. Kovalenko, O. V. Karpenko, V. O. Nikitin, L. M. Antypenko, *Helv. Chim. Acta* **2016**, *99*, 621–631. DOI:10.1002/hlca.201600062
19. J. C. Burbiel, W. Ghattas, P. Küppers, M. Köse, S. Lacher, A.-M. Herzner, C. E. Müller, *ChemMedChem* **2016**, *11*, 2272–2286. DOI:10.1002/cmdc.201600255
20. M. M. Zeydi, N. Montazeri, M. Fouladi, *J. Heterocycl. Chem.* **2017**, *54*, 3549–3553. DOI:10.1002/jhet.2979
21. W. A. Ewes, M. A. Elmersy, S. M. El-Messery, M. N. A. Nasr, *Bioorg. Med. Chem.* **2020**, *28*, 115373. DOI:10.1016/j.bmc.2020.115373
22. European convention for the protection of vertebrate animal used for experimental and other scientific purposes, Council of Europe, Strasbourg, **1986**.
23. J. C. Fehrenbacher, M. R. Vasko, D. B. Duarte, *Curr. Protoc. Pharmacol.* **2012**, *56*, 5.4.1–5.4.7. DOI:10.1002/0471141755.ph0506s56
24. S. N. Lapach, A. V. Chubenko, P. N. Babich, Statistical methods in biomedical research using EXCEL, Morion, Ukraine, **2001**, 408.
25. E. Breitmaier, Structure elucidation by NMR in organic chemistry: A practical guide, 3rd Ed., Wiley, Germany, **2002**, p. 270. DOI:10.1002/0470853069

## Povzetek

V prispevku opisujemo sintezo hidrazidov iz kinazolin-4(3H)-ilidenhidrazinov in dikarboksilnih kislin ter njihove nadaljnje transformacije. Pokazali smo, da tovrstne hidrazide lahko pripravimo s pomočjo aciliranja izhodnega kinazolin-4(3H)-ilidenhidrazina z ustreznimi acilhalidi, cikličnimi anhidridi in imidazoli monoestrov dikarboksilnih kislin. Pripravljene hidrazide smo pretvorili v [1,2,4]triazolo[1,5-c]kinazoline, ki smo jih uporabili kot izhodne spojine za nadaljnje kemijske modifikacije s ciljem uvedbe amidnega fragmenta v končne molekule. IR in <sup>1</sup>H NMR spektroskopija ter sklopljena kromatografsko-masna spektrometrija so omogočile študij strukture produktov. Za pripravljene spojine smo določili tudi protivnetno učinkovitost s pomočjo modela vnetja podganje tačke s karaginanom. Zaključimo lahko, da so ([1,2,4]triazolo[1,5-c]kinazolin-2-il)alkil karboksilne kisline obetavna skupina molekul s protivnetnim delovanjem, primerne za nadaljnje poglobljene študije sintez in protivnetnih aktivnosti.



Scientific paper

# Synthesis and Anticancer Activity of Triazole Linked Macrocycles and Heterocycles

Avula Srinivas<sup>1,\*</sup> and Enugala Kalyan Rao<sup>2</sup><sup>1</sup> Department of Chemistry, Vaagdevi Degree & PG College Kishanpura, Warangal, Telangana, India 506001<sup>2</sup> Department of Physical Sciences, Kakatiya Institute of Technological Sciences Warangal, Telangana, India 506015

\* Corresponding author: E-mail: avula.sathwikreddy@gmail.com

Received: 10-23-2020

## Abstract

Synthesis of macrocyclic enones starting from alkyl ether and triazole as a linker was achieved using click reaction and intramolecular aldol condensation. The newly synthesized macrocyclic enone was successfully utilized as a dipolarophile in 1,3-dipolar cycloaddition. The dipoles generated from hydrazine hydrochloride, hydroxylamine and guanidine hydrochloride were reacted with macrocyclic enone to give a new class of spiro aminopyrimidines, phenyl pyrazoles and isoxazoles grafted macrocycles in good yield. The structures of newly synthesized compounds were confirmed with IR, NMR and mass spectroscopy and evaluated for their anti cancer activity.

**Keywords:** Triazoles; click reaction; internal aldol condensation; macrocyclic enones; anticancer activity

## 1. Introduction

Carbohydrates are most important class of bio-molecules, their structural components have an important role in biological processes and organic synthesis.<sup>1</sup> In the chemical, pharmaceutical, food, cosmetic and detergent industries they act as readily available intermediates stocks for large scale applications<sup>2</sup> and also they have an important role in cell physiology in the form of glycoconjugates (glycolipids, glycoproteins and polysaccharides) and in many biological processes such as intercellular recognition, bacterial and viral infection, cancer metastasis, apoptosis and neuronal proliferation, etc.<sup>3</sup> The introduction of a carbohydrate moiety into a system often imparts interesting properties such as hydrophilicity, lowered noxious and escalated bioactivities;<sup>4</sup> organic chemists have linked carbohydrates to various biologically potent compounds to escalate their biological applications, such as steroids, amino acids and other therapeutic agents.<sup>5</sup> One of the methods used to link a carbohydrate moiety with a potential compound is *via* a triazole ring using the well known click-chemistry reaction.<sup>6</sup> The strategy of linking a carbohydrate moiety with another species *via* a triazole ring is gaining importance in organic synthesis, natural products chemistry and bio chemistry.<sup>7</sup> The stability, polar nature and possible hydrogen bonding ability of

a triazole ring combined with the biocompatibility and presence of stereogenic centers, the stereogenic centers of a carbohydrate moiety make glucal-based triazoles very interesting for organic synthetic chemists.

Macrocyclic compounds with large cavities are found to have potential application in chemistry, biology and nanotechnology.<sup>8,9</sup> With potent biological activities, heteroatoms-containing macro cyclic compounds are present in natural products.<sup>10</sup> Heterocyclic compounds are known to interact with various proteins and heterocyclic units are constituent parts of magnificent molecular ligands;<sup>12</sup> such compounds can also act as magic eye for chiral molecules and can be used for selective metal ion and anion remembrance.<sup>13,14</sup> The Cu(I)-catalyzed alkynes–azide cycloaddition is the most useful modality for the fashioning of diversification of 1,2,3-triazole grafted macrocycles.<sup>15</sup> In recent years 1,2,3-triazoles have large attraction in supramolecular chemistry because of their dual nature to act as both hydrogen bond donors and acceptors<sup>16,17</sup> due to their firmness and lyomorous properties, these triazoles can be of more conspicuous use as a non-peptide inhibitors.<sup>18</sup> Furthermore, they exhibit large variety of medical activities.<sup>19</sup> Triazole glycosides are also present in the structures of various antiviral drugs such as Ribavirin and  $\beta$ -D-ribofuranosyl-1,2,4-triazole-3-carboxamide.<sup>20</sup> Isoxazole derivatives are pertinent class of bioactive

molecules, which express glaring activities such as protein tyrosinephosphatase 1 inhibitors,<sup>21</sup> antiviral,<sup>22</sup> antihelminthic,<sup>23</sup> antiinflammatory,<sup>24</sup> anticonvulsant,<sup>25</sup> insecticidal,<sup>26</sup> antitubercular,<sup>27</sup> immunomodulatory,<sup>28</sup> and hypolipemic.<sup>29</sup> Moreover pyrazoles and their derivatives could be considered as possible antimicrobial agents,<sup>30</sup> activities of the other derivatives include antidepressant,<sup>31</sup> antiarthritic<sup>32</sup> and cerebroprotectors.<sup>33</sup> Some aryl pyrazoles were reported to act as non nucleoside human immunodeficiency virus (HIV-1) reverse transcriptase inhibitors,<sup>34</sup> COX-2 inhibitors,<sup>35–37</sup> activators of the nitric oxide receptors and soluble guanylate cyclase activity.<sup>38</sup> On the other hand, the pyrimidines have special place and have contributed exceptionally to biological and medicinal fields,<sup>39</sup> with activities such as antitubercular,<sup>40</sup> and calcium channel blockers,<sup>41</sup> and also many pyrimidines<sup>42</sup> have displayed diverse pharmaceutical activities depending upon the geometry and type of substituents attached to the ring.<sup>43</sup> 3-Azido-3-deoxythymidine (AZT),<sup>44</sup> a pyrimidine derivative, has been found to be an eloquent antiviral agent against HIV type 1 *in vitro*, and has been found to decrease mortality and opportunistic infections in patients with AIDS.

Following the successful introduction, inspired by the biological profile of triazoles, macrolides, isoxazoles, pyrazoles and pyrimidines, and in the continuation of our work on biologically active heterocycles<sup>45–52</sup> we have developed a series of novel triazole linked furanose pyranose macrocycles, their heterocyclic counterparts and evaluated their anticancer activity.

## 2. Results and Discussion

The key intermediate **8** required for the synthesis of compounds **9**, **10** and **11** was prepared according to the procedure outlined in the Scheme 1. 1-(2-(4-Bromobutoxy)phenyl)ethanone (**2**), prepared from 2-hydroxyacetophenone by treating with 1,4-dibromopropane in DMF in the presence of K<sub>2</sub>CO<sub>3</sub>, followed by sodium azide, gave its corresponding azide, is converted into triazole **7** (82%) by using 1,3-dipolar cycloaddition with propargyl ether **4** carried out at ambient temperature in the presence of CuSO<sub>4</sub> and sodium ascorbate in a mixture of 1:1 CH<sub>2</sub>Cl<sub>2</sub>–

H<sub>2</sub>O. Acid hydrolysis of **5** in 60% AcOH furnished the diol **6**, which on oxidative cleavage with NaIO<sub>4</sub> gave the aldehyde **7**, which is subjected to internal aldol condensation to give macrocycle<sup>53</sup> **8** (Scheme 1). Compound **8** was then reacted with hydroxylamine, hydrazine hydrochloride and guanidine hydrochloride at reflux temperature to give macrocyclic derivatives **9**, **10** and **11**.

The key intermediate **20** required for the synthesis of compounds **21**, **22** and **23** was prepared according to the procedure outlined in the scheme 2. 1-(2-(4-Bromobutoxy)phenyl)ethanone (**2**), prepared from 2-hydroxyacetophenone by treating with 1,4-dibromopropane in DMF in the presence of K<sub>2</sub>CO<sub>3</sub>, followed by sodium azide to give its corresponding azide, is converted into triazole **7** (82%) by using 1,3-dipolar cycloaddition with propargyl ether **16**, carried out at ambient temperature in the presence of CuSO<sub>4</sub> and sodium ascorbate in a mixture of 1:1 CH<sub>2</sub>Cl<sub>2</sub>–H<sub>2</sub>O, oxidation of compound **18** with IBX gave aldehyde, which is subjected to internal aldol condensation to give macrocycle<sup>53</sup> **20** (Scheme 2). Compound **20** was then reacted with hydroxylamine, hydrazine hydrochloride and guanidine hydrochloride at reflux temperature to give macrocyclic derivatives **21**, **22** and **23**. The structures of synthesized compounds were determined by IR, NMR, MS spectra and evaluated for their anticancer activity.

## 3. *In vitro* Cytotoxicity

Anticancer activity of the compounds **9**, **10**, **11**, **21**, **22** and **23** was determined on the basis of measurement of *in vitro* growth inhibition of tumor cell lines in 96 well plates by cell-mediated reduction of tetrazolium salt to the formation of water insoluble crystals using doxorubicin as a standard. The cytotoxicity was assessed against a panel of four different human tumor cell lines: A549 derived from human alveolar adenocarcinoma epithelial cells (ATCC No. CCL-185), HeLa derived from human cervical cancer cells (ATCC No. CCL-2), MDA-MB-231 derived from human breast adenocarcinoma cells (ATCC No. HTB22), MCF-7 (Michigan cancer Foundation cell line) and HEK 293 (normal human embryonic kidney cell line) using the MTT assays.<sup>54</sup> The IC<sub>50</sub> values were calculated

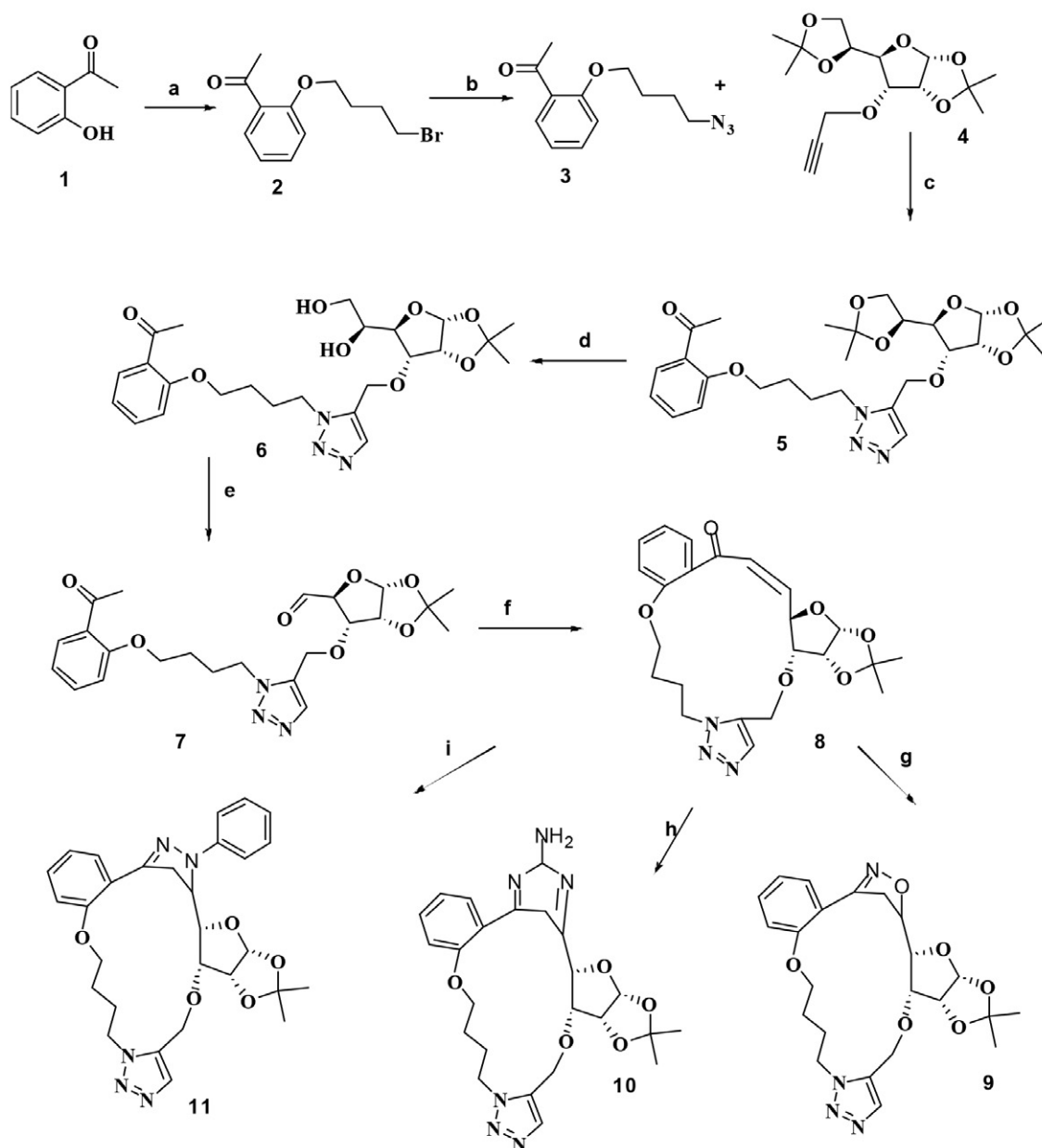
Table 1. *In vitro* anticancer activity of selected compounds

Compound	IC <sub>50</sub> values in μM				
	A549	Hela	MDAMB231	MCF-7	HEK 293
9	6.22	5.42	6.39	<b>1.82</b>	>100
10	7.02	3.92	4.01	10.07	>100
11	>100	3.76	4.21	>100	>100
21	12.09	2.98	3.97	>100	>100
22	>100	3.56	3.75	15.99	>100
23	6.01	5.05	6.05	<b>1.90</b>	>100
Doxorubicin	<b>0.459</b>	<b>0.509</b>	<b>0.91</b>	<b>1.07</b>	>100

from the plotted absorbance data for the dose-response curves.  $IC_{50}$  values (in  $\mu\text{M}$ ) are indicated as mean  $\pm$ SD of three independent experiments. From the data reported in Table 1, most of the prepared compounds possessed significant cytotoxicity effect on all the tested cell lines and potencies of some of the compounds were comparable to the standard doxorubicin, the most widely used drug for the treatment of tumors. Among the tested compounds **9** and **23** showed the most potent activity against MCF-7 cell line with  $IC_{50}$  value of 1.82 and 1.90  $\mu\text{M}$ , whereas **10**, **11**, **21** and **22** showed promising activity against MDA-MB-231 and HeLa cell lines.

## 4. Experimental

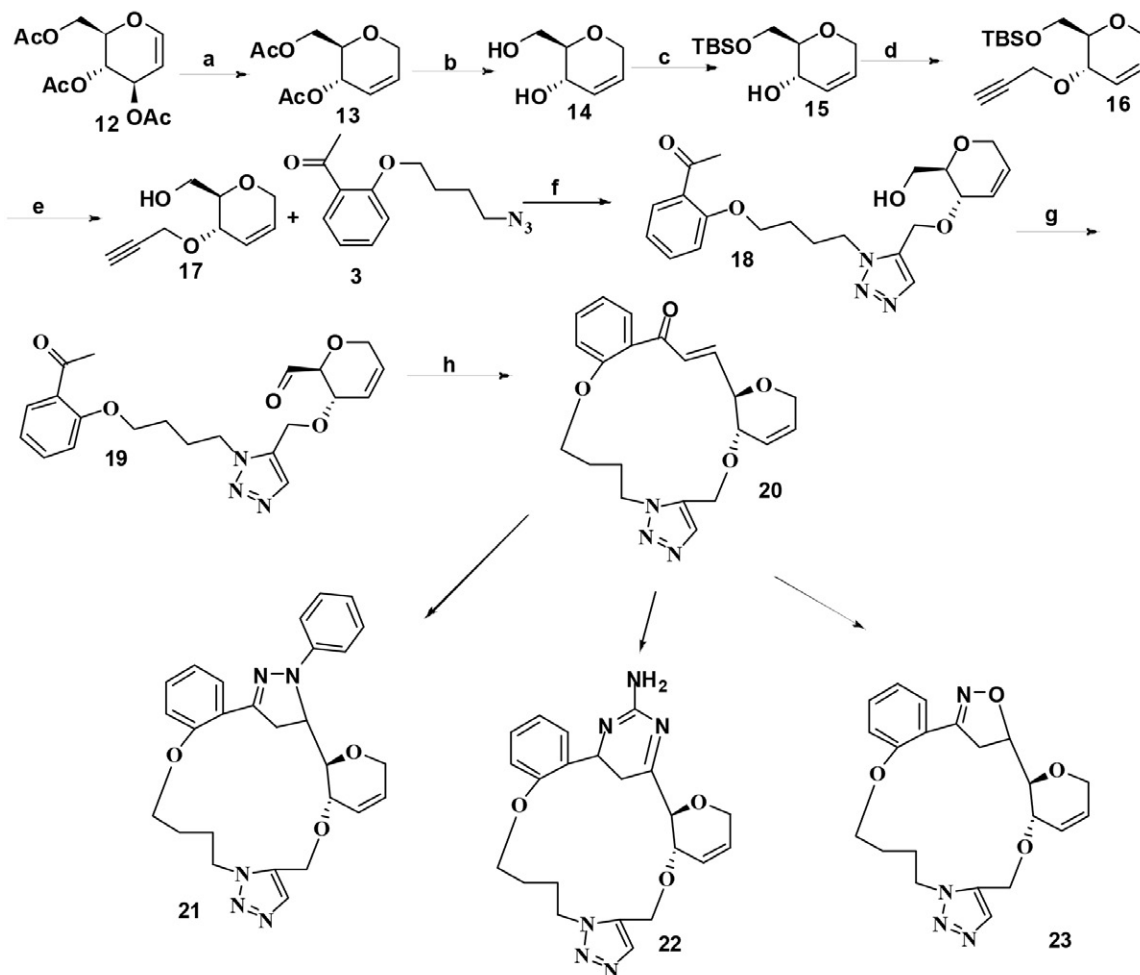
Commercial grade reagents were used as supplied, solvents (except those of analytical reagent grade) were dried and purified according to the literature when necessary. Reaction progress and purity of the compounds were checked by thin-layer chromatography (TLC) on pre-coated silica gel F254 plates from Merck and compounds were visualized either by exposure to UV light or by dipping in 1% aqueous potassium permanganate solution. Silica gel chromatographic columns (60–120 mesh) were used for the separations. By using Perkin–Elmer 141 polarimeter



**Scheme 1**

**Reagents and conditions:** (a) 1,4-dibromobutane,  $\text{K}_2\text{CO}_3$ , DMF; (b)  $\text{NaN}_3$ ; (c) sodium ascorbate,  $\text{CuSO}_4 \cdot 5\text{H}_2\text{O}$ ,  $\text{H}_2\text{O}$ ,  $\text{CH}_2\text{Cl}_2$ ; (d) 60% ACOH; (e)  $\text{NaIO}_4$ ,  $\text{CH}_2\text{Cl}_2$ ; (f)  $\text{KOH}$ ; (g)  $\text{NH}_2\text{OH} \cdot \text{HCl}$ ,  $\text{NaOAc}$ ,  $\text{AcOH}$ ; (h) guanidine hydrochloride; (i)  $\text{PhNHNH}_2$ ,  $\text{NaOAc}$ ,  $\text{AcOH}$ .





Scheme 2

**Reagents and conditions:** (a)  $\text{Et}_3\text{Si}$ ,  $\text{BF}_3$ , DMF; (b) NaOMe; (c) TBDMSCl,  $\text{Et}_3\text{N}$ , imidazole; (d) propargyl bromide,  $n\text{-Bu}_4\text{NHSO}_4$ ; (e) TBAF, THF; (f) sodium ascorbate,  $\text{CuSO}_4 \cdot 5\text{H}_2\text{O}$ ,  $\text{H}_2\text{O}$ ,  $\text{CH}_2\text{Cl}_2$ ; (g) IBX,  $\text{CH}_2\text{Cl}_2$ ; (h) KOH; (i)  $\text{PhNHNH}_2$ , NaOAc, AcOH; (j) guanidine hydrochloride; (k)  $\text{NH}_2\text{OH} \cdot \text{HCl}$ , NaOAc, AcOH.

optical rotations were measured on a 2 mL cell with a path length of 1 dm with  $\text{CHCl}_3$  or  $\text{CDCl}_3$  as the solvent. By using Fisher–Johns apparatus all melting points were measured and are uncorrected. IR spectra were recorded as KBr disks on a Perkin–Elmer FT IR spectrometer. The  $^1\text{H}$  NMR and  $^{13}\text{C}$  NMR spectra were recorded on a Varian Gemini spectrometer (300 MHz for  $^1\text{H}$  and 75 MHz for  $^{13}\text{C}$ ). Chemical shifts are reported as  $\delta$  ppm against TMS as the internal reference and coupling constants ( $J$ ) are reported in Hz units. Mass spectra were recorded on a VG micro mass 7070H spectrometer. Elemental analysis (C, H, N) were determined by a Perkin–Elmer 240 CHN elemental analyzer and were within  $\pm 0.4\%$  of theoretical values.

### 1-(2-(4-Bromobutoxy)phenyl)ethanone (2)

2-Hydroxyacetophenone (1.2 g, 8.8 mmol), a catalytic amount of potassium carbonate and 1,4-dibromobutane (1.9 g, 8.8 mmol) were stirred in DMF at  $0^\circ\text{C}$  to room temperature for 8 h, the reaction mixture was

quenched with  $\text{NH}_4\text{Cl}$ , thereafter the reaction mixture was concentrated under reduced pressure, the product was extracted with ethyl acetate, washed with brine and dried over sodium sulphate and purified by column chromatography (60–120 mesh, 12% ethyl acetate in hexane) to give compound **2** (2 g, 7.3 mmol, 84%). Mp  $189^\circ\text{C}$ .  $^1\text{H}$  NMR (300 MHz,  $\text{CDCl}_3$ ):  $\delta$  7.37–7.42 (m, 2H, Ar-H), 7.10–7.12 (m, 2H, Ar-H), 4.09 (m, 2H,  $\text{CH}_2$ ), 3.50 (m, 2H,  $\text{CH}_2$ ), 2.56 (s, 3H,  $\text{CH}_3$ ), 1.90–1.62 (m, 4H,  $\text{CH}_2$ );  $^{13}\text{C}$  NMR (75 MHz,  $\text{CDCl}_3$ ):  $\delta$  196.0, 162.1, 134.0, 122.5, 120.2, 117.9, 68.4, 30.5, 29.5, 29.1; MS:  $m/z$  ( $\text{M}^+\text{H}$ ) 271. Anal. Calcd for  $\text{C}_{12}\text{H}_{15}\text{BrO}_2$ : C, 53.15; H, 5.58; Found: C, 52.98; H, 5.45.

### 1-(2-(4-(5-(((3a*R*,5*R*,6*R*,6a*R*)-5-((*S*)-2,2-Dimethyl-1,3-dioxolan-4-yl)-2,2-dimethyltetrahydrofuro[2,3-*d*][1,3]dioxol-6-yloxy)methyl)-1*H*-1,2,3-triazol-1-yl)butoxy)phenyl)ethanone (5)

The compound **2** (1.90 g, 6.9 mmol) and sodium azide (0.500 g, 7.6 mmol) was stirred in methanol at reflux

temperature for 6 h, the reaction mixture was concentrated under reduced pressure, the product extracted with ethyl acetate and evaporated to give **3** (1.50 g) in quantitative yield as a yellow coloured liquid, which was used for the next reaction.

To the solution containing alkyne **4** (1.45 g, 4.8 mmol), azide **3** (1.50 g, 6.4 mmol) in dichloromethane (10 mL) and water (10 mL) were added  $\text{CuSO}_4 \cdot 5\text{H}_2\text{O}$  (0.110 g) and sodium ascorbate (0.114 g); the resulting suspension was stirred at room temperature for about 6 h, the mixture was diluted with 5 mL dichloromethane and 5 mL water. The organic phase was separated, washed with brine, dried over sodium sulphate and concentrated under reduced pressure; the crude product thus obtained was purified by column chromatography on silica gel (60–120 mesh, hexane/EtOAc 65:35) to afford **5** (3.290 g, 6.1 mmol, 76%) as a white powder. Mp 249 °C.  $^1\text{H}$  NMR (300 MHz,  $\text{CDCl}_3$ ):  $\delta$  8.04 (s, 1H, Ar-H), 7.32–7.10 (m, 4H, ArH), 5.56 (d,  $J = 3.7$  Hz, 1H,  $\text{C}_1\text{H}$ ), 4.63 (m, 1H,  $\text{C}_2\text{H}$ ), 4.59 (s, 2H,  $\text{CH}_2$ ), 4.41 (dd,  $J_1 = 3.1$  Hz,  $J_2 = 7.3$  Hz, 1H,  $\text{C}_5\text{H}$ ), 4.19–4.13 (m, 4H,  $\text{CH}_2$ ), 4.09–3.96 (m, 3H,  $\text{C}_4\text{H}$ ,  $2 \times \text{C}_6\text{H}$ ), 3.75 (dd,  $J_1 = 8.8$  Hz,  $J_2 = 4.1$  Hz, 1H,  $\text{C}_3\text{H}$ ), 2.52 (s, 3H,  $\text{CH}_3$ ), 1.78–1.75 (m, 4H,  $2 \times \text{CH}_2$ ), 1.51 (s, 3H,  $\text{CH}_3$ ), 1.40 (s, 3H,  $\text{CH}_3$ ), 1.36 (s, 6H,  $2 \times \text{CH}_3$ );  $^{13}\text{C}$  NMR (75 MHz,  $\text{CDCl}_3$ ):  $\delta$  196.0, 162.0, 142.4, 135.8, 129.4, 120.4, 117.9, 110.2, 106.2, 82.6, 79.4, 73.9, 68.6, 67.8, 65.1, 41.6, 27.5, 26.4, 25.4; MS:  $m/z$  ( $\text{M}^+\text{H}$ ) 532. Anal. Calcd for  $\text{C}_{27}\text{H}_{37}\text{N}_3\text{O}_8$ : C, 61.00; H, 7.02; N, 7.90; Found: C, 60.69; H, 6.95; N, 7.66.

**1-(2-(4-(5-(((3aR,5R,6R,6aR)-5-((S)-1,2-Dihydroxyethyl)-2,2-dimethyltetrahydrofuro[2,3-d][1,3]dioxol-6-yl)oxy)methyl)-1H-1,2,3-triazol-1-yl)butoxy)phenyl)ethanone (6)**

A mixture of **5** (3 g, 5.6 mmol) in 60% aq. AcOH (25 mL) was stirred at room temperature for 12 h. Reaction mixture was neutralized with anhydrous  $\text{NaHCO}_3$  (15 g) and extracted with EtOAc ( $3 \times 40$  mL). The combined organic layers were dried ( $\text{Na}_2\text{SO}_4$ ), evaporated and the residue was purified by column chromatography (60–120 mesh silica gel, 40% ethyl acetate in petroleum ether) to afford **6** (2.6 g, 5.2 mmol, 92%) as a pale yellow solid. Mp 256 °C.  $^1\text{H}$  NMR (300 MHz,  $\text{CDCl}_3$ ):  $\delta$  8.09 (s, 1H, Ar-H), 7.36–7.20 (m, 4H, ArH), 5.46 (d,  $J = 3.7$  Hz, 1H,  $\text{C}_1\text{H}$ ), 4.43 (m, 1H,  $\text{C}_2\text{H}$ ), 4.39 (s, 2H,  $\text{CH}_2$ ), 4.31 (d,  $J = 3.1$  Hz, 1H,  $\text{C}_5\text{H}$ ), 4.18–4.12 (m, 4H,  $\text{CH}_2$ ), 4.06–3.99 (m, 3H,  $\text{C}_4\text{H}$ ,  $2 \times \text{C}_6\text{H}$ ), 3.65 (dd,  $J_1 = 8.8$  Hz,  $J_2 = 4.1$  Hz, 1H,  $\text{C}_3\text{H}$ ), 2.44 (brs, 1H, OH), 1.78–1.75 (m, 4H,  $2 \times \text{CH}_2$ ), 1.52 (brs, 1H, OH), 1.41 (s, 3H,  $\text{CH}_3$ ), 1.30 (s, 3H,  $\text{CH}_3$ ), 1.26 (s, 3H,  $\text{CH}_3$ );  $^{13}\text{C}$  NMR (75 MHz,  $\text{CDCl}_3$ ):  $\delta$  196.5, 161.5, 142.4, 133.6, 127.9, 120.2, 117.9, 108.2, 98.6, 81.9, 79.6, 70.6, 47.4, 26.4, 25.1, 20.9; MS:  $m/z$  ( $\text{M}^+\text{Na}$ ) 514. Anal. Calcd for  $\text{C}_{24}\text{H}_{33}\text{N}_3\text{O}_8$ : C, 58.64; H, 6.77; N, 8.55; Found: C, 58.39; H, 6.55; N, 8.36.

**(5aS,9aR,Z)-8,9a,18,19,20,21-Hexahydro-4H-benzo[*l*]**

**pyrano[2,3-*o*][1,2,3]triazolo[5,1-*c*][1,9,4]dioxazacyclohexadecin-12(5aH)-one (8)**

To the solution of diol **6** (2.4 g, 4.88 mmol) in  $\text{CH}_2\text{Cl}_2$  (5 mL),  $\text{NaIO}_4$  (0.530 g, 2.48 mmol) was added at 0 °C and stirred at room temperature for about 6 h. The reaction mixture was filtered and washed with  $\text{CH}_2\text{Cl}_2$  ( $2 \times 10$  mL), dried over  $\text{Na}_2\text{SO}_4$  and evaporated to give keto aldehyde **7** (2 g) in quantitative yield as a yellow liquid, which was used for the next reaction.

The reaction mixture of keto aldehyde and KOH in methanol was stirred at reflux temperature for about 6 h, the methanol was then removed from the reaction mixture, the product was extracted with ethyl acetate and washed with brine, dried over sodium sulphate, evaporated and the residue was purified by column chromatography (60–120 mesh silica gel, 40% ethyl acetate in petroleum ether) to afford **8** (1.6 g, 3.62 mmol, 92%) as a pale yellow solid. Mp 226 °C.  $^1\text{H}$  NMR (300 MHz,  $\text{CDCl}_3$ ):  $\delta$  8.12 (s, 1H, Ar-H), 8.10–7.56 (m, 4H, Ar-H), 7.12 (d,  $J = 6.2$  Hz, 1H, =CH), 6.52 (d,  $J = 6.6$  Hz, 1H, =CH), 5.58 (d,  $J = 3.7$  Hz, 1H,  $\text{C}_1\text{H}$ ), 4.04–3.98 (m, 1H,  $\text{C}_4\text{H}$ ), 4.63 (m, 1H,  $\text{C}_2\text{H}$ ), 4.60 (s, 2H,  $\text{CH}_2$ ), 4.41 (d,  $J = 3.1$  Hz, 1H,  $\text{C}_5\text{H}$ ), 3.96–3.92 (m, 4H,  $\text{CH}_2$ ), 3.62 (dd,  $J_1 = 8.8$  Hz,  $J_2 = 4.1$  Hz, 1H,  $\text{C}_3\text{H}$ ), 1.75–1.72 (m, 4H,  $2 \times \text{CH}_2$ ), 1.24 (s, 6H,  $2 \times \text{CH}_3$ );  $^{13}\text{C}$  NMR (75 MHz,  $\text{CDCl}_3$ ):  $\delta$  187.5, 158.2, 146.0, 142.5, 136.7, 131.5, 128.9, 125.6, 120.9, 119.6, 114.6, 119.6, 103.4, 83.6, 73.0, 70.6, 66.9, 50.9, 26.4, 24.0; MS:  $m/z$  ( $\text{M}^+\text{H}$ ) 442. Anal. Calcd for  $\text{C}_{23}\text{H}_{27}\text{N}_3\text{O}_6$ : C, 62.57; H, 6.16; N, 9.52; Found: C, 62.39; H, 5.95; N, 9.26.

**(3<sup>3a</sup>R,3<sup>5</sup>S,3<sup>6</sup>R,3<sup>6a</sup>R)-3<sup>2</sup>,3<sup>2</sup>-Dimethyl-2<sup>4</sup>,2<sup>5</sup>,3<sup>3a</sup>,3<sup>5</sup>,3<sup>6</sup>,3<sup>6a</sup>-hexahydro-6<sup>1</sup>H-4,11-dioxa-2(3,5)-isoxazola-6(5,1)-triazola-3(5,6)-furo[2,3-*d*][1,3]-dioxola-1(1,2)benzenacycloundecaphane (9)**

A mixture of compound **8** (0.050 g, 0.113 mmol), hydroxylamine hydrochloride (0.020 g, 0.28 mmol) and sodium acetate (0.010 g, 0.12 mmol) in anhydrous glacial acetic acid (20 mL) was refluxed for 8 h. The reaction mixture was concentrated *in vacuo* and then poured into ice cold water, the solid thus separated was filtered off, washed with water and crystallized from ethanol to afford pure **10** (0.035 g, 0.07 mmol, 67%) as a brown solid. Mp 276 °C.  $^1\text{H}$  NMR (300 MHz,  $\text{CDCl}_3$ ):  $\delta$  8.04 (s, 1H, Ar-H), 7.62–7.49 (m, 4H, Ar-H), 5.42 (d,  $J = 3.7$  Hz, 1H,  $\text{C}_1\text{H}$ ), 4.69 (s, 2H,  $\text{CH}_2$ ), 4.60 (m, 1H,  $\text{C}_2\text{H}$ ), 4.41 (dd,  $J_1 = 3.1$  Hz,  $J_2 = 7.3$  Hz, 1H,  $\text{C}_4\text{H}$ ), 3.93–3.88 (m, 4H,  $\text{CH}_2$ ), 3.60 (dd,  $J_1 = 8.9$  Hz,  $J_2 = 4.1$  Hz, 1H,  $\text{C}_3\text{H}$ ), 3.59–3.55 (m, 1H, CH), 3.04 (m, 2H,  $\text{CH}_2$ ), 1.93–1.78 (m, 4H,  $2 \times \text{CH}_2$ ), 1.26 (s, 6H,  $2 \times \text{CH}_3$ );  $^{13}\text{C}$  NMR (75 MHz,  $\text{CDCl}_3$ ):  $\delta$  156.4, 142.5, 131.9, 128.9, 121.4, 117.8, 114.6, 111.6, 107.1, 83.6, 82.6, 81.6, 72.9, 66.5, 63.2, 50.6, 36.9, 26.9, 23.9. MS:  $m/z$  ( $\text{M}^+\text{H}$ ) 457. Anal. Calcd for  $\text{C}_{23}\text{H}_{28}\text{N}_4\text{O}_6$ : C, 60.52; H, 6.18; N, 12.27; Found: C, 59.99; H, 5.97; N, 12.01.

**(2<sup>4</sup>R,3<sup>a</sup>R,3<sup>5</sup>R,3<sup>6</sup>R,3<sup>6a</sup>R)-3<sup>2</sup>,3<sup>2</sup>-Dimethyl-2<sup>4</sup>,2<sup>5</sup>,3<sup>3a</sup>,3<sup>5</sup>,3<sup>6</sup>,3<sup>6a</sup>-hexahydro-6<sup>1</sup>H-4,11-dioxa-2(4,6)-pyrimi-**

**dana-6(5,1)-triazola-3(5,6)-furo[2,3-*d*][1,3]-dioxo-*la*-1(1,2)-benzenecycloundecaphane-2<sup>3</sup>-amine (10)**

To the solution of **8** (0.050 g, 0.113 mmol) and guanidine hydrochloride (0.029 g, 0.3 mmol) in ethanol (20 mL) was added aq. NaOH solution (5 mL). The reaction mixture was refluxed for about 6 h. Then it was poured in cold 10% HCl (50 mL) solution and the precipitate obtained was collected by filtration, washed with water until free from acid and recrystallized from toluene-ethanol (3:2) to give pure **10** as a brown solid (0.019 g, 0.04 mmol, 63%). Mp 266 °C. <sup>1</sup>H NMR (300 MHz, CDCl<sub>3</sub>): δ 8.02 (s, 1H, Ar-H), 7.12 (s, 2H, NH<sub>2</sub>), 6.94–7.10 (m, 4H, Ar-H), 5.49 (d, *J* = 3.7 Hz, 1H, C<sub>1</sub>H), 4.66 (s, 2H, CH<sub>2</sub>), 4.53 (m, 1H, C<sub>2</sub>H), 4.41 (m, 1H, C<sub>4</sub>H), 3.90–3.83 (m, 4H, 2×CH<sub>2</sub>), 3.62 (dd, *J*<sub>1</sub> = 3.1 Hz, *J*<sub>2</sub> = 7.3 Hz, 1H, C<sub>3</sub>H), 3.04 (m, 2H, CH<sub>2</sub>), 2.54 (m, 1H, CH), 1.78–1.90 (m, 4H, 2×CH<sub>2</sub>), 1.20 (s, 6H, 2×CH<sub>3</sub>); <sup>13</sup>C NMR (75 MHz, CDCl<sub>3</sub>): δ 164.5, 163.2, 154.5, 142.6, 128.9, 126.8, 120.4, 112.4, 105.9, 83.0, 77.6, 72.4, 65.8, 50.6, 43.6, 32.0, 27.0, 24.0; MS: *m/z* (M<sup>+</sup>+Na) 505. Anal. Calcd for C<sub>24</sub>H<sub>30</sub>N<sub>6</sub>O<sub>5</sub>: C, 59.74; H, 6.27; N, 17.42; Found: C, 59.59; H, 6.07; N, 17.01.

**(3<sup>3a</sup>R,3<sup>5</sup>R,3<sup>6</sup>R)-3<sup>2</sup>,3<sup>2</sup>-Dimethyl-2<sup>1</sup>-phenyl-2<sup>4</sup>,2<sup>5</sup>,3<sup>3a</sup>,3<sup>5</sup>,3<sup>6</sup>,3<sup>6a</sup>-hexahydro-2<sup>1</sup>H,6<sup>1H</sup>-4,11-dioxo-6(5,1)-triazola-2(3,5)-pyrazola-3(5,6)-furo-[2,3-*d*][1,3]-dioxo-*la*-1(1,2)-benzenecycloundecaphane (11)**

The mixture of compound **8** (0.050 g, 0.113 mmol), phenylhydrazine (0.025 g, 0.23 mmol) and anhydrous sodium acetate (0.012 g, 0.14 mmol) in glacial acetic acid (20 mL) was refluxed for about 7 h. The reaction mixture was concentrated *in vacuo* and cooled at room temperature, the solid thus separated was filtered off, then washed thoroughly with water, the unmilled product thus obtained was purified by column chromatography on silica gel with hexane-ethyl acetate as eluent to afford pure compound **11** (0.044 g, 0.08 mmol, 73%). Mp 276 °C. <sup>1</sup>H NMR (300 MHz, CDCl<sub>3</sub>): δ 8.09 (s, 1H, ArH), 7.25–7.10 (m, 5H, ArH), 6.95–7.14 (m, 4H, ArH), 5.40 (d, *J* = 3.7 Hz, 1H, C<sub>1</sub>H), 5.25 (d, *J* = 1.8 Hz, 1H, CHN), 4.54 (s, 2H, CH<sub>2</sub>), 4.50 (m, 1H, C<sub>2</sub>H), 4.38 (m, 1H, C<sub>4</sub>H), 3.90–3.85 (m, 4H, CH<sub>2</sub>), 3.59 (dd, *J*<sub>1</sub> = 3.1 Hz, *J*<sub>2</sub> = 7.3 Hz, 1H, C<sub>3</sub>H), 3.01 (m, 2H, CH<sub>2</sub>), 1.89–1.78 (m, 4H, 2×CH<sub>2</sub>), 1.24 (s, 6H, 2×CH<sub>3</sub>); <sup>13</sup>C NMR (75 MHz, CDCl<sub>3</sub>): δ 157.1, 151.5, 142.4, 131.5, 129.5, 128.6, 120.4, 116.9, 114.5, 112.0, 105.9, 85.0, 83.5, 82.3, 72.4, 66.5, 50.4, 48.1, 32.6, 27.1, 23.8; MS: *m/z* (M<sup>+</sup>+H) 532. Anal. Calcd for C<sub>29</sub>H<sub>33</sub>N<sub>5</sub>O<sub>5</sub>: C, 65.52; H, 6.26; N, 13.17; Found: C, 65.29; H, 5.97; N, 12.91.

**((2*R*,3*S*)-3-Acetoxy-3,6-dihydro-2*H*-pyran-2-yl)methyl Acetate (13)**

Tri-*O*-acetyl-D-glucal (**12**) (3.0 g, 11.0 mmol) was dissolved in anhydrous dichloromethane (5 mL), the solution was cooled to 0 °C, triethylsilane (1.53 g, 13.2 mmol) was added and the mixture was stirred for five minutes.

Boron trifluoride diethyl etherate (690 μL of a 40 w% solution in diethyl ether, 11.02 mmol) was added drop wise and the reaction mixture was stirred for 90 min. The mixture was poured into a saturated solution of NaHCO<sub>3</sub>. The organic layer was washed with water, dried over Na<sub>2</sub>SO<sub>4</sub> and concentrated under reduced pressure. Column chromatography on silica gel (PE/EtOAc, 3:1) yielded the title compound **13** (2.24 g, 10 mmol, 95%) as a colourless syrup. [α]<sub>D</sub><sup>20</sup>: +115.5 (*c* = 1.00, CHCl<sub>3</sub>). <sup>1</sup>H NMR (300 MHz, CDCl<sub>3</sub>): δ 5.87–5.84 (m, 2H, =CH), 4.95 (m, 1H, OCH), 4.03–3.99 (m, 1H, CH), 4.12–4.09 (m, 4H, OCH<sub>2</sub>), 2.20 (s, 6H, COCH<sub>3</sub>); <sup>13</sup>C NMR (75 MHz, CDCl<sub>3</sub>): δ 170.2, 127.2, 125.8, 73.6, 65.1, 64.0, 62.5, 21.1; MS: *m/z* (M<sup>+</sup>+H) 215. Anal. Calcd for C<sub>10</sub>H<sub>14</sub>O<sub>5</sub>: C, 56.07; H, 6.59; Found: C, 55.82; H, 6.35.

**(2*R*,3*S*)-2-((*tert*-Butyldimethylsilyloxy)methyl)-3,6-dihydro-2*H*-pyran-3-ol (15)**

At room temperature diacetate **13** (2.10 g, 9.8 mmol) was treated with a catalytic amount of sodium methoxide in methanol (100 mL). The free hydroxyl unsaturated glycoside was obtained after evaporation of the solvent in quantitative yield and used without further purification. This diol was treated with 2.50 equiv. of TBDMSCl (3.14 g, 20 mmol), 2.6 equiv. of NEt<sub>3</sub> (3.2 mL, 23 mmol), and 0.05 equiv. of imidazole (30 mg, 0.44 mmol) in CH<sub>2</sub>Cl<sub>2</sub> (30 mL) at room temperature for 24 h (until TLC analysis showed no more starting material). After addition of 25 mL of water and extraction with 3×30 mL of CH<sub>2</sub>Cl<sub>2</sub>, the organic layer was dried under reduced pressure. After evaporation of the solvent the residue was purified by column chromatography using petroleum ether/ethyl acetate as the eluent yielding the title compound **15** (1.94 g, 7.6 mmol, 85%) as a colourless syrup. <sup>1</sup>H NMR (300 MHz, CDCl<sub>3</sub>): δ 6.0–5.82 (m, 2H, =CH), 5.42 (d, *J* = 6.5 Hz, 1H, CH), 4.50 (brs, 1H, OH), 4.20–4.12 (m, 1H, CH), 3.91–3.80 (m, 4H, CH<sub>2</sub>), 0.98 (s, 9H, *t*-Bu), 0.24 (s, 6H, CH<sub>3</sub>); <sup>13</sup>C NMR (75 MHz, CDCl<sub>3</sub>): δ 127.5, 125.6, 84.6, 81.5, 73.6, 62.7, 25.6, 18.1; MS: *m/z* (M<sup>+</sup>+Na) 267. Anal. Calcd for C<sub>12</sub>H<sub>24</sub>O<sub>3</sub>Si: C, 58.97; H, 9.90; Found: C, 58.62; H, 9.75.

***tert*-Butyldimethyl(((2*R*,3*S*)-3-(prop-2-ynyloxy)-3,6-dihydro-2*H*-pyran-2yl)methoxy)silane (16)**

In toluene (1.6 mL) the solution of alcohol **14** (0.400 g, 1.63 mmol, 1.0 equiv.) was added, 35% aqueous solution of NaOH (1.6 mL), propargyl bromide (80% solution in toluene, 363 μL, 2.4 mmol, 1.5 equiv.), and *n*-Bu<sub>4</sub>N-HSO<sub>4</sub> (280 mg, 0.8 mmol, 0.5 equiv.) was added. After 6 h of vigorous stirring at room temperature, Et<sub>2</sub>NH (1.6 mL) was added. The reaction mixture was stirred for 1 h, poured into ice water, cautiously neutralized by addition of a 3M solution of hydrochloric acid, and extracted with EtOAc. The combined organic extracts were washed with brine, dried over MgSO<sub>4</sub>, filtered and concentrated under reduced pressure. The crude material was purified by flash

chromatography on silica gel (hexane/EtOAc 85:15) to afford propargyl ether as a colorless oil (0.345 g, 1.21 mmol, 75%). <sup>1</sup>H NMR (300 MHz, CDCl<sub>3</sub>): δ 6.03–5.80 (m, 2H, =CH), 4.69 (t, *J* = 3.9 Hz, 1H, CH), 3.68 (dd, *J*<sub>1</sub> = 8.9 Hz, *J*<sub>2</sub> = 4.1 Hz, 1H, OCH), 3.99–3.89 (m, 6H, CH<sub>2</sub>), 3.20 (s, 1H, CH), 0.96 (s, 9H, *t*-Bu), 0.23 (s, 6H, CH<sub>3</sub>); <sup>13</sup>C NMR (75 MHz, CDCl<sub>3</sub>): δ 127.2, 124.9, 78.0, 76.2, 74.2, 64.2, 63.2, 58.5, 25.3, 18.5; MS: *m/z* (M<sup>+</sup>+H) 283. Anal. Calcd for C<sub>15</sub>H<sub>26</sub>O<sub>3</sub>Si: C, 63.78; H, 9.28; Found: C, 63.62; H, 8.95.

**((2*R*,3*S*)-3-(Prop-2-ynoxy)-3,6-dihydro-2*H*-pyran-2-yl)methanol (17)**

In THF the stirred solution of **16** (0.325 g, 1.152 mmol), catalytic amount of TBAF was added and stirred the reaction mixture at room temperature for about 15 min, the product was extracted with ethyl acetate (20 mL). The combined organic extracts were washed with brine, dried over MgSO<sub>4</sub>, filtered, and concentrated *in vacuo*. The crude material was purified by flash chromatography on silica gel (60–120 mesh, hexane/EtOAc 70:30) to afford alcohol **17** as a yellow oil (0.285 g, 1.69 mol, 85%). <sup>1</sup>H NMR (300 MHz, CDCl<sub>3</sub>): δ 5.95–5.75 (m, 2H, =CH), 4.65 (d, *J* = 3.9 Hz, 1H, CH), 4.52 (brs, 1H, OH), 4.09–4.11 (m, 4H, OCH<sub>2</sub>), 3.64 (dd, *J*<sub>1</sub> = 4.1 Hz, *J*<sub>2</sub> = 8.9 Hz, 1H, OCH), 3.76 (d, *J* = 6.8 Hz, 2H, OCH<sub>2</sub>), 3.28 (s, 1H, CH); <sup>13</sup>C NMR (75 MHz, CDCl<sub>3</sub>): δ 127.2, 125.6, 78.3, 76.1, 74.1, 64.2, 61.4, 58.0; MS: *m/z* (M<sup>+</sup>+H) 169. Anal. Calcd for C<sub>9</sub>H<sub>12</sub>O<sub>3</sub>: C, 64.27; H, 7.10; Found: C, 64.02; H, 6.95.

**1-(2-(4-(5-(((2*R*,3*S*)-2-(Hydroxymethyl)-3,6-dihydro-2*H*-pyran-3-yloxy)methyl)-1*H*-1,2,3-triazol-1-yl)butoxy)phenyl)ethanone (18)**

To a solution containing alkyne **17** (0.250 g, 1.48 mmol), azide **3** (0.280 g, 1.20 mmol) in dichloromethane (10 mL) and water (10 mL) were added CuSO<sub>4</sub>·5H<sub>2</sub>O (0.110 g) and sodium ascorbate (0.114 g). The resulting suspension was stirred at room temperature for 6 h. After this time, the mixture was diluted with 5 mL dichloromethane and 5 mL water. The organic phase was separated, dried with sodium sulphate and concentrated at reduced pressure; the crude product thus obtained was purified by column chromatography on silica gel (60–120 mesh, hexane/EtOAc 60:40) to afford **18** (0.442 g, 1.10 mol, 77%) as a white powder. Mp 249–251 °C. <sup>1</sup>H NMR (300 MHz, CDCl<sub>3</sub>): δ 8.10 (s, 1H, Ar-H), 7.31–7.10 (m, 4H, ArH), 5.80–5.76 (m, 2H, =CH), 5.09 (brs, 1H, OH), 4.68 (s, 2H, CH<sub>2</sub>), 4.36–4.30 (m, 6H, CH<sub>2</sub>), 3.86 (m, 1H, CH), 3.58 (m, 2H, CH<sub>2</sub>), 3.28 (q, 1H, CH), 2.46 (s, 3H, CH<sub>3</sub>), 1.76–1.75 (m, 4H, CH<sub>2</sub>); <sup>13</sup>C NMR (75 MHz, CDCl<sub>3</sub>): δ 195.0, 165.2, 142.8, 134.8, 128.7, 127.8, 125.8, 120.2, 117.9, 78.6, 69.6, 64.8, 62.6, 47.9, 27.6, 26.8, 25.4; MS: *m/z* (M<sup>+</sup>+H) 402. Anal. Calcd for C<sub>21</sub>H<sub>27</sub>N<sub>3</sub>O<sub>5</sub>: C, 62.83; H, 6.78; N, 10.47; Found: C, 62.55; H, 6.57; N, 10.10.

**1-(2-(4-(5-(((2*R*,3*S*)-2-(Hydroxymethyl)-3,6-dihydro-2*H*-pyran-3-yloxy)methyl)-1*H*-1,2,3-triazol-1-yl)butoxy)phenyl)ethanone (20)**

In CH<sub>2</sub>Cl<sub>2</sub> (5 mL), IBX (0.100 g, 0.35 mmol) to a solution of keto alcohol **18** (0.400 g, 0.99 mmol) was added at 0 °C and stirred at room temperature for about 6 h. The reaction mixture was filtered and washed with CH<sub>2</sub>Cl<sub>2</sub> (2×10 mL). It was dried (Na<sub>2</sub>SO<sub>4</sub>) and evaporated to give keto aldehyde **19** (0.325 g) in quantitative yield as a yellow liquid, which was used as such for the next reaction.

The stirred reaction mixture of keto aldehyde **19** and NaOH (0.500 g, 12.5 mmol) in methanol (5 mL) was heated at reflux temperature for about 6 h, thereafter methanol was removed from the reaction mixture, the product was extracted with ethyl acetate and washed with brine, dried over sodium sulphate, volatile components were evaporated and the residue purified by column chromatography (60–120 mesh silica gel, 40% ethyl acetate in petroleum ether) to afford **20** (0.219 g, 0.57 mmol, 70.58%) as a pale yellow solid. Mp 269–271 °C. <sup>1</sup>H NMR (300 MHz, CDCl<sub>3</sub>): δ 8.09 (s, 1H, ArH), 7.36–7.18 (m, 4H, ArH), 7.12 (d, *J* = 3.2 Hz, 1H, =CH), 6.59 (d, *J* = 3.9 Hz, 1H, =CH), 5.87–5.84 (m, 2H, =CH), 4.68 (s, 2H, CH<sub>2</sub>), 3.99–3.95 (m, 4H, CH<sub>2</sub>), 3.87 (m, 2H, CH), 3.70 (m, 2H, CH<sub>2</sub>), 1.70–1.62 (m, 4H, CH<sub>2</sub>); <sup>13</sup>C NMR (75 MHz, CDCl<sub>3</sub>): δ 167.2, 157.6, 142.6, 140.6, 135.7, 131.6, 128.9, 126.4, 120.8, 115.2, 71.9, 67.6, 50.9, 24.1; MS: *m/z* (M<sup>+</sup>+H) 382. Anal. Calcd for C<sub>21</sub>H<sub>23</sub>N<sub>3</sub>O<sub>4</sub>: C, 66.13; H, 6.08; N, 11.02; Found: C, 65.89; H, 5.85; N, 10.86.

**(3<sup>2*R*</sup>,3<sup>3*S*</sup>)-Phenyl-2<sup>4</sup>,2<sup>5</sup>,3<sup>5</sup>,3<sup>6</sup>-tetrahydro-2<sup>1*H*</sup>,3<sup>2*H*</sup>,6<sup>1*H*</sup>-4,11-dioxo-6(5,1)-triazola-2(3,5)-pyrazola-3(2,3)-pyrane-1(1,2)-benzenacycloundecaphane (21)**

A mixture of compound **20** (0.200 g, 0.52 mmol), phenylhydrazine (0.100 g, 0.92 mmol) and anhydrous sodium acetate (0.100 g, 1.21 mmol) in glacial acetic acid (20 mL) was refluxed for 7 h. Then the reaction mixture was concentrated *in vacuo* and cooled at room temperature, the solid thus separated was filtered, washed thoroughly with water, the unprocessed product thus obtained was purified by column chromatography on silica gel with hexane–ethyl acetate as eluent to afford pure compound **21** (0.165 g, 0.33 mmol, 64%). Mp 219–221 °C. <sup>1</sup>H NMR (300 MHz, CDCl<sub>3</sub>): δ 8.16 (s, 1H, ArH), 7.67–7.49 (m, 4H, ArH), 7.28–7.24 (m, 5H, ArH), 5.80–5.72 (m, 2H, =CH), 4.69 (s, 2H, CH<sub>2</sub>), 3.99–3.94 (m, 6H, CH<sub>2</sub>), 3.84–3.80 (m, 2H, CH), 2.89 (m, 1H, CH), 1.84–1.78 (m, 6H, CH<sub>2</sub>); <sup>13</sup>C NMR (75 MHz, CDCl<sub>3</sub>): δ 157.8, 151.6, 142.6, 131.7, 129.9, 128.7, 126.1, 120.2, 117.6, 116.8, 115.6, 85.4, 74.1, 72.6, 66.1, 64.7, 51.2, 47.6, 32.6, 23.9; MS: *m/z* (M<sup>+</sup>+Na) 494. Anal. Calcd for C<sub>27</sub>H<sub>29</sub>N<sub>5</sub>O<sub>3</sub>: C, 68.77; H, 6.20; N, 14.85; Found: C, 68.59; H, 5.97; N, 14.51.

**(3<sup>2*R*</sup>-3<sup>3*S*</sup>)-2<sup>4</sup>,2<sup>5</sup>,3<sup>3</sup>,3<sup>6</sup>-Tetrahydro-3<sup>2*H*</sup>,6<sup>1*H*</sup>-4,11-dioxo-2(4,6)-pyrimidina-6(5,1)-triazola-3(2,3)-pyrana-1(1,2)-benzenacycloundecaphane-2-amine (22)**

To aq. NaOH (0.020 g, 0.5 mmol) solution (5 mL) the solution of **20** (0.050 g, 0.13 mmol) and guanidine hydrochloride (0.030 g, 0.31 mmol) in ethanol (20 mL) was added. The reaction mixture was refluxed, TLC (EtOAc : petroleum ether, 2:1) showed that the reaction was completed after 6 h. Then it was poured in cold 10% HCl (50 mL) solution and the obtained precipitate was collected by filtration, washed with water until free from acid and recrystallized from toluene-ethanol (3:2) to give pure **22** as a brown solid (0.039 g, 0.08 mmol, 68%). Mp 279–281 °C. <sup>1</sup>H NMR (300 MHz, CDCl<sub>3</sub>): δ 7.09 (brs, 2H, NH<sub>2</sub>), 8.02 (s, 1H, ArH), 7.10–6.88 (m, 4H, ArH), 5.82–5.74 (m, 2H, =CH), 4.69 (s, 2H, CH<sub>2</sub>), 4.09–3.94 (m, 6H, CH<sub>2</sub>), 3.74–3.70 (m, 2H, CH), 2.74 (m, 1H, CH), 1.78–1.74 (m, 4H, CH<sub>2</sub>), 1.54 (m, 2H, CH<sub>2</sub>); <sup>13</sup>C NMR (75 MHz, CDCl<sub>3</sub>): δ 164.9, 165.0, 154.9, 142.6, 128.4, 126.7, 120.4, 112.6, 81.6, 72.6, 66.7, 65.4, 50.9, 43.9, 31.6, 23.9; MS: *m/z* (M<sup>+</sup>+Na) 445. Anal. Calcd for C<sub>22</sub>H<sub>26</sub>N<sub>6</sub>O<sub>3</sub>: C, 62.54; H, 6.20; N, 19.89; Found: C, 62.29; H, 6.01; N, 19.61.

**(3<sup>2</sup>S,3<sup>3</sup>S)-2<sup>4</sup>,2<sup>5</sup>,3<sup>3</sup>,3<sup>6</sup>-Tetrahydro-3<sup>2</sup>H,6<sup>1</sup>H-4,11-dioxo-2(3,5)-isoxozola-6(5,1)-triazola-3(2,3)-pyrana-1(1,2)-benzacyclodecaphane (23)**

Mixture of compound **20** (0.050 g, 0.13 mmol), hydroxylamine hydrochloride (0.050 g, 0.71 mmol) and sodium acetate (0.010 g, 0.12 mmol) in anhydrous glacial acetic acid (20 mL) was refluxed for about 8 h. The reaction mixture was concentrated *in vacuo* and then poured into ice cold water, the solid thus separated was filtered off and washed with water and crystallized from ethanol to afford pure **23** (0.031 g, 0.08 mmol, 61%) as a brown solid. Mp 279–282 °C. <sup>1</sup>H NMR (300 MHz, CDCl<sub>3</sub>): δ 8.14 (s, 1H, ArH), 7.67–6.98 (m, 4H, ArH), 5.64–5.55 (m, 2H, =CH), 4.68 (s, 2H, CH<sub>2</sub>), 4.09–3.96 (m, 6H, CH<sub>2</sub>), 3.5 (m, 1H, CH), 3.87–3.85 (m, 2H, CH), 3.04 (m, 2H, CH<sub>2</sub>), 1.79–1.66 (m, 4H, CH<sub>2</sub>); <sup>13</sup>C NMR (75 MHz, CDCl<sub>3</sub>): δ 157.8, 156.4, 142.9, 131.7, 129.6, 128.4, 125.4, 120.6, 117.6, 114.6, 82.6, 72.6, 65.4, 64.2, 63.2, 50.8, 35.9, 23.9; MS: *m/z* (M<sup>+</sup>+H) 397. Anal. Calcd for C<sub>21</sub>H<sub>24</sub>N<sub>4</sub>O<sub>4</sub>: C, 63.62; H, 6.10; N, 14.13; Found: C, 63.39; H, 5.87; N, 13.91.

## 5. Conclusions

A series of novel furanose and pyranose macrocyclic enone heterocycles was prepared and evaluated for their anticancer activity. Among the tested compounds **9** and **23** showed the most potent activity against MCF-7 cell line with IC<sub>50</sub> value of 1.82 and 1.90 μM, whereas **10**, **11**, **21** and **22** showed promising activity against MDA-MB-231 and HeLa cell lines.

## Acknowledgements

The authors are thankful to CSIR-New Delhi for the financial support (Project funding No 02/247/15/EMR-II),

Director, CSIR- IICT, Hyderabad, India, for NMR and MS spectral analysis and Shanthy Research foundation for their moral support.

## 6. Reference

- (a) A. Farran, C. Cai, M. Sandoval, *Chem. Rev.* **2015**, *115*, 6811–6853. DOI:10.1021/cr500719h  
(b) A. Varki, *Glycobiology* **1993**, *3*, 97–130. DOI:10.1093/glycob/3.2.97
- N. Galonde, K. Nott, A. Debuigne, *J. Chem. Tech. Biotechnol.* **2012**, *87*, 451–471. DOI:10.1002/jctb.3745
- (a) M. E. Caines, H. Zhu, M. Vuckovic, *J. Bio. Chem.* **2008**, *283*, 31279–31283. DOI:10.1074/jbc.C800150200  
(b) H. Shirato, S. Ogawa, H. Ito, *J. Virol.* **2008**, *82*, 10756–10767. DOI:10.1128/JVI.00802-08  
(c) S. Nagaraj, K. Gupta, V. Pisarev, *Nat. Med.* **2007**, *13*, 828–835. DOI:10.1038/nm1609
- (a) C. R. Bertozzi, L. L. Kiessling, *Chem. Glyc. Bio. Sci.* **2001**, *291*, 2357–2364. DOI:10.1126/science.1059820  
(b) T. Angata, A. Varki, *Chem. Rev.* **2002**, *102*, 439–470. DOI:10.1021/cr000407m
- (a) V. K. Tiwari, R. C. Mishra, A. Sharma, R. P. Tripathi, *Mini Rev. Med. Chem.* **2012**, *12*, 1497–1519. DOI:10.2174/138955712803832654  
(b) V. K. Tiwari, B. B. Mishra, K. B. Mishra, N. Mishra, A. S. Singh, Chen, *Chem. Rev.* **2016**, *116*, 3086–3240. DOI:10.1021/acs.chemrev.5b00408  
(c) K. B. Mishra, B. B. Mishra, V. K. Tiwari, *Carbohydr. Res.* **2014**, *399*, 2–7. DOI:10.1016/j.carres.2014.09.001  
(d) D. Kumar, K. B. Mishra, B. B. Mishra, V. K. Tiwari, *Steroids* **2014**, *80*, 71–79. DOI:10.1016/j.steroids.2013.11.022
- R. Huisgen, G. Szeimies, L. Moebius, *Chem. Ber.* **1967**, *100*, 2494–2507. DOI:10.1002/cber.19671000806
- (a) F. G. Heras, R. Alonso, G. Alonso, *J. Med. Chem.* **1979**, *22*, 491–496. DOI:10.1021/jm00191a007  
(b) J. C. Morris, J. Chiche, C. Grellier, *J. Med. Chem.* **2011**, *54*, 6905–6918. DOI:10.1021/jm200892s
- (a) V. Balzani, A. Credi, F. M. Raymo, J. F. Stoddart, *Angew. Chem. Int. Ed.* **2000**, *39*, 3349–3391. DOI:10.1002/1521-3773(20001002)39:19<3348::AID-ANIE3348>3.0.CO;2-X  
(b) C. P. Collier, G. Mattersteig, E. W. Wong, Y. Luo, K. Beverley, J. Sampaio, F. M. Raymo, J. F. Stoddart, J. R. Heath, *Science* **2000**, *289*, 1172–1175. DOI:10.1126/science.289.5482.1172
- (a) E. M. Driggers, S. P. Hale, J. Lee, N. K. Terrett, *Nat. Rev. Drug. Discov.* **2008**, *7*, 608–624. DOI:10.1038/nrd2590  
(b) D. B. Amabilino, J. F. Stoddart, *Chem. Rev.* **1995**, *95*, 2725–2828. DOI:10.1021/cr00040a005  
(c) G. R. Pettit, Y. Kamano, C. L. Herald, *J. Nat. Prod.* **1986**, *49*, 661–664. DOI:10.1021/np50046a017
- P. Corvalin, *Antimicrob. Agents Chemother.* **1990**, *34*, 2291–2296. DOI:10.1128/AAC.34.12.2291
- (a) J. A. Wells, L. McClendon, *Nature* **2007**, *450*, 1001–1009. DOI:10.1038/nature06526

- (b) K. Ahsanullah, J. Rademann, *Angew. Chem. Int. Ed.* **2010**, *49*, 5378–5380. DOI:10.1021/jo2018203
12. (a) P. T. Quinn, P. D. Atwood, J. M. Tanski, T. F. Moore, F. Andersen, *J. Org. Chem.* **2011**, *76*, 10020–10030. (b) C. Nunez, A. Aldrey, V. García, R. Bastida, A. Macías, C. Lodeiro, *Inorg. Chim. Acta.* **2012**, *381*, 85–94. DOI:10.1016/j.ica.2011.05.031
13. (a) S. Camiolo, P. A. Gale, M. B. Hursthouse, M. E. Light, *Org. Biomol. Chem.* **2003**, *1*, 741–744. (b) C. Bazzicalupi, A. Bencini, I. Matera, S. Puccioni, B. Valtancoli, *Inorg. Chim. Acta* **2012**, *381*, 162–169. DOI:10.1016/j.ica.2011.08.057
14. (a) C. W. Tornøe, C. Christensen, M. Meldal, *J. Org. Chem.* **2002**, *67*, 3057–3064. DOI:10.1021/jo011148j  
(b) M. Meldal, C. W. Tornøe, *Chem. Rev.* **2008**, *108*, 2952–3015. DOI:10.1021/cr0783479
15. (a) Y. Hua, A. H. Flood, *Chem. Soc. Rev.* **2010**, *39*, 1262–1271. DOI:10.1039/b818033b  
(b) Y. Li, A. H. Flood, *Angew. Chem. Int. Ed.* **2008**, *47*, 2649–2652. DOI:10.1002/anie.200704717
16. (a) H. C. Kolb, K. B. Sharpless, *Drug Discovery Today* **2003**, *8*, 1128–1137. DOI:10.1016/S1359-6446(03)02933-7  
(b) J. Campbell, H. E. Blackwell, *J. Comb. Chem.* **2009**, *11*, 1094–1099. DOI:10.1021/cc900115x
17. J. T. Desai, C. K. Desai, K. R. Desai, *J. Iran. Chem. Soc.* **2008**, *5*, 67–73. DOI:10.1007/BF03245817
18. D. Milicevic, R. Kimmel, D. Urankar, A. Pevec, J. Košmrlj, S. Kafka, *Acta Chim. Slov.* **2020**, *67*, 421–434.
19. A. R. Aghakand, K. A. Dilmaghani, Z. D. Ghezlbash, B. Asghari, *Acta Chim. Slov.* **2019**, *66*, 344–350. DOI:10.17344/acsi.2018.4841
20. S. A. M. K. Nasser, *Carbohydr. Res.* **2006**, *341*, 2187–2199. DOI:10.1016/j.carres.2006.06.007
21. Y. C. Sung, H. A. Jin, D. H. Jae, K. K. Seung, Y. B. Ji, S. H. Sang, Y. S. Eun, S. K. Sang, R. K. Kwang, G. C. Hyae, K. C. Joong, *Bull. Kor. Chem. Soc.* **2003**, *24*, 1455–1459.
22. Y. S. Lee, S. M. Park, B. H. Kim, *Bioorg. Med. Chem. Lett.* **2009**, *19*, 1126–1128.
23. J. F. Hansen, S. A. Stronge, *J. Heterocycl. Chem.* **1977**, *14*, 1289–1294. DOI:10.1002/jhet.5570140734
24. T. K. Adhikari, A. Vasudeva, M. Girisha, *Indian J. Chem.* **2009**, *48B*, 430–437.
25. S. Balalie, A. Sharifi, A. Ahangarian, *Indian J. Heterocycl. Chem.* **2000**, *10*, 149–154.
26. H. Kai, T. Ichiba, M. Tomida, H. Nakai, K. Morita, *J. Pest. Sci.* **2000**, *25*, 267–273. DOI:10.1584/jpestics.25.267
27. V. V. Kachadia, M. R. Patel, S. H. Joshi, *J. Sci. I. R. Iran* **2004**, *15*, 47–52.
28. M. Marcin, Z. Machail, D. S. Eva, R. Stanislaw, *Cell. Mol. Biol. Lett.* **2005**, *10*, 613–619.
29. N. R. Nagar, V. H. Shan, *Indian J. Heterocycl. Chem.* **2003**, *13*, 173–179.
30. A. Srinivas, M. Sunitha, P. Karthik, G. Nikitha, K. Raju, B. Ravinder, S. Anusha, T. Rajasri, D. Swapna, D. Swaroopa, K. Srinivas, K. Vasumathi Reddy, *J. Heterocycl. Chem.* **2017**, *54*, 3250–3257. DOI:10.1002/jhet.2943
31. A. Srinivas, *Acta Chim. Slov.* **2016**, *63*, 173–179.
32. A. Srinivas, M. Sunitha, *Indian J. Chem. Sect. B* **2016**, *55B*, 102–109.
33. A. Srinivas, M. Sunitha, *Indian J. Chem. Sect. B* **2016**, *55B*, 1239–1242.
34. C. S. Reddy, A. Srinivas, M. Sunitha, A. Nagaraj, *J. Heterocycl. Chem.* **2010**, *47*, 1303–1309. DOI:10.1002/jhet.474
35. A. Srinivas, C. S. Reddy, A. Nagaraj, *Chem. Pharm. Bull.* **2009**, *57*, 685–693.
36. C. S. Reddy, A. Srinivas, A. Nagaraj, *J. Heterocycl. Chem.* **2009**, *46*, 497–502. DOI:10.1002/jhet.100
37. C. S. Reddy, A. Srinivas, A. Nagaraj, *J. Heterocycl. Chem.* **2008**, *45*, 1121–1125. DOI:10.1002/jhet.5570450428
38. C. S. Reddy, A. Srinivas, A. Nagaraj, *J. Heterocycl. Chem.* **2008**, *45*, 999–1003. DOI:10.1002/jhet.5570450409
39. K. Y. Lee, J. M. Kim, J. N. Kim, *Tetrahedron Lett.* **2003**, *44*, 6737–6740. DOI:10.1016/S0040-4039(03)01648-4
40. P. Erhan, A. Mutlu, U. Tayfun, E. Dilek, *Eur. J. Med. Chem.* **2001**, *36*, 539–543. DOI:10.1016/S0223-5234(01)01243-0
41. R. A. Nugen, M. Meghan, *J. Med. Chem.* **1993**, *36*, 134–139.
42. H. Kawazura, Y. Takahashi, Y. Shiga, F. Shimada, N. Ohto, A. Tamura, *Jpn. J. Pharmacology* **1997**, *73*, 317–324. DOI:10.1254/jjp.60.317
43. M. J. Genin, C. Bilers, B. J. Kieser, S. M. Poppe, S. M. Swaney, W. G. Tarpley, Y. Yagi, D. L. Romero, *J. Med. Chem.* **2000**, *43*, 1034–1040. DOI:10.1021/jm990383f
44. A. G. Habeb, P. N. P. Rao, E. E. Knaus, *J. Med. Chem.* **2001**, *44*, 3039–3042. DOI:10.1021/jm010153c
45. H. Hashimoto, K. Imamura, J. I. Haruta, K. Wakitani, *J. Med. Chem.* **2002**, *45*, 1511–1517. DOI:10.1021/jm010484p
46. M. Sakya, B. Rast, *Tetrahedron Lett.* **2003**, *44*, 7629–7632. DOI:10.1016/j.tetlet.2003.08.054
47. L. David, D. G. B. Selwood, *J. Med. Chem.* **2001**, *44*, 78–93.
48. J. M. Parmar, J. J. Modha, A. R. Parikh, *Indian J. Chem.* **1999**, *38B*, 440–444.
49. V. K. Ahluwalia, B. Madhu, *Indian J. Chem.* **1996**, *35B*, 742–746.
50. (a) K. S. Atwal, G. C. Roynyk, S. D. Kimball, D. M. Floyd, S. Moreland, *J. Med. Chem.* **1990**, *33*, 2629–2635. DOI:10.1021/jm00171a044  
(b) K. S. Atwal, B. N. Swanson, S. E. Unger, D. M. Floyd, S. Moreland, A. Hedberg, B. C. Orielly, J. E. T. Corrie, *J. Med. Chem.* **1991**, *34*, 806–811. DOI:10.1021/jm00106a048  
(c) G. C. Rovnyk, K. S. Atwal, S. D. Kimball, *J. Med. Chem.* **1992**, *35*, 3254–3263. DOI:10.1021/jm00095a023  
(d) G. C. Rovnyk, S. D. Kimball, B. Beyer, G. Cucinotta, J. D. Dimorco, J. Gougoutas, A. Hedberg, M. Molley, J. P. McCarthy, R. Zhang, S. Moreland, *J. Med. Chem.* **1995**, *38*, 119–129. DOI:10.1021/jm00001a017
51. V. K. Ahluwalia, M. Bala, *Indian J. Chem.* **1996**, *35B*, 742–748.
52. S. Kothari, R. Vyas, B. L. Verma, *Indian J. Heterocycl. Chem.* **1999**, *8*, 285–291.
53. S. Purushotham, R. Prasanna, R. Raghunathan, *Tetrahedron* **2013**, *69*, 9742–9750. DOI:10.1016/j.tet.2013.09.015
54. C. K. Chu, J. W. Beach, G. V. Ullas, Y. Kosugi, *Tetrahedron Lett.* **1988**, *29*, 5349–5352. DOI:10.1016/S0040-4039(00)82864-6

## Povzetek

Iz alkil etrov in triazolov kot distančnikov smo s kombinacijo klik reakcije in intramolekularne aldolne kondenzacije uspešno izvedli sintezo makrocikličnih enonov. Nove makrociklične enone smo uspešno uporabili tudi kot dipolarofile v 1,3-dipolarnih cikloadicijah. Dipole smo pripravili iz hidrazin hidroklorida, hidroksilamina in gvanidin hidroklorida ter jih reagirali z makrocikličnimi enoni; te reakcije so z dobrimi izkoristki vodile do nastanka novih spiro makrociklov substituiranih z aminopirimidini, fenil pirazoli in izoksazoli. Strukture novih produktov smo potrdili z IR, NMR in masno spektrometrijo ter določili njihovo aktivnost proti rakastim celicam.



Except when otherwise noted, articles in this journal are published under the terms and conditions of the Creative Commons Attribution 4.0 International License

Scientific paper

# Effects of Tryptophan on the Polymorphic Transformation of Calcium Carbonate: Central Composite Design, Characterization, Kinetics, and Thermodynamics

Sevgi Polat,\* Tuba Nur Ozalp-Sendur and Perviz Sayan

Department of Chemical Engineering, Faculty of Engineering, Marmara University, 34722, İstanbul, Turkey.

\* Corresponding author: E-mail: sevgi.polat@marmara.edu.tr

Phone: +90-2167773706, Fax: +90-2167773501

Received: 11-12-2020

## Abstract

The objectives of this study were to: (i) determine the effects of tryptophan on the polymorphic phase transformation of  $\text{CaCO}_3$ , (ii) investigate the thermal degradation characteristics of  $\text{CaCO}_3$  in terms of kinetics and thermodynamics using the Coats–Redfern method, and (iii) assess the influence of the experimental conditions on the vaterite composition of  $\text{CaCO}_3$  using response surface methodology based on central composite design. First, the  $\text{CaCO}_3$  crystals were prepared and analyzed using XRD, FTIR, SEM, BET, AFM, and zeta potential analysis. Based on the characterization results, the shape of the  $\text{CaCO}_3$  crystals changed from smooth cubic calcite crystals to porous irregular spherical-like vaterite crystals with increasing tryptophan concentration. Meanwhile, the kinetic results showed that the thermal degradation of  $\text{CaCO}_3$  followed the shrinkage geometrical spherical mechanism,  $R_3$  and the average activation energy was 224.6 kJ/mol. According to the results of the experimental design, the tryptophan concentration was the most influential variable affecting the relative fraction of vaterite in the produced crystals. It can be concluded that tryptophan is important for better understanding and controlling the polymorph, size, and morphology of  $\text{CaCO}_3$  crystals.

**Keywords:** Calcium carbonate; polymorphism; central composite design; kinetics; thermodynamics

## 1. Introduction

Calcium carbonate ( $\text{CaCO}_3$ ) is one of the most abundant natural minerals, comprising approximately 5% of the Earth's crust. It has a wide range of potential applications in industry and biomineralization.<sup>1,2</sup>  $\text{CaCO}_3$  takes various forms, including two hydrated crystal forms of ikaite ( $\text{CaCO}_3 \cdot 6\text{H}_2\text{O}$ ) and monohydrate ( $\text{CaCO}_3 \cdot \text{H}_2\text{O}$ ), an amorphous form, and three anhydrous crystalline polymorphs (calcite, aragonite, and vaterite).<sup>3–5</sup> The most abundant form of calcite in nature is as a stable thermodynamic phase in rhombohedral crystalline structure with cubic shaped.<sup>6</sup> Aragonite is metastable under ambient pressure and temperature and has a needle-like crystal shape with orthorhombic structure.<sup>7</sup> Vaterite is the thermodynamically least stable form of calcium carbonate and it has a spherical-like crystal shape with hexagonal structure.<sup>8</sup> All three of these forms of  $\text{CaCO}_3$  can be prepared by carbonation process under appropriate conditions and the order of abundance from high to low is calcite, arago-

nite, and vaterite in nature.<sup>9</sup> The vaterite polymorph is the least abundant in nature but it of particular interest for use in biomedical applications owing to its high specific surface area, good water solubility and dispersion, and lower density compared to the other two crystal polymorphs.<sup>10</sup>

The properties of  $\text{CaCO}_3$  are of particular importance in industrial applications, particularly the crystal structure, whiteness, chemical purity, specific surface area, particle size distribution, and morphology. Therefore, it is important to understand and have control of the different  $\text{CaCO}_3$  polymorphs formed during crystallization, which has recently attracted growing research interest.<sup>11</sup> To the best of our knowledge, various physicochemical factors have been found to be responsible for the polymorphic phase transformation process of  $\text{CaCO}_3$ , such as temperature,<sup>12</sup> solvent type,<sup>13</sup> pH,<sup>14</sup> and initial supersaturation.<sup>15</sup> In addition, different additives, such as barium, strontium, and magnesium ions,<sup>16,17</sup> graphene oxide,<sup>18</sup> biocompatible polymeric additives such as bovine serum albumin and polydopamine,<sup>19</sup> selenic acid, arsenic acid, and silicic



acid,<sup>20</sup> and various types of amino acids,<sup>21</sup> have been shown to greatly affect the morphology and polymorphic composition of CaCO<sub>3</sub> and the performance of the resulting product. CaCO<sub>3</sub> polymorphism has been investigated previously but more work is needed to fully understand the factors that control the structure and morphology of CaCO<sub>3</sub> during its polymorphic transformation. Thus, in this study, we systematically investigated the effects tryptophan on the polymorphic phase transformation of CaCO<sub>3</sub>. The structure, morphology, particle size, surface area, and surface charge of the polymorphs were analyzed in order to gain further understanding of the polymorphic transformation process for CaCO<sub>3</sub>. Tryptophan was selected for this study because of the limited number of studies using tryptophan as an additive to investigate the

CaCO<sub>3</sub> polymorphism and the influence of this additive on CaCO<sub>3</sub> structural and morphological properties has not yet fully studied yet. We employed the Coats–Redfern method to estimate the activation energy of CaCO<sub>3</sub> crystals and to ascertain the thermal decomposition mechanism of CaCO<sub>3</sub>. Moreover, experimental design was used to determine the effects of the process variables of temperature, stirring rate, and tryptophan concentration on the transformation of CaCO<sub>3</sub> polymorphs. The novelty of this work lies in the use of a suitable experimental design to investigate the variables that affect the polymorphic transformation of CaCO<sub>3</sub> and any possible interactions between the variables to determine the optimum conditions for maximizing the vaterite content. This in-depth investigation of the effects of the interactions between the process variables on CaCO<sub>3</sub> crystallization will provide very useful information for industry and researchers.

## 2. Experimental

### 2.1. Materials

Analytical-grade calcium chloride dihydrate (CaCl<sub>2</sub> · 2H<sub>2</sub>O), sodium carbonate (Na<sub>2</sub>CO<sub>3</sub>), and tryptophan (C<sub>11</sub>H<sub>12</sub>N<sub>2</sub>O<sub>2</sub>) were purchased from Merck. All solutions were prepared using distilled water.

### 2.2. Experimental Method

CaCO<sub>3</sub> was prepared by the reaction between CaCl<sub>2</sub> · 2H<sub>2</sub>O and Na<sub>2</sub>CO<sub>3</sub> in a glass crystallizer with an active volume of 1.0 L. At the beginning of the experiment, 0.2 M calcium chloride solution (0.4 L) was placed into the crystallizer. After thermal equilibrium was reached, a 0.2 M sodium carbonate solution (0.4 L) was fed into the crystallizer at a rate of 4 mL/min using a peristaltic pump. The suspension in the crystallizer was stirred at a rate of 500 rpm. During the polymorphic transformation process, the pH of the solution was continuously monitored via a pH probe inserted into the crystallizer and maintained at pH 8.5 by the addition of dilute sodium hydroxide or hydrochloric acid solution by an

automatic pH control system. The suspension temperature was maintained at a 30 ± 0.1 °C. At 30 and 100 min, 20-mL aliquots of the suspension were removed and used for crystal structure and morphology analysis.

The effect of tryptophan and its concentrations on the polymorphic transformation of CaCO<sub>3</sub> was investigated in this study. The specific amount of the tryptophan (corresponding to 50 ppm and 100 ppm) was added into the crystallizer at the beginning of the experiment. The product obtained was collected, filtered by using 0.45 µm membrane filters, washed with distilled water, and finally dried at room temperature. The prepared samples were treated prior to further analysis.

### 2.3. Analysis

The precipitated CaCO<sub>3</sub> were analyzed for structure, functional group, crystal size, morphology, surface charge and thermal characteristics. Firstly, X-ray diffraction (XRD, Bruker D2 Phaser Table-top Diffractometer) was used to determine the phase structures of the CaCO<sub>3</sub> polymorphs and scanned in the range of 10 to 70° with a scan rate of 3°/min. The calcite and vaterite polymorphs in the CaCO<sub>3</sub> were quantitatively determined using the Rietveld refinement method. Meanwhile, the polymorphic transformation was monitored by Fourier transform infrared spectroscopy (FTIR; Shimadzu IR Affinity-1) equipped with Attenuated Total Reflectance (ATR) accessories. The spectra were recorded with scanning range from 600 to 2000 cm<sup>-1</sup> at room temperature in transmission mode with a resolution of 4 cm<sup>-1</sup>. The crystal morphologies of the CaCO<sub>3</sub> were investigated by scanning electron microscopy (SEM/EDX; Zeiss EVO LS w10) and the particle size distributions were measured with a Malvern Mastersizer 2000 instrument. Zeta potential measurements were conducted using a Malvern Zeta Sizer Nano Series Nano-ZS. The thermal behavior of the CaCO<sub>3</sub> precipitated in pure and tryptophan media was determined using a Setaram LABSYS Evo thermogravimetric analyzer in a nitrogen atmosphere between 50 °C and 950 °C with a heating rate of 10 °C/min. Using the obtained data, the thermal decomposition kinetics for the CaCO<sub>3</sub> crystals precipitated in pure media were investigated and the kinetic parameters were calculated.

### 2.4. Coats–Redfern Method

The Coats–Redfern<sup>22</sup> model-fitting method is widely used for estimating the pre-exponential factor and activation energy to predict the order of a reaction. The basic equation for the Coats–Redfern method is as follows:

$$\ln \left[ \frac{g(\alpha)}{T^2} \right] = \ln \left[ \frac{AR}{\beta E_a} \left( 1 - \frac{2RT}{E_a} \right) \right] - \frac{E_a}{RT} \quad (1)$$

where  $\beta$  is the heating rate,  $R$  is the ideal gas constant (8.314 J/mol K), and  $g(\alpha)$  is a kinetic function of different

**Table 1.** Reaction mechanisms and symbols with their  $f(\alpha)$  and  $g(\alpha)$ .

Mechanisms	Symbol	$f(\alpha)$	$g(\alpha)$
<b>Reaction order</b>			
First-order	$F_1$	$(1-\alpha)$	$-\ln(1-\alpha)$
Second-order	$F_2$	$(1-\alpha)^2$	$(1-\alpha)^{-1}-1$
One and half order	$F_{1.5}$	$(1-\alpha)^{3/2}$	$2[(1-\alpha)^{-1/2}-1]$
<b>Diffusion phenomena</b>			
Parabolic Law	$D_1$	$0.5\alpha$	$\alpha^2$
Valensi equation	$D_2$	$[-\ln(1-\alpha)]^{-1}$	$\alpha+(1-\alpha)\ln(1-\alpha)$
<b>Phase interfacial reaction</b>			
Shrinkage geometrical column	$R_2$	$2(1-\alpha)^{1/2}$	$1-(1-\alpha)^{1/2}$
Shrinkage geometrical spherical	$R_3$	$3(1-\alpha)^{2/3}$	$1-(1-\alpha)^{1/3}$
<b>Exponential nucleation</b>			
Power law, $n = 1/2$	$P_2$	$2\alpha^{1/2}$	$\alpha^{1/2}$
Power law, $n = 1/3$	$P_3$	$3\alpha^{2/3}$	$\alpha^{1/3}$
<b>Nucleation and growth</b>			
Avrami-Erofeev two dimensional	$A_2$	$2(1-\alpha)[- \ln(1-\alpha)]^{1/2}$	$[- \ln(1-\alpha)]^{1/2}$
Avrami-Erofeev three dimensional	$A_3$	$3(1-\alpha)[- \ln(1-\alpha)]^{1/3}$	$[- \ln(1-\alpha)]^{1/3}$

reaction mechanisms that is obtained from integration of  $f(\alpha)$ . The activation energy ( $E_a$ ) can be determined by plotting a graph of  $1/T$  versus  $\ln [g(\alpha)/T^2]$  and determining the slope of the straight line of best fit. The intercept of the line gives the pre-exponential factor ( $A$ ) and  $g(\alpha)$  varies depending on the developed model and reaction mechanism. Most solid-state degradation reactions fall into one of five main categories, as detailed in Table 1.<sup>23,24</sup>

## 2. 5. Thermodynamic Analysis

The thermodynamic parameters of the  $\text{CaCO}_3$  crystals, including change in enthalpy ( $\Delta H$ ), change in Gibbs free energy ( $\Delta G$ ), and change in entropy ( $\Delta S$ ), were calculated based on kinetic data from the following equations<sup>25</sup>

$$\Delta H = E_a - RT \quad (2)$$

$$\Delta G = E_a + RT_{peak} \ln \left( \frac{K_B T_{peak}}{hA} \right) \quad (3)$$

$$\Delta S = \frac{\Delta H - T\Delta G}{T_{peak}} \quad (4)$$

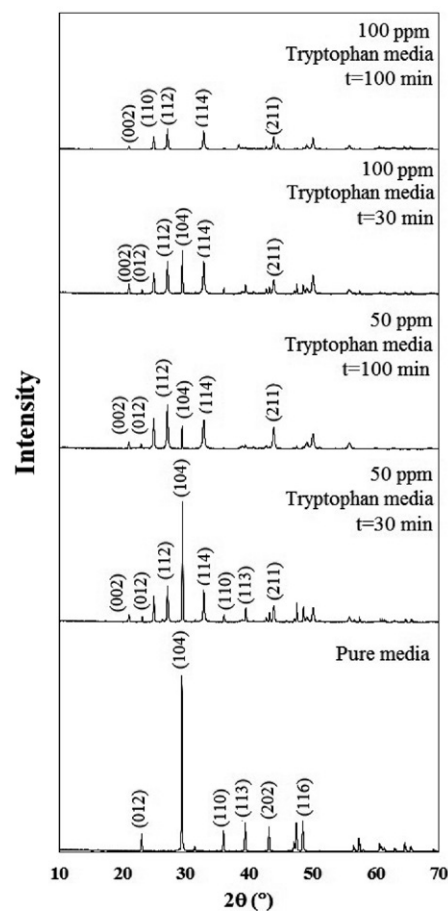
Where  $T_{peak}$  is the peak temperature of DTG curve,  $K_B$  is the Boltzmann constant, and  $h$  is the Planck constant.

## 3. Results and Discussion

### 3. 1. XRD Analysis

The XRD patterns of the samples at 30 and 100 min during the polymorphic transformation process from calcite to vaterite in the presence of 50 ppm and 100 ppm tryptophan are shown in Figure 1. The XRD results indicate that the  $\text{CaCO}_3$  crystals precipitated in pure media

were only in calcite form (JCPDS: 05-0586) and no intermediate phase was produced in pure media. The main peaks observed at  $2\theta$  of  $23.1^\circ$ ,  $29.4^\circ$ ,  $35.9^\circ$ , and  $39.3^\circ$  are diffraction peaks corresponding to the calcite crystals lat-



**Figure 1.** XRD results for  $\text{CaCO}_3$  crystals precipitated in pure media and media supplemented with 50 and 100 ppm tryptophan.

tice planes of (012), (104), (110), and (113), respectively. When 50 ppm tryptophan was added to media, the resulting crystals included both calcite and vaterite forms together. The solid sample taken at 30 min showed the appearance of new peaks at  $2\theta = 21.0^\circ$ ,  $24.9^\circ$ ,  $27.1^\circ$ ,  $32.7^\circ$ , and  $50.1^\circ$ , which were assigned to the (002), (110), (112), (114), and (118) lattice faces of vaterite, respectively (JCPDS: 33-0268). Rietveld refinement quantitative analysis determined the calcite and vaterite contents to be 74.84% and 25.16%, respectively, for the 30-min sample obtained from media supplemented with 50 ppm tryptophan. As the transformation process progressed further, more of the vaterite form (41.20%) was found in the crystal sample. The intensity of the characteristic diffraction peaks of vaterite was obviously increased and more of the vaterite polymorph was obtained with time.

When the tryptophan concentration was 100 ppm, both calcite and vaterite diffraction peaks were observed in the solid sample obtained at 30 min during the polymorphic transformation process and the mass fractions of calcite and vaterite were calculated to be 61.26% and 38.74%, respectively. The results of Rietveld refinement quantitative analysis showed that the vaterite content increased with the increasing tryptophan concentration. In the sample obtained at 100 min, the characteristic diffraction peaks of calcite had completely disappeared, showing that all the calcite crystals were completely transformed into the vaterite form. The XRD results indicated that tryptophan influenced the crystal structure of calcium carbonate.

### 3. 2. FTIR Analysis

The FTIR spectra for  $\text{CaCO}_3$  crystals precipitated with and without tryptophan at 30 and 100 min during the polymorphic phase transformation are presented in Figure 2.

The calcite and vaterite absorption peaks are at different positions in the FTIR spectra. The absorption peak at  $712\text{ cm}^{-1}$  is the characteristic peak of calcite, while the absorption peaks at  $1085\text{ cm}^{-1}$  and  $746\text{ cm}^{-1}$  correspond to vaterite.<sup>26</sup> The FTIR spectrum for the  $\text{CaCO}_3$  crystals precipitated in pure media displayed the characteristic band of the calcite polymorph at  $713\text{ cm}^{-1}$ . At  $t = 30\text{ min}$ , the two main characteristic peaks of vaterite were identified for the  $\text{CaCO}_3$  crystals precipitated in the presence of 50 ppm tryptophan. Meanwhile, the intensity of the absorption peak at  $713\text{ cm}^{-1}$  became obviously weaker. As the transformation progressed further, the intensity of the characteristic FTIR peaks of vaterite, especially that at  $746\text{ cm}^{-1}$ , obviously increased while the intensity of the absorption peak at  $713\text{ cm}^{-1}$  decreased. These FTIR results show the change of the crystal polymorphs from calcite only to a mixture of vaterite and calcite with a higher proportion of vaterite than calcite. With the higher tryptophan concentration, the intensity of the vaterite peak became stronger, while the corresponding peak of calcite became weaker. For the solid sample obtained at 100 min,

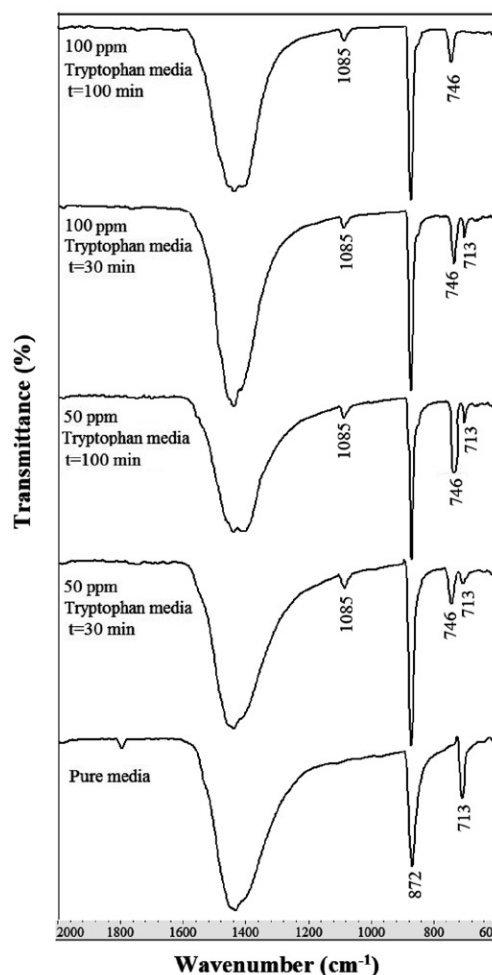


Figure 2. FTIR results for  $\text{CaCO}_3$  crystals precipitated in pure media and media supplemented with 50 and 100 ppm tryptophan.

the absorption peak at  $713\text{ cm}^{-1}$  had completely disappeared in the FTIR spectrum and the sample mainly consisting of the vaterite polymorph and water, which was consistent with the XRD results.

### 3. 3. SEM Analysis

The SEM image in Figure 3a shows that the surface of the  $\text{CaCO}_3$  crystals precipitated in pure media was smooth and non-porous and the crystals were composed of regular cubic-shaped particles with nearly uniform size, which was in agreement with the results of previous studies.<sup>27,28</sup> Energy dispersive X-ray (EDX) spectroscopy was applied to determine the elemental composition of the  $\text{CaCO}_3$  crystals. The EDX analysis showed a surface composition of Ca 40.12 wt%, C 11.97 wt%, and O 47.91 wt% for the crystals precipitated in pure media. The elemental content in  $\text{CaCO}_3$  was thus consistent with the theoretical values. The average particle size and BET surface area of the  $\text{CaCO}_3$  were  $32\text{ }\mu\text{m}$  and  $0.70\text{ m}^2/\text{g}$ , respectively. Based on the previous studies,<sup>29–32</sup>  $\text{CaCO}_3$  crystals precipitated without additive were generally characterized by small

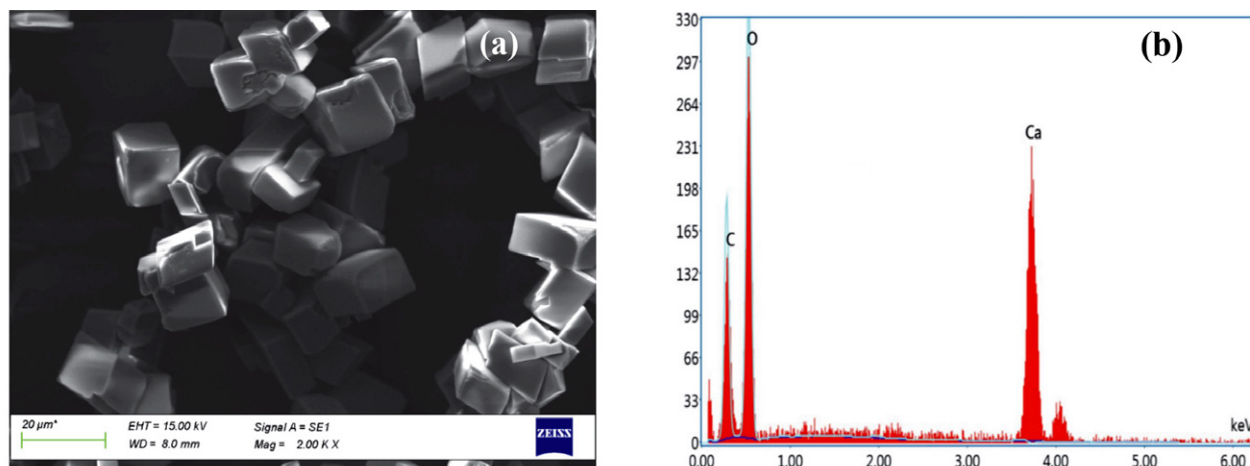


Figure 3. a) SEM and b) EDX results of  $\text{CaCO}_3$  crystals precipitated in pure media.

surface areas, below  $1 \text{ m}^2/\text{g}$ , which was consistent with our result.

The SEM images of the  $\text{CaCO}_3$  crystals precipitated in the presence 50 and 100 ppm tryptophan at different time points are presented in Figure 4.

At  $t = 30$  min, in addition to cubic-shaped calcite crystals with an irregular surface, some small spherical-shaped plate-like vaterite crystals were observed for the 50 ppm additive media. That is, calcite and vaterite

crystals were seen together, which was consistent with the XRD and FTIR results. With the increase of the transformation time to 100 min, the amount of cubic-shaped crystals decreased, surface deformations occurred on the calcite crystals, and some of the calcite was transformed to vaterite form. A similar outcome was also observed for crystals precipitated with 100 ppm tryptophan at 30 min. In addition to cubic calcite crystals, the sample also consisted of elliptical, intertwined, and compact agglomerates.

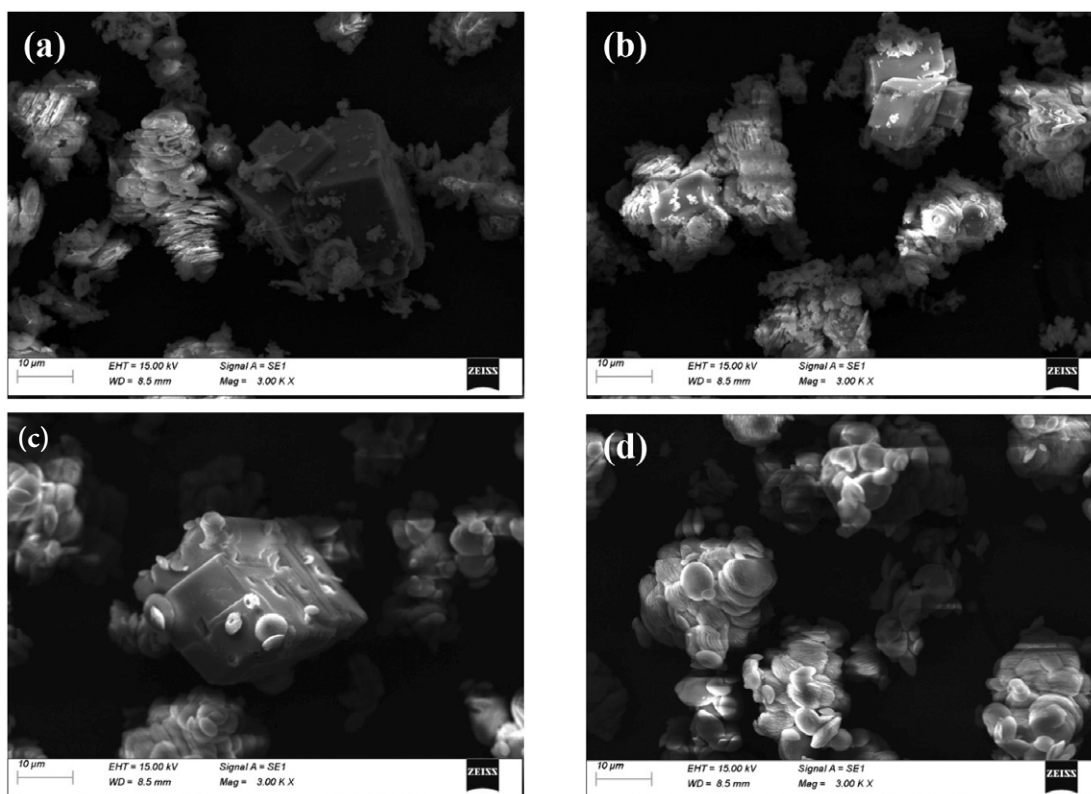


Figure 4. SEM images for  $\text{CaCO}_3$  crystals precipitated with 50 ppm tryptophan at  $t = 30$  min (a) and at  $t = 100$  min (b) and with 100 ppm tryptophan at  $t = 30$  min (c) and at  $t = 100$  min (d).

These agglomerates took a spherical form owing to the effects of the hydrodynamic conditions of the media. At  $t = 30$  min, both calcite and vaterite crystals were obtained. As the transformation process progressed, the cubic-shaped crystals disappeared completely and transformed into spherical-like vaterite crystals with an irregular crystal surface. With the completion of the transformation process, the obtained crystals had a spherical and ellipsoidal form, indicating that the calcite polymorph was completely converted into vaterite, which was also confirmed by the XRD and FTIR results. Meanwhile, the particle size and BET surface area of the samples precipitated in media supplemented with tryptophan were changed compared to the pure media due to the surface adsorption of the additive. The average particle sizes and BET surface areas of the samples precipitated in the presence of 50 and 100 ppm tryptophan were  $26 \mu\text{m}$  and  $3.8 \text{ m}^2/\text{g}$  and  $19 \mu\text{m}$  and  $6.4 \text{ m}^2/\text{g}$ , respectively. A higher additive concentration led to a decrease in the particle size and an increase in the specific surface area of the  $\text{CaCO}_3$ . Thus, more porous and rougher crystals with smaller sizes were produced in the presence of tryptophan.

To gain more insight into the effects of tryptophan on the topography of  $\text{CaCO}_3$ , AFM analysis was performed and 3D micrographs for the crystals precipitated with and

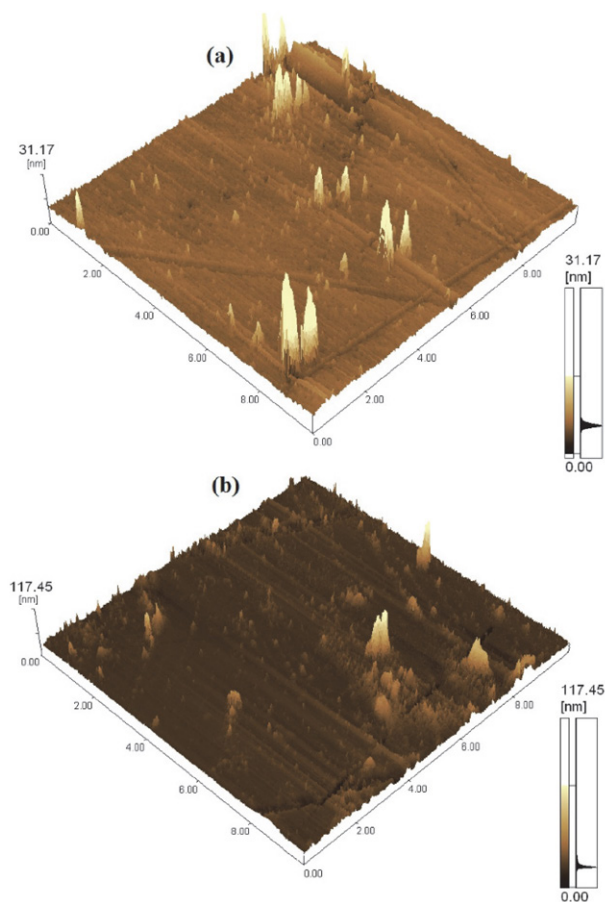
without tryptophan are shown in Figure 5. The surface topography of the  $\text{CaCO}_3$  crystals precipitated in pure media was flat and smooth with a maximum thickness of 31.17 nm. Compared to the crystals obtained in pure media, some ridges, defects, and irregularity occurred on the surface of  $\text{CaCO}_3$  crystals precipitated in 100 ppm tryptophan media and the thickness increased to 117.45 nm. These changes led to increased surface roughness, confirming the results obtained from the SEM images.

### 3. 4. Zeta Potential Analysis

The zeta potential of the  $\text{CaCO}_3$  crystals precipitated with and without tryptophan in the media was investigated to determine the surface charge and stability of a suspension of particles. The  $\text{CaCO}_3$  crystals prepared in pure media had a zeta potential of  $-8.1 \pm 2.1 \text{ mV}$ . Similar to pure media, the zeta potential of  $\text{CaCO}_3$  crystals precipitated in additive media had a negative value. The zeta potential values at 50 ppm were  $-15.7 \pm 1.0 \text{ mV}$ ,  $-17.4 \pm 1.8 \text{ mV}$  for  $t = 30$  and 100 mins, respectively. As the tryptophan concentration increased, the zeta potential value of the  $\text{CaCO}_3$  crystals showed a clear increase. The zeta potential values reached  $-19.2 \pm 1.3 \text{ mV}$  and  $-25.7 \pm 2.2 \text{ mV}$  at 100 ppm for  $t = 30$  and 100 mins, respectively, which obviously illustrated that the electrical surface charge of the  $\text{CaCO}_3$  crystals was more negative at a higher tryptophan concentration. This change in the zeta potential suggests that some tryptophan was adsorbed on the surface of  $\text{CaCO}_3$  crystals. In addition, the variations in zeta potentials in the additive media were associated with the changing agglomeration tendency of the crystals, which is supported with the results of SEM analysis.

### 3. 5. Filtration Analysis

Filtration is an important parameter for controlling the precipitation of  $\text{CaCO}_3$  since it affects both the properties of the crystalline products and process efficiency which is important from an economic point of view. In order to determine how tryptophan influences the filtration characteristics of  $\text{CaCO}_3$ , the average specific cake resistance and the average cake porosity of the crystals were analyzed based on Darcy's Law under 700 mbar constant pressure. The average specific cake resistance and the average cake porosity of the crystals precipitated in pure media were  $1.03 \times 10^{12} \text{ m/kg}$  and 0.548, respectively. The filtration characteristics of the  $\text{CaCO}_3$  are significantly changed by the addition of tryptophan to the media. Average specific cake resistances of  $9.65 \times 10^{11} \text{ m/kg}$  and  $4.24 \times 10^{11} \text{ m/kg}$  were obtained at the end of the polymorphic transformation process with tryptophan at 50 and 100 ppm, respectively. A higher concentration of tryptophan led to a lower specific cake resistance. Meanwhile, the average cake porosity increased from 0.658 to 0.712 as the tryptophan concentration increased from 50 to 100 ppm. This can be explained



**Figure 5.** 3D micrographs for the crystals precipitated without (a) and with 100 ppm tryptophan (b).

by the changes to the particle size, morphology, and polymorphic form, which have the greatest effect on these filtration characteristics. Fairly large differences in the sizes and shapes of the  $\text{CaCO}_3$  crystals that were formed in the presence of tryptophan could be seen in the SEM images; these changes had a direct impact on the filtration properties. Therefore, appropriately increasing the tryptophan concentration could be advantageous for increasing the filtration rate and improving the filtration characteristics.

### 3. 6. Thermogravimetric Analysis

The thermogravimetric (TG) and differential thermogravimetric (DTG) curves for the crystals precipitated in pure media and with 100 ppm tryptophan are presented in Figure 6. Considering the thermal degradation characteristics of  $\text{CaCO}_3$  crystals precipitated in pure media, a single DTG peak was observed, which showed that degradation occurred at a single stage, corresponding to the transformation of calcium carbonate to calcium oxide.<sup>33,34</sup> Thermal degradation occurred between 630 °C and 830 °C and the residual mass was 55.6 wt%, agreeing with the theoretical value. The weight loss from the  $\text{CaCO}_3$  crystals precipitated in tryptophan media was 45.2 wt%. The higher weight loss suggests that tryptophan had been adsorbed onto and interacted with the surface of the  $\text{CaCO}_3$  crystals. The addition of tryptophan had a slight effect on the temperature of the decomposition peak during the thermal decomposition of  $\text{CaCO}_3$ . While the maximum peak temperature was 809 °C for pure media, the value observed for the additive media was determined to be 821 °C. Thus, adding tryptophan to the crystallization media shifted the decomposition peak to higher temperature.

### 3. 7. Kinetic and Thermodynamic Analysis

In this study, the Coats–Redfern method was used to predict kinetic parameters such as activation energy and pre-exponential factor. The minimum energy required to initiate a reaction, known as the activation energy, can be determined by kinetic analysis. As shown in Table 2, the ac-

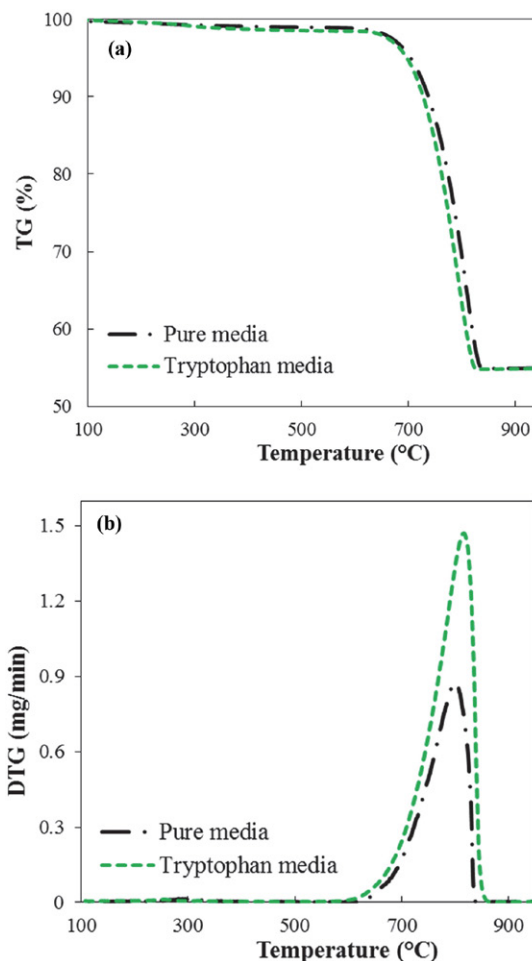


Figure 6. a) TG and b) DTG curves of  $\text{CaCO}_3$  crystals precipitated in pure media and with 100 ppm tryptophan.

tivation energies were between 56.6 and 442.6 kJ/mol, which was consistent with the results of previous studies.<sup>35,36</sup> The pre-exponential factors were in the range of  $3.08 \times 10^1$  to  $6.11 \times 10^{20} \text{ min}^{-1}$ , in good agreement with the literature.<sup>36</sup>

Linear adjustment using the different reaction mechanisms as shown in Table 1 was applied to estimate the reaction mechanism for the thermal degradation of  $\text{CaCO}_3$ .

Table 2. Kinetic calculation results for thermal decomposition of  $\text{CaCO}_3$  using the Coats–Redfern method.

Symbol	$E_a$ (kJ/mol)	A ( $\text{min}^{-1}$ )	$R^2$	$\Delta H$ (kJ/mol)	$\Delta G$ (kJ/mol)	$\Delta S$ (J/mol · K)
F <sub>1</sub>	242.8	$1.86 \times 10^{11}$	0.9891	233.8	286.4	-48.6
F <sub>2</sub>	281.0	$3.09 \times 10^{13}$	0.9813	272.0	278.6	-6.09
F <sub>1.5</sub>	257.8	$1.53 \times 10^{12}$	0.9908	248.8	282.4	-31.1
D <sub>1</sub>	423.1	$9.98 \times 10^9$	0.9772	414.1	285.8	118.5
D <sub>2</sub>	442.6	$6.11 \times 10^{20}$	0.9842	433.6	289.0	133.6
R <sub>2</sub>	218.9	$4.87 \times 10^9$	0.9865	209.9	295.3	-78.9
<b>R<sub>3</sub></b>	<b>224.6</b>	<b><math>6.88 \times 10^9</math></b>	<b>0.9954</b>	<b>215.6</b>	<b>297.9</b>	<b>-76.0</b>
P <sub>2</sub>	93.3	$4.27 \times 10^6$	0.9698	84.3	233.0	-137.4
P <sub>3</sub>	56.6	$3.08 \times 10^1$	0.9630	47.6	302.9	-235.8
A <sub>2</sub>	110.1	$2.93 \times 10^4$	0.9892	101.2	294.7	-178.8
A <sub>3</sub>	69.8	$1.98 \times 10^2$	0.9850	60.8	299.4	-220.4

It was found from Table 2 that the thermal degradation of  $\text{CaCO}_3$  predicted by the geometric spherical shrinkage mechanism (the  $R_3$  type model) fitted the experimental data best, which was consistent with previous research.<sup>35,36</sup> The regression coefficients ranged between 0.9630 and 0.9954 depending on the applied kinetic model. The  $R_3$  type model presented the highest accuracy ( $R^2 = 0.9954$ ) of the 11 models studied.

The thermodynamic parameters of enthalpy ( $\Delta H$ ), entropy ( $\Delta S$ ), and Gibbs free energy ( $\Delta G$ ) for the thermal decomposition of  $\text{CaCO}_3$  were calculated using different reaction mechanism models. According to the thermodynamic results presented in Table 2, the enthalpy change for the thermal decomposition of  $\text{CaCO}_3$  was between 47.6 and 433.6 kJ/mol depending on the model used. Diffusion models D1 and D2 gave higher  $\Delta H$  values than the other models tested, including the reaction, interfacial, exponential, nucleation, and growth models. The positive values of  $\Delta H$  obtained for the crystals confirmed that the main decomposition process was endothermic in nature. The entropy changes for the crystals were in the range of  $-235.8$  to  $133.6$  J/mol K. All of the tested models showed negative  $\Delta S$  values except for D1 and D2. The negative  $\Delta S$  values show that the disorder of the products obtained through bond dissociation was lower than that of the initial reactants. These negative values suggest that the disintegration product from the activated state has a more well-organized structure than before the thermal disintegration and that the reactions in the activated state proceed more gently than anticipated. The Gibbs free energy change was calculated to be between 233.0 and 302.9 kJ/mol. A positive value of  $\Delta G$  indicates that a reaction is unfavorable and thus energy needs to be supplied for the reaction to occur.

### 3. 8. Experiment Design Results

Response surface methodology (RSM) is a multivariate statistical technique that is used to optimize process variables and their responses by exploring the relationship between independent process variables and their observed responses. Box–Behnken design, central composite design (CCD), and three-level factorial design are examples of experimental design techniques, with CCD being the most effective and popular method. In this study, Design Expert software version 10 (Stat-Ease, Minneapolis, USA) was used for the experimental design using CCD.<sup>37</sup> We conducted 17 experiments with three center points using three variables of temperature (A), stirring rate (B), and tryptophan concentration (C), and the vaterite content was chosen as the response. Meanwhile, CCD with three factors and five levels was also applied to determine the correlation between the combined effects of individual variables. Tables 3 and 4 show the range and levels, respectively, of the investigated variables and their responses for all 17 optimized test experimental runs.

Thus, based on these results, the model equation for the vaterite content as a function of the process variables is:

**Table 3.** Experimental variables and their levels in central composite design matrix.

Parameters	Factors	Levels				
		-2	-1	0	+1	+2
Temperature ( $^{\circ}\text{C}$ )	A	20	25	30	35	40
Stirring rate (rpm)	B	400	450	500	550	600
Tryptophan concentration (ppm)	C	0	25	50	75	100

**Table 4.** Central composite design matrix and results.

Run	Temperature ( $^{\circ}\text{C}$ )	Actual level of factors		Concentration	Coded level of factors			Response Vaterite composition (%)
		Stirring rate (rpm)	(ppm)		A	B	C	
1	25	450		25	-1	-1	-1	19.2
2	35	450		25	+1	-1	-1	27.2
3	25	550		25	-1	+1	-1	25.4
4	35	550		25	+1	+1	-1	31.6
5	25	450		75	-1	-1	+1	60.6
6	35	450		75	+1	-1	+1	70.3
7	25	550		75	-1	+1	+1	64.4
8	35	550		75	+1	+1	+1	75.9
9	20	500		50	-2	0	0	34.7
10	40	500		50	+2	0	0	44.4
11	30	400		50	0	-2	0	40.6
12	30	600		50	0	+2	0	51.8
13	30	500		0	0	0	-2	0
14	30	500		100	0	0	+2	100
15	30	500		50	0	0	0	41.8
16	30	500		50	0	0	0	42.4
17	30	500		50	0	0	0	41.0

$$Y = 42.59 + 3.42A + 2.65B + 22.99C + 0.87AC - 0.15BC - 0.44A^2 + 1.22B^2 + 2.17C^2 \quad (5)$$

The lowest vaterite composition (19.2%) was obtained at 25 °C, 450 rpm, and 50 ppm tryptophan concentration (apart from the sample obtained in pure media at 30 °C and 500 rpm).

The model and factor significances with respect to vaterite content were examined by variance analysis (ANOVA) of the F test and p-values. The results are shown in Table 5. The obtained values of F and p suggest that the experimental values are significant and thus acceptable. The ANOVA results showed a large F of 63.59 and a small p-value  $\ll 0.0001$ , which verified that the model fit was statistically significant. The obtained correlation coefficient ( $R^2$ ) of 0.9879 showed that there was good correlation between the measured and predicted responses and confirmed that the model was suitable for the experimental data. The CCD analysis shows that the three independent process variables played an important role in determining the amounts of the  $\text{CaCO}_3$  polymorphs formed since its p-value was  $<0.05$  and had positive coefficients. Increasing the temperature, stirring rate, and tryptophan concentration increased the amount of vaterite formed and they were thus significant and favorable factors. However, the strength and significance of the effect varied for each parameter. The p-value of  $<0.0001$  for tryptophan concentration shows that it is the most important variable to control. However, the interaction of tryptophan concentration with other parameters had a less significant effect. Thus, this establishes tryptophan concentration as the most influential parameter during the polymorphic transformation of  $\text{CaCO}_3$ .

The effects of the independent variables and their interactions are presented in the three-dimensional (3D) response surface plots and contour plots in Figure 7.

According to the results, the 3D surface plots are flat with the slope being related to linear terms of the variables.

As shown in Figure 7, when more than one factor is changed at a time, different effects on the response are observed. The highest vaterite content was obtained with the highest additive concentration, temperature, and stirring rate. In comparison with temperature and stirring rate, tryptophan concentration had the most significant effect on the amount of vaterite produced.

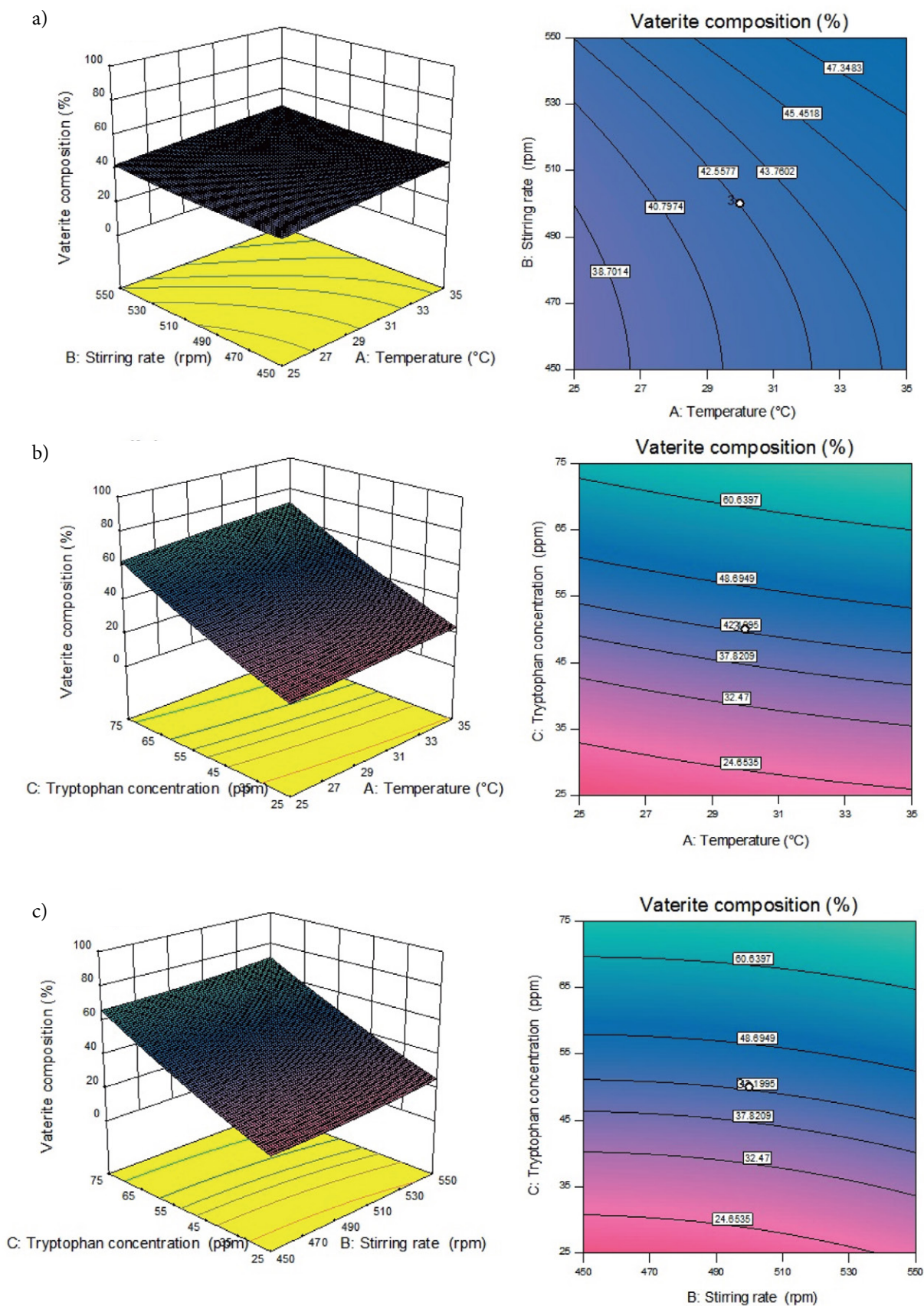
## 4. Conclusions

In this work, the precipitation of  $\text{CaCO}_3$  was investigated in the presence of different concentrations of tryptophan. XRD results showed that using 50 ppm tryptophan as an additive increased the vaterite content by 50.0% compared to pure media. In parallel with the XRD results, FTIR analysis demonstrated that the polymorphic transformation from calcite to vaterite was completely achieved in the presence of 100 ppm tryptophan. SEM images illustrated that tryptophan contributed to the formation of spherical vaterite crystals with a small crystal size. BET analysis showed that the addition of 100 ppm tryptophan increased the BET specific surface area from 0.7 to 6.4  $\text{m}^2/\text{g}$ . Zeta potential analysis suggested that the tryptophan tended to adsorb on the crystal surface. Filtration analysis showed that a higher tryptophan concentration led to a higher average cake porosity and a lower specific cake resistance. In this study, the thermal degradation kinetics of  $\text{CaCO}_3$  were also explored using the Coats–Redfern method. The thermal decomposition kinetics predicted by the  $R_3$  type model showed the best agreement with the experimental data out of the 11 tested models with high accuracy ( $R^2 = 0.9954$ ). Additionally, this study also provided a thermodynamic analysis of  $\text{CaCO}_3$  crystals. Based on the  $R_3$  type model, the  $\Delta H$ ,  $\Delta G$ , and  $\Delta S$  were calculated to be 215.6 kJ/mol, 297.9 kJ/mol, and  $-76.0$  J/mol K, respectively. CCD with RSM was applied successfully to determine how temperature, stirring rate, and tryptophan

Table 5. ANOVA results of the quadratic model for vaterite content.

Source	Sum of Squares	df	Mean Square	F-Value	p-value Prob > F
Model	8904.63	9	989.40	63.59	< 0.0001
A-Temperature	187.69	1	187.69	12.06	0.0104
B-Stirring rate	112.36	1	112.36	7.22	0.0312
C- Tryptophan concentration	8454.80	1	8454.80	543.43	< 0.0001
AB	0.000	1	0.000	0.000	1.0000
AC	6.13	1	6.13	0.39	0.5503
BC	0.18	1	0.18	0.012	0.9174
A <sup>2</sup>	3.73	1	3.73	0.24	0.6391
B <sup>2</sup>	28.99	1	28.99	1.86	0.2145
C <sup>2</sup>	91.49	1	91.49	5.88	0.0458
Residual	108.91	7	15.56		
Lack of Fit	107.92	5	21.58	43.75	0.0225
R <sup>2</sup>	0.9879				





**Figure 7.** 3D-surface and contour plots showing the effects of (a) temperature and stirring rate; (b) temperature and tryptophan concentration; and (c) stirring rate and tryptophan concentration on the vaterite composition.

concentration influenced the CaCO<sub>3</sub> polymorphic phase transformation in terms of the amount of vaterite produced. The experimental design results showed that among the investigated factors, additive concentration had the greatest effect on the vaterite content. The detailed information about the characterization, kinetics, thermodynamics, and optimization of CaCO<sub>3</sub> crystallization obtained in this work will provide a reference for the polymorphic transformation of calcium carbonate for scientific and industrial purposes.

## Acknowledgements

This work was supported by Marmara University Scientific Research Projects Commission under the funding FYL-2020-10025.

## 5. References

- Ç. M. Oral, B. Ercan, *Powder Technol.* **2018**, *339*, 781–788. DOI:10.1016/j.powtec.2018.08.066
- M. R. Abeywardena, R. K. W. H. M. K. Elkaduwe, D. G. G. P. Karunaratne, H. M. T. G. A. Pitawala, R. M. G. Rajapakse, A. Manipura, M. M. M. G. P. G. Mantilaka, *Adv. Powder Technol.* **2020**, *31*, 269–278. DOI:10.1016/j.appt.2019.10.018
- H. Cölfen, *Curr. Opin. Colloid Interface Sci.* **2003**, *8*, 23–31. DOI:10.1016/S1359-0294(03)00012-8
- J. D. Rodriguez-Blanco, S. Shaw, L. G. Benning, *Nanoscale.* **2011**, *3*, 265–271. DOI:10.1039/C0NR00589D
- J. Zhang, S. Yuzhu, Y. Jianguo, *J. Cryst. Growth.* **2017**, *478*, 77–84.
- H. Li, Q. Yao, F. Wang, Y. Huang, S. Fu, G. Zhou, *Geochim. Cosmochim. Acta.* **2019**, *256*, 35–48. DOI:10.1016/j.gca.2018.06.011
- N. Erdogan, H. Ali Eken, *Physicochem. Probl. Miner. Process.* **2017**, *53*, 57–68.
- T. Kato, A. Sugawara, N. Hosoda, *Adv. Mater.* **2002**, *14*, 869–877. DOI:10.1002/1521-4095(20020618)14:12<869::AID-ADMA 869>3.0.CO;2-E
- H. Saulat, M. Cao, M. M. Khan, M. Khan, K. Muhammad, M. M. Khan, A. Rehman, *Constr. Build. Mater.* **2020**, *236*, 117613. DOI:10.1016/j.conbuildmat.2019.117613
- L. H. Fu, Y. Y. Dong, M. G. Ma, W. Yue, S. L. Sun, R. C. Sun, *Ultrason. Sonochem.* **2013**, *20*, 1188–1193. DOI:10.1016/j.ulsonch.2013.03.008
- C. Carteret, A. Dandeu, S. Moussaoui, H. Muhr, B. Humbert, E. Plasari, *Cryst. Growth Des.* **2009**, *9*, 807–812. DOI:10.1021/cg800368u
- M. Kitamura, *J. Cryst. Growth.* **2002**, *237*, 2205–2214. DOI:10.1016/S0022-0248(01)02277-1
- E. Marie-Flaten, M. Seiersten, *J. Cryst. Growth.* **2009**, *311*, 3533–3538. DOI:10.1016/j.jcrysgro.2009.04.014
- Y. B. Hu, M. Wolthers, D. A. Wolf-Gladrow, G. Nehrke, *Cryst. Growth Des.* **2015**, *15*, 1596–1601. DOI:10.1021/cg500829p
- W. S. Kim, I. Hirasawa, W. S. Kim, *Ind. Eng. Chem. Res.* **2004**, *43*, 2650–2657. DOI:10.1021/ie034161y
- K. S. Raj, N. Devi, V.K. Subramanian, *Chem. Phys. Lett.* **2020**, *750*, 137502. DOI:10.1016/j.cplett.2020.137502
- Q. Yao, Y. Wang, Y. Zhang, H. Li, G. Zhou, *Sci. China Earth Sci.* **2019**, *62*, 1619–1629. DOI:10.1007/s11430-018-9336-6
- D. Zheng, H. Yang, F. Yu, B. Zhang, H. Cui, *Materials.* **2019**, *12*, 2045. DOI:10.3390/ma12132045
- M. L. P. Vidallon, F. Yu, B.M. Teo, *Cryst. Growth Des.* **2020**, *20*, 645–652. DOI:10.1021/acs.cgd.9b01057
- M. Kawano, T. Maeda, *J. Cryst. Growth.* **2020**, *535*, 125536. DOI:10.1016/j.jcrysgro.2020.125536
- L. Stajner, J. Kontrec, B. N. Dzakula, N. Maltar-Strmecki, M. Plodinec, D. M. Lyons, D. Kralj, *J. Cryst. Growth.* **2018**, *486*, 1–81. DOI:10.1016/j.jcrysgro.2018.01.023
- A. W. Coats, J. Redfern, *Nature.* **1964**, *201*, 68–69. DOI:10.1038/201068a0
- I. Mian, X. Li, Y. Jian, O. D. Dacres, M. Zhong, J. Liu, F. Ma, N. Rahman, *Bioresour. Technol.* **2019**, *294*, 122099. DOI:10.1016/j.biortech.2019.122099
- S. R. Naqvi, R. Tariq, Z. Hameed, I. Ali, M. Naqvi, W. H. Chen, S. Ceylan, H. Rashid, J. Ahmad, S. A. Taqvi, M. Shahbaz, *Renew. Energy.* **2019**, *131*, 854–860. DOI:10.1016/j.renene.2018.07.094
- Y. S. Kim, Y. S. Kim, S. H. Kim, *Environ. Sci. Technol.* **2010**, *44*, 5313–5317. DOI:10.1021/es101163e
- K. M. Choi, K. Kuroda, *Cryst. Growth Des.* **2012**, *12*, 887–893. DOI:10.1021/cg201314k
- Y. Liu, Y. Chen, X. Huang, G. Wu, *Mater. Sci. Eng. C.* **2017**, *79*, 457–464. DOI:10.1016/j.msec.2017.05.085
- N. L. Bolay, *Powder Technol.* **2003**, *130*, 450–455. DOI:10.1016/S0032-5910(02)00249-8
- S. Polat, *Adv. Powder Technol.* **2020**, *31*, 4282–4291. DOI:10.1016/j.appt.2020.09.003
- A. Bastrzyk, M. Fiedot-Tobola, I. Polowczyk, K. Legawiec, G. Plaza, *Colloids Surf. B.* **2019**, *174*, 145–152. DOI:10.1016/j.colsurfb.2018.11.009
- S. Kirboga, M. Oner, E. Akyol, *J. Cryst. Growth.* **2014**, *401*, 266–270. DOI:10.1016/j.jcrysgro.2013.11.048
- S. Polat, *J. Cryst. Growth.* **2019**, *508*, 8–18. DOI:10.1016/j.jcrysgro.2018.12.017
- M. A. Popescu, R. Isopescu, C. Matei, G. Fagarasan, V. Plesu, *Adv. Powder Technol.* **2014**, *25*, 500–507. DOI:10.1016/j.appt.2013.08.003
- K. S. P. Karunadasa, C. H. Manoratne, H. M. T. G. A. Pitawala, R. M. G. Rajapakse, *J. Phys. Chem. Solid.* **2019**, *134*, 21–28. DOI:10.1016/j.jpics.2019.05.023
- L. Fedunik-Hofman, A. Bayon, S.W. Donne, *Appl. Sci.* **2019**, *9*, 4601. DOI:10.3390/app9214601
- L. Yue, M. Shui, Z. Xu, *Thermochim. Acta.* **1999**, *335*, 121–126. DOI:10.1016/S0040-6031(99)00174-4
- Design-Expert software, Version 10 User's Guide, Stat-Ease.

## Povzetek

Cilji predstavljene študije so bili sledeči: (i) določitev vpliva triptofana na transformacijo polimorfnih faz  $\text{CaCO}_3$ , (ii) preučitev kinetike in termodinamike toplotne razgradnje  $\text{CaCO}_3$  s pomočjo Coats–Redfern-ove metode in (iii) določitev vpliva eksperimentalnih pogojev na delež vaterita pri  $\text{CaCO}_3$  z metodologijo odzivnih površin in centralnega kompozitnega oblikovanja. Pripravljene kristale  $\text{CaCO}_3$  smo analizirali z XRD, FTIR, SEM, BET, AFM in zeta potencialom. Rezultati karakterizacije so pokazali, da se oblika  $\text{CaCO}_3$  kristalov spreminja od gladkih kockastih kristalov kalcita do nepravilnih, poroznih kristalov vaterita, z višanjem koncentracije triptofana. Kinetična študija termične razgradnje je pokazala, da krčenje sledi volumskemu delčnemu mehanizmu, R3, s povprečno aktivacijsko energijo 224.6 kJ/mol. Na osnovi rezultatov iz načrtovanje eksperimentov lahko zaključimo, da je koncentracija triptofana najpomembnejši dejavnik, ki vpliva na delež vaterita v pripravljenih kristalih. Triptofan torej omogoča boljše razumevanje in nadzor tvorbe polimorfov, velikosti in morfologije  $\text{CaCO}_3$  kristalov.



Except when otherwise noted, articles in this journal are published under the terms and conditions of the Creative Commons Attribution 4.0 International License

Scientific paper

# Local Anesthetics Transfer Across the Membrane: Reproducing Octanol-Water Partition Coefficients by Solvent Reaction Field Methods

Hana Kavcic,<sup>1,3</sup> Nejc Umek,<sup>2</sup> Domen Pregeljč,<sup>4</sup> Neli Vintar<sup>1,3,5</sup> and Janez Mavri<sup>5,\*</sup><sup>1</sup> Clinical Department for Anesthesiology and Surgical Intensive Therapy of University Medical Center Ljubljana, Slovenia<sup>2</sup> Institute of Anatomy, Faculty of Medicine, University of Ljubljana, Slovenia<sup>3</sup> Department of Anesthesiology and Reanimatology, Faculty of Medicine, University of Ljubljana, Slovenia<sup>4</sup> Department of Chemistry, Imperial College London<sup>5</sup> Laboratory of Computational Biochemistry and Drug Design, National Institute of Chemistry, Ljubljana, Slovenia

\* Corresponding author: E-mail: janez.mavri@ki.si

Received: 11-18-2020

Presented at the Annual Meeting of the Slovenian Chemical Society 2020

## Abstract

Local anesthetics are one of the most widely used drug classes in clinical practice. Like many other biological molecules, their properties are altered depending on their protonation status, which is dependent on the pH of the environment. We studied the transport energetics of seven local anesthetics from the extracellular fluid across the biological membrane to the axoplasm in order to understand the effect of pH value on their efficacy and other pharmaco-dynamic properties. In this we applied three different methods of solvent reaction field in conjunction with quantum chemical calculations to reproduce experimental values of *n*-octanol/water partition coefficients for both neutral and protonated forms. Only the SMD method of Cramer and Truhlar was able to reproduce experimental partition coefficient values. The results are discussed in terms of the function of local anesthetics under physiological conditions and in the case of local acidosis.

**Keywords:** Local Anesthetics; solvent Reaction Field Methods; distribution Coefficient, protonation states

## 1. Introduction

Local anesthetics are a class of compounds originally developed from cocaine to expand its use as a numbing agent, while diminishing its unwanted side effects (e.g. disturbances in heart rhythm and heart attacks, neurological effects). They are currently the only drug class able to provide safe and effective local anesthesia and are widely used in medical and dental practice for pain control during surgical procedures and postoperative treatment.<sup>1,2</sup> They work by inhibiting voltage-dependent sodium channels and therefore blocking the transduction of the action potential along the neuronal axon.<sup>3</sup> While procedures done under local anesthesia are safer than general anesthesia, there remain possible complications, including the cardiotoxicity and neurotoxicity of certain local anesthetics.<sup>4</sup> The success rate of the

procedure is also substantially dependent on the skill level of the medical provider.<sup>5</sup> Broadening the therapeutic window, reducing the toxicity and fine-tuning the pharmacodynamic properties of local anesthetics are a few of the key goals that can be achieved by furthering research into the physiochemical characteristics of local anesthetics.

Most local anesthetics are weak bases with an acid dissociation constant ( $pK_a$ ) of 7 to 10, which means that at physiological pH, both the protonated and neutral forms are present.<sup>6</sup> In order to efficiently inhibit the channel, it is necessary for local anesthetics to first cross the biological membrane in their neutral form, diffuse to the receptor site and reprotonate before binding to the channel.<sup>7</sup> Membrane partitioning of local anesthetics has been determined by several methods, e.g. spectrophotometrically determining the *n*-octanol/water partition coefficient<sup>6</sup> or

by thermodynamic optometric studies of the interaction of a dipalmitoylphosphatidylcholine (DMPC) bilayer membrane with local anaesthetics.<sup>8</sup> Both found extensive partitioning of the neutral form of the local anaesthetic into the membrane. In recent years, computer modelling of local anaesthetic membrane transfer has been the method of choice, utilizing quantum chemistry calculations. Martin et al. examined the partitioning behaviour of the local anaesthetic benzocaine and found out that benzocaine favourably partitions into the lipid bilayer and is likely to accumulate just inside the lipid headgroups.<sup>9</sup> This has been reproduced by similar experiments for lidocaine, tetracaine and articaine, embedded in the DMPC lipid bilayer, with similar results.<sup>10–12</sup> These experiments confirm the idea that only the neutral form of local anaesthetics crosses the membrane in significant amounts. Membrane partitioning seems to be directly related to the potency(6,8) and duration of action<sup>13,14</sup> of local anaesthetics, however the mechanisms behind this observations are not clear. It should be emphasized that experimental techniques involving local anesthetic equilibrium properties and transport across the neuron membrane are extremely demanding and provide only a fraction of the necessary data. In this respect, *n*-octanol is a good approximation of a neuronal membrane and the *n*-octanol/water partition coefficient is an established property of a drug acting on the central nervous system needed to pass the hematocerebral (blood-brain) barrier.<sup>15</sup>

The aim of this article is to calculate the *n*-octanol/water partition coefficients for a few representative local anaesthetics in their neutral and protonated forms and critically compare them with the experimental values. We calculated the free energy of transfer using the experimentally determined partition coefficients provided by Strichartz et al.<sup>6</sup> We compared experimental values to the calculated values by using quantum chemical calculations and various solvent reaction field methods. The results are discussed in terms of their transport from the extracellular fluid to the axoplasm and in the opposite direction. The former determines onset of action and the latter defines the duration of action. The role of Schwann cells is also discussed.

## 2. Experimental

### 2.1. Quantum Chemical Calculations

We performed quantum chemical calculations of local anaesthetics along with various solvent reaction field methods. The structures of all local anaesthetics and their protonated analogs were built using the Molden v5.8 software package.<sup>16</sup> Calculations were performed using the Gaussian 16 software package.<sup>17</sup> The initial geometries of structures were optimized at the M06-2X/6-31+G(d,p) level, which is a good compromise between computational cost and reliability of results. For comparison, we performed the same calculations using the M06-2X/cc-PVDZ basis set

for lidocaine. The effects of solvation were considered by applying various solvent reaction field methods including an integral equation formalism variant (IEFPCM),<sup>18</sup> conductor-like polarizable continuum model (CPCM)<sup>19</sup> and universal solvation model, based on density (SMD) (20). Please note that the parameters of the SMD solvation models were obtained by fitting to reproduce solvation free energies for a large number of organic solutes in various solvents including *n*-octanol.<sup>20</sup> In the present study two solvents were considered: water with a dielectric constant of 78.30 and *n*-octanol with a dielectric constant of 9.86. The latter is an established model for a biological membrane.<sup>21,22</sup> In this respect, the solvation free energy of a substance in *n*-octanol versus the hydration free energy represents a standard measure of the ability of a drug to cross the membrane and is a standard procedure in the drug discovery process. All structures were optimized by including the solvent reaction field.<sup>23</sup> By inclusion of the solvent reaction field, the Born–Oppenheimer surface obtains meaning of a free energy surface. For all minimized structures, a vibrational analysis was performed in the harmonic approximation. The calculated frequencies allowed for thermodynamic corrections of free energies at 298.15 K.

### 2.2. Distribution Coefficient of Local Anaesthetics Between *n*-Octanol and Water

Because local anaesthetics are weak bases with pK<sub>a</sub> values between 7 and 10, their protonation states are pH dependent. Since protonated species have much more favorable solvation energy in water than in *n*-octanol, it is anticipated that at acidic pH values, local anaesthetics prefer to stay in the aqueous phase, while at neutral and basic pH values they show a higher tendency to stay in the *n*-octanol phase. Strichartz et al.<sup>6</sup> performed measurements of local anesthetic partition between *n*-octanol and water buffer at extremely acidic pH and extremely basic pH, providing partition coefficient data for protonated local anaesthetics [LA<sup>+</sup>] and neutral local anaesthetics [LA<sup>0</sup>]. For pH values between the two extreme cases, the distribution coefficients *Q* is pH and pK<sub>a</sub> dependent.

The distribution coefficient [*Q*] is an equilibrium constant and a measure of free energy. It is defined as the ratio of concentrations of local anaesthetics in water and in *n*-octanol, both protonated [LA<sup>+</sup>] and neutral [LA<sup>0</sup>]:

$$Q = \frac{[LA^0]_o + [LA^+]_o}{[LA^0]_w + [LA^+]_w} \quad (1)$$

where [LA<sup>0</sup>]<sub>o</sub> stands for concentration of the neutral form of local anesthetic in *n*-octanol, [LA<sup>0</sup>]<sub>w</sub> for its concentration in the aqueous solution, [LA<sup>+</sup>]<sub>o</sub> the concentration of the protonated form of local anesthetic in *n*-octanol, and [LA<sup>+</sup>]<sub>w</sub> the concentration in the aqueous solution.

If we expand the nominator and denominator on the right side of the equation by a factor of 1/[LA<sup>0</sup>]<sub>w</sub>, we obtain:

$$Q = \frac{[LA^0]_o/[LA^0]_w + [LA^+]_o/[LA^+]_w}{1 + [LA^+]_w/[LA^0]_w} \quad (2)$$

The partition coefficient of neutral species [ $P^0$ ] is the ratio of neutral local anesthetic in *n*-octanol and water;  $[LA^0]_o/[LA^0]_w$ . Similarly, the partition coefficient of protonated species [ $P^+$ ] is the ratio of protonated local anesthetic in *n*-octanol and water;  $[LA^+]_o/[LA^+]_w$ . When we introduce these variables, we get the compact form of the equation:

$$Q = \frac{P^0 + P^+ [LA^+]_w/[LA^0]_w}{1 + [LA^+]_w/[LA^0]_w} \quad (3)$$

By considering the relation  $\ln(x) = \ln(10)\log(x)$  and introducing a new variable  $\log \beta = pH - pK_a$ , it is possible to write an equation for the local anesthetic distribution coefficient as a function of pH and  $pK_a$ .

$$Q = \frac{P^0 + P^+ 10^{pK_a - pH}}{1 + 10^{pK_a - pH}} = \frac{P^0 + \beta P^+}{1 + \beta} \quad (4)$$

Since the distribution coefficient is an equilibrium constant, we can calculate the corresponding difference in free energy of transfer from an aqueous solution with a certain pH value to the membrane, which is also the difference between the two energies of solvation. The equation reads:

$$\begin{aligned} \Delta G &= -k_B T \ln Q = -k_B T \ln \frac{P^0 + P^+ 10^{pK_a - pH}}{1 + 10^{pK_a - pH}} = \\ &= -k_B T \ln \frac{P^0 + \beta P^+}{1 + \beta} \end{aligned} \quad (5)$$

### 3. Results

Experimental  $pK_a$  values, *n*-octanol/water partition coefficients and calculated free energy differences for the studied local anesthetics are collected in Table 1. Please note that all experimental values are from the article by Strichartz et al.<sup>6</sup>

Neutral local anesthetics generally prefer the membrane environment, whereas their protonated counterparts generally prefer water. Neutral etidocaine is 4900 times more likely to be in *n*-octanol than in water, while this number is only 304 for lidocaine. For protonated species, the situation is basically reversed as they prefer an aqueous environment. Protonated lidocaine is 16.7 times more likely to be in water than in *n*-octanol, while protonated etidocaine is 2.1 times more likely to be in water than in *n*-octanol. An exception is protonated bupivacaine, which still prefers the membrane environment. Ester linked local anesthetics share the same attributes with amide-linked ones. Neutral procaine and neutral 2-chloroprocaine are, respectively, 81 and 720 times more likely to be found in the membrane than in the aqueous environment. Protonated procaine is 500 times more likely to be in water than in *n*-octanol, while protonated 2-chloroprocaine is 38 times more likely to be in water than in *n*-octanol.

Calculated free energies for the transfer of neutral and protonated local anesthetics from water to *n*-octanol, calculated with three solvent reaction field methods (IEF-PCM, CPCM and SMD) are collected in Table 2. Free energies for the transfer from water to *n*-octanol, calculated from the experimental results of Strichartz, are added for comparison.

The range of difference between experimental results and the results from the IEFPCM method is between 4.31 and 6.46 kcal mol<sup>-1</sup> for the neutral form and between 2.05 and 5.19 kcal mol<sup>-1</sup> for the protonated form. The range of difference for the CPCM method is between 3.16 and 6.61 kcal mol<sup>-1</sup> for the neutral form and between 1.05 and 4.71 kcal mol<sup>-1</sup> for protonated form. The range of difference for the SMD method is between 0.16 and 2.96 kcal mol<sup>-1</sup> for the neutral form and between 0.03 and 5.15 kcal mol<sup>-1</sup> for the protonated form.

The same comparison between the three solvation field methods was done in a different basis set (M06-2X/cc-PVDZ) for lidocaine, with similar results. They are summarized in Table 3.

**Table 1. Experimental  $pK_a$  (acid dissociation constant) values, *n*-octanol/water partition coefficients and calculated free energy differences for studied local anesthetics.**  $pK_a^{\text{exp}}$  values refer to the experimentally calculated acid dissociation constants and were determined by the spectrophotometrical method. All experiments were performed at 25 °C.  $P^0$  is the *n*-octanol/water partition coefficient for the neutral form of local anesthetic,  $P^+$  is the protonated form.  $\Delta G_{wo}^0$  refers to free energy for transfer of unprotonated local anesthetics from water to *n*-octanol, while  $\Delta G_{wo}^+$  is the corresponding value for protonated species.

Local anesthetic	Type	$pK_a^{\text{exp}}$	$P^0$	$P^+$	$\Delta G_{wo}^0$ (kcal mol <sup>-1</sup> )	$\Delta G_{wo}^+$ (kcal mol <sup>-1</sup> )
Procaine	ester	9.06	81	0.002	-2.60	3.68
2-chloroprocaine	ester	9.30	720	0.026	-3.90	2.16
Lidocaine	amide	8.19	304	0.06	-3.38	1.66
Bupivacaine	amide	8.21	2565	1.5	-4.65	-0.24
Etidocaine	amide	8.11	4900	0.48	-5.03	0.43
Mepivacaine	amide	7.92	90	0.09	-2.66	1.43
Ropivacaine	amide	8.16	775	0.46	-3.94	0.46

**Table 2. Calculated free energies for the transfer of neutral and protonated local anesthetics from water to n-octanol.** Three solvent reaction field methods were used.  $\Delta G_{wo}^0$  and  $\Delta G_{wo}^+$  refer to the calculated free energies for the transfer of neutral and protonated local anesthetics from water to n-octanol. Experimental free energy values for the transfer of local anesthetics in their neutral and protonated form from water to n-octanol ( $\Delta G_{wo}^0(\text{exp})$  and  $\Delta G_{wo}^+(\text{exp})$ , respectively) are calculated from the experimental n-octanol/water partition coefficients.<sup>(6)</sup> All values are given in kcal mol<sup>-1</sup>.

Local Anesthetic	Solvent Reaction Field Method							
	M06-2X/6-31+G(d,p) IEFPCM		M06-2X/6-31+G(d,p) CPCM		M06-2X/6-31+G(d,p) SMD		$\Delta G_{wo}^0(\text{exp})$	$\Delta G_{wo}^+(\text{exp})$
	$\Delta G_{wo}^0$	$\Delta G_{wo}^+$	$\Delta G_{wo}^0$	$\Delta G_{wo}^+$	$\Delta G_{wo}^0$	$\Delta G_{wo}^+$		
Procaine	1.71	5.73	1.18	4.73	-1.78	1.08	-2.60	3.68
2-chloroprocaine	1.47	6.50	1.25	4.92	-0.94	-0.09	-3.90	2.16
Lidocaine	1.37	5.94	1.34	5.28	-4.14	1.69	-3.38	1.66
Bupivacaine	1.81	4.95	1.96	4.47	-3.68	-2.05	-4.65	-0.24
Etidocaine	1.21	5.62	0.79	4.93	-5.19	1.38	-5.03	0.43
Mepivacaine	1.09	6.11	0.50	4.94	-3.62	-3.72	-2.66	1.43
Ropivacaine	2.18	5.32	1.21	4.95	-3.61	-1.36	-3.94	0.46

**Table 3. Calculated free energies for the transfer of neutral and protonated lidocaine from water to n-octanol.**  $\Delta G_{wo}^0$  and  $\Delta G_{wo}^+$  refer to the calculated free energies for the transfer of neutral and protonated local anesthetics from water to n-octanol. Experimental free energy values for the transfer of local anesthetics in their neutral and protonated form from water to n-octanol ( $\Delta G_{wo}^0(\text{exp})$  and  $\Delta G_{wo}^+(\text{exp})$ , respectively) are calculated from experimental n-octanol water partition coefficients.

Lidocaine	Solvent Reaction Field Method							
	M06-2X/cc-PVDZ IEFPCM		M06-2X/cc-PVDZ CPCM		M06-2X/cc-PVDZ SMD		$\Delta G_{wo}^0(\text{exp})$	$\Delta G_{wo}^+(\text{exp})$
	$\Delta G_{wo}^0$	$\Delta G_{wo}^+$	$\Delta G_{wo}^0$	$\Delta G_{wo}^+$	$\Delta G_{wo}^0$	$\Delta G_{wo}^+$		
Lidocaine	1.16	16.31	0.80	4.62	-4.57	2.33	-3.38	1.66

The basis set cc-PVDZ, in conjunction with all applied solvation models, provided very similar results for lidocaine to those obtained with Pople's basis set 6-31+G(d,p).

## 4. Discussion

Our comparison of the free energies of solvation, calculated using three different solvation methods implemented in Gaussian 16, and free energies calculated from the experimental results of Strichartz et al., show that the best solvation model for predicting partition coefficients is the SMD method of Cramer and Truhlar.

Experimental data (Table 1) clearly demonstrate that all local anesthetics in their neutral form strongly prefer n-octanol over water. Therefore, at physiological conditions, the membrane does not represent a barrier to the transfer of local anesthetics from the extracellular liquid to the axoplasm since their population in the membrane is increased rather than decreased.

Local anesthetics are less effective when applied to inflamed tissue.<sup>24–26</sup> Under inflammatory conditions, the pH of the extracellular fluid is lowered by 0.5 to 1 pH unit giving rise to a shifted equilibrium for local anesthetics between the extracellular fluid and axoplasm.<sup>27</sup> Concomitantly, intracellular pH does not change significantly, but

stays at a pH value of around 7.1.<sup>28,29</sup> This results in the storage capacity of the membrane and Schwann cells constituting the myelin sheath and hydrophobic parts of other cells in the vicinity being significantly decreased. Preliminary calculations reveal that the storage capacity is decreased by a factor of about 3.5 relative to the physiological value. This is a plausible explanation for why local anesthetics are significantly less effective when applied to inflamed tissue. This conception is also supported by the clinical practice of co-administering sodium bicarbonate, which elevates the extracellular pH and allows for an increase in storage capacity of the surrounding tissue.<sup>30–32</sup> The body reacts to inflammation by vasodilation, increasing blood flow through the affected area, thus removing more local anesthetic molecules from the target tissue, which could provide an additional explanation for the diminished efficacy and duration of action in inflamed tissues.<sup>33</sup>

We performed the calculations with three solvent reaction field methods, namely IEFPCM, CPCM and SMD. The applied DFT method M06-2X was designed to reproduce thermochemical data including stabilities and barrier heights for chemical reactions. In conjunction with the flexible basis set 6-31+G(d,p), the applied quantum level of theory should faithfully reproduce the charge distribution as a necessary input for the solvation model. We also repeated the measurements for lidocaine for a different

basis set (M06-2X/cc-PVDZ). The results differ only slightly from the results obtained with the Pople's basis set and are within the error margin of the method used, as shown in Table 3. All three methods correctly assume that the neutral form has a lower free energy of transfer from water to *n*-octanol compared to the protonated counterpart, as shown in Table 2. The IEFPCM method and CPCM method both predict that all the differences in free energy are positive, which conflicts with the experimental results. The SMD method aligns better with the experimental results but overstates the partitioning of protonated local anesthetics in *n*-octanol, e.g. the differences in free energy are negative in three cases, whereas, according to the experimental results, they are positive. The SMD method was validated by a critical comparison between the experimental and calculated values of partition coefficients for both neutral and protonated local anesthetics (*vide infra*).

Our results indicate that only the SMD solvation model reasonably reproduces experimental free energies of transfer from aqueous solution to *n*-octanol. For most local anesthetics, SMD deviates less than 2 kcal mol<sup>-1</sup> from the experimental values. In contrast, both IEFPCM and CPCM failed significantly since they did not even qualitatively reproduce the experimental values *i.e.* preference for water versus *n*-octanol. It should be noted that the calculation of partition coefficients requires very accurate solvation models where two solvation free energies are subtracted from each other. Only the SMD model was properly parametrized for this demanding task since solvation parameters were adjusted to reproduce solvation free energy in several solvents including *n*-octanol. When determining the properties of other small organic compounds, the SMD model has proven to be the most precise solvation method as well.<sup>34–36</sup> In this respect, we recommend application of the SMD solvation model during the process of designing novel local anesthetics. The COSMO-RS solvation model, which also proved to yield comparably reliable *n*-octanol/water partition coefficients, is unfortunately not implemented in Gaussian 16.<sup>35</sup> It should be emphasized that among the applied solvent reaction field methods only SMD was parametrized to reproduce solvation free energy in *n*-octanol. The critical elements of parametrization are always nonbonding interactions with the solvent that include reversible work for cavity creation, a dispersion component of the solvation energy and an interaction between the charge distribution and dielectric continuum. PCM and CPCM did not reproduce the solvation energy in *n*-octanol and this is the main contribution to the discrepancy in the partition coefficient.

An alternative method for calculating the solvation free energy would be the treatment of several solvent molecules on the atomic level, inclusion of thermal averaging and application of one of the methods for free energy calculations, such as thermodynamic integration or perturbation. A critical component of such simulation are nonbonding solvent-solute interactions, especially atomic

charges and the dispersion component of van der Waals parameters. We did not proceed in this direction since such calculations are much more demanding in terms of complexity and CPU time.

The ultimate approach for modeling local anesthetics distribution between various parts of the neuron such as the extracellular fluid, membrane, axoplasm and myelin sheath and voltage-gated sodium channel is molecular simulation with atomic resolution. Contributions by Lyubartsev and coworkers represent a valuable starting point in the this regard.<sup>10,11</sup> It should be noted that Lyubartsev and coworkers<sup>10–12</sup> did not explicitly calculate the partition coefficients but rather the potential of mean force for transferring local anesthetics from the aqueous phase to a membrane composed of dimyristoylphosphatidylcholine (DMPC). Therefore, it is not possible to calculate the *n*-octanol-water partition coefficient from the calculated potential of mean force and compare it with the experimental value. They did, however, demonstrate the relevance of the boundary separating the aqueous phase and the bilayer, which is the preferred position for local anesthetics. Van der Spoel et al. developed a calculation protocol for determining *n*-octanol/water partition coefficients for a series of potential toxins by using molecular dynamics simulation.<sup>35</sup> It remains a challenge for the future to apply this approach to the studied local anesthetics. The structure of the voltage-gated sodium channel has been solved by cryo-electron microscopy with a resolution of 3.80 Å.<sup>(37)</sup> It remains a major challenge to model the binding of local anesthetics to the sodium channel binding site along with the associated conformational changes and decreased permeability to sodium ions. We are aware that correlation times for such conformational changes are long, which would require a very long simulation time.

In conclusion, our study represents a small step forward towards understanding the function of local anesthetics on a molecular level. We showed that the rate limiting step in the transport of local anesthetics from the point of bolus administration to the axoplasm is the macroscopic diffusion to and from the membrane, not the membrane crossing itself. Future challenges will include development of more sophisticated mathematical models of the process as well as clarification of the relevance of Schwann cells and other cells as lipid reservoirs and how they influence local anesthetic pharmacokinetics. The final goal is understanding the relationship between the structure of local anesthetics and their pharmacodynamic properties in order to design novel local anesthetics with the desired properties.

## 5. Conclusions

We demonstrated that local anesthetics flow from the compartment with a higher pH value to the compartment with a lower pH value since protonated local anesthetics have a more favorable solvation energy than their



neutral counterparts. This is consistent with clinical experience, i.e. in tissue acidosis, local anesthetics are less effective. Experimental data show that all local anesthetics in their neutral form strongly prefer *n*-octanol over water, whereas the protonated form mostly prefers the aqueous environment. In quantum chemical calculations, only the SMD solvent reaction field method was able to predict the same behavior and it seems to be the best model for prediction of the *n*-octanol/water partition coefficient.

## Acknowledgments

This work was supported by the Slovenian Research Agency (grant numbers P1-0012 and P3-0043). We would like to thank Tanja Gavranic of the National Institute of Chemistry, Ljubljana, Slovenia for her assistance with graphical work. We would also like to thank Ms. Charlotte Taft for proofreading the manuscript.

## 6. References

- Miller R, Eriksson L, Fleisher L, Wiener-Kronish J, Cohen N, Young W. Miller's anesthesia: Chapter 36 Local Anesthetics. In: Miller's Anesthesia. 8th Editio. ELSEVIER Churchill Livingstone, 2014.
- Becker DE, Reed KL. Local Anesthetics: Review of Pharmacological Considerations. *Anesth Prog.* 2012, 59(2), pp. 90–102. DOI:10.2344/0003-3006-59.2.90
- Kaplan MR, Meyer-Franke A, Lambert S, et al. Induction of sodium channel clustering by oligodendrocytes. *Nature.* 1997, 386(6626), pp. 724–728. DOI:10.1038/386724a0
- Markova L, Umek N, Horvat S, et al. Neurotoxicity of bupivacaine and liposome bupivacaine after sciatic nerve block in healthy and streptozotocin-induced diabetic mice. *BMC Vet Res.* 2020, 16, pp. 247. DOI:10.1186/s12917-020-02459-4
- Helander EM, Kaye AJ, Eng MR, et al. Regional Nerve Blocks—Best Practice Strategies for Reduction in Complications and Comprehensive Review. *Curr Pain Headache Rep.* 2019, 23(6), pp. 43. DOI:10.1007/s11916-019-0782-0
- Strichartz GR, Sanchez V, Arthur GR, Chafetz R, Martin D. Fundamental properties of local anesthetics. II. Measured octanol:buffer partition coefficients and pKa values of clinically used drugs. *Anesth Analg.* 1990, 71(2), pp. 158–170. DOI:10.1213/0000539-199008000-00008
- Wang G-K, Strichartz GR: State-dependent inhibition of sodium channels by local anesthetics: A 40-year evolution. *Biochemistry (Mosc).* 2012, 6, pp. 120–127. DOI:10.1134/S1990747812010151
- Hata T, Sakamoto T, Matsuki H, Kaneshina S. Partition coefficients of charged and uncharged local anesthetics into dipalmitoylphosphatidylcholine bilayer membrane: Estimation from pH dependence on the depression of phase transition temperatures. *Colloids Surf B Biointerfaces.* 2001, 22(1), pp. 77–84. DOI:10.1016/S0927-7765(01)00160-6
- Martin LJ, Chao R, Corry B. Molecular dynamics simulation of the partitioning of benzocaine and phenytoin into a lipid bilayer. *Biophys Chem.* 2014, 185, pp. 98–107. DOI:10.1016/j.bpc.2013.12.003
- Saeedi M, Lyubartsev AP, Jalili S. Anesthetics mechanism on a DMPC lipid membrane model: Insights from molecular dynamics simulations. *Biophys Chem.* 2017, 226, pp. 1–13. DOI:10.1016/j.bpc.2017.03.006
- Högberg CJ, Maliniak A, Lyubartsev AP. Dynamical and structural properties of charged and uncharged lidocaine in a lipid bilayer. *Biophys Chem.* 2007, 125(2–3), pp. 416–424. DOI:10.1016/j.bpc.2006.10.005
- Jalili S, Saeedi M. Study of procaine and tetracaine in the lipid bilayer using molecular dynamics simulation. *Eur Biophys J.* 2017, 46(3), pp. 265–282. DOI:10.1007/s00249-016-1164-8
- Thut PD, Turner MD, Cordes CT, Wynn RL. A rabbit tooth-pulp assay to quantify efficacy and duration of antinociception by local anesthetics infiltrated into maxillary tissues. *J Pharmacol Toxicol Methods.* 1995, 33(4), pp. 231–236. DOI:10.1016/1056-8719(95)00023-B
- Langerman L, Golomb E, Grant GJ, Benita S. Duration of spinal anaesthesia is determined by the partition coefficient of local anaesthetic. *Br J Anaesth.* 1994, 72(4), pp. 456–459. DOI:10.1093/bja/72.4.456
- Leo A, Hansch C, Elkins D. Partition coefficients and their uses. *Chem Rev.* 1971, 71(6), pp. 525–616. DOI:10.1021/cr60274a001
- Schaftenaar G, Noordik JH. Molden: a pre- and post-processing program for molecular and electronic structures. *J Comput Aided Mol Des.* 2000, 14(2), pp. 123–134. DOI:10.1023/A:1008193805436
- Gaussian 16, Revision B.01, M. J. Frisch, G. W. Trucks, H. B. Schlegel, G. E. Scuseria, M. A. Robb, J. R. Cheeseman, G. Scalmani, V. Barone, G. A. Petersson, H. Nakatsuji, X. Li, M. Caricato, A. V. Marenich, J. Bloino, B. G. Janesko, R. Gomperts, B. Mennucci, H. P. Hratchian, J. V. Ortiz, A. F. Izmaylov, J. L. Sonnenberg, D. Williams-Young, F. Ding, F. Lipparini, F. Egidi, J. Goings, B. Peng, A. Petrone, T. Henderson, D. Ranasinghe, V. G. Zakrzewski, J. Gao, N. Rega, G. Zheng, W. Liang, M. Hada, M. Ehara, K. Toyota, R. Fukuda, J. Hasegawa, M. Ishida, T. Nakajima, Y. Honda, O. Kitao, H. Nakai, T. Vreven, K. Throssell, J. A. Montgomery, Jr., J. E. Peralta, F. Ogliaro, M. J. Bearpark, J. J. Heyd, E. N. Brothers, K. N. Kudin, V. N. Staroverov, T. A. Keith, R. Kobayashi, J. Normand, K. Raghavachari, A. P. Rendell, J. C. Burant, S. S. Iyengar, J. Tomasi, M. Cossi, J. M. Millam, M. Klene, C. Adamo, R. Cammi, J. W. Ochterski, R. L. Martin, K. Morokuma, O. Farkas, J. B. Foresman, and D. J. Fox, Gaussian, Inc., Wallingford CT, 2016.
- Miertuš S, Scrocco E, Tomasi J. Electrostatic interaction of a solute with a continuum. A direct utilization of AB initio molecular potentials for the prevision of solvent effects. *Chem Phys.* 1981, 55(1), pp. 117–129. DOI:10.1016/0301-0104(81)85090-2
- Cossi M, Rega N, Scalmani G, Barone V. Energies, structures, and electronic properties of molecules in solution with the

- C-PCM solvation model. *J Comput Chem.* **2003**, *24*(6), pp. 669–681. DOI:10.1002/jcc.10189
20. Marenich A V, Cramer CJ, Truhlar DG. Universal solvation model based on solute electron density and on a continuum model of the solvent defined by the bulk dielectric constant and atomic surface tensions. *J Phys Chem B.* **2009**, *113*(18), pp. 6378–6396. DOI:10.1021/jp810292n
21. Pignatello R, Musumeci T, Basile L, Carbone C, Puglisi G. Biomembrane models and drug-biomembrane interaction studies: Involvement in drug design and development. *J Pharm Bioallied Sci.* **2011**, *3*(1), pp. 4–14. DOI:10.4103/0975-7406.76461
22. Ritter J, Flower R, Henderson G, Rang H. Rang & Dale's Pharmacology, 8th Edition. 8th Editio. Churchill Livingstone; **2015**.
23. Schutz CN, Warshel A. What are the dielectric "constants" of proteins and how to validate electrostatic models? *Proteins Struct Funct Genet.* **2001**, *44*(4), pp. 400–417. DOI:10.1002/prot.1106
24. Boronat López A, Peñarrocha Diago M. Failure of locoregional anesthesia in dental practice. Review of the literature. *Med Oral Patol Oral Cir Bucal.* **2006**, *11*(6), pp. E510–E513.
25. Potocnik I, Bajrović F. Failure of inferior alveolar nerve block in endodontics. *Endod Dent Traumatol.* **1999**, *15*(6), pp. 247–251. DOI:10.1111/j.1600-9657.1999.tb00782.x
26. Ueno T, Tsuchiya H, Mizogami M, Takakura K. Local anesthetic failure associated with inflammation: verification of the acidosis mechanism and the hypothetic participation of inflammatory peroxynitrite. *J Inflamm Res.* **2008**, *1*, pp. 41–48. DOI:10.2147/JIR.S3982
27. Punnia-Moorthy A. Evaluation of pH changes in inflammation of the subcutaneous air pouch lining in the rat, induced by carrageenan, dextran and *Staphylococcus aureus*. *J Oral Pathol.* **1987**, *16*(1), pp. 36–44. DOI:10.1111/j.1600-0714.1987.tb00674.x
28. Caldwell PC. Studies on the internal pH of large muscle and nerve fibres. *J Physiol.* **1958**, *142*(1), pp. 22–62. DOI:10.1113/jphysiol.1958.sp005998
29. Madshus IH. Regulation of intracellular pH in eukaryotic cells. *Biochem J.* **1988**, *250*(1), pp. 1–8. DOI:10.1042/bj2500001
30. Gupta S, Kumar A, Sharma AK, Purohit J, Narula JS. Sodium bicarbonate: an adjunct to painless palatal anesthesia. *Oral Maxillofac Surg.* **2018**, *22*(4), pp. 451–455. DOI:10.1007/s10006-018-0730-x
31. Guo J, Yin K, Roges R, Enciso R. Efficacy of sodium bicarbonate buffered versus non-buffered lidocaine with epinephrine in inferior alveolar nerve block: A meta-analysis. *J Dent Anesth pain Med.* **2018**, *18*(3), pp. 129–142. DOI:10.17245/jdapm.2018.18.3.129
32. Bailard NS, Ortiz J, Flores RA. Additives to local anesthetics for peripheral nerve blocks: Evidence, limitations, and recommendations. *Am J Heal Pharm.* **2014**, *71*(5), pp. 373–385. DOI:10.2146/ajhp130336
33. Huang AL, Vita JA. Effects of systemic inflammation on endothelium-dependent vasodilation. *Trends Cardiovasc Med.* **2006**, *16*(1), pp. 15–20. DOI:10.1016/j.tcm.2005.10.002
34. Umek N. Cyclization step of noradrenaline and adrenaline autoxidation: a quantum chemical study. *RSC Adv.* **2020**, *10*, pp. 16650–16658. DOI:10.1039/D0RA02713H
35. Van Der Spoel D, Manzetti S, Zhang H, Klamt A. Prediction of Partition Coefficients of Environmental Toxins Using Computational Chemistry Methods. *ACS Omega.* **2019**, *4*(9), pp. 13772–13781. DOI:10.1021/acsomega.9b01277
36. Bernales VS, Marenich A V., Contreras R, Cramer CJ, Truhlar DG. Quantum mechanical continuum solvation models for ionic liquids. *J Phys Chem B.* **2012**, *116*(30), pp. 9122–9129. DOI:10.1021/jp304365v
37. Shen H, Zhou Q, Pan X, Li Z, Wu J, Yan N. Structure of a eukaryotic voltage-gated sodium channel at near-atomic resolution. *Science.* **2017**, *355*, pp. 924. DOI:10.2210/pdb5x0m/pdb

## Povzetek

Lokalni anestetiki so eden najpogosteje uporabljenih razredov zdravil v klinični praksi. Tako kot pri mnogih drugih bioloških molekulah, se tudi njihove lastnosti spreminjajo glede na njihov protonacijski status, ki je odvisen od pH okolja. Proučevali smo transportno energetiko sedmih lokalnih anestetikov iz zunajcelične tekočine preko biološke membrane do aksoplazme, da bi razumeli vpliv vrednosti pH na njihovo učinkovitost in druge farmako-dinamične lastnosti. Pri tem smo uporabili tri različne metode reakcijskega polja topila v povezavi s kvantno-kemijskimi izračuni za reprodukcijo eksperimentalnih vrednosti koeficientov porazdelitve *n*-oktanol / voda za nevtralne in protonirane oblike. Samo SMD metoda Cramerja in Truhlarja je lahko reproducirala eksperimentalne vrednosti porazdelitvenih koeficientov. Rezultati so obravnavani v smislu funkcije lokalnih anestetikov v fizioloških pogojih in v primeru lokalne acidoze.



Except when otherwise noted, articles in this journal are published under the terms and conditions of the Creative Commons Attribution 4.0 International License

Scientific paper

# Isolation of Keratin from Waste Wool Using Hydrothermal Processes

Aleksandra Verdnik,<sup>1</sup> Maja Čolnik,<sup>1</sup> Željko Knez<sup>1,2</sup> and Mojca Škerget<sup>1,\*</sup><sup>1</sup> University of Maribor, Faculty of Chemistry and Chemical Engineering, Smetanova 17, 2000 Maribor, Slovenia<sup>2</sup> University of Maribor, Faculty of Medicine, Taborska ulica 8, 2000 Maribor, Slovenia

\* Corresponding author: E-mail: mojca.skerget@um.si

Received: 11-26-2020

## Abstract

The subcritical water (SubCW) extractions of waste wool to produce keratin were performed at temperatures of 150 °C to 250 °C and at different reaction times between 5 min to 75 min. The resulting proteins in the obtained products were confirmed with Fourier-transform infrared spectroscopy (FTIR). The molecular weight of the protein extracts was determined by using two different methods: with a polyacrylamide gel electrophoresis in the presence of sodium dodecyl sulphate (SDS-PAGE) and by using a gel permeation chromatography. The results show, that by using SubCW, keratin can be isolated from waste wool in very high yields, much higher than by other chemical methods. Maximal yield was achieved at 180 °C and 60 min and it was 90.3%. The molecular weight distributions of extracted proteins, which were generated from waste wool were between 14 kDa and 4 kDa, what is comparable to the results obtained by other chemical methods.

**Keywords:** Waste wool; keratin; isolation; SubCW; gel permeation chromatography; SDS-PAGE electrophoresis.

## 1. Introduction

The growing concerns regarding the environmental pollution and the increasing demand for safe and sustainable materials are encouraging the search for green processing methods that would allow exploitation of natural resources and development of bio-based products. By-products of the textile and meat industries, such as wool, horns, hooves and feathers contain a large proportion of keratin.<sup>1,2</sup> Keratin is a protein that has, due to its biodegradability and biocompatibility, recently become increasingly important.<sup>3</sup> Wool is often used in textile industry due to its excellent mechanical properties. More than 2.5 million tons of wool is produced every year all over the world, where Australia, China, New Zealand, Iran and Argentina represent five of the biggest producers of wool.<sup>4</sup> The problem is that during the shearing and weaving processes as well as by processing in abattoirs also a considerable amount of wool waste is generated. Wool contains up to 95% of pure keratin, which is an important secondary product.<sup>5</sup> In addition to proteins, wool contains small proportion of lipids, mineral salts, nucleic acid residues and carbohydrates.<sup>2</sup> Keratin has an extremely high potential to be used for the development of new products

in the pharmaceutical, medical, cosmetic and biotechnology industries. Keratin from wool can be used for several forms of gels, microfibrils, films, sponges, bulk materials, in wound healing, drug delivery, tissue engineering and medical devices.<sup>1,4,6,7</sup>

For the extraction of keratin from natural by-products different methods were used: reduction, oxidation, microwave radiation, sulfitolysis, alkaline extraction, ionic liquids and use of enzymes.<sup>8,9</sup> The disadvantage of these methods is that organic solvents and harmful chemicals are used, that could disrupt the structure of keratin and consequently have a negative influence on keratin properties. Organic solvents are expensive, toxic and non-renewable and pollute our environment.<sup>6,8,10</sup>

Recently, subcritical water (SubCW) has been increasingly used as a green medium for the extraction of value-added compounds from various materials, as it has many beneficial properties compared to other organic solvents.<sup>11</sup> SubCW is known as hot water under pressure with the critical point at 374 °C and 221 bar.<sup>12,13</sup> Under these conditions, the ionic product, diffusivity and thermal conductivity of water increase.<sup>11,14–16</sup> The advantages of the methods where SubCW is used as a medium are that they are performed rapidly and selectively without a catalyst,<sup>17</sup>

give high yields and high purity of products and water is easily removed from the decomposition products.<sup>18,19</sup>

SubCW was used for hydrolysis of biomass waste (fish waste, chicken waste, hair and feathers), to produce amino acids.<sup>20</sup> Isolation of keratin from waste wool with SubCW has not yet been published. Until now, superheated water<sup>9</sup> and steam explosion<sup>21</sup> have been used for the isolation of keratin from wool and the yields of keratin were quite low (up to 30%).<sup>9,21</sup>

The aim of this study was the development of SubCW isolation process of protein keratin from waste wool and to evaluate the performance of the process regarding the yield and molecular weight of the produced protein. The protein extracts were characterized with SDS-PAGE electrophoresis, gel permeation chromatography and FTIR analysis and new data about the molecular weight distribution of the keratin, isolated from wool with SubCW are presented.

## 2. Experimental

### 2.1. Materials

The waste wool of white traditional Slovenian sheep was kindly donated by local sheep farm. Trizma® base, sodium dodecyl sulfate, ammonium persulfate, glycine, methanol, 2-propanol, bovine serum albumin, trypsin, hydrochloric acid, dextran blue and Sephadex G-100 were supplied by Sigma-Aldrich. Coomassie brilliant blue G-250, sodium chloride, potassium chloride, disodium phosphate, potassium phosphate, monobasic, methylene blue and potassium chloride were supplied by Merck. Acetic acid was supplied by J.T.Baker. Lonza™ ProSieve™ protein marker was supplied by Fisher Scientific. 3X blue stained deposition buffer for SDS-PAGE electrophoresis and dithiothreitol were supplied by BioLabs Inc.

### 2.2. Isolation of Keratin from Waste Wool with SubCW

The high pressure and high temperature batch reactor (series 4740 Stainless Steel, Parr Instruments, Moline, IL, USA) was filled with 2 g of raw wool and 40 mL of distilled water. The ratio of solvent to wool was 20 mL/g. The filled reactor was purged three times with an inert nitrogen gas (N<sub>2</sub>) and the pressure in the reactor was set to 20 bar. The reactor was wrapped with a heating wire and

glass wool in order to prevent heat losses. The reactions were carried out at different temperatures and different reaction times, as shown in Table 1. After the extraction, the reactor was rapidly cooled down.

The post reaction mixture was filtered by vacuum permeation and the products were collected in the forms of aqueous solution and solid residue.

A portion of the aqueous solution (2 mL) was evaporated using a rotary evaporator to determine the yield of extracted keratin. The yield of keratin was calculated by the equation 1, where the initial mass of wool ( $m_{\text{wool}}$ ), mass of extracted products ( $m_{\text{products}}$ ) and a percent of keratin (95%) in wool ( $w$ ) were considered. The yields of keratin were calculated on assumption, that wool contains 95% of keratin.

$$\eta_{\text{keratin}} = \frac{m_{\text{products}}}{w \cdot m_{\text{wool}}} \cdot 100 \quad (1)$$

The remaining aqueous solution was stored in the freezer for further analysis.

### 2.3. Fourier Transformed Infrared Spectroscopy (FTIR)

The presence of functional groups characteristic of the extracted keratin (amide A, amide I, amide II, amide III) was confirmed using the technique of attenuated total reflection of infrared spectroscopy by Fourier transform (ATR-FTIR) in the wavelength range of 4000 cm<sup>-1</sup> and 400 cm<sup>-1</sup>. The data were analyzed with the high-performance IR solution software.<sup>9</sup>

### 2.4. Gel Permeation Chromatography

The molecular weight of extracted proteins was determined with gel permeation chromatography. For the preparation of stationary phase, 5% Sephadex G-100 gel was dissolved into deionized water and incubated at 95 °C for 5 h. Cooled Sephadex-G 100 was transferred into the glass separation column. 0.1 M phosphate buffered saline (PBS) at pH = 7.2 as the mobile phase were used.

The molecular weight determination of extracted proteins was done by comparing the ratio of  $V_e/V_0$  for the sample protein and the  $V_e/V_0$  of protein standards of known molecular weight, where  $V_e$  is the elution volume of standard protein and  $V_0$  is the void volume.<sup>22,23</sup> The  $V_0$  of a glass separation column is based on the volume of effluent required for the elution of 0.2% blue dextran (large molecule). The calibration curve was prepared based on the standard proteins with already known molecular weights in the range from 66000-360 Da. (Table 2).

The calibration curve of standards (equation 2) represents the dependence of the logarithm of the molecular weight (log M) on the ratio between the elution volume and the void volume of the column:

Table 1. SubCW reaction conditions

Temperature	Reaction time
150 °C	5 min, 15 min, 30 min, 60 min
180 °C	5 min, 15 min, 30 min, 60 min, 75 min
200 °C	5 min, 15 min, 30 min, 60 min
250 °C	5 min, 15 min, 30 min, 60 min

$$\log(M) = \frac{V_e}{V_0} \cdot k + n \quad (2)$$

where  $M$  is a molecular weight of keratin,  $V_e$  elution volume,  $V_0$  void volume of column (27 mL),  $k$  inclination of the curve and  $n$  section on the y axis.<sup>22,23</sup>

Table 2. Molecular weights of standards

Standard protein	Molecular weight (Da)
bovine serum albumin (BSA)	66 000
trypsin	23 800
methylene blue	360

Based on the equation 2 and elution volume of individual samples of isolated keratin the molecular weight of keratin was calculated.

In order to determine the elution volume of standards and samples, 1.4 mL of standards or sample solutions were loaded at the top of the column, the valve at the bottom was opened and the fractions of 1.5 mL were taken. The mobile phase (PBS buffer) was added at the top of the column throughout the experiment. The absorbance of the obtained fractions was measured by UV-Vis spectrophotometer at a wavelength of 280 nm.<sup>23</sup> The fraction with the highest absorbance represented the elution volume of an individual sample or standard.

## 2. 5. SDS-PAGE Electrophoresis

The molecular weight of the extracted keratin was determined by the SDS-PAGE gel electrophoresis. For the protein separation acrylamide/bisacrylamide (Acryl/Bis) separation gel with 1.5 M Tris-HCl buffer at pH 8.8 and 6% Acryl/Bis stacking gel with 0.5 M Tris HCl buffer at pH 6.8 were prepared. 20  $\mu$ L of extracted keratin sample was added to 20  $\mu$ L of loading buffer (mixture of SDS Blue Loading Buffer and dithiothreitol (DTT)). All prepared samples were incubated at 95 °C for 3-5 min and then centrifugated at 10,000 rpm for 2 min. Afterwards, 10  $\mu$ L of sample and protein marker (mixture of highly purified proteins with molecular weights from 4.6 to 300 kDa) were pipetted from the bottom of the vial and transferred into the bottom of the gel wells. The electrophoresis was run at 150 V for 90 min with tris-glycine-SDS running buffer (pH 8.3).

After electrophoresis, the gels well were washed with deionized water and colored with Coomassie blue, methanol and acetic acid water mixture. Then, the gels were discolored with methanol, acetic acid water mixture. After that all gels were dried on the filter paper with a vacuum pump.

The gels were analysed by using *ImageJ* free software, which was based on the calibration curve of the protein marker, where the distances ( $d$ , in pixels) from the boundary between the entry and separation gel to the protein

marker were measured. The calibration curve observes the dependence of  $\log M$  on the distance ( $d$ ).<sup>8</sup>

## 3. Results and Discussion

### 3. 1. Influence of Temperature and Reaction Time on Keratin Yield

The yield of keratin in the reaction mixture is affected by temperature and reaction time as it is shown in Table 3. At the low temperature of 150 °C and at short reaction times from 5-30 min the yield of keratin was the lowest and it was only between 1% and 26%. As can be seen from Figure 1 at these conditions also the highest amount of wool residue was found. Rajabinejad et al.<sup>9</sup> reported about similar yield of keratin (31%) obtained from wool with superheated water in a microwave at 170 °C and 30 min. In the present work however, by increasing the temperature to 180 °C, a much higher content of keratin in the liquid product was gained. The maximum yield of keratin (90.3%) was achieved at the temperature of 180 °C and reaction time of 60 min. Generally, the results show, that with increasing the temperature and prolonging the reaction time, the yield of keratin first increases and reaches a maximum and then it started to decrease. Namely, the high temperatures probably caused further decomposition of keratin to oligomers and free amino acids.<sup>9</sup>

Table 3. Yield of extracted keratin from waste wool with SubCW.

$t$ (min)	$T = 150$ °C	$T = 180$ °C	$T = 200$ °C	$T = 250$ °C
	$\eta_{\text{keratin}}$ (%)	$\eta_{\text{keratin}}$ (%)	$\eta_{\text{keratin}}$ (%)	$\eta_{\text{keratin}}$ (%)
5	1.7	23.8	73.0	73.3
15	5.4	57.9	81.1	75.3
30	16.1	71.4	87.6	80.5
60	25.6	90.3	86.0	63.2
75	/	73.6	/	/

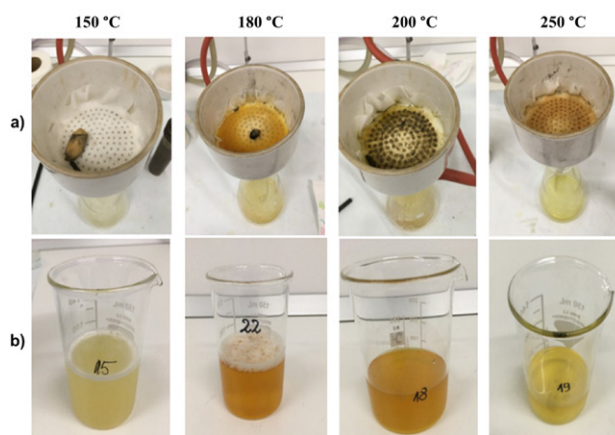


Figure 1. Reaction products at 150 °C, 180 °C, 200 °C and 250 °C at the reaction time (60 min); a) wool residues after filtration, b) liquid reaction product.

Furthermore, the differences in concentration of keratin in aqueous solutions obtained at different operating parameters are also visible by the color of the liquid product (Figure 1). The color of the aqueous solutions changed from a very pale yellow colored solutions obtained at the lowest and the highest temperatures (150 °C, 250 °C) to an intense yellow colored solution obtained at middle temperatures (180 °C and 200 °C) where the yield of keratin was near or at the maximum.

### 3. 2. FTIR Analysis of Isolated Keratin

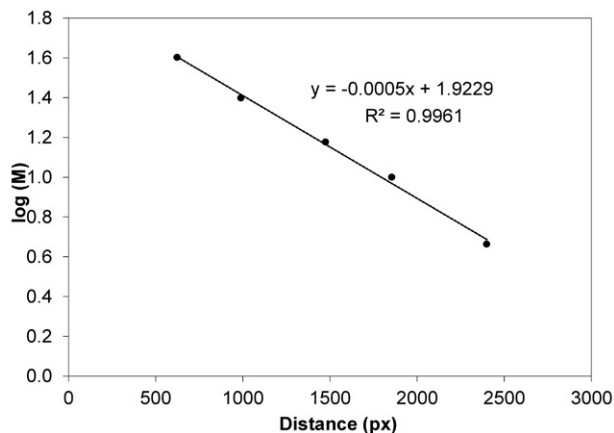
In order to characterize the extracted keratin obtained from waste wool in SubCW at 180 °C and 60 min, FT-IR spectra were recorded. The infrared absorption spectra show characteristic absorption bands attributed to the peptide bonds.<sup>24</sup>

In Figure 2, the major peaks represent peptide bonds characteristic for amides: amide A, amide I, amide II, amide III). Amide A peak at 3230 cm<sup>-1</sup> represents specific absorption bands for N-H bond while peak at 1635 cm<sup>-1</sup> (Amide I) is related to the C=O stretching vibration. Amide II (between 1480 cm<sup>-1</sup> and 1580 cm<sup>-1</sup>) shows elongation of C-N bond and bending of N-H functional groups, while amide III at wavelength 1242 cm<sup>-1</sup> is a combination of N-H, C-N and C=O groups. Peaks that appear in the range between 2800 cm<sup>-1</sup> and 3000 cm<sup>-1</sup> are attrib-

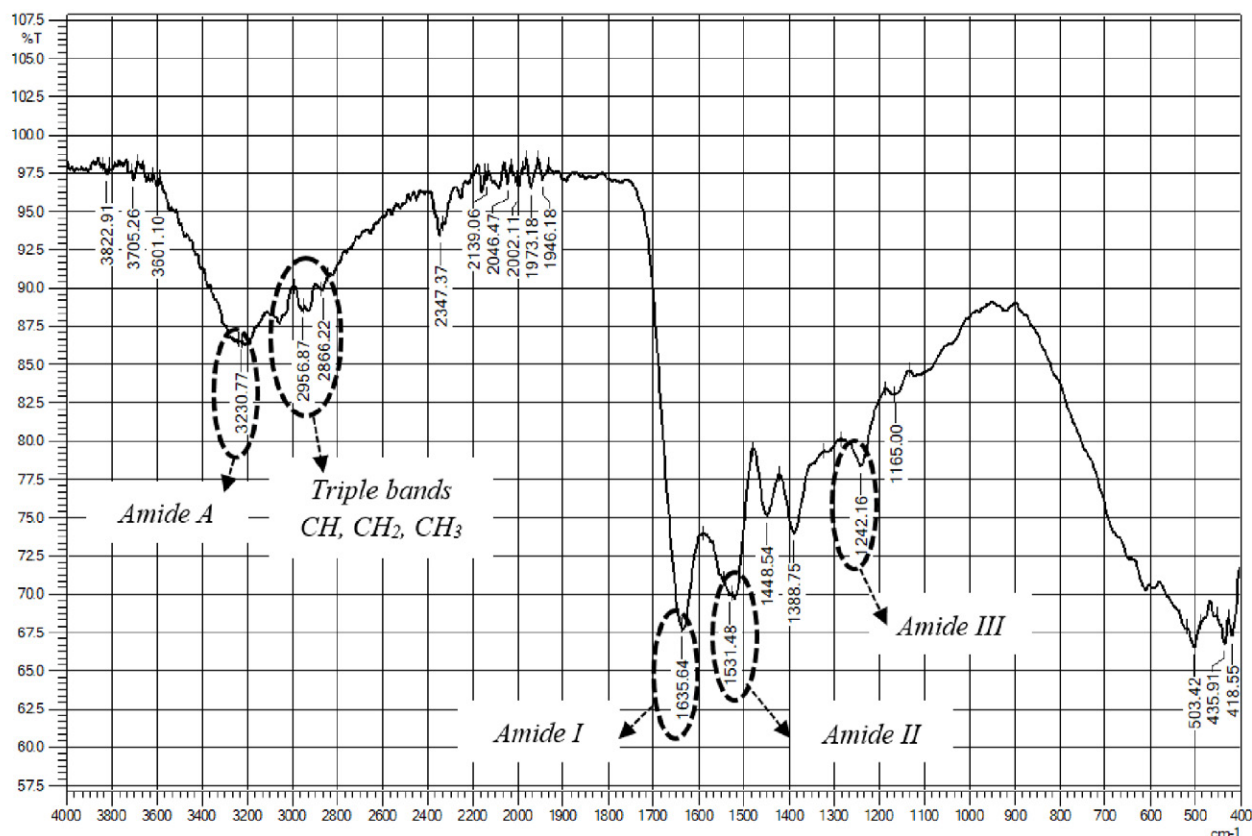
uted to the methylene stretching vibrations of the CH, CH<sub>2</sub> and CH<sub>3</sub> functional groups.<sup>24</sup>

### 3. 2. Molecular Weight of Isolated Keratin

The determination of the molecular weight of keratin with SDS-PAGE electrophoresis was done based on the calibration curve of protein standards (Figure 3) and by the elution of standards with known molecular weight



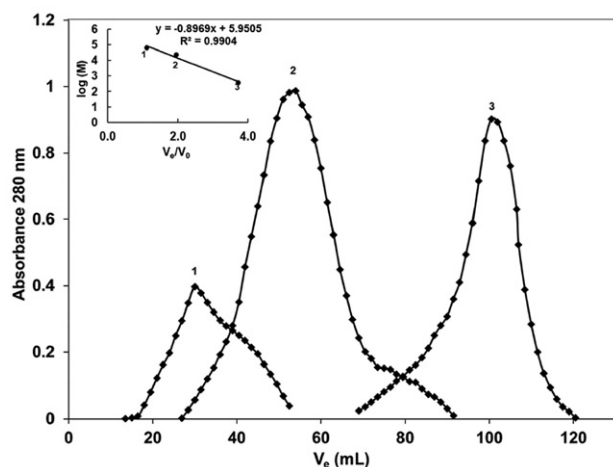
**Figure 3.** Standard curve of molecular weight markers using SDS-PAGE electrophoresis for molecular weight estimation of keratin samples, which are obtained by hydrothermal degradation of waste wool at 180 °C.



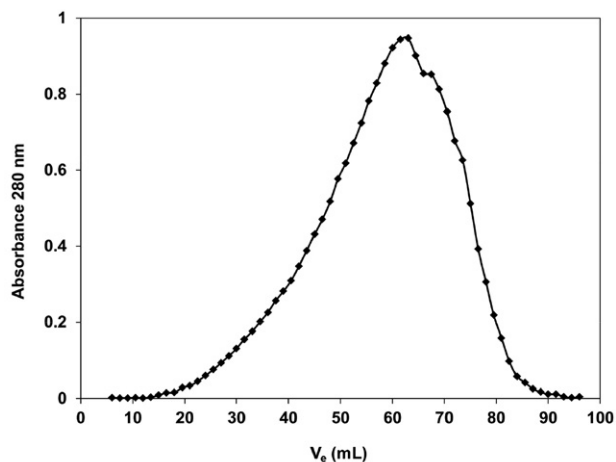
**Figure 2.** FTIR spectrum of keratin isolated from waste wool with SubCW at temperature of 180 °C and a reaction time of 60 min.

(Figure 4) in Sephadex G-100 gel under the same conditions as the sample of extracted keratin (Figure 5).

The molecular weight distributions of the extracted proteins are shown in Table 4 and Figure 6. Figure 6 shows the SDS-PAGE electropherograms of wool proteins isolated by SubCW at different temperatures and reaction times.



**Figure 4.** Gel permeation chromatography through Sephadex G-100 of standard proteins with known molecular weight: (1) BSA; (2) trypsin; (3) methylene blue.

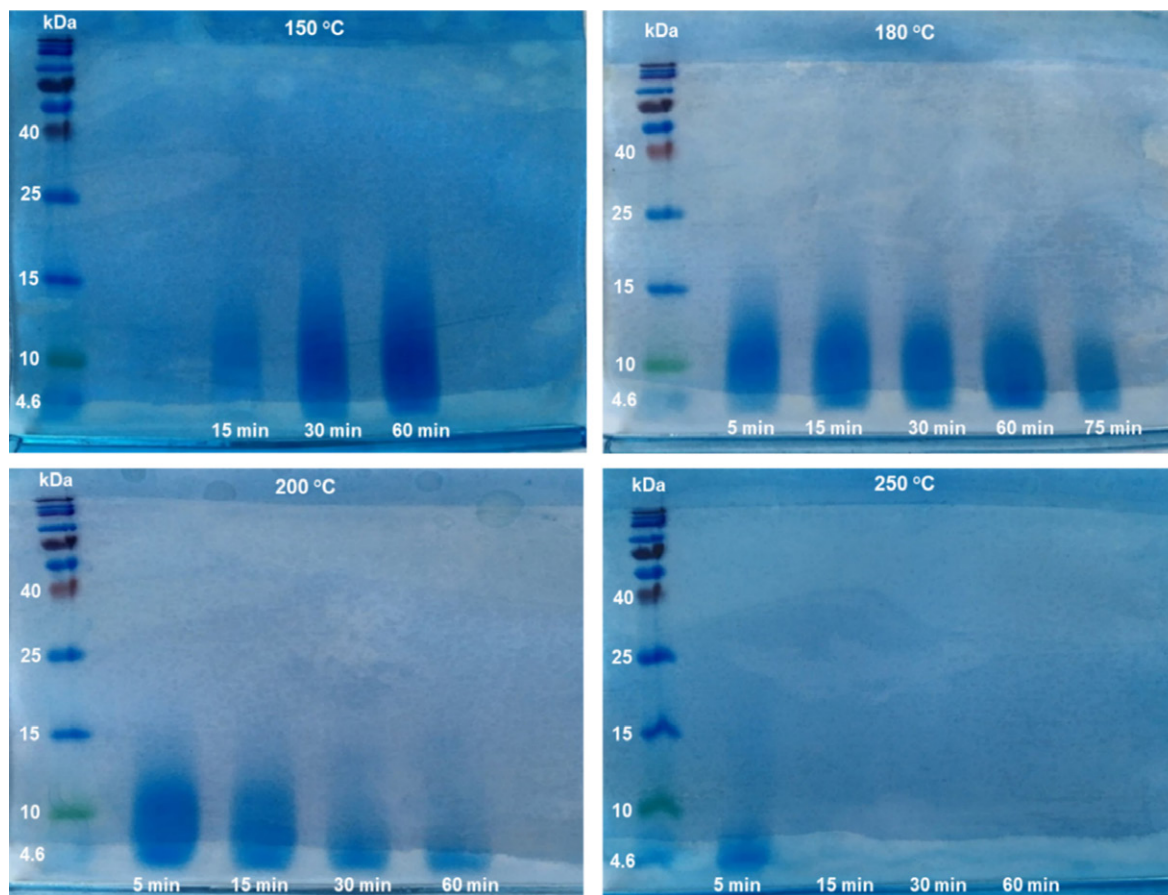


**Figure 5.** Gel permeation chromatography through Sephadex G-100 of isolated keratin at temperature of 180 °C and time 60 min.

Generally, the molecular weights of extracted proteins were quite low in all cases. A major protein fractions were in the range of 14 kDa and 4 kDa.

Molecular weight distribution of isolated keratin at temperature of 150 °C and at time 5 min has not been determined, while the yield of keratin was only 1.7%.

Table 4 shows, that molecular weight of extracted proteins decreased with increasing the temperature and



**Figure 6.** SDS-PAGE electrophoresis gels of isolated keratin.

Table 4. Molecular weight of keratin.

Temperature (°C)	Reaction time (min)	Molecular weight of keratin (kDa) (gel permeation chromatography)	Molecular weight of keratin (kDa) (SDS-PAGE)
150	15	9.2	5–14.0
150	30	8.3	4.6–14.0
150	60	8.2	4.6–13.9
180	5	7.5	4.6–12.5
180	15	7.4	4.6–12.0
180	30	7.3	4.6–11.5
180	60	7.2	4.6–11.3
180	75	6.6	4.6–10.4
200	5	6.5	4.6–10.8
200	15	5.9	4.6–8.8
200	30	5.2	4.6–6.5
200	60	4.7	4.6–6.3
250	5	4.6	4.6–5.0
250	15	4.2	/
250	30	4.1	/
250	60	3.7	/

reaction time due to further degradation of long chain proteins to smaller molecules.

As can be seen from Figure 6, the clear major fraction band between 14–8 kDa appeared after the hydrolysis of waste wool at 150 °C for reaction time of 30 and 60 min. Similar strong bands can be observed for products obtained at 180 °C that indicate molecular weight between 13 kDa and 7 kDa for all reaction times, while molecular weights at a higher temperature of 200 °C are much lower, only between 10.8 kDa and 5 kDa. In the case of 250 °C the major protein fraction in the range from 5 to 4.6 kDa results only for 5 min of reaction time, while at longer reaction times no bands were observed in the studied gels, which is a consequence of their degradation to very low molecular weight oligopeptides.<sup>8</sup> Low molecular weights of keratin indicated that structure of keratin was significantly affected with the high temperature of the SubCW treatment (cleavage of peptide bonds).

Based on the results it can be concluded that the optimal temperatures for isolation of keratin molecules of high molecular weights by using SubCW would be 150 °C or 180 °C, because at these two temperatures molecular weights of keratin obtained were the highest and were in the range of 14 kDa to 4.6 kDa.

### 3. 4. Comparison of Molecular Weights of Keratin Extracted from Wool by Different Methods

The molecular weight of keratin is influenced by the source from which the keratin is extracted due to structural differences, different content of sulphur and covalent intermolecular disulfide bonds, and by the method of keratin isolation.<sup>8,9,24</sup>

In Table 5 the molecular weights and yields of wool keratin obtained by different chemical methods reported in the literature are compared with the results obtained in the present work.

Table 5. Keratin molecular weights determined by SDS-PAGE electrophoresis and its yields isolated in different ways.

Extraction method	Molecular weight of keratin (kDa)	Yield of keratin (%)
Oxidation <sup>24</sup>	> 40	6
Alkaline hydrolysis <sup>24</sup>	< 10	25
Superheated water <sup>9</sup>	14–3	31
Sulfitolysis <sup>24</sup>	60–40 and 15–3.5	41
Ionic liquid <sup>24</sup>	60–3.5	51
Reduction <sup>24</sup>	55–40 and 10–3.5	53
H <sub>2</sub> O <sub>2</sub> <sup>8</sup>	36–6	54
<b>SubCW</b>	<b>14–4.0</b>	<b>90.3</b>

Shavandi and co-workers<sup>24</sup> studied five different extraction methods of keratin from wool of merino sheep. They used alkaline hydrolyses, reduction, oxidation, sulfitolysis and ionic liquid. For the reduction a solution of urea, sodium dodecyl sulphate and 2-mercaptoethanol was used, which gave the highest yield of keratin (53%). By using the ionic liquid, the yield of keratin was 51%. For sulfitolysis a solution of urea and sodium bisulfide was used and the yield of obtained keratin was 41%. Alkaline hydrolysis was done in the presence of 2% solution of sodium hydroxide, where only 25% of keratin was isolated. The oxidation reaction, where the 2% solution of acetic acid was used, the lowest yield of keratin (6%) was achieved. Keratin obtained by these various methods had different molecular weight and different physical-chemical proper-



ties.<sup>24</sup> In addition, keratin from wool and feathers was also extracted with different concentrations of hydrogen peroxide (H<sub>2</sub>O<sub>2</sub>), where the highest yield of keratin from wool was obtained with 1M H<sub>2</sub>O<sub>2</sub> at pH = 11 and it was 72.6%.<sup>8</sup>

All chemical methods for keratin isolation presented in Table 5, except the oxidation method, gave keratin with molecular weights in a similar range as SubCW, which is between 14 kDa and 4 kDa, however all the methods gave much lower yields as SubCW method, where the highest yield was 90.3%. This is an important advantage over other extraction methods, which use additional organic solvents and harmful chemicals, which pollute and cause negative effects on our environment. The use of SubCW for isolation of keratin from wool is a much greener alternative.

#### 4. Conclusion

Keratin isolation from waste wool was performed in a high pressure and high temperature batch reactor with SubCW at temperatures of 150 °C–250 °C and at different reaction time from 5 min to 75 min. At the lowest temperature of isolation (150 °C) the yields of keratin were very low (between 1% and 26%). The highest yield of keratin was achieved at 180 °C and at a reaction time of 60 min and it was 90.3%. At a temperature of 250 °C, the yield of keratin was lower than at a temperature 200 °C. The presence of keratin in reaction product was confirmed by FTIR spectroscopy. Molecular weights of extracted keratin were determined by gel permeation chromatography and SDS-PAGE electrophoresis. It was found that the molecular weight distribution of protein extracts was between 14 kDa and 4 kDa. The molecular weight of protein decreased with increasing temperature, due to degradation of long chain keratin to oligomers and amino acids. The optimum operating conditions for keratin isolation from waste wool with SubCW are temperature 180 °C and reaction time of 60 min where the yield of isolation was high and the molecular weight distribution of proteins was between 11.3 and 4.6 kDa.

The results of this study indicate that extraction of keratin from waste wool with SubCW represents an important alternative to the conventional extraction processes and provide an important basis for further development of keratin based bioactive materials.

#### Acknowledgements

Special thanks to the Slovenian Research Agency (ARRS) for financial support of research programme group P2-0046: Separation processes and production design.

#### 5. References

1. A. Shavandi, T. H. Silva, A. A. Bekhit and A. E.-D. A. Bekhit, *Biomater. Sci.*, **2017**, 5, 1699–1735. DOI:10.1039/C7BM00411G
2. P. Staroń, M. Banach and Z. Kowalski, *Chemik*, **2011**, 65, 1019–1026.
3. S. Sharma, A. Gupta, S. Sharma and A. Gupta, *Braz. Arch. Biol. Technol.*, **2016**, 59, 1–14. DOI:10.1590/1678-4324-2016150684
4. P. Mokrejs, O. Krejci, P. Svoboda and V. Vasek, *Rasayan J. Chem.*, **2011**, 4, 728–735.
5. J. M. Cardamone, *J. Mol. Struct.*, **2010**, 969, 97–105. DOI:10.1016/j.molstruc.2010.01.048
6. S. Zheng, Y. Nie, S. Zhang, X. Zhang and L. Wang, *ACS Sustainable Chem. Eng.*, **2015**, 3, 2925–2932. DOI:10.1021/acssuschemeng.5b00895
7. J. G. Rouse and M. E. Van Dyke, *Materials (Basel)*, **2010**, 3, 999–1014. DOI:10.3390/ma3020999
8. B. Fernández-d'Arlas, *Eur. Polym. J.*, **2018**, 103, 187–197. DOI:10.1016/j.eurpolymj.2018.04.010
9. H. Rajabinejad, M. Zoccola, A. Patrucco, A. Montarsolo, G. Rovero and C. Tonin, *Text. Res. J.*, **2018**, 88, 2415–2424. DOI:10.1177/0040517517723028
10. G. Zhu, X. Zhu, Z. Xiao, R. Zhou, N. Feng and Y. Niu, *Biomass Conv. Bioref.*, **2015**, 5, 309–320. DOI:10.1007/s13399-014-0153-3
11. I. Pavlovič, Ž. Knez and M. Škerget, *J. Agric. Food Chem.*, **2013**, 61, 8003–8025. DOI:10.1021/jf401008a
12. Ž. Knez, M. K. Hrnčič, M. Čolnik and M. Škerget, *J. Supercrit. Fluids*, **2018**, 133, 591–602. DOI:10.1016/j.supflu.2017.08.011
13. H. Qu, J.-H. Gong, X.-C. Tan, P.-Q. Yuan, Z.-M. Cheng and W.-K. Yuan, *Chem. Eng. Sci.*, **2019**, 195, 958–967. DOI:10.1016/j.ces.2018.10.042
14. F. Ondze, O. Boutin, J.-C. Ruiz, J.-H. Ferrasse and F. Charton, *Chem. Eng. Sci.*, **2015**, 123, 350–358. DOI:10.1016/j.ces.2014.11.026
15. X. Su, Y. Zhao, R. Zhang and J. Bi, *Fuel Process. Technol.*, **2004**, 85, 1249–1258. DOI:10.1016/j.fuproc.2003.11.044
16. H. Zhang, X. Su, D. Sun, R. Zhang and J. Bi, *J. Fuel Chem. Technol.*, **2007**, 35, 487–491. DOI:10.1016/S1872-5813(07)60030-9
17. A. Cata, M. Miclau, I. Ienascu, D. Ursu, C. Tanasie and M. N. Stefanuta, *Rev. Roum. Chim.*, **2015**, 60, 579–585.
18. M. Ravber, Ž. Knez and M. Škerget, *J. Supercrit. Fluids*, **2015**, 104, 145–152. DOI:10.1016/j.supflu.2015.05.028
19. S. Jokić, T. Gagić, Ž. Knez, M. Banožić and M. Škerget, *J. Supercrit. Fluids*, **2019**, 153, 104593. DOI:10.1016/j.supflu.2019.104593
20. H. Cheng, X. Zhu, C. Zhu, J. Qian, N. Zhu, L. Zhao and J. Chen, *Bioresour. Technol.*, **2008**, 99, 3337–3341. DOI:10.1016/j.biortech.2007.08.024
21. C. Tonin, M. Zoccola, A. Aluigi, A. Varesano, A. Montarsolo, C. Vineis and F. Zimbardi, *Biomacromolecules*, **2006**, 7, 3499–3504. DOI:10.1021/bm060597w
22. K. C. Duong-Ly and S. B. Gabelli, *Meth. Enzymol.*, **2014**, 541, 105–114. DOI:10.1016/B978-0-12-420119-4.00009-4
23. J. R. Whitaker, *Anal. Chem.*, **1963**, 35, 1950–1953. DOI:10.1021/ac60205a048
24. A. Shavandi, A. E.-D. A. Bekhit, A. Carne and A. Bekhit, *J. Bioact. Compat. Polym.*, **2017**, 32, 163–177. DOI:10.1177/0883911516662069

## Povzetek

Pri temperaturah med 150 in 250 °C in reakcijskih časih med 5–75 min smo izvedli subkritično vodno ekstrakcijo (SubCW) odpadne volne s ciljem pridobivanja keratina. Dobljene proteine prisotne v nastalih produktih smo potrdili z infrardečo spektroskopijo s Fourierovo Transformacijo (FTIR). Molekulsko maso ekstrahiranih proteinov smo določili z dvema tehnikama: poliakrilamidno elektroforezo z natrijevim dodecil sulfatom (SDS-PAGE) ter izključitveno kromatografijo. Rezultati so pokazali, da lahko s SubCW iz odpadne volne pridobimo keratin z zelo visokim izkoristkom, precej višjim kot z ostalimi kemijskimi metodami. Maksimalni izkoristek smo dosegli pri 180 °C in 60 minutah in je znašal 90.3 %. Porazdelitev velikosti proteinov ekstrahiranih iz odpadne volne je bila med 14 kDa in 4 kDa, kar je primerljivo z rezultati ostalih kemijskih metod.



Except when otherwise noted, articles in this journal are published under the terms and conditions of the Creative Commons Attribution 4.0 International License

Scientific paper

# Synthesis, X-Ray Crystal Structures and Catalytic Epoxidation of Oxidovanadium(V) Complexes with Aroylhydrazone and Ethyl Maltolate Ligands

Dong-Hui Zou,<sup>1,\*</sup> Min Liang<sup>2</sup> and Wei Chen<sup>2</sup><sup>1</sup> College of Food and Bio-Engineering, Qiqihar University, Qiqihar 161006, P. R. China<sup>2</sup> School of Chemistry and Chemical Engineering, Qiqihar University, Qiqihar 161006, P. R. China

\* Corresponding author: E-mail: zoudongh1000@163.com

Received: 11-30-2020

## Abstract

Two oxidovanadium(V) complexes, [VOL<sup>1</sup>L] (1) and [VOL<sup>2</sup>L] (2) (L = ethyl maltolate), derived from the aroylhydrazones 4-bromo-*N*'-(2-hydroxy-5-methylbenzylidene)benzohydrazide (H<sub>2</sub>L<sup>1</sup>) and *N*'-(3,5-dibromo-2-hydroxybenzylidene)-4-methoxybenzohydrazide (H<sub>2</sub>L<sup>2</sup>), respectively, have been synthesized and characterized by elemental analysis, infrared and electronic spectroscopy. Structures of the complexes were further confirmed by single crystal X-ray determination. The V atoms in the complexes are coordinated by the ONO donor atoms of the aroylhydrazone ligand, OO donor atoms of the ethyl maltolate ligand, and one oxido O atom, forming octahedral coordination. The complexes function as effective olefin epoxidation catalysts with hydrogen peroxide as terminal oxidant and sodium hydrogen carbonate as a co-catalyst.

**Keywords:** Aroylhydrazone; vanadium complex; catalytic activity; crystal structure

## 1. Introduction

Schiff base complexes have gained remarkable attention due to their interesting applications in the development of new materials like catalysts, and biological applications like DNA cleavage, antibacterial, antiviral and antifungal agents.<sup>1</sup> Metal complexes of hydrazone type Schiff bases were used as catalysts for the organic synthesis, such as olefin polymerization and epoxidation reactions.<sup>2</sup> Among the various metal ions, the complexes of vanadium have received considerable interest in their biochemical significance and industrial catalytic processes.<sup>3</sup> For instance, the use of vanadium complexes in asymmetric synthesis, in C–C bond formation as well as in C–C, C–O and C–H bond cleavages, catalytic oxidation of various olefins, oxidative halogenation and selective epoxidation of unsaturated hydrocarbons and allyl alcohols.<sup>4</sup> Aroylhydrazones bearing typical –CO–NH–N=CH– group are interesting ligands in the preparation of various metal complexes which have considerable biological and catalytic properties.<sup>5</sup> To date, a number of vanadium complexes have been obtained. However, the vanadium complexes with hydrazones are rarely reported with catalytic

oxidation of olefins. Recently, our research group has reported some vanadium complexes and their catalytic epoxidation property.<sup>6</sup> As a continuation of such work, we report in this paper two new vanadium(V) complexes [VOL<sup>1</sup>L] (1) and [VOL<sup>2</sup>L] (2) (L = ethyl maltolate), derived from the aroylhydrazones 4-bromo-*N*'-(2-hydroxy-5-methylbenzylidene)benzohydrazide (H<sub>2</sub>L<sup>1</sup>) and *N*'-(3,5-dibromo-2-hydroxybenzylidene)-4-methoxybenzohydrazide (H<sub>2</sub>L<sup>2</sup>).

## 2. Experimental

### 2.1. Materials and Methods

5-Methylsalicylaldehyde, 3,5-dibromosalicylaldehyde, 4-bromobenzohydrazide and 4-methoxybenzohydrazide were purchased from Sigma-Aldrich. VO(acac)<sub>2</sub> and the solvents with analytical reagent grade were purchased from Xiya Chemicals Co. Ltd. Microanalyses for C, H, N were carried out using a Perkin Elmer 2400 CHNS/O elemental analyzer. <sup>1</sup>H NMR spectra were recorded on a Bruker AVANCE 500 MHz spectrometer. FT-IR spectra were recorded on a FT-IR 8400-Shimadzu as KBr discs in

the range of 400–4000  $\text{cm}^{-1}$ . UV-Vis spectra were recorded on a Lambda 35 spectrometer. X-ray diffraction data were collected using a Bruker Smart 1000CCD diffractometer.

## 2. 2. Synthesis of 4-bromo-*N'*-(2-hydroxy-5-methylbenzylidene)benzohydrazide ( $\text{H}_2\text{L}^1$ )

An ethanolic solution (20 mL) containing 2-hydroxy-5-methylbenzaldehyde (1.0 mmol, 0.14 g) was added dropwise to an ethanolic solution of 4-bromobenzohydrazide (1.0 mmol, 0.22 g) with constant stirring. The mixture was refluxed for 30 min, after which the solvent was removed by rotary evaporator. The white precipitate was re-crystallized from ethanol and obtained by filtration. Yield: 0.25 g, 76%. For  $\text{C}_{15}\text{H}_{13}\text{BrN}_2\text{O}_2$ : anal. calcd., %: C, 54.07; H, 3.93; N, 8.41. Found, %: C, 54.26; H, 4.02; N, 8.32. FT-IR (KBr),  $\text{cm}^{-1}$ :  $\nu(\text{OH})$  3427,  $\nu(\text{NH})$  3241,  $\nu(\text{CH})$  2820–3100,  $\nu(\text{C}=\text{O})$  1645,  $\nu(\text{C}=\text{N})$  1612,  $\nu(\text{C}-\text{O})$  1157. UV-Vis data in ethanol ( $\lambda$ , nm ( $\epsilon$ ,  $\text{M}^{-1}\text{cm}^{-1}$ )): 231 (19,270), 285 (18,125), 303 (17,430), 345 (12,653).  $^1\text{H}$  NMR (500 MHz,  $\text{DMSO}-d_6$ , ppm):  $\delta$  = 12.03 (s, 1H; OH), 11.12 (s, 1H; NH), 8.62 (s, 1H; CH=N), 7.87 (d, 2H; ArH), 7.73 (d, 2H; ArH), 7.45 (s, 1H, ArH), 7.12 (d, 1H; ArH), 6.95 (d, 1H, ArH), 2.32 (s, 3H,  $\text{CH}_3$ ).

## 2. 3. Synthesis of *N'*-(3,5-dibromo-2-hydroxybenzylidene)-4-methoxybenzohydrazide ( $\text{H}_2\text{L}^2$ )

An ethanolic solution (20 mL) containing 3,5-dibromo-2-hydroxybenzaldehyde (1.0 mmol, 0.28 g) was added dropwise to an ethanolic solution of 4-methoxybenzohydrazide (1.0 mmol, 0.17 g) with constant stirring. The mixture was refluxed for 30 min, after which the solvent was removed by rotary evaporator. The white precipitate was re-crystallized from ethanol and obtained by filtration. Yield: 0.31 g, 72%. For  $\text{C}_{15}\text{H}_{12}\text{Br}_2\text{N}_2\text{O}_3$ : anal. calcd., %: C, 42.09; H, 2.83; N, 6.54. Found, %: C, 41.85; H, 2.92; N, 6.46. FT-IR (KBr),  $\text{cm}^{-1}$ :  $\nu(\text{OH})$  3447,  $\nu(\text{NH})$  3221,  $\nu(\text{CH})$  2820–3100,  $\nu(\text{C}=\text{O})$  1653,  $\nu(\text{C}=\text{N})$  1612,  $\nu(\text{C}-\text{O})$  1153. UV-Vis data in ethanol ( $\lambda$ , nm ( $\epsilon$ ,  $\text{M}^{-1}\text{cm}^{-1}$ )): 221 (21,250), 272 (17,610), 310 (15,455), 332 (16,820).  $^1\text{H}$  NMR (500 MHz,  $\text{DMSO}-d_6$ , ppm):  $\delta$  = 12.02 (s, 1H; OH), 11.13 (s, 1H; NH), 8.67 (s, 1H; CH=N), 7.88 (d, 2H; ArH), 7.79 (s, 1H; ArH), 7.71 (s, 1H, ArH), 7.13 (d, 2H; ArH), 3.80 (s, 1H,  $\text{CH}_3$ ).

## 2. 4. Synthesis of the complexes [VOL<sup>1</sup>L] (1) and [VOL<sup>2</sup>L] (2)

The aroylhydrazones  $\text{H}_2\text{L}^1$  (0.10 mmol, 33 mg) or  $\text{H}_2\text{L}^2$  (0.10 mmol, 43 mg) was dissolved in ethanol (15 mL). To each solution an ethanolic solution (10 mL) of VO(acac)<sub>2</sub> (0.10 mmol, 26 mg) and ethyl maltol (0.10 mmol, 14 mg) was added with stirring. Mixtures were stirred at room temperature for 30 min to give deep brown

solution. Brown block-shaped single crystals suitable for X-ray analysis were obtained after slow evaporation of the solvent over a few days. The crystals were isolated by filtration.

**Complex 1:** Yield: 0.18 g, 33%. For  $\text{C}_{22}\text{H}_{18}\text{BrN}_2\text{O}_6\text{V}$ : anal. calcd., %: C, 49.18; H, 3.38; N, 5.21. Found, %: C, 49.35; H, 3.31; N, 5.12. FT-IR (KBr),  $\text{cm}^{-1}$ :  $\nu(\text{C}=\text{N})$  1611,  $\nu(\text{C}-\text{O})$  1176,  $\nu(\text{V}=\text{O})$  971. UV-Vis data in ethanol ( $\lambda$ , nm ( $\epsilon$ ,  $\text{M}^{-1}\text{cm}^{-1}$ )): 271 (18,223), 325 (10,370), 410 (2,738). **Complex 2:** Yield: 0.26 g, 41%. For  $\text{C}_{22}\text{H}_{17}\text{Br}_2\text{N}_2\text{O}_7\text{V}$ : anal. calcd., %: C, 41.80; H, 2.71; N, 4.43. Found, %: C, 41.61; H, 2.83; N, 4.51. FT-IR (KBr),  $\text{cm}^{-1}$ :  $\nu(\text{C}=\text{N})$  1608,  $\nu(\text{C}-\text{O})$  1173,  $\nu(\text{V}=\text{O})$  972. UV-Vis data in ethanol ( $\lambda$ , nm ( $\epsilon$ ,  $\text{M}^{-1}\text{cm}^{-1}$ )): 265 (19,560), 332 (12,451), 413 (3,890).

## 2. 5. X-Ray Structure Determination

Crystal structures of complexes were measured on a Bruker SMART 1000CCD diffractometer using Mo-K $\alpha$  radiation ( $\lambda = 0.71073$  Å) and a graphite monochromator at 25 °C. Unit cell and reflection data were obtained by standard methods and are summarized in Table 1.<sup>7</sup> The structures were solved, refined, and prepared for publication using the SHELXTL package (structure solution refinements and molecular graphics),<sup>8</sup> and using full-matrix least-squares techniques by using  $F^2$  with anisotropic displacement factors for all non-hydrogen atoms. The amino H atoms were located from difference Fourier maps and

Table 1. Crystal data and structure refinement for the complexes

Parameters	1	2
Molecular formula	$\text{C}_{22}\text{H}_{18}\text{BrN}_2\text{O}_6\text{V}$	$\text{C}_{22}\text{H}_{17}\text{Br}_2\text{N}_2\text{O}_7\text{V}$
Formula weight	537.23	632.13
Crystal system	Triclinic	Triclinic
Space group	$P-1$	$P-1$
$a$ (Å)	7.4116(9)	9.7299(8)
$b$ (Å)	11.8466(11)	11.1554(10)
$c$ (Å)	13.2718(12)	11.4937(11)
$\alpha$ (°)	107.525(1)	69.303(1)
$\beta$ (°)	93.496(1)	88.575(1)
$\gamma$ (°)	90.253(1)	88.952(1)
$V$ (Å <sup>3</sup> )	1108.8(2)	1166.6(2)
$Z$	2	2
$D_{\text{calc}}$ (g/cm <sup>3</sup> )	1.609	1.800
$\mu$ (mm <sup>-1</sup> )	2.290	3.897
$F(000)$	540	624
Reflections collected	5921	10918
Independent reflection	4075 (0.0134)	4312 (0.0405)
( $R_{\text{int}}$ )		
Reflections observed ( $I > 2\sigma(I)$ )	3102	3227
Data/restraints/parameters	4075/0/291	4312/0/309
Goodness-of-fit on $F^2$	1.025	1.049
Final $R$ indices ( $I > 2\sigma(I)$ )	0.0537, 0.1333	0.0399, 0.0829
$R$ indices (all data)	0.0740, 0.1465	0.0644, 0.0926
Max/min $D\rho$ (e Å <sup>-3</sup> )	1.034, -1.007	0.530, -0.449

refined isotropically, with N–H distances restrained to 0.90(1) Å. Positions of the remaining hydrogen atoms were calculated from the structure of the molecular skeleton and their displacement parameters were refined isotropically on a group-wise basis.

## 3. Results and Discussion

### 3.1. Synthesis and Spectral Characterization

The two complexes were readily prepared from the reaction of the corresponding aroylhydrazone ligands and  $\text{VO}(\text{acac})_2$ . The single crystals of the complexes are stable at ambient condition.

The  $\nu(\text{C}=\text{N})$  absorptions are observed at  $1611\text{ cm}^{-1}$  for **1** and  $1608\text{ cm}^{-1}$  for **2**.<sup>9</sup> The intense bands indicative of the C=O vibrations and the sharp bands indicative of the N–H vibrations are absent in the complexes, indicating the enolization of the aroylhydrazone ligands. The weak peaks in the low wave numbers in the region  $450\text{--}700\text{ cm}^{-1}$  may be attributed to V–O and V–N bonds in the complexes. The complexes exhibit typical bands at  $971\text{--}972\text{ cm}^{-1}$ , which are assigned to the V = O vibrations.<sup>10</sup>

The UV-Vis spectra of the complexes were recorded in  $10^{-5}\text{ mol L}^{-1}$  in ethanol, in the range  $200\text{--}500\text{ nm}$ . The weak bands centered at  $325\text{--}332\text{ nm}$  for the complexes are attributed to intramolecular charge transfer transitions from the  $p_\pi$  orbital on the nitrogen and oxygen to the empty  $d$  orbitals of the metal.<sup>10</sup> The intense bands observed at  $265\text{--}270\text{ nm}$  are assigned to intraligand  $\pi\text{--}\pi^*$  transition. The bands centered at about  $410\text{ nm}$  are attributed to the ligand-to-metal charge transfer transitions (LMCT).<sup>11</sup>

### 3.2. Structure Description of the Complexes

The molecular structures of complexes **1** and **2** are shown in Figs. 1 and 2, respectively. Selected bond lengths

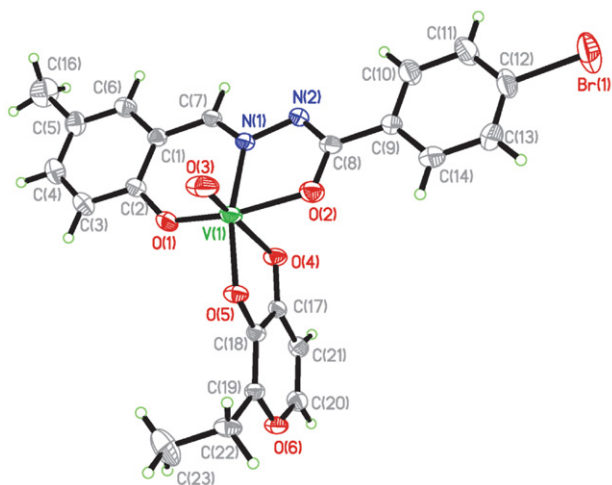


Fig. 1. An ORTEP diagram of complex **1** with atom labeling scheme and 30% probability thermal ellipsoids for all non-hydrogen atoms.

and angles are reported in Table 2. The V atoms in both complexes are six-coordinated in octahedral geometry, with the phenolate oxygen (O(1)), the enolate oxygen (O(2)) and the imine nitrogen (N(1)) of the aroylhydrazone ligands, and the hydroxylate oxygen (O(5)) of the ethyl maltolate ligand in the equatorial plane, and with the oxido group (O(3)) and the carbonyl oxygen (O(4)) in the axial positions. The V atoms deviated from the least-squares planes defining by the four equatorial donor at-

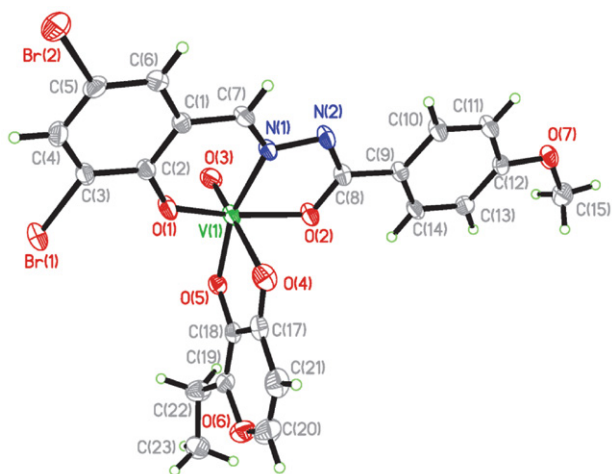


Fig. 2. An ORTEP diagram of complex **2** with atom labeling scheme and 30% probability thermal ellipsoids for all non-hydrogen atoms.

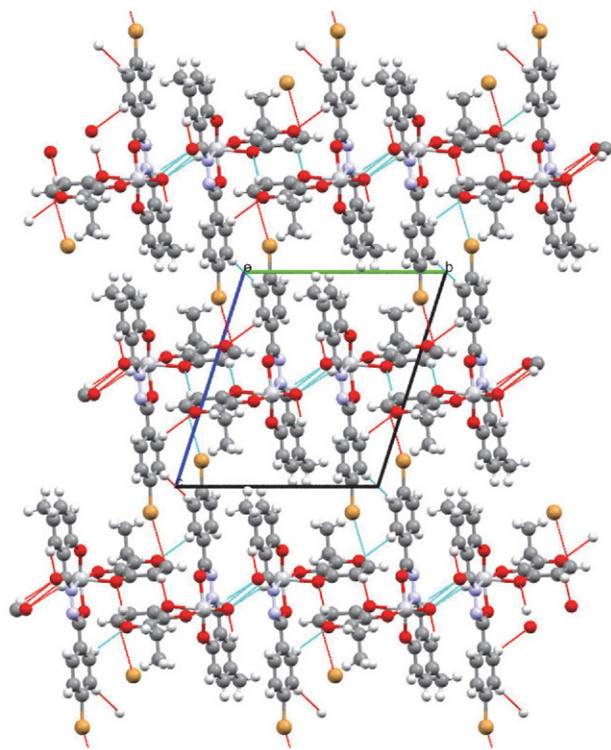


Fig. 3. Hydrogen bonds linked structures of complex **1**, viewed along the  $a$  axis. Hydrogen bonds are shown as dashed lines.

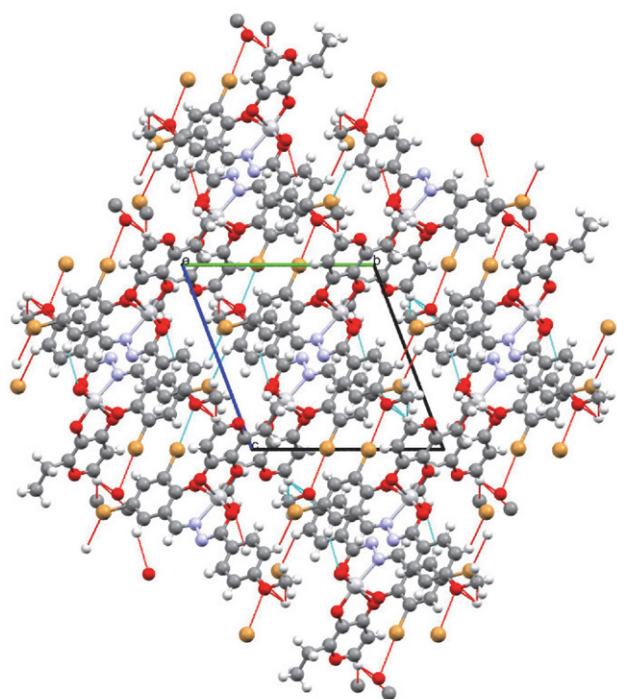


Fig. 4. Hydrogen bonds linked structures of complex 2, viewed along the *a* axis. Hydrogen bonds are shown as dashed lines.

oms by 0.295(2) Å for **1** and 0.290(2) Å for **2**. The bond lengths related to the V atoms are comparable to the similar vanadium complexes.<sup>6b,12</sup> The benzene rings C(1)–C(6) and C(9)–C(14) form dihedral angles of 2.1(3)° for **1** and 2.7(3)° for **2**. There exists weak Br(1)···O(7)<sup>i</sup> (*i*: -1 + *x*, *y*, 1 + *z*) contact with distance of 2.96(5) Å representing 87.8 % of the sum of van der Waals radii in complex **2**.

In the crystal structure of complex **1**, the vanadium complex molecules are linked through C–H···O hydrogen bonds (Table 3) to form layers along the *ab* plane (Fig. 3). In the crystal structure of complex **2**, the vanadium complex molecules are linked through C–H···O and C–H···Br hydrogen bonds (Table 3) to form three-dimensional network (Fig. 4).

Table 3. Hydrogen bonding interactions (Å, °)

<i>D</i> –H··· <i>A</i>	<i>d</i> ( <i>D</i> –H)	<i>d</i> (H··· <i>A</i> )	<i>d</i> ( <i>D</i> ··· <i>A</i> )	Angle( <i>D</i> –H··· <i>A</i> )
<b>1</b>				
C(6)–H(6)···O(3) <sup>ii</sup>	0.93	2.50(3)	3.367(5)	154(6)
C(7)–H(7)···O(3) <sup>iii</sup>	0.93	2.53(3)	3.143(5)	124(6)
C(14)–H(14)···O(6) <sup>iv</sup>	0.93	2.57(3)	3.399(5)	148(6)
C(21)–H(21)···O(4) <sup>v</sup>	0.93	2.42(3)	3.246(5)	148(6)
<b>2</b>				
C(6)–H(6)···O(3) <sup>vi</sup>	0.93	2.56(3)	3.237(4)	130(5)
C(11)–H(11)···Br(2) <sup>vii</sup>	0.93	2.80(3)	3.563(4)	140(5)
C(19)–H(19)···O(7) <sup>viii</sup>	0.93	2.47(3)	3.340(4)	156(5)

Symmetry codes: ii) 1 + *x*, *y*, *z*; iii) 1 - *x*, 1 - *y*, 1 - *z*; (iv) -*x*, -*y*, 1 - *z*; (v) 1 - *x*, -*y*, 1 - *z*; (vi) -*x*, 1 - *y*, 1 - *z*; (vii) 1 + *x*, -1 + *y*, *z*; (viii) *x*, *y*, 1 + *z*.


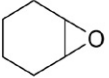
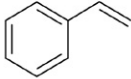
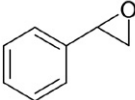

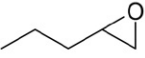
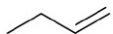
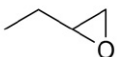
Table 2. Selected bond lengths (Å) and angles (°) for the complexes

	<b>1</b>	<b>2</b>
Bond lengths (Å)		
V(1)–O(1)	1.841(3)	1.847(2)
V(1)–O(3)	1.580(3)	1.583(3)
V(1)–O(5)	1.871(3)	1.863(2)
V(1)–O(2)	1.941(3)	1.921(2)
V(1)–O(4)	2.261(3)	2.259(3)
V(1)–N(1)	2.097(3)	2.090(3)
Bond angles (°)		
O(3)–V(1)–O(1)	100.96(19)	99.93(13)
O(1)–V(1)–O(5)	98.68(13)	100.77(11)
O(1)–V(1)–O(2)	155.11(14)	154.62(11)
O(3)–V(1)–N(1)	101.16(14)	99.60(13)
O(5)–V(1)–N(1)	160.03(12)	160.64(12)
O(3)–V(1)–O(4)	173.29(17)	175.04(13)
O(5)–V(1)–O(4)	77.53(10)	77.60(10)
N(1)–V(1)–O(4)	82.89(11)	84.41(11)
O(3)–V(1)–O(5)	97.98(14)	98.05(12)
O(3)–V(1)–O(2)	95.33(17)	97.23(12)
O(5)–V(1)–O(2)	97.53(12)	95.16(10)
O(1)–V(1)–N(1)	83.29(13)	83.99(11)
O(2)–V(1)–N(1)	75.14(12)	74.78(11)
O(1)–V(1)–O(4)	84.75(14)	83.34(11)
O(2)–V(1)–O(4)	80.45(12)	80.93(11)

### 3. 3. Catalytic Property

The catalytic experiment was carried out according to the literature method.<sup>6b</sup> A mixture of CH<sub>3</sub>OH/CH<sub>2</sub>Cl<sub>2</sub> (V:V = 7:3, 1.2 mL) was used for the reactions at 25 °C. The molar ratios for the catalyst:substrate:NaHCO<sub>3</sub>:H<sub>2</sub>O<sub>2</sub> are 1:298:117:1170. The conversion was measured after 74.5 min. Both vanadium complexes have good property in the olefin oxidation processes with epoxides as the products. The results are summarized in Table 4. Interestingly, both complexes have similar catalytic properties with high epoxide yields and good selectivity toward the aliphatic and aromatic substrates. However, when H<sub>2</sub>O<sub>2</sub> was used as single oxidant the catalytic efficiency is not good. When NaHCO<sub>3</sub> was added as a co-catalyst to the above reactions,

Table 4. The catalytic oxidation results

Substrate	Product		Conversion (%) (TON) <sup>a</sup>
		1	> 99 (351)
		2	> 99 (367)
		1	98 (343)
		2	> 99 (327)
		1	93 (310)
		2	96 (307)
		1	95 (282)
		2	97 (291)

<sup>a</sup> TON = (mmol of product)/mmol of catalyst.

the efficiency of the catalytic property can increase obviously. This might be attributed to the equilibrium process between H<sub>2</sub>O<sub>2</sub> and hydrogen carbonate to produce peroxymonocarbonate, HCO<sub>4</sub><sup>-</sup>, which is a more reactive nucleophile than H<sub>2</sub>O<sub>2</sub> and facilitated the epoxidation reactions. The two vanadium complexes have better catalytic properties than the cobalt(II) complex derived from 2-bromo-*N*<sup>2</sup>-(2-hydroxy-5-methylbenzylidene)benzohydrazide,<sup>13</sup> and similar catalytic properties with the oxido-vanadium(V) and dioxidomolybdenum(VI) complexes of hydrazones and Schiff bases.<sup>14</sup>

## 4. Conclusion

Two new similar oxidovanadium(V) complexes with aroylhydrazone ligands have been prepared and structurally characterized using X-ray structure analysis. The complexes have octahedral geometry with positions around the central atom being occupied with donor atoms of the aroylhydrazone ligand, the ethyl maltolate ligand and one oxido group. The complexes show effective catalytic property in the oxidation of various olefins to their corresponding epoxides.

## Supplementary Material

CCDC reference numbers 2043121 and 2043122 contain the supplementary crystallographic data for this article. These data can be obtained free of charge at <http://www.ccdc.cam.ac.uk>, or from Cambridge Crystallographic Data Center, 12 Union Road, Cambridge CB2 1EZ, UK; Fax: +44 1223 336 033; Email: [deposit@ccdc.cam.ac.uk](mailto:deposit@ccdc.cam.ac.uk).

## Acknowledgments

This work was financially supported by the Fundamental Research Funds in Heilongjiang Provincial Universities (Project No. 135409307).

## 5. References

- (a) H. Zakeri, S. Rayati, G. Zarei, A. Parsa, F. Adhami, *Iran. J. Catal.* **2020**, *10*, 71–78;  
(b) M. Gillard, J. Weynand, H. Bonnet, F. Loiseau, A. Decotignies, J. M. Dejeu, E. Defrancq, B. Elias, *Chem. Eur. J.* **2020**, *26*, 13849–13860; DOI:10.1002/chem.202001409  
(c) A. Arunadevi, N. Raman, *J. Coord. Chem.* **2020**, *73*, 2095–2116; DOI:10.1080/00958972.2020.1824293  
(d) J. M. Galvan-Hidalgo, D. M. Roldan-Marchan, A. Gonzalez-Hernandez, T. Ramirez-Apan, A. Nieto-Camacho, S. Hernandez-Ortega, E. Gomez, *Med. Chem. Res.* **2020**, *29*, 2146–2156; DOI:10.1007/s00044-020-02630-4  
(e) S. Kumari, S. Ray, *New J. Chem.* **2020**, *44*, 14953–14963; DOI:10.1039/D0NJ01590C  
(f) S. Q. T. Pham, C. Richardson, C. Kelso, A. C. Willis, S. F. Ralph, *Dalton Trans.* **2020**, *49*, 10360–10379. DOI:10.1039/D0DT01370F
- (a) R. Ramachandran, G. Prakash, P. Viswanathamurthi, J. G. Malecki, *Inorg. Chim. Acta* **2018**, *477*, 122–129; DOI:10.1016/j.ica.2018.03.007  
(b) M. Ghorbanloo, A. M. Alamooti, *J. Porous Mater.* **2017**, *24*, 769–777; DOI:10.1007/s10934-016-0314-9  
(c) S. Selvamurugan, R. Ramachandran, G. Prakash, P. Viswanathamurthi, J. G. Malecki, A. Endo, *J. Organomet. Chem.* **2016**, *803*, 119–127; DOI:10.1016/j.jorganchem.2015.11.017  
(d) S. Muthumari, R. Ramesh, *RSC Advances* **2016**, *6*, 52101–52112; DOI:10.1039/C6RA06734D  
(e) Y.-J. Cai, Y.-Y. Wu, F. Pan, Q.-A. Peng, Y.-M. Cui, *Acta Chim. Slov.* **2020**, *67*, 896–903; DOI:10.17344/acsi.2020.5895  
(f) S. Aslkhademi, N. Noshiranzadeh, M. S. Sadjadi, K. Mehriani, N. Farhadyar, *Polyhedron* **2019**, *160*, 115–122. DOI:10.1016/j.poly.2018.12.023
- (a) J. Szklarzewicz, A. Jurowska, M. Hodorowicz, R. Grybos, K. Kruczala, M. Gluch-Lutwin, G. Kazek, *J. Coord. Chem.* **2020**, *73*, 986–1008; (b) L.-P. Lu, F.-Z. Suo, Y.-L. Feng, L.-L. Song, Y. Li, Y.-J. Li, K.-T. Wang, *Eur. J. Med. Chem.* **2019**, *176*, 1–10; (c) F. Heidari, S. J. A. Fatemi, S. Y. Ebrahimipour, H. Ebrahimnejad, J. Castro, M. Dusek, V. Eigner, *Inorg. Chem. Commun.* **2017**, *76*, 1–4; (d) M. Sutradhar, L. M. D. R. S. Martins, M. F. C. Guedes da Silva, A. J. L. Pombeiro, *Coord. Chem. Rev.* **2015**, *301–302*, 200–239.
- (a) L. Schober, M. Sako, S. Takizawa, H. Groger, H. Sasai, *Chem. Commun.* **2020**, *56*, 10151–10154; DOI:10.1039/D0CC02621B  
(b) U. Das, P. Pattanayak, M. K. Santra, S. Chattopadhyay, *J. Chem. Res.* **2018**, *1*, 57–62; DOI:10.3184/174751918X15168821806597  
(c) Y. Sekiguchi, K. Arashiba, H. Tanaka, A. Eizawa, K. Na-

- kajima, K. Yoshizawa, Y. Nishibayashi, *Angew. Chem. Int. Ed.* **2018**, *57*, 9064–9068; DOI:10.1002/anie.201802310
- (d) M. R. Maurya, N. Jangra, F. Avecilla, I. Correia, *Eur. J. Inorg. Chem.* **2019**, *2*, 314–329; DOI:10.1002/ejic.201801243
- (e) J. C. Pessoa, M. R. Maurya, *Inorg. Chim. Acta* **2017**, *455*, 415–428. DOI:10.1016/j.ica.2016.04.012
5. (a) D. Sadhukhan, A. Ray, G. Pilet, C. Rizzoli, G. M. Rosair, C. J. Gomez-Garcia, S. Signorella, S. Bellu, S. Mitra, *Inorg. Chem.* **2011**, *50*, 8326–8339; DOI:10.1021/ic200846j
- (b) M. Bagherzadeh, M. Zare, T. Salemnoush, S. Ozkar, S. Akbayrak, *Appl. Catal. A-General* **2014**, *475*, 55–62; DOI:10.1016/j.apcata.2014.01.020
- (c) V. Vrdoljak, J. Pisk, D. Agustin, P. Novak, J. P. Vukovic, D. Matkovic-Calogovic, *New J. Chem.* **2014**, *38*, 6176–6185; DOI:10.1039/C4NJ01394H
- (d) M. Ghorbanloo, R. Bikas, G. Malecki, *Inorg. Chim. Acta* **2016**, *445*, 8–16; DOI:10.1016/j.ica.2016.02.018
- (e) Z. Moradi-Shoeili, M. Zare, S. Akbayrak, S. Ozkar, *Transition Met. Chem.* **2017**, *42*, 357–363. DOI:10.1007/s11243-017-0139-7
6. (a) D.-H. Zou, N. Sun, W. Chen, *J. Struct. Chem.* **2019**, *60*, 1101–1109; DOI:10.1134/S0022476619070114
- (b) M. Liang, D.-H. Zou, *Acta Chim. Slov.* **2016**, *63*, 180–185; DOI:10.17344/acsi.2015.2169
- (c) M. Liang, D.-H. Zou, *Inorg. Nano-Met. Chem.* **2017**, *47*, 110–115; DOI:10.1080/15533174.2016.1149730
- (d) M. Liang, N. Sun, D.-H. Zou, *Acta Chim. Slov.* **2018**, *65*, 964–969. DOI:10.17344/acsi.2018.4625
7. Bruker, SMART (Version 5. 624) and SAINT (Version 6. 04) programs using the windows NT system, Bruker AXS Inc., Madison, WI, USA, **2001**.
8. G. M. Sheldrick, *Acta Crystallogr.* **2008**, *A64*, 112–122. DOI:10.1107/S0108767307043930
9. D. Sadhukhan, M. Maiti, E. Zangrando, S. Pathan, S. Mitra, A. Patel, *Polyhedron* **2014**, *69*, 1–9. DOI:10.1016/j.poly.2013.11.007
10. A. Sarkar, S. Pal, *Polyhedron* **2006**, *25*, 1689–1694. DOI:10.1016/j.poly.2005.11.009
11. S. Roy, T. N. Mandal, K. Das, R. J. Butcher, A. L. Rheingold, S. K. Kar, *J. Coord. Chem.* **2010**, *63*, 2146–2157. DOI:10.1080/00958972.2010.499457
12. (a) J.-X. Lei, J. Wang, Y. Huo, Z. You, *Acta Chim. Slov.* **2016**, *63*, 670–677;
- (b) L. Xu, Y. Li, M. Duan, Y. Li, M. Han, J. Wu, Y. Wang, K. Dong, Z. You, *Polyhedron* **2019**, *165*, 138–142; DOI:10.1016/j.poly.2019.03.016
- (c) Q.-C. Zhou, T.-R. Wang, H. Li, L. Chen, J.-J. Xin, S. Guo, G.-H. Sheng, Z.-L. You, *J. Inorg. Biochem.* **2019**, *196*, 110680; DOI:10.1016/j.jinorgbio.2019.03.020
- (d) Z.-Q. Sun, S.-F. Yu, X.-L. Xu, X.-Y. Qiu, *Acta Chim. Slov.* **2020**, *67*, 1281–1289; DOI:10.17344/acsi.2020.6236
- (e) D. L. Peng, *Russ. J. Coord. Chem.* **2020**, *46*, 276–282; DOI:10.1134/S1070328420040065
- (f) L. Li, K.-W. Lu, Y.-T. Li, G.-F. Jiang, Y. Xin, L. Ye, Y. Zhang, H. Liu, C.-N. Shang, Z.-L. You, *Chin. J. Inorg. Chem.* **2017**, *33*, 905–912; DOI:10.1007/s40242-017-7240-5
- (g) Y. M. Cui, Y. Q. Wang, X. X. Su, H. Huan, P. Zhang, *J. Struct. Chem.* **2019**, *60*, 1299–1305. DOI:10.1134/S0022476619080092
13. F.-M. Wang, *Acta Chim. Slov.* **2016**, *63*, 406–410. DOI:10.1109/TCSII.2015.2505038
14. (a) H.-Y. Liu, Y.-S. Yin, L.-J. Yang, X.-L. Zhou, Y.-F. Ye, *Acta Chim. Slov.* **2020**, *67*, 130–136; DOI:10.17344/acsi.2019.5286
- (b) Q.-A. Peng, X.-P. Tan, Y.-D. Wang, S.-H. Wang, Y.-X. Jiang, Y.-M. Cui, *Acta Chim. Slov.* **2020**, *67*, 644–650; DOI:10.17344/acsi.2019.5650
- (c) Q. Yang, P. Wang, Y. Lei, *Acta Chim. Slov.* **2020**, *67*, 927–933; DOI:10.17344/acsi.2020.5932
- (d) M. Abdi, A. F. Shojaei, M. Ghadermazi, Z. Moradi-Shoeili, *Acta Chim. Slov.* **2020**, *67*, 476–486. DOI:10.17344/acsi.2019.5466

## Povzetek

Sintetizirali smo dva oksidovanadijeva(V) kompleksa, [VOL<sup>1</sup>L] (**1**) in [VOL<sup>2</sup>L] (**2**) (L = etil maltolat), pripravljena z aroilhidrazonoma 4-bromo-*N*<sup>2</sup>-(2-hidroksi-5-metilbenziliden)benzohidrazidom (H<sub>2</sub>L<sup>1</sup>) in *N*<sup>2</sup>-(3,5-dibromo-2-hidroksibenzilidene)-4-metoksibenzohidrazidom (H<sub>2</sub>L<sup>2</sup>) ter ju okarakterizirali z elementno analizo, infrardečo in elektronsko spektroskopijo. Strukturi kompleksov smo nadalje potrdili z monokristalno rentgensko difrakcijo. Vanadijev atom v obeh kompleksih je koordiniran z ONO donorskimi atomi aroilhidrazonskega liganda, OO donorskimi atomi etil maltolatnega liganda in z enim oksido O atomom, ki skupaj tvorijo oktaedrično koordinacijo. Kompleksa sta učinkovita katalizatorja za epoksidacijo olefinov z vodikovim peroksidom kot oksidantom in natrijevim hidrogenkarbonatom kot kokatalizatorjem.



Except when otherwise noted, articles in this journal are published under the terms and conditions of the Creative Commons Attribution 4.0 International License



Scientific paper

# Impact of High Temperature and Pressure to Steel Passivation in CO<sub>2</sub> Atmosphere

Mojca Slemnik\*

University of Maribor, Faculty of Chemistry and Chemical Engineering, Smetanova 17, 2000 Maribor, Slovenia

\* Corresponding author: E-mail: [mojca.slemnik@um.si](mailto:mojca.slemnik@um.si)

Received: 12-10-2020

## Abstract

The corrosion behaviour of AISI 347 in 0.1 M sulfuric acid at temperatures 50 and 75 °C and pressures up to 300 bar in a CO<sub>2</sub> atmosphere was studied by surface analysis and electrochemical methods. Corrosion reactions in which CO<sub>2</sub> is present accelerate the formation of a protective FeCO<sub>3</sub> layer, but the success of such a passivation depends on the saturation concentration and the corresponding temperature. Significantly better results compared to untreated steels were obtained at lower temperatures by increasing the pressure. To explain the differences in corrosion rates between samples, the activation energy for the layer dissolution was also discussed. It can be assumed that the compressibility of the CO<sub>2</sub> at different pressures has an influence on the formation of the protective iron carbonate layer and its properties and thus on the corrosion behaviour.

**Keywords:** Stainless steel, EIS, CO<sub>2</sub> corrosion, high pressure

## 1. Introduction

The steel AISI 347 is generally used in extreme conditions, e.g. aggressive media, at high temperatures and/or high pressures, mostly in pipeline systems, in the gas industry, especially for industrial gas cylinders, etc. It belongs to the group of steels with the low carbon content, which can be additionally protected with inhibitors or coatings.<sup>1</sup> The niobium content improves the mechanical properties of the steel by increasing hardness and the corrosion properties by reducing pitting.<sup>2</sup> It has a great affinity to carbon, which precipitates as a carbide. Niobium carbides are more stable than those of chromium, they remove carbon from the solid solution and stabilize the steel.<sup>3</sup> Niobium also refines the grain size, promotes the formation of chromium oxides and accelerates the formation of an iron oxide enriched passive layer in the outer layer and chromium, manganese and iron oxides in the inner layer at high temperature.<sup>4</sup> Carbon dioxide is useful as a supercritical fluid in several chemical processes as it changes its properties such as density, diffusivity, viscosity, compressibility, and surface tension by changing temperature and/or pressure. When it is used in a corrosive environment, it changes its parameters such as pH, partial pressure, temperature, concentration, compressibility etc. and influences the formation of a protective passive layer on the surface of the metal and thus its protective properties. To reduce the cor-

rosion rate, some authors suggest different coatings, pre-passivation<sup>5–8</sup> or the use of efficient inhibitors<sup>9–11</sup> for steel in CO<sub>2</sub> and also aggressive environments. Not many CO<sub>2</sub> corrosion studies have been carried out on low carbon steels,<sup>12</sup> but the fact is that steel exposed to the CO<sub>2</sub> environment triggers a spontaneous passivation process as it causes the formation of the FeCO<sub>3</sub> layer that protects the metal surface and reduces the corrosion rate.

Dugstad<sup>13–16</sup> explains how the term CO<sub>2</sub> corrosion covers a wide range of electrochemical mechanisms and complex processes. The interaction between protective FeCO<sub>3</sub> layer formation, corrosion rate and iron ion concentration in water was described in detail. CO<sub>2</sub> corrosion reactions are divided into anodic and cathodic processes. It was also found that ferritic-perlitic microstructures can be covered with a porous carbide phase which was related to high carbon content on the steels. In principle, corrosion reactions in CO<sub>2</sub> create a chemical environment that accelerates the formation of iron carbonate, which is often oxidized in air.<sup>17</sup> Such a layer is formed by the precipitation of iron carbonate when its saturation concentration is exceeded.<sup>18,19</sup> The concentrations of iron and carbonate ions must locally exceed the solubility limit. The precipitation rate is low at low temperatures, so that in this case a very small amount of layer is formed and a higher temperature is required for process efficiency. If the rate of iron

and carbon precipitation is equal to or higher than the corrosion rate, a dense protective layer is formed, but if the corrosion process is faster, the layer becomes porous and unprotective.<sup>20</sup> Therefore, special attention has been paid to the study of iron carbonate solubility under different conditions. W. Sun and S. Nešič<sup>21</sup> developed a uniform equation for iron carbonate solubility that is valid for a wide range of parameters and is based on literature data. In the case of CO<sub>2</sub> corrosion, however, many effects must be taken into account.<sup>22</sup> As expected, the temperature increases the corrosion rate, especially at low pH values, when no precipitation of iron carbonate can occur. On the other hand, the solubility of iron carbonate increases with rising temperature, and when it finally exceeds the solubility limit of iron carbonate, its protective scale formation reduces the rate of corrosion. In addition to temperature and many other effects, the effect of the CO<sub>2</sub> partial pressure was also investigated.<sup>23</sup> Y. Sun and S. Nešič<sup>24</sup> studied an increase in  $P_{\text{CO}_2}$  from 3 to 20 bar and concluded, that  $P_{\text{CO}_2}$  generally leads to an increase in the corrosion rate due to an increased concentration of H<sub>2</sub>CO<sub>3</sub>, which further accelerates the cathodic reaction and thus the corrosion rate. However, when the conditions for the formation of iron carbonate are favourable, a higher  $P_{\text{CO}_2}$  value increases the carbonate ion concentration, which further leads to higher supersaturation and scale precipitation.<sup>25</sup> Y. Zhang et al.<sup>26</sup> studied CO<sub>2</sub> corrosion behaviour between low partial pressure (1 MPa) and supercritical conditions (9.5 MPa) at various temperatures (from 50 to 130 °C) and immersion times. It was concluded that the change in partial pressure does not alter the corrosion mechanism, but only affects the corrosion rate, so that the rate is higher under supercritical conditions. X. Li et al.<sup>27</sup> investigated the nature of corrosion scales in extremely aggressive environments at high temperature and CO<sub>2</sub> high pressure and found that the corrosion resistance performance of corrosion scales decreases with increasing temperature and CO<sub>2</sub> pressure, finding the decreasing pitting and repassivation potential with increasing density and diffusivity of the acceptor in the scales. Z. M. Wang et al.<sup>28</sup> succeeded in the *in situ* observation of the CO<sub>2</sub> corrosion process under high pressure from active dissolution, the formation of a defective corrosion layer up to local layer dissolution and pitting.

In general, corrosion protection methods include the use of corrosion resistant materials, coatings, corrosion inhibitors, electrochemical protection, rust preventing oils or greases and surface treatments.<sup>29</sup> The most natural and spontaneous phenomenon in the surface treatment of metals is passivation process, which can also be accelerated with a suitable approach. In our previous study we worked on improving the surface passivation at 25 °C by forming a stable protective layer of iron carbonate by exposing the system only to elevated pressures of up to 300 bar<sup>30</sup> in acidic environment. In the following we were interested in the corrosion behaviour of steel in sulphuric acid at elevated pressures of up to 300 bar and simultane-

ously elevated temperatures of 50 and 75 °C, since AISI 347 is commonly used for industrial gas cylinders operating under high pressure. We also investigated the temperature dependence and the values of the activation energies required for the dissolution process of protective layer.

## 2. Experimental

### 2.1. Material and Sample Preparation

Stainless steel AISI 347 made in Železarna Ravne, Slovenia, has been investigated, with following chemical composition in wt%: Fe 69.882%, C 0.05%, Si 0.53%, Mn 1.32%, P 0.024%, S 0.024%, Cr 17.95%, Ni 9.66% in Nb 0.56%.

Samples were mechanically polished with 400–1200 grit abrasive paper, polished with diamond pastes to a mirror – like quality, and degreased in acetone, p.a. (Fluka).

The high pressure experiments were performed in a thermostated autoclave with 65 mL volume, which is designed for a maximum temperature of 200 °C and pressure to 400 bar. The temperature was kept constant with the outdoor thermostat Lauda RC6 CP and measured with the Greisinger thermometer GMH 3230 with an accuracy of ± 0.1 °C. For the evacuation of the autoclave the vacuum pump with a provided underpressure of 3.45 Pa was used. CO<sub>2</sub> was dosed into the autoclave with the pump PM101. The pressure was measured with the sensor Wika (PI) with an accuracy of 0.01 MPa.

Samples were immersed in 40 mL of 0.1 M H<sub>2</sub>SO<sub>4</sub> prepared from 96% acid, p.a. (Carlo Erba), previously bubbled for 10 min with CO<sub>2</sub> of 99.995% purity (Messer Slovenija). The autoclave was evacuated and charged with CO<sub>2</sub> to the desired pressure. The solution was stirred with a magnetic stirrer at a frequency of 800 min<sup>-1</sup> for 1 hour.

After pressure relief, the samples, which were already covered with the resulting layer, were analysed with the Sirion 400 NC (SEM – Scanning Electron Microscopy) and EDS (Energy Dispersive X-ray Spectroscopy) INCA 350 analyser.

### 2.2. Electrochemical Tests

The electrochemical measurements were performed in a standard three-electrode cell with sample as working electrode, a platinum counter electrode and reference SCE (standard calomel electrode, with the potential + 2,44 V vs. standard hydrogen electrode). The cell was filled with 300 mL 0.1 M sulfuric acid. The data were collected with Electrochemical Interface Solartron1287 and Frequency Response Analyzer Solartron 1250.

The samples were stabilised at OCP (open circuit potential) until the system reached stability and then the impedance curves were recorded in the frequency range between 60 kHz and 1 mHz. The amplitude of the excitation voltage was 10 mV. Measurements were made three times

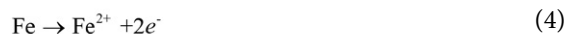
for each sample and the mean value was considered with the standard deviation max. 3%.

Potentiodynamic curves from 0.6 V to 1.0 V<sub>SCE</sub> were recorded at a sampling rate of 1 mVs<sup>-1</sup>. All data were acquired and processed with the ZPlot, ZView, CorrWare and CorrView instruments developed by Scribner Associates, Inc.<sup>31</sup>

## 3. Results and Discussion

### 3.1. Surface Analysis

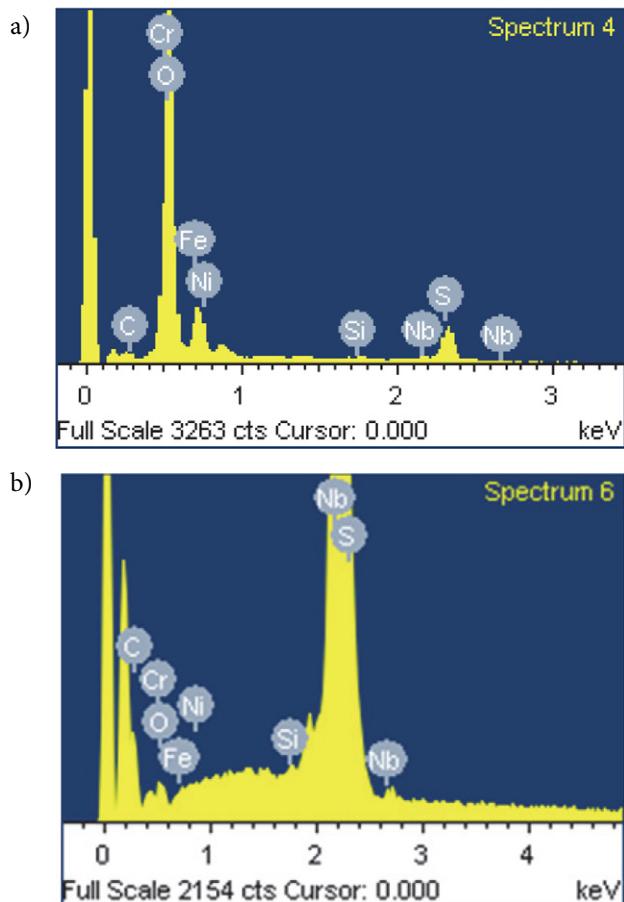
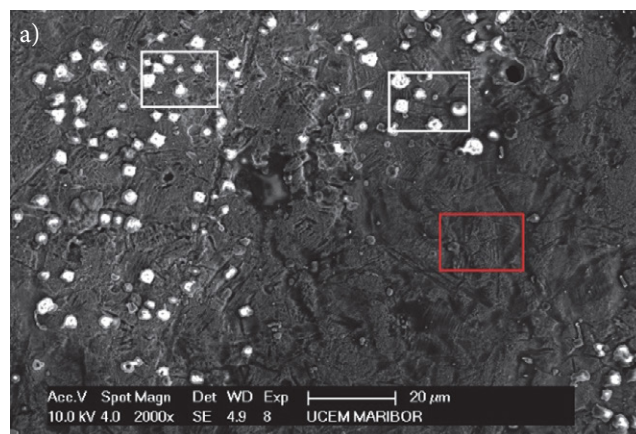
It is generally known that during CO<sub>2</sub> corrosion of steel the system first leads to the formation of H<sub>2</sub>CO<sub>3</sub> and further to the formation of FeCO<sub>3</sub> (siderite):<sup>26,32,33</sup>



Layer growth is caused by precipitation after exceeding the saturation concentration under suitable conditions. Our samples, which were exposed to CO<sub>2</sub> in a closed autoclave system under different pressure and temperature values, were covered with a layer whose morphology was further investigated with SEM and EDS.

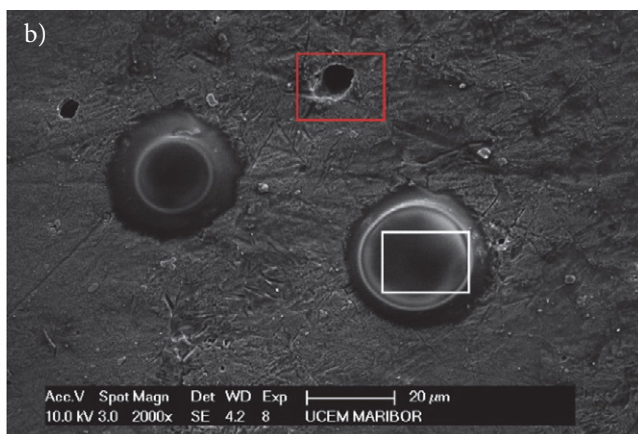
#### 3.1.1. Temperature: 50 °C

White spots (white rectangles in Figure 1a and EDS in Figure 2a) were detected as precipitants with a high oxygen content (43%) in a 3:1 ratio with iron (16%), which clearly indicates the formation of FeCO<sub>3</sub>, while at the same time a high chromium content was detected. Dark



**Figure 2.** EDS results for AISI 347 from Figure 1a): a) white precipitants and b) dark area.

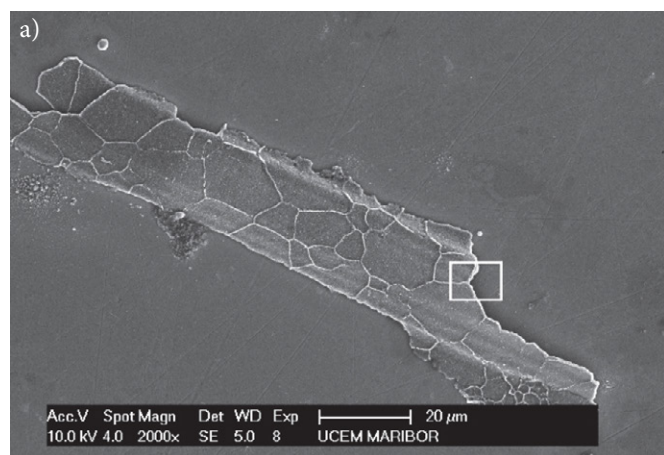
precipitants (red rectangle in Figure 1a and EDS in Figure 2b) indicate a high content of niobium (91%). The sample treated at 300 bar (white rectangle in Figure 1b) shows large particles with a high content of oxygen (43%), iron (16%) and some chromium (13%). Some large pits (red rectangle in Figure 1b) are also visible in the dark area (pitting corrosion). It was found,<sup>34</sup> that the FeCO<sub>3</sub> layer



**Figure 1.** SEM images for AISI 347 at 50 °C and pressure a) 100 bar, b) 300 bar.

on the steel surface grows even in pits of locally corroded samples.

### 3. 1. 2. Temperature: 75 °C



## 3. 2. Electrochemical Impedance Spectroscopy (EIS)

The passivity imposed on the system by the potential difference has values between Flade potential and trans-

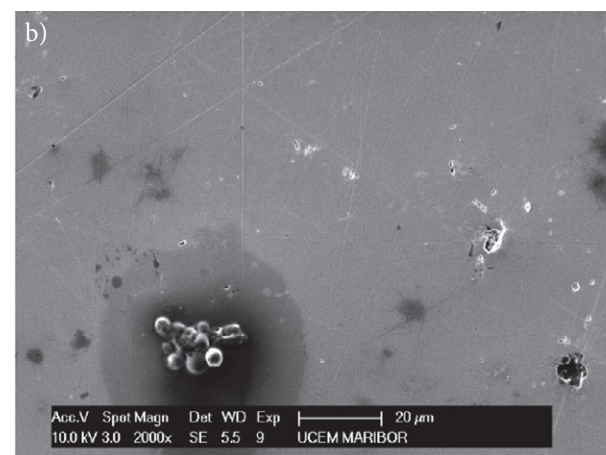


Figure 3. SEM images for AISI 347 at 75 °C and pressure: a) 100 bar and b) 300 bar.

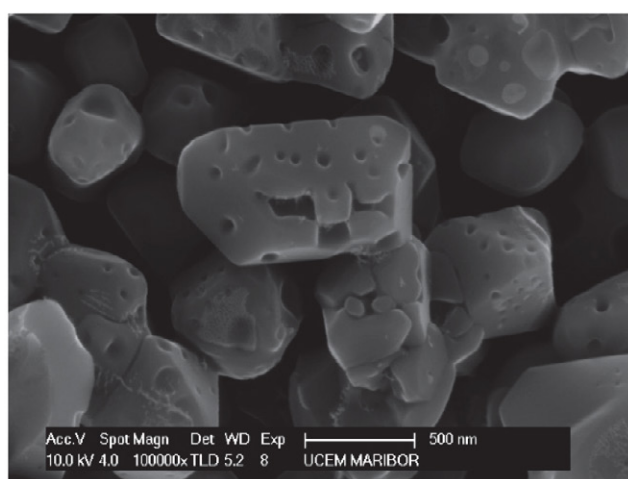
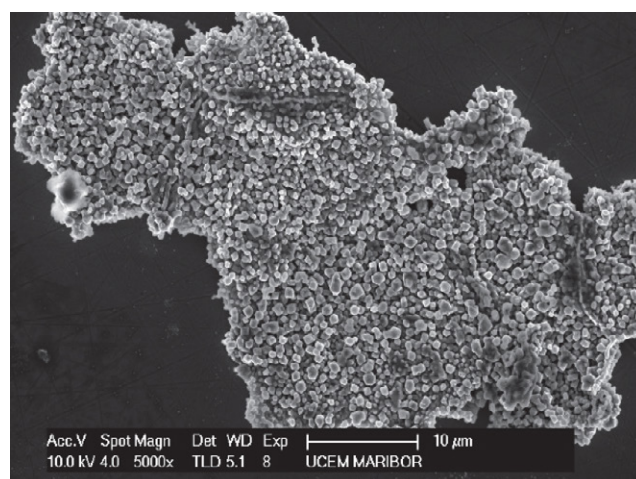


Figure 4. SEM images for AISI 347 at 75 °C and 100 bar at different magnifications (white borders from Figure 3).

At 75 °C (Figures 3, 4) and 100 bar some large structures of particles on the steel surface are visible. With EDS we detected high content of oxygen, iron and also chromium, in %: O 35.40, Fe 20.23 and Cr 41.82. Apparently, iron and chromium oxides precipitated and niobium accelerates their formation in the passive layer. A formation shown in Figure 3b (75 °C at 300 bar) was identified as a carbide. The EDS analysis shows a high content of carbon, in %: C 29.18, O 12.85, Si 1.19, S 6.65, Cr 10.50, Fe 32.38, Ni 6.82 and Nb 0.43. In corrosion systems the carbides are always the worst option, as their formation leads to accelerated pitting corrosion. The formation of porous carbide layer in CO<sub>2</sub> environments have been also reported by other authors.<sup>16,35,36</sup>

passivity potential. The effect of this process can be deduced from the resistance values, which decrease at the Flade potential and remain low and almost constant, and then increase sharply in the area of transpassivity. With EIS the passive layer can be examined at any potential value. Impedance curves, which are measured during the corrosion process, lead to the construction of equivalent circuits, which illustrate and evaluate chemical processes on the examined material.<sup>20,37,38</sup>

The RC equivalent circuit has been designed on the basis of the measured impedance curves shown in Fig. 5, where  $R_s$  represents the solution resistance,  $R_{cl}$  and  $R_{ct}$  the carbonate (pore) resistance and the charge transfer resistance, respectively.  $Q_{cl}$  and  $Q_{dl}$  are respectively  $Q$  of the car-

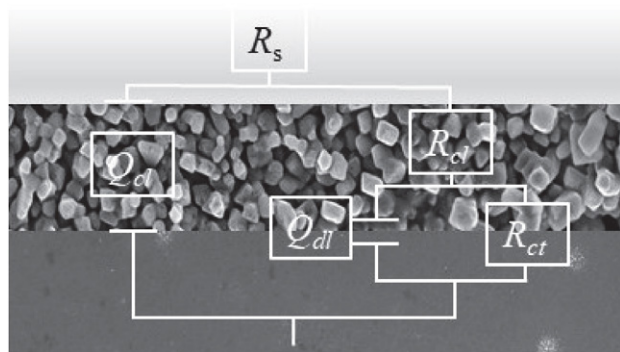


Figure 5. Equivalent circuit used for modelling the EIS results.

bonate (pore) and  $Q$  of double layer.  $Q$  is a frequency dependent element calculated from the CPE (constant phase element), which allows a better agreement between experimental and theoretical data.

The impedance of the CPE is defined:<sup>20,37</sup>

$$Z_{CPE} = [Q(j\omega)^\alpha]^{-1} \quad (6)$$

where  $Z$  is the electrode impedance, the frequency independent constant  $Q$  is a combination of properties related to the surface and the electroactive species,  $\alpha$  is related to a slope of  $\log Z$  vs.  $\log f$  in the Bode plot, and is attributed to the surface heterogeneity,  $\omega$  is the angular frequency.<sup>39</sup>

The parameter  $Q$  ( $s^\alpha \Omega^{-1} \text{cm}^{-2}$ ) can be converted to the capacitance  $C$  ( $s \Omega^{-1} \text{cm}^{-1}$ ) at  $\alpha < 1$  to quantitatively de-

termine the system parameters, in particular the thickness, which is inversely proportional to the capacitance. When  $\alpha = 1$ ,  $Q$  simply represents capacitance  $C$ .<sup>40</sup>

Nyquist diagrams (Figures 6 and 7) show curves for samples treated at 1, 100 and 200 bar, which are typical for passive systems with high impedance values, and show two time constants, while the curves at 300 bar and untreated samples show classic semi-circular shapes. For the data collected for untreated steel and for sample at 50 °C and 300 bar, only one time constant is visible in the impedance diagram. The high frequency part of the diagram can refer to the  $\text{FeCO}_3$  layer or even to the mixture of  $\text{FeCO}_3$  and  $\text{F}_3\text{C}$  carbide layers, which was also detected by other authors.<sup>16,36,41</sup> They all have proved that  $\text{FeC}_3$  can act as a substrate for iron carbonate precipitation.

The low frequency part corresponds to the charge transfer process. From Figures 6 and 7 it can be seen that the highest charge transfer resistance shows steel treated at 100 bar, lower, but still similar are the values for samples treated at 1 and 200 bar, while the  $R_{ct}$  value for the 300 bar sample decreases significantly, but is still slightly higher than for untreated steel.

Data from equivalent circuits are collected in Table 1.

The comparison between the working temperatures is clear and to be expected: temperature accelerates corrosion, which is expressed in lower impedance values and lower  $R_{ct}$  values, Figure 8.

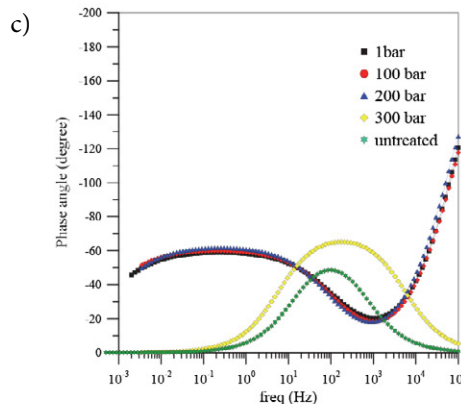
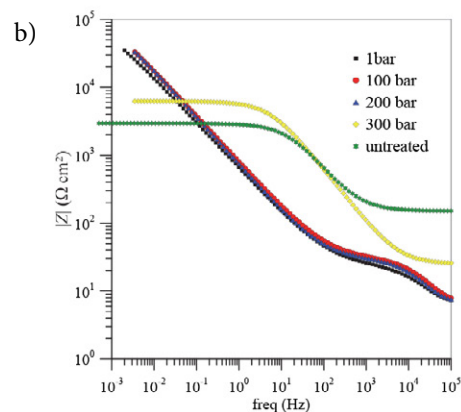
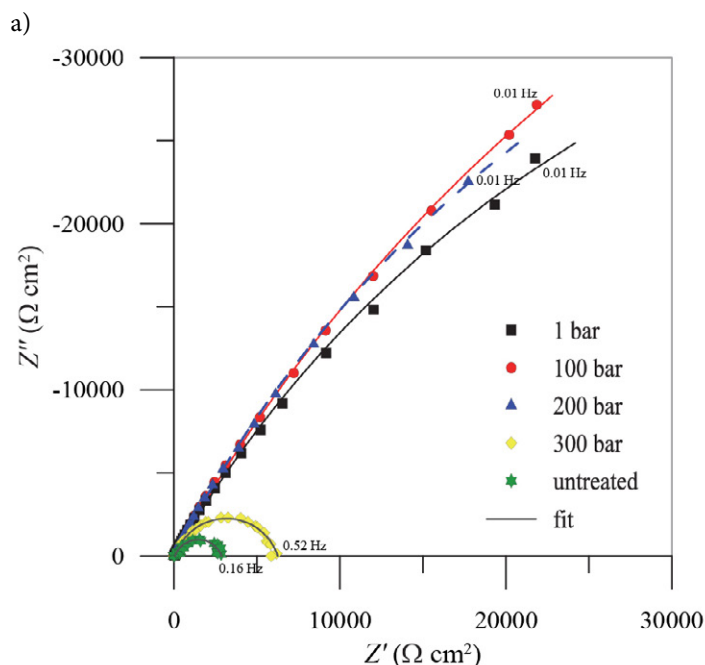
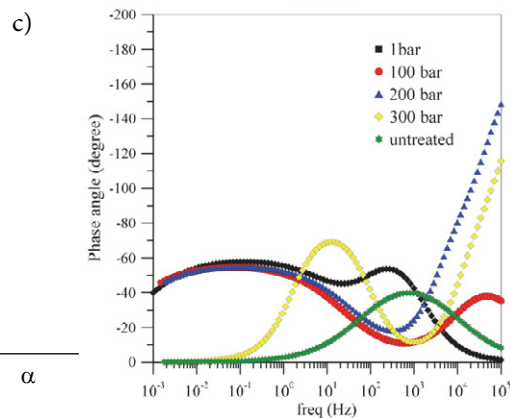
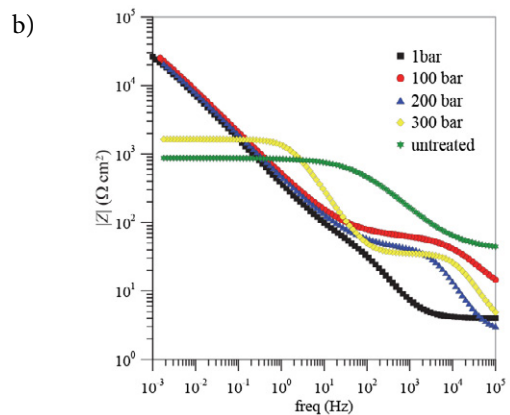
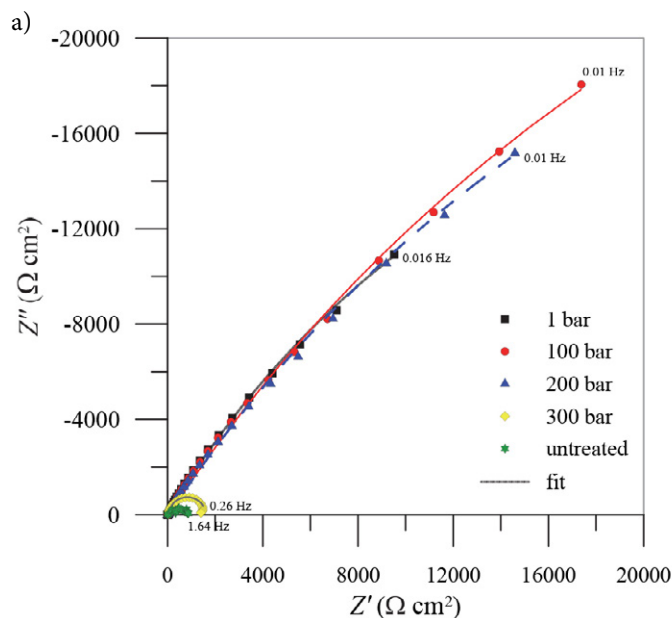


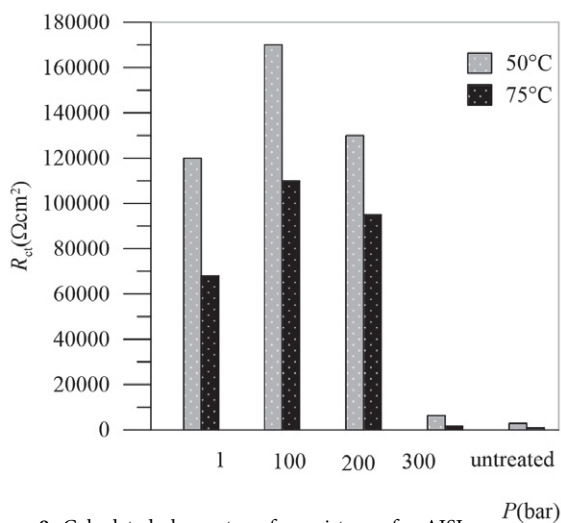
Figure 6. Impedance spectra for AISI 347 at 50 °C: a) Nyquist plot, b) and c) Bode plot



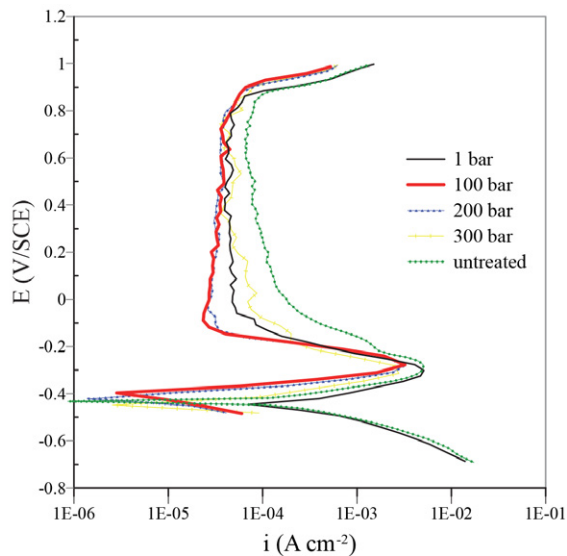
**Figure 7.** Impedance spectra for AISI 347 at 75 °C: a) Nyquist plot, b) and c) Bode plot

**Table 1.** Parameter values from EIS measurements for AISI 347 at 50 and 75 °C.

	<i>P</i> (bar)	<i>R</i> <sub>po</sub> (Ωcm <sup>2</sup> )	<i>Q</i> <sub>c</sub> ·10 <sup>-6</sup> (s <sup>α</sup> Ω <sup>-1</sup> cm <sup>-2</sup> )	<i>α</i>	<i>R</i> <sub>ct</sub> (kΩcm <sup>2</sup> )	<i>Q</i> <sub>dl</sub> ·10 <sup>-6</sup> (s <sup>α</sup> Ω <sup>-1</sup> cm <sup>-2</sup> )	<i>α</i>
50 °C	1	34	8.40	0.71	120	440	0.67
	100	39	3.78	0.77	170	360	0.68
	200	38	4.00	0.78	130	370	0.76
	300				6.20	9.20	0.80
	untreated				2.80	9.99	0.77
75 °C	1	60	93	0.80	68	750	0.65
	100	56.27	3.7	0.76	110	650	0.63
	200	45	1.3	0.98	95	700	0.63
	300	38	0.46	0.98	1.6	67	0.95
	untreated				0.83	22.6	0.65



**Figure 8.** Calculated charge transfer resistance for AISI 347 at 50 and 75 °C depending on the pressure treatment.



**Figure 9.** Polarization curves for AISI 347 at 50 °C.

**Table 2.** Parameter values from potentiodynamic curves for AISI 347.

	<i>P</i> (bar)	$i_{\text{corr}} \cdot 10^{-5}$ (A cm <sup>-2</sup> )	$i_{\text{crit}} \cdot 10^{-3}$ (A cm <sup>-2</sup> )	$E_{\text{pas}}$ (V/SCE)	$E_{\text{trans}}$ (V/SCE)	$E_{\text{pas}} - E_{\text{trans}}$ (V/SCE)	$r_{\text{corr}}$ (mm y <sup>-1</sup> )
50 °C	1	1.680	2.80	-0.130	0.794	0.924	0.196
	100	0.821	3.53	-0.164	0.831	0.996	0.096
	200	1.174	3.36	-0.154	0.812	0.966	0.137
	300	9.372	2.89	-0.144	0.768	0.912	1.090
	untreated	13.05	5.10	-0.048	0.759	0.804	1.525
75 °C	1	5.624	4.67	-0.171	0.739	0.910	0.657
	100	2.744	1.87	-0.175	0.748	0.924	0.320
	200	4.600	4.56	-0.172	0.741	0.913	0.537
	300	15.24	1.33	-0.164	0.738	0.902	1.780
	untreated	22.08	9.86	-0.013	0.731	0.744	2.581

### 3. 3. Potentiodynamic Polarization

From polarization curves presented in Figure 9 (example at 50 °C), the parameters listed in Table 2 were read out.

On the basis of Tafel extrapolation<sup>42</sup> from corrosion currents,  $i_{\text{corr}}$  corrosion rates in mm per year were calculated, which are listed in Table 2 and also shown in Figure 10 including values for the corrosion rates at 25 °C.<sup>30</sup> The  $E_{\text{pas}}$  values are the highest (shifted towards more positive values) for a sample treated at 100 bar, these samples also show the lowest  $i_{\text{corr}}$  the largest passive range ( $E_{\text{pas}} - E_{\text{trans}}$ ) and the lowest corrosion rates.

From Figure 10, we can determine the best results for measured system at 50 °C and 100 bar.

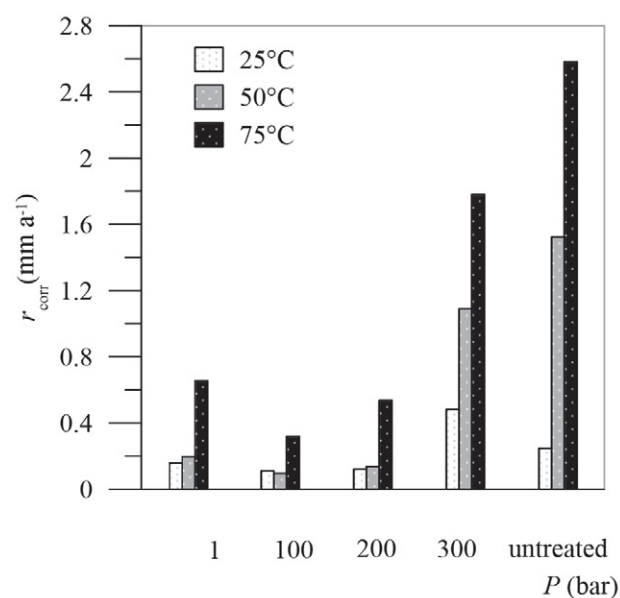
As explained in the Introduction section, the growth of the FeCO<sub>3</sub> layer occurs only after the saturation concentration is exceeded, and this requires a higher temperature,

> 60 °C.<sup>20</sup> This means that obviously at this combination 25 °C and 100 bar, is still a low temperature, which implies that the corrosion rate is higher than the rate of FeCO<sub>3</sub> precipitation. At 50 °C and 100 bar, the circumstances of precipitation are so favourable that the corrosion rate is lower. At 75 °C and 100 bar, the temperature is so high that it accelerates the corrosion rate regardless of the FeCO<sub>3</sub> precipitation rate.

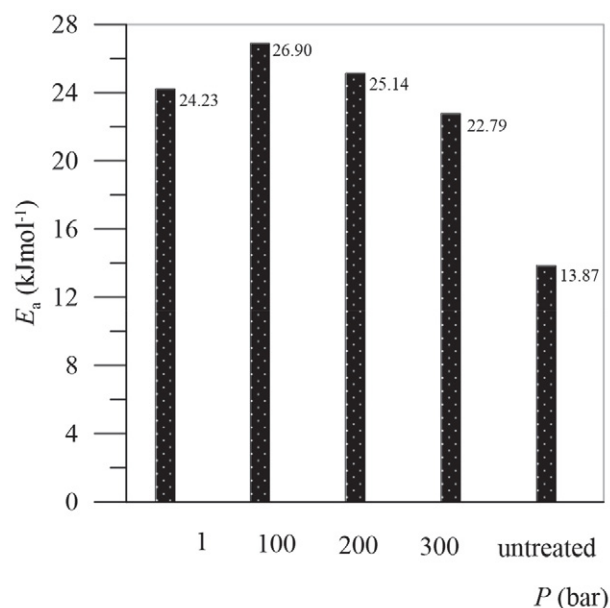
### 3. 4. Activation Energy Calculation

The temperature dependence of the corrosion current density at different pressure values was further determined. Data at 25 °C (published in earlier work<sup>30</sup>), 50 and 75 °C were considered. The values of the activation energy were calculated using the Arrhenius equation:<sup>43, 44</sup>

$$\ln i_{\text{corr}} = \ln A - \frac{E_a}{RT}, \quad (7)$$



**Figure 10.** Corrosion rate for AISI 347 at 25<sup>30</sup>, 50 and 75 °C in dependence of pressure.



**Figure 11.** Activation energy values for AISI 347 in dependence of pressure treatment.

where  $A$  is pre-exponential factor,  $E_a$  is activation energy and  $R$  is a gas constant. Activation energy values are given in Figure 11.

The activation energy represents the minimum energy that the reactants must have to form a product. In our case, the passive layer has already been formed, so that the activation energy can be related to the process of dissolving the layer. From the data obtained it can be concluded that the highest corrosion rate would be that of untreated steel, since the process of dissolution of the passive layer requires a minimum energy of 13.87 kJ/mol, unlike steel treated at 100 bar, which has the highest value of activation energy of 26.9 kJ/mol and would therefore corrode at the lowest rate.

## 4. Discussion

SEM images and in especially EDS analyses show that at 100 bar and 50 °C treated steel (which indicates the best corrosion results) the content of oxygen incorporated in the passive layer to build up protective compounds increases by up to 30 wt % determined on a dark, more or less uniformly corroded surface, without precipitates.

At 50 °C, the oxygen content increases considerably: from 2 to 9 wt.% and the carbon content increases from 1.1 to 2.3 wt.%. The oxygen content in precipitated white particles increases up to 43 wt.% (in relation to Fe – 15.8 wt.%, which clearly indicates the formation of  $\text{FeCO}_3$ , and the chromium content also increases up to 20 wt.%, (Figure 1a). By increasing the operating temperature to 75 °C of the sample treated at 100 bar, the oxygen content decreases to 35 wt.% but at the same time increases the carbon content. For the sample treated at 300 bar, which indicates the highest corrosion rate between the treated samples, the EDS data are as follows: the oxygen content on the dark surface decreased from 24.7% at 50 °C to 1.7% at 75 °C. White precipitates, which are clearly visible in Figures 2b) and 3b), contain 41.4 wt.% oxygen at 50 °C, which decreases to 8 wt.% at 75 °C, while the carbon content increases from 0.46 wt.% to 9.5 wt.% as the temperature rises. A significant pressure increase obviously leads to an accelerated precipitation of carbon or carbon compounds.

It is obvious that the corrosion behaviour at increasing pressure and temperature depends on the  $\text{FeCO}_3$  precipitation mechanism. Choi et al.<sup>45</sup> found that the concentrations of  $\text{CO}_2$ ,  $\text{H}_2\text{CO}_3$  and  $\text{HCO}_3^-$  in the water –  $\text{CO}_2$  system for transport pipelines increase with increasing pressure but decrease with increasing temperature. The solubility of  $\text{CO}_2$  in water reaches its almost lowest value at 55 °C (compared to 55 and 75 °C) and 100 bar. It was also found that the reduced grain size of  $\text{FeCO}_3$  forms a denser and therefore more efficient protective layer. These results are also in good agreement with our findings. The comparison between images a) and b) in Fig. 1 shows the small grain sizes that have grown at 100 bar compared to the

large grain size at 300 bar, indicating slower layer growth at 300 bar, which leads to a porous layer and thus to a higher corrosion rate. Pfennig et al.<sup>32</sup> also confirmed that the corrosion rates at 100 bar are lower compared to the ambient pressure, assuming that this could be due to an open capillary system within the corrosion layer that is not present in the high pressure system and thus prevents rapid mutual diffusion of the ionic species. We can assume that at 1 and 200 bar the mechanism of protective layer growth is the same as at 100 bar, as also indicated by Zhang et al.<sup>26</sup> (studied at 10 and 95 bar). One would expect the corrosion rate to decrease steadily with pressure, but at 300 bar it changes significantly. At high pressures, the amount of  $\text{CO}_2$  dissolved in water and some other  $\text{CO}_2$  properties should be considered, for example the compressibility factor.

The compressibility factor for  $\text{CO}_2$ , calculated with a modified Redlich-Kwong equation according to Spycher et al.<sup>46</sup> and Lemmon et al.<sup>47</sup> showed the lowest value exactly between 100 and 200 bar at about 50 °C compared to about 70 °C. At 300 and up to 600 bar it increases linearly. At 100 bar, the value of the compressibility factor is about 0.38 compared to 300 bar, which indicates a value of 0.6, meaning that at 300 bar the  $\text{CO}_2$  molecules collide more often and hardly move at all. This can explain the slower diffusion and thus the formation of a porous layer with large particles which consequently leads to a high corrosion rate.

## 5. Conclusions

In this study the corrosion behaviour of AISI 347 in 0.1 M sulphuric acid at temperatures of 50 and 75 °C and pressures 1, 100, 200 and 300 bar in  $\text{CO}_2$  atmosphere was investigated. An increased pressure significantly reduced the corrosion rate compared to untreated steel. The decisive points of our contribution are:

A surface analysis was used to detect both the  $\text{FeCO}_3$  layers and the precipitated grains, whose size varies according to the  $\text{CO}_2$  pressure level.

The corrosion rate determined by electrochemical methods decreases from 1 to 200 bar, is lowest at 100 bar, but increases significantly at 300 bar.

We attribute this sudden change to a compressibility factor of the  $\text{CO}_2$ , which allows us to explain the movement and collision of the molecules with each other, leading to their slower diffusion and consequently to the formation of a porous layer with large grains, which is noticeable as an increase in the corrosion rate.

The best conditions for the lowest corrosion rate were found at 50 °C and 100 bar. This combination shows the following results:

A small grain size precipitates, causing them to adhere closely together, resulting in a denser and thicker protective layer of  $\text{FeCO}_3$ , which is therefore more resistant to further dissolution.



Charge transfer resistance showed the highest value, which confirmed the lowest corrosion rate.

The activation energy for dissolution of the protective layer showed the highest value, confirming the best passivation.

All conclusions are in good agreement with the value of the compressibility factor of CO<sub>2</sub> at 100 bar, which allows us to explain the movements of its molecules on which the formation and the properties of the protective layer depend.

## Acknowledgements

This work was supported by Slovenian Research Agency, grant P2-006.

## 6. References

1. A. Assarian, S. M., Improving Polyaspartic Anti-Corrosion Coating Protective Properties with the use of Nano-silica. *Acta Chim. Slov.* **2018**, *65*, 569–577. DOI:10.17344/acsi.2018.4187
2. Itman Filho, A.; Silva, R.; Cardoso, W.; Casteletti, L. C., Effect of Niobium in the Phase Transformation and Corrosion Resistance of One Austenitic-ferritic Stainless Steel. *Materials Research* **2014**, *17*, 801–806. DOI:10.1590/1516-1439.190113
3. A. C. Gonzaga, C. Barbosa, S. S. M. Tavares, A. Zeemann, J. C. Payão, Influence of post welding heat treatments on sensitization of AISI 347 stainless steel welded joints. *Journal of Materials Research and Technology* **2020**, *9* (1), 908–921. DOI:10.1016/j.jmrt.2019.11.031
4. S. Y. Huang, W.-T. Tsai, Y.-T. Pan, J.-C. Kuo, H.-W. Chen, Lin, Effect of Niobium Addition on the High-Temperature Oxidation Behavior of 22Cr25NiWCoCu Stainless Steel in Air. *Metals - Open Access Metallurgy Journal* **2019**, *9*, 975. DOI:10.3390/met9090975
5. M. F. Morks, P. Corrigan, N. Birbilis, I. S. Cole, A green Mn-MgZn phosphate coating for steel pipelines transporting CO<sub>2</sub> rich fluids. *Surface and Coatings Technology* **2012**, *210*, 183–189. DOI:10.1016/j.surfcoat.2012.09.018
6. M. F. Morks, N. F. Fahim, T. H. Muster, I. S. Cole, Cu-based Fe phosphate coating and its application in CO<sub>2</sub> pipelines. *Surface and Coatings Technology* **2013**, *228*, 167–175. DOI:10.1016/j.surfcoat.2013.04.025
7. Q.-Y. Wang, X.-Z. Wang, H. Luo, J.-L. Luo, A study on corrosion behaviors of Ni–Cr–Mo laser coating, 316 stainless steel and X70 steel in simulated solutions with H<sub>2</sub>S and CO<sub>2</sub>. *Surface and Coatings Technology* **2016**, *291*, 250–257. DOI:10.1016/j.surfcoat.2016.02.017
8. Y. Zhao, W. Liu, W. Banthukul, Y. Fan, X. Li, Effect of silty sand on the pre-passivation behaviour of 1Cr steel in a CO<sub>2</sub> aqueous environment. *Corrosion Engineering, Science and Technology* **2020**, *55* (3), 205–216. DOI:10.1080/1478422X.2020.1713533
9. H. Cen, J. Cao, Z. Chen, X. Guo, 2-Mercaptobenzothiazole as a corrosion inhibitor for carbon steel in supercritical CO<sub>2</sub>-H<sub>2</sub>O condition. *Applied Surface Science* **2019**, *476*, 422–434. DOI:10.1016/j.apsusc.2019.01.113
10. H.-H. Zhang, X. Pang, K. Gao, Localized CO<sub>2</sub> corrosion of carbon steel with different microstructures in brine solutions with an imidazoline-based inhibitor. *Applied Surface Science* **2018**, *442*, 446–460. DOI:10.1016/j.apsusc.2018.02.115
11. A. Singh, Y. Lin, K. R. Ansari, M. A. Quraishi, E.E. Ebenso, S. Chen, W. Liu, Electrochemical and surface studies of some Porphines as corrosion inhibitor for J55 steel in sweet corrosion environment. *Applied Surface Science* **2015**, *359*, 331–339. DOI:10.1016/j.apsusc.2015.10.129
12. D. A. López, T. Pérez, S. N. Simison, The influence of microstructure and chemical composition of carbon and low alloy steels in CO<sub>2</sub> corrosion. A state-of-the-art appraisal. *Materials & Design* **2003**, *24* (8), 561–575. DOI:10.1016/S0261-3069(03)00158-4
13. A. Dugstad, Fundamental Aspects of CO<sub>2</sub> Metal Loss Corrosion – Part I: Mechanism. *NACE – International Corrosion Conference Series* **2006**, 2015.
14. A. Dugstad, The Importance of FeCO<sub>3</sub> Super-saturation on CO<sub>2</sub> Corrosion of Carbon Steels *CORROSION/1992, Paper No.14, (Houston, TX: NACE International, 1992)*
15. A. Dugstad, H. H., M. Seiersten, Effect of Steel Microstructure on Corrosion Rate and Protective Iron Carbonate Film Formation. *Corrosion* **2001**, *47* (4), 369–378. DOI:10.5006/1.3290361
16. A. Dugstad, Mechanism of protective film formation during CO<sub>2</sub> corrosion of carbon steel. *Corrosion/98* **1998**, (Paper no. 31), NACE, Huston, TX.
17. J. K. Heuer, J. F. Stubbins, An XPS characterization of FeCO<sub>3</sub> films from CO<sub>2</sub> corrosion. *Corrosion Science* **1999**, *41* (7), 1231–1243. DOI:10.1016/S0010-938X(98)00180-2
18. W. Sun, S. Nesic, Basics Revisited: Kinetics of Iron Carbonate Scale Precipitation in CO<sub>2</sub> Corrosion. In *CORROSION 2006*, NACE International: San Diego, California, 2006; p 21.
19. S. N. Yoon-Seok Choi, Corrosion Behavior Of Carbon Steel In Supercritical CO<sub>2</sub>-Water Environments. *CORROSION 2009, 22–26 March, Atlanta, Georgia* **2009**.
20. S. Nešić, K. L. J. Lee, A Mechanistic Model for Carbon Dioxide Corrosion of Mild Steel in the Presence of Protective Iron Carbonate Films—Part 3: Film Growth Model. *Corrosion* **2003**, *59* (7), 616–628. DOI:10.5006/1.3277592
21. W. Sun, S. Nešić, R.C. Woollam, The effect of temperature and ionic strength on iron carbonate (FeCO<sub>3</sub>) solubility limit. *Corrosion Science* **2009**, *51* (6), 1273–1276. DOI:10.1016/j.corsci.2009.03.009
22. S. Nešić, Key issues related to modelling of internal corrosion of oil and gas pipelines – A review. *Corrosion Science* **2007**, *49* (12), 4308–4338. DOI:10.1016/j.corsci.2007.06.006
23. C. De Waard, D. E. Milliams, Carbonic Acid Corrosion of Steel. *CORROSION* **1975**, *31* (5), 177–181. DOI:10.5006/0010-9312-31.5.177
24. S. Nešić, S. W. Keith George, High Pressure CO<sub>2</sub> Corrosion Electrochemistry and the Effect of Acetic Acid. *CORROSION*

- 2004, 28 March-1 April, New Orleans, Louisiana 2004.
25. Y. Sun, S. Nešić, A parametric study and modeling on localized CO<sub>2</sub> corrosion in horizontal wet gas flow. *NACE Meeting Papers* 2004.
26. Y. Zhang, X. Pang, S. Qu, X. Li, K. Gao, Discussion of the CO<sub>2</sub> corrosion mechanism between low partial pressure and supercritical condition. *Corrosion Science* 2012, 59, 186–197. DOI:10.1016/j.corsci.2012.03.006
27. X. Li, Y. Zhao, W. Qi, J. Xie, J. Wang, B. Liu, G. Zeng, T. Zhang, F. Wang, Effect of extremely aggressive environment on the nature of corrosion scales of HP-13Cr stainless steel. *Applied Surface Science* 2019, 469, 146–161. DOI:10.1016/j.apsusc.2018.10.237
28. Z. M. Wang, X. Han, J. Zhang, Z. L. Wang, In situ observation of CO<sub>2</sub> corrosion under high pressure. *Corrosion Engineering, Science and Technology* 2014, 49 (5), 352–356. DOI:10.1179/1743278213Y.0000000144
29. I. Milošev, Contemporary Modes of Corrosion Protection and Functionalization of Materials. *Acta Chimica Slovenica* 2019, 66, 511–533. DOI:10.17344/acsi.2019.5162
30. M. Slemnik; D. Pečar, High-pressure CO<sub>2</sub> pretreatment as a method for stainless steel passivation. *Anti-Corrosion Methods and Materials* 2010, 57 (6), 290–296. DOI:10.1108/00035591011087145
31. ZView, ZPlot, CorrView, CorrWare, version 2.8. *Scribner Associates, Inc, Southern Pines, NCD, USA 1990–1999*.
32. A. Pfennig, A. Kranzmann, Effect of CO<sub>2</sub> and pressure on the stability of steels with different amounts of chromium in saline water. *Corrosion Science* 2012, 65, 441–452. DOI:10.1016/j.corsci.2012.08.041
33. G. Zhang, M. L.C. Chai, Y. Wu, Effect of HCO<sub>3</sub><sup>-</sup> concentration on CO<sub>2</sub> corrosion in oil and gas fields. *Journal of University of Science and Technology Beijing, Mineral, Metallurgy, Material* 2006, 13 (1), 44–49. DOI:10.1016/S1005-8850(06)60012-1
34. A. Pfennig, A. Kranzmann, The Role Of Pit Corrosion In Engineering The Carbon Storage Site At Ketzin, Germany. *WIT Transactions on Ecology and the Environment* 2010, 136, 109–119. DOI:10.2495/AIR100101
35. Staicopolus, N., The role of cementite in the acidic corrosion of steel. *J. Electrochem. Soc.* 1963, 110. DOI:10.1149/1.2425602
36. S. Al-Hassan, B. Mishra, D. L. Olson, M. M. Salama, , Effect of microstructure on corrosion of steels in aqueous solutions containing carbon dioxide. *Corrosion* 1998, 54 (6), 480. DOI:10.5006/1.3284876
37. A. S. Hamdy, E. El-Shenawy, T. El-Bitar, Electrochemical Impedance spectroscopy of the corrosion behaviour of some niobium bearing stainless steels in 3.5% NaCl. *International Journal of Electrochemical Science* 2006, Vol.1, 171–180. DOI:10.1016/j.matlet.2006.10.043
38. Z. Tan, L. Yang, D. Zhang, Z. Wang, F. Cheng, M. Zhang, Y. Jin, Development mechanism of internal local corrosion of X80 pipeline steel. *Journal of Materials Science & Technology* 2020, 49, 186–201. DOI:10.1016/j.jmst.2019.10.023
39. M. E. Orazem, I. Frateur, B. Tribollet, V. Vivier, S. Marcelin, N. Pebere, A.L. Bunge, E. A.White, D.P. Riemer, M. Musiani, Dielectric Properties of Materials Showing Constant-Phase-Element (CPE) Impedance Response. *Journal of The Electrochemical Society* 2013, 160 (6), C215–C225. DOI:10.1149/2.033306jes
40. B. Hirschorn, M. E. Orazem, B. Tribollet, V. Vivier, I. Frateur, M. Musiani, Determination of effective capacitance and film thickness from constant-phase-element parameters. *Electrochimica Acta* 2010, 55 (21), 6218–6227. DOI:10.1016/j.electacta.2009.10.065
41. F. Farelas, M. Galicia, B. Brown, S. Nestic, H. Castaneda, Evolution of dissolution processes at the interface of carbon steel corroding in a CO<sub>2</sub> environment studied by EIS. *Corrosion Science* 2010, 52 (2), 509–517. DOI:10.1016/j.corsci.2009.10.007
42. Corrosion: Third Edition. Shreir, L. L.; Jarman, R. A.; Burstein, G. T., Eds. 1994; Vol. 1, pp 1–2815.
43. P. W. Atkins, *Physical Chemistry*. Eight ed.; Oxford University Press Oxford, USA, 2006.
44. F. Mohammadinejad, S. M. A. Hoseini, M. S. Zandi, M. J. Bahrami, Z. Golshani, Metoprolol: New and Efficient Corrosion Inhibitor for Mild Steel in Hydrochloric and Sulfuric Acid Solutions. *Acta Chim. Slov.* 2020, 67, 710–719. DOI:10.17344/acsi.2019.5301
45. Y.-S. Choi, S. Nešić, Determining the corrosive potential of CO<sub>2</sub> transport pipeline in high pCO<sub>2</sub>-water environments. *International Journal of Greenhouse Gas Control* 2011, 5 (4), 788–797. DOI:10.1016/j.ijggc.2010.11.008
46. N. Spycher, K. Pruess, J. Ennis-King, CO<sub>2</sub>-H<sub>2</sub>O mixtures in the geological sequestration of CO<sub>2</sub>. I. Assessment and calculation of mutual solubilities from 12 to 100 °C and up to 600 bar. *Geochimica et Cosmochimica Acta* 2003, 67 (16), 3015–3031. DOI:10.1016/S0016-7037(03)00273-4
47. E. W. Lemmon, M. O. McLinden, D. G. Friend, National Institute of Standards and Technology, US, Thermophysical properties of fluid systems. 1998.

## Povzetek

S površinsko analizo in elektrokemijskimi metodami smo proučevali korozijske lastnosti jekla AISI 347 v 0,1 M raztopini žveplove kisline. Jeklo smo izpostavili CO<sub>2</sub> atmosferi pri 50 in 75 °C in tlakih vse do 300 barov. Prisotnost CO<sub>2</sub> pospešuje nastanek zaščitne plasti iz FeCO<sub>3</sub>, vendar je uspešnost takšnega pasiviranja odvisna od njegove nasičenosti in ustrezne temperature. Ne samo podobni, celo boljši rezultati so bili doseženi pri nižjih temperaturah s povišanjem tlaka. Razlike v korozijski hitrosti med vzorci smo potrdili tudi z določitvijo vrednosti aktivacijskih energij, ki jih sistem potrebuje za nadaljnje raztapljanje zaščitne plasti. Predpostavimo lahko, da stisljivost CO<sub>2</sub> pri različnih tlakih vpliva na poroznost zaščitne plasti železovega karbonata in posledično njenih korozijskih lastnosti.



Except when otherwise noted, articles in this journal are published under the terms and conditions of the Creative Commons Attribution 4.0 International License

Scientific paper

# Synthesis and Cytotoxicity of Thieno[2,3-*b*]Pyridine Derivatives Toward Sensitive and Multidrug-Resistant Leukemia Cells

Salah A. Al-Trawneh,<sup>1,\*</sup> Amer H. Tarawneh,<sup>2</sup> Anastassiya V. Gadetskaya,<sup>3</sup>  
Ean-Jeong Seo,<sup>4</sup> Mohammad R. Al-Ta'ani,<sup>1</sup> Samir A. Al-Taweel<sup>1</sup>  
and Mustafa M. El-Abadelah<sup>5</sup>

<sup>1</sup> Chemistry Department, Faculty of Science, Mu'tah University, Karak 61710, Jordan

<sup>2</sup> Chemistry and Chemical Technology Department, Faculty of Science, Tafila Technical University, Tafila 61610, Jordan

<sup>3</sup> School of Chemistry and Chemical Technology, Al-Farabi Kazakh National University, Almaty 050040, Kazakhstan

<sup>4</sup> Department of Pharmaceutical Biology, Institute of Pharmaceutical and Biomedical Sciences, Johannes Gutenberg University, Staudinger Weg 5, 55128 Mainz, Germany

<sup>5</sup> Chemistry Department, Faculty of Science, The University of Jordan, Amman 11942, Jordan

\* Corresponding author: E-mail: laratr@mutah.edu.jo

Phone: +96232372380/4561

Received: 12-17-2020

## Abstract

A new series of substituted ethyl 7-cyclopropyl-2-(2-aryloxo)-3-nitro-4-oxo-4,7-dihydrothieno[2,3-*b*]pyridine-5-carboxylates **3a–e** were prepared by utilizing ethyl 2-chloro-7-cyclopropyl-3-nitro-4-oxo-4,7-dihydrothieno[2,3-*b*]pyridine-5-carboxylate (**1**) and replacing of the 2-chlorine with anions obtained from phenol (**2a**), salicylaldehyde derivatives **2b–d** or thiophenol (**2e**), leading to the respective ethyl 7-cyclopropyl-2-(2-aryloxo)-3-nitro-4-oxo-4,7-dihydrothieno[2,3-*b*]pyridine-5-carboxylates **3a–e**. The new compounds were evaluated for their *in vitro* cytotoxicity towards sensitive CCRF-CEM and multidrug-resistant CEM/ADR5000 leukemia cells. The screening revealed that compounds **3a**, **3b**, and **3e** inhibited the growth of both cell lines. Compound **3b**, with a phenol moiety, exhibited the highest growth inhibitory activity against CEM/ADR5000 and CCRF-CEM cells with IC<sub>50</sub> values 4.486 ± 0.286 and 2.580 ± 0.550 μM, respectively. Collectively, the presented results demonstrate that the synthesized thieno[2,3-*b*]pyridines warrant further exploration for potential use as anti-cancer agents.

**Keywords:** Thieno[2,3-*b*]pyridine, Multidrug resistance, Cytotoxicity.

## 1. Introduction

Thieno[2,3-*b*]pyridines were mentioned for the first time in 1913.<sup>1</sup> The chemistry of thieno[2,3-*b*]pyridines has been well documented during the past decades.<sup>1</sup> Various biological activities of this heterocyclic compounds class were described,<sup>2</sup> such as antimicrobial,<sup>3–6</sup> anti-inflammatory,<sup>7–9</sup> antioxidant,<sup>6</sup> antituberculosis,<sup>4</sup> and antimalarial activities.<sup>10</sup> Moreover, the incorporation of the *N*-cyclopropyl group with 4-oxothieno[2,3-*b*]pyridines showed a higher potency against *Escherichia coli* ATCC10536 than the *N*-ethyl and *N*-*tert*-butyl analogs.<sup>11</sup> It is important to

mention that compounds containing thieno[2,3-*b*]pyridines moieties attracted considerable interest regarding their potency as anti-cancer agents.<sup>12–14</sup>

Despite severe undesired side effects, chemotherapeutics are considered effective treatments of primary and metastatic tumors (Figure 1).<sup>15</sup>

One serious problem of cancer chemotherapy is the development of resistance towards multiple structurally and functionally unrelated anti-cancer drugs.<sup>16–18</sup> This phenomenon defined as multidrug resistance (MDR), where chemotherapy fails even at high drug, which leads to toxic side effects.<sup>19</sup> MDR is frequently caused by the

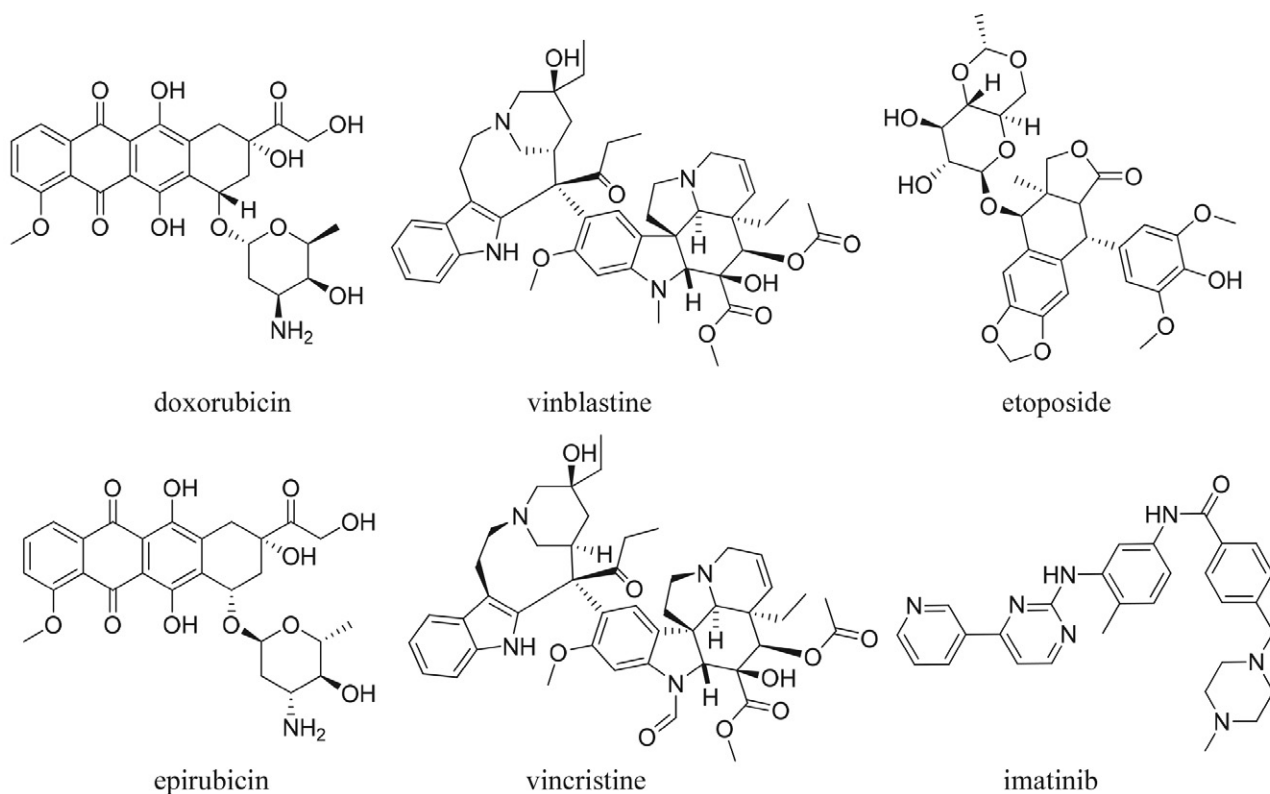
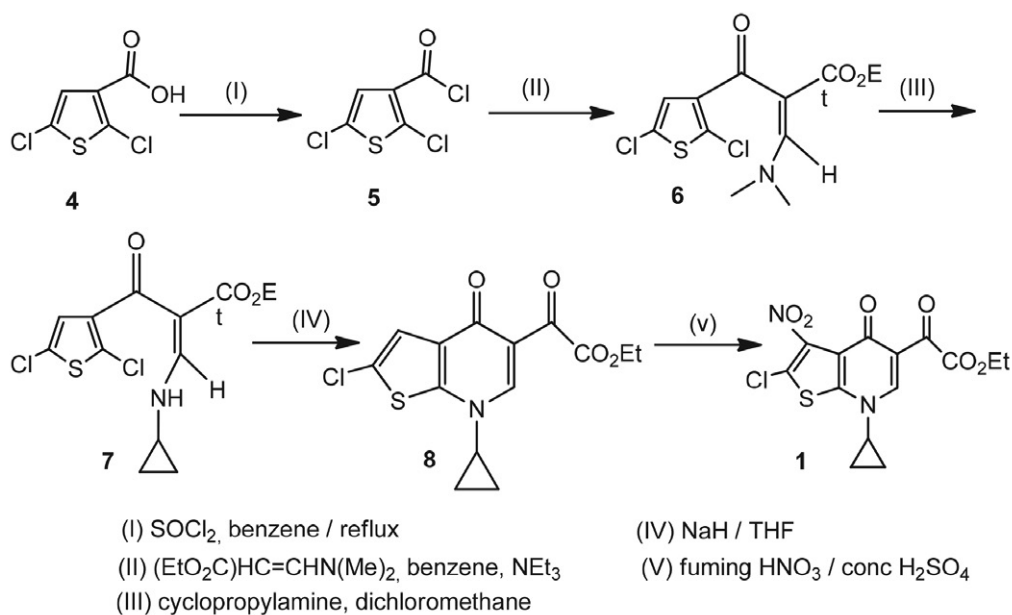


Figure 1. Representative samples of chemotherapy in market.

overexpression of membrane efflux pumps of the ATP-binding cassette (ABC) transporter family. The best characterized ABC-transporter in this context is P-glycoprotein (Pgp), which causes increased transport of chemotherapeutic agents out of the cells.<sup>20,21</sup>

Thieno[2,3-*b*]pyridines have been reported to exhibit chemopreventive effects suppressing carcinogenesis of

numerous tumor types including breast, prostate, non-small cell lung, melanoma, leukemia, ovarian, liver, and colon cancer.<sup>22,23</sup> As a part of our continuing search for novel biological agents,<sup>24–27</sup> newly synthesized 4,7-dihydrothieno[2,3-*b*]pyridine derivatives were evaluated for their growth inhibitory activity towards multidrug-resistant CEM/ADR5000 cells in comparison to their pa-



Scheme 1. Preparation of ethyl 3-nitro-4-oxothieno[2,3-*b*]pyridine-5-carboxylate 1.

rental sensitive cell line, CCRF-CEM. This is the first report on the cytotoxicity of 4,7-dihydrothieno[2,3-*b*]pyridine against sensitive and multidrug resistance leukemia cells. Moreover, the structure-activity relationship of the synthesized set was also studied.

## 2. Results and Discussion

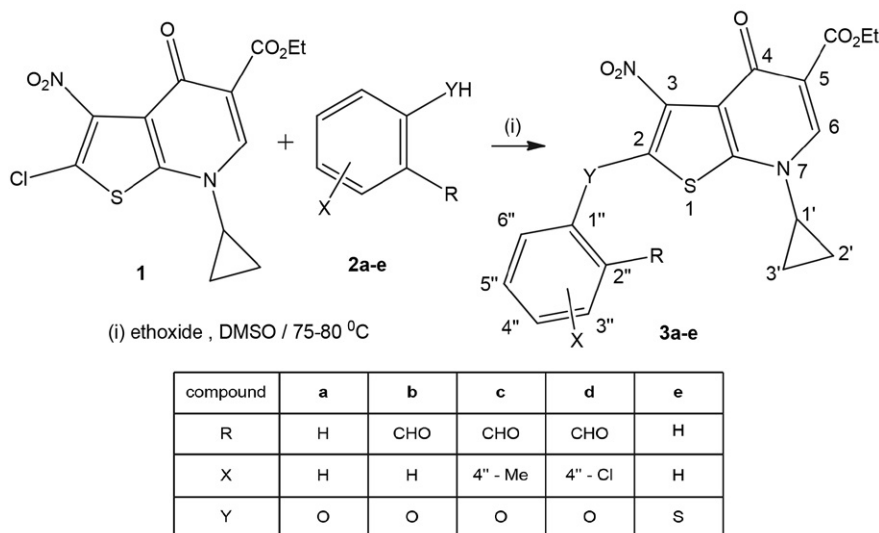
### 2.1. Chemistry

The synthesis of a selected set of 4,7-dihydrothieno[2,3-*b*]pyridine derivatives **3a–e** has been accomplished in two-step reactions as illustrated in Schemes 1 and 2. The first step involves the formation of ethyl 3-nitro-4-oxothieno[2,3-*b*]pyridine-5-carboxylate **1**. The latter synthon

was prepared by starting with 2,5-dichlorothiophene-3-carboxylic acid (**4**). The following successive steps were performed according to a reported procedure.<sup>11</sup>

Freshly prepared oxyanions from phenol (**2a**), salicylaldehyde (**2b**), 5-methylsalicylaldehyde (**2c**), and 5-chlorosalicylaldehyde (**2d**) took part in subsequent nucleophilic aromatic substitution ( $S_NAr$ ) reactions of chloro substituent in compound **1** as shown in Scheme 2. Whereas, compound **3e** was prepared according to the same procedure by sulfur anion obtained from benzenethiol (**2e**) and then reacted with compound **1** in the same manner as phenol derivatives (see Scheme 2).

The new compounds **1** and **3a–e** were characterized by IR, MS, and NMR spectral data. These data, given in the



**Scheme 2.** Synthesis of ethyl 2-(aryloxy)-7-cyclopropyl-3-nitro-4-oxo-4,7-dihydrothieno[2,3-*b*]pyridine-5-carboxylic acids **3a–e**.

**Table 1.** NMR spectroscopic data (500 MHz,  $CDCl_3$ ) for compound **3a**.

Ethyl 7-cyclopropyl-3-nitro-4-oxo-2-phenoxy-4,7-dihydrothieno[2,3- <i>b</i> ]pyridine-5-carboxylate ( <b>3a</b> )			
position	$\delta_c$ , type	$\delta_H$ ( <i>J</i> in Hz)	HMBC
1	–	–	–
2	130.39, C	–	–
3	141.39, C	–	–
3a	121.43, C	–	–
4	167.76, C	–	–
5	116.00, C	–	–
6	145.73, CH	8.36, s	3, 4, 1', CO <sub>2</sub> Et
7a	150.81, C	–	–
1'	36.56, CH	3.47, m	–
2'	7.85, CH <sub>2</sub>	1.22, m	1'
3'	7.85, CH <sub>2</sub>	1.28, m	1'
1''	157.16, C	–	–
2'', 6''	118.42, CH	7.25, d	1'', 2'', 6'', 4''
3'', 5''	130.38, CH	7.45, t	1'', 3'', 5''
4''	126.28, CH	7.30, t	2'', 6''
-OCH <sub>2</sub> CH <sub>3</sub>	14.37, CH <sub>3</sub>	1.39, t	CH <sub>2</sub>
-OCH <sub>3</sub> CH <sub>2</sub>	61.34, CH <sub>2</sub>	4.36, q	CO <sub>2</sub> Et
C-COOEt	164.81, C	–	–

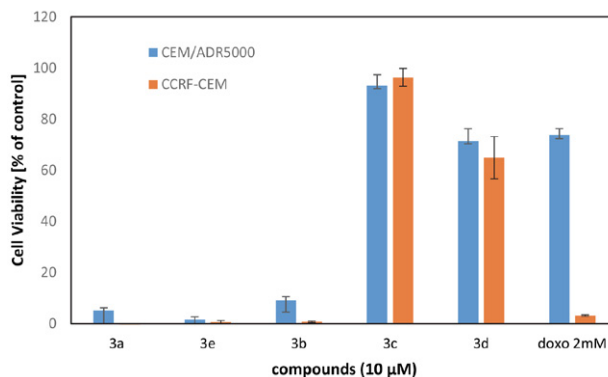
experimental section, were in compliance with the assigned structures. HMBC correlations allowed the complete assignments: the protons at position H-5" showed a common strong correlation in all compounds **3a–e** with the carbons at positions C-1", C-3" and a weak one with the carbons at positions C-4" and C-6", while in compound **3c** an additional correlation of the protons at  $\delta_{\text{H}}$  7.54 (d,  $J = 8.0\text{Hz}$ , 1H, H-5") with the carbons of the methyl group at  $\delta_{\text{C}}$  20.69 (C-CH<sub>3</sub>) was observed. The presence of the aldehyde group at position C-2" enabled to differentiate the correlation in compounds **3b–d** for the protons at position H-3" which showed a correlation with the carbons at positions C-1", C-5" and with the aldehyde carbon itself at  $\delta_{\text{C}}$  186.22–188.9 (C-CHO). In addition, in compound **3c** the correlation between the signal at  $\delta_{\text{H}}$  7.84 (s, 1H, H-3") and the signal at  $\delta_{\text{C}}$  20.69 (C-CH<sub>3</sub>) for the methyl group was detected. The correlation of proton at position H-4" with the carbons at positions C-2" and C-6" was presented in all compounds, except for compounds **3c–d** due to substituted position C-4" to methyl and chloro, respectively. The NMR data of the compound **3a**, as a representative of the title compounds **3a–e**, are shown in Table 1.

Thus, the mass spectra display the correct molecular ion peaks, for which the measured high-resolution mass spectra (HRMS) data were in good agreement with the calculated values. DEPT and 2D (COSY, HMQC, HMBC) experiments showed correlations that helped in the <sup>1</sup>H and <sup>13</sup>C signal assignments to the different carbons, and they are attached and/or neighboring hydrogens. H-6 proton resonating at 8.36 as a sharp singlet made a long-range correlation with C-3, C-4, C-1' and CO<sub>2</sub>Et. In addition, protons 2', 3' show correlation with C-1'. On the other hand, the phenol ring correlated with aldehyde functionality (Table 1).

## 2. 2. Biological Evaluation. Cytotoxic Activities Against Lymphoblastic Leukemia Cells

As the first step, all compounds were tested at a fixed concentration of 10  $\mu\text{M}$  (Figure 2) in CCRF-CEM and CEM/ADR5000 cells. Compounds **3a**, **3e**, and **3b** significantly inhibited cell viability (reduction to less than 10% growth).

From the structure-activity relationship (SAR) point of view, incorporating salicylaldehyde moiety to thieno[2,3-*b*]pyridine (**3b**) exhibited good activity against CCRF-CEM and CEM/ADR5000 cells with IC<sub>50</sub> values of 4.76 and 5.11  $\mu\text{M}$ , respectively. However, incorporating the phenol moiety (**3a**) increased activity against CCRF-CEM and CEM/ADR5000 (Table 2). Changing the hydrogen on the *para* position of **3b** with a halogen in **3d** or with methyl in **3c** led to reduced biological activity against both cell lines. While replacement of the phenol moiety with thiophenol in **3e** retrieved biological activity against CCRF-CEM and CEM/ADR5000 cells with IC<sub>50</sub>



**Figure 2.** Growth percentage (%) of drug-sensitive lymphoblastic leukemia CCRF-CEM cells and multidrug-resistant P-glycoprotein-overexpressing subline CEM/ADR5000 cells treated with compounds **3a–e** at a concentration of 10  $\mu\text{M}$ . Doxorubicin (doxo) was used as control. Results of three independent experiments with every six parallel measurements are shown.

values of 4.00 and 4.59  $\mu\text{M}$  for **3e**, respectively (Table 2). This is a remarkable result since CEM/ADR cells are more than 1000-fold resistant to the established anti-cancer drug doxorubicin.<sup>28</sup> Hence, these compounds inhibited multidrug-resistant cells with similar efficacy as sensitive cells, possibly qualifying them as candidates for further development as treatment of unresponsive cancers.

**Table 2.** Cytotoxicity of active compounds towards sensitive human lymphoblastic CCRF-CEM and multidrug-resistant CEM/ADR5000 leukemia cells as determined by the resazurin assay.

Com- pounds	IC <sub>50</sub> [ $\mu\text{M}$ ] <sup>a</sup>		Degree of resistance <sup>b</sup>
	CCRF- CEM	CEM/ ADR5000	
<b>3a</b>	2.580 ± 0.550	4.486 ± 0.286	1.74
<b>3b</b>	4.763 ± 0.160	5.109 ± 0.294	1.07
<b>3e</b>	4.009 ± 0.154	4.591 ± 0.017	1.15

<sup>a</sup> The lymphoblastic leukemia cells were treated with different concentrations of each compound. Mean values and standard deviation of three independent experiments with every six parallel measurements are shown. <sup>b</sup> The degrees for resistance were calculated by division of the IC<sub>50</sub> values of the compounds for CEM/ADR5000 by the corresponding IC<sub>50</sub> values for CCRF-CEM cells.

## 3. Experimental

### 3. 1. Chemicals and Equipment

2,5-Dichlorothiophene, cyclopropylamine, 3-acetyl-2,5-dichlorothiophene, phenol, 2-hydroxybenzaldehyde, 2-hydroxy-5-methylbenzaldehyde, 5-chloro-2-hydroxybenzaldehyde, and thiophenol were purchased from Aldrich. Sodium hydride, sodium hydroxide, magnesium sulfate, triethylamine, dimethylformamide, dimethyl sulfoxide, thionyl chloride (SOCl<sub>2</sub>), and ethyl 3-(*N,N*-dimethylamino)acrylate were purchased from Acros. Benze-

ne and tetrahydrofuran were dried over sodium metal and distilled, then collected under the nitrogen atmosphere. Thin-layer chromatography plates (Macherey-Nagel GmbH & Co. KG Xtra-SIL G/UV254, 20 × 20 cm, 0.20 mm silica gel 60, 0.06–0.2 mm (70–230 mesh ASTM) for column chromatography. Ultraviolet Fluorescence Analysis Cabinet was used to visualize the colorless spots. Melting points (uncorrected) were determined on the Electrothermal IA6304 Melting Point apparatus in open capillary tubes. <sup>1</sup>H and <sup>13</sup>C NMR spectra were recorded on a 500 MHz (Bruker 500 MHz Avance III) and 400 MHz (Bruker Avance III 400 MHz) spectrometers with TMS as the internal standard. High-resolution mass spectra (HRMS) were measured (in positive or negative ion mode) using the electrospray ion trap (ESI) technique by collision-induced dissociation on a Bruker APEX-IV (7 Tesla) instrument. IR spectra were recorded on a Nicolet Impact 400 FT-IR spectrophotometer.

### 3. 2. Synthesis of Ethyl 2-Chloro-7-cyclopropyl-3-nitro-4-oxo-4,7-dihydrothieno[2,3-*b*]pyridine-5-carboxylate (1)

A mixture of 2,5-dichlorothiophene-3-carboxylic acid **4** (5 g, 25.4 mmol), and thionyl chloride (SOCl<sub>2</sub>) (12.0 g, 101 mmol) were dissolved in dry benzene (60 mL), then refluxed for 4–5 h under anhydrous conditions. The solvent and excess thionyl chloride were distilled under reduced pressure, dry benzene (20 mL) was then added to remove the trace of thionyl chloride, and re-distilled. The resulting 2,5-dichloro-3-thionobenzoyl chloride **5** was used for the next step without further purification. To a stirred and cooled (5–10 °C) solution of ethyl 3-(*N,N*-dimethylamino)acrylate (4.3 g, 30 mmol) and triethylamine (5.1 g, 51 mmol) in dry benzene (50 mL) was added dropwise a solution of **5** in dry benzene (20 mL).

The resulting mixture was refluxed at 85 °C for 2 h, then cooled to room temperature, and washed with water (3 × 2 mL). The organic layer was separated, dried over MgSO<sub>4</sub> and the solvent was then evaporated to dryness to obtain the desired product **6**. A stirred solution of **6** in dichloromethane (50 mL) was treated dropwise with cyclopropyl amine (2.85 g, 50 mmol) at 2–4 °C. The resulting mixture was then stirred at 25 °C for 24 h. The solvent was evaporated and the residue was soaked with hexane to obtain a yellow precipitate product **7**. Sodium hydride (0.8 g, 17.5 mmol, 55%) in dry THF (60 mL) was added to the pure **7**. The reaction mixture was stirred at room temperature for 30 min. Then, the temperature was increased to 60 °C for 3 h. The solvent was evaporated, and the residual white precipitate **8** was washed with water and dried. The product crystallized from the CHCl<sub>3</sub>/ethanol mixture (1:2).<sup>11</sup>

Finally, the nitration of **8** was achieved by dissolving **8** in concentrated sulfuric acid (6 mL). The latter solution

was slowly and dropwise added for 30 min to –5 °C stirred solution of fuming nitric acid (2 mL) and concentrated sulfuric acid (5 mL). The mixture was allowed to warm to 5 °C and poured into the ice bath (50 mL). The solid product **1** was filtered and crystallized from DMF/ethanol (1:9) [mp 180–182 °C dec., total yield 30%]. <sup>1</sup>H NMR (500 MHz, CDCl<sub>3</sub>) δ 1.26 (m, 2H) and 1.29 (m, 2H) (H<sub>2</sub>-2' + H<sub>2</sub>-3'), and 1.36 (t, *J* = 7.1 Hz, 3H, CH<sub>3</sub>CH<sub>2</sub>O-), 3.49 (m, 1H, H-1'), 4.35 (q, *J* = 7.1 Hz, 2H, -OCH<sub>2</sub>CH<sub>3</sub>), 8.36 (s, 1H, H-6).<sup>11</sup>

### 3. 3. General Procedure for Synthesis of Ethyl 2-(Aryloxo/arylthio)-7-cyclopropyl-3-nitro-4-oxo-4,7-dihydrothieno[2,3-*b*]pyridine-5-carboxylates 3a–e

To a stirred solution of **1** (0.2 g, 0.6 mmol) in dimethyl sulfoxide (2 mL) the appropriate sodium salt of phenol (**2a**), salicylaldehydes **2b–d** or thiophenol (**2e**) (0.9 mmol) [prepared from the reaction of compounds **2a–e** (0.9 mmol) with sodium ethoxide (0.06 g, 0.9 mmol) in ethanol] was slowly added. The resulting mixture was then heated at 70–80 °C for 12 h. The reaction mixture was cooled and poured onto ice-water (20 mL), then extracted with chloroform (20 mL), the organic layer washed with water (2 × 20 mL) and brine (2 × 20 mL), dried over anhydrous sodium sulfate Na<sub>2</sub>SO<sub>4</sub> and the solvent was evaporated to yield a yellow, solid substance. This crude product was purified by column chromatography using silica gel and eluting with chloroform/ethyl acetate (1:1, *v/v*) to give solid products (Scheme 2).

**Ethyl 7-Cyclopropyl-3-nitro-4-oxo-2-phenoxy-4,7-dihydrothieno[2,3-*b*]pyridine-5-carboxylate (3a)**. This compound was prepared from **1** (0.2 g, 0.6 mmol) and phenol (**2a**) (0.10 g, 0.9 mmol) by following the general procedure and reaction conditions as described above. Reaction time 12 h; yield 0.20 g (87%), mp 260–262 °C. HRMS (ESI) *m/z* [M+Na] calcd for C<sub>19</sub>H<sub>16</sub>N<sub>2</sub>O<sub>6</sub>SNa: 423.06213; found: 423.06182. IR 3900, 3089, 2952, 1728, 1688, 1615, 1559, 1486, 1453, 1395, 1344, 1320, 1229, 1199, 1146, 1070, 1044, 922, 875, 836, 800, 761, 694, 597, 554 cm<sup>-1</sup>. <sup>1</sup>H NMR (500 MHz, CDCl<sub>3</sub>) δ 1.22 (m, 2H) and 1.28 (m, 2H) (H<sub>2</sub>-2' + H<sub>2</sub>-3'), and 1.39 (t, *J* = 7.0 Hz, 3H, CH<sub>3</sub>CH<sub>2</sub>O-), 3.47 (m, 1H, H-1'), 4.36 (q, *J* = 7.0 Hz, 2H, -OCH<sub>2</sub>CH<sub>3</sub>), 7.25 (d, *J* = 7.6 Hz, 2H, H-2'' + H-6''), 7.30 (t, *J* = 6.8 Hz, 1H, H-4''), 7.45 (t, *J* = 8.0 Hz, 2H, H-3'' + H-5''), 8.36 (s, 1H, H-6). <sup>13</sup>C NMR (125 MHz, CDCl<sub>3</sub>) δ 7.85 (C-2' + C3'), 14.37 (-OCH<sub>2</sub>CH<sub>3</sub>), 36.56 (C-1'), 61.34 (-OCH<sub>2</sub>CH<sub>3</sub>), 116.00 (C-5), 118.42 (C-2'' + C-6''), 121.43 (C-3a), 126.28 (C-4''), 130.38 (C-3'' + C-5''), 130.39 (C-2), 141.39 (C-3), 145.73 (C-6), 150.81 (C-7a), 157.16 (C-1''), 164.81 (C-COOEt), 167.76 (C-4).



**Ethyl 7-Cyclopropyl-2-(2-formylphenoxy)-3-nitro-4-oxo-4,7-dihydrothieno[2,3-*b*]pyridine-5-carboxylate (3b).** This compound was prepared from **1** (0.2 g, 0.6 mmol) and salicylaldehyde (**2b**) (0.12 g, 0.9 mmol) by following the general procedure and reaction conditions as described above. Reaction time 12 h; yield 0.22 g (85%), mp 200–202 °C. HRMS (ESI)  $m/z$  [M+Na] calcd for  $C_{20}H_{16}N_2O_7SNa$ : 451.05704; found: 451.05789. IR 3853, 3745, 2983, 2354, 1687, 1620, 1542, 1448, 1389, 1335, 1229, 1030, 835, 780, 536  $cm^{-1}$ .  $^1H$  NMR (500 MHz, DMSO- $d_6$ )  $\delta$  1.05 (m, 2H) and 1.19 (m, 2H) ( $H_2-2'$  +  $H_2-3'$ ), and 1.23 (t,  $J = 7.1$  Hz, 3H,  $CH_3CH_2O-$ ), 3.64 (m, 1H,  $H-1'$ ), 4.18 (q,  $J = 7.1$  Hz, 2H,  $-OCH_2CH_3$ ), 7.39 (d,  $J = 8.3$  Hz, 1H,  $H-6''$ ), 7.46 (t,  $J = 7.5$  Hz, 1H,  $H-4''$ ), 7.76 (t,  $J = 7.4$  Hz, 1H,  $H-5''$ ), 7.90 (d,  $J = 7.1$  Hz, 1H,  $H-3''$ ), 8.32 (s, 1H,  $H-6$ ), 10.26 (s, 1H, CHO).  $^{13}C$  NMR (125 MHz, DMSO- $d_6$ )  $\delta$  7.68 ( $C-2'$  +  $C3'$ ), 14.65 ( $-OCH_2CH_3$ ), 37.16 ( $C-1'$ ), 60.83 ( $-OCH_2CH_3$ ), 116.06 ( $C-5$ ), 118.66 ( $C-6''$ ), 119.91 ( $C-3a$ ), 126.48 ( $C-2''$ ), 126.90 ( $C-4''$ ), 130.46 ( $C-3''$ ), 131.44 ( $C-2$ ), 137.06 ( $C-5''$ ), 143.72 ( $C-3$ ), 146.15 ( $C-6$ ), 149.33 ( $C-7a$ ), 158.24 ( $C-1''$ ), 164.39 ( $C-COOEt$ ), 167.56 ( $C-4$ ), 188.9 ( $C-CHO$ ).

**Ethyl 7-Cyclopropyl-2-(2-formyl-4-methylphenoxy)-3-nitro-4-oxo-4,7-dihydrothieno[2,3-*b*]pyridine-5-carboxylate (3c).** This compound was prepared from **1** (0.2 g, 0.6 mmol) and 2-hydroxy-5-methylbenzaldehyde (**2c**) (0.14 g, 0.9 mmol) by following the general procedure and reaction conditions as described above. Reaction time 12 h; yield 0.16 g (62%), mp 203–205 °C. HRMS (ESI)  $m/z$  [M+Na] calcd for  $C_{21}H_{18}N_2O_7SNa$ : 465.07269; found: 465.07196. IR 1625, 1566, 1532, 1497, 1449, 1394, 1343, 1240, 1192, 1144, 1070, 796  $cm^{-1}$ .  $^1H$  NMR (500 MHz,  $CDCl_3$ )  $\delta$  1.30 (m, 2H) and 1.40 (m, 2H) ( $H_2-2'$  +  $H_2-3'$ ), and 1.45 (t,  $J = 7.0$  Hz, 3H,  $CH_3CH_2O-$ ), 2.50 (s, 3H,  $C(4'')$ - $CH_3$ ), 3.57 (m, 1H,  $H-1'$ ), 4.42 (q,  $J = 7.0$  Hz, 2H,  $-OCH_2CH_3$ ), 7.38 (d,  $J = 8.4$  Hz, 1H,  $H-6''$ ), 7.54 (d,  $J = 8.0$  Hz, 1H,  $H-5''$ ), 7.84 (s, 1H,  $H-3''$ ), 8.43 (s, 1H,  $H-6$ ), 10.48 (s, 1H, CHO).  $^{13}C$  NMR (125 MHz,  $CDCl_3$ )  $\delta$  7.83 ( $C-2'$  +  $C3'$ ), 14.34 ( $-OCH_2CH_3$ ), 20.69 ( $C-CH_3$ ), 36.70 ( $C-1'$ ), 61.30 ( $-OCH_2CH_3$ ), 116.04 ( $C-5$ ), 118.24 ( $C-6''$ ), 121.21 ( $C-3a$ ), 126.25 ( $C-2''$ ), 129.60 ( $C-3''$ ), 131.46 ( $C-2$ ), 136.65 ( $C-4''$ ), 136.84 ( $C-5''$ ), 141.99 ( $C-3$ ), 145.88 ( $C-6$ ), 149.58 ( $C-7a$ ), 156.63 ( $C-1''$ ), 164.49 ( $C-COOEt$ ), 167.63 ( $C-4$ ), 187.66 ( $C-CHO$ ).

**Ethyl 2-(4-Chloro-2-formylphenoxy)-7-cyclopropyl-3-nitro-4-oxo-4,7-dihydrothieno[2,3-*b*]pyridine-5-carboxylate (3d).** This compound was prepared from **1** (0.2 g, 0.6 mmol) and 2-hydroxy-5-chlorobenzaldehyde (**2d**) (0.16 g, 0.9 mmol) by following the general procedure and reaction conditions as described above. Reaction time 12 h; yield 0.18 g (67%), mp 202–205 °C. HRMS (ESI)  $m/z$  [M+Na] calcd for  $C_{20}H_{15}ClN_2O_7SNa$ : 485.01807; found: 485.01986; [M+H] calcd for  $C_{20}H_{16}ClN_2O_7S$ : 463.03613; found: 463.03778. IR 1683, 1623, 1555, 1526, 1487, 1448, 1394, 1323, 1245, 1160, 1136, 1067, 1030, 934, 866, 832, 797, 721,

630  $cm^{-1}$ .  $^1H$  NMR (500 MHz,  $CDCl_3$ )  $\delta$  1.18 (m, 4H) ( $H_2-2'$  +  $H_2-3'$ ), and 1.29 (t,  $J = 7.0$  Hz, 3H,  $CH_3CH_2O-$ ), 3.45 (m, 1H,  $H-1'$ ), 4.25 (q,  $J = 6.8$  Hz, 2H,  $-OCH_2CH_3$ ), 7.20 (d,  $J = 8.4$  Hz, 1H,  $H-6''$ ), 7.53 (dd,  $J_1 = 2.4$  Hz,  $J_2 = 8.8$  Hz, 1H,  $H-5''$ ), 7.83 (d,  $J = 2.4$  Hz, 1H,  $H-3''$ ), 8.28 (s, 1H,  $H-6$ ), 10.31 (s, 1H, CHO).  $^{13}C$  NMR (100 MHz,  $CDCl_3$ )  $\delta$  7.92 ( $C-2'$  +  $C3'$ ), 14.35 ( $-OCH_2CH_3$ ), 36.79 ( $C-1'$ ), 61.41 ( $-OCH_2CH_3$ ), 116.12 ( $C-5$ ), 119.21 ( $C-6''$ ), 121.04 ( $C-3a$ ), 127.16 ( $C-2''$ ), 128.99 ( $C-3''$ ), 132.11 ( $C-4''$ ), 132.59 ( $C-2$ ), 135.89 ( $C-5''$ ), 142.61 ( $C-3$ ), 146.12 ( $C-6$ ), 147.76 ( $C-7a$ ), 157.06 ( $C-1''$ ), 164.37 ( $C-COOEt$ ), 167.67 ( $C-4$ ), 186.22 ( $C-CHO$ ).

**Ethyl 7-Cyclopropyl-3-nitro-4-oxo-2-(phenylthio)-4,7-dihydrothieno[2,3-*b*]pyridine-5-carboxylate (3e).** This compound was prepared from **1** (0.2 g, 0.6 mmol) and thiophenol (**2e**) (0.07 g, 0.65 mmol) by following the general procedure and reaction conditions as described above. Reaction time 12 h; yield 0.12 g (50%), mp 208–209 °C. HRMS (ESI)  $m/z$  [M+Na] calcd for  $C_{19}H_{16}N_2O_5S_2Na$ : 439.03928; found: 439.03896. IR 3900, 3089, 2952, 1728, 1688, 1615, 1559, 1486, 1453, 1395, 1344, 1320, 1229, 1199, 1146, 1070, 1044, 922, 875, 836, 800, 761, 694, 597, 554  $cm^{-1}$ .  $^1H$  NMR (500 MHz,  $CDCl_3$ )  $\delta$  1.15–1.22 (m, 4H,  $H_2-2'$  +  $H_2-3'$ ), and 1.33 (t,  $J = 7.0$  Hz, 3H,  $CH_3CH_2O-$ ), 3.41 (m, 1H,  $H-1'$ ), 4.29 (q,  $J = 7.0$  Hz, 2H,  $-OCH_2CH_3$ ), 7.36 (m, 3H,  $H-2''$  +  $H-6''$  +  $H-4''$ ), 7.49 (m, 2H,  $H-3''$  +  $H-5''$ ), 8.26 (s, 1H,  $H-6$ ).  $^{13}C$  NMR (125 MHz,  $CDCl_3$ )  $\delta$  7.78 ( $C-2'$  +  $C3'$ ), 14.35 ( $-OCH_2CH_3$ ), 36.05 ( $C-1'$ ), 61.34 ( $-OCH_2CH_3$ ), 116.00 ( $C-5$ ), 129.31 ( $C-4''$ ), 129.64 ( $C-2''$  +  $C-6''$ ), 121.43 ( $C-3a$ ), 132.45 ( $C-3''$  +  $C-5''$ ), 130.39 ( $C-2$ ), 141.39 ( $C-3$ ), 145.42 ( $C-6$ ), 150.81 ( $C-7a$ ), 157.16 ( $C-1''$ ), 164.81 ( $C-COOEt$ ), 167.76 ( $C-4$ ).

### 3. 4 Resazurin Reduction Assay

The cytotoxic effects of compounds on drug-sensitive leukemia CCRF-CEM and multidrug-resistant P-glycoprotein-overexpressing CEM/ADR5000 cells were evaluated by the resazurin assay as previously described.<sup>29–33</sup> All compounds were first tested at a single concentration of 10  $\mu M$  (Figure 2) against CCRF-CEM and CEM/ADR5000 cells. Compounds **3a**, **3e**, and **3b**, which significantly inhibited cell viability (reduction to less than 10% growth) were further tested in a concentration range from 0.001 to 10  $\mu M$  to determine the 50% inhibitory concentrations (for  $IC_{50}$ ) in both, CCRF-CEM and CEM/ADR5000 cell lines. The fluorescence was measured using an Infinite M2000 Pro<sup>TM</sup> plate reader (Tecan, Crailsheim, Germany) at an excitation wavelength of 544 nm and an emission wavelength of 590 nm. All experiments were performed three times with every six parallel measurements. The viability was evaluated based on a comparison with untreated cells. The  $IC_{50}$  values represent the concentrations of the compounds required to inhibit 50% of cell viability and were determined from a calibration curve by linear regression using Microsoft Excel.

## 4. Conclusion

A series of novel thieno[2,3-*b*]pyridine derivatives have been synthesized and screened for their *in vitro* cytotoxicity towards sensitive CCRF-CEM and multidrug resistance CEM/ADR5000 leukemia cells. Compounds **3a**, **3b**, and **3e** inhibited the growth of both cell lines incorporating phenol without substitution at *para* position, which can be considered as lead structures for further drug development.

## Acknowledgments

We gratefully thank the Deanship of Scientific Research at Mutah University, Al-Karak, Jordan for financial support. Also, the support of Prof. Dr. Thomas Efferth from Department of Pharmaceutical Biology, Institute of Pharmaceutical and Biomedical Sciences, Johannes Gutenberg University, Mainz, Germany in providing laboratory equipment for the biological assay and measurements is greatly acknowledged.

## Appendix A. Supplementary Material

Supplementary data to this article includes <sup>1</sup>H, <sup>13</sup>C, DEPT, 2D NMR and HRMS spectra of the synthesized ethyl 2-(aryloxo/arylthio)-7-cyclopropyl-3-nitro-4-oxo-4,7-dihydrothieno[2,3-*b*]pyridine-5-carboxylate **3a–e** compounds which are described in this article.

## 5. References

- V. P. Litvinov, V. V. Dotsenko, S. G. Krivokolysko, *Russ. Chem. Bull.* **2005**, *54*, 864–904. DOI:10.1007/s11172-005-0333-1
- A. E. Mekky, S. M. Sanad, A. Y. Said, M. A. Elneairy, *Synth. Commun.* **2020**, *50*, 2376–2389. DOI:10.1080/00397911.2020.1778033
- R. M. Kumbhare, T. L. Dadmal, R. Pamanji, U. B. Kosurkar, L. R. Velatooru, K. Appalanaidu, Y. K. Rao, J. V. Rao, *Med. Chem. Res.* **2014**, *23*, 4404–4413. DOI:10.1007/s00044-014-1006-0
- F. M. Shaikh, N. B. Patel, G. Sanna, B. Busonera, P. La Colla, D. P. Rajani, *Med. Chem. Res.* **2015**, *24*, 3129–3142. DOI:10.1007/s00044-015-1358-0
- M. Singh, S. K. Singh, M. Gangwar, G. Nath, S. K. Singh, *Med. Chem. Res.* **2016**, *25*, 263–282. DOI:10.1007/s00044-015-1479-5
- M. Bhat, S. L. Belagali, *Res. Chem. Intermediat.* **2016**, *42*, 6195–6208. DOI:10.1007/s11164-016-2454-6
- C. Kharbanda, M. S. Alam, H. Hamid, K. Javed, S. Bano, A. Dhulap, Y. Ali, S. Nazreen, S. Haider, *Bioorg. Med. Chem.* **2014**, *22*, 5804–5812. DOI:10.1016/J.BMC.2014.09.028
- T. I. Chaban, V. V. Ogurtsov, V. S. Matiychuk, I. G. Chaban, I. L. Demchuk, I. A. Nektegayev, *Acta Chim. Slov.* **2019**, *66*, 103–111. DOI:10.17344/acsi.2018.4570
- T. I. Chaban, J. E. Matiychuk, O. Y. Shyyka, I. G. Chaban, V. V. Ogurtsov, I. A. Nektegayev, V. S. Matiychuk, *Acta Chim. Slov.* **2020**, *67*, 1035–1043. DOI:10.17344/acsi.2019.5439
- S. S. Thakkar, P. Thakor, A. Ray, H. Doshi, V. R. Thakkar, *Bioorg. Med. Chem.* **2017**, *25*, 5396–5406. DOI:10.1016/j.bmc.2017.07.057
- M. M. El-Abadelah, S. S. Sabri, H. A. Al-Ashqar, *Heterocycles* **1997**, *2*, 255–264. DOI:10.3987/COM-96-7613
- M. E. Abdelaziz, M. M. El-Miligy, S. M. Fahmy, M. A. Mahran, A. A. Hazzaa, *Bioorg. Chem.* **2018**, *80*, 674–692. DOI:10.1016/J.BIOORG.2018.07.024
- C. Eurtivong, I. Reynisdóttir, S. Kuczma, D. P. Furkert, M. A. Brimble, J. Reynisson, *Bioorg. Med. Chem.* **2016**, *24*, 3521–3526. DOI:10.1016/J.BMC.2016.05.061
- J. M. Hung, H. J. Arabshahi, E. Leung, J. Reynisson, D. Barker, *Eur. J. Med. Chem.* **2014**, *86*, 420–437. DOI:10.1016/j.ejmech.2014.09.001
- S. Singh, B. Sharma, S. S. Kanwar, A. Kumar, *Front. Plant Sci.* **2016**, *7*, 1667. DOI:10.3389/fpls.2016.01667
- M. M. Gottesman, T. Fojo, S. E. Bates, *Nat. Rev. Cancer.* **2002**, *2*, 48–58. DOI:10.1038/nrc706
- T. Efferth, M. Volm, *Arch. Toxicol.* **2017**, *91*, 2515–2538. DOI:10.1007/s00204-017-1938-5
- N. Erin, J. Grahovac, A. Brozovic, T. Efferth, *Drug Resist. Update* **2020**, *53*, 100715. DOI:10.1016/j.drug.2020.100715
- C. H. Choi, *Cancer Cell Int.* **2005**, *5*, 30. DOI:10.1186/1475-2867-5-30
- T. Efferth, *Curr. Mol. Med.* **2001**, *1*, 45–65. DOI:10.2174/1566524013364194
- J. P. Gillet, T. Efferth, D. Steinbach, J. Hamels, F. De Longueville, V. Bertholet, J. Remacle, *Cancer Res.* **2004**, *64*, 8987–8993. DOI:10.1158/0008-5472.CAN-04-1978
- X. X. Zeng, R. L. Zheng, T. Zhou, H. Y. He, J. Y. Liu, Y. Zheng, A. P. Tong, M. L. Xiang, X. R. Song, S. Y. Yang, L. T. Yu, *Bioorg. Med. Chem. Lett.* **2010**, *20*, 6282–6285. DOI:10.1016/j.bmcl.2010.08.088
- R. Zhou, W. J. Huang, Z. Y. Guo, L. Li, X. R. Zeng, Y. Q. Deng, F. Y. Hu, A. P. Tong, L. Yang, J. L. Yang, *Oncol. Rep.* **2012**, *28*, 225–231. DOI:10.3892/or.2012.1776
- S. A. Al-Trawneh, M. M. El-Abadelah, J. A. Zahra, S. A. Al-Taweel, F. Zani, M. Incerti, A. Cavazzoni, P. Vicini, *Bioorg. Med. Chem.* **2011**, *19*, 2541–2548. DOI:10.1016/j.bmc.2011.03.018
- S. A. Al-Trawneh, S. A. Al-Dawdieh, N. S. Abutaleb, A. H. Tarawneh, E. A. Salama, M. M. El-Abadelah, M. N. Seleem, *Chem. Pap.* **2020**, *74*, 1241–1252. DOI:10.1007/s11696-019-00974-9
- A. H. Tarawneh, F. León, S. K. Jain, A. V. Gadetskaya, S. T. Abu-Orabi, B. L. Tekwani, S. J. Cutler, *Med. Chem. Res.* **2018**, *27*, 1269–1275. DOI:10.1007/s00044-018-2146-4
- A. H. Tarawneh, F. León, S. Pettaway, K. M. Elokely, M. L. Klein, J. Lambert, A. Mansoor, S. J. Cutler, *J. Nat. Prod.* **2015**, *78*, 1461–1465. DOI:10.1021/acs.jnatprod.5b00218
- T. Efferth, V. B. Konkimalla, Y. F. Wang, A. Sauerbrey, S. Meinhart, F. Zintl, J. Mattern, M. Volm, *Clin. Cancer Res.* **2008**, *14*, 2405–2412. DOI:10.1158/1078-0432.CCR-07-4525

29. J. O'Brien, I. Wilson, T. Orton, F. Pognan, *Eur. J. Biochem.* **2000**, 267, 5421–5426.  
DOI:10.1046/j.1432-1327.2000.01606.x
30. S. Abdelfatah, M. Böckers, M. Asensio, O. Kadioglu, A. Klinger, E. Fleischer, T. Efferth, *Phytomedicine* **2020**, 153196.  
DOI:10.1016/j.phymed.2020.153196
31. N. Mahmoud, M. E. M. Saeed, Y. Sugimoto, A. Klinger, E. Fleischer, T. Efferth, *Phytomedicine* **2020**, 77, 153271.  
DOI:10.1016/j.phymed.2020.153271
32. A. T. Mbaveng, G. F. Chi, I. N. Bonsou, S. Abdelfatah, A. N. Tamfu, E. M. O. Yeboah, V. Kuete, T. Efferth, *Phytomedicine* **2020**, 76, 153261. DOI: 10.1016/j.phymed.2020.153261
33. G. Yan, M. Dawood, M. Böckers, S. M. Klauck, C. Fottner, M. M. Weber, T. Efferth, *Phytomedicine* **2020**, 79, 153332.  
DOI:10.1016/j.phymed.2020.153332

## Povzetek

Iz ključnega intermediala etil 7-ciklopropil-2-kloro-3-nitro-4-okso-4,7-dihidrotieno[2,3-*b*]piridin-5-karboksilata (**1**) smo s substitucijo 2-klorovega substituenta z anioni, pripravljenimi iz fenola (**2a**), salicilaldehidnih derivatov **2b–d** in tiofenola (**2e**), sintetizirali serijo novih substituiranih 7-ciklopropil-2-(2-ari-  
lokso)-3-nitro-4-okso-4,7-dihidrotieno[2,3-*b*]piridin-5-karboksilatov **3a–e**. Za nove spojine smo določili *in vitro* citotoksično delovanje proti občutljivim CCRF-CEM levkemičnim celicam in proti CEM/ADR5000 levkemičnim celicam, odpornim na več različnih učinkovin. Testiranje je pokazalo, da so spojine **3a**, **3b** in **3e** inhibirale obe celični liniji. Spojina **3b**, ki vsebuje fenolni fragment, pa je pokazala največjo inhibitorno aktivnost rasti pri celicah CEM/ADR5000 in CCRF-CEM z  $IC_{50}$  vrednostmi  $4.486 \pm 0.286 \mu\text{M}$  (za prvo celično linijo) in  $2.580 \pm 0.550 \mu\text{M}$  (za drugo celično linijo). Skupno gledano rezultati kažejo, da pripravljene tieno[2,3-*b*]piridini izkazujejo potencialno uporabnost kot protirakave učinkovine in da si zato zaslužijo, da so predmet nadaljnjih raziskav.



Except when otherwise noted, articles in this journal are published under the terms and conditions of the Creative Commons Attribution 4.0 International License

Scientific paper

# A Novel Cd(II) Isophthalate Complex with Triethanolamine: Crystal Structure, Fluorescence and Antimicrobial Activity

Zuhal Yolcu,<sup>1,\*</sup> Sinem Yurtcan<sup>2</sup> and Meryem Çıtlakoglu<sup>1</sup><sup>1</sup> Department of Chemistry, Faculty of Art and Science, Giresun University, Giresun, Turkey<sup>2</sup> Giresun University Central Research Laboratory Application and Research Center

\* Corresponding author: E-mail: zuhal.yolcu@giresun.edu.tr

Received: 12-22-2020

## Abstract

A mixed ligand Cd(II) complex [Cd(IsoPht)(TEA)H<sub>2</sub>O]·3H<sub>2</sub>O was synthesized for the first time by using isophthalic acid (H<sub>2</sub>IsoPht) and tetradentate triethanolamine (TEA) and characterized by X-ray single-crystal diffraction, FT-IR, and thermogravimetric analysis (TGA). This novel complex crystallizes in the triclinic system with *P*-1 space group and distorted monocapped trigonal prismatic geometry. The Cd(II) has seven coordinates with bidentate IsoPht, a TEA in the tetradentate mode, and an aqua ligand. The fluorescence properties of the Cd(II) complex and TEA ligand were investigated at room temperature. The present Cd(II) complex was also tested for its antimicrobial activity by *in vitro* agar diffusion method against some Gram-positive and Gram-negative bacteria and a fungus.

**Keywords:** Isophthalic acid; triethanolamine; Cd(II) complex; X-ray single crystal; antimicrobial activity

## 1. Introduction

Triethanolamine (TEA) is a potential ligand that can interact with metal ions to form supramolecular complexes with different structures, and many coordination compounds containing TEA ligands have been reported for the last two decades.<sup>1–6</sup> TEA is also used as a pH regulator in cosmetology, as a corrosion inhibitor in metal-cutting fluids, as a curing agent for epoxy and rubber polymers, in adhesives, antistatic agents, or as a pharmaceutical intermediate.<sup>7–9</sup> TEA generally acts as the tri- or tetradentate ligand, but some metal complexes with mono- or bidentate TEA coordination modes are also known.<sup>10,11</sup> Metal complexes containing TEA ligand can be (neutral or cationic) mono-, bi- and polynuclear structures.<sup>12,13</sup> Some mononuclear mixed ligand complexes were reported for Ni(II) with TEA and orotic acid,<sup>14</sup> Cu(II) with TEA and malonic acid,<sup>15</sup> Zn(II) and Cd(II) with TEA and *p*-nitrobenzoic acid,<sup>16</sup> Zn(II) with TEA and aqua ligand,<sup>17</sup> Cu(II) with TEA, aqua and 1H-imidazole ligands,<sup>18</sup> aqua ligand.<sup>19</sup> Based on the collaborative use of TEA and phthalic acid, mononuclear complexes for Ni(II),<sup>20</sup> Zn(II),<sup>21</sup> Cd(II),<sup>22</sup> and coordination polymer for Cd(II)<sup>23</sup> were also reported. Although TEA has no specific physiological effects except

for its low antibacterial activity, as an auxiliary ligand TEA may increase the physiological effect of bioactive substances in mixed ligand metal complexes.<sup>8,9,24</sup> There are preliminary pharmacological studies demonstrating that the transition metal complexes of TEA protect animals from ethanol and carbon monoxide poisoning and have immune-modulating and antiproliferative properties.<sup>25–27</sup> Also, the mixed ligand zinc complex containing TEA has been reported to have anti-angiogenic and anti-atherogenic effects.<sup>28</sup>

Coordination compounds may combine a metal ion, a biocompatible ligand, and some auxiliary ligands in the same molecule to form mixed-ligand coordination types to achieve the desired properties.<sup>29,30</sup> Apart from the TEA ligand, isophthalic acid (H<sub>2</sub>IsoPht) has been selected as a good candidate for this purpose. Dicarboxylic acids have important advantages in design of coordination compounds compared with other organic ligands. Isophthalic acid has two carboxyl groups that can lose one or two protons to form various coordination modes, act as a hydrogen bond acceptor and donor. So it is a versatile and variable ligand that can bind metal ions in different directions.<sup>31–38</sup> The synthesis of coordination compounds containing O and/or N-donor ligands are very significant

and intriguing in the field of pharmacology due to the discovery of their antimicrobial properties. The biological activity of coordination compounds with O-donor ligand isophthalato (IsoPht) has been studied.<sup>39–42</sup> Antimicrobial activities of Zn-IsoPht complexes were displayed *in vitro* against some Gram-positive, some Gram-negative bacteria and fungus by Radovanović and co-workers, who showed that the most potent inhibitory effect of [Zn(dipya)(IsoPht)]<sub>n</sub> (dipya = 2,2'-dipyridylamine) against all the tested microorganisms.<sup>39</sup> Devereux and co-workers demonstrated high antibacterial activity of Mn-phen-pht/IsoPht complexes against *Candida albicans*.<sup>40</sup>

Cadmium coordination compounds containing O and/or N-donor ligands can show promising fluorescence properties.<sup>43–49</sup> In this study, a novel mixed ligand Cd(II) complex with TEA and IsoPht was synthesized and the structure of the complex was identified by using X-ray single-crystal diffraction and FT-IR. Thermal properties of the complex were also examined in detail. The fluorescence and antimicrobial properties of the complex were investigated, too.

## 2. Experimental

### 2.1. Materials and Instrumentations

Triethanolamine (TEA), Isophthalic acid (H<sub>2</sub>IsoPht), and Cd(NO<sub>3</sub>)<sub>2</sub> · 4H<sub>2</sub>O were purchased from Sigma Aldrich Ltd. IR spectra were obtained with an FT/IR-100 type A Spectrophotometer. Thermal degradation of the complex was performed using a TA Instruments SII-EXTAR-6000 TG/DTA. Experiments were conducted from 30 to 900 °C, with a heating rate of 10 °C min<sup>-1</sup>, under nitrogen atmosphere using platinum crucibles. Fluorescence spectra of the complex were taken on Agilent Cary Eclipse Fluorescence Spectrophotometer.

### 2.2. Synthesis of [Cd(IsoPht)(TEA)H<sub>2</sub>O] · 3H<sub>2</sub>O

5 mmol of Cd(NO<sub>3</sub>)<sub>2</sub> · 4H<sub>2</sub>O (1540 mg) was dissolved in 30 mL of water. Then, 10 mmol (1.33 mL) TEA was added and reaction solution was stirred for 10 min at 70 °C. After that, 5 mmol (830 mg) of H<sub>2</sub>IsoPht was added to the solution and stirred for more 3 hours. 4 weeks later, colorless crystals were obtained by slow evaporation of the clear solution that appeared after filtration at room temperature.

### 2.3. X-Ray Crystallography

The reflection intensities of the Cd(II) complex were collected at 296 K using Agilent SuperNova single-crystal diffractometer with Mo-K $\alpha$  radiation ( $\lambda = 0.71073$  Å). The structure was solved using the program SHELXT<sup>50</sup> by direct methods, and all non-hydrogen atoms were refined with anisotropic displacement parameters by full-matrix

least-squares methods based on F<sup>2</sup> using SHELXL.<sup>51</sup> The molecular graphics were prepared using OLEX<sup>2</sup> program.<sup>52</sup> Detailed information about the crystal data and structure determination are summarized in Table 1. Selected experimental and calculated interatomic distances and bond angles are given in Table 2.

### 2.4. Computational Protocol

Quantum chemical calculation of the complex was performed using Gaussian 09 program suits running under Windows.<sup>53</sup> Ground state geometry optimization of the complex was performed by using Minnesota M062X hybrid density functional method with appropriate basis set combinations, 6-31g(d,p) for non-metal atoms and pseudo potential-included SDD for metal atom.

Table 1. Crystallographic data for [Cd(IsoPht)(TEA)H<sub>2</sub>O] · 3H<sub>2</sub>O

Empirical formula	C <sub>14</sub> H <sub>27</sub> CdNO <sub>11</sub>
Formula weight	497.76
Temperature/K	293(2)
Crystal system	Triclinic
Space group	<i>P</i> $\bar{1}$
a/Å	9.0749(3)
b/Å	10.7120(3)
c/Å	12.2025(5)
$\alpha$ /°	66.944(3)
$\beta$ /°	72.272(3)
$\gamma$ /°	67.510(3)
Volume/Å <sup>3</sup>	991.61(7)
Z	1
$\rho_{\text{calc}}$ /cm <sup>3</sup>	1.667
$\mu$ /mm <sup>1</sup>	1.157
F(000)	508.0
Crystal size/mm <sup>3</sup>	0.13 × 0.15 × 0.17
Radiation	MoK $\alpha$ ( $\lambda = 0.71073$ )
2 $\theta$ range for data collection/°	6.684 to 52.742
Reflections collected	13143
Independent reflections	4050 [R <sub>int</sub> = 0.0400, R <sub>sigma</sub> = 0.0352]
Data/restraints/parameters	4050/3/258
F <sup>2</sup>	1.067
Final R indexes [I > 2 $\sigma$ (I)]	R <sub>1</sub> = 0.0325, wR <sub>2</sub> = 0.0817
Final R indexes [all data]	R <sub>1</sub> = 0.0325, wR <sub>2</sub> = 0.0838
Largest diff. peak/hole / e Å <sup>-3</sup>	1.44/−0.78

### 2.5. Antimicrobial Activity

*In vitro* antimicrobial screening test of the synthesized compound were carried out for antibacterial and antifungal activity. Antibacterial activity was tested against three bacterial strains; two gram-positive [*Bacillus cereus* (ATCC 10876), *Staphylococcus aureus* (ATCC 29213)] and one gram-negative [*Escherichia coli* (ATCC 25922)] and antifungal activity was tested against one fungal strain [*Candida albicans* (ATCC10231)]. The agar well diffusion method was used in these assays. After nutrient agar was

sterilized in an autoclave at 121 °C for 15 min, it was transferred into sterile Petri plates. Then the agar medium solidified, 8 mm diameter wells were drilled with a sterile metallic applicator. 20  $\mu\text{L}$  of the sample at different concentrations prepared in DMSO was poured into the wells. DMSO served as a negative control, Ampicillin and Flucanazole served as a positive control. The plates were incubated aerobically at 37 °C for 24 h. The diameters of inhibition zones were measured by using a zone reader and were given as millimeters. Evaluation of the inhibition zone was made by averaging the three test results.

### 3. Results and Discussion

#### 3.1. The Crystal Structure of $[\text{Cd}(\text{IsoPht})(\text{TEA})\text{H}_2\text{O}]\cdot 3\text{H}_2\text{O}$

X-ray single-crystal analysis reveals that complex crystallized in the triclinic system with space group  $P\bar{1}$ . The complex has an interesting monomeric molecular structure which is rarely found for cadmium polycarboxylate complexes. In the complex,  $\text{H}_2\text{IsoPht}$  acts as a bidentate ligand by losing hydrogen atoms while the TEA ligand acts as a tetradentate ligand using all its donor atoms. The Cd1 atom is coordinated by six oxygen atoms and one nitrogen atom, two of which are from IsoPht ligand (O1 and O2), three oxygen atoms, and one nitrogen atom from a TEA ligand (O5, O6, O7, and N1), together with one oxygen atom of aqua ligand, O8W. In crystallization, uncoordinated three water molecules are also part of the molecular structure (Figure 1). Thus, Cd(II) ions are in distorted monocapped trigonal prismatic geometry environments

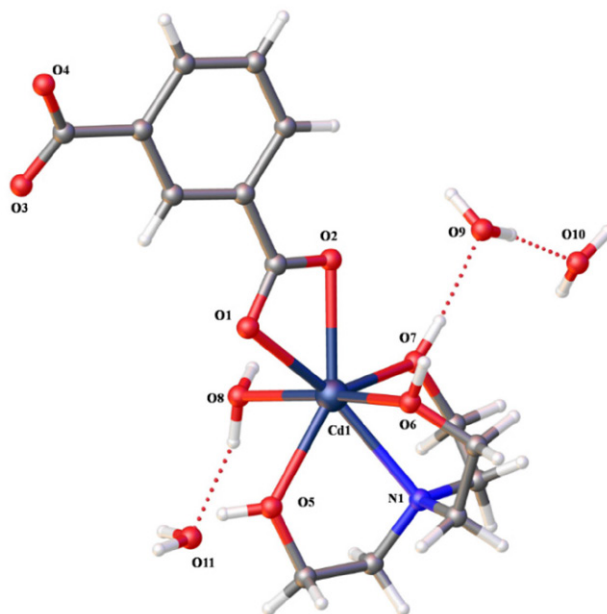


Figure 1. A view of the  $[\text{Cd}(\text{IsoPht})(\text{TEA})\text{H}_2\text{O}]\cdot 3\text{H}_2\text{O}$  compound showing the atom-labeling

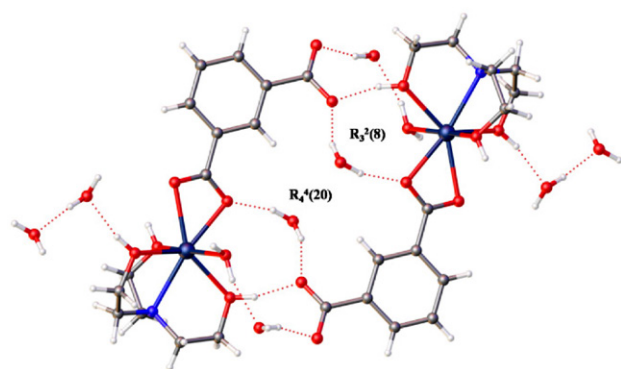
with  $\text{CdO}_6\text{N}$  chromophores. This seven-coordinate geometry around the Cd(II) ion in the titled complex is similar to the other reported Cd(II) complexes.<sup>1,2</sup>

The Cd1-O bonds are in the range 2.300 (2)–2.399 (2) Å and Cd1-N bond is 2.434 (2) Å (Table 2). The bond lengths between Cd1 and O atoms of IsoPht (O1, O2), 2.329(2) and 2.399(2) Å are comparable to the other Cd(II)-IsoPht complexes.<sup>46,54,55</sup> The bond distances of Cd1-O and Cd1-N between Cd1 and TEA, which are in the range of 2.300(2)–2.353(2) Å (O5, O6, O7) and

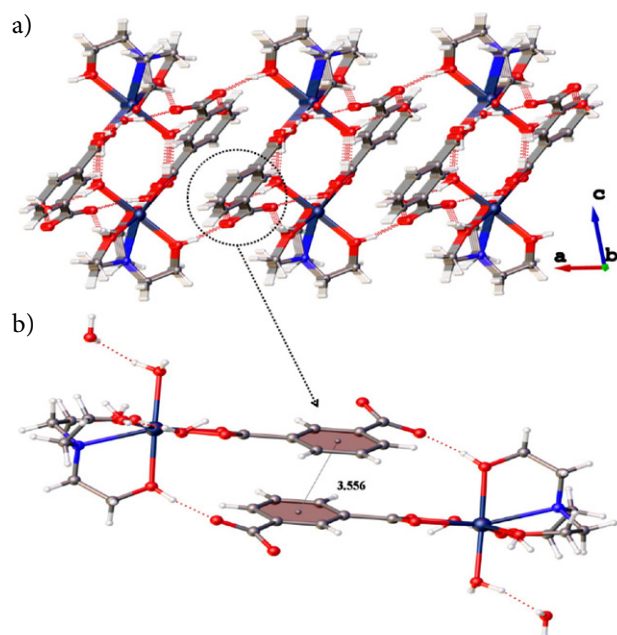
Table 2. Selected experimental and calculated coordination bonds and angles of  $[\text{Cd}(\text{IsoPht})(\text{TEA})\text{H}_2\text{O}]\cdot 3\text{H}_2\text{O}$

Bond lengths (Å)					
Bond	Exp.	Calc.	Bond	Exp.	Calc.
Cd1-O1	2.329(2)	2.2216	Cd1-O6	2.353(2)	2.5327
Cd1-O2	2.399(2)	2.2723	Cd1-O7	2.325(3)	2.3801
Cd1-O5	2.300(2)	2.4193	Cd1-O8	2.324(2)	2.4119
Cd1-N1	2.434(2)	2.4485			
Bond angles (°)					
Angle	Exp.	Calc.	Angle	Exp.	Calc.
O1-Cd1-O2	55.12(7)	58.86	O5-Cd1-O7	131.11(10)	126.59
O1-Cd1-O6	86.17(9)	92.92	O7-Cd1-O2	80.08(8)	103.19
O8-Cd1-O2	94.06(8)	131.99	O7-Cd1-O1	134.14(8)	132.58
O8-Cd1-O1	88.16(9)	87.74	O7-Cd1-O6	103.78(11)	123.19
O8-Cd1-O6	170.64(9)	152.86	O1-Cd1-N1	150.55 (8)	152.40
O8-Cd1-O7	85.50(11)	73.38	O2-Cd1-N1	140.73 (7)	127.47
O6-Cd1-O2	88.80(8)	69.16	O5-Cd1-N1	70.83 (8)	74.03
O5-Cd1-O2	146.41(8)	130.20	O6-Cd1-N1	72.15 (8)	69.51
O5-Cd1-O1	91.61(8)	83.14	O7-Cd1-N1	72.00 (8)	74.64
O5-Cd1-O8	78.85(9)	69.84	O8-Cd1-N1	110.61(8)	98.47
O5-Cd1-O6	93.86(10)	83.29			

2.434(2) Å (N1), are similar within the reported seven-coordinated mixed ligand complexes.<sup>16,23</sup> However, these bond lengths are shorter than those of the reported eight-coordinated complexes.<sup>3,22</sup> In addition, the bond angles between the Cd1 and O atoms vary between 55.12° (7) and 170.64° (9) in Table 2. The bond angles of the complex are normal compared with those of the related complexes.<sup>1,2,16</sup> The crystal structure is further stabilized by multiply intermolecular hydrogen bonds. The uncoordinated water molecules play an important role in the supramolecular architecture. The hydrogen-bonding interactions, which are assembled into 2D layers parallel to by O-H...O weak hydrogen bonds (Table 3), formed where the TEA donate hydrogen atoms to the neighboring carboxylate and water oxygens (Figure 2). It can be seen from Figure 2 that the hydrogen bonds between the TEA ligands and the car-



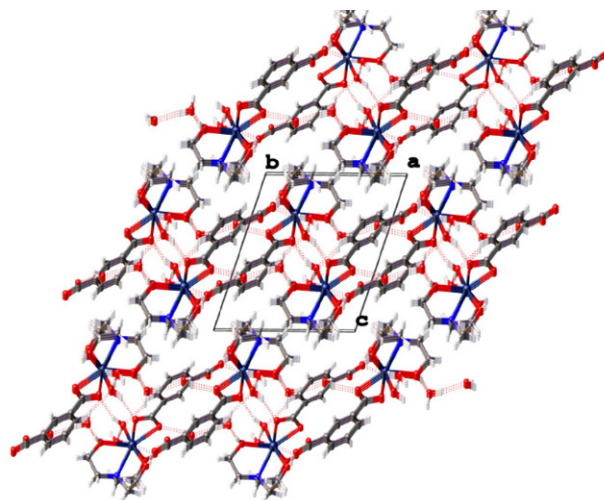
**Figure 2.** Part of the crystal structure of [Cd(IsoPht)(TEA)H<sub>2</sub>O]·3H<sub>2</sub>O, showing the formation of R<sub>3</sub><sup>2</sup>(8), and R<sub>4</sub><sup>4</sup>(20) rings by the O-H...O hydrogen bonds



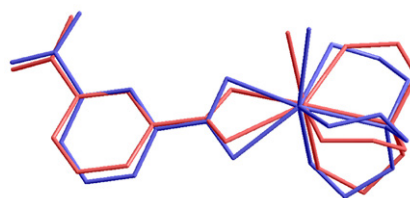
**Figure 3.** ((a) 2-D supramolecular network along the [010] direction in [Cd(IsoPht)(TEA)H<sub>2</sub>O]·3H<sub>2</sub>O complex. (b)  $\pi$ ... $\pi$  interaction

boxylate groups of IsoPht, giving rise to R<sub>3</sub><sup>2</sup>(8) and R<sub>4</sub><sup>4</sup>(20) ring motives. The molecules located along the [010] direction (Figure 3(a)), are linked by  $\pi$ ... $\pi$  stacking [ $\pi$ ... $\pi$  d = 3.556 Å] (Figure 3(b)). The  $\pi$ ... $\pi$  stacking interaction between the benzene ring of the IsoPht ligand is stronger than in the related {[Cd(HFlu)(IsoPht)(H<sub>2</sub>O)]·H<sub>2</sub>O}<sub>n</sub> (HFlu = fluconazole) complex [ $\pi$ ... $\pi$  d = 3.705 Å] in literature.<sup>46</sup>

An extensive network of hydrogen bonds,  $\pi$ ... $\pi$  stacking, and van der Waals interactions embed the complex in a three-dimensional lattice. Figure 4 shows the packing diagram of the complex along the [100] direction.



**Figure 4.** Packing diagram of [Cd(IsoPht)(TEA)H<sub>2</sub>O]·3H<sub>2</sub>O complex along the [100] direction



**Figure 5.** Superimposition of X-ray (red) and optimized (blue) geometries of [Cd(IsoPht)(TEA)H<sub>2</sub>O]·3H<sub>2</sub>O

**Table 3.** Hydrogen bond interactions for [Cd(IsoPht)(TEA)H<sub>2</sub>O]·3H<sub>2</sub>O

Hydrogen-bonds				
D-H...A	D-H	H...A	D...A	D-H...A
O8-H8-O9 <sup>i</sup>	0.85	2.08(4)	2.895(4)	161.9
O8-H8-O11	0.85	1.98	2.818(4)	167.2
O6-H6-O4 <sup>ii</sup>	0.89(5)	1.71(5)	2.598(3)	176(5)
O5-H5-O3 <sup>iii</sup>	0.73(5)	1.81(5)	2.536(4)	169(6)
O9-H9-O10	0.85	1.84	2.693(4)	176.2
O9-H9-O8 <sup>i</sup>	0.85	2.26	2.895(4)	132.0
O10-H10-O1 <sup>iv</sup>	0.85	2.01	2.808(3)	156.1
O10-H10-O3 <sup>i</sup>	0.85	1.91	2.743(4)	165.0
O11-H11-O4 <sup>iii</sup>	0.85	2.11	2.928(4)	162.5

Symmetry transformations used to generate equivalent atoms: (i) x, 1-y, 1-z; (ii) x, 2-y, 1-z; (iii) 1-x, 2-y, 1-z; (iv) +z, -1+y, +z

Quantum chemical optimized geometry of the complex exhibited reasonable accordance with experimental X-ray geometry with a RMSE deviation of 0.622 Å. Superimpositions of the X-ray and calculated geometries of the complex are given in Figure 5. In general, there is a pleasant consistence between optimized and X-ray geometries according to the results and as expected, the general tendency of gas-phase optimizations in favour of somewhat extending the bond distances was introduced.

### 3. 2. FT-IR Study

In the FT-IR spectrum of the Cd(II) complex, the broad absorption band between 3500 and 3100  $\text{cm}^{-1}$  with maxima at 3427, 3385 and 3146  $\text{cm}^{-1}$ , which are assigned to stretching vibrations  $\nu(\text{O-H})$  of uncoordinated water molecules, aqua and TEA ligand (Figure S1). The FT-IR stretching band at 3373  $\text{cm}^{-1}$  belongs to the hydroxyl group (O-H) of the TEA ligand and has been observed to shift to lower wavelength (3146  $\text{cm}^{-1}$ ) during complexation. The FT-IR bands identified at 3079, 2975, 2898 and 2844  $\text{cm}^{-1}$  are associated with aromatic and aliphatic  $\nu(\text{C-H})$  stretching vibrations. The bands in the spectral region 1700–1300  $\text{cm}^{-1}$  of complex shows five peaks with frequencies 1601, 1538, 1479, 1442 and 1390  $\text{cm}^{-1}$ . These bands can be attributed to stretching vibrations of aromatic ring  $\nu(\text{C}_{\text{Ar}})$  and carboxylate groups  $\nu(\text{C=O})$ . The peaks corresponding to a strong asymmetric stretching  $\nu_{\text{asym}}(\text{C=O})$  as 1689  $\text{cm}^{-1}$  and a weak symmetric stretching  $\nu_{\text{sym}}(\text{C=O})$  as 1417  $\text{cm}^{-1}$  of the  $\text{H}_2\text{IsoPht}$  were observed at lower frequencies (1538  $\text{cm}^{-1}$  and 1390  $\text{cm}^{-1}$ , respectively). This situation demonstrates that the IsoPht ligand coordinated to the Cd(II) via the oxygen atoms of the car-

boxylate group. The difference between the  $\nu_{\text{asym}}(\text{C=O})$  and  $\nu_{\text{sym}}(\text{C=O})$  stretching vibrations observed in the IR spectra of the complexes ( $\Delta\nu$ ), [ $\Delta\nu = \nu_{\text{asym}}(\text{C=O}) - \nu_{\text{sym}}(\text{C=O})$ ] is used to determine the coordination type of the carboxylate group. The frequency difference,  $\Delta\nu > 200 \text{ cm}^{-1}$  generally associated with unidentate coordination, a possible exception involving highly unsymmetrical bridging, i.e. “pseudo-unidentate” coordination.  $\Delta\nu > 105 \text{ cm}^{-1}$  and  $< 200 \text{ cm}^{-1}$  indicates chelating and/or bridging carboxylate groups. Accordingly, the value of  $\Delta\nu$  148  $\text{cm}^{-1}$  for the complex indicated that the chelate coordination mode of the carboxyl group of the IsoPht.<sup>56,57</sup> The coordination mode of IsoPht ligand is also approved by the single-crystal X-ray structure examined. The band observed at 434  $\text{cm}^{-1}$  is due to the metal-oxygen (M-O) bond.<sup>58</sup>

### 3. 3. Thermal Analysis

Thermal stability and behavior of the Cd(II) complex were examined by simultaneous TG/DTG/DTA in nitrogen atmosphere. The TG-DTG and DTA curves of the complex are shown in Figure 6. The complex underwent complete degradation in two main stages. The first stage (44–118 °C), is related to the removal of both crystal water and aqua ligand at  $\text{DTG}_{\text{max}}$  88 °C with a 13.98% mass loss. This exhibits an endothermic peak at 89 °C in the DTA curve. The anhydrous complex stays stable up to 179 °C. Over this temperature, it can be suggested that the TEA and IsoPht ligands removed successively from the structure in the temperature range of 179–657 °C ( $\text{DTG}_{\text{max}}$ : 378 °C). The final solid product of thermal decomposition is associated with CdO formation (found 27.7, calcd. 25.8%).

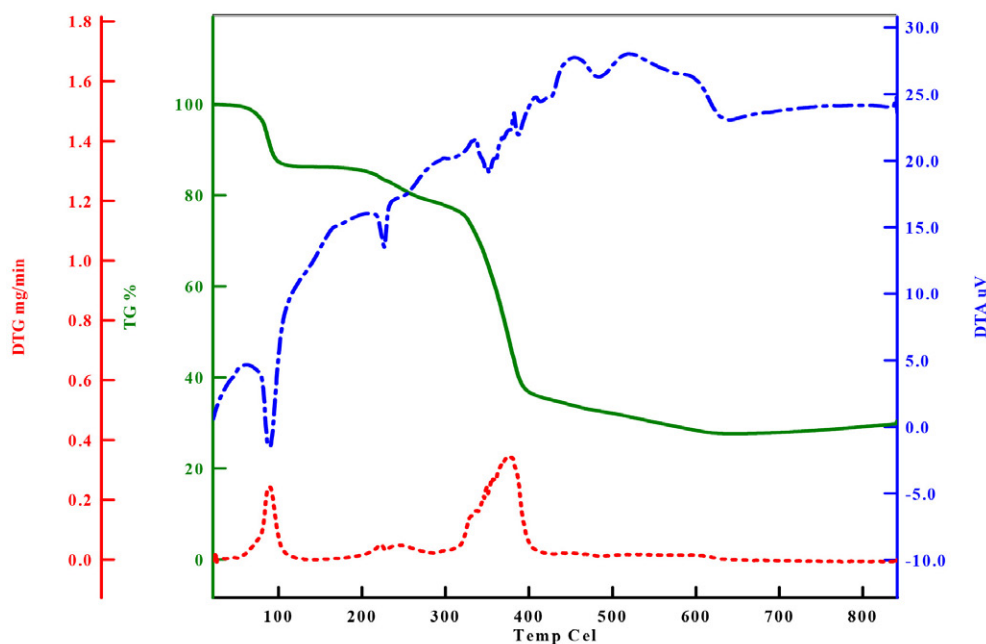


Figure 6. TGA curves of  $[\text{Cd}(\text{IsoPht})(\text{TEA})\text{H}_2\text{O}] \cdot 3\text{H}_2\text{O}$  complex



### 3. 4. Fluorescence Properties

The fluorescent properties of the TEA ligand and Cd(II) complex have been examined at room temperature. The resulting emission spectrum is given in Figure 7. Due to the fluorescence quenching of carboxyl groups of IsoPht (which are strong electron-attracting groups), this ligand shows very low fluorescence emission at room temperature.<sup>48,59</sup> While the TEA ligand shows the emission peaks at 312 and 346 nm with the excitation at 270 nm, the complex exhibits emission bands at 357 and 423 nm with the excitation at 270 nm. Compared with the emission of the TEA ligand, the emission peaks of the complex were observed to redshift (ca.45 nm and 77 nm). The solid-state fluorescence of the complex may be assigned to MLCT or LMCT transitions.<sup>60</sup>

### 3. 5. Antimicrobial Activity

The antimicrobial activity of the prepared [Cd(IsoPht)(TEA)H<sub>2</sub>O]·3H<sub>2</sub>O complex against three bac-

teria and one fungus was studied. Saturated solution and inhibition zones (mm) of the Cd(II) complex are given in Table 4. In the different concentrations of the complex, various inhibition values were observed for *B. cereus*, *S. aureus*, *E. coli*, and *C. albicans* between 10–25 mm, 7–20 mm, 16–18 mm, and 8–15 mm respectively. It was shown more efficacy than positive control against all three bacterial zones, especially at concentrations of 40000 and 20000 ppm.

Recently, it has been reported that Cu(II) complexes of TEA with salts of salicylic, cinnamic, and succinic acids,<sup>6</sup> Zn(II) and Cu(II) cinnamate with TEA complexes<sup>61</sup> showed antimicrobial activity against bacteria *E. coli*, *S. aureus*, *M. smegmatis*, fungi *C. albicans* and *A. niger*. In addition, it has been shown that TEA with Cu(II) picrate and Ag(I) complexes appeared to exhibit mild to moderate activity towards *S. marcescens*, *S. japonicum*, *S. maltophilia* and *S. aureus*.<sup>62,10</sup> Compared to these previous studies, it can be said that the Cd(II) complex synthesized in this study has a moderate inhibitory activity against similar strains.

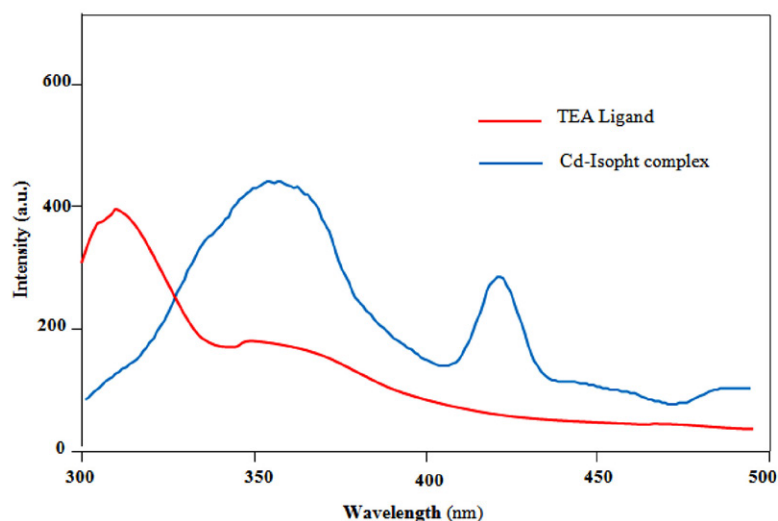


Figure 7. Fluorescence spectrum of [Cd(IsoPht)(TEA)H<sub>2</sub>O]·3H<sub>2</sub>O complex and TEA ligand in the solid-state ( $\lambda_{\text{ex}} = 270 \text{ nm}$ )

Table 4. Diameter of zones of inhibition (mm) of [Cd(IsoPht)(TEA)H<sub>2</sub>O]·3H<sub>2</sub>O complex

ppm	<i>S.aureus</i>	<i>B.cereus</i>	<i>E.coli</i>	<i>C.albicans</i>
40000	20	25	18	15
20000	20	25	16	15
10000	15	20	0	12
5000	13	16	0	8
2500	9	15	0	0
1250	7	15	0	0
625	0	14	0	0
312.5	0	10	0	0
<sup>a</sup> DMSO	–	–	–	–
<sup>b</sup> Ampicilin (10 $\mu\text{g/mL}$ )	18	20	15	–
<sup>b</sup> Flukonozol (25 $\mu\text{g/mL}$ )	–	–	–	20

a: negative control; b: positive control

The antimicrobial activity of mixed ligand metal complex was determined by various factors such as the chelate effect, i.e. bidentate, tridentate or tetradentate ligands, the nature of ligand, the total charge of the complex, and metal ion located in the center.<sup>63</sup> In light of this information, it can be said that despite the weak antimicrobial activity of TEA alone,<sup>8,9</sup> the complex formed by combining with Cd(II) ion shows moderate antimicrobial activity against all tested strains.

## 4. Conclusions

A novel mixed ligand [Cd(IsoPht)(TEA)H<sub>2</sub>O]·3H<sub>2</sub>O complex was synthesized and structurally characterized. The revealed X-ray structure clearly showed that the complex has a distorted monocapped trigonal prismatic geometry by binding to Cd(II) ion as TEA tetradentate and IsoPht bidentate. Thermal stability and behavior of the complex in the nitrogen atmosphere were investigated. The complex was completely degraded in two main stages. Fluorescence properties of cadmium complex having d<sup>10</sup> electron configuration at room temperature were also measured. In the fluorescence spectrum, the red-shift of the peaks of the complex may be attributed to the LMCT or MLCT transitions. In addition, the antimicrobial properties of the complex were investigated against three bacteria and one fungus. Data on the antimicrobial activity of the Cd(II) chelate complex formed by the tetradentate TEA and bidentate IsoPht ligands shows supported that it demonstrated moderate activity to inhibit the growth of all tested strains.

## Supplementary Data

Crystallographic data have been deposited with the Cambridge Crystallographic Data Centre as supplementary publication No. CCDC 1977619. Copies of the data can be obtained, free of charge, on application to CCDC, 12 Union Road, Cambridge CB2 1EZ, UK (fax: +44-1223-336033 or e-mail: deposit@ccdc.cam.ac.uk).

## Acknowledgments

The authors would like to thank Dr. Esra Deniz Candan for the assistance of antimicrobial activity determination, and Assoc. Prof. Dr. Serkan Demir for his helpful advice on theoretical calculations.

## 5. References

- O. Andac, Y. Topcu, V. T. Yilmaz, K. Guven, *Acta Cryst.* **2001**, C57, 1381–1384. DOI:10.1107/S0108270101015049
- I. Ucar, O. Z. Yesilel, A. Bulut, H. Icbudak, H. Ölmez, C. Kazak, *Acta Cryst.* **2004**, C60, 392–394. DOI:10.1107/S0108270104013174
- J. M. Ashurov, *Acta Cryst.* **2016**, E72, 526–529. DOI:10.1107/S2056989016004515
- M. Rubab, M. N. Akhtar, W. Zierkiewicz, M. Michalczyk, R. Nadeem, M. Shahid, M. N. Tahir, M. Akram, M. A. Hanif, M. A. AlDamen, *Res. Chem. Intermed.* **2019**, 45, 5649–5664. DOI:10.1007/s11164-019-03927-9
- Z. Bousourani, G. D. Geromichalos, K. Repana, E. Yiannaki, V. Psycharis, C. P. Raptopoulou, D. Hadjipavlou-Litina, E. Pontiki, C. Dendrinou-Samara, *J. Inorg. Biochem.* **2011**, 105, 839–849. DOI:10.1016/j.jinorgbio.2011.03.007
- Y. Kondratenko, A. A. Zolotarev, I. Ignatyev, V. Ugolkov, T. Kochina, *Transit. Met. Chem.* **2020**, 45, 71–81. DOI:10.1007/s11243-019-00359-7
- T. Esker, A. DeBoo, Y. Ishiwa, Ethanolamines. CEH Report, SRI Consulting, California, USA, **1999**.
- K. H. Beyer, W. F. Bergfeld, W. O. Berndt, R. K. Boutwell, W. W. Carlton, D. K. Hoffmann, A. L. Schroeder, *J. Am. Coll. Toxicol.* **1983**, 2, 183–235.
- J. B. Knaak, H. W. Leung, W. T. Stott, J. Busch, J. Bilsky, *Rev. Environ. Contam. Toxicol.* **1997**, 149, 1–86. DOI:10.1007/978-1-4612-2272-9\_1
- R. Kumar, S. Obrai, A. Kaur, M. S. Hundal, H. Meehnian, A. K. Jana, *New J Chem.* **2014**, 38, 1186–1198. DOI:10.1039/c3nj00729d
- G. M. Kapteijn, P. J. Baesjou, P. L. Alsters, D. M. Grove, W. J. J. Smeets, H. Kooijman, A. L. Spek, G. Koten, *Chem. Ber.* **1997**, 130, 34–44. DOI:10.1002/cber.19971300106
- I. Ignatyev, Y. Kondratenko, V. Fundamensky, T. Kochina, *Transit. Met. Chem.* **2018**, 43, 127–136. DOI:10.1007/s11243-017-0199-8
- A. C. Dumitriu, M. Cazacu, A. Bargan, S. Shova, C. Turta, *Polyhedron*, **2013**, 50, 255–263. DOI:10.1016/j.poly.2012.11.009
- O. Z. Yesilel, H. Ölmez, I. Ucar, A. Bulut, C. Kazak, *Z. Anorg. Allg. Chem.* **2005**, 631, 3100–3103. DOI:10.1002/zaac.200500297
- V. T. Yilmaz, E. Senel, *Transit. Met. Chem.* **2004**, 29, 336–342. DOI:10.1023/B:TMCH.0000020381.99658.ac
- J. M. Ashurov, A. B. Ibragimov, B. T. Ibragimov, *Polyhedron*, **2015**, 102, 441–446. DOI:10.1016/j.poly.2015.05.044
- Y. Kondratenko, V. Fundamenskaya, I. Ignatyev, A. Zolotarev, T. Kochina, V. Ugolkova, *Polyhedron*, **2017**, 130, 176–183. DOI:10.1016/j.poly.2017.04.022
- S. Gao, J. W. Liu, J. R. Li, L. H. Huo, H. Zhao, *Acta Cryst.* **2004**, E60, m94–m95. DOI:10.1107/S1600536803028630
- H. Guo, S. K. Huang, X. Z. Li, *Acta Cryst.* **2009**, E65, m891. DOI:10.1107/S1600536809026166
- M. Haukka, A. M. Kirillov, M. N. Kopylovich, A. J. L. Pombeiro, *Acta Cryst.* **2005**, E61, m2746–m2748. DOI:10.1107/S1600536805039127
- Y. P. Li, H. Zang, D. Sun, J. Ming, G. F. Sua, *Acta Cryst.* **2014**, E70, m361–m362. DOI:10.1107/S1600536814021771
- Y. P. Li, L. Y. Han, J. Ming, G. F. Su, *Acta Cryst.* **2014**, E70, m371. DOI:10.1107/S1600536814022375
- X. He, J. Lv, G. Xu, *Acta Cryst.* **2012**, C68, m109–m112.
- A. Dicko, P. Tardi, X. Xie, L. Mayer, *Int. J. Pharm.* **2007**, 337, 219–228.

25. M. G. Voronkov, G. A. Kuznetsova, A. Y. Fedorin, G. G. Yshkov, A. V. Mashanov, N. A. Malishkina, M. M. Rasulov, Pat. RF. No 2418580, **2009**.
26. M. G. Voronkov, A. Y. Fedorin, V. Mashanov, N. A. Malishkina, G. A. Kuznetsova, G. G. Yshkov, Pat. RF. No 2425676, **2010**.
27. O. P. Kolesnikova, A. N. Mirskova, S. N. Adamovich, R. G. Mirskov, O. T. Kudaeva, M. G. Voronkov, *Dokl. Biol. Sci.* **2009**, 425, 556–560. DOI:10.1134/S0012496609020070
28. M. M. Rasulov, M. G. Voronkov, M. K. Nurbekov, M. V. Zvereva, A. N. Mirskova, S. N. Adamovich, R. G. Mirskov, *Dokl. Biochem. Biophys.* **2012**, 444, 147–148. DOI:10.1134/S1607672912030064
29. T. Hambley, *Science*. **2007**, 318, 1392–1393. DOI:10.1126/science.1150504
30. T. Storr, K. H. Thompson, C. Orvig, *Chem. Soc. Rev.* **2006**, 35, 534–544. DOI:10.1039/b514859f
31. S. Zhan, Y. Sun, S. Li, G. Tang, Y. Wang, Y. Cui, *Polyhedron*, **2017**, 121, 252–263. DOI:10.1016/j.poly.2016.10.016
32. X. Shi, P. Chen, Z. Yin, T. Li, M. Wu, L. Tian, *Polyhedron*, **2018**, 141, 87–93. DOI:10.1016/j.poly.2017.11.019
33. S. L. Cai, L. Lu, W. P. Wu, J. Wang, Y. C. Sua, A. Q. Ma, A. Singh, A. Kumar, *Inorg. Chim. Acta*, **2019**, 484, 291–296. DOI:10.1016/j.ica.2018.09.066
34. M. Antonijević Nikolić, J. Antić-Stanković, B. Dražić, S. Tanasković, *J. Mol. Struct.* **2019**, 1184, 41–48. DOI:10.1016/j.molstruc.2018.10.027
35. Z. Lin, J. Luo, M. Hong, R. Wang, L. Han, R. Cao, *J. Solid State Chem.* **2004**, 177, 2794–2498. DOI:10.1016/j.jssc.2004.04.005
36. Y. Wang, L. Wang, X. Zhou, Y. Li, J. Li, *J. Mol. Struct.* **2018**, 1173, 612–619. DOI:10.1016/j.molstruc.2018.07.025
37. J. Ge, J. Cheng, P. Wang, Q. Liu, Y. Dong, *J. Mol. Struct.* **2014**, 1056–1057, 127–134. DOI:10.1016/j.molstruc.2013.10.029
38. W. Song, X. Cui, X. Wang, L. Liang, E. Yang, X. Zhao, *Polyhedron*, **2017**, 127, 266–277. DOI:10.1016/j.poly.2017.02.012
39. L. Radovanović, J. Rogan, D. Poletti, M. Milutinović, M. V. Rodić, *Polyhedron*, **2016**, 112, 18–26. DOI:10.1016/j.poly.2016.03.054
40. M. Devereux, M. McCann, V. Leon, M. Geraghty, V. McKee, J. Wikaira, *Met. Based Drugs*, **2000**, 7, 275–288.
41. M. Geraghty, V. Sheridan, M. McCann, M. Devereux, V. McKee, *Polyhedron*, **1999**, 18, 2931–2939. DOI:10.1016/S0277-5387(99)00201-6
42. P. K. Panchal, M. N. Patel, *Synth. React. Inorg. Met. Org. Chem.* **2004**, 34, 1277–1289. DOI:10.1081/SIM-120039271
43. K. Yue, S. Zhao, R. Zhao, Y. Wang, *Adv. Mater. Res.* **2012**, 399–401, 896–899. DOI:10.4028/www.scientific.net/AMR.399-401.896
44. X. C. Cheng, X. H. Zhu, H. W. Kuai, Z. Naturforsch, *B J. Chem. Sci.* **2013**, 68, 1000–1006. DOI:10.5560/znb.2013-3165
45. H. W. Kuai, X. Y. Xu, X. C. Cheng, L. D. Feng, X. H. Zhu, *J. Coord. Chem.* **2013**, 66, 4304–4315. DOI:10.1080/00958972.2013.867025
46. G. Pan, J. Tang, X. Yin, W. Tian, Z. Huang, Z. Naturforsch *B: J. Chem. Sci.* **2013**, 68, 1333–1339. DOI:10.5560/znb.2013-3185
47. L. Liu, S. Zhang, Y. Wang, X. Guo, L. Wu, B. Wu, *Inorg. Chim. Acta* **2014**, 423, 176–183. DOI:10.1016/j.ica.2014.08.010
48. H. Lin, F. Sui, P. Liu, X. Wang, G. Lin, *Bull. Korean Chem. Soc.* **2013**, 34, 2138–2142. DOI:10.5012/bkcs.2013.34.7.2138
49. X. Yi, W. Chen, J. Huang, D. Zhang, Y. Wang, *Acta Chim Slov.* **2017**, 64, 1042–1047.
50. G. M. Sheldrick, *Acta Cryst.* **2015**, A71, 3–8. DOI:10.1107/S2053229614024218
51. G. M. Sheldrick, *Acta Cryst.* **2015**, C71, 3–8. DOI:10.1107/S2053229614024218
52. O. Dolomanov, L. Bourhis, R. Gildea, J. Howard, H. Puschmann, *J. Appl. Crystallogr.* **2009**, 42, 339–341. DOI:10.1107/S0021889808042726
53. M. J. Frisch, G. W. Trucks, H. B. Schlegel, G. E. Scuseria, M. A. Robb, J. R. Cheeseman, G. Scalmani, V. Barone, B. Menonucci, G. A. Petersson, H. Nakatsuji, M. Caricato, X. Li, H. P. Hratchian, A. F. Izmaylov, J. Bloino, G. Zheng, J. L. Sonnenberg, M. Hada, M. Ehara, K. Toyota, R. Fukuda, J. Hasegawa, M. Ishida, T. Nakajima, Y. Honda, O. Kitao, H. Nakai, T. Vreven, J. A. Montgomery, Jr., J. E. Peralta, F. Ogliaro, M. Bearpark, J. J. Heyd, E. Brothers, K. N. Kudin, V. N. Staroverov, R. Kobayashi, J. Normand, K. Raghavachari, A. Rendell, J. C. Burant, S. S. Iyengar, J. Tomasi, M. Cossi, N. Rega, J. M. Millam, M. Klene, J. E. Knox, J. B. Cross, V. Bakken, C. Adamo, J. Jaramillo, R. Gomperts, R. E. Stratmann, O. Yazyev, A. J. Austin, R. Cammi, C. Pomelli, J. W. Ochterski, R. L. Martin, K. Morokuma, V. G. Zakrzewski, G. A. Voth, P. Salvador, J. J. Dannenberg, S. Dapprich, A. D. Daniels, Ö. Farkas, J. B. Foresman, J. V. Ortiz, J. Cioslowski, D. J. Fox, Gaussian 09, Revision A.1, Gaussian, Inc., Wallingford CT, **2009**.
54. J. Tao, X. M. Chen, R. B. Huang, L. S. Zheng, *J. Solid State Chem.* **2003**, 170, 130–134.
55. L. Tian, L. Yan, S. Y. Liu, *J. Coord. Chem.*, **2011**, 64, 16, 2945–2952. DOI:10.1080/00958972.2011.609594
56. G. B. Deacon, R. J. Phillips, *Coord. Chem. Rev.* **1980**, 33, 227–250. DOI:10.1016/S0010-8545(00)80455-5
57. K. Nakamoto, Handbook of Vibrational Spectroscopy. **2006**, pp. 1872–1892.
58. K. Anandhan, R. Thilak Kumar, *Spectrochim. Acta, Part A.* **2015**, 149, 476–480. DOI:10.1016/j.saa.2015.04.035
59. X. Shi, G. Zhu, Q. Fang, G. Wu, G. Tian, R. Wang, D. Zhang, M. Xue, S. Qiu, *Eur. J. Inorg. Chem.* **2004**, 1, 185–191. DOI:10.1002/ejic.200300390
60. G. Sun, H. Huang, X. Tian, Y. Song, Y. Zhu, Z. Yuan, W. Xu, M. Luo, S. Liu, X. Feng, F. Luo, *Cryst. Eng. Comm.* **2012**, 14, 6182–6189. DOI:10.1039/c2ce25602a
61. Y. A. Kondratenko, V. L. Ugolkov, D. Y. Vlasov, T. A. Kochina, *Mendeleev Commun.*, **2020**, 30, 639–641. DOI:10.1016/j.mencom.2020.09.029
62. R. Kumar, S. Obrai, A. Kaur, G. Hundal, H. Meehnan, A.K. Jana, *Polyhedron*, **2013**, 56, 55–61. DOI:10.1016/j.poly.2013.03.043

63. M. Rizzotto, Metal Complexes as Antimicrobial Agents. In: Bobbarala V (ed) A Search for Antibacterial Agents, IntechOpen, Rijeka, 2012, pp. 73–86. DOI:10.5772/45651

## Povzetek

Z uporabo izoftalne kisline ( $H_2IsoPht$ ) in tetradentatnega trietanolamina (TEA) smo sintetizirali nov kadmijev(II) kompleks s formulo  $[Cd(IsoPht)(TEA)H_2O] \cdot 3H_2O$  in dobljeno spojino karakterizirali z monokristalno rentgensko difrakcijo, FT-IR in termogravimetrično analizo (TGA). Spojina kristalizira triklinsko v prostorski skupini  $P-1$  s popačeno trikotno prizmo z dodatnim ligandom nad stransko ploskvijo. Cd(II) je sedemštevno koordiniran z bidentatnim IsoPht, tetradentatnim TEA in akva ligandom. Preučevali smo fluorescenčne lastnosti kadmijevega kompleksa in liganda TEA. Raziskovali smo tudi antimikrobno aktivnost sintetiziranega Cd(II) kompleksa z *in vitro* metodo difuzije v agarju proti gram pozitivnim in gram negativnim bakterijam ter glivam.



Scientific paper

# New Zinc Coordination Compound with Simple Salicylato and Pyridine Ligands: Synthesis, Crystal Structure and Hirshfeld Surface Analysis

Nives Kitanovski and Marta Počkaj\*

Faculty of Chemistry and Chemical Technology, University of Ljubljana, Večna pot 113, SI-1000 Ljubljana, Slovenia.

\* Corresponding author: E-mail: marta.pockaj@fkkt.uni-lj.si

Received: 12-08-2020

## Abstract

A novel mononuclear zinc coordination compound with formula  $[\text{Zn}(\text{Hsal})_2(\text{Py})_2]$  ( $\text{H}_2\text{sal}$  = salicylic acid,  $\text{Py}$  = pyridine) was prepared by mixing aqueous solutions of sodium salicylate and zinc sulfate in 1:1 molar ratio, and to the resulting solution pyridine was added dropwise. The obtained compound was characterized by elemental analysis, IR spectroscopy, and its crystal structure was determined by single-crystal X-ray diffraction method. X-ray structure analysis has shown that the central zinc ion is four-coordinated by two monodentate salicylato ligands and two pyridine molecules, forming a distorted tetrahedron. Since the asymmetric unit consists of two halves of coordination molecules, orthorhombic *Ibca* space group symmetry leads to two coordination molecules with slightly different geometry. The comparison between the two is given in terms of interatomic distances and angles, and also in terms of differences in intermolecular interactions obtained as a result of Hirshfeld surface analysis. With the assistance of  $\text{C}-\text{H}\cdots\text{O}$  interactions, the adjacent molecules are linked into chains and further connected into three-dimensional network.

**Keywords:** Coordination chemistry; zinc; salicylic acid; crystal structure; Hirshfeld surface analysis.

## 1. Introduction

Although zinc is deemed to be a trace element in the human body, it is present in all organs, tissues and fluids, in total 2–4 grams. Its importance for the growth and existence of all living organisms has been known for more than hundred years.<sup>1</sup> The research on zinc coordination chemistry has been initiated in the early 1940s by the discovery of erythrocyte carbonic anhydrase which is involved in the transport of carbon dioxide in blood. Apart from being a part of enzymatic active sites of all six different enzyme classes with catalytic and regulatory functions (oxidoreductases, transferases, hydrolases, lyases, isomerases, and ligases), zinc also plays structural roles and as such contributes to the stability of proteins. With its  $d^{10}$  electron configuration, zinc is not subject to reduction or oxidation reactions. Furthermore, its crystal-field stabilization energy is zero, resulting in a remarkably adoptable coordination sphere which allows to accommodate a broad range of coordination numbers and geometries.<sup>2</sup> All of listed characteristics of zinc as a central ion in combination with various ligands lead to new compounds with interesting antimicrobial, antidiabetic, optical, magnetic and other physical properties.<sup>3–10</sup>

On the other hand, salicylic acid ( $\text{H}_2\text{sal}$ ; Fig. 1) has been found in numerous plant species where it acts as a phytohormone necessary for plant growth and development. Its salts and esters, salicylates, are widely used in medicine. With their two functional groups, i.e. hydroxylic and carboxylic, salicylates are of great importance as ligands in coordination chemistry with their versatile coordination modes.<sup>11</sup> For example, zinc acetylsalicylate with formula  $[\text{Zn}(\text{acsal})_2(\text{H}_2\text{O})_2]$  is used as anti-inflammatory agent.<sup>12</sup>

Despite the numerous researches in zinc chemistry, there are not as many reports on crystal structures containing the unsubstituted salicylato ligand and additional pyridine-like ligands as one might expect.<sup>13</sup> Only four

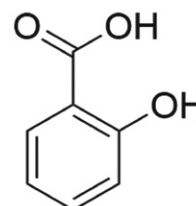


Figure 1. Salicylic acid.

such crystal structures were reported till now<sup>14–17</sup> which might indicate considerable difficulties with the crystallization of mononuclear coordination compounds of the entitled class. However, we have managed to prepare the new zinc coordination compound with two salicylate and two additional pyridine ligands. In the present work, its synthesis and characterization, including the single crystal structure determination and Hirshfeld surface analysis, is described.

## 2. Experimental

### 2.1. Materials and Physical Measurements

All reagents and chemicals were purchased from commercial sources and used without further purification.

CHN elemental analyses were performed with a PerkinElmer 2400 CHN Elemental Analyzer. The infrared spectra were measured on solid samples using a Perkin-Elmer Spectrum 100 series FT-IR spectrometer equipped with an ATR sampling accessory.

### 2.2. Synthesis

To the solution of sodium salicylate,  $C_7H_5NaO_3$ , (178 mg, 1.11 mmol in 2 mL water) the solution of  $ZnSO_4$  (300 mg, 1.04 mmol of  $ZnSO_4 \cdot 7H_2O$  in 5 mL water) was added. To the obtained colourless solution, pyridine was added dropwise (15 droplets, i.e. ~0.7 mL). The white solid, hydrated  $ZnSO_4$ , appeared immediately after the addition of pyridine. The reaction mixture including the fine white solid was left in an open Erlenmeyer flask at ambient temperature. The quantity of white solid decreased with time and after its disappearance, colourless single crystals suitable for the structural analysis grew out of the solution in 18 days. Yield: 50 mg (10%). Anal. Calcd. for  $C_{24}H_{20}N_2O_6Zn$ : C, 57.90%; H, 4.05%; N, 5.63%. Found: C, 56.89%; H, 4.14%; N, 6.08%.  $\nu_{max}$ : 3077 (vw), 1632 (w, C=N from pyridine ring), 1601 (s,  $\nu_{as}(OCO)$ ), 1567 (s), 1541 (s), 1487 (s), 1468 (s), 1450 (s), 1394 (vs,  $\nu_s(OCO)$ ), 1319 (s), 1239 (s), 1220 (s), 1156 (s), 1098 (w), 1071 (w), 1044 (s), 1015 (w), 957 (w), 885 (s), 864 (s), 831 (s), 755 (w), 697 (vs), 670 (s), 638 (s).

### 2.3. X-Ray Crystallography

For X-ray structural analysis, single crystal of the title compound was dipped into silicon grease, mounted onto the tip of glass fibres and transferred to the goniometer head in the liquid nitrogen cryostream. Data were collected on a SuperNova diffractometer equipped with Atlas detector using CrysAlis software and monochromated Mo K $\alpha$  radiation (0.71073 Å) at 150 K.<sup>18</sup> The initial structural model was obtained via direct methods using the Superflip structure solution program.<sup>19</sup> A full-matrix least-squares refinement on  $F^2$  magnitudes with anisotropic displace-

ment parameters for all nonhydrogen atoms using *SHELXL-2018/3* was employed.<sup>20</sup> All H atoms were initially located in difference Fourier maps; those residing on C-atoms were further treated as riding on their parent atoms with C(aromatic)–H distance of 0.95 Å. On the other hand, the hydrogens bonded to oxygen atoms (i.e. H3 and H6) were refined freely. Details on crystal data, data collection and structure refinement are given in Table 1. Figures depicting the structures were prepared with *Mercury*.<sup>21</sup>

Table 1. Crystal data, data collection and refinement.

Crystal data	[Zn(Hsal) <sub>2</sub> Py <sub>2</sub> ]
Formula	C <sub>24</sub> H <sub>20</sub> N <sub>2</sub> O <sub>6</sub> Zn
$M_r$	497.79
Cell setting, space group	Orthorhombic, <i>Ibca</i>
$a / \text{Å}$	15.2247(5)
$b / \text{Å}$	15.5719(6)
$c / \text{Å}$	37.7204(17)
$V / \text{Å}^3$	8942.7(6)
$Z$	16
$D_x / \text{Mg m}^{-3}$	1.479
$\mu / \text{mm}^{-1}$	1.142
$F(000)$	4096
Crystal form, colour	prism, colourless
Crystal size / mm <sup>3</sup>	0.25 × 0.15 × 0.15
<b>Data collection</b>	
$T / \text{K}$	150(2)
No. of measured, independent and observed reflections	24914, 6220, 4140
$R_{int}$	0.0373
<b>Refinement</b>	
$R$ (on $F_{obs}$ ), $wR$ (on $F_{obs}$ ), $S$	0.0339, 0.0801, 1.025
No. of contributing reflections	6220
No. of parameters	307
No. of restraints	none
$\Delta\rho_{max}, \Delta\rho_{min} / e\text{Å}^{-3}$	0.732, -0.733

$$R = \frac{\sum |F_o| - |F_c|}{\sum |F_o|}; wR_2 = \frac{\{\sum [w(F_o^2 - F_c^2)^2] / \sum [w(F_o^2)^2]\}^{1/2}}{\{\sum [w(F_o^2 - F_c^2)^2] / (n - p)\}^{1/2}}$$

where  $n$  is the number of independent reflections and  $p$  is the total number of parameters refined.

### 2.4. Hirshfeld Surface Analysis

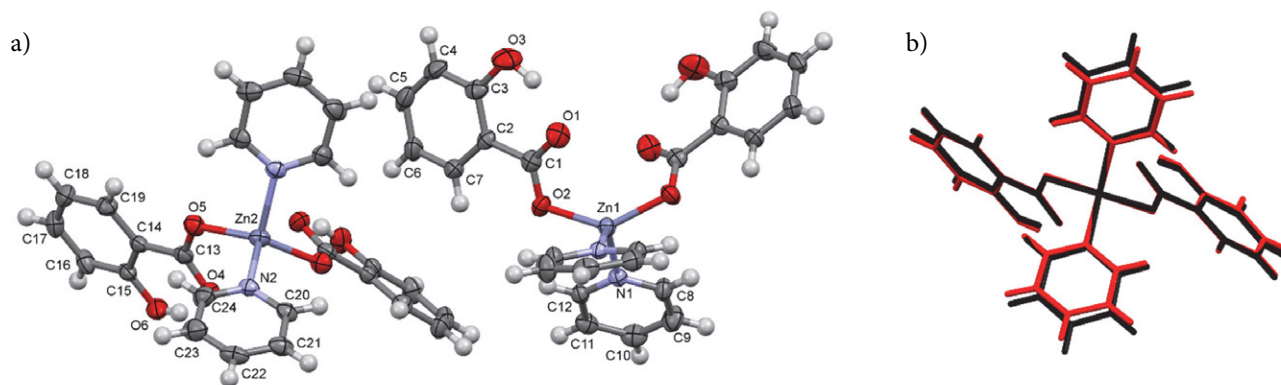
The Hirshfeld surface of the molecule is defined as a set of points in three-dimensional space where the contribution to the electron density of the molecule of interest is equal to the contribution from all other molecules.<sup>22</sup> The Hirshfeld surface analyses were performed and fingerprint plots were drawn using Crystal Explorer, both based on the results of previous single crystal X-ray diffraction study.<sup>23</sup> The Hirshfeld surfaces were plotted over three quantities: a)  $d_{norm}$ , plotted in red-white-blue colour code, representing shorter/close to the sum of van der Waals radii/longer contacts between the molecules; b) shape index;

the red colour represents concave and the blue convex regions; and c) curvedness. Furthermore, the 2D fingerprint plots, i.e. plots of  $d_i$  over  $d_e$  are provided to recognize and evaluate different intermolecular contacts in the crystal.  $d_i$  and  $d_e$  represent distances from the isosurface to the nearest atom inside or outside to the Hirshfeld surface, respectively.

## 3. Results and Discussion

### 3.1. Crystal structure

Single crystal X-ray structure determination has shown that the title compound crystallizes in orthorhombic *Ibca* space group (no. 73). The asymmetric unit consists of two central zinc ions, each surrounded by a pyridine molecule and a salicylate ligand. The aforementioned space group symmetry leads to two similar but not completely identical coordination molecules with formula  $[\text{Zn}(\text{Hsal})_2(\text{Py})_2]$  (Fig. 2a), hereinafter referred to molecule1 (containing Zn1) and molecule2 (containing Zn2); their overlay is shown in Fig. 2b.



**Figure 2.** a) Two similar coordination molecules  $[\text{Zn}(\text{Hsal})_2(\text{Py})_2]$ . The displacement ellipsoids of non-hydrogen atoms are drawn at the 50% probability level while the hydrogen atoms are drawn as spheres of arbitrary radii and their labels are omitted for clarity. b) Overlay of the coordination molecules; molecule1 (i.e. containing Zn1) is black while the molecule2 (containing Zn2) is red.

In both symmetrical coordination molecules, a central Zn is positioned on a twofold axis running parallel to *x* (Zn1, Wyckoff site 8c) or *y* axis (Zn2, Wyckoff site 8d), respectively, and is surrounded by two pyridine molecules and two monodentately bound salicylate ligands *via* its deprotonated carboxylic oxygen. The obtained coordination number is four, and the values of  $\tau_4'$  parameter<sup>24,25</sup> of 0.70 for Zn1 and 0.74 for Zn2 confirm the distorted tetrahedra around both central ions. Data on selected bond lengths and angles around the central zinc ions are given in Table 2; values are in accordance with the previously reported Zn complexes with salicylate ligand and its derivatives.<sup>13</sup>

Although bond lengths and angles are quite similar in both molecules, there are some distinctions between them as already seen from their overlay (Fig. 2b). The an-

**Table 2.** Selected bond lengths and angles (Å, °) for 1.

Molecule1		Molecule2	
Zn1–O2	1.9502(13)	Zn2–O5	1.9533(14)
Zn1–N1	2.0256(15)	Zn2–N2	2.0405(16)
O2–Zn1–O2 <sup>i</sup>	134.83(9)	O5–Zn2–O5 <sup>ii</sup>	133.95(8)
N1–Zn1–N1 <sup>i</sup>	119.61(9)	N2–Zn2–N2 <sup>ii</sup>	111.42(9)
O2–Zn1–N1	97.83(6)	O5–Zn2–N2	105.38(6)
O2 <sup>i</sup> –Zn1–N1	104.48(6)	O5 <sup>ii</sup> –Zn2–N2	100.11(6)

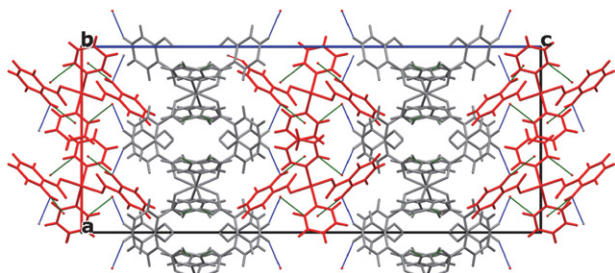
Symmetry codes: (i)  $x, -y, -z + \frac{1}{2}$ ; (ii)  $-x + \frac{1}{2}, y, -z$ .

gles between the meanplane defined by carboxylate group and the salicylate ring are similar, with values of 7.1(1)° in molecule1 and 6.4(1)° in molecule2, respectively. However, the angles between the meanplane of pyridine and salicylate rings differ significantly, with values 50.49(8)° in molecule1 and 82.21(6)° in molecule2, respectively. This difference is further reflected in the packing of the coordination molecules and also in slightly different hydrogen bonding schemes / close contacts of both molecules (Table 3). In molecule1 two intramolecular hydrogen bonds of

O–H...O and C–H...O type are present. On the other hand, if considering the classical criterion for C–H...O hydrogen bonds, i.e. C–H...O angle > 110° and C...O distance < 3.22 Å, in molecule2 only the intramolecular O–H...O hydrogen bond appears, while there is no C–H...O hydrogen bond due to geometric differences in between the molecules. The corresponding distance between the same atoms in molecule2 is significantly larger than the sum of van der Waals radii (i.e. C24...O6, 3.440(3) Å).

Additional C–H...O contact can be found between two adjacent molecules1 (C11–H11...O1) or two adjacent molecules2 (C20–H20...O6), respectively, connecting the molecules with the same numerical label into chains that run parallel to *a* axis (Fig. 3). The C–H...O hydrogen bonds between molecule1 and molecule2 are slightly longer than is the sum of van der Waals radii (C5–

H5...O6) but still connect the aforementioned chains into three-dimensional structure. The difference in hydrogen bonding schemes between both coordination molecules can be also revealed in fingerprint plots of both molecules (see Section 3.2).



**Figure 3.** The packing of exchanging chains of hydrogen-bonded molecules1 (grey) and molecules2 (red) that run parallel to *a* direction. A view down *b* axis. The hydrogen bonds between molecules1 or molecules2 are given in green while those between molecule1 and molecule2 (C5–H5...O6) are depicted in blue.

the classical crystallographic analysis with which the molecule packing is studied by elucidating atom-to-atom or residue-to-residue contacts. Fig. 4a represents Hirshfeld surface of molecule containing Zn1 (molecule1) mapped over  $d_{\text{norm}}$  in a range from  $-0.179$  to  $+1.501$  arbitrary units. The bright red spots ‘1’ and ‘2’ in the vicinity of hydrogen (H11) and oxygen (O1) indicate donors and acceptors of C–H...O interaction while the diminutive-red spot ‘3’ near hydroxylic oxygen (O3) claims its cooperation in a relatively weak C–H...O interaction.

HS mapped over shape index (Fig. 4b) clearly shows red hollows and blue bumps which in a close look from different perspectives can reveal the way the molecules (i. e. their Hirshfeld surfaces) touch each other. Together with HS mapped over curvedness (Fig. 4c), the absence of broad, flat regions can be observed and consequently there is no evidence of planar stacking arrangements of molecules1, e.g.  $\pi$ - $\pi$  stacking.<sup>26</sup>

To overcome the trouble of presenting 3D Hirshfeld surfaces in two dimensions, a quantitative 2D fingerprint

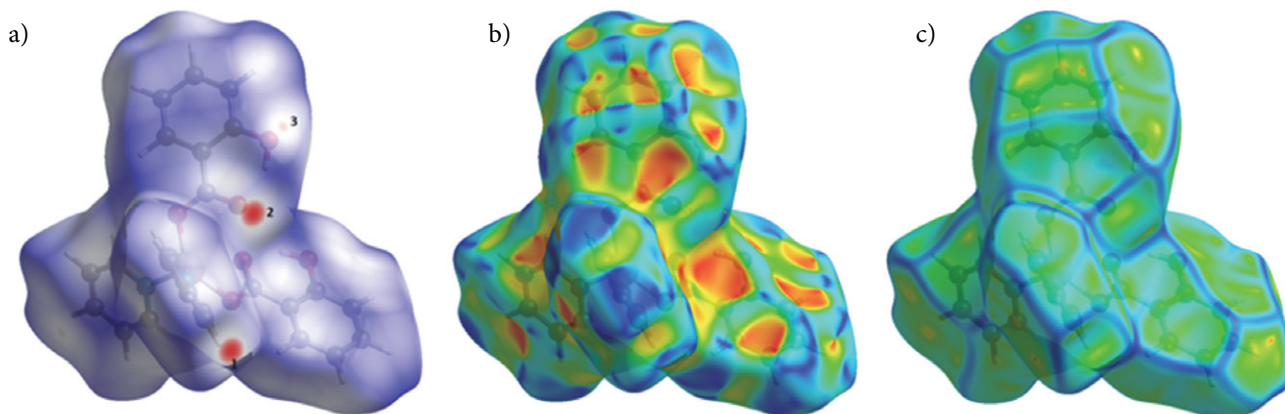
**Table 3.** Hydrogen bond geometry in 1.

D–H...A	D–H (Å)	H...A (Å)	D...A (Å)	D–H...A (°)	Symmetry code of A
O3–H3...O1	0.95(3)	1.67(3)	2.546(2)	151(3)	<i>x, y, z</i>
C12–H12...O2	0.95	2.60	3.111(2)	114	<i>x, y, z</i>
C11–H11...O1	0.95	2.46	3.203(2)	135	$-x + \frac{1}{2}, y + \frac{1}{2}, z$
O6–H6...O4	0.84(3)	1.78(3)	2.542(2)	150(3)	<i>x, y, z</i>
C20–H20...O6	0.95	2.57	3.027(2)	110	<i>x, y - 1/2, -z</i>
C5–H5...O6	0.95	2.48	3.331(3)	149	$x - \frac{1}{2}, -y + \frac{1}{2}, -z$

### 3.2. Hirshfeld Surface Analysis

Hirshfeld surface (HS) analysis is an invaluable tool that enables us to understand and describe weak intermolecular interactions in the crystal structure that are crucial in the packing of molecules in crystals. By means of this method, the molecule is treated as a whole, opposing to

plot of molecule1 is presented in Fig. 5. Only the dominant contributions to the Hirshfeld surface, i.e. H...H, C...H/H...C and O...H/H...O contacts which together contribute more than 92% to the total HS, are shown. Two symmetrical spikes at  $(d_i + d_e) \sim 2.3$  Å represent C–H...O interactions observed as red spots of different intensities in Fig.



**Figure 4.** Hirshfeld surface of molecule1 a) plotted over  $d_{\text{norm}}$  in the range from  $-0.179$  to  $+1.501$  arbitrary units; b) plotted over shape-index property (range from  $-1.000$  to  $1.000$ ), and c) plotted over curvedness (range from  $-4.000$  to  $0.400$ ).



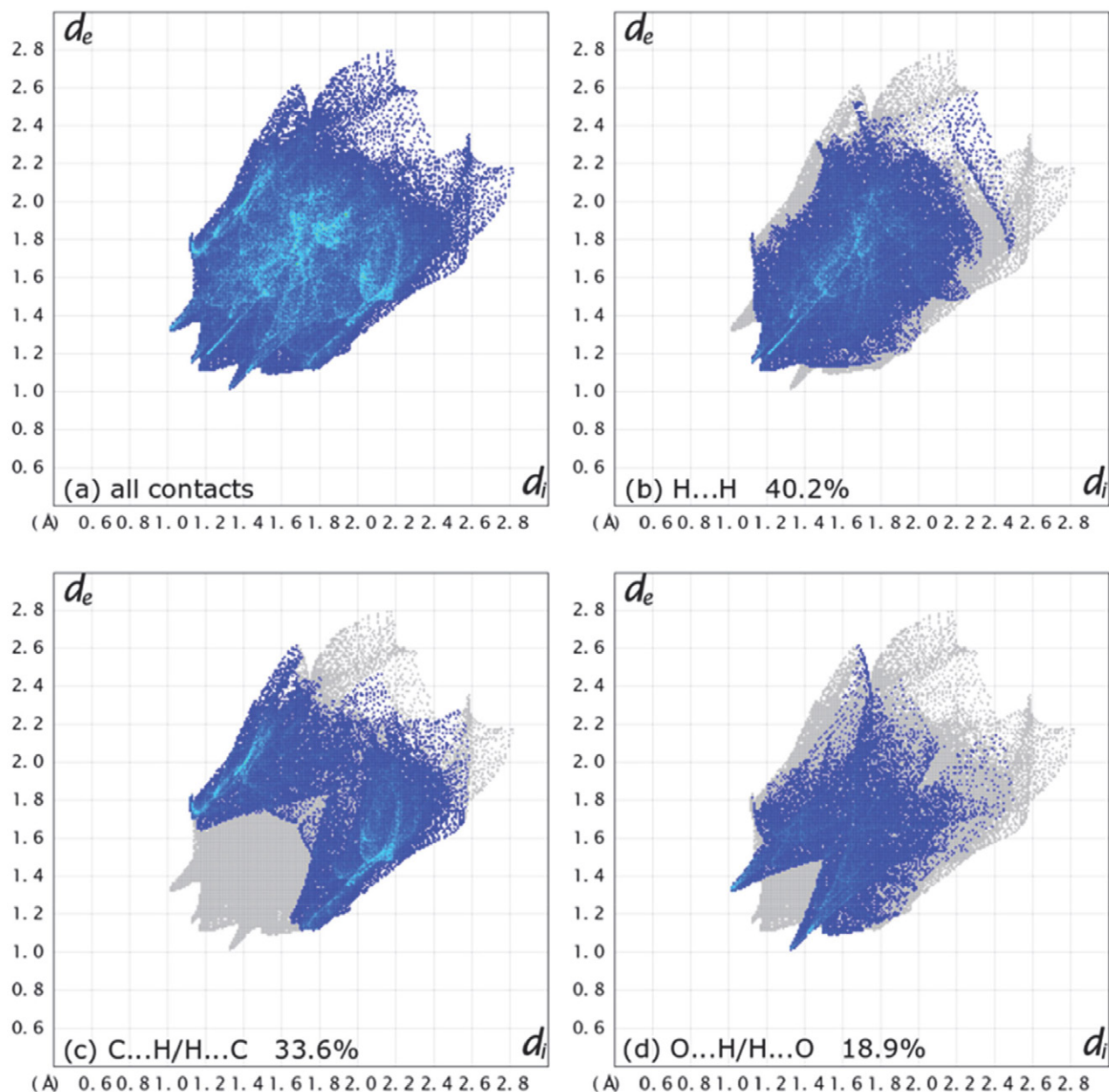


Figure 5. a) A full 2D fingerprint plot of molecule1, together with those delineated into b) H...H, c) C...H / H...C and d) O...H / H...O contacts.

4a. All other features that should indicate other important short contacts such as  $\pi$ - $\pi$  stacking are absent from 2D fingerprint plots of molecule1.

Since the asymmetric unit consists of two halves of the coordination molecule and the HS analysis can reveal differences between the two symmetrically independent molecules, it was performed also on the molecule2. The HS mapped over  $d_{\text{norm}}$ , shape index and curvedness are shown in ESI (Fig. S1). The observations are very similar to those of molecule1. However, slight differences can be observed from 2D fingerprint plots (Fig. 6). The dominant contacts in molecule2 are the same as in molecule1, and

also their contribution to the total HS is similar (>92%). However, the percentage contributions do differ slightly as a result of subtle geometry differences of both molecules (Fig. 7).

## 4. Conclusions

Crystal structure of a new zinc coordination compound with salicylato and pyridine ligand, *i.e.*  $[\text{Zn}(\text{H-sal})_2(\text{Py})_2]$  was determined by single-crystal X-ray diffraction at 150 K, and it was further evaluated by Hirshfeld

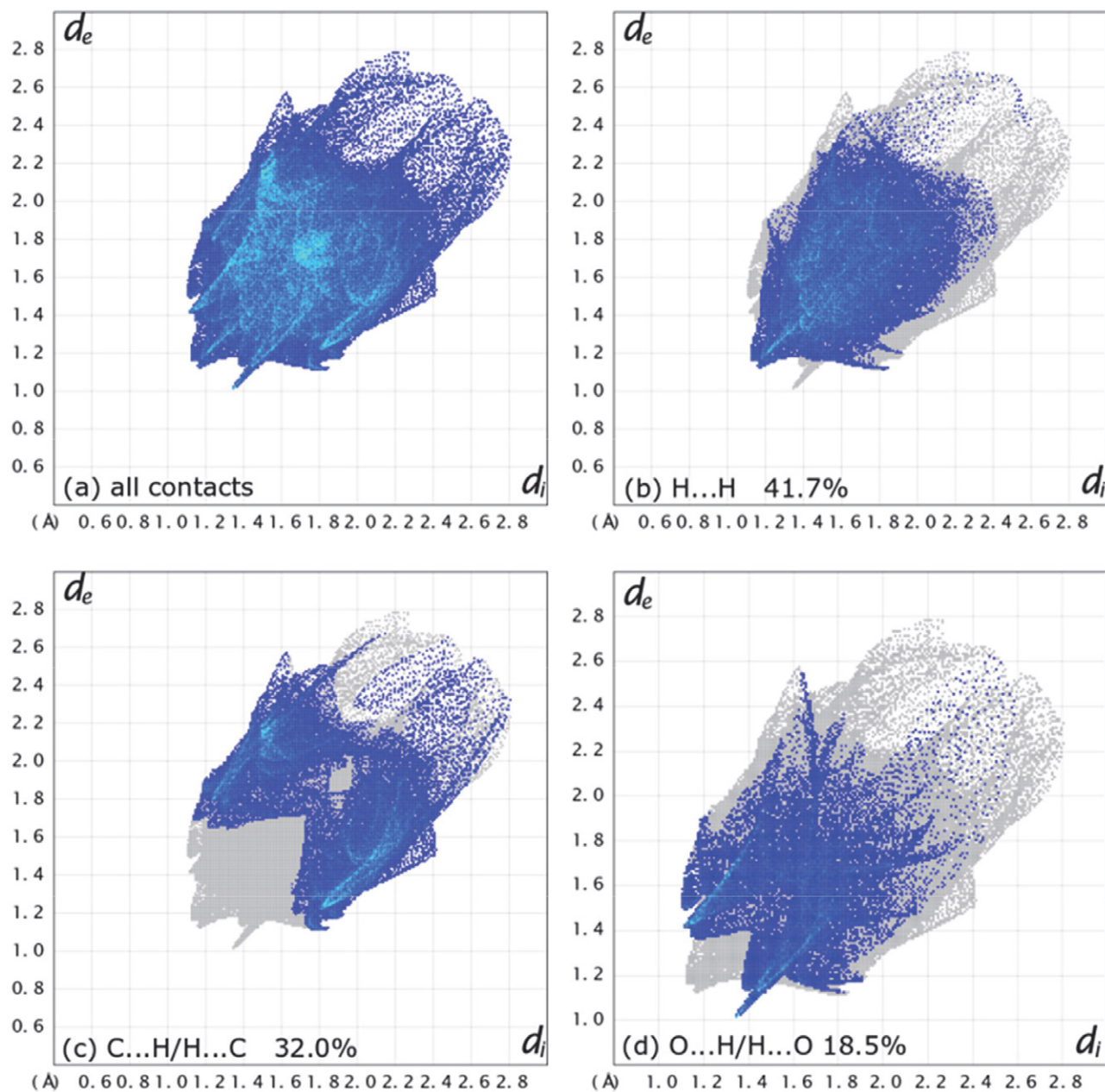


Figure 6. a) A full 2D fingerprint plot of molecule 2, together with those delineated into b) H...H, c) C...H / H...C and d) O...H / H...O contacts.

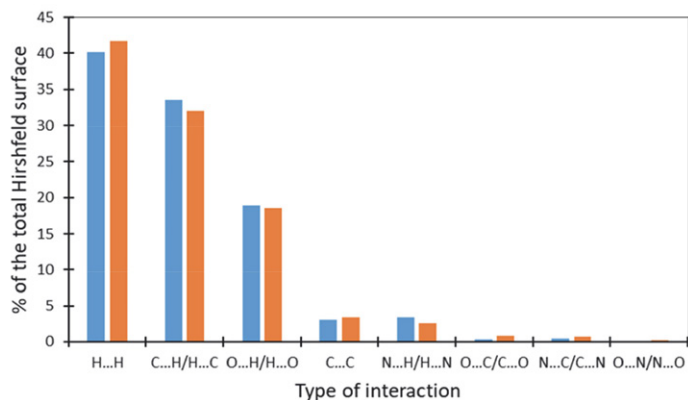


Figure 7. The proportions of different interactions to the total Hirshfeld surface in molecule1 (blue) and molecule2 (orange columns).

surface analysis. The central Zn(II) is four-coordinated in a shape of distorted tetrahedron. Since the asymmetric unit consists of two halves of coordination molecule, there are subtle differences between symmetrically independent coordination molecules. In both coordination molecules, H...H, C...H/H...C and O...H/H...O contacts contribute the most to molecular packing but the percentage of each of the aforementioned interactions to the total Hirshfeld surface differ as a consequence of slight geometrical differences between two coordination molecules. As a result of C–H...O interactions between the adjacent molecules, the three-dimensional network is formed.

## 5. Supplementary Information

CCDC 2014661 contains the supplementary crystallographic data. These data can be obtained free of charge from The Cambridge Crystallographic Data Centre via [www.ccdc.cam.ac.uk/data\\_request/cif](http://www.ccdc.cam.ac.uk/data_request/cif).

## Acknowledgments

This work was financially supported by Slovenian research agency (grant P1-0175). The authors thank Eva Judež for the synthesis and EN-FIST Centre of Excellence for the use of SuperNova diffractometer.

## 6. References

- M. J. Jackson in: C. F. Mills (Ed.): Zinc in human biology; Springer, London, UK, **1989**, pp. 1–10.
- J. Burgess, R. H. Prince: Zinc: Inorganic & Coordination Chemistry, in: Encyclopedia of Inorganic Chemistry, 2nd edition, John Wiley & Sons Ltd., **2006**.
- Y.-L. Sang, X.-S. Lin, W.-D. Sun, *Acta Chim. Slov.* **2020**, *67*, 581–585. DOI:10.17344/acsi.2019.5595
- A. Erxleben, *Coord. Chem. Rev.* **2003**, *246*, 203–228. DOI:10.1016/S0010-8545(03)00117-6
- X.-G. Yi, X.-N. Fang, J. Guo, J. Li, Z.-P. Xie, *Acta Chim. Slov.* **2020**, *67*, 507–515. DOI:10.17344/acsi.2019.5532
- X. Meng, Y. Song, H. Hou, Y. Fan, G. Li, Y. Zhu, Yu Zhu, *Inorg. Chem.* **2003**, *42*, 1306–1315. DOI:10.1021/ic0259282
- D. A. Shultz, S. H. Bodnar, *Inorg. Chem.* **1999**, *38*, 591–594. DOI:10.1021/ic981092k
- T. Koleša-Dobravec, K. Maejima, Y. Yoshikawa, A. Meden, H. Yasui, F. Perdih, *New J. Chem.* **2018**, *42*, 3619–3632. DOI:10.1039/C7NJ04189F
- T. Koleša-Dobravec, K. Maejima, Y. Yoshikawa, A. Meden, H. Yasui, F. Perdih, *New J. Chem.* **2017**, *41*, 735–746. DOI:10.1039/C6NJ02961B
- N. Podjed, B. Modec, M. M. Alcaide, J. López-Serrano, *RSC Adv.* **2020**, *10*, 18200–18221. DOI:10.1039/D0RA03192E
- K. Praveen, D. S. S. Madhavi, A. Anil Kumar, Y. Kranthi Kumar, *Int. J. Eng. Sci. Invention Res. Dev.* **2016**, *5*, 8–10.
- P. Lemoine, B. Viosat, G. Morgant, F. T. Greenaway, A. Thomas, N.-H. Dung, J. R. J. Sorenson, *J. Inorg. Biochem.* **2002**, *89*, 18–28. DOI:10.1016/S0162-0134(01)00324-5
- C. R. Groom, I. J. Bruno, M. P. Lightfoot, S. C. Ward, *Acta Crystallogr.* **2016**, *B72*, 171–179. DOI:10.1107/S2052520616003954
- H. Necefoglu, W. Clegg, A. J. Scott, *Acta Crystallogr.* **2001**, *E57*, m462–m464. DOI:10.1107/S1600536801015021
- T. Hokelek, H. Necefoglu, *Anal. Sci.* **2001**, *17*, 1241–1242. DOI:10.2116/analsci.17.1241
- D. Kose, A. Ay, O. Sahin, O. Buyukgungor, *J. Iran. Chem. Soc.* **2013**, *9*, 591–597. DOI:10.1007/s13738-012-0072-9
- K.-H. Lin, F.-F. Zhang, Z.-Y. Yu, S. Min, *Acta Crystallogr.* **2007**, *E63*, m1930. DOI:10.1107/S1600536807028322
- CrysAlisPRO, Oxford Diffraction /Agilent Technologies UK Ltd, Yarnton, England.
- L. Palatinus, G. Chapuis, *J. Appl. Cryst.* **2007**, *40*, 786–790. DOI:10.1107/S0021889807029238
- G. M. Sheldrick, *Acta Crystallogr.* **2015**, *C71*, 3–8.
- C. F. Macrae, P. R. Edgington, P. McCabe, E. Pidcock, G. P. Shields, R. Taylor, M. Towler, J. van de Streek, *J. Appl. Crystallogr.* **2006**, *39*, 453–457. DOI:10.1107/S002188980600731X
- M. J. Turner, J. J. McKinnon, S. K. Wolff, D. J. Grimwood, P. R. Spackman, D. Jayatilaka, M. A. Spackman, CrystalExplorer17. University of Western Australia, 2017. DOI:10.1039/B818330A
- M. A. Spackman, D. Jayatilaka, *CrystEngComm* **2009**, *11*, 19–32.
- A. Okuniewski, D. Rosiak, J. Chojnacki, B. Becker, *Polyhedron* **2015**, *90*, 47–57. DOI:10.1016/j.poly.2015.01.035
- D. Rosiak, A. Okuniewski, J. Chojnacki, *Polyhedron* **2018**, *146*, 35–41. DOI:10.1016/j.poly.2018.02.016
- S. L. Tan, M. M. Jotani, E. R. T. Tiekink, *Acta Crystallogr.* **2019**, *E75*, 308–318. DOI:10.1107/S2056989019001129

## Povzetek

Pri reakciji med vodnima raztopinama natrijevega salicilata in cinkovega sulfata v množinskem razmerju 1:1 in dodatku piridina po kapljicah v nastalo raztopino je nastala nova enojedrna koordinacijska spojina s formulo  $[Zn(Hsal)_2(Py)_2]$  ( $H_2sal$  = salicilna kislina,  $Py$  = piridin). Okarakterizirali smo jo s pomočjo elementne analize, infrardeče spektroskopije ter z rentgensko difrakcijo na monokristalu določili njeno kristalno strukturo. Koordinacijsko število centralnega cinkovega iona je štiri, in sicer je koordiniran s po dvema enoveznima salicilatnima ligandoma ter dvema molekulama piridina, koordinacijski polieder je popačen tetraeder. V asimetrični enoti sta dve polovici koordinacijskih molekul, kot posledica ortorombske prostorske skupine *Ibca* pa se tvorita dve koordinacijski molekuli z nekoliko različno geometrijo. Podana je primerjava med njima, in sicer tako v smislu medatomskih razdalj in kotov kot tudi v opažanju razlik v medmolekulskih interakcijah, dobljenih s pomočjo analize Hirshfeldovih površin. S pomočjo  $C-H\cdots O$  interakcij so sosednje molekule povezane v verige, te pa še naprej tako, da se tvori tridimenzionalna struktura.



Except when otherwise noted, articles in this journal are published under the terms and conditions of the Creative Commons Attribution 4.0 International License

Short communication

# Investigation of Photochemical Reactions of some Metal Carbonyls with N'-(2-Hydroxy-6-Methylbenzylidene)Methanesulfonylhydrazide and 5-Methyl-2-Hydroxyacetophenonemethanesulfonylhydrazone

Sema Sert<sup>1</sup><sup>1</sup> Department of Chemistry, Faculty of Science, Ege University, İzmir, Turkey

\* Corresponding author: E-mail: semasertkimya@hotmail.com

Received: 05-08-2019

## Abstract

Eight new complexes,  $[M(\text{CO})_5(5\text{msalmsh})]$  [ $M=\text{Cr};(1\text{a}), \text{Mo};(2\text{a}); \text{W}(3\text{a})$ ],  $[\text{Re}(\text{CO})_4\text{Br}(5\text{msalmsh})]$  (4a),  $[M(\text{CO})_5(5\text{mafms})]$  [ $M=\text{Cr};(1\text{b}), \text{Mo};(2\text{b}); \text{W}(3\text{b})$ ],  $[\text{Re}(\text{CO})_4\text{Br}(5\text{mafms})]$  (4b), have been synthesized by the photochemical reaction of the metal carbonyls  $[M(\text{CO})_6]$  ( $M=\text{Cr}, \text{Mo}, \text{W}$ ) and  $[\text{Re}(\text{CO})_5\text{Br}]$  with N'-(2-Hydroxy-6-Methylbenzylidene) Methanesulfonylhydrazide (5msalmsh) and 5-methyl-2-hydroxyacetophenonemethanesulfonylhydrazone (5mafms). The complexes have been characterized by elemental analysis, LC-MS, FT-IR, <sup>1</sup>H NMR spectroscopy. Spectroscopic studies show that 5msalmsh and 5mafms behave monodentate ligand and coordinate via an imine N donor atom to the central metal atom in (1a)–(4a) and (1b)–(4b).

**Keywords:** Hydrazones; monodentate ligands; metal carbonyls; photochemical reactions.

## 1. Introduction

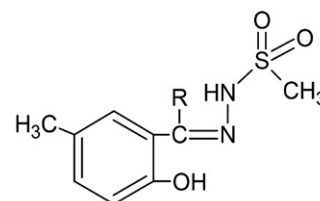
Sulfonylhydrazones and sulfonamides have been shown to be active in several pharmacological tests, demonstrating antibacterial, antitumor, diuretic, antiviral, and antinociceptive activity.<sup>1–5</sup> These compounds have gained importance in bioinorganic and metal based drug chemistry because of their lower cost, lower toxicity and most activity against bacterial diseases.<sup>6,7</sup> Moreover, they are used in agriculture field as well as insecticides and herbicides. They are less toxic as compared to other drugs and are scalable.<sup>8,9</sup>

In chemical synthesis, photochemical reactions are usually cleaner and more efficient than other types of reactions because the key reagent is light of particular energy. In fine chemical synthesis and pharmaceutical productions, photochemical reaction steps offer shorter routes for many synthetic schemes, e.g. synthesis of vitamin D. In addition, photocleavage has also become one of the more effective methods for removing protective groups. The use of photochemistry is limited by concerns about scalability, efficiency, and safe operations of the processes.<sup>10</sup>

Metal carbonyl complexes are among the most photoreactive transition metal complexes known.<sup>11</sup> The commonly known carbonyls of Cr(0), Mo(0), and W(0) are

six-coordinate octahedral complexes,  $M(\text{CO})_6$ . Other stable complexes containing only the central metal and CO include the dimers  $M_2(\text{CO})_{10}^{2-}$  having a single M–M bond. Numerous compounds of the  $M(\text{CO})_n(\text{L})_{6-n}^-$  variety have been prepared, many photochemically.<sup>12</sup>

In this work, eight new complexes  $[M(\text{CO})_5(5\text{msalmsh})]$  [ $M=\text{Cr};(1\text{a}), \text{Mo};(2\text{a}); \text{W}(3\text{a})$ ],  $[\text{Re}(\text{CO})_4\text{Br}(5\text{msalmsh})]$  (4a),  $[M(\text{CO})_5(5\text{mafms})]$  [ $M=\text{Cr};(1\text{b}), \text{Mo};(2\text{b}); \text{W}(3\text{b})$ ],  $[\text{Re}(\text{CO})_4\text{Br}(5\text{mafms})]$  (4b) as shown in Scheme 1 were synthesized by the photochemical reactions of



5msalmsh; R=H

5mafms; R=CH<sub>3</sub>

Figure 1. The structure of ligands.

[M(CO)<sub>6</sub>] (Cr, Mo, W) with 5msalmsh and 5mafms (shown in Figure 1) and characterized by elemental analysis, MS, IR and <sup>1</sup>H NMR spectroscopy. According to all the spectroscopic data, 5msalmsh and 5mafms are monodentate and coordinated via the imine nitrogen donor atom.

## 2. Experimental

### 2.1. Physical Measurements

Reactions were carried out under dry nitrogen using Schlenk techniques. All solvents were dried and degassed prior to use. Elemental analyses were performed according to standard micro analytical procedures (TÜBİTAK Laboratories, Ankara). The infrared spectra of the compounds as KBr disks were recorded in the range of 4000–400 cm<sup>-1</sup> with a Mattson 1000 FT spectrometer. <sup>1</sup>H NMR spectra of dimethylsulfoxide-d<sub>6</sub> (DMSO-d<sub>6</sub>) solutions of the compounds were recorded on a 400 MHz digital FT-NMR at TÜBİTAK. Electron impact mass spectra were recorded on a Micromass VG Platform-II LC-MS at TÜBİTAK. Photochemical reactions were carried out in an immersion-well apparatus by using a medium pressure 400W Mercury lamp. All solvents and silica gel were purchased from Merck. M(CO)<sub>6</sub> (M=Cr, Mo, W) and Re(CO)<sub>5</sub>Br were purchased from Aldrich. These reagents were used as supplied. 5msalmsh and 5mafms were prepared by the literature method.<sup>13</sup>

### 2.2. Synthesis

Complexes (1a)–(4a) and (1b)–(4b) were prepared by photochemical reactions of metal carbonyls M(CO)<sub>6</sub> (M = Cr, Mo, W) and Re(CO)<sub>5</sub>Br with 5msalmsh and 5mafms, and were obtained in 50–70% yields. The methods employed for the preparation of the complexes are very similar, so that the preparation of [Cr(CO)<sub>5</sub>(5msalmsh)] (1a) is given in detail as a representative example.

#### 2.2.1. [Cr(CO)<sub>5</sub>(5msalmsh)], (1a).

Cr(CO)<sub>6</sub> (0.44 g, 2 mmol) and 5msalmsh (0.44 g, 2 mmol) were dissolved in THF (80–100 mL). The solution was irradiated for 2 h at room temperature. During irradiation, the reaction mixture changed from colorless to dark yellow. After dissolving in dichloromethane (10 cm<sup>3</sup>), petroleum ether (50 cm<sup>3</sup>) was added, resulting in the precipitation of a dark yellow solid which was washed with petroleum ether and dried under vacuum. Yield (60%). Found (%): C, 38.8; H, 2.5; N, 6.4; S, 7.2. Calcd. for CrC<sub>14</sub>H<sub>12</sub>N<sub>2</sub>SO<sub>8</sub> (%): C, 40.0; H, 2.9; N, 6.7; S, 7.6. IR (ν, KBr): 2067 (m, CO), 1978 (m, CO), 1950 (s, CO), 1928 (s, CO), 1873 (s, CO), 3158 (s, N-H), 1602(s, C=N), 1315 (s, C-O), 1274 (s, (SO<sub>2</sub>)<sub>as</sub>), 1152 (s, (SO<sub>2</sub>)<sub>sym</sub>) cm<sup>-1</sup>. <sup>1</sup>H NMR (δ, DMSO-d<sub>6</sub>): 2.10 (s, 3H, CH<sub>3</sub>-C<sub>6</sub>H<sub>5</sub>), 2.94 (s, 3H, CH<sub>3</sub>-SO<sub>2</sub>), 6.56–7.20 (m, H, (CH)<sub>Ar</sub>), 7.95 (s, 1H, HC=N-), 9.98

(s, H, NH), 11.87 (s, 1H, OH). MS(LC,70 eV): m/z (%) = 405 (25) [M<sup>+</sup>-(Me)], 377 (15) [M<sup>+</sup>-(Me+CO)], 349 (30) [M<sup>+</sup>-(Me+2CO)], 321 (25) [M<sup>+</sup>-(Me+3CO)], 293 (15) [M<sup>+</sup>-(Me+4CO)], 265 (10) [M<sup>+</sup>-(Me+5CO)].

#### 2.2.2. [Mo(CO)<sub>5</sub>(5msalmsh)], (2a).

Yield (64%). Found (%): C, 35.6; H, 2.5; N, 5.6; S, 6.5. Calcd. for MoC<sub>14</sub>H<sub>12</sub>N<sub>2</sub>SO<sub>8</sub> (%): C, 36.1; H, 2.6; N, 6.0; S, 6.9. IR (ν, KBr): 2066 (m, CO), 1990 (m, CO), 1950 (s, CO), 1925 (s, CO), 1871 (s, CO), 3160 (s, N-H), 1602(s, C=N), 1315 (s, C-O), 1274 (s, (SO<sub>2</sub>)<sub>as</sub>), 1152 (s, (SO<sub>2</sub>)<sub>sym</sub>) cm<sup>-1</sup>. <sup>1</sup>H NMR (δ, DMSO-d<sub>6</sub>): 2.08 (s, 3H, CH<sub>3</sub>-C<sub>6</sub>H<sub>5</sub>), 2.96 (s, 3H, CH<sub>3</sub>-SO<sub>2</sub>), 6.58–7.14 (m, H, (CH)<sub>Ar</sub>), 7.93 (s, 1H, HC=N-), 9.96 (s, H, NH), 11.88 (s, 1H, OH). MS (LC,70 eV): m/z (%) = 436 (15) [M<sup>+</sup>-(CO)], 408 (25) [M<sup>+</sup>-(2CO)], 380 (25) [M<sup>+</sup>-(3CO)], 352 (15) [M<sup>+</sup>-(4CO)], 324 (10) [M<sup>+</sup>-(5CO)].

#### 2.2.3. [W(CO)<sub>5</sub>(5msalmsh)], (3a).

Yield (62%). Found (%): C, 29.4; H, 2.0; N, 5.0; S, 5.2. Calcd. for WC<sub>14</sub>H<sub>12</sub>N<sub>2</sub>SO<sub>8</sub> (%): C, 30.4; H, 2.2; N, 5.1; S, 5.8. IR (ν, KBr): 2065 (m, CO), 1991 (m, CO), 1955 (s, CO), 1922 (s, CO), 1872 (s, CO), 3158(s, N-H), 1602(s, C=N), 1315 (s, C-O), 1274 (s, (SO<sub>2</sub>)<sub>as</sub>), 1152 (s, (SO<sub>2</sub>)<sub>sym</sub>) cm<sup>-1</sup>. <sup>1</sup>H NMR (δ, DMSO-d<sub>6</sub>): 2.14 (s, 3H, CH<sub>3</sub>-C<sub>6</sub>H<sub>5</sub>), 2.92 (s, 3H, CH<sub>3</sub>-SO<sub>2</sub>), 6.58–7.14 (m, H, (CH)<sub>Ar</sub>), 7.94(s, 1H, HC=N-), 9.94 (s, H, NH), 11.85 (s, 1H, OH). MS (LC,70 eV): m/z (%) = 537 (15) [M<sup>+</sup>-(Me)], 509 (10) [M<sup>+</sup>-(Me+CO)], 481 (10) [M<sup>+</sup>-(Me+2CO)], 453 (20) [M<sup>+</sup>-(Me+3CO)], 397 (15) [M<sup>+</sup>-(Me+5CO)].

#### 2.2.4. [Re(CO)<sub>4</sub>Br(5msalmsh)], (4a).

Yield (58%). Found(%): C, 25.4; H, 21.8; N, 4.2; S, 5.1. Calcd. for ReC<sub>13</sub>H<sub>12</sub>N<sub>2</sub>SO<sub>7</sub>Br (%): C, 25.7; H, 2.0; N, 4.6; S, 5.3. IR (ν, KBr): 2112 (w, CO), 2016 (m, CO), 1965 (m, CO), 1932 (s, CO), 3158 (s, N-H), 1602(s, C=N), 1315 (s, C-O), 1274 (s, (SO<sub>2</sub>)<sub>as</sub>), 1152 (s, (SO<sub>2</sub>)<sub>sym</sub>) cm<sup>-1</sup>. <sup>1</sup>H NMR (δ, DMSO-d<sub>6</sub>): 2.12 (s, 3H, CH<sub>3</sub>-C<sub>6</sub>H<sub>5</sub>), 2.90 (s, 3H, CH<sub>3</sub>-SO<sub>2</sub>), 6.56–7.12 (m, H, (CH)<sub>Ar</sub>), 7.92 (s, 1H, HC=N-), 9.96 (s, H, NH), 11.86 (s, 1H, OH). MS (LC,70 eV): m/z (%) = 578 (15) [M<sup>+</sup>-(CO)], 550 (15) [M<sup>+</sup>-(2CO)], 494 (20) [M<sup>+</sup>-(4CO)].

#### 2.2.5. [Cr(CO)<sub>5</sub>(5mafms)], (1b).

Yield (62%). Found(%): C, 41.2; H, 2.9; N, 6.0; S, 7.0. Calcd. for CrC<sub>15</sub>H<sub>14</sub>N<sub>2</sub>SO<sub>8</sub> (%): C, 41.5; H, 3.2; N, 6.4; S, 7.4. IR (ν, KBr): 2071 (m, CO), 1970 (m, CO), 1946 (s, CO), 1936 (s, CO), 1872 (m, CO), 3204 (s, N-H), 1608 (m, C=N), 1323 (s, C-O), 1254 (s, (SO<sub>2</sub>)<sub>as</sub>), 1150 (s, (SO<sub>2</sub>)<sub>sym</sub>) cm<sup>-1</sup>. <sup>1</sup>H NMR (δ, DMSO-d<sub>6</sub>): 2.20 (s, 3H, CH<sub>3</sub>-C<sub>6</sub>H<sub>5</sub>), 2.98 (s, 3H, CH<sub>3</sub>-SO<sub>2</sub>), 6.76–7.28 (m, H, (CH)<sub>Ar</sub>), 2.20 (s, 3H, CH<sub>3</sub>-C=N-), 10.86 (s, H, NH), 11.50 (s, 1H, OH). MS (LC,70 eV):

$m/z$  (%) = 433 (10) [ $M^+-(3H)$ ], 418 (15) [ $M^+-(3H+Me)$ ], 390 (15) [ $M^+-(3H+Me+CO)$ ], 362 (20) [ $M^+-(3H+Me+2CO)$ ], 334 (15) [ $M^+-(3H+Me+3CO)$ ], 306 (10) [ $M^+-(3H+Me+4CO)$ ], 278 (15) [ $M^+-(3H+Me+5CO)$ ].

### 2. 2. 6. [ $Mo(CO)_5(5mafmsH)$ ], (2b).

Yield (66%). Found(%): C, 36.8; H, 2.7; N, 5.4; S, 6.2. Calcd. for  $MoC_{15}H_{14}N_2SO_8$  (%): C, 37.6; H, 2.9; N, 5.8; S, 6.7. IR ( $\nu$ , KBr): 2070 (m, CO), 1971 (m, CO), 1944 (s, CO), 1925 (s, CO), 1872 (m, CO), 3203 (s, N-H), 1608 (m, C=N), 1323 (s, C-O), 1252 (s,  $(SO_2)_{as}$ ), 1152 (s,  $(SO_2)_{sym}$ )  $cm^{-1}$ .  $^1H$  NMR ( $\delta$ , DMSO- $d_6$ ): 2.18 (s, 3H,  $CH_3-C_6H_5$ ), 3.02 (s, 3H,  $CH_3-SO_2$ ), 6.77–7.20 (m, H,  $(CH)_{Ar}$ ), 2.24 (s, 3H,  $CH_3-C=N^-$ ), 10.87 (s, H, NH), 11.58 (s, 1H, OH). MS (LC,70 eV):  $m/z$  (%) = 420 (20) [ $M^+-(2Me+CO)$ ], 492 (15) [ $M^+-(2Me+2CO)$ ], 364 (15) [ $M^+-(2Me+3CO)$ ], 336 (25) [ $M^+-(2Me+4CO)$ ], 308 (20) [ $M^+-(2Me+5CO)$ ].

### 2. 2. 7. [ $W(CO)_5(5msalmsh)$ ], (3b).

Yield (64%). Found(%): C, 31.2; H, 2.3; N, 4.4; S, 5.2. Calcd. for  $WC_{15}H_{14}N_2SO_8$  (%): C, 31.8; H, 2.5; N, 4.9; S, 5.6. IR ( $\nu$ , KBr): 2064 (m, CO), 1972 (m, CO), 1932 (s, CO), 1921 (s, CO), 1875 (m, CO), 3204 (s, N-H), 1609 (m, C=N), 1324 (s, C-O), 1253 (s,  $(SO_2)_{as}$ ), 1150 (s,  $(SO_2)_{sym}$ )  $cm^{-1}$ .  $^1H$  NMR ( $\delta$ , DMSO- $d_6$ ): 2.22 (s, 3H,  $CH_3-C_6H_5$ ), 3.01 (s, 3H,

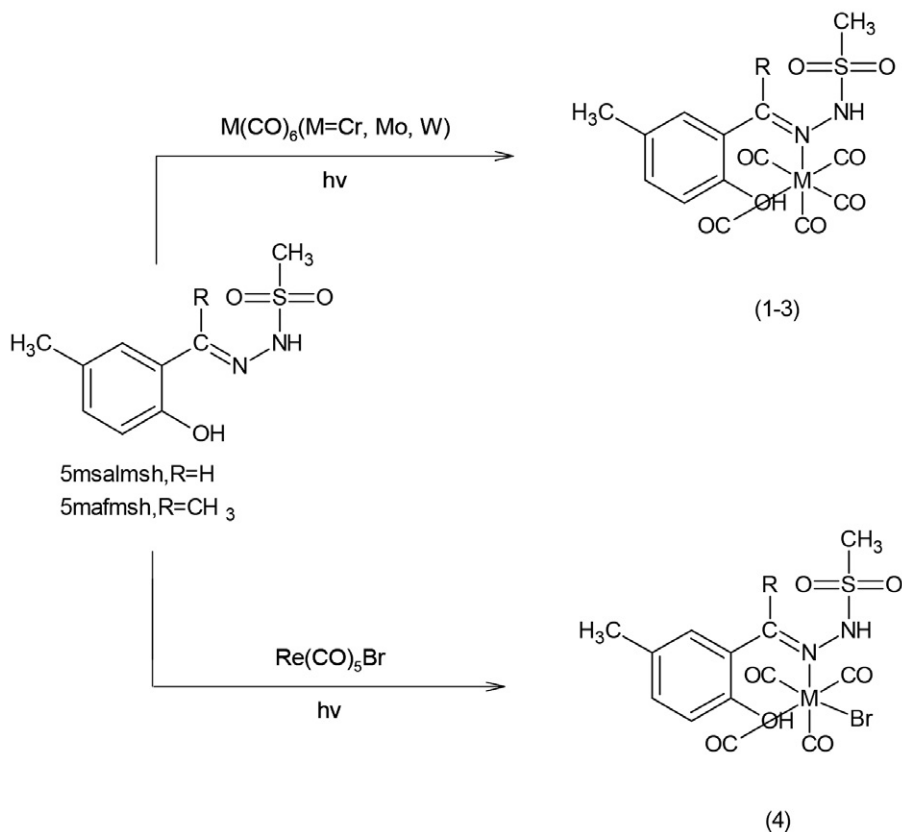
$CH_3-SO_2$ ), 6.75–7.28 (m, H,  $(CH)_{Ar}$ ), 2.22 (s, 3H,  $CH_3-C=N^-$ ), 10.88 (s, H, NH), 11.56 (s, 1H, OH). MS (LC,70 eV):  $m/z$  (%) = 551 (10) [ $M^+-(Me)$ ], 523 (10) [ $M^+-(Me+CO)$ ], 495 (15) [ $M^+-(Me+2CO)$ ], 467 (20) [ $M^+-(Me+3CO)$ ], 439 (25) [ $M^+-(Me+4CO)$ ], 411 (10) [ $M^+-(Me+5CO)$ ].

### 2. 2. 8. [ $Re(CO)_4Br(5mafmsH)$ ], (4b).

Yield (60%). Found(%): C, 26.8; H, 2.0; N, 4.0; S, 5.0. Calcd. for  $ReC_{14}H_{14}N_2SO_7Br$  (%): C, 27.1; H, 2.2; N, 4.5; S, 5.2. IR ( $\nu$ , KBr): 2113 (w, CO), 2022 (m, CO), 1920 (m, CO), 1908 (s, CO), 3204 (s, N-H), 1610 (m, C=N), 1324 (s, C-O), 1253 (s,  $(SO_2)_{as}$ ), 1152 (s,  $(SO_2)_{sym}$ )  $cm^{-1}$ .  $^1H$  NMR ( $\delta$ , DMSO- $d_6$ ): 2.16 (s, 3H,  $CH_3-C_6H_5$ ), 2.96 (s, 3H,  $CH_3-SO_2$ ), 6.76–7.25 (m, H,  $(CH)_{Ar}$ ), 2.28 (s, 1H,  $CH_3-C=N^-$ ), 10.84 (s, H, NH), 11.58 (s, 1H, OH). MS (LC,70 eV):  $m/z$  (%) = 617 (20) [ $M^+-(3H)$ ], 602(10)[ $M^+-(3H+Me)$ ], 546 (25) [ $M^+-(3H+Me+2CO)$ ], 518 (25) [ $M^+-(3H+Me+3CO)$ ], 490 (15) [ $M^+-(3H+Me+4CO)$ ].

## 3. Results and Discussion

Complexes (1a–4a) and (1b–4b) were prepared by a photochemical reaction as shown in Scheme 1. The photo-generation of  $M(CO)_5$  from  $M(CO)_6$  ( $M=Cr, Mo, W$ ) has been extensively studied. The 16-electron  $M(CO)_5$  frag-



**Scheme 1.** The photochemical reaction of  $M(CO)_6$  ( $M=Cr, Mo, W$ ) and  $Re(CO)_5Br$  with the 5msalmsh and 5mafmsH ligands.

ments react quickly with any available donor atom to form a  $M(\text{CO})_5\text{L}$  species. If L is a bidentate ligand,  $M(\text{CO})_4\text{L}$  chelate or bridging  $M_2(\text{CO})_{10}(\mu\text{-L})$  compounds may occur.<sup>14–16</sup> In this study, photochemical reactions of  $M(\text{CO})_6$  ( $M=\text{Cr}$ ,  $\text{Mo}$ ,  $\text{W}$ ), and  $\text{Re}(\text{CO})_5\text{Br}$  with 5msalmsh and 5mafmslh ligands proceed in this expected manner and give a series of complexes (1a–4a) and (1b–4b).

The strong C=N stretching vibration, found at  $1618\text{ cm}^{-1}$  in 5msalmsh, shifts to lower wavenumber in (1a–4a) and the strong C=N stretching vibration, found at  $1628\text{ cm}^{-1}$  in 5mafmslh, shifts to lower wavenumber in (1b–4b), showing that 5msalmsh and 5mafmslh ligands coordinate to the metal via the imine donor atom.<sup>16</sup> These shifts have been explained as a weakening of the CN bond resulting from the loss of electron density from the nitrogen to the metal atom.<sup>17</sup> No shifting upon complex formation was observed for the  $\nu_{\text{as}}(\text{SO}_2)$ ,  $M_{\text{sym}}(\text{SO}_2)$ ,  $\nu(\text{NH})$  and  $\nu(\text{CO})$  stretching vibrations indicating that  $\text{SO}_2$ ,  $\text{NH}$  and  $\text{CO}$  groups were not coordinated to metal atom in (1a–4b) and (1b–4b). The OH stretching vibration was not observed in both free ligand as well as in (1a–4a) and (1b–4b) because of hydrogen bonding with the imine nitrogen atom.<sup>18</sup>

According to number of carbonyl bands, provides important clues to the environment of the metal centers.<sup>19</sup> Five carbonyl stretching bands in (1a–3a) and (1b–3b) are attributed to local  $C_{4v}$  symmetry  $M(\text{CO})_5$ . Similarly four CO stretching absorptions in (4a,4b) indicate to local  $C_{2v}$  symmetry<sup>20</sup> (shown in Figure 1). The  $\nu(\text{CO})$  modes in (1a–4a) and (1b–4b) move also to lower wave numbers when compared with the starting carbonyl complexes.<sup>13,14</sup>

In the  $^1\text{H}$  NMR spectra of (1a–4a) and (1b–4b), the signal for the NH hydrogen of free ligands remain unchanged. No shift of hydroxyl protons with complex formation shows that OH group does not coordinate to metal atoms. The signals of the  $\text{HC}=\text{N}$  and  $\text{CH}_3=\text{N}$  protons show a small upfield shift, which may be related to changing  $\pi$ -electron density in the C=N bond complex formation in (1a–4a) and (1b–4b). According to these data, 5msalmsh and 5mafmslh behave as monodentate ligands via the imine N donor atom in (1a–4a) and (1b–4b).

The mass spectra show fragmentation via successive loss of CO groups and fragmentation of the organic ligands.

## 4. Conclusions

Eight new metal carbonyl complexes,  $[M(\text{CO})_5(5\text{msalmsh})]$  [ $M=\text{Cr}$ ; (1a),  $\text{Mo}$ ; (2a);  $\text{W}$ (3a)],  $[\text{Re}(\text{CO})_4\text{Br}(5\text{msalmsh})]$  (4a),  $[M(\text{CO})_5(5\text{mafmslh})]$  [ $M=\text{Cr}$ ; (1b),  $\text{Mo}$ ; (2b);  $\text{W}$ (3b)],  $[\text{Re}(\text{CO})_4\text{Br}(5\text{mafmslh})]$  (4b), have been characterized using elemental analysis,  $^1\text{H}$  NMR, LC-MS and IR spectra. 5msalmsh and 5mafmslh behave as monodentate ligands via the N imine donor atom in (1a–4a) and (1b–4b). IR and NMR spectra of the compounds show that the 5msalmsh and 5mafmslh ligands coordinate to the metal

atom for compounds (1a–4a) and (1b–4b) only via an imine N donor atom behaving as a monodentate neutral ligand.<sup>13</sup>

## Acknowledgments

We thank BP (Turkey) for the provision of the photochemical apparatus and the Research Foundation of Ege University for funds and TUBITAK for allocation of time at the NMR, Mass Spectra and Elemental Analyses.

## 5. References

1. S. Rollas, N. Gulerman, H. Erdeniz, *Farmaco*, **2002**, 57(2), 171–174. DOI:10.1016/S0014-827X(01)01192-2
2. Y. Ozama, N. H. Sugi, T. Nagasu, T. Owa, T. Watanabe, N. Koyanagi, H. Yoshino, K. Kitoh, K. Yoshimatsu, *Eur. J. Cancer*, **2001**, 37, 2275–2282. DOI:10.1016/S0959-8049(01)00275-1
3. U. A. K. Betz, R. Fischer, G. Kleymann, M. Hendrix, H. Rübnsamen-Waigmann, *Antimicrob. Agents Chemother.*, **2002**, 46, 1766–1772. DOI:10.1128/AAC.46.6.1766-1772.2002
4. G. Bhattacharya, J. Herman, D. Delfin, M. M. Salem, T. Barszcz, M. Mollet, G. Riccio, R. Brun, K. A. Werbovetz, *J. Med. Chem.*, **2004**, 47, 1823–1832. DOI:10.1021/jm0304461
5. L. M. Lima, E. G. Amarante, A. L. P. Miranda, C. A. M. Fraga, E. J. Barreiro, *Pharm. Pharmacol. Commun.*, **1999**, 5, 673–678. DOI:10.1211/146080899128734370
6. Ü. Ö. Özdemir, F. İlbiz, A. B. Gündüzalp et. al., *Journal of Molecular Structure*, **2015**, 1100, 464–474. DOI:10.1016/j.molstruc.2015.07.054
7. S. Özçelik, M. Dinçer, M. Şekerci, A. Balaban, Ü. Özdemir, *Acta Crystallogr. Sect. E*, **2004**, 60(9), 1552–1553. DOI:10.1107/S1600536804019932
8. L. L. Silva, K. N. Oliveria, R. J. Nunes, *Arxivoc*, **2006**, 13, 124–129. DOI:10.3998/ark.5550190.0007.d12
9. X. He, L. Tang, L. He, P. Xu, *Hua Xi Yi Da Xue Bao*, **1988**, 19(3), 317–319. DOI:10.1039/b104037p
10. H. Lu, M. A. Schmidt, K. F. Jensen, *Royal Society of Chemistry*, **2001**, 1, 22–28.
11. G. Orhan, O. S. Senturk, U. O. Ozmen, S. Sert, E. Subası, *Journal of Coord. Chem.*, **2014**, 67(19), 3216–3225. DOI:10.1080/00958972.2014.963569
12. Marc Wrighton, *Chemical Reviews*, **1974**, 74(4), 401–430. DOI:10.1021/cr60290a001
13. Ü. Ö. Özdemir, P. Güvenç, E. Şahin, F. Hamurcu, *Inorganic Chimica Acta*, **2009**, 362, 2613–2618. DOI:10.1016/j.ica.2008.11.029
14. M. J. Almond, F. Sarıkahya, O. S. Şentürk, *Polyhedron*, **1997**, 16, 1101. DOI:10.1016/S0277-5387(96)00384-1
15. F. Sarıkahya, O. S. Şentürk, *Synth. React. Inorg. Met.-Org. Chem.*, **2001**, 31, 1843–1851.
16. F. A. Cotton, G. Wilkinson, G., *Advanced Inorganic Chemistry*, **1988**, 5<sup>th</sup> Ed., Wiley Interscience, New York, 1047.



17. J. E. Kovacic, *Spectrochim. Acta Part A: Molecular Spectroscopy*, **1967**, 23, 183–187. DOI:10.1016/0584-8539(67)80219-8
18. N. I. Dodoff, Ü. Özdemir, N. Karacan, M. Georgieva, S. M. Konstantinov, M. E. Stefanova, *Z. Naturforsch.*, **1999**, 54(12), 1553–1562. DOI:10.1515/znb-1999-1213
19. G. L. Miessler, D. A. Tarr, *Inorganic Chemistry*, **2000**, 2<sup>nd</sup> ed., Prentice Hall, New Jersey, 471.
20. U. Mazzi, A. Binmondo, N. Kotsev, D.A. Clemente, *Journal of Organomet. Chem.*, **1977**, 135(2), 177–182. DOI:10.1016/S0022-328X(00)80858-X

## Povzetek

Osem novih kompleksnih spojin  $[M(CO)_5(5msalmsh)]$  [ $M=Cr$ ; (1a), Mo; (2a); W(3a)],  $[Re(CO)_4Br(5msalmsh)]$  (4a),  $[M(CO)_5(5mafms)]$  [ $M=Cr$ ; (1b), Mo; (2b); W(3b)] in  $[Re(CO)_4Br(5mafms)]$  (4b) smo sintetizirali s fotokemijsko reakcijo med kovinskimi karbonili,  $[M(CO)_6]$  ( $M=Cr, Mo, W$ ),  $[Re(CO)_5Br]$  in ligandoma (5msalmsh in 5mafms). Spojine smo karakterizirali z elementno analizo, s tekočinsko kromatografijo sklopljeno z masno spektroskopijo (LC-MS), infrardečo spektroskopijo (FT-IR) in NMR spektroskopijo ( $^1H$  NMR). Rezultati spektroskopskih metod kažejo, da sta monodentatna liganda 5msalmsh in 5mafms na kovinski center v spojinah (1a)–(4a) in (1b)–(4b) koordinirana z atomom dušika, ki pripada imino skupini.



Except when otherwise noted, articles in this journal are published under the terms and conditions of the Creative Commons Attribution 4.0 International License

*Technical paper*

# First Estimation of Reference Intervals for Thyroid-Stimulating Hormone and Thyroid Hormones in Slovenian Population

Adrijana Oblak,<sup>1</sup> Ajda Biček,<sup>1</sup> Edvard Pirnat,<sup>1</sup> Katja Zaletel<sup>1,2</sup>  
and Simona Gabersček<sup>1,2,\*</sup>

<sup>1</sup> Department of Nuclear Medicine, University Medical Centre Ljubljana, Zaloška 7, 1525 Ljubljana, Slovenia

<sup>2</sup> Faculty of Medicine, University of Ljubljana, Vrazov trg 2, 1000 Ljubljana, Slovenia

\* Corresponding author: E-mail: [simona.gaberscek@kclj.si](mailto:simona.gaberscek@kclj.si)  
telephone: +386 1 522 35 51, fax: +386 1 522 22 37

Received: 02-17-2020

## Abstract

For thyroid function estimation and clinical decision making, use of appropriate reference intervals for thyroid-stimulating hormone (TSH), free thyroxine (fT<sub>4</sub>) and free triiodothyronine (fT<sub>3</sub>) is crucial. For each laboratory, establishment of own reference intervals is advised. For the first Slovenian estimation of reference intervals for thyroid hormones a large group of 1722 healthy individuals without thyroid disease was established retrospectively. Hormone analyses were performed on automated analyser Advia Centaur XP Immunoassay System (Siemens Healthineers), which reference intervals for TSH, fT<sub>4</sub> and fT<sub>3</sub> were 0.55–4.78 mIU/L, 11.5–22.7 pmol/L, and 3.5–6.5 pmol/L, respectively. Statistical analysis followed non-parametric percentile method. Our laboratory reference intervals for TSH, fT<sub>4</sub> and fT<sub>3</sub> are mostly narrower than intervals given by manufacturer. Median value, lower and upper limit for TSH, fT<sub>4</sub> and fT<sub>3</sub> were 1.98 (0.59–4.23) mIU/L, 14.5 (11.3–18.8) pmol/L and 4.82 (3.79–6.05) pmol/L, respectively. Most likely, an inclusion of a high number of healthy individuals without thyroid disease was a reason for such results.

**Keywords:** reference intervals; thyroid-stimulating hormone; thyroid hormones; immunoassays; interferences

## 1. Introduction

Biochemical parameters obtained from blood sampling are an important part of clinical decision-making. However, a path from ordering a test by a clinician to the value of an analyte in blood is long and is facing several important and critical steps which can influence the end result and, consequently, a clinical decision. Important part of this process is preanalytics which combines different aspects – from biological variability to sample collection and sample handling prior to analysis.<sup>1</sup> Preanalytics is a source of majority of errors and should therefore be carefully executed.<sup>2</sup> The primary goal of every medical examination is to cause no harm to a patient. Incorrect test results expose a patient to diagnostic errors and an institution to unnecessary additional costs.<sup>3</sup> As a part of a good laboratory practice our laboratory follows Clinical Laboratory Standard Institute (CLSI) guidelines which propose each laboratory should determine its own reference intervals on its own population in their own laboratory environment.<sup>4</sup> When laboratory prepares reference intervals for any kind of hormones in a

population, it is facing several problems. Excretion of hormones differs on daily, weekly, monthly, seasonally basis, and also depends on sex, age, drugs, and different physiological states like pregnancy or puberty. Inclusion of a large number of individuals in the establishment of reference intervals may overcome those problems. It is also important to set the time of blood withdrawal to prevent incorrect interpretation of results, especially for hormones following circadian rhythm like thyroid-stimulating hormone (TSH).<sup>5</sup> Studies have shown that the time of sample collection has an impact on serum TSH value and should therefore be standardized to minimize the impact of false TSH values on clinical decisions especially in subclinical hypothyroidism, which is defined as elevated TSH, and normal free thyroxine (fT<sub>4</sub>) and free triiodothyronine (fT<sub>3</sub>) values.<sup>6</sup> This fact was confirmed by our study from 2016 which showed that 23% of patients sent to our department from periphery laboratories because of mildly elevated TSH (up to 10 mIU/L) had normal thyroid gland, and only 22% really had elevated TSH after the complete thyroid examination.<sup>7</sup> Other 55% had Hashimoto's thyroiditis in euthyroid phase. A possible

explanation for such differences could be too early blood collection in the periphery laboratories. Generally, preferable time of blood collection for various tests is in fasting state from 7 a.m. to 9 a.m.<sup>8</sup> If within the same timeframe also a blood sample for thyroid function assessment is taken, a falsely elevated TSH level could be measured.<sup>9</sup> Increased TSH level may be associated with unnecessary treatment or with unnecessary referral to thyroid specialist that prolongs waiting list of patients for examination.

Reference intervals for each assay are given by manufacturer in the Instructions for use (IFU). Given data, however, usually lack information regarding health of reference population, median values and the time of collection of samples. The data that are obtained on samples chosen by manufacturer are from apparently healthy adult individuals. However, no data on their actual health or thyroid status is available.

In several studies, reference values were established in various populations. In most studies, the exclusion criteria were not such that individuals with thyroid disorders could be excluded or the values were obtained from databases only. Thyroid diseases were mostly excluded by patient's history, or by laboratory tests only and not by complete clinical examination.<sup>10,11,12</sup>

Therefore, the aim of our work was to establish laboratory-own reference intervals for TSH,  $fT_4$  and  $fT_3$  on a method we are using in our laboratory considering the time frame in which TSH has the lowest values according to circadian rhythm – from 9 a.m. to 3 p.m. in a large group of clinically examined individuals without thyroid disease.

## 2. Experimental

We reviewed medical records of all adult patients who were examined by thyroid specialist for the first time in their life between January 1, 2011, and December 31, 2014, at the Department of Nuclear Medicine, University Medical Centre Ljubljana, Slovenia. In all patients, a routine clinical examination including thyroid ultrasound was performed followed by the measurement of serum concentration of TSH,  $fT_4$ ,  $fT_3$ , thyroglobulin antibodies (Tg-Ab), and thyroid peroxidase antibodies (TPO-Ab). Reference intervals given by manufacturer at the time of analysis were for TSH 0.55–4.78 mIU/L,  $fT_4$  11.5–22.7 pmol/L,  $fT_3$  3.5–6.5 pmol/L, and for Tg-Ab and TPO-Ab, up to 60 kU/L. We only included data of patients with a normal thyroid gland, with no associated diseases and without amiodarone or other drugs influencing the level of TSH,  $fT_4$  and  $fT_3$  such as glucocorticoids or psychotropic medication. Data from pregnant individuals were not included in the study. We found 2073 reference individuals from 15 to 93 years of age who met these criteria. Following CLSI<sup>3</sup> guidelines only those from 18 to 65 years of age were included into reference group, which made a group of 1722 reference individuals.

### 2. 1. Sample Preparation

Venous blood was collected following standardized protocol of venous blood sampling used at the department.<sup>13</sup> Blood was taken from 9 a.m. to 3 p.m. into serum collective tubes (BD Vacutainer® blood collection tubes) by trained nurses. Transportation was made across the hall since laboratory is a part of the department. Blood was coagulating for 30 min and was centrifuged afterwards at 4 °C for 10 min at 3000 rpm. Measurements of all parameters were performed on the day of collection using serum from primary tube.

### 2. 2. Analysis

All biochemical analyses were performed on automated analyser Advia Centaur XP Immunoassay System (Siemens Medical Solutions Diagnostics, Dublin, Ireland) using chemiluminescent principle. All analyses on Advia Centaur are traceable to standardization. The TSH3-Ultra assay standardization is traceable to the World Health Organization (WHO) 3<sup>rd</sup> International Standard for human TSH (IRP 81/565), which is the last generation of tests available on the market.<sup>14</sup> The  $fT_4$  and  $fT_3$  assays are traceable to an internal standard manufactured using U.S.P. (United States Pharmacopeia).<sup>15</sup> The Tg-Ab standardization is traceable to the WHO Reference Preparation MRC 65/93 and the TPO-Ab standardization is traceable to the WHO Reference Preparation MRC 66/387.<sup>16</sup> Performance characteristics for all assays are as follows. TSH limit of detection is 0.008 mIU/L, linearity of the assay is in the range from 0.008 to 150.0 mIU/L with the recovery range from 96.3 to 105.0%. TSH intra-assay and inter-assay coefficients of variation ranged from 2.4% to 4.9% and from 1.5% to 4.4%, respectively. Limits of detection for  $fT_4$  and  $fT_3$  are 1.3 pmol/L and 0.3 pmol/L, respectively, linearities of the assays are in the range from 1.3 to 155.0 pmol/L, and 0.3 to 30.8 pmol/L, respectively. Intra-assay and inter-assay coefficient of variations for free thyroid hormones,  $fT_4$  and  $fT_3$ , ranged from 2.22% to 4.69% and from 1.58% to 4.59% for  $fT_4$  and from 2.35% to 3.08% and from 2.76% to 4.05% for  $fT_3$ . Limits of detection for TPO-Ab and Tg-Ab are 28 kU/L and 15 kU/L, respectively, while linearities of the assays are in the range from 28 to 1300 kU/L and from 15 to 500 kU/L, respectively. TPO-Ab and Tg-Ab intra-assay and inter-assay coefficient of variations ranged from 1.3% to 6.8% and from 2.8% to 3.4% for TPO-Ab and from 2.9% to 5.5% and from 1.8% to 2.0% for Tg-Ab, respectively. Cross-reactivity of TSH assay was shown non-detectable for human chorionic gonadotropin (hCG), follicle-stimulating hormone (FSH), and luteinizing hormone (LH) tested at 200.000 mIU/L, 1500 mIU/L, and 600 mIU/L, respectively. Cross-reactivity for  $fT_4$  and  $fT_3$  assays was below 1.0% for diiodotyrosine, monoiodotyrosine, and reverse  $T_3$ . Quality controls (QC) for TSH,  $fT_4$ , and  $fT_3$  were performed using independent control material, Liquicheck Immuno-

assay Plus Control, Trilevel #360 (Bio-Rad Laboratories, Inc.). As for Tg-Ab and TPO-Ab control material Advia Centaur Systems QC anti-TG and anti-TPO 1,2 (Siemens Healthcare Diagnostics, Inc.) based on LOT of reagent were used, low and high level.

### 2. 3. Estimation of Reference Intervals

Reference values for TSH,  $fT_4$ , and  $fT_3$  from data of reference individuals were estimated using statistical program MedCalc Statistical Software version 14.8.1 (MedCalc Software bvba, Ostend, Belgium, 2014). Reference intervals were determined by non-parametric percentile method following CLSI EP28-A3 with 95% reference interval, double sided. Outliers were analysed using Reed et al. and none were detected.<sup>17</sup> Results are presented as lower and upper limit of reference values for each parameter for all individuals and separately for men and women.

### 2. 4. Ethical Approval

Study was approved by the Republic of Slovenia National Medical Ethics Committee (number 47/08/14, October 24, 2014).

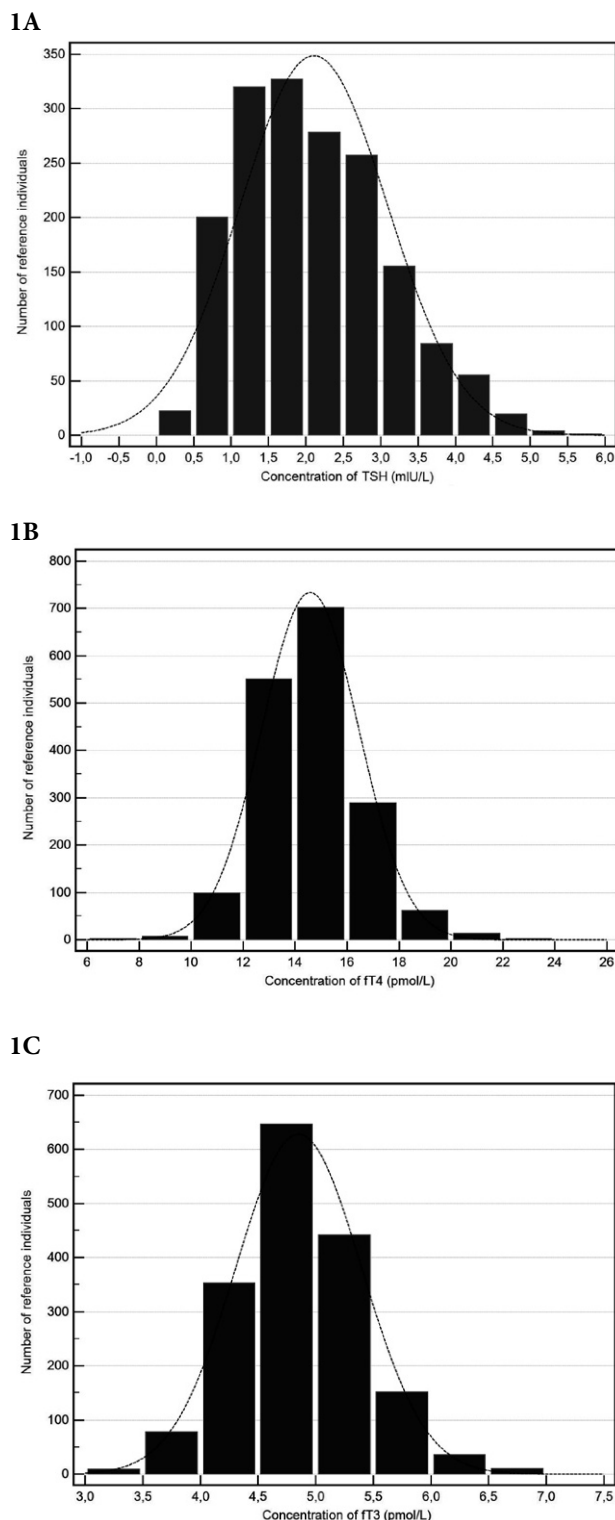
## 3. Results and Discussion

Into the reference group, 398 men and 1324 women were included with the average age of 43 years for men and 38 years for women, respectively. The data are not symmetrically distributed ( $P < 0.0001$ ), therefore, a non-parametric percentile method was used. The obtained intervals from 2.5th to 97.5th percentile are presented in Table 1 including 90% coefficient interval and histograms of the distribution of results are followed below in Figure 1. For comparison, manufacturer's intervals are also given.

**Table 1.** Reference intervals for serum concentration of TSH,  $fT_4$  and  $fT_3$  obtained from 1722 reference individuals, given also separately for men (398) and women (1324). Comparison of laboratory-own and manufacturer's reference intervals.

Parameter	TSH (mIU/L)	$fT_4$ (pmol/L)	$fT_3$ (pmol/L)
<b>Lower limit<sup>a</sup></b>	<b>0.59</b>	<b>11.3</b>	<b>3.79</b>
CI 90% <sup>a</sup>	0.56–0.62	11.1–11.4	3.74–3.85
<b>Upper limit<sup>a</sup></b>	<b>4.23</b>	<b>18.8</b>	<b>6.05</b>
CI 90% <sup>a</sup>	4.16 – 4.44	18.4 – 19.0	5.91–6.16
Men <sup>a</sup>	0.59–4.45	11.3–19.4	3.83–6.30
Women <sup>a</sup>	0.58 – 4.18	11.3–18.5	3.78–5.90
Advia Centaur XP <sup>b</sup>	0.55–4.78	11.5–22.7	3.5–6.5

<sup>a</sup> laboratory-own data; <sup>b</sup> manufacturer's data TSH, thyroid-stimulating hormone;  $fT_4$ , free thyroxine;  $fT_3$ , free triiodothyronine; CI, confidence interval



**Figure 1.** Histograms showing distribution of reference values in a population of 1722 reference individuals. 1A: TSH distribution of reference values with Coefficient of Skewness 0.5308 ( $P < 0.0001$ ) and Coefficient of Kurtosis  $-0.2141$  ( $P = 0.0469$ ); 1B:  $fT_4$  distribution of reference values with Coefficient of Skewness 0.4014 ( $P < 0.0001$ ) and Coefficient of Kurtosis 0.7660 ( $P < 0.0001$ ); 1C:  $fT_3$  distribution of reference values with Coefficient of Skewness 0.3044 ( $P < 0.0001$ ) and Coefficient of Kurtosis 0.5839 ( $P = 0.0001$ ).

We did not observe significant changes in reference ranges between men and women.

Distribution of reference values is not normal which is confirmed with Coefficients of Skewness and Kurtosis and with D'Agostino-Pearson test.

Establishment of laboratory-own reference intervals and their use in routine clinical practice should be performed cautiously. All factors influencing these values should be taken into account – preanalytical as well as analytical. Not only they will prevent us from an impact they would have to the calculation of lower and/or upper limits of intervals but they will also help us with setting the time of the day blood samples should be taken and in which it is appropriate to use them. This is very important when measuring serum levels of various hormones due to present biological variations such as pulsatile secretion and/or circadian rhythm.

In general, measurement of various hormones is complex. First, differences between different immunoassays due to usage of different detecting antibodies exist. This is a consequence of the nature of the individual analyte and of the prepared antibodies. Thus, the comparison of values between different immunoassay methods can mislead a clinician. This holds true especially for the measurements of peptide and protein hormones which lack standardization and, therefore, equivalency between assays is not possible. Second, methods have detection limits. Third, endogenous and exogenous interferences may importantly influence immunoassays and final concentrations.<sup>18</sup> Endogenous substances are usually well known since they arrive from properties of the specimen. Nowadays, reagents are tested against some obvious interferences like molecules showing similar structure to analyte although an impact of autoantibodies, binding proteins, heterophile antibodies, human anti-animal antibodies always exists and one should always keep this in mind while evaluating results. On the other hand exogenous interferences are usually not known or at least not known to the laboratory due to lack of patient's history and any prior testing of interferences. This includes drugs, which can influence the measurement of an analyte, and can lead to false positive or negative test results. An important problem is also different food supplements, which - with the expansion of usage – impact the detection of hormones. They are also very hard to detect. Some interferences have been discovered lately, like biotin, which shows an important impact on immunoassays, especially those which are using biotin streptavidin reaction.<sup>19,20,21</sup> Furthermore, associated diseases may influence test results. Thus, during the diagnostic procedure, it is important to standardize as many procedures as possible to minimize known influences. Therefore, the collaboration between a clinician and a laboratory is absolutely necessary. An important part of collaboration is also a special proximity of the laboratory and clinical part which is an advantage at our department.

While preparing reference intervals it is very important to know what kind of intervals you wish to prepare –

healthy or unhealthy adults, children, pregnant women. Considering that, inclusion and exclusion criteria should be selected cautiously. Individuals with known associated diseases or medications could influence the end results and should not be included into the reference group.

In most methods, the exact data of health status of reference individuals are not given by manufacturer. However, for TSH and thyroid hormones, it is very important that we know health and thyroid status of reference individuals. In our study, we have established reference values for TSH and free thyroid hormones, which is the first such study performed in Slovenian adult population. All individuals were clinically examined by thyroid specialists. Therefore, presented data are based on really healthy population. We did not find this size of clinically and biochemically proven healthy reference population in the available literature. All the preanalytical and analytical influences were limited. The use of third generation TSH assay enabled us to determine values with good precision and reproducibility. We did not find any statistical difference in reference intervals between men and women, therefore reference intervals for the whole population were implemented. The significant differences in reference ranges between men and women were observed in Chinese population.<sup>22</sup> By contrast, in the study from Brasil, no gender-related differences in reference ranges were found.<sup>23</sup> This indicates the differences between populations and the necessity for determination of population-based reference intervals.

Our study showed narrower reference intervals as those proposed by manufacturer with the exception of the slightly lower limit for  $fT_4$ . Most likely, an inclusion of a high number of thyroid-healthy individuals only was a reason for such results. Narrower reference intervals for TSH and  $fT_4$  were also found in the literature.<sup>24</sup> Differences from reference intervals proposed by manufacturer were observed in all three analytes. The most pronounced change was observed in the upper level of  $fT_4$ , which decreased from 22.7 pmol/L to 18.8 pmol/L. This change enables detection of more patients with manifest hyperthyroidism (decreased level of TSH, increased level of  $fT_4$  or  $fT_3$ ). Generally, narrower reference intervals for TSH,  $fT_4$  and  $fT_3$  help clinician not to overlook subclinical forms of thyroid disorders. Since these also have an important health impact, our results contribute to better management of thyroid patients.

Children and pregnant women were excluded from the study. For both populations, reference intervals should be prepared separately due to different physiology of thyroid hormone synthesis and secretion.

## 4. Conclusions

Laboratory-own reference intervals for TSH,  $fT_4$  and  $fT_3$  on a method we are using in our laboratory consider-

ing the time frame in which TSH has the lowest values according to circadian rhythm were established. These intervals are mostly narrower than intervals proposed by manufacturer and therefore improve management of thyroid patients by better detection of patients with subclinical thyroid disorders. Laboratories in the area which use the same methodology could take over the established reference intervals. If laboratory or manufacturer changes methodology, it is laboratory's responsibility to verify those changes and, if necessary, repeat the establishment of reference intervals.

## Acknowledgements

The work has been supported by University Medical Center Ljubljana, Slovenia.

## Conflict of Interest

The authors declare no conflict of interest.

## 5. References

1. S. Narayanan, *Indian J. Clin. Biochem.* **1996**, *11*, 7–11. DOI:10.1007/BF02868404
2. A. Atay, L. Demir, S. Cuhadar, G. Saglam, H. Unal, S. Aksun, B. Arslan, A. Ozkan, R. Sutcu, *Biochemia Medica.* **2014**, *24*, 376–382. DOI:10.11613/BM.2014.040
3. M. L. Graber, N. Franklin, R. Gordon, *Arch. Intern. Med.* **2005**, *165*, 1493–1499. DOI:10.1001/archinte.165.13.1493
4. Clinical Laboratory Standard Institute. Defining, establishing, and verifying reference intervals in the clinical laboratory; Approved Guideline, 3rd edition. CLSI Document EP28-A3c. Wayne, PA, **2010** [https://clsi.org/media/1421/ep28a3c\\_sample.pdf](https://clsi.org/media/1421/ep28a3c_sample.pdf) (assessed: February 16, 2020).
5. C. Lucke, R. Hehrmann, K. von Mayersbach, A. von zur Mühlen, *Acta Endocrinol. (Copenh).* **1977**, *86*, 81–88. DOI:10.1530/acta.0.0860081
6. B. Mirjanic-Azaric, T. Stojakovic-Jelisavac, B. Vukovic, D. Stojanovic, M. Vujnic, S. Uletilovic, *Clin. Biochem.* **2015**, *48*, 1347–1349. DOI:10.1016/j.clinbiochem.2015.08.020
7. S. Gaberšček, L. Petek-Hojker, S. Hojker, *Zdrav. Vestn.* **2002**, *71*, 485–486.
8. A. M. Simundic, M. Cornes, K. Grankvist, G. Lippi, M. Nybo, *Clin. Chim. Acta.* **2014**, *432*, 33–37. DOI:10.1016/j.cca.2013.11.008
9. J. Ehrenkranz, P. R. Bach, G. L. Snow, A. Schneider, J. L. Lee, S. Ilstrup, S. T. Bennett, S. Benvenega, *Thyroid.* **2015**, *25*, 954–961. DOI:10.1089/thy.2014.0589
10. T. Vadiveloo, P. T. Donnan, M. J. Murhpy, G. O. Leese, *J. Clin. Endocrinol. Metab.* **2013**, *98*, 1147–1153. DOI:10.1210/jc.2012-3191
11. J. H. Barth, A. Luvai, N. Jassam, W. Mbagaya, E. S. Kilpatrick, D. Narayanan, S. Spoor, *Ann. Clin. Biochem.* **2018**, *55*, 107–112. DOI:10.1177/0004563217691549
12. S. Y. Park, H. I. Kim, H.-K. Oh, T. H. Kim, H. W. Jang, J. H. Chung, M.-H. Shin, S. W. Kim, *PLoS. ONE.* **2015**, *13*, e0190738.
13. M. Piskar. Priporočeni postopek za odvzem venske krvi. *Slovenian association for clinical chemistry and laboratory medicine, 1st ed.* Ljubljana, **1999**. <https://www.szklm.si/si/vsebi-na/eflm-48/nova-eflm-priporocila-za-odvzem-venske-krvi> (assessed: February 16, 2020)
14. Thyroid Stimulating Hormone, Human. WHO International Standard 81/565. [https://www.nibsc.org/products/brm\\_product\\_catalogue/detail\\_page.aspx?catid=81/565](https://www.nibsc.org/products/brm_product_catalogue/detail_page.aspx?catid=81/565) (assessed: March 27, 2021).
15. United States Pharmacopeia. <https://www.usp.org/> (assessed: March 27, 2021).
16. WHO International Biological Reference Preparation. [https://www.who.int/bloodproducts/ref\\_materials/catalogue\\_miscellaneous.pdf](https://www.who.int/bloodproducts/ref_materials/catalogue_miscellaneous.pdf) (assessed: March 27, 2021).
17. A. H. Reed, R. J. Henry, W. B. Mason, *Clin. Chem.* **1971**, *17*, 275–284. DOI:10.1093/clinchem/17.4.275
18. J. Tate, G. Ward, *Clin. Biochem. Rev.* **2004**, *25*, 105–120.
19. A. Clerico, M. Plebani, *Clin. Chem. Lab. Med.* **2017**, *55*, 777–779. DOI:10.1515/cclm-2017-0070
20. M. L. Piketty, M. Polak, I. Flechtner, L. Gonzales-Briceño, J. C. Souberbielle, *Clin. Chem. Lab. Med.* **2017**, *55*, 780–788. DOI:10.1515/cclm-2016-0606
21. C. Trambas, Z. Lu, T. Yen, K. Sikaris, *Ann. Clin. Biochem.* **2018**, *55*, 205–215. DOI:10.1177/0004563217701777
22. Z.-Z. Li, B.-Z. Yu, J.-L. Wang, Q. Yang, J. Ming, Y.-R. Tang, *J. Clin. Lab. Anal.* **2020**, *34*, e23197.
23. M. H. C. Gurgel, C. M. M. Ponte, R. Fontes, I. V. Rocha, L. A. A. Batista, T. C. S. Sousa, R. M. Montenegro Junior, *Arch. Endocrinol. Metab.* **2020**, *64*, 362–368.
24. N. Reix, C. Massart, M. d'Herbomez, F. Gasser, B. Heurtault, A. Agin, *Clin Biochem.* **2013**, *46*, 1305–1308. DOI:10.1016/j.clinbiochem.2013.04.015e

## Povzetek

Za oceno delovanja ščitnice in klinično odločanje je ključnega pomena uporaba ustreznih referenčnih intervalov za tirotropin (TSH), prosti tiroksin ( $pT_4$ ) in prosti trijodtironin ( $pT_3$ ). Priporočljivo je, da vsak laboratorij pripravi lastne referenčne intervale. Za prvo slovensko postavitev referenčnih intervalov za ščitnične hormone smo retrospektivno zbrali veliko skupino 1722 zdravih posameznikov brez ščitnične bolezni. Analizo hormonov smo izvedli na avtomatiziranem analizatorju Advia Centaur XP Immunoassay System (Siemens Healthineers). Proizvajalčevi referenčni intervali za TSH so bili 0,55–4,78 mIU/L, za  $pT_4$  11,5–22,7 pmol/L in za  $pT_3$  3,5–6,5 pmol/L. Za statistično obdelavo podatkov smo uporabili neparametrično metodo. Naši laboratorijski referenčni intervali za TSH,  $pT_4$  in  $pT_3$  so bili v glavnem ožji kot tisti, ki jih je predlagal proizvajalec. Mediana vrednost in razpon sta bila za TSH 1,98 (0,59–4,23) mIU/L, za  $pT_4$  14,5 (11,3–18,8) pmol/L in za  $pT_3$  4,82 (3,79–6,05) pmol/L. Najverjetnejši vzrok za takšen rezultat raziskave je bila vključenost velikega števila zdravih posameznikov brez ščitnične bolezni.



Except when otherwise noted, articles in this journal are published under the terms and conditions of the Creative Commons Attribution 4.0 International License

Technical paper

# Degradation of Plasticized Poly(1-chloroethylene) Waterproofing Membranes used as a Building Material

Gregor Kravanja,<sup>1,2\*</sup> Andrej Ivanič<sup>2</sup> and Samo Lubej<sup>2\*</sup>

<sup>1</sup> University of Maribor; Faculty of Chemistry and Chemical Engineering; Laboratory of separation processes and product design, Smetanova ul. 17, 2000 Maribor, Slovenia

<sup>2</sup> University of Maribor, Faculty of Civil Engineering, Transportation and Architecture, Smetanova 17, 2000 Maribor, Slovenia

\* Corresponding author: E-mail: gregor.kravanja@um.si and samo.lubej@um.si

Received: 10-23-2020

## Abstract

In the present work, both unused plasticized poly(1-chloroethylene) membranes and membranes taken from a flat roof area were comprehensively analysed. First, tensile strength and elongation at breaking points were determined, followed by measurements of wettability. Secondly, morphological changes were analysed using scanning electron microscopy (SEM). To study chemical changes in aged membranes, Fourier transform infrared spectroscopy (FTIR) analysis in the attenuated total reflection mode (ATR) was used. Finally, thermogravimetric analysis and differential scanning calorimetry (TGA-DSC) were performed simultaneously to study thermal degradation. The results show obvious changes in the mechanical, physical and chemical properties of membranes caused by plasticizer loss. Surface microstructure becomes stiffer, which leads to contractions and the prevalence of voids. In cross-sectional area, average thickness values decrease. Due to the degradation of the plasticized waterproofing membranes, the roofing area had to be completely replaced.

**Keywords:** degradation; waterproofing membranes; plasticized PVC; SEM; FTIR; TGA-DSC

## 1. Introduction

Poly(1-chloroethylene) (PVC) is formed by the polymerization of vinyl chloride monomers. It is one of the most commonly used thermoplastics in construction, automotive, electrical parts and packaging.<sup>1</sup> The properties of PVC can be significantly improved by adding plasticizers to make it more flexible and durable, which greatly expands its applications.<sup>2, 3</sup> Plasticized PVC membranes are among the most commonly used waterproofing materials for roofing and geotechnical applications. However, practice shows that roofing membranes undergo chemical and physical changes when exposed to the combined effects of heat from solar radiation, near ultraviolet radiation, atmospheric oxidation, moisture and air pollution over long periods of time.<sup>4</sup> As a result, plasticizers escape from the membranes through evaporation, leaching, and migration into other materials, causing significant changes in material flexibility, hardness, mass and elasticity.<sup>5</sup>

Despite extensive research in recent years in the field of testing of waterproofing membranes, there is still a

shortage of specific studies on the durability, repairability and performance of such materials in roofing applications. The performance of plasticized PVC membranes has been evaluated by Dunn et al.<sup>6</sup> who exposed the membranes to different climatic conditions for 4.5 years and reported the loss of plasticizer by evaporation. Similarly, Audouin et al.<sup>7</sup> showed that increased temperature affects the migration of plasticizer from the membranes. They analysed the mass loss kinetics of plasticized PVC between 85 °C and 120 °C. Ito and Nagai<sup>8</sup> investigated the influence of artificial ageing conditions on plasticized PVC. They found obvious changes in mechanical properties and microstructure through the thickness difference caused by plasticizer loss. Beer et al.<sup>9</sup> investigated the long-term behaviour of plasticized PVC at different locations in Europe and North America. They confirmed reduced low-temperature flexibility and elongation at break points following plasticizer migration. Blanco et al.<sup>10</sup> investigated the long-term behaviour of high-density polyethylene (HDPE), ethylene-propylene-diene monomer (EPDM) and plasticized PVC membranes, and reported that the shear strength of



joints remained relatively unaffected by ageing despite the loss of plasticiser. Kositchaiyong et al.<sup>11</sup> studied anti-fungal performance and mechanical-morphological properties of PVC and wood/PVC composites under the influence of soil and UV light, and concluded that UV weathering reduced the antifungal performance of the material from 81.4% to 28.3%. Recently, environmental and economic comparisons of the life cycle performance of bituminous, synthetic, liquid and cement-based membranes suitable for flat roofs were reviewed by Goncalves et al.<sup>12</sup> Paolini et al.<sup>13</sup> investigated twelve roofing membrane products made of modified bitumen, PVC and polyolefin with different spectral reflectances in terms of energy demand for building cooling. It was found that weathering, soiling and biological growth significantly affect their solar reflectance and thus increase the energy consumption for air conditioning. Furthermore, as shown in our previous study, natural ageing under high humidity and thermal fluctuations can strongly influence the surface morphology and chemical composition of fibrous insulation material covered with plasticized PVC.<sup>14</sup> A probable reason for the deterioration of the insulation was the damaged waterproofing PVC membrane. To ensure a fully functional and repair-free lifetime of a building, the degradation and durability estimation of covering water-repellent PVC-P membranes must be considered.

The objectives of this study were to evaluate the basic properties of plasticized PVC membranes and to measure

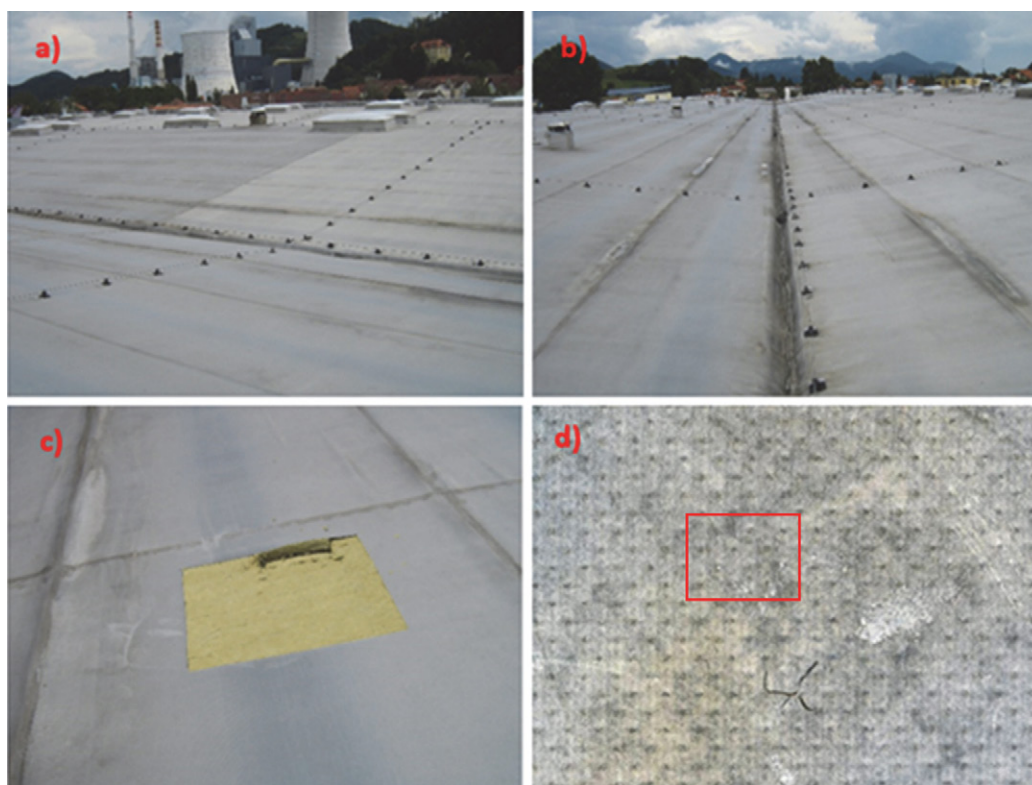
the level of degradation by comparing unused membranes and weathered (aged) membranes from a flat roofing area. To the best of the authors knowledge, little information was reported in the literature on plasticized PVC membranes reinforced with a polyester mesh that can be used for mechanically fixed roof systems above thermal insulation. First, the mechanical properties and wettability of these membranes were comprehensively evaluated. Secondly, morphological changes in the microstructure were evaluated to determine the thickness and prevalence of voids that were probably created by plasticizer loss. To explain such plasticizer loss in the material, chemical changes were identified and quantified. Finally, the thermal stability of the samples was examined to determine the degree of thermal degradation

## 2. Material and Characterization Methods

New plasticized PVC membranes and membranes from the flat roof area, which are about 10 years old, were comprehensively analysed in a laboratory using various techniques.

### 2. 1. Samples from the Case Study

1.2 mm thin Standard Grey RAL 7047 plasticized PVC membranes reinforced with polyester mesh (Flagon



**Figure 1.** Plasticized PVC waterproofing membranes were taken from a flat industrial roof located in Slovenia, Central Europe (a, b) Extraction at sampling location 1 (c). Naturally aged and locally damaged plasticized PVC membrane (d).

SR, Soprema, Italy) were obtained from the unvented roof of an industrial building located in Slovenia, Central Europe, which is characterized by a Cfb climate zone (Figure 1 a,b,c). Membranes are made of 51% pure PVC, 46% additives and 3% reinforcing material. The roof construction consisted of several layers: on top, a 1.2 mm thick plasticized PVC membrane; below, a 200 mm thick layer of thermal insulation with a density of 150 kg/m<sup>3</sup>, followed by a 0.3 mm thick vapor barrier and trapezoidal sheet metal cladding anchored in steel roof beams (Appendix 1). An inspection revealed that the waterproofing membranes were damaged at several points where the photovoltaic modules were installed; the damage was visible as star-shaped cracks (Figure 1. d).

Samples exposed to natural outdoor weathering were taken from various sampling locations, as shown in Appendix 2. Location 1 is an area with many visible star-shaped cracks on the surface of membranes. Location 2 is an area where a strong colour variation of the membranes was observed. Location 3 is a softening roofing area where a significant deterioration in the strength of the insulation has been observed. Plasticized PVC membranes were taken from each of these roofing areas, immediately wrapped in polyethylene, and transported to the laboratory for further analysis.

Plasticized PVC membranes are produced by cast spreading, whereby a spreading head applies a substrate of a liquid-viscosity raw material called “plastisol”. The spreading and gelation process is repeated four times, creating a membrane of four differently formulated layers. Between the second and third layers an inner reinforcing layer of polyester mesh is inserted. This process creates a molecular bond between the layers, resulting in a homogeneous, elastic, single-layer membrane.<sup>15</sup>

## 2. 2. Mechanical Testing

The mechanical performance of new, unused PVC membranes and aged membranes from the roof area was measured with a Zwick/Roell Z010 universal testing machine according to standard EN 12311-2. The length of the samples was 200 mm and width 50 mm. At an elongation of 1% and 2%, the secant modulus of elasticity was measured at a cross-head speed of 1.25 mm/min. After exceeding a deformation of 2%, samples were measured with a test cross-head speed of 200 mm/min until they broke. All specimens were tested in longitudinal and transverse directions using the same test method under laboratory conditions  $T = 393.15 \pm 2$  K, RH (relative humidity) = 50 ± 5 %.

## 2. 3. Contact Angle Measurement

The wettability of plasticized membranes was assessed with an exact experimental procedure. Droplets of milli-Q water (a specific resistance of 18.2 μΩ) with exact sizes of 10 μl were formed on a membrane with a micropi-

ette. Droplets were filmed with a Basler Aca1300-200um digital camera equipped with a Basler Premium Lens with C-mount, connected to a computer using the OpenDrop algorithm to calculate the contact angles.<sup>16</sup> To avoid optical aberrations and the fake reflections from other sources that can occur at the drop edge, the drop of was lit from the opposite side with a diffusion light, which was achieved by placing a glass diffuser between the light source and the sessile drop. The undesired effect of drop oscillation was minimized by using an anti-vibration table.

## 2. 4. Thickness Evaluation, Surface Morphology and Chemical Characterization

The thickness evaluation and morphological changes in aged membrane microstructure were scanned using ESEM (Environmental Scanning Electron Microscopy) Quanta 200 3D (FEI Company, Hillsboro, OR). Chemical modifications were identified and quantified using Fourier Transform Infrared Spectroscopy (FTIR) analysis on a Bruker Tensor 27 DTGS spectrometer in attenuated total reflection (ATR) mode between 4000 and 450 cm<sup>-1</sup> with an average of 32 consecutive scans and a resolution of 4 cm<sup>-1</sup>.

## 2. 5. Low-temperature Flexibility

Low-temperature flexibility is an important membrane property, especially during the application phase. Normally, the flexibility of membranes decreases significantly along with the surrounding temperature.<sup>9</sup> A test of low-temperature resistance was carried out according to the SIST EN 495-5 standard. This European Standard specifies a method for the determination of the behaviour of plastic and rubber sheets for waterproofing to folding after exposure at a low temperature. The examined samples were folded at 180° and conditioned for 12 h at low temperatures in a chamber. The occurrence of cracks in the samples indicates that the material is not resistant to low temperatures.

## 2. 6. Thermal Degradation

Thermogravimetric analysis and thermal transition of material samples were carried out using a TGA/DSC (Differential Scanning Calorimetry) instrument (Mettler Toledo). The investigated material was placed in separate vials and heated in an N<sub>2</sub> atmosphere at a rate of 20 K/min from 298 K to 1273 K. Mass loss was measured as a consequence of thermal degradation of membrane layers.

# 3. Results and Discussion

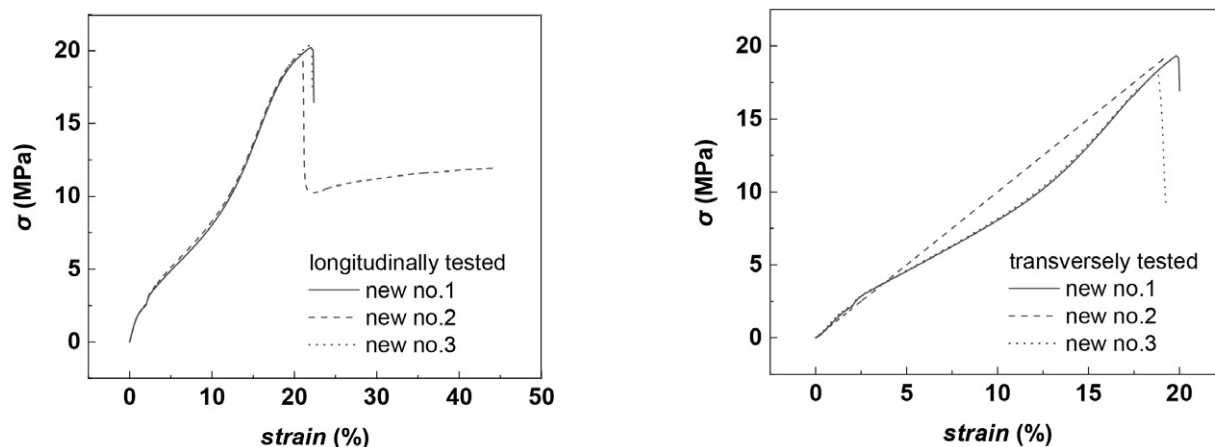
## 3. 1. Mechanical Performance

The maximum tensile strength in MPa ( $\sigma$ ) and the elongation at break in % ( $\epsilon$ ) were determined for samples

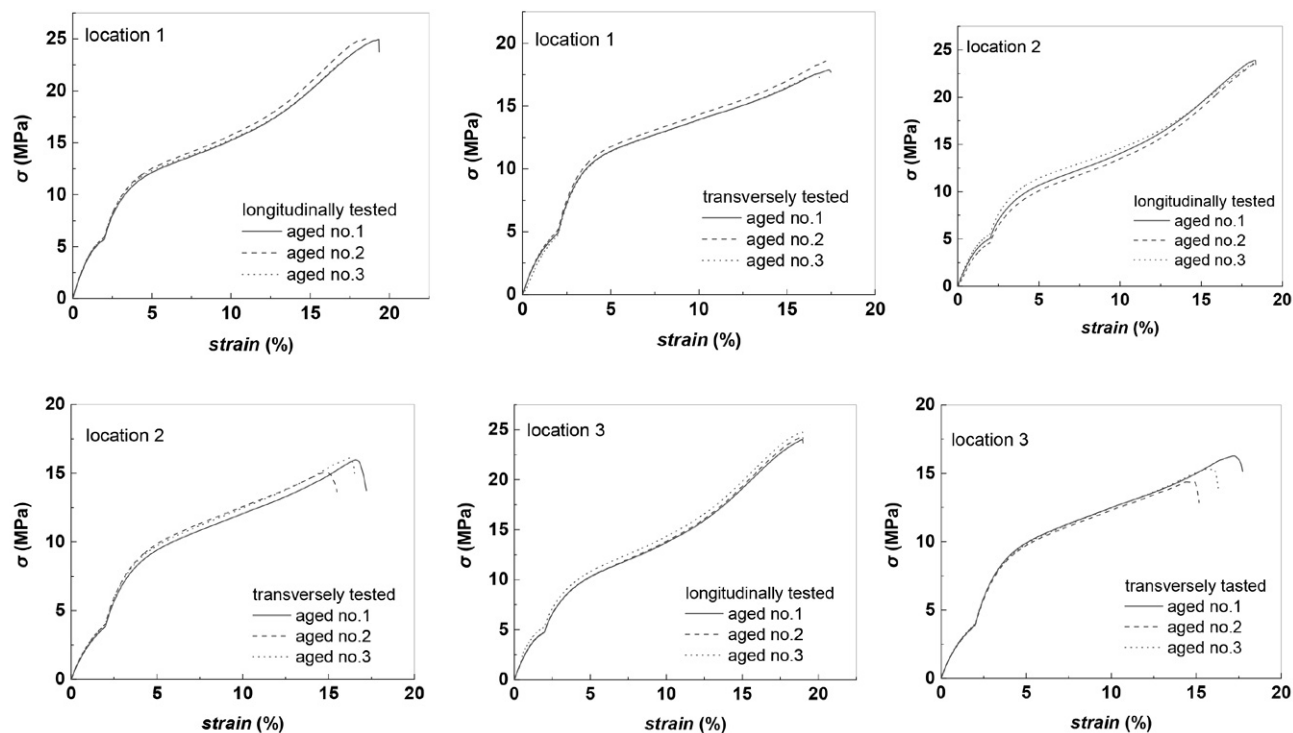
after 10 years of use and the values were compared with those of new samples (Figures 2 and 3). Three samples were tested from each sampling location. As can be seen in Figure 3, there is a small variation in tensile strength in the longitudinal direction of aged membranes. It appears that the polyester mesh is well encapsulated within the membrane matrix and has not degraded over time. In addition, there is a tendency for tensile strength to increase with age, as the membrane loses flexibility over time.<sup>9</sup> Similar observations were made in a study by Blanco et al.<sup>10</sup>, where both load and tensile strength in longitudinal and transversal

directions were evaluated for 35-year-old geomembranes with reinforced polyester.

On the other hand, the strength of aged membranes decreases in the transverse directions compared to the strength of a new membrane. As shown in Table 1, aged membrane samples showed a shorter elongation at break than that of the new membrane. This indicates a loss of flexibility caused by natural aging under high humidity and thermal fluctuations. The deterioration in elastic properties is caused by the loss of plasticizers as a result of a long period of combined exposure to heat from solar



**Figure 2.** Tensile strength and elongation at break (load/strain curves) for new plasticized PVC membrane samples tested longitudinal (left) and transverse (right) directions at conditions:  $T = 393.15 \pm 2$  K, RH (relative humidity) =  $50 \pm 5$  %.



**Figure 3.** Tensile strength and elongation at break (load/strain curves) for aged, plasticized PVC membrane samples tested longitudinal (left) and transverse (right) directions at conditions:  $T = 393.15 \pm 2$  K, RH (relative humidity) =  $50 \pm 5$  %.

radiation, ear-ultraviolet radiation, atmospheric oxidation, humidity and air pollution.<sup>17</sup> It was found that the influence of plasticizer content has a certain influence on elongation, but a mixed influence on the tensile strength of membranes reinforced with polyester mesh. Despite sufficient tensile strength, the wettability properties of these membranes were strongly influenced by age.

**Table 1.** Tensile strength and elongation at break.

Sample	$\sigma$ (MPa)		$\epsilon$ (%)	
	longitudinally		transversely	
New	20.23	<b>22.36</b>	19.17	<b>20.01</b>
	18.68	<b>44.54</b>	19.27	<b>20.51</b>
	20.43	<b>22.16</b>	18.17	<b>19.28</b>
Location 1	24.94	<b>19.34</b>	17.88	<b>17.48</b>
	25.16	<b>18.79</b>	18.57	<b>17.16</b>
	22.53	<b>16.76</b>	17.54	<b>16.83</b>
Location 2	23.90	<b>18.36</b>	15.91	<b>17.21</b>
	23.55	<b>17.31</b>	15.04	<b>15.49</b>
	23.70	<b>18.39</b>	16.12	<b>16.51</b>
Location 3	24.01	<b>19.96</b>	16.26	<b>18.96</b>
	24.26	<b>19.99</b>	14.38	<b>17.73</b>
	25.27	<b>19.96</b>	15.29	<b>16.29</b>

### 3. 2. Contact Angle and Wettability

The surface wettability of the membranes was evaluated by measuring the contact angles of sessile droplets. As can be seen from Table 2, the contact angles of new

plasticized PVC membranes remain almost constant within 180 seconds and have a significantly higher initial contact angle compared to the aged samples. In contrast, the contact angle for aged membranes is significantly reduced from  $56.1^\circ \pm 2.5^\circ$  at 10s to  $16.5^\circ \pm 4.5^\circ$  at 30 seconds and becomes zero after 120 seconds (Table 3, 4 and 5). Despite the good mechanical performance, the water repellence of these membranes is strongly impaired. Increasing the hydrophilicity of the aged membrane increases the unwanted water permeability and can cause damage in other roof layers.<sup>18</sup>

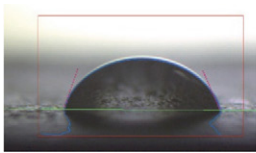
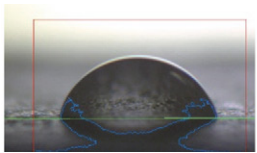
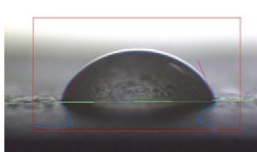
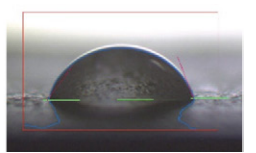
### 3. 3. Surface Morphology

As mentioned above, the distribution and loss of plasticizer in the membrane can play an important role in tensile strength and elongation at break as well as in wettability properties. Change in surface of membranes that may result in the loss of plasticizer was also demonstrated by observation of micrographs from scanning electron microscopes (SEM).

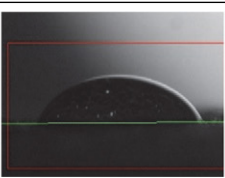
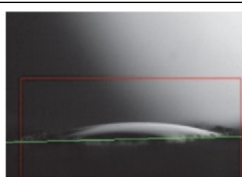
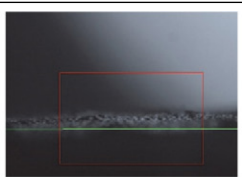
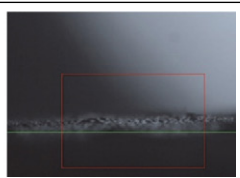
#### 3. 3. 1. Microstructure

Microphotographs of new and aged membranes taken by SEM show significant differences between them. As shown in Figure 4, new membranes have a smooth surface, without cracks. Locally, only the grains of filler can be observed. In contrast, aged membranes that have been exposed to natural weathering show irritated surfaces with many cracks, agglomerates and craters as a result of plasticizer loss. The material becomes stiffer, which leads to

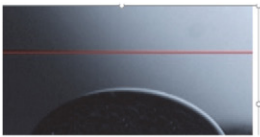
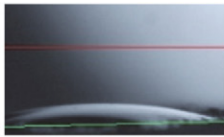
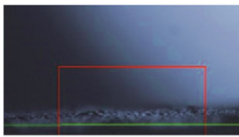
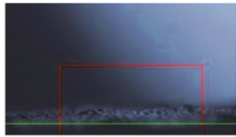
**Table 2.** Time-dependent contact angles of water droplets on new plasticized PVC membranes.

CA	$69.4^\circ \pm 1.1^\circ$	$68.2^\circ \pm 1.5^\circ$	$66.5^\circ \pm 0.8^\circ$	$65.11^\circ \pm 0.5^\circ$
				
t (s)	10 s	30 s	120 s	180 s

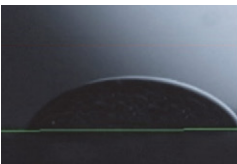
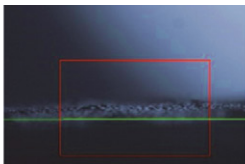
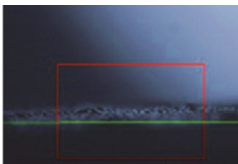

**Table 3.** Time-dependent contact angles of water droplets on naturally aged and damaged plasticized PVC membranes (location 1).

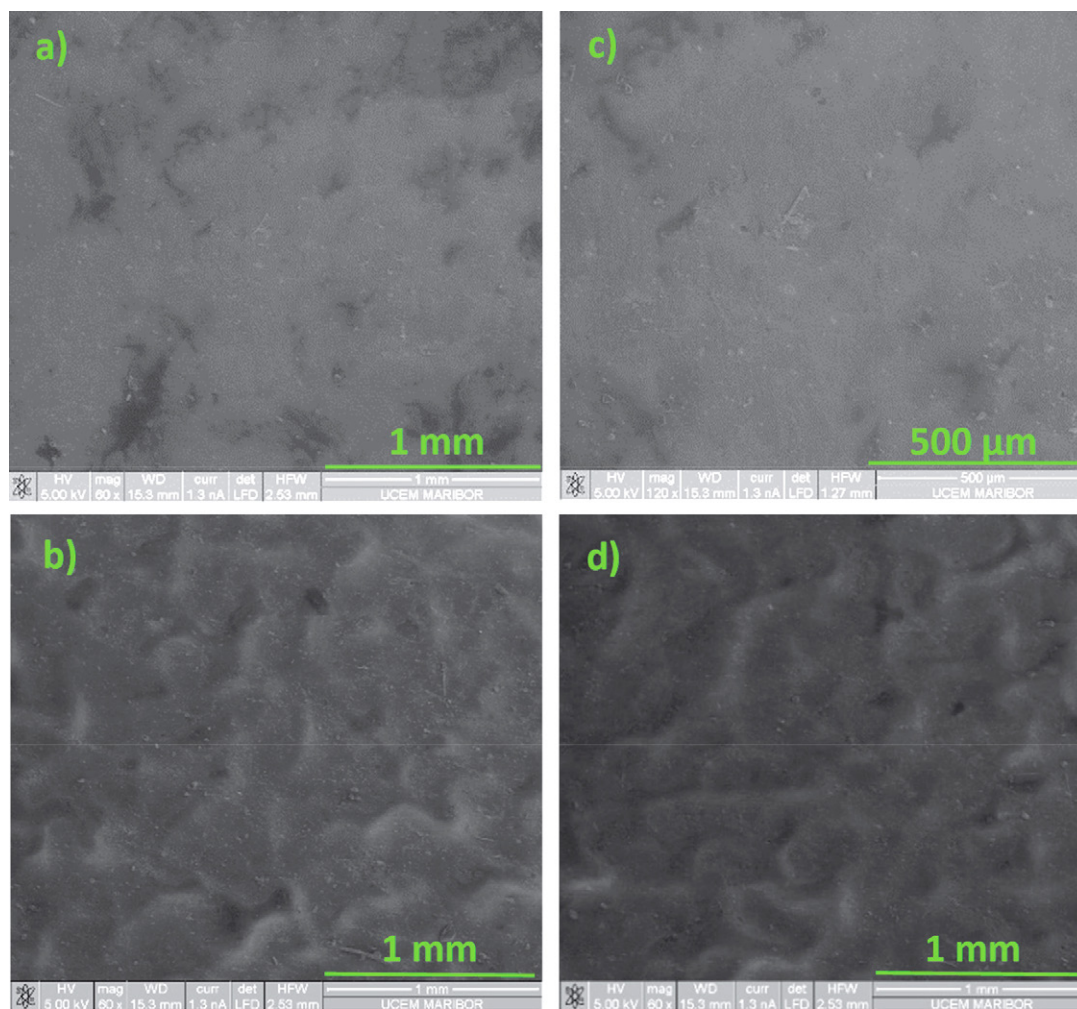
CA	$56.1^\circ \pm 2.5^\circ$	$16.5^\circ \pm 4.5^\circ$	/	/
				
t (s)	10 s	30 s	120 s	180 s

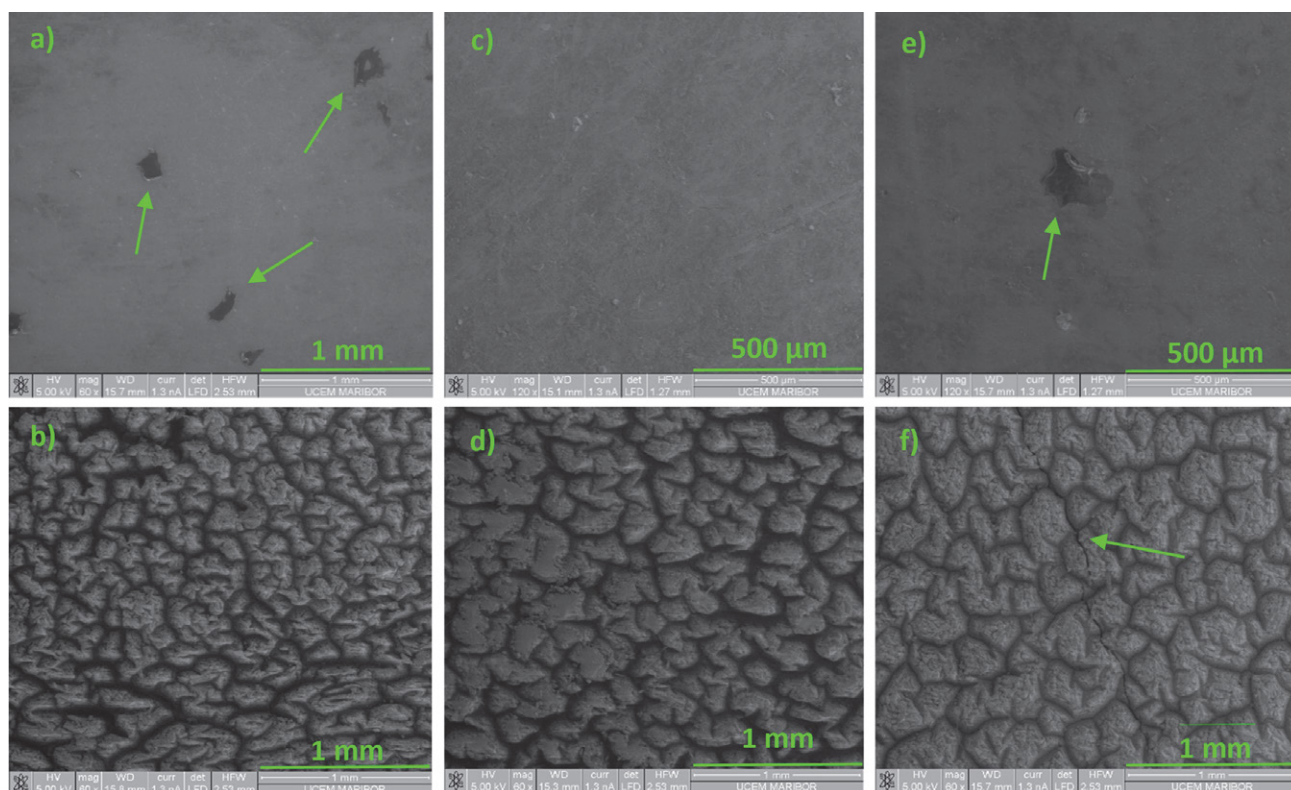
**Table 4:** Time-dependent contact angles of water droplets on naturally aged and damaged plasticized PVC membranes (location 2).

CA	$54.1^{\circ} \pm 1.5^{\circ}$	$18.5^{\circ} \pm 3.5^{\circ}$	/	/
				
t (s)	10 s	30 s	120 s	180 s

**Table 5:** Time-dependent contact angles of water droplets on naturally aged and damaged plasticized PVC membranes (location 3).

CA	$52.1^{\circ} \pm 4.5^{\circ}$	/	/	/
				
t (s)	10 s	30 s	120 s	180 s

**Figure 4.** Microstructure of new membranes' upper layer (a, c) and lower layer (b, d).



**Figure 5.** The microstructure of aged membranes extracted from different sampling locations: 1 (a, b), 2 (c, d), and 3 (e, f). The surface is more heterogeneous, with many craters, cracks, agglomerates, and voids.

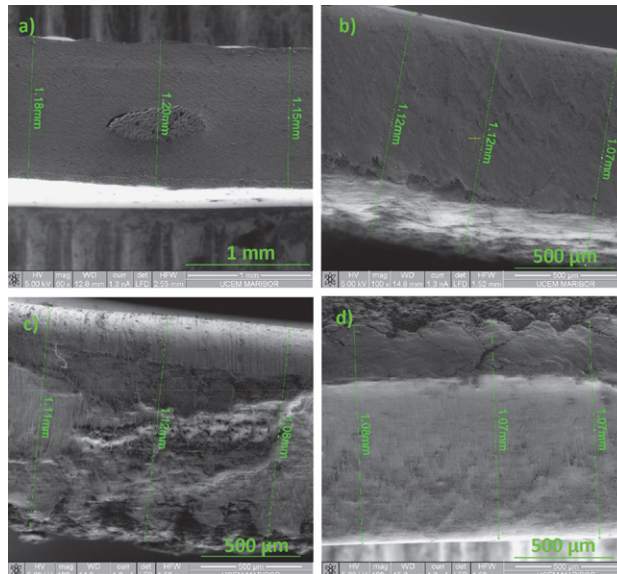
contractions and the prevalence of voids (Figure 5). It is assumed that the rearrangement and aggregation of molecular chains are the main mechanisms of membrane degradation.<sup>19</sup> Pedrosa et al.<sup>20</sup> presented an interesting study using X-ray spectroscopy and SEM analysis of membranes exposed to different weathering conditions. They reported that aged membranes show numerous cracks and fractures and there is a significant decrease in chlorine content. Therefore, they suggested that dehydrochlorination may be the main mechanism of deterioration.

### 3. 3. 2. Thickness Evaluation

Cross-sectional microphotographs with thickness evaluations of the investigated plasticized PVC membranes are presented in Figure 6 and Table 6. It can be seen that the thickness of the aged membranes is decreased. As can be seen in Figure 6, there is also a visible difference in cross-sectional area between new and aged membranes.

**Table 6.** Thickness of the new and aged membranes.

Samples	Average value (mm)	Standard deviation (%)
Location 1	1.17	1.25
Location 2	1.11	1.63
Location 3	1.09	1.63
New	1.18	2.05

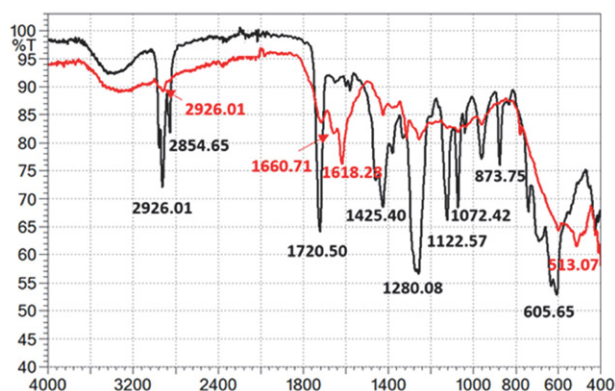


**Figure 6.** Microphotographs in cross section with thickness evaluation for new membrane (a) and aged membranes (a, b, c).

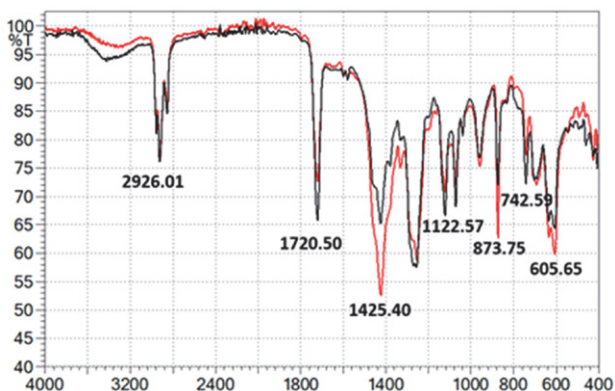
For example, the average thickness values for location 3 decrease from 1.18 mm to 1.09 mm. Changes in material thickness might be because of the reduction of plasticizer content. To justify plasticizer loss in material, chemical changes were identified and quantified using ATR/FTIR analysis.

### 3. 4. ATR/FTIR Analysis

FTIR spectra were recorded to investigate the chemical changes in the aged membranes from location 3 (with the highest exposed to solar radiation, near-ultraviolet radiation, atmospheric oxidation and moisture. Both the front (directly exposed to weathering) and side (inverted next to the insulation material) surfaces of the membranes were examined (Table 7, Figure 7 and 8). In FTIR, the spectra appearance of several characteristic bands can be seen. In particular, the C=O stretching vibration of the ester function from plasticizer is detected at  $1720.50\text{ cm}^{-1}$ . O-H bending is detected at  $1425.40\text{ cm}^{-1}$  and symmetric and antisymmetric vibrations of the ester C-O-C group in the region  $1072.42 - 1280.08\text{ cm}^{-1}$ . At the front side of aged membrane new peaks appear at  $1660.71-1618.28\text{ cm}^{-1}$  that are associated with the stretching of the C=C bonds of the aromatic ring, indicating that chemical degradation appeared in the membrane molecules<sup>21</sup>. Compared to the front side of new membranes, the characteristic C-Cl stretching vibration at  $642.95-605.65\text{ cm}^{-1}$  is not visible. This suggests that UV aging could have caused a dehydrochlorination reaction. These data are consistent with changes in the



**Figure 7.** FTIR spectra at the front side of the new plasticized membranes (black line) and aged membranes (red line) operating in attenuated total reflection (ATR) mode.



**Figure 8.** FTIR spectra at the back side of the plasticized membranes (black line) and aged membranes (red line) operating in attenuated total reflection (ATR) mode.

membrane morphology and elongation properties. On the back side of the membranes there is no visible difference in spectra between new and aged samples. The C-H stretching mode can be observed at  $2954.95-2852.72\text{ cm}^{-1}$  and the *trans* C-H wagging mode at  $873.75\text{ cm}^{-1}$ <sup>22</sup>.

**Table 7:** Main FTIR bands for the front and back sides of plasticized PVC membranes.

	Wavenumber, $\text{cm}^{-1}$	Chemical Group
<b>Front side (new)</b> vibration	2954.95–2854.65	C-H stretching
	1720.50	C=O stretching
	1425.40–1379.10	O-H bending
	1280.08	C-O stretching
	1122.57–1039.63	C-O stretching
	873.75	C-H bending
<b>Front side (aged)</b>	740.67–605.65	C-Cl stretching
	2926.01	C-H stretching
	1660.71–1618.28	C=C stretching
<b>Back side (new and aged)</b>	1253.73	C-O stretching
	2954.95–2852.72	C-H stretching
	1720.50	C=O stretching
	1425.40	O-H bending
	1122.57	C-O stretching
	742.95–605.65	C-Cl stretching

### 3.5 Low-temperature Flexibility

Three 50 mm wide rectangular samples from each sampling location were folded between two metal plates and then stored in a chamber to allow them to cool to the desired test temperature. In the first experiment, all samples were subjected for 12 h to the temperature of 248 K ( $-25\text{ }^{\circ}\text{C}$ ). New samples meet the requirement according to the standard SIST EN 495-5 and stay unaltered after  $180^{\circ}$  bending around a small radius. In contrast, the flexibility of all aged membranes decreased significantly. Visible cracks were observed on the surface of the membranes and it was also possible to see into the polyester reinforcement in the upper layer of the membrane.

In the second experiment, the lowest temperature at which aged samples stay visually unaltered (without cracking) was recorded (Figure 9 a). The reproducibility of the test method was  $\pm 5\text{ K}$ . There is a clear difference in low temperature flexibility between new and aged membranes. As can be seen in Figure 9, aged membranes are resistant to low temperature bending up to  $278 \pm 5\text{ K}$ , while new ones are resistant to 238 K. The results are in accordance with those in a study by Beer et al., who performed similar tests on PVC membranes after long-term exposure.<sup>9</sup> Although flexibility is mainly an issue during installation and roof maintenance, the obtained results are important to understand the long-term behaviour of membranes.

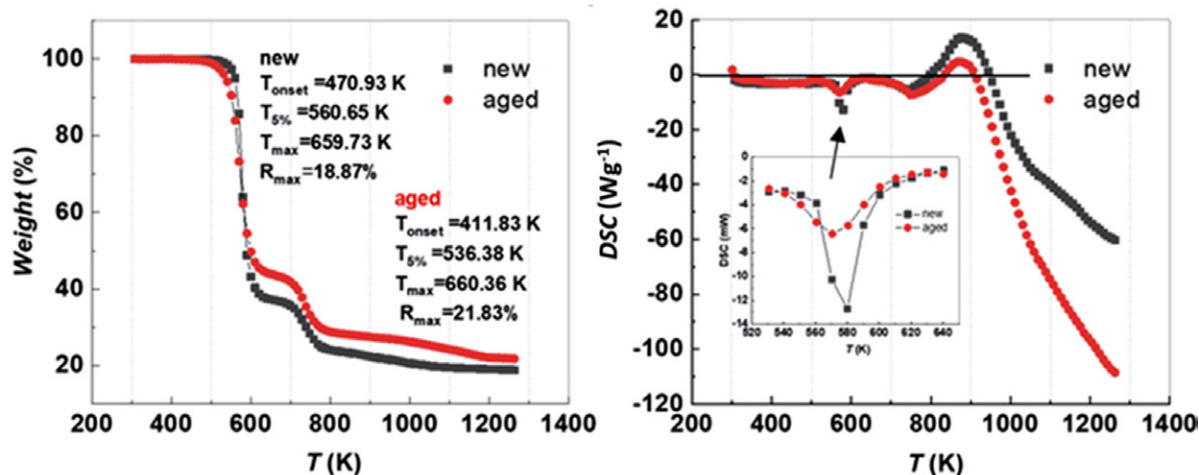


Figure 9. The lowest temperature at which aged samples stay visually unaltered (a). Cracks were observed along the upper layer of aged membranes after exposure to the temperature of 248 K ( $-25\text{ }^{\circ}\text{C}$ ) (b).

### 3. 6. TGA-DSC Analysis

Figure 10 shows the thermal properties of a new membrane and an aged membrane (from location 3) heated in nitrogen at a temperature range from 298 K up to 1273 K. The TG characteristic temperatures of the membranes are illustrated in Figure 10, including the onset temperature ( $T_{\text{onset}}$ ), 5% weight loss temperature ( $T_{5\%}$ ), the temperature at the maximum degradation rate ( $T_{\text{max}}$ ), and the maximum degradation rate ( $R_{\text{max}}$ ). It can be observed that new membranes have relatively high thermal stability below 470.93 K. In the case of aged membranes, the weathering effects led to a decrease in the  $T_{\text{onset}}$  value from 470.93 K to 411.83 K, and for  $T_{5\%}$  from 560.65 K to 536.38 K. This seems to confirm that weathering aging over a long period of time resulted in degradation of the membrane molecules, as suggested by FTIR analysis.

The initial negative heat flux shows that the decomposition reactions occur due to the heating of PVC,

plasticizers and polyester mesh. In this step, dehydrochlorination takes place, producing HCl molecules.<sup>23</sup> In the temperature range from 540 K to 650 K, both membranes show a characteristic endothermic deviation from baseline, which is more evident in a new sample (Figure 10). The increase in heat flux at about 880 K could correspond to an exothermic transformation caused by crystallization of the samples. HCl is released from the melt and the molecules are rearranged by cross-linking reactions. Above 1273 K, the total charring of the membranes corresponds to a high negative heat flux.

## 4. Conclusions

The results of the measurements reaffirmed the sensitivity of plasticized PVC membranes reinforced with polyester mesh used for mechanically fixed unvented roof

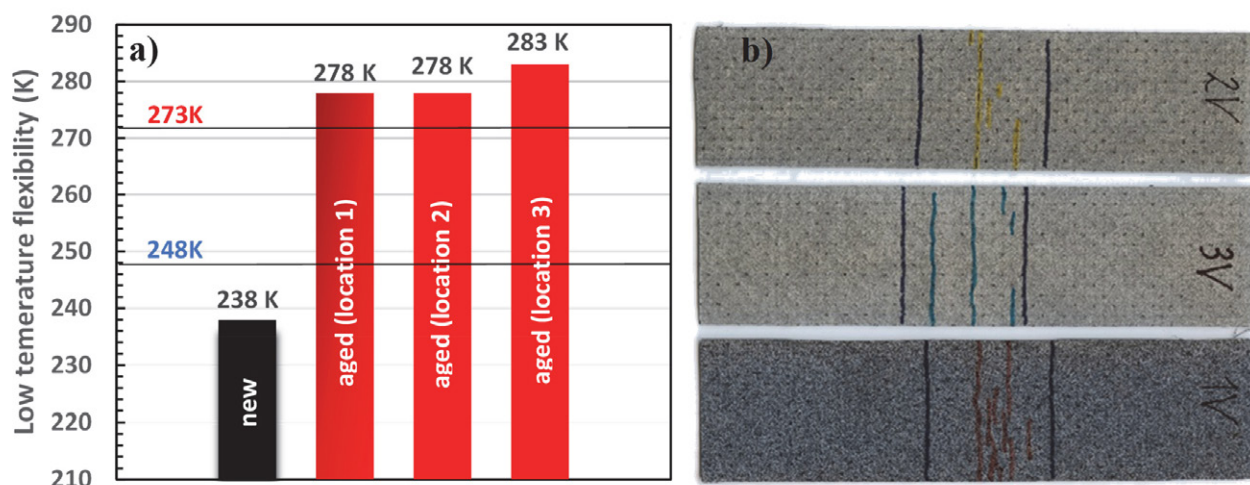


Figure 10. Results of the TGA-DSC analysis for new and aged membranes from location 3.



systems over thermal insulation. During 10 years of use, plasticized PVC gradually degraded, and its primary physical, chemical and mechanical properties changed. This tendency was observed in all three sampling locations. Therefore, the roofing area had to be completely replaced. The main conclusions are:

- there is a tendency for tensile strength to increase with age. It appears that the polyester mesh is well encapsulated within the membrane matrix,
- aged membrane samples exhibited shorter elongation at break than new ones. This indicates a loss of flexibility under high humidity and thermal fluctuations,
- wettability properties of examined membranes were highly affected by age,
- the surface of aged membranes is more heterogeneous than that of new ones, containing many craters, cracks, agglomerates, and voids. Similarly, the thickness of the aged membranes decreased probably due to the migration of plasticizer content,
- FTIR analysis confirmed the chemical changes in aged membranes. New peaks appear at 1660.71–1618.28  $\text{cm}^{-1}$ , indicating that chemical degradation had occurred in the membrane molecules,
- when low-temperature flexibility tests were performed, visible cracks were observed along the aged membranes,
- thermal analysis revealed that the weathering aging effects resulted in reductions of  $T_{\text{onset}}$  and  $T_{5\%}$ .

To reduce degradation and increase the durability of PVC membranes, new durable additives and plasticizers that are resistant to heat from solar radiation, near-ultraviolet radiation, atmospheric oxidation and moisture should be used. In future studies, we will use time-temperature superposition models to assess the effect of aging on waterproofing membranes.

## Acknowledgments

The authors would like to acknowledge the Slovenian Research Agency (ARRS) for partly financing this research within the frame of program P2-0046.

## Conflicts of Interest

The authors declare no conflict of interest.

## 5. References

1. Y. Ma, S. Liao, Q. Li, Q. Guan, P. Jia and Y. Zhou, *React Funct Polym.* **2020**, *147*, 637–642.
2. Z. Kormosh, I. Hunka and Y. Bazel, *Acta Chim. Slov.* **2008**, *55*, 261–267. DOI:10.1002/jccs.200800052
3. M. Shamsipur, S. Sahari, M. Payehghadr and K. Alizadeh, *Acta Chim. Slov.* **2011**, *58*, 555–562.
4. M. Zagorodnikova, V. Yartsev and V. Rupyshev, *Adv. Mater. Technol.* **2019**, *2*, 41–47.
5. M. Londschien and M. Bonnet, *J. Appl. Polym. Sci.* **2018**, *135*, 46689. DOI:10.1002/app.46689
6. P. Dunn, D. Oldfield and R. Stacewicz, *J. Appl. Polym. Sci.* **1970**, *14*, 2107–2116. DOI:10.1002/app.1970.070140818
7. L. Audouin, B. Dalle, G. Metzger and J. Verdu, *J. Appl. Polym. Sci.* **1992**, *45*, 2091–2096. DOI:10.1002/app.1992.070451204
8. M. Ito and K. Nagai, *Polym. Degrad. Stab.* **2007**, *92*, 260–270. DOI:10.1016/j.polymdegradstab.2006.11.003
9. H. Beer, A. Delgado, R. Paroli and S. Graveline: 10DBMC International Conference On 10. Durability of Building Materials and Components LYON, International AG, Industriestrasse, Lyon, France **2005**, 1–7.
10. M. Blanco, N. Touze-Foltz, M. Pérez Sánchez, M. Redón-Santafé, F.-J. Sánchez Romero, J. B. Torregrosa Soler and F. A. Zapata Raboso, *Geosynth. Int.* **2018**, *25*, 85–97. DOI:10.1680/jgein.17.00035
11. A. Kositchaiyong, V. Rosarpitak, H. Hamada and N. Sombatsompop, *Int. Biodeterior. Biodegradation* **2014**, *91*, 128–137. DOI:10.1016/j.ibiod.2014.01.022
12. M. Gonçalves, J. D. Silvestre, J. de Brito and R. Gomes, *J. Build. Eng.* **2019**, *24*, 100710. DOI:10.1016/j.job.2019.02.002
13. R. Paolini, M. Zinzi, T. Poli, E. Carnielo and A. G. Mainini, *Energy Build.* **2014**, *84*, 1 333–343. DOI:10.1016/j.enbuild.2014.08.008
14. A. Ivanič, G. Kravanja, W. Kidess, R. Rudolf and S. Lubej, *Materials*, **2020**, *13*, 2392. DOI:10.3390/ma13102392
15. Flagon, <https://pdf.archiexpo.com/pdf/soprema/flagon/3193-66009.html>.
16. E. Huang, A. Skoufis, T. Denning, J. Qi, R. R. Dagastine, R. F. Tabor and J. D. Berry, *J. Open Source Softw.* **2021**, *58*, 2604
17. M. Lenartowicz, B. Swinarew, A. Swinarew and G. Rymarz, *Int. J. Polym. Anal. Charact.* **2014**, *19*, 611–624. DOI:10.1080/1023666X.2014.933071
18. A. Behboudi, Y. Jafarzadeh and R. Yegani, *Chem. Eng. Res. Des.* **2016**, *114*, 96–107. DOI:10.1016/j.cherd.2016.07.027
19. Y. Fu and J. R. Lakowicz, *Nature*, **2011**, *472*, 178–179. DOI:10.1038/472178a
20. A. Pedrosa and M. Del Río, *Materiales de Construcción* **2017**, *67*, 109. DOI:10.3989/mc.2017.08915
21. A. Royaux, I. Fabre-Francke, N. Balcar, G. Barabant, C. Bollard, B. Lavédrine and S. Cantin, *Polym. Degrad. Stab.* **2017**, *137*, 109–121. DOI:10.1016/j.polymdegradstab.2017.01.011
22. S. Ramesh, K. H. Leen, K. Kumutha and A. K. Arof, *Spectrochim. Acta A Mol. Biomol. Spectrosc.* **2007**, *66*, 1237–1242.
23. A. Marongiu, T. Faravelli, G. Bozzano, M. Dente and E. Ranzi, *J. Anal. Appl. Pyrolysis.* **2003**, *70*, 519–553. DOI:10.1016/S0165-2370(03)00024-X

## Povzetek

Z namenom ugotoviti vzroke degradacije in preučiti vplivov naravnega staranja na obstojnost plastificiranih polivinilkloridnih membran, smo izvedli vzorčenje poškodovanih membran iz industrijskih strešnih kritin in jih primerjali z novimi. Določili smo natezne trdnosti, stopnjo elongacije do pretrga, in omočljivost membran. Nato smo z uporabo skenirane elektronske mikroskopije (SEM) analizirali morfološke mikrostrukturne spremembe in določili debeline membran. Za preučevanje kemijskih sprememb v starih membranah smo uporabili Fourierevo analizo z infrardečo spektroskopijo (FTIR). Z namenom preučevanja toplotne razgradnje smo uporabili termogravimetrično analizo in diferenčno dinamično kalorimetrijo (TGA-DSC). Rezultati nakazujejo na očitne spremembe mehanskih, fizikalnih in kemijskih lastnosti poškodovanih membran, kar nakazuje na zmanjšanje vsebnosti plastifikatorja. Površina membran postane trša, kar povzroči krčenje in razširjenost praznin. Povprečne debeline membran na preseku se zmanjšajo. Zaradi degradacije hidroizolacije iz plastificiranega PVC-ja, je bilo strešno kritino potrebno zamenjati v celoti.



Except when otherwise noted, articles in this journal are published under the terms and conditions of the Creative Commons Attribution 4.0 International License

**DRUŠTVENE VESTI IN DRUGE AKTIVNOSTI**  
**SOCIETY NEWS, ANNOUNCEMENTS, ACTIVITIES**

**Vsebina**

Boris Krajnc in drugi kemiki na dachauskih procesih .....	S45
Poročilo o delu v letu 2020 .....	S67
Navodila za avtorje .....	S72

**Contents**

Boris Krajnc and other chemists involved in 1948/49 Dachau Trials in Slovenia .....	S45
Report for 2020 .....	S67
Instructions for authors .....	S72



Chemical education

# Boris Krajnc in drugi kemiki na dachauskih procesih

Marko Dolinar

Univerza v Ljubljani, Fakulteta za kemijo in kemijsko tehnologijo, Katedra za biokemijo, Večna pot 113, 1000 Ljubljana, Slovenija

\* Corresponding author: E-mail: marko.dolinar@fkkt.uni-lj.si

Received: 06-03-2021

## Povzetek

Boris Krajnc je bil prvi habilitirani učitelj ljubljanske univerze za področje biokemije – imenovanje v naziv docenta je datirano s 5. januarjem 1946. Vendar se je Krajncova življenjska pot zelo hitro končala, saj so ga 27. oktobra 1947 aretirali in 26. aprila 1948 na montiranem dachauskem procesu obsodili na smrt. Ustrelili naj bi ga 12. maja 1948, starega 34 let. Krajncova življenjska zgodba je tesno povezana z delom več slovenskih kemikov, ki so bili kot zaporniki v koncentracijskem taborišču Dachau izbrani za tehnično pomoč pri izvedbah poskusov na ljudeh ali pri delu v kliničnem laboratoriju. Na povojnih dachauskih procesih v Ljubljani je bilo skupaj obsojenih 8 kemikov, od teh jih je bilo 5 obsojenih na smrt in ustreljenih. V kasnejših presoajah dachauskih procesov se je izkazalo, da so bile obtožnice skonstruirane, priznanja pa pridobljena s krutimi zasliševalskimi metodami, zato so bile vse sodbe razveljavljene. Po emigraciji encimatika Richarda Klemna ter pregonu Maksa Samca in Marte Blinc z univerze je bil Boris Krajnc tisti, ki naj bi skrbel za biokemijo na Tehniški fakulteti. Po njegovi smrti je nekaj let biokemijo predaval Krajncov mlajši kolega Dušan Stucin z Medicinske fakultete, potem pa biokemije več let ni bilo v kemijskem kurikulumu.

**Ključne besede:** biokemija; dachauski procesi; Polygal; strjevanje krvi

## 1. Uvod

Dachauski procesi je skupno ime za politične procese v letih 1948 in 1949, v katerih je bilo skupaj obsojenih več kot 30 ljudi, med njimi številni na smrtno kazen. Med žrtvami teh procesov je bilo kar 9 kemikov<sup>1</sup>. Predhodnik dachauskih procesov je bilo sojenje za delovno nesrečo v hrastniški steklarni, ki jo je oblast želela prikazati kot sabotažo, vendar takrat tožilcu ni uspelo dovolj dobro utemeljiti obtožnice, zato so sodbo razveljavili. V nadaljevanju so preiskovalci natančno preverili pred- in medvojno delovanje tistih, ki so bili povezani s hrastniško steklarno in pri tem opazili povezave med strokovnjaki na nekaterih pomembnih položajih, ki jim je bilo skupno to, da so preživeli obdobje internacije v koncentracijskem taborišču Dachau (in nekateri Buchenwald), ter večinoma sodelovali kot tehnično osebje pri poskusih na ljudeh ali v laboratoriju taboriščne bolnišnice. Zaradi ustreznih znanj so to pogosto bili kemiki, zaradi pomembnosti dela, ki so ga opravljali, pa so v primerjavi z ostalimi interniranci imeli ugodnejše življenj-

ske razmere. Obtožnica jih je prikazala kot tajne agente Gestapa, ki so jih nemške oblasti poslale na prešolanje v taborišča, da bi se tam pomešali med rojake, pridobivali podatke in se kasneje vrnili v Slovenijo ter nadaljevali z delom kot agenti. Po vojni naj bi tujim agenturam posredovali podatke o stanju v Sloveniji in izvajali sabotaže. Hkrati naj bi se ti „agenti“ medsebojno podpirali pri pridobivanju vodilnih položajev v gospodarstvu in politiki.

Eden od obtoženih kemikov je bil Boris Krajnc, ki je komaj dobro leto in pol pred aretacijo postal docent za področje biokemije na Tehniški fakulteti ljubljanske univerze. Po Richardu Klemnu, ki je emigriral že leta 1942<sup>1</sup>, je bil Krajnc naslednji učitelj ljubljanske univerze, ki se je ukvarjal z biokemijskimi temami, vendar je Klemen po imenovanju za privatnega docenta predaval predvsem encimatiko in kmetijsko kemijo, Krajnc pa prav biokemijo, zato ga Fakulteta za kemijo in kemijsko tehnologijo Univerze v Ljubljani vodi kot docenta za področje biokemije (ob njegovem imenovanju področje habilitacije ni bilo definirano).

Sojenje Borisu Krajncu in drugim obsojenim na dachauskih procesih je bilo v naslednjih desetletjih večkrat strokovno obdelano in večina sodb je bila končno razveljavljenih leta 1976. Čeprav je res, da so nekateri slovenski

<sup>1</sup> Obtoženi so bili kemiki Karel Barle, Branko Diehl, Boris Fakin, Mirko Košir, Boris Krajnc, Vladimir Ličen, Mitja Sark in Milan Stepišnik. Mirko Pibernik je umrl med preiskavo, torej pred vložitvijo obtožnice.

kemiki sodelovali v psevdomedicinskih raziskavah v taborišču Dachau, njihovo sodelovanje pri tem ni bilo prostovoljno, oziroma dela niso mogli zapustiti po lastni želji, kot neutemeljene pa so se izkazale tudi druge točke obtožnic.

## 2. Življenjska pot Borisa Krajnc

Boris Krajnc (slika 1) se je rodil 25. decembra 1913 na Reki na Hrvaškem, kjer je bil oče Ivan posojilniški uradnik. Družina se je kmalu preselila v Celje, od koder je bila mati Franja, rojena Božič. Boris je v Celju opravil 5 razredov osnovne šole (1925) in nato 8 razredov realne gimnazije (maturiral je junija 1933 kot Borislav Krajnc). Oče je umrl decembra 1931, tako da je Boris ostal sam z mamo.



**Slika 1:** Fotografija B. Krajnc iz osebne izkaznice, datirane s 3. 3. 1946. Vir: Arhiv Republike Slovenija, SI AS 1931, RSNZ SRS, Dachauski procesi, šk. 512.

Leta 1933 se je vpisal na ljubljansko univerzo, kjer je na Tehniški fakulteti študiral kemijo. Diplomiral je pod mentorstvom Maksa Samca z nalogo »Metiliranje škrobvih substanc«. Strokovni del diplomske naloge je zagovarjal 29. septembra 1938, diplomska listina pa je datirana s 3. julijem 1939.

Študijski kolega Borisa Krajnc je bil Mirko (Friedrik) Dermelj (1914–2018), nečak Maksa Samca. Ko sta zaključila študij (na isti dan), je Samec Dermelja poslal

na izpopolnjevanje v Heidelberg<sup>II</sup>, njegovega prijatelja Krajnc pa v Berlin. S štipendijo v okviru mednarodne izmenjave študentov je od novembra 1938 do maja 1939 deloval na Kemijskem inštitutu cesarja Wihelma (nem.: Kaiser-Wilhelm-Institut für Chemie) v laboratoriju dr. Kurta Hessa (1888–1961), ki je bil zagret pristaš nacionalsocializma<sup>III</sup>. Skupaj s Hessom je Krajnc leta 1940 v reviji nemškega kemijskega društva »Berichte der deutschen chemischen Gessellschaft« objavil najprej kratek članek o določanju končnih skupin sestavin škroba<sup>2</sup>, nato pa v isti reviji še članek<sup>3</sup> z naslovom »O visokometiliranem škrobu in vprašanje njegovih cepitvenih sladkorjev« (soavtor tudi Hans Albrecht Schulze). V drugem članku je Krajnc zapisan napačno (Kranjc) in brez afilicije ljubljanske univerze.

Mirko Dermelj je ostal v Nemčiji do septembra, Krajnc pa le do maja 1939, torej 7 mesecev<sup>IV</sup>. Nato je Krajnc v starojugoslovanski vojski odslužil 9-mesečni »dijaški rok« v Kruševcu v Srbiji in to s položenim izpitom za rezervnega oficirja<sup>V</sup>; njegov zadnji čin je bil podnarednik. Vojaški rok sta služila z Dermeljem v isti vojašnici in sočasno, prav tako sta se leta 1940 oba zaposlila v železarni na Jesenicah. Krajnc je 15. septembra 1940 postal obratni asistent v Kranjski industrijski družbi (KID), ki je upravljala z železarno, vendar je bilo njegovo delovno mesto v opekarni. Pred izbruhom 2. svetovne vojne sta bila z Dermeljem in verjetno še nekaterimi drugimi slovenskimi kemiki mobilizirana v vojno-tehnični zavod Obiličevo v Kruševcu (Srbija). Ker pa so Kruševac že prvi dan vojne bombardirali, so se vojaki odpravili proti Sara-

II Dermelj se je usposabljal pri dr. Karlu Freudenbergu na Raziskovalnem inštitutu za kemijo lesa in polisaharidov na Univerzi v Heidelbergu do avgusta 1939. Za bivanje v Nemčiji je prejel nemško štipendijo. Ob izbruhu 2. svetovne vojne je moral zapustiti Heidelberg zaradi bližine Francije, ki je vstopila v vojno z Nemčijo<sup>4,5,6</sup>. Na zaslišanju novembra 1947 pa je Dermelj izjavil, da sta imela s Krajncem štipendijo ljubljanske univerze in da se je vrnil v Ljubljano že junija 1939. Ko so ga preiskovali zaradi očitane medvojnega oportunitizma, je izjavil, da je v Heidelbergu »zagovarjal svojo diplomsko nalogo« in da se Samec in Freudenberg strokovno nista dobro razumela.

III Hess je na inštitut prišel leta 1921 in ustanovil oddelek za kemijo celuloze. Leta 1931 je odšel v industrijo (IG Farben), a je ohranil status gostujočega sodelavca in še naprej vodil oddelek. Njegova nacistična usmerjenost se kaže s tem, da je prijavil fizičarko Lise Meitner, ki je bila avstrijska judinja – sicer pa tesna sodelavka direktorja inštituta, nobelovca Otta Hahna – verjetno v želji, da bi zamenjal Hahna na direktorskem mestu<sup>7</sup>.

IV V času izpopolnjevanja v Berlinu je prišlo verjetno do nekega nesoglasja, kar je mogoče razbrati iz navedbe Borisa Krajnc, ko je med preiskavo za Diehl-Oswaldov proces opisal značaj Maksa Samca. Tam je omenil, da so se stiki med Samcem in Hessom ohladili prav zaradi Krajncovega dela v Berlinu.

V Rekruti s končano srednjo šolo so do leta 1940 lahko za 9 mesecev vstopili v šolo za rezervne vojaške starešine, potem pa so polagali izpit. Če ga niso opravili, so morali nadaljevati s služenjem do dopolnjenih 14 mesecev (običajni rok je trajal 18 mesecev, v letalstvu in mornarici pa 2 leti). Septembra 1940 so z uredbo dijaški rok podaljšali na 12 mesecev, če so bili naborniki neuspešni pri končnem izpitu, pa so morali ostati v vojski skupaj 18 mesecev, medtem ko je bil redni rok v vseh rodovih vojske 2 leti<sup>8</sup>.

jevu<sup>VI</sup>. Ob kapitulaciji jugoslovanske armade 17. 4. 1941 sta bila Krajnc in Dermelj torej v Sarajevu, od koder sta se uspela preko Zagreba vrniti na Jesenice. Od oktobra 1941 je bil Krajnc povezan z delovanjem Osvobodilne fronte na Jesenicah, a so ga nekaj mesecev kasneje aretirali. Od 22. januarja do 16. marca 1942 je bil zaprt v Begunjah, kjer so ga pogosto zasliševali, od tam pa je bil interniran v Dachau.

V koncentracijsko taborišče Dachau je prispel 18. marca 1942 in ostal zaprt do 22. decembra 1943. Po Krajncu navedbi v službenem listu<sup>VII</sup> je bil zapor v Dachau spremenjen v konfinacijo, od koder naj bi pobegnil novembra 1944 in se vrnil na Jesenice. Pridružil se je partizanskemu Jeseniško-bohinjskemu odredu, od decembra 1944 pa je bil referent za industrijo pri Okrožnem odboru Osvobodilne fronte Jesenice.

V času, ko je bil Krajnc v taborišču Dachau, ga je verjetno trikrat obiskal študijski kolega in prijatelj Mirko Dermelj<sup>VIII</sup>, prvič za novo leto 1944. Ob tem je Krajnc dobil prost dan, ko je lahko odšel v München in tam tudi prespal. Dermelju je ob prvem obisku pripovedoval o poskusih s podhlajevanjem, pri katerih je sodeloval. Drugič je z Dermeljem potovala tudi 'starejša kemičarka Zakrajškova iz Maribora' (Marija Zakrajšek, diplomirala 1936, torej dve leti pred Krajncem in Dermeljem)<sup>IX</sup>. Iz zapisnikov zaslišanj Borisa Krajncja v letih 1947/48 je razvidno, da sta ga obiskali tudi mama in kasnejša žena in da je ob teh priložnostih vedno lahko prespal v Münchnu v hotelu.

O njegovem delu v Dachau, ki je podrobneje razloženo v nadaljevanju, je znano, da je večino časa sodeloval pri razvoju preparata za strjevanje krvi v skupini, ki jo je vodil Sigmund Rascher, kasneje pa je vodenje prevzel Kurt Plötner.

Da status Borisa Krajncja ni ustrezal klasični predstavi o nekom, ki je bil zaprt v taborišču Dachau, govori podatek, da je bil konec maja 1944 na dopustu doma, a se je nato vrnil v Dachau. V Slovenijo se je dokončno vrnil 7. novembra 1944 na osnovi ponarejenega dokumenta<sup>X</sup>, ki so

VI Vodja generalštaba je z odhodom jugoslovanske vlade in kralja v Grčijo prevzel general Kalafatović, vrhovno poveljstvo pa je bilo nameščeno v bližini Sarajeva<sup>9</sup>. Nemško letalstvo je Sarajevo bombardiralo 12. in 13. aprila, 15. aprila pa so nemške enote vkorakale v mesto<sup>10</sup>.

VII Personalna mapa v arhivu Univerze v Ljubljani št. 87/1167.

VIII V prepisu zasebnega pogovora z Mirkom Dermeljem iz leta 2012, ki mi ga je posredovala dr. Tatjana Peterlin-Neumeier, sta omenjena dva obiska, v zaslišanjih po 2. svetovni vojni pa je izjavil, da je bil na obisku trikrat.

IX Po Dermeljevem pripovedovanju (novembra 2012) je ob drugem obisku Krajnc iz taborišča pretihotopil revolver, ki naj bi ga dobil v zameno za kos kruha pri zaporniku, ki je delal zunaj taborišča pri čiščenju posledic letalskih bombardiranj, in majhen radijski sprejemnik, ki so ga zaporniki naredili iz elektrotehniškega materiala, zbranega iz sestreljenih letal. Radijski aparat je Dermelj kasneje predal partizanom. Krajncjeva žena pa omenja v zaslišanju dne 22. 11. 1949 dve ali tri pištole, ki naj bi jih preskrbel profesor kemije Boris Škerlj iz Kranja (ki je med vojno delal v Münchnu) in preko Borisa Krajncja posredoval Dermelju.

X V Janžekovičevem poročilu<sup>11</sup> iz leta 1970 je napačno navedeno, da

mu ga organizirali sodelavci OF z Jesenic in mu ga je prinesel Milan Stepišnik, ko se je oktobra 1944 vrnil z dopusta. Takoj po prihodu na Jesenice je Krajnc odšel preko zveze na Črnem vrhu nad Jesenicami k partizanom<sup>XI</sup>.

Po osvoboditvi je bil Boris Krajnc od 25. 5. 1945 do 31. 1. 1946 vršilec dolžnosti šefa odseka za kemijsko industrijo na Ministrstvu za industrijo in rudarstvo Ljudske republike Slovenije. Kaže, da se je tam zavzemal za odprtje tovarne za predelavo magnezita (iz njega bi lahko pridobivali magnezijev oksid, uporaben za proizvodnjo ognjeodporne opeke za plavže), ohranjen pa je tudi njegov referat o hidrolizi lesa. Junija 1945 se je na Jesenicah poročil z Ivanko Zvezda (1919–2012).

Doktorsko disertacijo z naslovom »Končne skupine in struktura škrobovih komponent« je Boris Krajnc zagovarjal 10. novembra 1945<sup>XII</sup>. V nalogi je Maks Samec, ki po osvoboditvi ni več smel delovati na univerzi, naveden kot delovni mentor, Marij Rebek pa kot 'referent' (mentor). Zagovor je bil samo en mesec pred predčasno upokojitvijo Marija Rebeka, po kateri se je odselil v Gradec, kjer je še naprej predaval. Nenavadno je, da Krajnc po vrnitvi iz Berlina maja 1939 sploh ni več delal na tematiki svoje doktorske naloge, tako da disertacija temelji na rezultatih, dobljenih v obdobju 7-mesečnega podiplomskega usposabljanja. Njegova disertacija, ki jo hrani NUK, ima le 8 strani<sup>XIII</sup> in vključuje 5 tabel, 1 shemo in 15 virov. Vendar je v

je uporabil ponarejeno potrdilo, ki mu ga je priskrbel Stepišnik za dopust maja 1944. V resnici je to potrdilo dobil šele po Stepišnikovi vrnitvi z dopusta konec oktobra 1944, uporabil pa ga je za pobeg iz Dachaua. Kot je izjavil v preiskovalnem postopku, je pobeg izvedel v času, ko je bil vodja skupine, dr. Plötner, v 'Berlinu', z 'Lebersdorferjem' pa se je dogovoril, da bi v primeru, če bi kdo po telefonu preverjal Krajncjev odhod, rekel, da je vse v redu. Gre za Josefa (Seppa) Leberstorferja (roj. 1912), študenta medicine v Dunaju, ki je kot zapornik delal na rentgenskem in zobnem oddelku, sicer pa je bil predvojni komunist, ki so ga v Dachau privedli že junija 1941 (izpuščen je bil 10. 11. 1944). Od maja 1944 je Leberstorfer bil kapo (nadzorni zapornik) v stavbi, kjer je bila taboriščna bolnišnica z laboratoriji. Plötner je poleg vodenja raziskovalne skupine v Dachau bil na mestu taboriščnega zdravnika v Sachsenhausnu nedaleč od Berlina. Vendar tam ni zdravil, pač pa je verjetno zgolj opravljal poskuse na zapornikih<sup>12</sup>. Da je bil 'v Berlinu', verjetno pomeni, da je bil v taborišču Sachsenhausen.

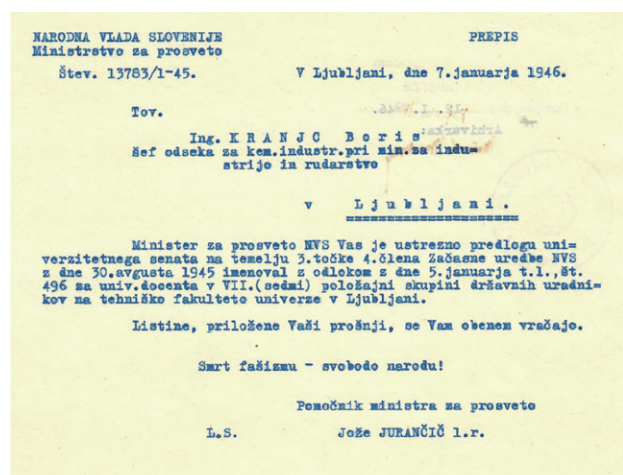
XI Kot opisuje Mirko Dermelj (gl. opombo VIII), je prenočil v počitniški hiši družine Zvezda, od tam pa je ponj prišel nekdo od partizanskih sodelavcev. Enota naj bi se kasneje zadrževala na področju Pokljuke.

XII Promocija doktorata je bila šele 5. oktobra 1946, ko je bil Krajnc že docent. V seznamu doktorjev UL je listina vpisana pod št. 649, z dopisom THF (Tehniška fakulteta).

XIII Za primerjavo sem preveril nekaj drugih doktoratov Tehniške fakultete iz tistega obdobja. Istega leta (20. decembra 1945) je iz kemije doktoriral Božo Težak (1907–1980), kasnejši profesor zagrebške univerze, in sicer z disertacijo »Istraživanje taložnih struktura barium sulfata«. Težak je do takrat objavil 11 strokovnih in znanstvenih člankov, a je njegova naloga obsegala 69 strani<sup>13</sup>, NUK pa pod tem naslovom in z letnico 1945 hrani samo 3-stranski separat, ki nima značilnosti disertacije. Eno leto prej je doktoriral Ludvik Žagar z nalogo »Primerjava amilopektinov koruznega in krompirjevega škroba«, NUK pa pod tem naslovom hrani »odlomke iz invaguralne disertacije« v obsegu 5 strani. Disertacij (niti izvlečkov) kemikov, ki so promovirali do leta 1955, NUK ne hrani, z izjemo nekaterih, ki so razširjene izvlečke objavili v Razpravah SAZU (Dušan Hadži, Drago Lebez).

predvojnem in zgodnjem povojnem obdobju bilo običajno, da kot tiskana publikacija izide le kratek izvleček, ki ga knjižničarji včasih označujejo kot 'odlomki iz avguralne disertacije'.

Senat Univerze v Ljubljani je 11. decembra 1945 sprejel pobudo Tehniške fakultete in predlagal »šefa oddelka za kemično industrijo pri min. industrije in rudarstva tov. ing. Borisa Krajncja za univerzitetnega docenta za biokemijo«. Nato je 5. januarja 1946 minister za prosveto<sup>XIV</sup> Krajncja z odlokom imenoval za univerzitetnega docenta na Tehniški fakulteti ljubljanske univerze (slika 2). S februarjem 1946 se je Krajnc zaposlil kot docent, razvrščen v VII. položajno skupino, novembra 1947 (ko je bil že v zaporu) pa je napredoval v docenta II. Univerzi je predložil potrdilo o nekaznovanju, datirano s 25. 3. 1947.



Slika 2: Dopis Ministrstva za prosveto o imenovanju Borisa Krajncja za docenta na predlog senata ljubljanske univerze. Vir: Zgodovinski arhiv in muzej Univerze v Ljubljani (ZAMU) IV - 87/1167, personalna mapa Borisa Krajncja.

V seznamu predavanj Univerze v Ljubljani za poletni semester 1945/46 je Boris Krajnc naveden kot edini član Inštituta za biokemijo z redno zaposlitvijo, ob njem pa je kot honorarni predavatelj še inž. Josip Šlajmer, zadolžen za predmet Tehnična mikrobiologija. Krajnc je naveden s predmetom Izbrana poglavja iz biokemije (2 h predavanj tedensko in 15 h biokemijskega praktikuma, ki se je izvajal v laboratoriju za organsko kemijo).

Na ravni države je bil avgusta 1946 predpisan učni načrt, ki je za študente kemije predvideval v 2. letniku predmet Tehnično mikroskopiranje, v 4. letniku pa Izbrana poglavja iz biokemije in encimatike ter Tehnično mikrobiologijo. Določen je bil tudi učni načrt za ločen dvoletni študij farmacije, ki pa takrat še ni vseboval biokemije. V zimskem semestru 1946/47 je Krajnc tako naveden pri

predmetu Izbrana poglavja iz biokemije in encimatike (2 h predavanj, 5 h vaj), v poletnem semestru pa pri predmetu Tehnična kataliza (2 h predavanj).

V zimskem semestru 1947/48 je Krajnc pokrival predmet Tehnologija katalitskih procesov (3 h predavanj, 20 h vaj). Bolj biološke in biokemijske vsebine so v tem semestru poleg inž. Šlajmerja izvajali še drugi zunanji predavatelji: Jože Lazar Botanične mikroskopsko-anatomske vaje ter vaje iz Sistematike rastlin, Peter Lenče Anatomijo in fiziologijo človeka za farmacevte, Albin Seliškar z Medicinske fakultete pa Fiziološko kemijo.

Glede Krajncčevega raziskovalnega dela v letih 1946–47 ni veliko podatkov, iz naslovov diplomskih nalog<sup>XV</sup> pa je razvidno, da je nadaljeval raziskave o vlogi pektina na strjevanje krvi, kar je bila glavna tema pri njegovem strokovnem delu v Dachauu. Prvo ohranjeno diplomsko delo (Bojan Držaj, Vpliv pektina na koagulacijo krvi po mikrometodi, 1947) vključuje izolacijo in karakterizacijo pektina iz jabolčnih tropin ter frakcioniranje različno dolgih fragmentov pektina, čemur je sledila analiza delovanja na strjevanje krvi. Rezultati so pokazali, da strjevanje krvi pospešujejo le razgradni produkti pektina, ne pa sam pektin, ne glede na dolžino njegove verige. Drugo diplomsko delo (Jelka Ružič: Vpliv razgradninskih produktov pektina na I. fazo koagulacije krvi, 1949) je vključevalo kislinsko hidrolizo pektina, s čimer je nastala digalakturonska kislina. Nato je študentka preverjala njen vpliv na hitrost strjevanja krvi v razmerah in vitro. Dodatno je izolirala še trombin in trombokinazo in ugotavljala morebitno spremembo hitrosti strjevanja krvi. V delu, kjer je določila optimalno koncentracijo digalakturonske kisline, je omenila, da se rezultat ujema z rezultati njenega predhodnika (verjetno Držaja).

Iz obveščevalnih podatkov Udbe (obveščevalec »Milko«, prim. opombo XV) je razvidno, da se je Krajnc zavezal tudi za razvoj postopkov aromatizacije nafte, kar naj bi bil osnovni problem slovenske kemijske industrije. Sprva je bil doc. Škerlak<sup>XVI</sup> temu nenaklonjen, ker naj bi bilo zelo negotovo, če je v doglednem času možno doseči zadovoljive rezultate, kasneje pa je podprl Krajncja in prevzel pobudo pri pogovorih s predstavnikom republiške planske komisije, tako da je ta tema prišla v petletni plan. Obveščevalec meni, da bi uspeh aromatizacije velenjskega lignita predstavljal za slovensko industrijo pomemben dosežek.

XV V knjižnici UL FFKT sta arhivirani samo dve nalogi, pri katerih je Krajnc omenjen kot mentor, čeprav je iz obveščevalnih podatkov (23.4.1948, obveščevalec 'Milko', ki je moral biti zaposlen na fakulteti, saj je natančno poznal vsebino pogovorov med Krajncem in Škerlakom) [SI AS 1931, dosje B. Kranjca, str. 365] mogoče razumeti, da je pod njegovim mentorstvom bilo izvedenih 5 diplomskih nalog na temo pektina. Glede morebitnih ostalih treh nalog ni mogoče ugotoviti, ali so sploh obstajale.

XVI Tibor Škerlak (1913–1992) je doktoriral na Tehniški visoki šoli v Münchnu, leta 1945 pa je postal docent za teoretično in fizikalno kemijo na Tehniški fakulteti UL. Zaradi podpore resoluciji Informbiroja je bil zaprt na Golem otoku (1949–1951). Kasneje se je preselil v Sarajevo, kjer je bil na univerzi leta 1954 izvoljen v naziv izrednega profesorja. Ustanovil je katedro za fizikalno kemijo, ki jo je tudi vrsto let vodil. V času vojne v Bosni in Hercegovini ga je smrtno ranil ostrostrelec<sup>15</sup>.

XIV Glede na izjavo Borisa Fakina med preiskavo in obravnavo na dachauskem procesu naj bi si Krajnc želel priti na univerzo, zato ga je »priporočil ministru za prosveto kot najboljšega znanstvenega delavca in partijca«<sup>14</sup>.



Krajnca so aretirali 27. oktobra 1947. Na Diehl-Oswaldovem procesu aprila 1948 so ga obsodili na smrt. Sodbo naj bi izvršili 12. maja 1948<sup>XVII</sup>, a obstajajo indici, ki kažejo, da so nekateri obsojenci s tega procesa ostali zaprti do leta 1950, ko so jih ustrelili na območju Kočevskega Roga. Za Krajnca se je zdelo, da je podatek o izvršeni sodbi leta 1948 verodostojen. Pokopali naj bi ga bržkone na neoznačenem mestu na ljubljanskih Žalah<sup>16</sup>. Vendar pa sem v Arhivu Republike Slovenije našel rokopis<sup>XVIII</sup> Borisa Krajnca iz zapora, datiran z 20. majem 1948<sup>XIX</sup>. To je tudi zadnji Krajnčev tekst v arhivu, vsekakor pa je bila izjava podana dober teden po tem, ko naj bi Krajnca usmrtili.

Zaradi obsodbe je pristojni minister izdal odločbo o prenehanju delovnega razmerja, rektor pa je na seji senata UL 22. junija 1948 lahko samo sporočil, da sta Boris Krajnc in Mirko Košir prenehala biti člana profesorskega kolegija<sup>17</sup>.

S Krajnčevo aretacijo ni jasno, kdo, če sploh, je prevzel njegove predmete v študijskem letu 1947/48. Iz seznamov predavanj UL je razvidno, da se je predmet Izbrana poglavja iz biokemije in encimatike ponovno izvajal v študijskem letu 1948/49, ko je predmet predaval Dušan Stucin z Medicinske fakultete, enako naslednja tri leta, potem pa je prišlo do reorganizacije študijev kemije, po kateri biokemije niso več predavali do 1956/57, ko se ponovno pojavi, tokrat kot ‚višji kurz‘ (Izbrana poglavja iz biokemije in encimatike, D. Stucin z Medicinske fakultete).

### 3. Krajnčevo delovanje v taborišču Dachau

Kot sledi iz analize dachauskih procesov<sup>11</sup>, ki jo je pripravila takoimenovana »Janžekovičeva komisija«<sup>XX</sup>, je

XVII Vojaško sodišče v Ljubljani je 16. junija 1948 poslalo matičnemu uradu na Reki dopis, ki naj bi služil za vpis Krajnca v knjigo umrlih. V dopisu je navedeno, da je bil Krajnc justificiran 12. maja 1948. Z Reke so sporočili, da za vpis v knjigo umrlih niso pristojni, temveč morajo to izvesti v Ljubljani. V izpisku iz mrliške matične knjige iz Ljubljane je navedeno, da je Krajnčeva smrt bila vpisana leta 1950. Datum smrti je 12.5.1948, kraj smrti pa Miklošičeva 4, to je naslov nekdanjih ljubljanskih zaporov za sodno palačo (danes sta tam parkirna hiša in hotel).

XVIII Vprašanja so se nanašala izključno na eno osebo, ‚Žukova‘, ki je bil med vojno zaprt v taborišču Dachau, po Krajnčevem vedenju pa naj bi bil po osvoboditvi ‚direktor na radiu Beograd‘. Jevgenij Andrejevič Žukov (1898-1959) je bil predvojni novinar, ki je iz Beograda pokrival področje Balkana. Že leta 1925 je bil med soustanovitelji Zveze ruskih pisateljev in novinarjev v Jugoslaviji, leta 1928 pa je ustanovil koncertno agencijo Jugokonzert, ki je organizirala gostovanja številnih vidnih umetnikov v Beogradu in drugod po Jugoslaviji. Med vojno je bil interniran v Dachau, po vojni pa je nadaljeval z novinarskim in organizacijskim delom na področju kulture v Beogradu. Žukov je bil v rednih stikih z Justinom Ažmanom iz Kroke, prav tako nekdanjim internirancem v Dachau. V času Krajnčevega zadnjega zaslivanja so Žukova preverjali glede delovanja v Dachau, kjer je bil sobni starešina. Obtožb je bil oproščen šele po letu 1950<sup>18</sup>.

XIX Naknadno sem ugotovil, da je zapisnik našla že Emilija Snój, ki je leta 2001 zagovarjala diplomsko nalogo na temo dachauskih procesov<sup>19</sup>.

XX Gre za petčlansko komisijo, ki so jo sestavljali pravnik Ivo Janžekovič (predsednik komisije, sicer predsednik Republiškega sveta Zveze sindika-

bil Krajnc po prihodu v Dachau sprva dodeljen v različne taboriščne delovne skupine, nato pa je bil januarja 1943 premeščen v ‚raziskovalno postajo‘ v skupino dr. Sigmunda Rascherja, kjer naj bi najprej opravljal analize krvi, kasneje pa sodeloval pri testiranju preparata za strjevanje krvi.

Krajnc je v okviru preiskave za dachauski proces povedal, da je po prihodu v Dachau tri mesece delal v skupini za gradnjo barak, nakar ga je Martin Presterl<sup>XXI</sup> uspel premestiti na zajčjo farmo, kjer je dva meseca prevažal krmo in gnoj. Sledilo je delo v proizvodnji, kjer naj bi izdelovali lesene igrače, in v mizarski delavnici, nato pa je bil premeščen k dr. Rascherju po navodilu taboriščne pisarne za razporejanje dela (Arbeitseinsatz). V argumentaciji razveljavitve sodbe v Diehl-Oswaldovem procesu (razveljavitev je datirana s 7. aprilom 1976) je natančneje navedeno, da je bil Krajnc premeščen v gospodarske obrate taborišča septembra 1942, sredi januarja 1943 pa v skupino dr. Rascherja, kjer je po Krajnčevi navedbi izvajal »določitve mlečne

tov in v predhodnem mandatu poslanec v republiškem zboru slovenske skupščine), Francka Strmole (nekdanja predsednica Ljudske mladine Slovenije, pravnica, v predhodnem mandatu poslanka v republiškem zboru, kasneje predsednica vrhovnega sodišča SRS od 1981 do 1993), Ivan Ros (pravnik, poslanec, predsednik skupščinskega odbora za organizacijsko-politična vprašanja), Savo Šifer (pravnik, sodnik, poslanec v predhodnem sklicu skupščine, član Višjega gospodarskega sodišča SRS, kasneje, leta 1959, predsednik sodnega senata, ki je obsodil Jožeta Pučnika zaradi protidržavnega delovanja) in Rihard Knez (pravnik, sodnik, od leta 1947 član vrhovnega sodišča SRS, član sodnega senata 1948 na sojenju proti »Bitenčevi skupini«, obtoženi protidržavnega delovanja – prim. <http://nzsveza.github.io/articles/9-slike-iz-zadnjega-dejanja/>), tajnik komisije za prošnje in pritožbe pri republiškem izvršnem svetu). Komisija je z delom začela 26. maja 1969 in končno poročilo izdala 30. marca 1970. Sestavo komisije je določil predsednik izvršnega sveta slovenske skupščine Stane Kavčič, ki je dobil nalogo, da razišče nejasnosti glede dachauskih procesov, od vodstva Zveze komunistov Slovenije. Pri delu je imela komisija dostop do celotnega gradiva, okrog 30.000 tipkanih strani, in do predhodnih analiz procesov, ki sta jih pripravila leta 1951 major Udbe Anton Debevec (1923-2002) in 1968 major Stane Škraba (prav Škraba, takrat še v rangju kapetana, je opravil hišno preiskavo ob aretaciji Borisa Krajnca leta 1947). Janžekovičeva komisija je imela 9 sej, vsak član pa si je moral na osnovi gradiva izdelati najprej lastno mnenje o procesih. Na osnovi teh neodvisnih mnenj so oblikovali končno poročilo, v katerem opisujejo predvsem značilnosti taborišč in njihovo upravljanje, povojne gospodarske sabotaže, ki so bile povod za začetek preiskave, značilnosti preiskovalnega postopka in glavne obravnave, nato pa so se člani posvetili posameznim obsojencem in se kritično opredelili do dokazov, uporabljenih v procesih. Kot je nakazala že Škrabova analiza, je tudi Janžekovičeva komisija ugotovila, da preiskave in sojenja niso bili izvedeni ustrezno.

XXI **Josef (Martin) Presterl** (1916–1948?) je bil soobtoženec na dachauskem procesu, sicer pa je bil avstrijski predvojni komunist, španski borec in novinar. Po vojni je simpatiziral z jugoslovansko uradno politiko. Po preiskovalnem zaporu v Gradcu je bil od 22. 2. 1942 zaprt v taborišču Dachau. Leta 1946 je z jugoslovansko pomočjo v Avstriji ustanovil založbo Kristall-Verlag in leta 1947 izdal brošuro »2000 kilometrov po novi Jugoslaviji«, v kateri je poudarjal naprednost in zanos, ki naj bi vladal v takratni Jugoslaviji. Avgusta istega leta je v dogovoru z jugoslovanskim konzulatom ustanovil tiskovno agencijo, ki naj bi dvakrat mesečno izdajala bilten, ki bi ‚ustrezno‘ predstavljal dosežke v Jugoslaviji in sosednjih socialističnih državah. Aretili so ga na železniški postaji v Mariboru 27. oktobra 1947. Več o njegovem delu je razvidno iz članka Heima Halbrainerja<sup>20</sup>. Postal je ključna priča tožilstva, saj je trdil, da je v vlogi agenta tuje obveščevalne službe razpredel agenturne stike z drugimi obtoženimi, ki so pred tem bili agenti Gestapa, tako kot on sam.

kislina, klora, krvnega sladkorja, beljakovin, števila rdečih krvnih teles in drugih sestavin v krvi«. Meril naj bi tudi temperaturo in sodeloval pri izdelavi pektinskih preparatov.

Čprav je Krajnc v svojem življenjepis, ki ga je pripravil ob zaposlitvi na ljubljanski univerzi, iz dachauskega obdobja omenjal samo delo na preparatu za strjevanje krvi, je torej gotovo sodeloval tudi pri zadnjih poskusih ohlajanja in ponovnega ogrevanja (t.i. hipotermični poskusi), po katerih je Rascher verjetno najbolj znan<sup>XXII</sup>.

Krajncova vključenost v poskuse s podhlajevanjem je zelo verjetna glede na časovni razpored raziskav Rascherjeve skupine v koncentracijskem taborišču Dachau. V času, ko naj bi Krajnc začel delati pod Rascherjevim vodstvom (januar 1943) so potekali še zadnji poskusi s hipotermijo, predvsem v povezavi z različnimi postopki ogrevanja po izpostavitvi mrazu. Večina predhodnih raziskav s potapljanjem v mrzlo vodo naj bi namreč bila zaključena že septembra ali oktobra 1942, kot je mogoče razbrati iz korespondence Rascherja s Himmlerjem. Oktobra je namreč Rascher oddal zaključno poročilo o opravljenih poskusih, v katerem navaja, da bi bilo treba zgolj še natančneje ugotoviti, kateri načini ogrevanja bi bili najprimernejši, kar je Himmler nato tudi izrecno podprl. Vsi poskusi naj bi bili zaključeni do maja 1943. Da hipotermični poskusi v Krajncem obdobju niso več intenzivno potekali, priča tudi to, da so vodje raziskave o hipotermiji (prof. dr. Holzlöhner, dr. Finke in dr. Rascher) o rezultatih poročali že konec oktobra 1942 na sestanku v Nürnbergu.

V hipotermičnih poskusih so zapornike potapljali v mrzlo vodo in analizirali njihove odzive: merili so telesno

temperatura na različnih delih telesa, določali krvno sliko in podobno<sup>21</sup>. Potapljanju naj bi sledili poskusi, ki naj bi pokazali, kateri postopek ponovnega segrevanja je najboljši. Zapornike, moške, so potapljali oblečene ali gole, zavestne ali anestezirane, v bazene s hladno vodo (2–12 °C). Eksperimentalne podatke so v glavnem uničili, ostaja pa precej informacij, ki izhajajo iz korespondence med vodji poskusov in Heinrichom Himmlerjem, šefom SS-a. Takoj po vojni so podatke zbrali v obliki 228 strani dolgega poročila<sup>XXIII</sup>. Poskusov naj bi bilo med 360 in 400, na 280 do 300 ljudeh; 80–90 jih je zaradi teh poskusov umrlo. Glede na to poročilo kaže, da raziskava ni bila dovolj sistematična, da so zanemarili številne pomembne podatke za interpretacijo itd. Z medicinskega stališča so hipotermični poskusi, pa tudi večinsko odklonilen odnos stroke do vrednosti teh poskusov, bili obdelani leta 1990<sup>21</sup>.

Krajnc naj bi predvsem sodeloval v »pektinskih poskusih«, ki so bili namenjeni pripravi formulacije in testiranju preparata »Polygal-10« za strjevanje krvi. Poskusi s tem preparatom naj bi potekali v letih 1943 in 1944<sup>22</sup>.

Razvoj sredstva za strjevanje krvi je zadnji obsežnejši projekt Rascherjeve skupine<sup>XXIV</sup> in je tekel sočasno z manj obsežnima poskusoma priprave krompirja v prahu oz. v tabletah ter sredstva proti rjavenju z manjšo vsebnostjo linolne kisline. Sredstvo za strjevanje krvi naj bi raziskovali od jeseni 1943, že decembra istega leta pa naj bi ga dali v uporabo dachauskemu zaporniškem zdravniku dr. Kahru. Glede na to, da so Rascherja marca 1944, ob izbruhu afere, povezane z otroci, ki naj bi jih rodila njegova žena, v resnici pa so bili ugrabljeni, premestili v München, raziskav ni več mogel nadaljevati, njegov Oddelek R pa je s 1. majem 1944 prevzel dr. Kurt Plötner<sup>XXV</sup>.

XXII **Sigmund Rascher** (1909–1945) je opravil državni zdravniški izpit v Münchnu leta 1936. Ob tem je pridobil tudi doktorski naziv na osnovi raziskovalnega dela, ki je bilo s področja diagnostike nosečnosti na osnovi oblike kristala bakrovega klorida (CuCl<sub>2</sub>). Ta v prisotnosti organskih snovi kristalizira v paličasti obliki, a naj bi bila oblika odvisna od tipa organske snovi. Tako naj bi določeni hormoni v vzorcih urina nosečnic dali specifične oblike kristalov. To naj bi bilo mogoče samo ob izredno natančni izvedbi kristalizacij in je bilo praktično neponovljivo. Prvo delovno mesto je dobil kot neplačani asistent na oddelku za kirurgijo ene od münchenskih bolnišnic, tako da je konec leta 1937 dobil dovoljenje za opravljanje zdravniškega poklica. Že pred tem pa je prejel enoletno štipendijo raziskovalnega sklada za izvedbo raziskave na temo diagnostike raka na osnovi kristalizacijskega vzorca CuCl<sub>2</sub>. Dobljenim rezultatom že ob objavi veliko strokovnjakov ni verjelo, danes pa velja, da so potvorjeni. Rascherjeva partnerka Karoline Diehl je bila prijateljica vodje SS-a Heinricha Himmlerja in je preko njega uspela urediti nekatere privilegije za Rascherja. Od maja 1939 je kot član ustanove Ahnenerbe raziskoval raka, od avgusta istega leta pa je bil zaposlen kot zdravnik pri nemškem letalstvu. Decembra 1940 je začel sodelovati z zdravniki iz taborišča Dachau, leta 1941 pa je dobil od Himmlerja dovoljenje, da na zapornikih izvede raziskave, povezane z višinskimi poletji, torej pri znižanem zračnem tlaku. Takoimenovani hipobarični poskusi so potekali v Dachau od februarja do maja 1942. Sledili so poskusi s podhlajevanjem in drugi, ki so natančneje opisani v nadaljevanju. Karoline Diehl je dobila prvega otroka pri svojih 47 letih, nato pa še tri. Navzven sta z Rascherjem prikazovala, kot da jih je Karoline sama rodila, in o naraščanju sta tekoče obveščala Himmlerja. Leta 1944 pa se je izkazalo, da so bili vsi štirje otroci ugrabljeni kot dojenčki in nekateri celo naknadno zamenjani. Zato so Karoline Rascher odpeljali v taborišče Ravensbrück, kjer so jo usmrtili že leta 1944, Sigmunda Rascherja pa konec aprila 1945 v Dachau.

XXIII Sestavil ga je avstrijsko-ameriški psihiater in nevrolog Leo Alexander (1905–1980), sicer glavni medicinski svetovalec sodišča pri Nürnberških procesih, med vojno pa v činu majorja sodelavec ameriške armade v Evropi.

XXIV Hubert Rehm v knjigi o Rascherju meni, da je bil projekt Polygal po zaključku poskusov s podhlajevanjem za Rascherjevo skupino najpomembnejši projekt in edini, ki je temeljil na lastni ideji, zato je bil pod pritiskom, da projekt uspe. To naj bi vplivalo tudi na interpretacijo rezultatov, če ne celo na izvedbo poskusov.

XXV **Kurt Plötner** (1905–1984) je leta 1930 zaključil študij kemije in leta 1934 opravil državni izpit iz medicine. Doktoriral je leta 1939 s področja serumskih proteinov in naslednje leto postal docent na univerzi v Leipzigu<sup>40</sup>. Leta 1941 je delal kot vodja internističnega oddelka v bolnišnici vojnega letalstva v Dachau, nato pa je leto in pol služboval v bolnišnici v zasedenem Minsku. Konec leta 1943 je prevzel mesto asistenta Klause Schillinga pri poskusih, povezanih z malarijo, maja 1944 pa je postal vodja nekdanjega 'Oddelka R' Sigmunda Rascherja, ki se je ob tem preimenoval v 'Oddelek P'. Sočasno je bil na mestu taboriščnega zdravnika v Sachsenhausnu. Poleg preizkušanja sredstva za strjevanje krvi naj bi sodeloval pri preizkusih dveh nevarnih spojin na zapornikih: potencialnega bojnega strupa z delovnim imenom N-Stoff (klorov trifluorid)<sup>23</sup> in psihoaktivne spojine 3,4,5-trimetoksifenetilamin (meskalin, po izvoru iz kaktusa pejočla). Pri meskalinu naj bi opazoval obnašanje poskusnih oseb; predvsem naj bi poskusil ugotoviti, če deluje kot 'serum resnice'. Leta 1945 naj bi v zvezi s temi poskusi začel sodelovati z ameriško Cio in prevzel priimek Schmitt, s čimer se je zavaroval pred aretacijo francoske uprave. Leta 1952 si je vrnil stari priimek in dobil zaposlitev na Freiburški univerzi, kjer je predaval v nazivu izrednega profesorja.

Ta se je v veliki meri posvetil sredstvu za strjevanje krvi, ki ga je preimenoval v Styptoral. O nadaljevanju poskusov s podhladitvijo naj bi potekali pogovori, a jih najverjetneje niso izvajali<sup>24</sup>.

V osnovi naj bi preparat Polygal oz. Styptoral sestavljal ekstrakt sladkorne pese, a se je njegova sestava v procesu optimizacije spreminjala, saj je sprva bila surovina jabolčni pektin iz ostankov po stiskanju soka. Preventivno jemanje tega preparata naj bi zmanjšalo krvavitve, ki bi bile posledica bojevanja, pa tudi pri operacijah ali zaradi notranjih krvavitev pljuč ali prebavil. Na nekaterih taboriščnih naj bi poskus opravili tako, da so jim dali preparat, nato pa amputirali zdravo okončino, ali jih ustrelili v vrat ali trup.

Ideja za preparat je Rascher dobil od dachauskega zapornika, avstrijskega kemika Roberta Feixa (1893–1973), ki je pred vojno razvil tekoče želirno sredstvo Opekta za uporabo v gospodinjstvih. Sodeloval je tudi pri njegovi proizvodnji v Kölnu. Za medicinsko uporabo pa naj bi pod Rascherjevim vodstvom razvili preparat v tabletah. Feix je najverjetneje vložil patentno prijavo za medicinski pektinski preparat že leta 1942, preden so ga zaprli in kasneje internirali v Dachau (tja je prispel konec januarja 1943), patent pa je bil odobren oktobra 1943.

Izkazalo se je, da je že v 30-tih letih pektinski preparat za strjevanje krvi Sango-Stop<sup>XXVI</sup> proizvajalo neko nemško podjetje. Šlo je za tekočino za intramuskularno ali podkožno injiciranje. Tudi v Franciji so že pred tem uporabljali pektinske injekcije za zaustavljanje krvavitev<sup>25</sup>. Ideja o pektinskem preparatu torej ni bila nova, je pa prišla pobuda v pravem času, ko se je pokazala potreba po zaustavljanju krvavitev pri vojaki na frontni črti, pri čemer je bila dodana vrednost to, da bi preparat bil na voljo v obliki tablet.

Patent za Polygal je pri nemškem patentnem uradu v Berlinu datiran z 2. oktobrom 1943. Da je preparat praktično obstajal že jeseni 1943, in da so načrtovali njegovo proizvodnjo, dokazuje pisni dogovor oz. predpogodba (z dne 12. 10. 1943) med Rascherjem in Feixom<sup>26</sup> glede proizvodnje in delitve dobička od prodaje preparata<sup>XXVII</sup>. Še marca 1944 je Wolfram Sievers, predstojnik ustanove Ahnenerbe<sup>XXVIII</sup>, predvideval zagon proizvodnje Polygala v

bližini Bodenskega jezera ob pomoči nekaterih privilegiranih zapornikov. Pristojni odbor pa je proizvodnjo zavrnil, češ da ta ni v pristojnosti raziskovalnih oddelkov, je pa odobril razvoj *postopkov za proizvodnjo* tega zdravila. Kasneje je proizvodni del projekta prevzelo podjetje Deutsche Heilmittel<sup>24</sup>, a so bile priprave na proizvodnjo vezane na objekt v Schlachtersu, ki je bil podružnica (včasih imenovana tudi podružnica Biesings) taborišča Dachau, ustanovljena 4. aprila 1944 prav za zagon proizvodnje<sup>27</sup>. Za proizvodnjo so izbrali opuščeno sirarno, v bližini pa je bil tudi objekt, nekakšen skedenj, ki so ga preuredili za nastanitev osebja, kasneje pa so najeli in preuredili za bivanje nekdanje kegljišče v vaški gostilni. Del proizvodnje naj bi potekal v tamkajšnji žganjarni Nikolodi, zadnji del sušenja pa v mlekarni Edelweiss. Delalo naj bi med 6 in 8 zapornikov, ki sta jih čuvala dva SS-ovca, a so se kljub prepovedi večkrat sprehajali po vasi in bili v občasnih stikih z domačini<sup>28</sup>. Kasneje so zaradi bližajočih se francoskih enot proizvodnjo preselili v nekdanjo pivovarno Reiner v kraju Lochau pri Bregenzu. Tam je bila izpostava taborišča Dachau že leta 1942, ko je v njej delovalo kovinsko podjetje s prisilnimi delavci in ujetniki. Isto poslopje so usposobili za delovanje in uradno odprli kot enoto za proizvodnjo pektinskega preparata 7. aprila 1945, delavci pa bi bili zaporniki in sodelavci (nekdanje) skupine Sigmunda Rascherja oziroma Kurta Plötnerja. Tam naj bi delalo med 5 in 20 zapornikov iz Nemčije, Poljske in Slovenije, varovalo pa jih je 5 starejših SS-ovcev<sup>32</sup>. Koliko tablet so izdelali, ni jasno, obstajajo pa podatki, da so preparat preizkušali na več klinikah.

Kljub temu, da je osnovna formulacija preparata bila znana že jeseni 1943, so potekale raziskave v smeri optimizacije sestave in postopka priprave še v jeseni 1944. Pri iskanju podatkov o drugih kemikih, obsojenih na dachauskih procesih, sem dobil kopijo laboratorijskih zapiskov<sup>XXIX</sup> iz Dachaua, ki predstavljajo dober vpogled v raziskave, opravljene poleti in jeseni leta 1944. Avtor teh zapiskov je bil po vsej verjetnosti Milan Stepišnik, ki je delal v Plötnerjevi skupini skupaj s Krajncem. Natančnejši prikaz vsebine teh zapiskov bo tema enega od kasnejših člankov, saj gre za prvi verodostojen opis postopkov priprave pektinskega preparata v Dachauu, kot tudi za pregled rezultatov testiranja na zapornikih.

XXVI Preparat Sango-Stop je na primer strokovno obravnavan v članku Geoga Sacka<sup>29</sup> iz leta 1935 z opisom zdravljenja treh primerov nenadne krvavitve pri hemofilikih. Uporaben naj bi bil tudi pri obolenjih prebavil, pri katerih pride tudi do driske. Opis preparata in doziranje sta opisana tudi v kratkem prispevku E. Gohrbandta<sup>30</sup> iz leta 1936. Pod tem imenom ga je prodajalo podjetje Turon iz Frankfurta<sup>31</sup>.

XXVII Proizvodnja naj bi potekala v navezavi s podjetjem Sicabo na Predarlberškem, za prodajo pa bi ustanovili posebno podjetje. Feix naj bi imel proizvodne in prodajne pravice, ob tem pa bi mu pripadalo 5 % prihodkov za čas trajanja patenta. Udeležba pri dobičku bi bila taka, da bi 33 % pripadlo Rascherju, ravno toliko Feixu in 34 % družbenikom. Enaka delitev bi veljala tudi pri šele načrtovanih patentih v tujini.

XXVIII Ahnenerbe je bila sprva organizacija za strokovno obravnavo arijske zgodovine. Ustanovili so jo leta 1935 in je delno delovala kot društvo, a je bila del SS-a. V njej je imel vsaj od leta 1937 glavno besedo vodja

SS-a, Heinrich Himmler, ki je praktične zadeve vodil preko generalnega tajnika Wolframa Sieversa. Ta je tudi vodil Inštitut za namenske vojaško-znanstvene raziskave, ki je bil ustanovljen julija 1942. Večino psevdomedicinskih raziskav je Rascherjeva skupina opravila v okviru tega inštituta, ki je omogočal tudi zaposlitve nekdanjih taboriščnikov.

XXIX V lasti družine Stepišnik je rokopisni zvezek, ki predstavlja zanimiv in dragocen dokument o raziskovalnem delu v skupini Kurta Plötnerja, ki pa je logično nadaljevanje prvotnih raziskav iz obdobja, ko je skupino vodil Sigmund Rascher. Na osnovi rokopisa je mogoče reči, da zvezka ni pisal Krajnc, pač pa bolj verjetno Stepišnik. Da je Stepišnik iz taborišča prinesel zapiske, je navedla njegova žena v pismu slovenskemu izvršnemu svetu, ko se je zavzemala za rehabilitacijo obsojenih. Tam je tudi zapisala, da so bili zapiski zaplenjeni ob hišni preiskavi, zato ni jasno, kako so se ponovno znašli v lasti Stepišnikovih.

V zvezku so navedeni osnovni pristopi k pripravi ekstrakta iz rezin sladkorne pese, kar je vključevalo kislodrolizo pektina in kasnejše umiljenje z dodatkom NaOH. V nadaljevanju je predstavljen del raziskav o vlogi morebitnih dodatkov, ki bi lahko čas strjevanja krvi še skrajšali, med drugim različne kisline biološkega izvora. Pri ovrednotenju učinkovitosti so izvajali tudi teste na ljudeh. Nekateri so dobili preprat oralno, drugi intravenozno, tretji intramuskularno. Čas strjevanja krvi so določali v rednih časovnih intervalih, običajno do 7 h po doziranju preparata oz. dodatka. Kri so jemali iz žile (venska) in iz uhlja (kapilarna), čas strjevanja pa so določali na vbodni rani na uhlju. Ena serija poskusov je bila namenjena spremljanju hitrosti strjevanja krvi v odvisnosti od vremena, tako da so na treh ljudeh izvajali meritve vsak dan skozi več kot en mesec in vzporedno beležili vremenske podatke. Preizkusne osebe so navedene z začetnicami imena in priimka, starostjo, telesno težo in višino. Zadnji poskusi, opisani v zvezku, so od 11. oktobra 1944. Kot vemo, je Krajnc pobegnil iz ujetništva v začetku novembra 1944, pa tudi Stepišnik naj bi ostal v Dachauu samo do konca oktobra. Zato je bilo sprva težko reči, kdo je bil avtor zvezka<sup>XXX</sup>. Na osnovi primerjave rokopisa s Krajncem iz arhivskega gradiva Univerze v Ljubljani<sup>XXXI</sup> in Arhiva RS je mogoče reči, da avtor teh zapiskov ni Krajnc. Zapiski so v slovenščini, torej je avtor moral biti Slovenec. Glede na veliko število preizkušancev (okrog 80), se zdi najbolj verjetno, da so meritve opravili v taborišču Dachau in ne v podružnici Schlachters, kjer naj bi bilo vsega skupaj manj kot 10 ljudi. Od Slovencev so bili v Rascherjevi skupini Krajnc, Stepišnik, Barle (vsi kemiki) ter Ravnikar (krojač) in Pufler (steklar). Barle je bil od poletja 1944 v Schlachtersu, zato ni mogel sodelovati pri izvedbi opisanih poskusov. Zato je utemeljeno sklepati, da gre za Stepišnikov zvezek. Glede znanstvene vrednosti zbranih meritev velja pripomniti, da so v veliki večini teste izvajali z istim preparatom na samo enem človeku, kar je z današnjega stališča nesprejemljivo.

Naknadno sem v Krajncem dosjeju v Arhivu RS odkril tipkopis, ki vključuje večino tistih poskusov, ki so opisani v Stepišnikovih zapiskih, pa tudi nekaj dodatnih. Pri pisanju je bil uporabljen pisalni stroj s slovenskimi znaki, zato je verjetno, da gre za prepis rezultatov, ki jih je Krajnc ob pobegu prinesel iz Dachaua, a so bili takrat rokopisni. Vsebina omenjenega tipkopisa bo predmet kas-

XXX Zapiske Borisa Krajncja je omenjala njegova žena v pogovoru za časopis Dnevnik. Po mnenju Ivanke Krajnc naj bi njen mož zvezek s podatki iz Dachaua odnesel na fakulteto, kjer se je zaposlil in nadaljeval delo na pektinskih preparatih, vendar zvezka na fakulteti ne hranijo. V knjigi Bore Krivokapiča<sup>33</sup> je v delu, ki opisuje njegov pogovor z Ivanko Krajnc in njeno borbo za razjasnitev okoliščin, povezanih s smrtno obsodbo njenega moža, zapisano, da je Boris Krajnc med poskusi v Dachauu vodil tajne zapiske, ki jih je ob pobegu iz taborišča prinesel s seboj. Nekaj naj bi jih zasegli med hišno preiskavo, nekaj pa jih je v času, ko je podala izjavo, še hranila.

XXXI Arhiv hrani vpisni list v 1. semester študija (september 1933). Primerjal sem značilen način pisanja pisanih črk B, K, S, p, r in z, ki so drugačne kot v zvezku s podatki iz Dachaua.

nejše analize, ki bo predstavila tudi Stepišnikove zapiske (članek v pripravi).

#### 4. Boris Krajnc v gradivih, povezanih s taboriščem Dachau

V Arolsenkem arhivu (International tracking service, Bad Arolsen, Nemčija) hranijo malo gradiva o Krajncu. Iz taboriščnega vpisnega lista za B. Krajncja je razvidno, da je bil Krajnc pripeljan v taborišče Dachau 18. marca 1942 in izpuščen 22.12.1943. Tik pred izpustitvijo, 10.12., naj bi bil ‚prepeljan‘ in 16.12. ‚vrnjen‘, a iz arhiva ni jasno kje bi bil v vmesnem času. Možno je, da gre za obdobje, ko naj bi ga premestili v Berlin, o čemer je več napisanega v nadaljevanju. Kategorija zapora je bila *Schutzhäftling*, torej varnostni pripornik, kar je pomenilo zapor brez sojenja in brez določenega trajanja zapora. To je bil pogost način odstranitve politično neprimernih ljudi.

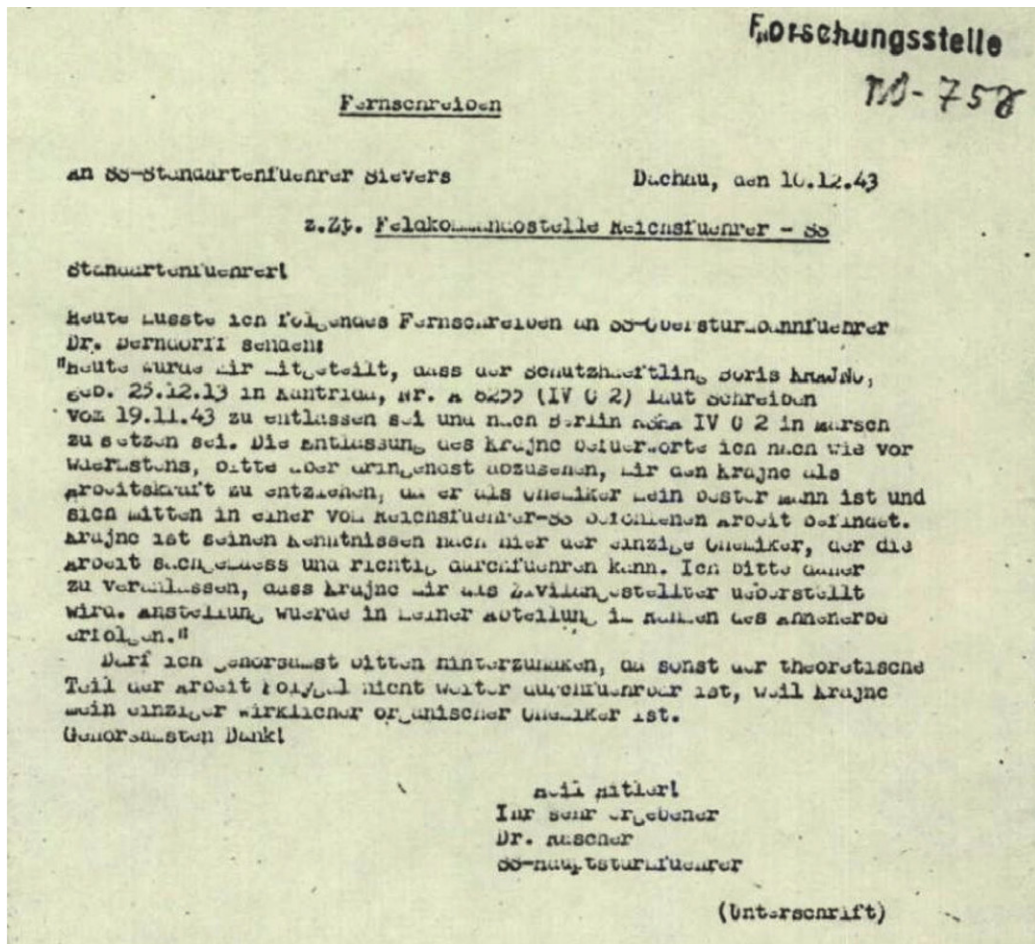
Kot je razvidno iz naloga za oddajo telegrama, ki ga hrani Arolsenki arhiv, razvidno pa je tudi iz zapisnika sojenja v Nürnbergu (2. 1. 1947) je 10. 12. 1943 Rascher pisal svojemu nadrejenemu v ustanovi Ahnenerbe (slika 3) glede Borisa Krajncja, za katerega je zvedel, da naj bi ga izpustili v skladu z odločitvijo od 19. 11. 1943 in ga premestili v nemški glavni varnostni urad v Berlinu<sup>XXXII</sup>. Sicer da podpira njegovo izpustitev, a nujno prosi, da bi Krajnc ostal pri njem, kajti je sredi dela, ki ga je naročil načelnik SS, Krajnc pa je Rascherjev najboljši kemik, ki zna delo opraviti strokovno in korektno. V nasprotnem teoretičnega dela raziskave na poligalu ne bo mogoče dokončati, saj je Krajnc njegov edini organski kemik<sup>34</sup>.

Ostalo gradivo v Arolsenkem arhivu ne razkriva Krajncjeve vloge v (psevdo)medicinskih poskusih. Izrecno je omenjen kot kemik samo pri poskusih strjevanja krvi in sicer v zbirnem poročilu<sup>35</sup>, pripravljenem po vojni na osnovi primarnih virov, predvsem korespondence dr. Rascherja in delovnega poročila o preparatu. Arolsenka arhivska služba ni našla podatkov o tem, da bi Krajnc sodeloval pri drugih poskusih v Dachauu.

Gradiva o Krajncu je v Arolsenkem arhivu leta 1970 preverjalo javno tožilstvo pri deželnem sodišču München II v povezavi s preiskavo proti nekdanjim članom SS, ki so sodelovali pri medicinskih poskusih v koncentracijskem taborišču Dachau. Iskali so morebitne priče poskusov, predvsem preživele poskusne osebe, pa tudi morebitne sodelavce pri poskusih. Med temi so iskali tudi podatke o Vladimiru Premruju<sup>XXXIII</sup>, saj naj bi iz arhivskih dokumen-

XXXII V zapisniku je navedena oznaka urada RSHA LV C 2, a gre verjetno za napako in bi namesto LV moralo pisati IV, kar bi pomenilo Urad IV, to je bil protiobveščevalni urad, oddelek za kartoteke, pisarna za taboriščne zadeve. Urad LV ni obstajal. V Rehmovi knjigi o Rascherju je naveden urad IVC2.

XXXIII Več o Premruju je navedenega v nadaljevanju, ob obravnavi ostalih slovenskih kemikov, ki so sodelovali pri poskusih v nemških taboriščih.



**Slika 3:** Dopis S. Rascherja vodji organizacije Ahnenerbe, dr. Sieversu. V telegramu, ki je bil tudi del dokaznega gradiva proti Sieversu na Nürnberškem procesu, Rascher prosi, da bi Krajinca po odpustu iz varnostnega pripora zaposlil kot kemika v okviru raziskovalne skupine, ki jo je Rascher vodil. V ključnem delu dopisa pravi: »Krajinčičovo izpustitev še naprej najtopleje zagovarjam, vseeno pa najmanj prosim, da se odpravite temu, da bi Krajinčič zapustil delovno mesto pri meni, ker je kot kemik moj najboljši mož in sredi dela, ki ga je ukazal državni vodja SS-a. Krajinčič je po svojih znanjih tu edini kemik, ki zna opraviti delo strokovno in natančno. Zato prosim, da poskrbite, da bi Krajinčiča premestili k meni kot civilnega uslužbenca. Zaposlitev bi bila na mojem oddelku v okviru Ahnenerbe. Dovolite, da najpokorneje prosim, da se zavzamete za to zadevo, sicer teoretični del projekta Polygal ne bi bil več izvedljiv, saj je Krajinčič moj edini pravi organski kemik.« Vir: Digitalni arhiv ITS, Bad Arolsen, št. dokumenta 4.2 / 82231970.

tov javni tožilec ugotovil, da je bil marca 1944 dodeljen skupini dr. Rascherja.

V zborniku o taborišču Dachau je v poglavju o jugoslovanskih komunistih<sup>36</sup> navedeno, da naj bi Krajinčič konec maja 1944 (očitno ob odhodu na dopust) v Slovenijo v tubi zobne paste pretihotapilo poročilo slovenskih komunistov o stanju v taborišču. Poročilo sta napisala Bogdan Švent in Jože Zakovšek, namenjeno pa je bilo Rudiju Janhubi<sup>XXXIV</sup>, ki je bil takrat v Beli Krajini. Pri posredovanju poročila Krajinčiču je sodeloval Branko Diehl.

O Sigmundu Rascherju je leta 2006 izšel roman z naslovom »Der Untergang des Hauses Rascher« (Konec

XXXIV **Rudi Janhuba** (1914–1976) je bil španski borec, ki je po porazu republikancev bil interniran v Franciji, nato pa je bil na prisilnem delu v Nemčiji, od koder je leta 1941 ušel in se pridružil partizanom, kjer je dosegel čin podpolkovnika. Bil je delegat centralnega komiteja Komunistične partije Slovenije pri organiziranju partizanov na Štajerskem in Koroškem, nato pa je deloval v varnostno-obveščevalni službi v Ljubljani<sup>37</sup>. Po vojni je deloval kot časnikar in diplomat. Med špansko državljansko vojno je nekaj časa deloval v mestu Albaceta, tako kot Branko Diehl.

Rascherjeve hiše<sup>XXXV</sup>), ki v največji meri temelji na zgodovinskih gradivih. Ta so v romanu tudi citirana. Avtor romana je Hubert Rehm<sup>XXXVI</sup>, a je pri tem delu uporabil psevdonim Siegfried Bär. V tem dokumentarnem romanu se Krajinčič pojavlja na več mestih, a roman ne daje natančnejšega vpogleda v njegovo delo. Več je napisanega o drugem Rascherjevem sodelavcu iz današnje Slovenije,

XXXV Kot navaja avtor v 5. izdaji (2020)<sup>25</sup>, je naslov parafraziran po zgodbi Edgarja Allana Poeja The Fall of the House of Usher, v nemškem prevodu Der Untergang des Hauses Usher. Zgodba govori o R. Usherju, kar se izgovori podobno kot Rascher. V slovenščini so prevodi za Poejevo delo različni, zadnji prevod Jožeta Udoviča pa ima naslov Konec Usherjeve hiše, zato sem temu ustrezno prevedel tudi naslov Rehmovega romana.

XXXVI **Hubert Rehm** (roj. 1951) je leta 1983 doktoriral iz biokemije in je nato deloval kot raziskovalec, a se je kasneje posvetil pisanju in založniškemu delu. Je soizdajatelj nemške strokovne revije Laborjournal in je avtor ali soavtor več učbenikov oz. laboratorijskih priročnikov s področja biokemije. Piše tudi satirično prozo, npr. o tem, kako postati univerzitetni profesor, in kritična dela o financiranju raziskovalnega dela v Nemčiji. Roman o dr. Rascherju je doživel že 5. izdajo in je bil preveden tudi v angleščino.

Rudiju Punzengruberju<sup>XXXVII</sup>. Krajnc je obširneje omenjen predvsem v kontekstu njegove premetitve iz statusa zapornika v sodelavca, zaposlenega preko ustanove Ahnenerbe, decembra 1943<sup>XXXVIII</sup>. Nadalje je navedeno, da je oktobra 1944 pobegnil iz Schlachtersa, vse nadaljnje omembe pa so povezane s sojenjem v Ljubljani. Schlachters je ime kraja, kjer je Rascher organiziral proizvodnjo preparata Polygal in je bil uradno delovna podružnica taborišča Dachau. Šlo je za zakup mlekarne, ki je bil pravno urejen konec marca 1944, takrat že brez Rascherja. Tam je najprej delalo okrog 5 zapornikov, kasneje pa verjetno nekaj več.

Poleg Krajnc (in Punzengruberja, ki pa se ni imel za Slovenca), Rehmovega knjiga od slovenskih kemikov omenja samo še Vladimira Premruja, ki naj bi ga Rascher vključil v delo svoje skupine po tem, ko je od Punzengruberjeve mame Dore zvedel, da je zaprt v Dachauu.

Slovenski kemiki so omenjeni tudi v knjigi Julijana Reitzensteina o raziskavah pod Himmlerjevim okriljem in v okviru ustanove Ahnenerbe<sup>40</sup>. Na seznamu ‚kdo je kdo‘ na Inštitutu za namenske vojaškoznanstvene raziskave (priloga v knjigi) so omenjeni Krajnc (zapisano napačno: Krajic in brez akademskega naziva, zgolj kot sodelavec-zapornik), Punzengruber in Stepišnik (zapisano napačno: Stepinski).

Uradni nemški in zavezniški viri iz povojnega obdobja ne vsebujejo podatkov o tehničnem osebju, ki je delalo v Rascherjevi skupini.

XXXVII **Rudolf Emanuel Punzengruber** je bil rojen leta 1900 v Črni na Koroškem (Schwarzenbach). Kot navaja Rehm<sup>25</sup>, je na graški univerzi študiral kemijo in tam doktoriral decembra 1925 z disertacijo o alkalni hidrolizi etilestrov očetne kisline s karbonati enovalentnih kationov Li<sup>+</sup>, Na<sup>+</sup> in Rb<sup>+</sup>. Doma so imeli kmetijo, žago in trgovino. Bili so pronemško usmerjeni in so podpirali nacionalsocializem, čeprav je bila njegova mama Slovenka. Med obema vojnama se je zapletel v finančne škandale, ob izbruhu vojne pa je bil verjetno zaposlen pri kraljevi vojski v Beogradu, kjer je bil prijavljen v hotelu Astoria. Maja 1941 so ga pripripi in v preiskovalnem zaporu je ostal do konca junija 1942, ko so ga premestili v taborišče Dachau. S posredovanjem Rascherjevega sodelavca Neffa je prišel v raziskovalno skupino dr. Rascherja, kjer je sodeloval pri poskusih podhlajevanja, vzporedno pa je razvijal zaščitni premaz proti rji. Postal je nekakšen vodja kemikov in pod njegovim vodstvom jih je delalo 5<sup>72</sup>, med njimi Krajnc. Punzengruber je dajal videz premožnega človeka, čeprav to ni bil. Z Rascherjem sta se dobro razumela, tako da je Rascher septembra 1943 preživel dopust v Mežiški dolini. Istega meseca je bil Punzengruber izpuščen iz taborišča, a je nadaljeval delo v Rascherjevi skupini, čeprav je bil formalno dodeljen policiji kot rezervist, zato ga niso vpoklicali na fronto. Marca 1944 se je izkazalo, da sredstvo proti rji še ni primerno za proizvodnjo, zato so nadaljevali z njegovo optimizacijo, a neuspešno, tako da so julija 1944 umaknili patentno prijavo zanj. Oktobra 1945 se je Punzengruber poročil s Giso Schäfer, roj. Wagner, tehničarko na univerzitetni kliniki v Münchnu, kamor je prej prinašal vzorce v analizo. Po vojni so Američani Punzengruberja aretirali in najprej zaprli v Dachau, nato pa preselili v zaporniško krilo sodišča v Nürnbergu. Priča je proti Rascherju in na vsak način poskusil zmanjšati svojo vlogo v Rascherjevi skupini<sup>38,39</sup>. Iz neznanega razloga je v ameriških sodnih virih naveden kot zdravnik (tako je omenjen tudi v knjigi nekdanjega bolničarja v Dachauu, zgodovinarja Stanislava Zamečnika Das war Dachau). Kasneje se je podpisoval tudi kot Rolf Punzengruber. Do leta 1966 je živel v Münchnu, kjer je tudi pokopan.

XXXVIII Krajnceva mesečna plača je bila 385 mark<sup>40</sup>.

V Arolsenkem arhivu hranijo kopijo dokumenta od 11. januarja 1944, ki so ga iz taborišča poslali na policijsko upravo (verjetno mesta Dachau), v njem pa je navedeno, da je bil Boris Krajnc z dnem 22. 12. 1943 izpuščen iz zapore in sočasno sprejet v delovno razmerje v Uradu A<sup>XXXIX</sup> Personalnega štaba SS-a – to je bil urad, pod katerega je sodil Rascherjev oddelek v okviru Inštituta za namenske vojaškoznanstvene raziskave. Policijsko upravo prosijo, da Krajncu izročijo ustrezne papirje, med drugim tudi karte za hrano in oblačila. Da je šlo za delovno razmerje, potrjuje tudi seznam tujcev<sup>XL</sup>, ki so med vojno bivali na področju kasnejše ameriške zasedbene cone in so ga lokalne oblasti kmalu po vojni pripravile za zavezniške sile z namenom razjasnitve usode tujcev. Na tem seznamu<sup>XLI</sup> je navedeno, da je bil Krajnc 26. 3. 1944 zaveden v kartoteki Urada za delo München, izpostava Dachau. Kot je razvidno iz po vojni pripravljenega seznama prebivalcev občine Dachau<sup>XLII</sup>, je bil Krajnc tam prijavljen od 22. 12. 1943, za dopust konec maja 1944 pa se je začasno odjavil.

Zanesljivih dokumentov o njegovem bivanju v obdobju od junija do novembra 1944, ko naj bi se vrnil na Jesenice<sup>XLIII</sup>, sprva ni bilo mogoče najti. Možno bi bilo, da je po vrnitvi z dopusta živel in delal v Schlachtersu kjer so v tistem času pripravljali obrat za proizvodnjo tablet Polygal. Prav tako maja 1944 naj bi v Schlachters iz Dachaua bil premeščen Janko Ravninar, še en Slovenec iz Rascherjeve skupine, kjer je sodeloval kot pomožni delavec, po poklicu pa je bil krojač. V Rehmovem dokumentarnem romanu je

XXXIX Od leta 1940 naprej je pod to oznako treba razumeti SS-ovo organizacijo Ahnenerbe.

XL V povojnem času so zavezniške zasedbene sile sistematično zbirale podatke o dogajanju v Nemčiji med 2. svetovno vojno, odkriti pa so želeli tudi usodo številnih zapornikov, prisilnih delavcev in drugih, ki so jih nemški okupatorji prepeljali v Nemčijo. Tako so med drugim morali lokalni uradi sestaviti popise vseh tujcev, ki so med vojno bivali v Nemčiji in sezname zaposlenih tujcev v nemških podjetjih.

XLI Seznam jugoslovanskih delavcev, ki ga je pripravil Urad za delo iz Münchna, str. 3 seznama izpostave Dachau, interna oznaka strani ITS 074. Na istem seznamu (str. 6 oz. ITS 077) je tudi Milan Stepišnik (več o njem v nadaljevanju) z datumom evidentiranja 15. 9. 1944. Gre za takoi-menovani Formular 11.

XLII Na seznamu tujcev ‚jugoslovanske narodnosti‘, ki so ga pripravili na občini Dachau avgusta 1946, je Boris Krajnc vpisan s priimkom Kraync. Prebivališče (Formular 7; stran ITS 090) je prijavil z datumom 22. 12. 1943 in datumom objave 24. 5. 1944. Na formularju za popis dokumentov (Formular 10, stran ITS 224) pa je navedeno, da je bila personalna mapa za zaposlitev odprta 14. 1. 1944. Kartotečna kartica navaja naslednje podatke: Kraync Boris, dipl. inž. kemije, rojen 25. 12. 1913 v Kantridi (prej Italija, zdaj nemško), vera rk (rimskokatoliška), priselitev iz KL (koncentracijskega taborišča) Dachau 22. 12. 1943, odselitev 24. 5. 1944 v Cilli (Celje), ponovna priselitev 6. 6. 1944 iz Cilli; državljanstvo: nekdanja Jugoslavija, narodna pripadnost: Slovenija. Stepišnik je v isti evidenci zaveden z datumom prijave 21. 7. 1944 (prihod iz koncentracijskega taborišča Dachau) in objave 1. 11. 1944. Na evidenčni kartici je navedeno, da se je odselil v Aßling/Oberkrain (Jesenice na Gorenjskem).

XLIII Po mnenju Huberta Rehma naj bi Krajnc pobegnil iz Schlachtersa oktobra 1944, vendar je po naknadnem preverjanju (osebna komunikacija) ugotovil, da ni nobenega zanesljivega podatka o tem, da je res bil del ekipe za pripravo preparata Polygal v Schlachtersu.

navedeno, da je Krajnc pobegnil domov iz Schlachtersa oktobra 1944, čeprav je iz povojnih slovenskih virov, predvsem številnih zaslišanj, mogoče ugotoviti, da se je vrnil na Jesenice novembra tega leta. Iz zapisnikov preiskovalnega postopka pred dachauskim procesom je razvidno, da je Krajnc pobegnil iz Dachaua na osnovi ponarejenega dokumenta, ki ga je z Jesenic prinesel Milan Stepišnik, zato je podatek o pobegu iz Schlachtersa dvomljiv. Prav tako je v romanu navedeno, da naj bi bil Krajnc španski borec. Res se pojavlja v nekaterih knjigah o mednarodnih brigadah v španski državljanski vojni<sup>XLIV</sup>, ni pa ga na seznamih, ki so jih sestavili jugoslovanski prostovoljci v tej vojni.

## 5. Krajnc kot obdolženec na Diehl-Oswaldovem procesu

V preiskavi, ki ji je sledil prvi dachauski proces v Ljubljani, je bil Krajnc aretiran 27. 10. 1947 (podatek iz obtožnice vojaškega sodišča od 16. 4. 1948). Ohranjen je zapi-

snik hišne preiskave na dan aretacije. Trajala je eno uro, v njej pa so zasegli med drugim dve mapi korespondence in dve mapi strokovnega gradiva.

Obtožnica je Krajncu bremenila, da je februarja 1942 v begunjskih zaporih prostovoljno začel sodelovati z Gestapom in mu priznal svoje sodelovanje z Osvobodilno fronto ter s tem izpostavil svoje sodelavce; da se je v Dachauu marca 1942 povezal z agentom Martinom Presterlom, mu poročal o sointernirancih in sodeloval v lažni protifašistični provokatorski organizaciji; da je od januarja 1943 do novembra 1944 v poizkusni postaji aktivno sodeloval s krvnikom Rascherjem in Plötnerjem pri najgrozovitejših zločinih; da je kot agent Gestapa posredoval pri vodstvu taborišča, da so bili na poizkusne postaje pritegnjeni še Stepišnik, Barle, Ličen in drugi, s čimer je soodgovoren tudi za njihove zločine. Obtožen je bil tudi oddaje lažne biografije, da bi se po vojni vrnil na vplivno mesto, od koder bi črpal tajne podatke kot bivši gestapovski agent in da bi protežiral gestapovske agente s pisanjem pozitivnih karakteristik. Nadalje je bil obtožen za povezavo s tujo obveščevalno službo

g. major, ne zavezite me! Z najtežjimi deli, z  
nimitejnjo najtežjimi naloz bi hotel dobiti, da me pripravijo  
iskano sodelovati. Občan sem, ki ne vidim ribode. Iskano  
bi hotel privedati kaj mi o koncu, pa me ne vidite ni.  
Ne maram se mi tako lahkimino iskat. s mojo usodo kot  
dostoj. Verjete, da me ni vel se ferd, da bom gornik  
samo mesico. Spuhalat me moj polotaj dostoj jeno, da me  
prijel do tope delepa. ~~.....~~  
~~.....~~  
Boris Krajnc

Takrat, ko bi mogel opraviti vaše zavezanje, me se iskat  
z napi. kadej, ko bi ga ne fufetoval, pa vidim, da me  
ga iskat.

**Slika 4:** Rokopisna izjava Borisa Krajncu iz časa preiskave za Diehl-Oswaldov proces. Dokument ni datiran, verjetno pa sodi v obdobje malo pred sojenjem aprila 1948. Vir: Arhiv Republike Slovenija, SI AS 1931, RSNZ SRS, Dachauski procesi, šk. 512.

XLIV Krajnc je naveden v knjigi Las brigadas internacionales de la guerra de España (Andreu Castells, Esplugues de Llobregat: Editorial Ariel, 1974), vendar le kot soobtoženi na dachauskem procesu, kjer so sodili tudi številnim španskim borecem. Edina zgolj teoretična možnost, da bi kakor koli sodeloval pri zadevah, povezanih s špansko državljansko vojno, bi bila v času študija, saj so mednarodne brigade razpustili septembra 1938.

junija 1945 ter da ji je poročal o dogajanju na univerzi in da je izvajal škodljive aktivnosti po navodilu tuje obveščevalne službe. Obtožnica je bila vložena 2. 12. 1947.

V knjigi o dachauskih procesih<sup>33</sup> je Boro Krivokapić citiral pritožbo Krajncve žene Ivanke Komisiji za prošnje in pritožbe Centralnega komiteja Zveze komunistov Slove-

nije z dne 12. 4. 1969. V tem dolgem pismu je navedeno, da je pod Krajnčevim mentorstvom opravljala diplomsko nalogo Jelka Ružič<sup>XLV</sup>, takrat svakinja, kasneje pa druga žena<sup>XLVI</sup> Borisa Kraigherja (v času sojenja je bil minister za notranje zadeve LR Slovenije). S posredovanjem Jelke Ružič je Krajnčevi uspelo priti na zasebni obisk k Borisu Kraigherju, ki ji je povedal, da bo Boris Krajnc nekaj časa zaprt in da se je to zgodilo na zahtevo tuje velesile. Nekateri menijo, da je šlo za Sovjetsko zvezo, neposrednih dokazov za to pa ni.

Sojenje pred vojaškim sodiščem<sup>XLVII</sup> je potekalo med 20. in 24. aprilom 1948, razglasitev sodbe pa je bila dva dni kasneje. To je bil prvi izmed dachauskih procesov in hkra-ti največji. Pogosto ga poimenujejo po dveh prvoobtoženih Diehl-Oswaldov proces. Danes velja, da je šlo za montiran proces, pri katerem so obdolžence s fizičnim in psihičnim nasiljem prisilili v priznanje dejanj, ki jih niso zagrešili. Nazoren prikaz postopkov, ki so jih uporabljali v zasliševanjih, je pričevanje Vlasta Kopača<sup>41</sup>, ki je bil na Diehl-Oswaldovem procesu obsojen na smrt, a so mu po pritožbi omilili kazen na 20 let zapor, nato pomilostili na 10 let in ‚začasno‘ izpustili aprila 1951. Na sojenju je bil pogosto edini dokaz za očitano dejanje lastno priznanje obdolženca, obramba, ki je bila imenovana, pa ni imela vpogleda v obtožnico in je bila pod pritiskom oblasti. Redkih dokazov v prid obdolžencem sodišče ni upoštevalo, večinoma pa odvetnikom niso dovolili povabiti prič, ki bi koristile obdolžencem. Na tem nepoštenem sojenju so izrekli izredno visoke kazni, saj so od 14 obdolžencev kar enajstim izrekli smrtno kazen. Upoštevati pa je treba še tri preiskovance, ki so umrli med preiskavo.

Krajnc je med zaslišanji priznal sodelovanje z Gestapom, ki naj bi ga podpisal v zaporu v Begunjah, in še nekatera druga očitana dejanja, vendar teh izjav ni mogoče šteti za verodostojne. Pod kakšnim pritiskom so bili preiskovanci, je mogoče razbrati iz Krajnčevega pisma majorju (verjetno preiskovalcu), ki ga hrani Arhiv Republike Slovenije (slika 4). Pri uporabi gradiv iz časa preiskave in s sojenja je potrebna posebna previdnost, podobno kot velja tudi pri arhivskih dokumentih tajnih služb<sup>42</sup>.

## 6. Drugi kemiki na dachauskih procesih

**Milan Stepišnik** (1910–1950?) je bil tako kot Krajnc kemik (diplomiral 1935, tri leta pred Krajncem) in je bil obsojen na istem dachauskem procesu kot Krajnc. Stepišnik je diplomiral na Tehniški fakulteti z nalogo »Analogi-

ja med nikotinsko in m-nitrobenzojevo kislino« pod mentorstvom Marija Rebka. Znan je bil tudi kot vrhunski atlet. Med drugim se je udeležil olimpijskih iger v Berlinu leta 1936, kjer je bil zastavonoša jugoslovanske reprezentance, bil pa je tudi večkratni balkanski prvak<sup>XLVIII</sup>. Znana je fotografija treh prvovršenih atletov na tekmovanju v jeseni 1941<sup>XLIX</sup>, kjer na zmagovalnem odru prvi in tretji pozdravljata s fašističnim pozdravom, Stepišnik kot drugi pa stoji mirno.

Do začetka vojne je bil zaposlen v tovarni Zogmeier-Gruber v Slovenski Bistrici, nato pa je bil do junija zaprt v Mariboru, čemur je sledila izselitev v Lazarevac v Srbiji. Od tam se je kmalu vrnil, saj so mu odobrili preselitev v Ljubljansko pokrajino, tako da je že 2. julija 1941 prišel v Ljubljano in se avgusta zaposlil v papirnici v Vevčah. Zaradi sodelovanja z Osvobodilno fronto so ga novembra 1943 belogardisti<sup>1</sup> aretirali, kasneje pa so ga internirali v Dachau. V ameriški bazi Holocaust Survivors and Victims Database je zaveden s priimkom Stepiniks, datum prihoda v Dachau 7. december 1943, datum odpusta 21. julij 1944, kar verjetno sovпада z njegovo redno zaposlitvijo v Dachau, podobno kot pri Krajncu. Že nekaj dni po prihodu v taborišče so ga kot kemika vključili v delo Rascherjeve skupine, nadaljeval pa ga je tudi kasneje, ko je skupino prevzel Plötner. Delal naj bi izključno pri pripravi tablet za strjevanje krvi, skupaj z Jankom Puflerjem<sup>LI</sup>. V dokumen-

XLVIII V metu kladiva je osvojil kolajne na 6 predvojnih Balkanskih igrah, od tega 3 zlate. Štirikrat je izboljšal državni rekord v tej disciplini. Tudi po vojni je še tekmoval in je bil zastavonoša slovenske atletske reprezentance na prvem povojnem jugoslovanskem atletskem prvenstvu (Zagreb, 1945), kjer je osvojil 6. mesto v metu diska, v metu kladiva pa je bil drugi. Leta 1946 je na balkanskih igrah v Tirani osvojil bronasto medaljo v metu kladiva<sup>43</sup>.

XLIX Fotografija je nastala 14. 9. 1941 na atletskem mitingu za pokal Iva Scapola na stadionu v mestu Schio pri Vicenzi, ki ga je dve leti prej otvoril Benito Mussolini. Na tem tekmovanju so nastopili vsi najboljši italijanski lahkoatleti, v dogovoru z njihovo atletsko zvezo pa prvič po priključitvi Ljubljanske pokrajine Italiji tudi trije naši tekmovalci. V metu kladiva je zmagal italijanski prvak Teseo Taddia, Stepišnik je bil drugi, tretji pa je bil Cecchini.

L V dopisu Stepišnikove žene Poldke je navedeno, da so v njihovo stanovanje vdrli oboroženi belogardisti in odpeljali moža ter dve sosedki. Kot sodelavca OF so ga nameravali še isto noč ustreliti na Urhu, vendar so ga zato, ker je sama doživela živčni zlom in so jo morali odpeljati v bolnišnico, na koncu odpeljali v zapor, ne na streljanje.

LI **Janko Pufler** (1905–1950?) je bil steklar v Hrastniku, kjer so ga že leta 1926 sprejeli v komunistično partijo, leta 1928 pa so ga izgnali, tako da je naslednja leta preživel v različnih državah Evrope. Spomladi 1937 je prišel iz Sovjetske zveze kot prostovoljec v Španijo, kjer je bil v vlogi inštruktorja. Po koncu državljanske vojne je bil v več francoskih taboriščih. Julija 1942 ga je aretiralo Gestapo v Gradcu, februarja 1943 pa so ga zaprli v taborišče Dachau. Po nekaj tednih so ga dodelili za steklopahača v ‚poskusni postaji‘, kasneje pa naj bi kot laborant sodeloval pri razvoju tablet za strjevanje krvi, a je verjetno, da je bil predvsem zadolžen za pripravo in čiščenje steklovine. Leta 1944 so ga preselili v podružnico Schlachters in tik pred koncem vojne v Lochau. V nekaterih virih je naveden kot Hans Puffer ali Janco Puffer. Decembra 1945 so ga postavili za direktorja steklarne Hrastnik, a so ga oktobra 1946 razrešili zaradi spora s političnimi organizacijami v podjetju. Proti koncu tega meseca je v nočni izmeni izbruhnil požar, zaradi katerega je prišlo do zastoja v proizvodnji. To so oblasti prikazale kot sabotažo in so zato na celjskem okrožnem so-

XLV Jelka Marija Ružič je diplomirala šele leta 1949, torej več kot eno leto po Krajnčevi aretaciji.

XLVI Boris Kraigher je bil najprej poročen s sestro Jelke Ružič, arhitektko Miro Ružič<sup>71</sup>.

XLVII Samo prvi dachauski proces je potekal pred vojaškim, vsi naslednji pa pred civilnim sodiščem.



taciji za obnovo procesa piše, da naj bi pomagal Puflerju pri pripravi pektinskih tablet<sup>LII</sup> in da naj ne bi sodeloval pri poskusih na internirancih.

V drugi polovici oktobra 1944 je bil na dopustu v Ljubljani in na Jesenicah, kjer je pridobil potrdilo, da so ga pripravljene zaposliti v železarni na področju, pomembnem za nemško vojaško industrijo. Na osnovi tega so mu v Dachau dovolili, da se s 1. novembrom 1944 vrne domov. Iste meseca se je zaposlil v šamotarni železarne na Jesenicah. Po vojni so ga postavili za ‚delegata‘ Ministrstva za industrijo in rudarstvo v Industriji metalnih polizdelkov (kasnejši Impol) v Slovenski Bistrici, kar je ustrezalo funkciji direktorja. Kot član državne delegacije je v začetku leta 1947 nekaj mesecev pregledoval nemška kemična podjetja glede vojnih reparacij. V času pomanjkanja materialov je sam poskrbel za pripravo mase za šamotno oblogo talilne peči v Impolu, ki pa, verjetno zaradi nekakovostnih surovin, ni zdržala dolgo, kar so oblasti prikazale kot sabotažo. Aretirali so ga 30. septembra 1947 in na Diehl-Oswaldovem procesu obsodili na smrt. Zdi se verjetno, da so kazni izvršili šele leta 1950<sup>LIII</sup>, obstajale pa naj bi tudi pričbe, ki so se oglasile svojcem in naj bi ga videle še kasneje, tako da naj bi po mnenju nekaterih umrli šele leta 1974 (izročilo družine Stepišnik).

**Karel Barle** (1910–1948) iz Šmartnega pri Slovenj Gradcu je bil inženir kemije. Študij je začel v Ljubljani, zaključil pa v Avstriji, kamor je leta 1934 emigriral po nalogu Komunistične partije Jugoslavije. Bil je prostovoljec Španske državljanske vojne, ko se je ta končala pa je bil v več francoskih in nemških taboriščih. Aretirali so ga v Brestu v Franciji konec novembra 1941, v Dachau pa je prispel 22. avgusta 1942 in od marca 1943 delal kot kemik najprej pri ohlajevalnih poskusih, kasneje pa je sodeloval pri ra-

dišču izvedli sojenje proti Puflerju, njegovemu delavcu Jožetu Bengaliji in še dvema sodelavcema. Po pritožbi je višje sodišče sodbo razveljavilo in vrnilo zadevo prvostopenjskemu sodišču pod spremenjenim senatom. Na Diehl-Oswaldovem procesu so Puflerju poleg sabotaže očitali še vrsto drugih dejanj iz časa vojne in pred njo. Tako so ga na primer obdolžili, da je bil sodelavec Gestapa že od leta 1928 (kar je priznal), pri čemer so Gestapo ustanovili šele leta 1933. Obsojen je bil na smrt. Jože Benegalija je bil na istem procesu obsojen na 18 let prisilnega dela, a so ga iz zapora izpustili leta 1954.

LII Dokaj nelogično se zdi, da bi Stepišnik, ki je bil kemik z izkušnjami, pomagal Puflerju, steklarju, pri pripravi pektinskih preparatov. Bolj verjetno je obratno. Navedeno je tudi, da naj bi stika s poskusnimi osebami sploh ne imel, kar je prav tako malo verjetno, glede na najdene njegove zapiske o rezultatih preiskav na poskusnih osebah.

LIII Po uradnem zapisniku naj bi vse na smrt obsojene na prvem dachauskem procesu usmrtili 12. maja 1948, a so v osebni arhivu Borisa Kraigherja<sup>44</sup> našli rokovnik za vpenjanje listov manjšega formata, ki je vseboval predvsem kratke zabeleške. Pri 18. oktobru 1952 je najprej navedeno ime Nikič, kar bi lahko pomenilo Boris Nikič (s pravim imenom Niko Šilih, pomočnik načelnika Udbe za Slovenijo), sledijo priimki 24 zapornikov, obsojenih na smrt. Pri nekaterih je za imenom znak +, kar bi bilo mogoče razumeti kot oznako za likvidacijo, ne pa nujno. Nekatera imena nimajo te oznake, nekatera so zapisana v oklepaju, nekatera z znakom – pred imenom, nekatera pa so podčrtana. Kaj bi to pomenilo, ni znano. Poleg Stepišnika so bili navedeni in označeni s + še dachauski obsojenci Diehl, Oswald, Juranič, Ličen in Pufler. Krajnc na tem seznamu ni, prav tako ne Barleta.

zvoju pektinskih tablet. Boris Krajnc je v preiskovalnem postopku natančno opisal Barletov prihod v Rascherjevo skupino. Pri tem je omenil tudi to, da mu je Barle povedal, da je v Španiji (v Albaceti) kot kemik izvajal mikrobiološke preiskave vode. Nadalje je povedal, da se je za vključitev Barleta v raziskave zelo zavzemal Rudolf Punzengruber (gl. op. XXXVII), ki je bil tudi s Koroške, ker je mislil, da bosta prijateljevala, a kasneje nista. Barle je bil v taborišču član prvega jugoslovanskega taboriščnega komiteja<sup>LIV</sup>. Kot kemik je sodeloval pri tehničnem delu priprave poročila o stanju v koncentracijskem taborišču Dachau<sup>LV</sup>. Aprila 1945 je v Schlachtersu, kjer so vzpostavljali proizvodni obrat za pektinske tablete, spoznal bodočo ženo Reziko (Theresia, roj. Brüstle, 1925–1949) in se z njo poročil junija 1945. Osoboditev je dočakal v dachauski podružnici Lochau na Predarlberškem v današnji Avstriji in se v domovino vrnil šele septembra 1945. Zaposlil se je na Ministrstvu za industrijo in rudarstvo, kasneje pa v Centralnem komiteju KPS, kjer je bil sekretar ekonomske komisije. Aretiran je bil 8. avgusta 1947 in bil zaradi domnevnega sodelovanja s tujo obveščevalno službo in medvojnega

LIV Taboriščni komiteji so bile po nacionalnostih organizirane ilegalne protifašistične organizacije, ki jih je povezoval mednarodni taboriščni komite. Slovenski komunisti so organizirali jugoslovanski taboriščni komite (med jugoslovanskimi taboriščniki so namreč prevladovali Slovenci). Pomembna vloga taboriščnega komiteja je bila pomoč tistim rojakom, ki niso dobivali paketov pomoči od doma in tistim, ki so rabili zdravstveno pomoč, hkrati pa je odbor razširjal informacije o dogajanju v domovini in skrbel za moralno med zaporniki. Če je bilo mogoče, so svoje zanesljive člane razporejali na delovne naloge, kjer bi lahko pomagali drugim, ali poskušali preprečiti transporte svojih članov v uničevalna taborišča. Konec leta 1944 so se odločili ustanoviti širšo organizacijo taboriščnikov s protifašistično usmeritvijo, a je do ustanovitve prišlo šele aprila 1945. Z osvoboditvijo taborišča Dachau 29. aprila 1945 se je jugoslovanski narodnoosvobodilni odbor preoblikoval v Jugoslovanski nacionalni odbor<sup>36</sup>. Na dachauskih procesih je tožilstvo nastopalo s pozicije, da je bil taboriščni komite podaljšek Gestapa oz. da je šlo za ‚provokatorsko‘ antifašistično organizacijo. To je bila ena od točk obtožnice pri Karlu Barletu, Borisu Krajncu in nekaterim drugim obtožencem na dachauskih procesih.

LV Šlo je za dve poročili, napisani v žepno beležnico z nevidnim črnilom, ki ga je izdelal Karel Barle. Prvo poročilo je napisal takratni sekretar taboriščnega jugoslovanskega partijskega komiteja Vlasto Kopač in v njem prosil KPS za usmeritve glede delovanja komunistov v taborišču. Drugo poročilo je pripravil sovjetski taboriščni partijski komite v ruščini, namenjeno pa je bilo sovjetskemu predstavniku v glavnem štabu NOV in POS. Beležnico s poročilom je ob vrnitvi v Slovenijo v jeseni 1944 s seboj prinesel Milan Stepišnik<sup>36</sup>. Iz izvlečkov izjav Borisa Krajnc in Milana Stepišnika med preiskavo v letih 1947/1948 je mogoče ugotoviti, da je Stepišnik ob odpustu iz Dachaua s seboj prinesel manjši zvezek (‘notez’), ki naj bi ga z nevidno pisavo popisal ‘DiI’ (Branko Diehl), namenjen pa naj bi bil Krajncu. Stepišnik je povedal, da je v Dachau skupaj z Barletom dodelal postopek, pri katerem je besedilo napisano z raztopino svinčevega nitrata, nevidno pisavo pa nato razvijejo z vodikovim sulfidom. Krajncova bodoča žena naj bi zvezek poslala Krajncu na Pokljuko, kjer se je pridružil partizanom, a tam ni bilo pogojev, da bi pisavo razvil. Pisavo naj bi kasneje razvila Neža Exel (inž. kemije, diplomirala 1939 kot Agneza Hillinger), ki je pisavo prepoznala kot Diehlovo, a je bila slabo čitljiva. Po mnenju Krajncove žene (zaslišanje 22. 11. 1947) naj bi v zvezku bili »važni podatki o delu in poskusih v lagerju«. Glede na to, da je bil Kopač soavtor članka, v katerem je opisana beležnica<sup>36</sup>, je bolj verjetno, da je poročilo pripravil on, kot pa da je bil avtor Diehl, kot je na osnovi pisave ocenila Neža Exel.

»sodelovanja pri zločinških poskusih« na prvem Dachauskem procesu obsojen na smrt z ustrelitvijo. Verjetno je umrl zaradi neznosnih razmer v zaporu še pred izvršitvijo smrtne obsodbe<sup>19,45</sup>. Njegovo ženo so na 6. dachauskem procesu avgusta 1948 obsodili na smrt zaradi domnevnega vohunstva. V Arhivu Republike Slovenije je v Barletovem dosjeju iz obdobja preiskave za Diehl-Oswaldov proces shranjen njegov opis priprave različnih pektinskih preparatov, predvsem njihov razvoj v Dachauu, zelo malo pa o proizvodnji v Schlachtersu. Ti podatki so, glede na to, da je bil Barle kemik, gotovo bolj verodostojni od tistih, ki jih je v svojih spominih podal Franz Jauk (1904–1995)<sup>LV1</sup>, po poklicu barvarski pomočnik, v Dachauu pa taboriščni pisar bloka 5 in kasneje sodelavec v skupini Sigmunda Rascherja<sup>46</sup>.

**Branko Diehl** (1905–1950?) iz Celja je po maturi na celjski Realki leta 1923 začel s študijem kemije na Dunaju in ga naslednje leto nadaljeval v Ljubljani na Tehniški fakulteti, kasneje pa je diplomiral iz fizike in kemije na Filozofski fakulteti UL (1931). Leta 1933 so ga zaradi delovanja v Komunistični partiji Jugoslavije obsodili na 3 leta zapora. Po povratku se je za kratko zaposlil v rudniku v Mežici, a so ga kmalu ponovno aretirali, po 4-mesečni preiskavi pa se je vrnil v rudnik. Konec junija 1941 so ga v Žerjavu aretirali in kot znanega komunisto zaprli, nato pa poslali v taborišče Dachau, kamor je prišel 15. septembra istega leta kot eden prvih Slovencev oz. Jugoslovancev. Nekaj časa je delal v laboratoriju taboriščne bolnišnice, sodeloval pa je tudi pri delu takoimenovane ‚malarične postaje‘, kjer so izvajali poskuse na taboriščnikih. Vendar naj bi Diehl opravljal samo mikroskopske analize krvi in komarjev<sup>LVII</sup>.

V Dachauu je bil ob osvoboditvi tajnik Jugoslovanskega narodnega odbora, skupine predstavnikov različnih narodov, v kateri so bili predvsem člani Komunistične partije, za glavno nalogo pa je imela organizacijo povratka jugoslovanskih internirancev<sup>LVIII</sup>. Po vojni je bil ‚delegat Ministrstva industrije in rudarstva‘ (direktor) v rudniku v Mežici, glavni inšpektor za gozdarstvo pri Kontrolni komisiji Predsedstva vlade LR Slovenije in član ekonomske komisije Centralnega komiteja Komunistične partije Slovenije. Skupaj z Oskarjem Juraničem (ki je bil prav tako član Jugoslovanskega narodnega odbora) je pripravil povojno oceno delovanja KPJ v koncentracijskem taborišču Dachau. Aretirali so ga 16. septembra 1947 in na Dachauskem procesu obsodili na smrt zaradi domnevnega sodelovanja z Gestapom, dela na ‚malarični

LV1 Več o življenjski poti Franza Jauka je v sestavku<sup>47</sup> H. Halbreinerja.

LVII Vlasto Kopač je v intervjuju s Petrom Vodopivcem<sup>50</sup> leta 1986 povedal, da naj Barle sploh ‚ne bi sodeloval pri poskusih‘ in da je samo ‚seciral komarje in uši‘.

LVIII Ob tem je odbor tudi evidencial tiste internirance, ki so pred aretacijo sodelovali z belo gardo ali okupatorji. Zaslisevali so jih že v Dachauu, nato pa organizirali njihov ločen transport v domovino, kjer so številne ustrelili brez sojenja, proti drugim pa so organizirali sodne procese z izredno nizkimi pravnimi standardi (prim. sestavek<sup>51</sup> Tineta Velikonje iz leta 1995).

postaji, povojnega ustanavljanja vohunske mreže in povojne sabotaže.

**Mirko Pibernik** (1905–1947) se je po maturi na Ljubljanski realki leta 1924 vpisal na Tehniško fakulteto in iz kemije je diplomiral 1928 pod imenom Bogomir. Tema njegove diplomske naloge je bila oksidacija škroba za pripravo topnih oblik, o čemer je naslednje leto izšel članek Maksa Samca v reviji *Kolloidchemische Beihefte*<sup>48</sup>. Bil je tudi aktiven član Sokola in soavtor telovadnega priročnika<sup>49</sup> (izšel 1933). Po odsluženem vojaškem roku v šoli za rezervne oficirje se je poročil in zaposlil v podjetju Medič-Zankl, tovarni olja, lakov in barv, ki je imelo en proizvodni obrat v Medvodah (kasnejši Color) in enega v Domžalah (kasnejši Helios). Pibernik je delal v obeh sočasno, tako da se je redno vozil med obema tovarnama. Marca 1941 so ga mobilizirali v enoto v Srbiji, a se je po kapitulaciji Jugoslavije uspel vrniti v Medvode, kjer je še naprej delal v istem podjetju. Med vojno je stanoval v Medvodah, kjer so v upravni stavbi podjetja poleg kemijskega laboratorija bila tudi stanovanja za zaposlene. Sodeloval je z Osvobodilno fronto in med drugim ilegalno tiskarno preskrboval s tiskarsko barvo, ki so jo delali v tovarniškem laboratoriju. V začetku leta 1944 je bil za kratko zaprt v Ljubljani, morda v povezavi z delovanjem Miklavčeve skupine<sup>LIX</sup> v Medvodah.

Pibernikova družina je med vojno živela v Šiški (sprva pod italijansko zasedbo), tako da jo je le občasno obiskoval s kolesom. Ob povratku je večkrat s seboj vozil pakete za dachauske zapornike in jih oddal na pošti v Medvodah, ki so bile pod nemško zasedbo. Tudi po vojni je ostal zaposlen v tovarni barv in lakov v Medvodah, kjer je bil direktor do prihoda Vladimira Lična na ta položaj, Pibernik pa je postal referent direktorije kemične industrije pri slovenski vladi. Leta 1946 je bil član komisije za povojne reparacije pri jugoslovanski vojni misiji v Berlinu. Aretirali so ga 3. 11. 1947, v času preiskave pa je – po uradni verziji – naredil samomor, a je verjetneje, da je 19. novembra umrl zaradi posledic mučenja. Objavljeni so odlomki z zaslišanj, iz katerih je razvidno, da je (verjetno pod prisilo) menjal izpovedi, tako da so bile v skladu s sugestijami zasliševalcev. V Dachauu ni bil nikoli in njegovo ime se ne pojavlja v gradivih, ki jih hrani največji arhiv za obdobje nacizma v Nemčiji<sup>LX</sup>, zato je absurdno, da je bil osumljen sodelovanja

LIX **Ivan Miklavc** (1890–1944) je bil podjetnik iz Medvod, ki si je med vojno prizadeval za ustanovitev pokrajinskega odbora Osvobodilne fronte za Gorenjsko in s skupino somišljenikov pripravljala organizacijske korake za vzpostavitev oblastnih struktur še pred pregonom Nemcev. Predvideli so tudi že nekatere kadrovske zasedbe, pri čemer so vključevali pripadnike krščanskih socialistov, članov Sokola in komunistov (ki so bili v manjšini), zato nekateri menijo, da Miklavc ni bil po volji takratnega vodstva OF<sup>52</sup>.

LX Na proizvodnje v Arolsenkih arhivih sem dobil podatek, da Pibernika ni v nobenih dokumentih, povezanih z Dachauom, niti kje drugeje v arhivskem gradivu in da ni jasno, zakaj se njegovo ime pojavlja na jetniški evidenčni kartici Vladimira Lična. V zborniku Dachauski procesi<sup>54</sup> je navedeno, da naj bi bil med vojno v Dachauu, a kaže, da navedba ni pravilna (Anton Pibernik, osebna komunikacija). Možna razlaga, zakaj je bil Pibernik naveden na Ličnovi jetniški kartici, je, da mu je redno pošiljal pakete, vendar taki pripisi na karticah niso bili običajni.

z Gestapom. Očitani so mu tudi sodelovanje s tujo obveščevalno službo in sabotažne dejavnosti v povezavi z vžigom ricinusovega olja, kot je razloženo v nadaljevanju.

**Vladimir Ličen** (1912–1950?) je bil rojen v Trstu, a se je družina po italijanski zasedbi po prvi svetovni vojni preselila v Slovenijo. Maturiral je na ljubljanski realki leta 1930, diplomiral pa je na Filozofski fakulteti v Ljubljani iz kemije leta 1936. Vojaški rok je služil v Kruševcu v Srbiji. Leta 1938 se je zaposlil v tovarni barv in lakov Medič-Zankl v Medvodah. Tik pred začetkom vojne v Jugoslaviji je bil mobiliziran, a so ga v Sarajevu ujeli in odpeljali v taborišče v Osnabrücku, nato pa so ga predali italijanskim oblastem, kjer je bil zaprt v več taboriščih za vojne ujetnike, od koder je ušel septembra 1943 in se vrnil v Trst<sup>53</sup>. Tam so ga zaradi ponarejenih dokumentov aretirali in poslali v taborišče Dachau (prispel je 24. novembra).

V taborišču je delal v bolnišničnem laboratoriju do 25. aprila 1944, ko so ga izpustili, za kar naj bi posredoval tudi Leon Rupnik (takratni ljubljanski župan in komandant domobranskih enot). Na zaporniški kartici je (ni jasno, zakaj) pripisano ime inž. Mirka Pibernika. Po izpustitvi je delal v Celovcu v tovarni kvasa in špirta, po osvoboditvi pa se je vrnil v Medvode, kjer je bil najprej obratovodja in kasneje direktor tovarne. Uvedel je nekatere spremembe v postopkih proizvodnje, za kar je bil tudi večkrat nagrajen. Ker je bilo težko dobiti dovolj lanenega olja iz uvoza, je v proizvodnjo vpeljal domače ricinusovo olje, o čemer naj bi se predhodno posvetoval s strokovnjaki z univerze in inštitutov, opravili pa naj bi tudi več preliminarnih analiz. Ko je 3. oktobra 1947 v tovarni prišlo do samovžiga ricinusovega olja, so oblasti to označile kot sabotažo v navezi s tujimi vohunskimi agenturami. Na Dachauskem procesu je bil med drugim obtožen, ker »je dobil nalogo organizirati bakteriološki laboratorij« v taboriščni bolnišnici. Po odpustu ga je tam nasledil Mirko Košir. V preiskovalnem zaporu je bil od 3. oktobra 1947, aprila 1948 pa je bil obsojen na smrt.

**Mirko (Miroslav Jožef) Košir** (1905–1951) je na Filozofski fakulteti UL diplomiral iz kemije, fizike in fizikalne kemije leta 1929. Kemijo je učil najprej dve leti v Kikindi, potem pa v Kranju. Po sojenju mladim komunistom leta 1934, kjer je bil oproščen, se je zaposlil v škrobarni v Domžalah, kasneje pa v Rudarski družbi Trojane, kjer so kopali antimonit. Pred 2. svetovno vojno je bil aktiven v delavskem gibanju in je postal član vodstva Komunistične partije Slovenije. Ob izbruhu 2. svetovne vojne so ga zajeli Nemci, odpeljali v svoja taborišča, nato pa predali Italijanom, ki so ga zaprli v svoja. Po kapitulaciji Italije se je pridružil partizanom, kjer so ga vključili v kulturniško skupino, med nemško ofenzivo pa se je vrnil v Ljubljano. Po aretaciji so ga poslali v Dachau, kamor je bil sprejet 12. 2. 1944. Ko so aprila 1944 iz taborišča Dachau izpustili Vladimira Lična, je prišel na njegovo mesto v taboriščni bolnišnici, kjer je opravljal analize krvi, urina in sputuma. Nato so ga 11. 10. 1944 prepeljali v Sachsenhausen, kjer je kot kemik delal v tovarni granat.

Ob koncu vojne se je preko Prage, Budimpešte in Beograda vrnil v Ljubljano. Deloval je kot prevajalec in predavatelj na ljubljanski univerzi, kjer je bil od 1946 izredni profesor na Tehniški fakulteti in honorarni predavatelj za družbene vede na Gospodarski fakulteti in Akademiji upodablajočih umetnosti<sup>17</sup>. Aretirali so ga 9. aprila 1948 in še isti mesec obsodili na 20 let zaporov. Iz slovenskih zaporov so ga kasneje premestili na Goli otok, kjer so ga ob prihodu pretepli in je 11. 3. 1951 zaradi posledic poškodb umrl.

**Vladimir Premru** (1902–1949) je bil prvotno osumljenec v dachauskih procesih, a so ga zaradi pomanjkanja dokazov izpustili, kasneje pa obsodili zaradi domnevnega sodelovanja z Informburojem in zaprli na Goli otok, kjer je umrl oktobra 1949. Na Medicinsko fakulteto UL se je vpisal v študijskem letu 1920/21, s študijem pa je nadaljeval v Zagrebu in Gradcu. Leta 1924 se je prepisal na Filozofsko fakulteto v Ljubljani, kjer je diplomiral iz kemije in fizike leta 1929. Najprej je poučeval na Državni tehniški srednji šoli, kjer je leta 1930 izšel njegov učbenik Elektrokemija. Od ustanovitve Banovinskega inštituta za raziskovanje in zdravljenje novotvorb (1938) je kot neplačan sodelavec vodil tudi kemijski laboratorij (inštitut je imel »klinični, kemični in kemobiološki« laboratorij<sup>55</sup>, ki jih je verjetno vse, glede na skromno kadrovsko sestavo inštituta, vodil Premru). Znan je tudi kot prevajalec leposlovja in ekspresionistični pesnik. Leta 1941 je v soavtorstvu z dr. Leom Šavnikom objavil kratko preliminarno raziskovalno poročilo o karcinogenem delovanju različnih preparatov na osnovi stilbena (1,2-difeniletena)<sup>56</sup> v reviji Zeitschrift für Krebsforschung, naslednje leto pa v isti reviji celovitejše poročilo<sup>57</sup> o isti temi. Novembra 1943 so ga aretirali in poslali v taborišče Dachau, kamor je bil sprejet 8. januarja 1944. V sprejemnem listu v taborišče je zaveden kot učitelj kemije iz Ljubljane. Rojen je bil v Boštanju, njegovi starši pa so kasneje živeli v Celju, tako kot Krajnci. Iz Dachaua, kjer je od marca 1944 delal v skupini dr. Rascherja, je bil kasneje premeščen v podružnico Lochau.

Ko se je po osvoboditvi peš vračal domov, so ga zajeli Francozi in zaprli v njihovo prehodno taborišče Tisis, tako da se je vrnil šele avgusta 1945. Po povratku je najprej delal kot pomočnik ravnatelja srednje tehniške šole, maja 1946 pa je postal načelnik oddelka za strokovno šolstvo na Ministrstvu za industrijo in rudarstvo LRS<sup>58</sup>. Njegov sin Lev Premru (1931–2005) je bil prav tako interniran na Goli otok, a je preživel jetništvo in doktoriral iz kemije 1965. V naziv docenta je bil izvoljen 1971 in v naziv izrednega profesorja 1974, kariero pa je nadaljeval v industriji. Znan je predvsem kot direktor Leka v času njegove intenzivne širitve (1980–88)<sup>59</sup>.

**Mitja Sark** (1919–2000) je maturiral na ljubljanski realki leta 1939 in se istega leta vpisal na študij kemije na Tehniški fakulteti. Že kot študent je bil vključen v delo Osvobodilne fronte v Ljubljani, kjer so ga belogardisti januarja 1943 aretirali, italijanska uprava pa ga je marca poslala v taborišče Visco pri Palmanovi. Konec julija se je vrnil v Ljubljano, kjer

so ga 5. novembra ponovno aretirali in poslali v taborišče Dachau, kamor je prispel 28. 11. 1943. Od aprila 1944 naprej je delal kot kemik na „malarični postaji“ in ostal v taborišču do začetka junija 1945, ko se je s prvim organiziranim transportom vrnil v Slovenijo. Takoj se je zaposlil v laboratoriju za nadzor živil pri Ministrstvu za ljudsko zdravstvo v Ljubljani, ob delu pa je nadaljeval s študijem.

Tik pred koncem študija je bil 19. septembra 1947 aretiran in 22. maja 1948 obsojen na 18,5 let zapore. Obsojen je bil za sodelovanje pri poskusih na taboriščnikih pod vodstvom dr. Klause Schillinga, ter ker naj bi po vojni dajal lažne informacije o svojem delovanju v Dachau<sup>LXI</sup>. Kazen so mu kasneje dvakrat znižali, z amnestijo novembra 1954 pa je bil izpuščen. Kmalu se je zaposlil kot kemik na Inštitutu za elektrozeve. Diplomiral je šele leta 1956 z novo nalogo »Pridobivanje lahkih luknjičavih apnenih betonov iz apna in kremenca oziroma silikatov v avtoklavu«, ki jo je pripravil pod mentorstvom prof. Janka Kavčiča. Decembra 1961 se je zaradi politično motiviranih konfliktov<sup>LXII</sup> odločil, da zapusti Slovenijo in je za kratek čas delal v Nemčiji kot nekvalificiran delavec<sup>LXIII</sup>, kasneje pa se je preselil na Švedsko, kjer je živel v okolici Stockholma.

Od februarja 1962 naprej je delal kot kemik v industrijskem laboratoriju, nato je bil asistent na švedskem državnem inštitutu za javno zdravje, kjer je bil predvsem zadolžen za kontrolo izdelkov (predvsem živil), ki so prihajali iz uvoza, zadnjih 5 let do upokojitve (1988) pa kot razvojni inženir na tehniški visoki šoli v Stochkolmu. Sodba z dachauskega procesa je bila razveljavljena leta 1971. Po osamosvojitvi Slovenije je Sark dobil slovenski potni list in je večkrat prišel na obisk v domovino, kjer je med drugim na Televiziji Slovenija sodeloval na omizju o povojnih montiranih procesih<sup>62</sup>. Tridesetstranski pogovor z Mitjem Sarkom je izšel leta 1996 v Novi reviji<sup>63</sup>.

**Boris Fakin** (bolj znan pod psevdonimom Igor Torcar; 1913–2004) je diplomiral iz kemije 1942 in sicer z nalogo »Grignardove sinteze propionske, izomaslene, valerianske in izovalerianske kisline« (mentor prof. Ladislav Klinc). Zaradi sodelovanja z Osvobodilno fronto je bil v Ljubljani konec leta 1943 aretiran in od 20. 1. 1944 zaprt v Dachau, od koder je bil 11. 10. 1944 premeščen v Sachsenhausen (kasneje v podružnico Klinkerwerk Oranienburg)<sup>64</sup>, kjer je ostal do konca vojne. V Dachauu je delal v kliničnem laboratoriju taboriščne bolnišnice. Med drugim naj bi opravljal analize urina in blata, pri čemer obstaja pričanje več zapornikov, da je, če je bilo treba, potvoril rezultate preiskav, da bi zadržal slovenske internirance dalj časa v bolnišnici in jih s tem rešil transporta ali težkega dela.

Po vojni je bil zaposlen na republiškem ministrstvu za industrijo in rudarstvo, nazadnje kot direktor direkcije za kemično industrijo. Aprila 1948 je bil aretiran in obsojen zaradi domnevnega sodelovanja z Gestapom, katerega agent naj bi bil. Obsojen je bil na 8 let in 9 mesecev zapore s prisilnim delom, po pritožbi pa so kazni podaljšali na 12 let in naknadno znižali na 6 let strogega zapore, od katerih je preostal 4 leta, nato pa so ga pogojno izpustili. Sodba je bila razveljavljena leta 1971. Od leta 1954 je bil učitelj na Akademiji uporabljajočih umetnosti UL, kjer je predaval predmet Tehnologija slikarskih, kiparskih in grafičnih materialov. O svojih izkušnjah s povojnimi procesi je napisal roman Umiranje na obroke (1984), ki je verjetno njegovo najbolj znano delo.

Po vojni je bil zaposlen na republiškem ministrstvu za industrijo in rudarstvo, nazadnje kot direktor direkcije za kemično industrijo. Aprila 1948 je bil aretiran in obsojen zaradi domnevnega sodelovanja z Gestapom, katerega agent naj bi bil. Obsojen je bil na 8 let in 9 mesecev zapore s prisilnim delom, po pritožbi pa so kazni podaljšali na 12 let in naknadno znižali na 6 let strogega zapore, od katerih je preostal 4 leta, nato pa so ga pogojno izpustili. Sodba je bila razveljavljena leta 1971. Od leta 1954 je bil učitelj na Akademiji uporabljajočih umetnosti UL, kjer je predaval predmet Tehnologija slikarskih, kiparskih in grafičnih materialov. O svojih izkušnjah s povojnimi procesi je napisal roman Umiranje na obroke (1984), ki je verjetno njegovo najbolj znano delo.

## 7. Razveljavitev obsodbe

Do razveljavitve sodb iz dachauskih procesov je prišlo postopoma, saj je sprva moralo dozoreti spoznanje o krivičnosti sojenja, kasneje pa so morali rešiti vprašanje, kako s čim manj politične škode za vladajočo elito predstaviti ničnost sodb. Da so se o tem sploh sprožala vprašanja, gre v prvih letih po procesu v veliki meri zasluga vdovam obsojenih na smrt<sup>LXIV</sup>, kasneje pa tudi tistim, ki so bili obsojeni na zaporne kazni, a so bili po nekaj letih pomiloščeni in/ali začasno izpuščeni. Pomembne so bile tudi aktivnosti združenj taboriščnikov, ki so pozivala k rehabilitaciji

LXI Vprašanje je, zakaj Sarku niso sodili že na Diehl-Oswaldovem procesu, saj so ga aretirali kmalu po Barletu in Diehlu, mesec in pol pred Krajncem. Obtožnica je bila dokaj podobna (sodelovanje z Gestapom, izvajanje poskusov na taboriščnikih, neresnično navajanje podatkov o medvojnem delovanju), le da mu niso očitali povojnega delovanja za tuje obveščevalne službe in/ali sabotaž. Možna razlaga za Sarkovo ločeno sojenje bi bila, da je v vodstvu državne varnosti delal **Dušan Bravničar** (191–2004), rojen istega leta kot Sark, prav tako študent kemije (vpisan v 1. letnik 1937) in član vodstva KP v Ljubljani že leta 1941. Vsi ostali kemiki na dachauskih procesih so bili starejši. Bravničar je sodeloval pri preiskavi proti Martinu Presterlu, ključni priči tožilstva na Diehl-Oswaldovem procesu<sup>60</sup>. Morda je Bravničar vedel, kako stroge bodo sodbe na prvem procesu in je Sarku kot kolegu in revolucionarno usmerjenemu študentu namenil ločeno sojenje. Bravničar je zaključil študij kemije na 1. stopnji leta 1966, pred tem pa je opravljal nekatere vidne politične in administrativne funkcije v Sloveniji. Nazadnje je bil direktor Inštituta za zgodovino delavskega gibanja; upokojil se je leta 1962<sup>61</sup>.

LXII Sark je imel abonirano kosilo v gostilni Bellevue v Šiški. Neka dne mu je direktorica sporočila, da mu ne smejo več postreči. Gostinsko podjetje je namreč dobilo od partijskega komiteja iz Šentvida (v tistem času je Sark delal v tovarni Keramika v Šentvidu oz. Vižmarjih pri Ljubljani – to je bila ena od proizvodnih enot Inštituta za elektrozeve) ukaz, da kot bivši gestapovec in zapornik ne sme več dobivati hrane. Sarka je to razjezilo in je tožil partijski komite in dva posameznika za razžalitev časti, ob tem pa se je skliceval na člen iz kazenskega zakonika, da tistega, ki bivšemu zaporniku očita prestano zaporno kazeno, lahko kaznujejo z enim letom zapore. Tožbo so mu večkrat odsvetovali in mu grozili s posledicami, odvetnik Ljuba Prenner, ki je bil sam večkrat preganjan zaradi opozaranja na nepravilnosti v slovenskem sodstvu, pa ga je podprl. Sodišče je razsodilo, da obtoženci niso krivi in pri tem utemeljevalo dopustnost očitka prav s Sarkovo obsodbo na dachauskem procesu. Vse pritožbe na sodbo (celo na jugoslovansko ustavno sodišče in maršalu Titu) so bile odbite.

LXIII F. Derganc navaja<sup>65</sup>, da je Sark živel v Belgiji, vendar je bil tam morda le kratek čas pred selitvijo na Švedsko ali pa sploh ne.

LXIV Ivanka Krajnc je na primer skupaj z drugimi vdovami umorjenih na dachauskih procesih pisala pismo ženi jugoslovanskega predsednika, Jovanki Broz, glede (verjetno obnove) procesa proti njihovim možem. To pismo in vlogo za rehabilitacijo B. Krajnc je v šestdesetih prinesla tudi na vodstvo študentske organizacije UL, ker je v času razcveta študentskih gibanj po letu 1968 računala na njihovo pomoč<sup>66</sup>.

nekdanjih sojetnikov, in združenja nekdanjih španskih borcev, saj so številni obsojenci bili nekdanji prostovoljci španske državljanske vojne.

V analizi obsodbe Borisa Krajnc, ki je bila osnova za razveljavitev sodbe (podobno pa bi lahko navedel še za druge v tem članku omenjene kemike, pa tudi druge obsojene) je jasno navedeno, da o agentski navezavi na Gestapo ne more biti govora. Glede pridobivanja agentov Gestapa obstaja vrsta zgodovinskih virov. Resnični agenti Gestapa bi namreč morali biti evidentirani na drugačen način, o njih bi morala obstajati evidenca nalog, poročanj in izplačil, tega pa za obsojene na dachauskih procesih ni bilo. Poleg tega so agente pridobivali predvsem za protiobveščevalno delo na terenu in agentov ne bi pošiljali v taborišča, taborišča pa so imela tako ali tako vzpostavljen svoj sistem pridobivanja podatkov in urejanja odnosov med zaporniki. Bolj verjetno je, da je Krajnc v Begunjah pod grožnjo streljanja podpisal splošno izjavo o lojalnosti, čeprav je med zaslišanjem navedel, da se je s podpisom obvezal, da bo delal za veliko Nemčijo po direktivah Gestapa. Izjavo o lojalnosti, ki naj bi jo podpisal v Begunjah, je omenil npr. Stane Oswald v zaslišanjih, vendar ta ne šteje kot soglasje k sodelovanju z Gestapom v vlogi agenta.

Obtožnica je Krajncu in drugim, ki so delali v poskusni postaji taborišča Dachau, očitala kaznivo dejanje vojnega zločinstva. V razveljavitvi sodbe je utemeljeno zapisano, da pri poskusih niso sodelovali naklepoma. Naveden je tudi sklic na povojne procese v Nemčiji, kjer so sodelavce pri poskusih na ljudeh sodišča vabila zgolj kot prič, ne pa kot storilce dejanj. Nelogično bi tudi bilo, da bi sodili tehničnim sodelavcem, medtem ko številnim njihovim nadrejenim niso sodili. Pri tem je prevladalo spoznanje, da nekdanji taboriščniki tudi po izpustitvi niso imeli možnosti izbire in so bili prisiljeni še naprej delati v skupinah, ki so jih rekrutirale, čeprav ne več v statusu zapornika. Sicer so s tem pridobili nekatere privilegije, ki jih taboriščniki niso imeli (boljšo hrano, občasne izhode iz taborišča, manjše tveganje za premestitev in delo do popolne izčrpanosti), kar pa ne pomeni, da so delo opravljali po lastni želji.

Poleg tega so v sedemdesetih letih zaslišali še številne dodatne prič, ki so kar po vrsti omenjale, da so jim Krajnc in ostali v taborišču pomagali. Krajnc je na primer dobival pakete z zdravili, ki so jih dobili oboleli taboriščniki mimo zaporniške bolnišnice. V prid Krajncu so pričali Tibor Škerlak, ki je Krajnc opisal kot zelo delavnega, poštenega in skromnega, Dušan Stucin, ki je pohvalil Krajnc trden značaj in revolucionarno usmerjenost, in Bojan Držaj, Krajnc diplomant, ki ga je pohvalil kot predavatelja in ga prikazal kot ,revolucionarja iz prepričanja‘.

Kot posreden dokaz, kako je Krajnc položaj bil privilegiran, so na montiranem procesu navedli, da je lahko prišel domov na dopust in se potem prostovoljno vrnil na delo v skupino dr. Rascherja. Pred razveljavitvijo sodbe je sodišče pridobilo pisma, ki jih je Krajnc pisal svoji mami. Iz tistega, ki je datiran s 17. decembrom 1943, je razvidno, da je edini dopust, ki ga je dobil maja 1944, verjetno zakasnen dopust

za tistega, ki mu ga je Rascher obljubil za božič 1943, ko mu je uspelo Krajncu dobiti nazaj v svojo skupino. Ker so bili čez praznike dopusti prepovedani, je Rascher obljubil, da ga bo poslal na dopust ,čim bo zopora v januarju ukinjena‘.

V pismu, ki ga je materi poslal 31. 12. 1943, pa je Krajnc opisal dogajanje v zvezi z njegovim odpustom iz taborišča in zaposlitvijo v skupini dr. Rascherja. Opisal je, kako je verjel, da se bo z odpustom lahko vrnil domov, da pa so mu zadnji hip sporočili, da mora z vlakom v Berlin, kjer se mora najprej javiti policiji, potem pa skupini za razporejanje dela. Ravno ko je zvedel, da mora v Berlin, je baje prišel mimo dr. Rascher in se zelo razburil, ker je menil, da bodo Krajncu v Berlinu uporabili za odkopavanje ruševin. Z avtom ga je odpeljal nazaj na poskusno postajo ter začel urejati zadeve. Šele 22. 12. je Rascher dobil dovoljenje za zaposlitev Krajncu v svoji skupini, do takrat pa je bil Krajnc še naprej jetnik v taborišču.

Sodišče ob razveljavitvi sojenja ni videlo dokazov za vojno zločinstvo, poleg tega naj bi večino časa delal na pektinskih preparatih. O delovanju ,poskusnih postaj‘ naj bi že takoj, ko se je pridružil partizanom, pripravil poročilo za vojaško sodišče IX. korpusa, o razmerah v taborišču pa naj bi poročal že iz Dachaua, a teh poročil sodišče leta 1948 ni pridobilo in ne preverjalo.

Glede ,špijonskih podatkov in poročila o delu na univerzi, ki naj bi jih posredoval tuji obveščevalni službi, na sojenju ni bilo podanih nobenih dokazov, prav tako ne za škodljivo delovanje po direktivah tuje obveščevalne službe. To bi lahko bila britanska služba v navezavi s Krajncovo udeležbo na sestanku trgovske delegacije za področje kemijske industrije v Veliki Britaniji. Na ta sestanek naj Krajnc sploh ne bi želel iti, ker ni znal angleško, a je vseeno moral, skupaj s še tremi kemiki iz drugih republik (od katerih je samo eden znal angleško).

Na osnovi kritične obravnave obtožb in novih dejstev je Javno tožilstvo SRS 7. aprila 1976 Vrhovnemu sodišču SRS predlagalo obnovo kazenskega postopka proti obtoženim v Diehl-Oswaldovem procesu. Vrhovno sodišče je predlog tožilstva sprejelo 22. junija 1976, pri tem pa zadevo predalo v obravnavo Okrožnemu sodišču v Ljubljani. To je 26. julija, po umiku prvotne obtožnice s strani javnega tožilstva, razveljavilo sodbo in ustavilo kazenski postopek. Politika se je uspela poenotiti in opredeliti do dachauskih procesov šele leta 1984, ko je bilo 11. julija objavljeno skupno sporočilo predsedstva Centralnega komiteja Zveze komunistov Slovenije (CK ZKS) in predsedstva Republiške konference Socialistične zveze delovnega ljudstva (RK SZDL). Aprila 1986 se je 10. kongres ZKS zavzel za popolno odpravo posledic obsodb v dachauskih procesih, kar so nekateri interpretirali kot politično rehabilitacijo obsojencev<sup>LXV</sup>.

LXV Nekateri kritiki postopka razveljavitve procesa menijo, da umik obtožnice ne pomeni ustrezne razjasnitve dejstev in oprostitve za očitana dejanja, prav tako pa ni ustrezno enačenje ,zavzemanja za popolno odpravo posledic‘ s pravo politično rehabilitacijo. Po mnenju nekaterih bi bila pravična razrešitev šele obsodba tistih, ki so krivi, da je do procesa in obsodbe sploh prišlo<sup>68</sup>.

Obsodbe so prizadele številne družine: Sarkova družina je razpadla, Barletova sta imela dve leti starega sina, ki so ga vzgajali sorodniki in rejniki. Ko so Stepišnikove pregnali iz stanovanja v Slovenski Bistrici, so prišli živeti v Ljubljano h Krajncovi ženi Ivanki, kasneje pa so izselili tudi njo. Razveljavitev sodbe je prišla, ko so bile žene obsojenih stare že 55 let in več. Vrnili so jim nekaj odvzetega premoženja, niso pa jim mogli vrniti svojcev. Še več: za točne datume in kraje usmrtitve in pokopa svojci večine obsojencev še vedno ne vedo, čeprav je po slovenski osamosvojitvi Arhiv Republike Slovenije poskušal najti ustrezne podatke. Krajncova žena naj bi bila zaradi nenehnih prizadevanj za doseg rehabilitacije pod stalnim policijskim nadzorom vse do leta 1983<sup>19</sup>. O življenju po obsodbi moža je iskreno spregovorila<sup>67</sup> z novinarko Ranko Ivelja<sup>LXVI</sup> leta 2003. V sestavku so omenjeni tudi dotlej javnosti neznan arhivski podatki o tem, da naj bi bili nekateri domnevno ustreljeni obsojenci živi še leta 1952. Za Krajncu je bolj verjeten podatek iz pričevanja Antona Debevca, ki je pripravil prvo analizo dachauskih procesov (sicer interni dokument Udbe). Povedal je, da se je ob pripravi poročila (1951) dve leti srečeval z na smrt obsojenimi, da pa je Barle umrl zaradi bolezni in izčrpanosti že nekaj dni po obsodbi, Krajnc pa po kakšnem letu<sup>19</sup>.

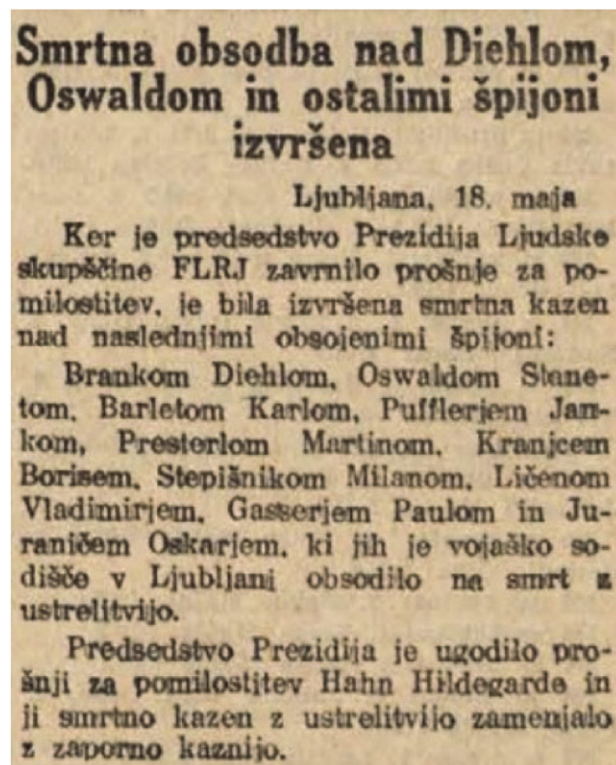
Univerza v Ljubljani je maja 1997 ustanovila komisijo za rehabilitacijo univerzitetnih učiteljev. Ta komisija je zbrala gradiva in za senat pripravila izhodišča za razpravo in predlog sklepa. Točko so obravnavali na seji senata 15. 1. 1998 in na njej rehabilitirali vse iz političnih razlogov odstranjene učitelje UL, med njimi tudi Borisa Krajncu in Mirka Koširja. Ker seznam takrat še ni bil popoln, je komisija z delom nadaljevala<sup>69</sup>.

## 8. Zaključek

V psevdomedicinske poskuse v nemških koncentracijskih taboriščih so vključili več kot 27 000 jetnikov, od katerih jih je zaradi poskusov umrlo skoraj 4400<sup>70</sup>. Številni teh poskusov so potekali v taborišču Dachau, kjer sta bili najbolj znani skupini dr. Rascherja in dr. Schillinga, v obojih pa so kot tehnično in pomožno osebje sodelovali tudi nekateri Slovenci, med njimi več kemikov. Po vojni so jim sodili na takoimenovanih dachauskih procesih v Ljubljani, kjer so jih, tudi zaradi sodelovanja pri teh poskusih, obsodili za vojno hudodelstvo. Hkrati so od njih izsilili še priznanja za druga

LXVI V tem članku je Branko Diehl napačno naveden kot filozof, kar se pojavlja tudi v nekaterih drugih virih. Vendar pa je Diehl diplomiral iz kemije in fizike na Filozofski fakulteti. Naravoslovci, ki so študirali na tej fakulteti, so bili večinoma kasnejši profesorji v srednjih šolah, za razlikovanje od inženirjev kemije, ki so študirali na Tehniški fakulteti, pa so jih nekateri imenovali kar 'filozofi'. V istem članku je Milan Stepišnik označen kot doktor kemije, vendar to ne drži. Tekmovanje v Italiji, na katerem Stepišnik ni želel pozdraviti s fašističnim pozdravom, je njegov sin datiral s 'tik pred začetkom vojne', vendar gre za tekmovanje septembra 1941.

dejanja, predvsem za sodelovanje z Gestapom v vlogi agentov, povezovanje s tujimi obveščevalnimi službami, spodbujanje delovanja naprednih taboriščnih združenj, povojne sabotaže v podjetjih, pisanje lažnih biografij in neutemeljenih priporočil nekdanjim sojetnikom itd.



Slika 5: Novica, objavljena v časopisu Ljudska pravica dne 19. maja 1948. Istega dne je podobno kratka novica izšla tudi v Slovenskem poročevalcu, le da je bila datirana s 17. majem. Čeprav v članku ni navedeno, naj bi usmrtitev izvedli 12. maja, o čemer obstaja več pisnih virov. Vendar pa je ta datum usmrtitve vprašljiv, saj Arhiv RS hrani rokopisno Krajncovo izjavo iz centralnih zaporov Udbe, datirano z 20. majem 1948.

Na prvem in največjem procesu aprila 1948 je bilo obsojenih 14 ljudi, od tega 11 na smrtno kazen (slika 5). Šest obtoženih je bilo kemikov, od tega so jih pet obsodili na smrt. Trije preiskovanci so med zaslišanji umrli, med njimi en kemik. V kasnejših dachauskih procesih so na zaporno kazen obsodili še dva kemika. Kemiki so s svojim strokovnim znanjem, hkrati pa obvladanjem nemškega jezika (znanstvene objave vodilnih slovenskih kemikov v predvojnem času so bile pretežno v nemščini) bili zanesljiv kader za pomoč pri eksperimentalnem delu, v zameno za sodelovanje pa so imeli ugodnejše življenjske razmere v taborišču, nekateri pa tudi mesečno plačo in možnost izhodov iz taborišča. Ne glede na to pa je po preučitvi očitanih jim dejanj že v 60-tih letih prejšnjega stoletja prevladalo mnenje, da so bili k sodelovanju v poskusih prisiljeni in niso imeli možnosti, da bi to delo odklonili. V drugih toč-

kah obtožnic je bilo po ponovni preučitvi procesov stališče javnega tožilstva, da so bila priznanja izsiljena, sojenja pa nepoštena, zato so bile sodbe razveljavljene. Ponovnih sojenj ni bilo, saj je tožilstvo odstopilo od pregona. Ne glede na to pa so posledice dachauskih procesov zaznamovale ne samo družin obsojenih, pač pa so sojenja negativno vplivala tudi na veteranska združenja španskih borcev in taboriščnikov, nenazadnje pa so posledice bile, vsaj posredno, tudi za kemijsko stroko in njen ugled.

Med obsojenci na smrt na Diehl-Oswaldovem procesu je za biokemijsko stroko še posebej pomemben Boris Krajnc, ki je manj kot dve leti pred aretacijo bil izvoljen v naziv docenta. Pokrival je področje biokemije, kar lahko razumemo kot prvo habilitacijo za to področje na ljubljanski univerzi. S Krajnčevu usmrtitvijo je tehniška fakulteta ostala brez edinega biokemika, predavanja iz biokemije pa je prevzel Dušan Stucin z Medicinske fakultete. Šele v začetku 60-tih let se je biokemija na takratni Fakulteti za naravoslovje in tehnologijo ponovno vzpostavila, medtem pa so druge kemijske discipline skoraj 15 let napredovale sorazmerno neovirano, tako kadrovske kot raziskovalno.

## 9. Zahvala

Osnovni podatki o dachauskih zapornikih so iz Arolsenkega arhiva (The Arolsen Archives – International Center on Nazi Persecution). Tatjani Peterlin-Neumeier se zahvaljujem predvsem za prepis tistega dela pogovora z Mirkom Dermeljem iz leta 2012, v katerem se spominja Borisa Krajnc, ter za nekatere informacije, povezane z Maksom Samcem in Mirkom Dermeljem. Za nekatera dodatna pojasnila glede dela Rascherjeve skupine in osebnosti njegovih sodelavcev se zahvaljujem Hubertu Rehm. Zdaj že pokojnemu Pavlu Ledineku se zahvaljujem za nekatere podatke o Milanu Stepišniku in njegovi družini, Katarini Stepišnik pa predvsem za dostop do dachauskega laboratorijskega dnevnika Milana Stepišnika, izvlečkov iz zaslišanj Milana Stepišnika in nekaterih pisem iz arhiva družine Stepišnik. Antonu Piberniku se zahvaljujem za dopolnitev podatkov o pred- in medvojnem delovanju njegovega očeta Mirka Pibernika, Primožu Sarku pa za nekatere informacije o njegovem očetu Mitji Sarku. Arhivska služba UL mi je posredovala kopijo rokopisa Borisa Krajnc in Branka Diehla, podatek o seji senata UL decembra 1945 ter kopije korespondence o imenovanju v docentski naziv. Fakultetna knjižnica mi je omogočila vpogled v diplomski nalogi Bojana Držaja in Jelke Ružič. Obema se zahvaljujem za pomoč. Za dostop do arhivskega gradiva, povezanega z dachauskimi procesi, se zahvaljujem Arhivu Republike Slovenije, še posebej Tadeju Cankarju. Hvala tudi Saši Florjančič iz Kovaškega muzeja Kropa za podatke o povezavi med družinama Ažman in Žukov. Prav tako se zahvaljujem Nataliji Štular iz Slovenskega planinskega muzeja, ki mi je posredovala podatke, povezane z Ivanko Krajnc, in Ani Logar za nekatere podatke o zapuščini Bo-

risa Krajnc, ki jo je hranila Ivanka Krajnc. Emiliji Snoj se zahvaljujem za pojasnilo glede pridobitve izjave Antona Debevca o življenju Borisa Krajnc po uradnem dnevu usmrtitve.

## 10. Viri

1. M. Dolinar, Richard Klemen, the first lecturer of enzymology at the University of Ljubljana, *Acta Chim. Slov.* **2020**, *67*, S49–S61. DOI:10.17344/acsi.2020.6152
2. K. Hess, B. Krajnc, Die Endgruppenbestimmung bei den Stärkekomponenten (X. Mitteil. über Stärke), *Berichte der deutschen chemischen Gesellschaft* **1940**, *73*, 976–979. DOI:10.1002/cber.19400730909
3. K. Hess, H. A. Schulze, B. Kranjc, Über höchstmethylierte Stärke und die Frage ihrer Spaltzucker (XI. Mitteil. über Stärke), *Berichte der deutschen chemischen Gesellschaft* **1940**, *73*, 1067–1076. DOI:10.1002/cber.19400731008
4. V. Zimmermann, Eine Deutsche hat mich beim Kapitän denunziert, *Südoschweiz*, 5. 4. **2011**. Dostopno na <https://www.suedostschweiz.ch/zeitung/eine-deutsche-hat-mich-beim-kapitan-denunziert> (datum dostopa 4.1.2021).
5. T. Škarja, Odličen zgled in vzornik. Mirko Dermelj – stolecnik. *Planinski vestnik* **2104**, *11*, 26–27.
6. J. Petrovec, Mirko Dermelj – Neobvezno v nedeljo (intervju). 19. 10. **2014**, dostopno na <https://4d.rtvlo.si/arhiv/neobvezno-v-nedeljo/174300165> (datum dostopa 4. 1. 2021).
7. M. Walker, O. Hahn, Verantwortung und Verdrängung, Ergebnisse, 10. zvezek raziskovalnega programa »Geschichte der Kaiser-Wilhelm-Gesellschaft im Nationalsozialismus«, Berlin: Max-Planck-Gesellschaft, **2003**.
8. Spremembe v vojaški službi. *Novine Slovenske krajine* **1940**, *27* (38), str. 2. (datum objave 22. 9. 1940)
9. D. Siter, Kapitulacija jugoslovanske kraljeve vojske. Objavljeno 17. 4. **2017** na <http://zgodovina.si/kapitulacije-jugoslovanske-kraljeve-vojske/> (datum ogleda 4.1.2021).
10. H. Kamberović, Nasilje kao sudbina? Sarajevo na razmeđu carstava i država u 20. stoljeću. V: Između rata i mira – Sarajevo u prelomnim godinama 20. stoljeća. Sarajevo: Udruženje za modernu historiju, **2020**, str. 9–28.
11. I. Janžekovič, R. Knez, I. Ros, F. Strmole, S. Šifrer, Analiza dachauskega procesa in obdelava posameznikov, obsojenih v tem procesu. V: Dachauski procesi (ur. M. Ivanič). Ljubljana: ČZDO Komunist, **1990**, str. 382–503.
12. M. Pukrop, SS-Mediziner zwischen Lagerdienst und Fronteinsatz. Die personelle Besetzung der Medizinischen Abteilung im Konzentrationslager Sachsenhausen 1936 – 1945. Doktorska disertacija. Hannover: Gottfried Wilhelm Leibniz Universität Hannover, **2015**, str. 36 in 375.
13. Znanstveno djelo Bože Težaka, Božo Težak (1907–2017): vizionar informacijskih i komunikacijskih znanosti 21. stoljeća / Visionary of information and communication science of the 21st century, *Informatol.* **2017**, *50*, 1–13.
14. Dokumenti o razveljavitvi sodbe Fakina in Mrzela. V: Da-

- chauski procesi (ur. M. Ivanič). Ljubljana: ČZDO Komunist, **1990**, str. 766–827.
15. M. Cacan, Tibor Škerlak – In memoriam. *Glasnik hemičara i tehnologa Bosne i Hercegovine* **2012**, 38, 69–71.
  16. B. Zihel, Promemorija. V: Dachauski procesi (ur. M. Ivanič). Ljubljana: ČZDO Komunist, **1990**, str. 25–32.
  17. A. Gabrič, Odpuščanje profesorjev Univerze v Ljubljani iz službe zaradi politično-ideoloških vzrokov, Univerza v Ljubljani, *Objave* **2000**, 6, 12–32.
  18. S. Florjančič, Justin in Rika Ažman iz Krope. Življenje pred in med drugo svetovno vojno. Vigenjc **2015**, 15, 7–51.
  19. E. Snoj, Dachauski procesi kot primer nemoči posameznika na montiranem procesu totalitarnega sistema. Diplomsko delo. Ljubljana: Univerza v Ljubljani, Filozofska fakulteta, Oddelek za sociologijo, **2001**.
  20. H. Halbrainer, Josef Martin Presterl. Ein Grazer Spanienkämpfer und Verleger als Opfer der Schauprozesse 1948. V: Alfred Klahr Gesellschaft – Mitteilungen, **2016**, 23(3), 9–13.
  21. R. L. Berger, Nazi Science — The Dachau Hypothermia Experiments. *N. Engl. J. Med.* **1990**, 322, 1435–1440.  
DOI:10.1056/NEJM199005173222006
  22. A. Riedle, Medizinische Humanexperimente im KZ Dachau am Beispiel der Versuche von Dr. Sigmund Rascher und Prof. Dr. Claus Schilling. Betrifft Widerstand **2015**, 129, 12–23.
  23. F. Schmaltz, Kampfstoff-Forschung im Nationalsozialismus: Zur Kooperation von Kaiser-Wilhelm-Instituten, Militär und Industrie. Göttingen: Wallstein Verlag, **2005**, str. 174–177.
  24. M. H. Kater, Das „Ahnenerbe“ der SS 1935–1945, Ein Beitrag zur Kulturpolitik des Dritten Reiches, 4. izdaja. München: R. Oldenbourg Verlag, **2006**, str. 231–264  
DOI:10.1524/9783486594683
  25. S. Bär, Der Untergang des Hauses Rascher. Das bizarre Leben des Dachauer KZ-Arzt, 5. izdaja. Rottweil: Siegfried Bär, samozaložba, **2020**.
  26. National Archives Catalog, Case Number 000-50-2, Vol 1: Freezing experiments carried out by Dr Rasher..., **1942–1944**; Category: Medical Experiments and Reports, Fold3, File #232070885, str. 18. Dostopno na <https://catalog.archives.gov/id/40947627> (datum ogleda 2.6.2021).
  27. HLS Nuremberg Trials Project (zapisnik sojenja na Nürnbergskem procesu 2. 1. **1947**), str. 973. Dostopno na <http://nuremberg.law.harvard.edu/transcripts/1-transcript-for-nmt-1-medical-case?seq=993> (datum ogleda 2. 6. 2021).
  28. G. Römer, Schlachters. V: Wolfgang Benz, Barbara Distel (ur.): Der Ort des Terrors. Geschichte der nationalsozialistischen Konzentrationslager. Band 2: Frühe Lager, Dachau, Emslandlager. München: C.H. Beck, **2005**, 481–482.
  29. G. Sack, Über die Hämolytische Wirkung der Pektine, Insbesondere bei Hämophilie. *Klinische Wochenschrift*, **1935**, 14, 1536–1538. DOI:10.1007/BF01780472
  30. E. Gohrbandt, Die Einwirkung der Pektine auf die Blutgerinnung, *Deutsche medizinische Wochenschrift*, 2. 10. **1936**, 1625–1626. DOI:10.1055/s-0028-1141334
  31. World Trade News on Chemicals and Allied Products, United States Bureau of Foreign and Domestic Commerce 11(52), 25. 12. **1937**, str. 863.
  32. A. Knoll, Lochau. V: Wolfgang Benz, Barbara Distel (ur.): Der Ort des Terrors. Geschichte der nationalsozialistischen Konzentrationslager. Band 2: Frühe Lager, Dachau, Emslandlager. München: C.H. Beck, **2005**, 385–387.
  33. B. Krivokapić, Dahauski procesi, Beograd: Prosveta, **1986**.
  34. Digitalni arhiv ITS, Bad Arolsen, št. dokumenta 4.2/82231970 (**1943**).
  35. Pseudo-medizinische Versuche in KL Dachau. Erprobung des Blutstillmittels »Polygal 10«. Digitalni arhiv ITS, Bad Arolsen, št. dokumentov 4.2 / 82231949- 82231953 (**1969**).
  36. V. Kopač, F. Žemva, B. Albaneze, Delo jugoslovanskih komunistov v taborišču. V: Dachau, zbornik (ur. L. Bukovac). Ljubljana: Založba Borec, **1981**, str. 253–289.
  37. Pogrebni govor – Rudi Janhuba. Avtor neznan. **1976**. Objavila Mestna knjižnica Ljubljana 21. 5. 2016. Dostopno na <https://www.kamra.si/mm-elementi/item/pogrebni-govor-rudi-janhuba.html> (datum ogleda 27. 1. 2021).
  38. C. Kohl: The Witness House: Nazis and Holocaust Survivors Sharing a Villa during the Nuremberg Trials. New York: Other Press, **2010**.
  39. HLS Nuremberg Trials Project (zapisnik sojenja na Nürnbergskem procesu 21. 3. **1947**), str. 2344. Dostopno na <http://nuremberg.law.harvard.edu/transcripts/2-transcript-for-nmt-2-milch-case?seq=2935> (datum ogleda: 2. 6. 2021).
  40. J. Reitzenstein, Himmlers Forscher: Wehrwissenschaft und Medizinverbrechen im „Ahnenerbe“ der SS. Paderborn: Verlag Ferdinand Schöningh, 2. izdaja, **2020**.
  41. V. Kopač, Izjava Vlasta Kopača o preiskovalnem postopku. V: Dachauski procesi (ur. M. Ivanič). Ljubljana: ČZDO Komunist, **1990**, str. 347–354.
  42. M. Jeraj, O rabi in zlorabi arhivskega gradiva tajnih služb (na primeru pripovedi o Milovanu Ilichu, objavljene v Koroških vojnih zgodbah). *Prispevki za novejšo zgodovino* **2018**, 58(2), 190–205.
  43. E. Djogič, Razvoj slovenske atletike od leta 1945 do 1950. Univerza v Ljubljani, Fakulteta za šport, diplomsko delo, **2007**.
  44. Arhiv Republike Slovenije, SI AS 1529, škatla 24.
  45. M. Horvat, V. Kopač, Vlasto Kopač: »Nič nisem zagrešil in tudi milosti ne bom prosil«, *Delo, Sobotna priloga* 31. 8. **2013** (dostopno na spletu <https://old.delo.si/zgodbe/sobotnapriloga/vlasto-kopac-nic-nisem-zagresil-in-tudi-milosti-ne-bom-prosil.html>, datum ogleda 13.11.2020).
  46. F. Jauk, Wir haben die Losung von Dachau gelernt. Hundert Monate in Dachau und Gestapohaft. Graz: KPÖ Steiermark, **1988**.
  47. H. Halbreiner, Franz Jauk. Ein Grazer Widerstandskämpfer als Zeuge der NS-Medizinverbrechen im KZ Dachau. *Alfred-Klahr-Gesellschaft Mitteilungen* **2016**, 16(2), 22–24.
  48. M. Samec, Studien über Pflanzenkolloide XXIII.: Lösliche Stärken erhalten durch Einwirkung von Oxydationsmitteln / nach Versuchen von M. Pibernik, *Kolloidchemische Beihefte* **1929**, 28, 155–166. DOI:10.1007/BF02557607
  49. M. Pibernik, B. Gregorka, Proste vežbe za I pokrajinski slet u Ljubljani i za međusletske utakmice 1933 = Proste vaje za I. pokrajinski slet v Ljubljani in za medzletne tekme 1933, Načelnništvo Saveza sokola kraljevine Jugoslavije. Ljubljana: Učiteljska tiskarna, **1933**.



50. P. Vodopivec, Prispevek za zgodovino represije na Slovenskem po 2. svetovni vojni, Neobjavljen intervju v Vlastom Kopačem iz leta 1986. *Prispevki za novejšo zgodovino* LII **2012**, 52(2), 274–294.
51. T. Velikonja, Zarja miru in mrak božičnega procesa, Zaveza 19, **1995**; dostopno na <http://nzszeva.github.io/articles/19-zarja-miru-in-mrak-bozicnega-procesa/> (datum ogleda 2.6.2021).
52. I. Žajdela, Da bi bili složni, *Reporter* **2019**, 12(18), 56–57 (datum objave 6. maj 2019). Povzeto po Biltenu Inštituta za narodnostna vprašanja 209 (3.–9. 5. 2019).
53. L. Malec, Ličen, Vladimir. V: Primorski slovenski biografski leksikon. Gorica : Goriška Mohorjeva družba, 1993. 19. snopič. Dostopno na: Primorci.si, spletni biografski leksikon znanih Primork in Primorcev, <http://www.primorci.si/osebe/li%C4%8Den-vladimir/903/>, zadnja sprememba 6. 3. **2013** (datum dostopa 19. 8. 2020).
54. M. Ivanič, Kronološki prikaz poteka in razveljavitve dachauskih procesov (1946–1986). V: Dachauski procesi (ur. M. Ivanič). Ljubljana: ČZDO Komunist, **1990**, str. 33–51.
55. F. Novak, Banovinski institut za raziskovanje in zdravljenje novotvorb, *Radiološki glasnik* **1938**, 3–4, 122–124.
56. L. Šavnik, V. Premru, Ein Beitrag zur cancerogenen Wirkung der Stilbenpräparate. *Zeitschrift für Krebsforschung* **1941**, 51, 337–343. DOI:10.1007/BF01621005
57. L. Šavnik, V. Premru, Experimentelle Ergebnisse über die krebserzeugende Wirkung der Stilbenpräparate. *Zeitschrift für Krebsforschung* **1942**, 52, 83–90. DOI:10.1007/BF01621318
58. F. Koblar, Premru, Vladimir (1902–1949). Slovenska biografija. Slovenska akademija znanosti in umetnosti, Znanstvenoraziskovalni center SAZU, 2013. Dostopno na <http://www.slovenska-biografija.si/oseba/sbi460489/#slovenski-biografski-leksikon> (datum ogleda 29. junij 2020). Izvirna objava v: Slovenski biografski leksikon: 8. zv., ur. F. K. Lukman, Ljubljana: Slovenska akademija znanosti in umetnosti, **1952**.
59. N. Troha, Poročilo notranjega ministra LRS Borisa Kraigherja na seji Politbiroja Centralnega komiteja Komunistične partije Slovenije, 9. marec 1950 (komentirana objava rokopisnih beležk). *Prispevki za novejšo zgodovino*, 2018, 58 (3), 151–170. Dostopno tudi na <https://ojs.inz.si/pnz/article/view/307/1270> (datum ogleda 3. 6. 2021).
60. Vmesno poročilo o povojnih množičnih pobojih. 16. seja, 9. 6. 1994 – Dušan Bravničar, Franc Konobelj. *Poročevalec Državnega zbora Republike Slovenije* **1996**, 42, 38–39.
61. Z. Čepič, Od Inštituta za zgodovino delavskega gibanja do Inštituta za novejšo zgodovino. V: Zgodovinske pisane v zrcalu zgodovine: 50 let Inštituta za novejšo zgodovino, ur. A. Gabrič. Ljubljana: Inštitut za novejšo zgodovino, str. 49–126, **2009**.
62. T. Kukovica, Gledanje med vrsticami, Sladka lažnost demokratičnega bivanja. *Gorenjski glas*, 9.3.1991, str. 12.
63. M. Kocjan-Barle, Pogovor z Mitjem Sarkom, *Nova revija* **1994**, 143, 58–87.
64. M. Jevnikar, Torkar Igor. V: Primorski Slovenski biografski leksikon, 16. snopič, ur. M. Jevnikar, Gorica: Goriška Mohorjeva družba, **1990**, str. 32–34.
65. F. Derganc, Kakor tujca, Zgodba iz življenja. *Dolenjski list* **1991**, 41 (19), 8. (datum objave 10. 5. 1991)
66. F. Pivec, Osamosvajanje študentske skupnosti. Slovensko študentsko gibanje v šestdesetih letih. V: Slovenija – Jugoslavija, krize in reforme 1968/1988 (ur. Zdenko Čepič). Ljubljana: Inštitut za novejšo zgodovino, **2010**, str. 295–304.
67. R. Ivelja, Usoda na smrt obsojenih še vedno ovita v skrivnost. *Dnevnik*, 26. 4. **2003**. Dostopno na <https://www.dnevnik.si/49206> (datum ogleda 3. 6. 2021).
68. R. Kocjančič, Kot so bili montirani dachauski procesi, tako so bile montirane tudi rehabilitacije obsojencev (2.), *Reporter*, 1. 6. **2015**. Dostopno na <https://reporter.si/clanek/kolumnisti/rudi-kocjancic-kot-so-bili-montirani-dachauski-procesi-tako-so-bile-montirane-tudi-rehabilitacije-obsojencev-2-480347> (datum ogleda 3. 6. 2021).
69. T. Wraber, Poročilo o delu 1. komisije za rehabilitacijo univerzitetnih učiteljev, Univerza v Ljubljani, Objave 6/2000, 11.
70. P. Weindling, A. von Villiez, A. Loewenau, N. Farron, The victims of unethical human experiments and coerced research under National Socialism. *Endeavour* **2016**, 40(1), 1–6. DOI:10.1016/j.endeavour.2015.10.005
71. P. Pahor, Kraigherjeva živela vsak na svojem koncu. *Dnevnik*, 29. 10. **2011**. Dostopno na <https://www.dnevnik.si/1042484192> (datum ogleda 3. 6. 2021).
72. P. Weindling: Victims and Survivors of Nazi Human Experiments: Science and Suffering in the Holocaust. London: Bloomsbury Academic, **2015**.

## Abstract

At the University of Ljubljana, Boris Krajnc was the first habilitated teacher to cover the subject of biochemistry: he was appointed on January 5, 1946. However, Krajnc's life ended abruptly. He was arrested on October 17, 1947 and sentenced to death on April 26, 1948 in the mounted Dachau Trial in Ljubljana. He was reportedly shot on May 12, 1948, at the age of 34. The life story of Boris Krajnc is closely linked to the work of several Slovenian chemists who were selected as prisoners at Dachau Concentration Camp to provide technical assistance in human experiments or in the clinical laboratory of the camp hospital. In the post-war period Dachau Trials in Ljubljana, a total of 8 chemists were convicted, 5 of whom were sentenced to death and executed by firing squad. In later evaluations of Dachau Trials it turned out that the charges were constructed and the confessions were obtained by cruel interrogation methods, therefore all judgements were annulled. After the emigration of the enzymologist Richard Klemen (1942) and the expulsion of Maks Samec and Marta Blinc from the university (1945), Boris Krajnc was to supervise biochemistry at the Technical Faculty. After his death, the lecturer of biochemistry was Dušan Stucin from the Medical Faculty. Later, biochemistry was absent from the chemistry curriculum for several years.



## POROČILO PREDSEDNIKA SLOVENSKEGA KEMIJSKEGA DRUŠTVA O DELU DRUŠTVA V LETU 2020

V letu 2020 je bilo društvo aktivno na številnih področjih. Izvajali smo redne letne aktivnosti, pri katerih je bil glavni poudarek na rednem izdajanju društvene revije *Acta Chimica Slovenica* (ACSi) ter organizaciji največjega letnega dogodka društva, konference "Slovenski kemijski dnevi 2020" in EFCATS poletne šole.

**Slovenski kemijski dnevi 2020** so bili organizirani v Portorožu, v Kongresnem centru Grand hotela Bernardin, in sicer v dneh od 16. do 18. septembra 2020. Programskemu in organizacijskemu odboru je predsedoval predsednik društva, znan. svet. dr. Albin Pintar, skupaj s člani odbora v zasedbi prof. dr. Romana Cerc-Korošec, prof. dr. Zorka Novak Pintarič, prof. dr. Darja Lisjak, doc. dr. Matic Lozinšek, prof. dr. Matjaž Valant in dr. Silvo Zupančič. Na posvetovanju je bilo predstavljenih več kot 120 prispevkov v obliki predavanj in posterjev. Delo je potekalo plenarno in v dveh vzporednih sekcijah. Udeleženci konference so bili zelo zadovoljni s kakovostjo znanstvenih in strokovnih prispevkov ter spremljevalnim programom srečanja. Na konferenci je sodelovalo 17 razstavljalcev. Sponzorji dogodka so bili abcr GmbH, Mikro+polo, Hidden Analytical, Primakem, Omega, Optik instruments, Krka, Chemass, Mettler Toledo in Laboratorijum. Objavili smo Zbornik povzetkov konference, ki je dostopen na USB ključu ter na voljo v NUK-u in strokovnih knjižnicah po Sloveniji. Plenarni predavatelji so bili prof. **dr. Nives Ogrinc** (Institut "Jožef Stefan", Ljubljana), **prof. dr. Klaus Müllen** (Max-Planck-Institut für Polymerforschung, Mainz, Nemčija) in **prof. dr. Bert Weckhuysen** (Univerza Utrecht, Nizozemska). Poleg treh plenarnih predavanj so udeleženci poslušali šest »keynote« vabljenih predavanj, ki so jih izvedli **prof. dr. Iztok Arčon** (Univerza v Novi Gorici), **prof. dr. Andreja Benčan Golob** (Institut "Jožef Stefan", Ljubljana), **izr. prof. dr. Nejc Hodnik** (Kemijski inštitut, Ljubljana), **prof. dr. Ksenija Kogej** (Fakulteta za kemijo in kemijsko tehnologijo, Univerza v Ljubljani), **prof. dr. Marjana Simonič** (Fakulteta za kemijo in kemijsko tehnologijo, Univerza v Mariboru) in **dr. Krunoslav Užarevič** (Inštitut Ruđer Bošković v Zagrebu, Hrvaška). Podelili smo nagrade študentom za najboljša predavanja in posterske predstavitve.

V letu 2020 smo v reviji *Acta Chimica Slovenica* (ACSi) izdali 4 številke revije, v katerih je bilo skupaj objavljenih 133 originalnih znanstvenih člankov na skupno 1147 straneh z dvokolonskim tiskom. Članki pokrivajo vsa področja kemije, kemije materialov in kemijskega in biokemijskega inženirstva. Spremembe uredniške politike in s tem vsebine revije ni bilo. Od objavljenih člankov so bili trije tako imenovani »Feature Articles« (FA) in eden »Review Article« (RA). Vsi članki so objavljeni na spletu in prosto dostopni. Člani Slovenskega kemijskega društva in avtorji člankov prejmejo elektronsko obvestilo o izidu nove številke. Vseh člankov, ki so bili leta 2019 oddani v ure-

dniški sistem, je bilo 828, kar pomeni, da jih je bilo na koncu sprejetih okoli 16 %. Za namene promocije revije so člani uredniškega odbora izdelali predstavitveno zgibaniko. Prvič smo jo zainteresirani javnosti razdelili na srečanju Slovenski kemijski dnevi v Portorožu septembra 2020. V letu 2020 se je uredniškemu odboru na področju »Analizna kemija«, kjer je število oddanih člankov med najvišjimi, pridružil dodaten urednik, dr. Alen Albreht. S tem smo pospešili obravnavo člankov na tem področju. Reviji ACSi se vztrajno viša faktor vpliva. Za leto 2019 je faktor vpliva zrastel na 1,223 (iz 1,076 v letu 2018). Spremembe uredniške politike in s tem vsebine revije ni bilo, zato v letu 2021 nadaljujemo po isti poti.

V društvenih vesteh smo objavili seznam diplomskih, magistrskih in doktorskih del FKKT UL, FKKT UM ter podiplomskega študijskega programa »Znanosti o okolju« Fakultete za znanosti okolju, UNG v letu 2019. Na slovenskih straneh revije je bil objavljen tudi koledar važnejših znanstvenih srečanj, a je bil v letu 2020 zelo okrnjen zaradi vplivov pandemije COVID-19 na organizacijo tovrstnih dogodkov. Objavili smo tudi letna poročila sekcij. V letu 2020 so društvene vesti obsegale 105 strani. Na društvenih straneh sta bila poleg ostalih novic objavljena dva zanimiva strokovna članka avtorja dr. M. Dolinarja in predstavitev nove znanstvene monografije avtorjev dr. J. Faganelija ter dr. A. Malej.

Zahvaljujem se tudi vsem inštitucijam, ki so v letu 2020 finančno podprle izdajanje revije *Acta Chimica Slovenica*. Te so Fakulteta za kemijo in kemijsko tehnologijo Univerze v Ljubljani, Fakulteta za kemijo in kemijsko tehnologijo Univerze v Mariboru, Kemijski inštitut in Inštitut »Jožef Stefan«. Sponzorja revije sta bila z objavo oglasa Donau Lab d.o.o. Ljubljana in Helios Domžale, d.o.o.

V letu 2020 smo nadaljevali z aktivnostmi za pridobivanje novih članov. Medse smo jih privabili 23, od tega 16 študentov. Za ta namen smo že konec leta 2017 pričeli s prenovno grafične podobe društva ter s pomočjo grafične oblikovalke izdelali plakate, ki nagovarjajo nove člane k vpisu. Plakate smo razobesili po številnih inštitucijah, s to aktivnostjo smo nadaljevali tudi v letu 2020. Za nove člane smo uvedli simbolno darilo (reprezentančne kemične svinčnike) ob njihovem vpisu v društvo. Člane smo o aktivnostih v letu 2020 še pogosteje obveščali preko elektronske pošte in preko spletne strani društva, za namene promocije in obveščanja pa prav tako tudi preko vzpostavljenih Facebook in Twitter profilov društva, ki sta hitro in dobro zaživela.

Člani Slovenskega kemijskega društva so bili dejavni tudi **na področju mednarodnega sodelovanja**. Predvsem je potrebno omeniti članstvo društva v mednarodnih združenjih IUPAC, ECTN, IUCr, EURACHEM, EuChemS, EFCE, EPF, ECA in EFCATS.

V letu 2019 smo pridobili tudi organizacijo poletne šole Evropske federacije katalitskih združenj (EFCATS), ki smo jo izpeljali septembra letos sočasno s konferenco »Slovenski kemijski dnevi 2020« v Portorožu in sicer od 15. – 19. septembra 2020. Poletna šola je potekala pod naslovom **“ENGINEERING MATERIALS FOR CATALYSIS”**. Organizirali smo jo skupaj z Avstrijskim katalitskim združenjem. Privabila je preko 90 študentov in mladih doktorjev. Poletna šola je potekala na hibriden način, saj se vsi prijavljeni udeleženci, zaradi epidemije COVID-19, niso mogli udeležiti šole v živo.

Društvo se je v letu 2020 uspešno prijavilo na Javni razpis ARRS za sofinanciranje delovanja v mednarodnih znanstvenih združenjih v letu 2020, kjer smo bili uspešni pri vseh oddanih vlogah.

*V Ljubljani, dne 17. marca 2021*

*znan. svet. dr. Albin Pintar predsednik društva*



## Poročilo Sekcije za kristalografijo za leto 2020

Podobno kot vse druge dejavnosti, je tudi delo Sekcije za kristalografijo pri Slovenskem kemijskem društvu v letu 2020 zaznamovala pandemija COVID-19.

V prvih dveh mesecih so sicer po ustaljenem postopku potekale priprave na tradicionalno Hrvaško-Slovensko kristalografsko srečanje z mednarodno udeležbo, ki bi moralo biti junija 2020 v Rabcu. Člani sekcije smo, kot običajno, sodelovali v organizacijskem odboru, ki je mednaroden (poleg slovenskih in hrvaških so vključeni tudi kristalografi iz tretjih držav). Program je bil že sestavljen, povabili smo plenarne predavatelje in se s sponzorji dogovorili za sodelovanje, potem pa je marca nastopila negotovost zaradi naglega širjenja COVID-19 po svetu in po zgledu svetovne in evropske kristalografske zveze, s katerima smo tudi redno sodelovali dopisno in na sejah preko videokonferenčnih orodij, smo izvedbo srečanja preložili na čas po pandemiji.

Preloženi so bili svetovni kristalografski kongres, evropsko kristalografsko srečanje in evropska konferenca o praškovni difrakciji. Slednja bi morala biti v Šibeniku v maju 2020, organizirajo jo kolegi iz Hrvaške, nekateri člani Sekcije za kristalografijo pri Slovenskem kemijskem društvu sodelujemo kot svetovalci

V času pisanja tega poročila je že znano, da bo letos (avgusta 2021) potekal svetovni kristalografski kongres v Pragi na hibridni način. Zasedanj skupščine svetovne kristalografske zveze se bom kot nacionalni predstavnik udeležil na daljavo, enako zasedanja skupščine evropske kristalografske zveze. Usoda hrvaško-slovenskega kristalografskega srečanja je še negotova, evropska konferenca o praškovni difrakciji pa naj bi se v živo izvedla v Šibeniku letos jeseni.

*prof. dr. Anton Meden*

## Sekcija za analizno kemijo

Osnovna dejavnost sekcije za Analizno kemijo v okviru Slovenskega kemijskega društva je organiziranje mednarodnih in domačih znanstvenih ter strokovnih srečanj, predavanj domačih in tujih strokovnjakov ter izvedba različnih delavnic. Člani sekcije pa sodelujejo tudi znotraj delovnih skupin Eurachem in drugih združenj v evropskem prostoru (DAC, FECS) in tako pomembno prispevajo k prepoznavnosti Slovenskega kemijskega društva.

Delo sekcije za Analizno kemijo je bilo v letu 2020 popolnoma v znamenju epidemije Sars-Covid 19, kar je v praksi pomenilo, da se je večina dogodkov preselila v novo obliko – popolnoma digitalizirano spletno okolje ali pa so bili odpovedani oz. prestavljeni. Takšno usodo je doletelo tudi tradicionalno mednarodno srečanje podiplomskih študentov in njihovih mentorjev YISAC (Young Investigators Seminar on Analytical Chemistry), ki bi moralo pote-

kati junija 2020 na Univerzi v Lodzu na Poljskem. Ker srečanja junija in septembra ni bilo mogoče organizirati, je obveljala dokončna odpoved. Izvedba naslednje konference Yisac je tako planirana v Beogradu leta 2021. Med redkimi aktivnostmi sekcije, ki so bile izvedene, kot običajno, velja izpostaviti 26. jubilejno konferenco »Slovenski kemijski dnevi 2020«, ki se je odvijala septembra 2020 v Portorožu. Posebej vzpodbudna je številčna aktivna udeležba mlajših kolegov iz različnih institucij, ki so na zavidljivem nivoju predstavili raznolike in zanimive raziskave na področju elektrokemije, materialov, okolja, spektroskopije in kromatografije.

V prihodnje želimo v sekcijo aktivno vključiti mlajše kolege in nadaljevati z organizacijo domačih ter tujih srečanj, predavanj in konferenc. Posebej želimo okrepiti povezovanje pri prenosu znanja iz univerzitetnih in raziskovalnih laboratorijev v industrijo.

*Mitja Kolar*

## Poročilo Sekcije za keramiko za leto 2020

V okviru založbe Elsevier je v letu 2020 začela izhajati nova mednarodna recenzirana revija Evropskega keramičnega združenja (ECerS) Open Ceramics, katere glavni urednik je prof. Paolo Colombo. Gre za hčerinsko revijo odprtega tipa vodilne revije s keramičnega področja Journal of the European Ceramic Society (JECS). Open Ceramics objavlja rezultate izvirnih raziskav, kakor tudi pregledne znanstvene članke in razglede, vezane na vse vrste keramičnih materialov, od tradicionalne do napredne keramike, od stekel do ognjevzdržnih materialov, od biokeramike do kompozitov s keramično matrico. Revija obsega rezultate raziskav, ki se osredotočajo na surovine, prahove, vlakna, prevleke, sintrane komponente ali porozne strukture. Dobrodošli so prispevki, ki se ukvarjajo z bazičnimi aspekti ali uporabnimi raziskavami ter podajajo teoretične in eksperimentalne rezultate dela. Poudarek je na prihajajočem znanstvenem ali tehnološkem razvoju, ki podaja razmerje med procesiranjem, mikrostrukturno in lastnostmi keramike, stekel in drugih nekovinskih anorganskih materialov, pa tudi njihovo sintezo, izdelavo in uporabo. Revija je namenjena široki javnosti, od akademskih krogov do industrije. Revija je lansirala številne posebne izdaje, da bi takoj pritegnila čim več kvalitetnih objav. Eno izmed bolj uspešnih po številu prejetih in objavljenih člankov je bila posebna izdaja »Young Ceramists in the Spotlight«, pri kateri je bil eden od gostujočih urednikov tudi doc. dr. Andraž Kocjan z Inštituta »Jožef Stefan«.

V okviru delovanja ECerS-ove mreže mladih keramikov Young Ceramists Network (YCN), ki se praviloma oglašuje preko socialnih omrežij in predstavitev na konferencah, je bila izpeljana serija webinarjev. V letu 2020 sta bila izpeljana dva. Serijo je otvoril glavni urednik JECS prof. Richard Todd z webinarjem na temo kako uspešno objaviti znanstveni članek. Sledil je webinar na temo krožnega gospodarstva z gostoma Carlos Velazquez (Direktor Sustainability - ROCA Group) in Francisco Veiga Simão (štipendist sheme Marie Curie). Vsak webinar je imel okoli 100 gledalcev. Organizacija webinarjev je bila kot odgovor na situacijo pandemije COVID-19, zaradi katere je odpadla planirana YCN-jeva druga delavnica za mreženje mladih keramikov, ki bi morala biti izpeljana v portugalski Viana do Castelo. YCN je področje oglaševanja in informi-

ranja razširil iz že obstoječe spletne strani (<https://youngceramists.eu/>), LinkedIn ter Facebook platform še na Instagram ter Twitter. Celokupno ima že več kot 1700 članov/sledilcev po celem svetu.

Na področju keramičnih materialov je bila v letu 2020 v okviru Evropskega keramičnega združenja organizirana konferenca Electroceramics XVII, ki je zaradi pandemije COVID-19 potekala prvič in v celoti virtualno in sicer med 24. in 28. 8. 2020. Konferenci sta predsedovala Jurij Koruza in Andreas Klein iz TU Darmstadt, Nemčija. Po številu prispevkov je bila konferenca primerljiva s prejšnjimi leti, s 325 udeleženci iz 41 držav, kar v oteženih razmerah organizacije znanstvenih srečanj predstavlja velik uspeh. Izpeljana je bila še yCAM, konferenca mladih keramikov, ki se ukvarja z aditivnim oblikovanjem keramike. Tudi slednja je potekala v celoti virtualno med 28. in 30. 10. 2020.

Evropsko keramično združenje sporoča, da so XVII Konferenca in razstava ECerS, 9. Mednarodna konferenca o keramiki (ICC9) in konferenca Electroceramics XVIII načrtovane kot skupna konferenca v Krakovu na Poljskem od 10. do 14. julija 2022. Na ta način se bo pomagalo pri reševanju problema prestavljanja številnih konferenc v leto 2022, kot posledica pandemije COVID-19. Skupna konferenca se bo imenovala »Keramika v Evropi 2022« in bo organizirana kot ena konferenca s skupnimi znanstvenimi simpoziji o keramiki, pa tudi z nekaterimi posebnimi tematikami, povezanimi z vsebinami združenih konferenc. Skupno organizacijo podpirajo Evropsko keramično združenje, Mednarodna keramična zveza (ICF), Fraunhofer IKTS in Elektrokeramična mreža združenja ECerS. Tekmovanje predstavitev najboljših študentov (Student Speech Contest), izbranih predstavnikov pridruženih članic ECerS, ki poteka vsake dve leti v okviru konference ECerS, ki je bila v letu 2020 odpovedana, bo izpeljano v letu 2021 v okviru bienalne konference mladih keramikov, ki poteka jeseni v srbskem Novem Sadu. Če bo konferenca odpovedana, bo tekmovanje izpeljana virtualno. Slovenijo bo zastopala Hermina Hudelja, doktorandka z Odseka za Nanostrukturne materiale Inštituta Jožef Stefan.

*doc. dr. Matjaž Spreitzer in  
doc. dr. Andraž Kocjan*



# Acta Chimica Slovenica

## Author Guidelines

### Submissions

Submission to ACSi is made with the implicit understanding that neither the manuscript nor the essence of its content has been published in whole or in part and that it is not being considered for publication elsewhere. All the listed authors should have agreed on the content and the corresponding (submitting) author is responsible for having ensured that this agreement has been reached. The acceptance of an article is based entirely on its scientific merit, as judged by peer review. There are no page charges for publishing articles in ACSi. The authors are asked to read the Author Guidelines carefully to gain an overview and assess if their manuscript is suitable for ACSi.

### Additional information

- Citing spectral and analytical data
- Depositing X-ray data

### Submission material

Typical submission consists of:

- full manuscript (PDF file, with title, authors, abstract, keywords, figures and tables embedded, and references)
- supplementary files
  - **Full manuscript** (original Word file)
  - **Statement of novelty** (Word file)
  - **List of suggested reviewers** (Word file)
  - **ZIP file containing graphics** (figures, illustrations, images, photographs)
  - **Graphical abstract** (single graphics file)
  - **Proposed cover picture** (optional, single graphics file)
  - **Appendices** (optional, Word files, graphics files)

Incomplete or not properly prepared submissions will be rejected.

### Submission process

Before submission, authors should go through the checklist at the bottom of the page and prepare for submission.

Submission process consists of 5 steps.

#### Step 1: Starting the submission

- Choose one of the journal sections.
- Confirm all the requirements of the **checklist**.
- Additional plain text comments for the editor can be provided in the relevant text field.

#### Step 2: Upload submission

- Upload full manuscript in the form of a Word file (with title, authors, abstract, keywords, figures and tables embedded, and references).

#### Step 3: Enter metadata

- First name, last name, contact email and affiliation for all authors, in relevant order, must be provided. Corresponding author has to be selected. Full postal address and phone number of the corresponding author has to be provided.

- **Title and abstract** must be provided in plain text.
- Keywords must be provided (max. 6, separated by semicolons).
- Data about contributors and supporting agencies may be entered.
- **References** in plain text must be provided in the relevant text filed.

#### Step 4: Upload supplementary files

- Original Word file (original of the PDF uploaded in the step 2)
- **List of suggested reviewers** with at least five reviewers with two recent references from the field of submitted manuscript must be uploaded as a Word file. At the same time, authors should declare (i) that they have no conflict of interest with suggested reviewers and (ii) that suggested reviewers are experts in the field of the submitted manuscript.
- All **graphics** have to be uploaded in a single ZIP file. Graphics should be named Figure 1.jpg, Figure 2.eps, etc.
- **Graphical abstract image** must be uploaded separately
- **Proposed cover picture** (optional) should be uploaded separately.
- Any additional **appendices** (optional) to the paper may be uploaded. Appendices may be published as a supplementary material to the paper, if accepted.
- For each uploaded file the author is asked for additional metadata which may be provided. Depending of the type of the file please provide the relevant title (Statement of novelty, List of suggested reviewers, Figures, Graphical abstract, Proposed cover picture, Appendix).

#### Step 5: Confirmation

- Final confirmation is required.

### Article Types

**Feature Articles** are contributions that are written on editor's invitation. They should be clear and concise summaries of the most recent activity of the author and his/her research group written with the broad scope of ACSi in mind. They are intended to be general overviews of the authors' subfield of research but should be written in a way that engages and informs scientists in other areas. They should contain the following (see also general directions for article structure in ACSi below): (1) an introduction that acquaints readers with the authors' research field and outlines the important questions to which answers are being sought; (2) interesting, new, and recent contributions of the author(s) to the field; and (3) a summary that presents possible future directions. Manuscripts normally should not exceed 40 pages of one column format (letter size 12, 33 lines per page). Generally, experts in a field who have made important contribution to a specific topic in recent years will be invited by an editor to contribute such an **Invited Feature Article**. Individuals may, however, send a proposal (one-page



maximum) for an Invited Feature Article to the Editor-in-Chief for consideration.

**Scientific articles** should report significant and innovative achievements in chemistry and related sciences and should exhibit a high level of originality. They should have the following structure:

1. Title (max. 150 characters),
2. Authors and affiliations,
3. Abstract (max. 1000 characters),
4. Keywords (max. 6),
5. Introduction,
6. Experimental,
7. Results and Discussion,
8. Conclusions,
9. Acknowledgements,
10. References.

The sections should be arranged in the sequence generally accepted for publications in the respective fields and should be successively numbered.

**Short communications** generally follow the same order of sections as Scientific articles, but should be short (max. 2500 words) and report a significant aspect of research work meriting separate publication. Editors may decide that a Scientific paper is categorized as a Short Communication if its length is short.

**Technical articles** report applications of an already described innovation. Typically, technical articles are not based on new experiments.

## Preparation of Submissions

**Text** of the submitted articles must be prepared with Microsoft Word. Normal style set to single column, 1.5 line spacing, and 12 pt Times New Roman font is recommended. Line numbering (continuous, for the whole document) must be enabled to simplify the reviewing process. For any other format, please consult the editor. Articles should be written in English. Correct spelling and grammar are the sole responsibility of the author(s). Papers should be written in a concise and succinct manner. The authors shall respect the ISO 80000 standard [1], and IUPAC Green Book [2] rules on the names and symbols of quantities and units. The Système International d'Unités (SI) must be used for all dimensional quantities.

**Graphics** (figures, graphs, illustrations, digital images, photographs) should be inserted in the text where appropriate. The captions should be self-explanatory. Lettering should be readable (suggested 8 point Arial font) with equal size in all figures. Use common programs such as MS Excel or similar to prepare figures (graphs) and ChemDraw to prepare structures in their final size. Width of graphs in the manuscript should be 8 cm. Only in special cases (in case of numerous data, visibility issues) graphs can be 17 cm wide. All graphs in the manuscript should be inserted in relevant places and **aligned left**. The same graphs should be provided separately as images of appropriate resolution (see below) and submitted together in a ZIP file (Graphics ZIP). Please do not submit figures as a Word file. In **graphs**, only the graph area determined by both axes should be in the frame, while a frame around the whole graph should be omitted. The graph area should be white. The legend should be inside the graph area. The style of all graphs should be the same. **Figures and illustrations** should be of sufficient quality for the

printed version, i.e. 300 dpi minimum. **Digital images and photographs** should be of high quality (minimum 250 dpi resolution). On submission, figures should be of good enough resolution to be assessed by the referees, ideally as JPEGs. High-resolution figures (in JPEG, TIFF, or EPS format) might be required if the paper is accepted for publication.

**Tables** should be prepared in the Word file of the paper as usual Word tables. The captions should appear above the table and should be self-explanatory.

**References** should be numbered and ordered sequentially as they appear in the text, likewise methods, tables, figure captions. When cited in the text, reference numbers should be superscripted, following punctuation marks. It is the sole responsibility of authors to cite articles that have been submitted to a journal or were in print at the time of submission to ACSi. Formatting of references to published work should follow the journal style; please also consult a recent issue:

1. J. W. Smith, A. G. White, *Acta Chim. Slov.* **2008**, *55*, 1055–1059.
2. M. F. Kemmere, T. F. Keurentjes, in: S. P. Nunes, K. V. Peinemann (Ed.): *Membrane Technology in the Chemical Industry*, Wiley-VCH, Weinheim, Germany, **2008**, pp. 229–255.
3. J. Levec, Arrangement and process for oxidizing an aqueous medium, US Patent Number 5,928,521, date of patent July 27, **1999**.
4. L. A. Bursill, J. M. Thomas, in: R. Sersale, C. Collela, R. Aiello (Eds.), *Recent Progress Report and Discussions: 5th International Zeolite Conference*, Naples, Italy, 1980, Gianini, Naples, **1981**, pp. 25–30.
5. J. Szegezdi, F. Csizmadia, Prediction of dissociation constant using microconstants, [http://www.chemaxon.com/conf/Prediction\\_of\\_dissociation\\_constant\\_using\\_microconstants.pdf](http://www.chemaxon.com/conf/Prediction_of_dissociation_constant_using_microconstants.pdf), (assessed: March 31, 2008)

Titles of journals should be abbreviated according to Chemical Abstracts Service Source Index (CASSI).

## Special Notes

- Complete characterization, **including crystal structure**, should be given when the synthesis of new compounds in crystal form is reported.
- Numerical **data should be reported with the number of significant digits corresponding to the magnitude** of experimental uncertainty.
- **The SI system of units and IUPAC recommendations** for nomenclature, symbols and abbreviations should be followed closely. Additionally, the authors should follow the general guidelines when citing spectral and analytical data, and depositing crystallographic data.
- **Characters** should be correctly represented throughout the manuscript: for example, 1 (one) and l (ell), 0 (zero) and O (oh), x (ex), D7 (times sign), B0 (degree sign). Use Symbol font for all Greek letters and mathematical symbols.
- The rules and recommendations of the **IUBMB** and the **International Union of Pure and Applied Chemistry (IUPAC)** should be used for abbreviation of chemical names, nomenclature of chemical compounds, enzyme nomenclature, isotopic compounds, optically active isomers, and spectroscopic data.

- **A conflict of interest** occurs when an individual (author, reviewer, editor) or its organization is involved in multiple interests, one of which could possibly corrupt the motivation for an act in the other. Financial relationships are the most easily identifiable conflicts of interest, while conflicts can occur also as personal relationships, academic competition, etc. **The Editors** will make effort to ensure that conflicts of interest will not compromise the evaluation process; potential editors and reviewers will be asked to exempt themselves from review process when such conflict of interest exists. When the manuscript is submitted for publication, **the authors** are expected to disclose any relationships that might pose potential conflict of interest with respect to results reported in that manuscript. In the Acknowledgement section the source of funding support should be mentioned. The statement of disclosure must be provided as Comments to Editor during the submission process.
- **Published statement of Informed Consent.** Research described in papers submitted to ACSi must adhere to the principles of the Declaration of Helsinki (<http://www.wma.net/e/policy/b3.htm>). These studies must be approved by an appropriate institutional review board or committee, and informed consent must be obtained from subjects. The Methods section of the paper must include: 1) a statement of protocol approval from an institutional review board or committee and 2), a statement that informed consent was obtained from the human subjects or their representatives.
- **Published Statement of Human and Animal Rights.** When reporting experiments on human subjects, authors should indicate whether the procedures followed were in accordance with the ethical standards of the responsible committee on human experimentation (institutional and national) and with the Helsinki Declaration of 1975, as revised in 2008. If doubt exists whether the research was conducted in accordance with the Helsinki Declaration, the authors must explain the rationale for their approach and demonstrate that the institutional review body explicitly approved the doubtful aspects of the study. When reporting experiments on animals, authors should indicate whether the institutional and national guide for the care and use of laboratory animals was followed.
- To avoid conflict of interest between authors and referees we expect that not more than one referee is from the same country as the corresponding author(s), however, not from the same institution.
- Contributions authored by **Slovenian scientists** are evaluated by non-Slovenian referees.
- Papers describing **microwave-assisted reactions** performed in domestic microwave ovens are not considered for publication in *Acta Chimica Slovenica*.
- *Manuscripts that are not prepared and submitted in accord with the instructions for authors are not considered for publication.*

## Appendices

Authors are encouraged to make use of supporting information for publication, which is supplementary ma-

terial (appendices) that is submitted at the same time as the manuscript. It is made available on the Journal's web site and is linked to the article in the Journal's Web edition. The use of supporting information is particularly appropriate for presenting additional graphs, spectra, tables and discussion and is more likely to be of interest to specialists than to general readers. When preparing supporting information, authors should keep in mind that the supporting information files will not be edited by the editorial staff. In addition, the files should be not too large (upper limit 10 MB) and should be provided in common widely known file formats to be accessible to readers without difficulty. All files of supplementary materials are loaded separately during the submission process as supplementary files.

## Proposed Cover Picture and Graphical Abstract Image

**Graphical content:** an ideally full-colour illustration of resolution 300 dpi from the manuscript must be proposed with the submission. Graphical abstract pictures are printed in size 6.5 x 4 cm (hence minimal resolution of 770 x 470 pixels). Cover picture is printed in size 11 x 9.5 cm (hence minimal resolution of 1300 x 1130 pixels)

Authors are encouraged to submit illustrations as candidates for the journal Cover Picture\*. The illustration must be related to the subject matter of the paper. Usually both proposed cover picture and graphical abstract are the same, but authors may provide different pictures as well.

\* The authors will be asked to contribute to the costs of the cover picture production.

### Statement of novelty

Statement of novelty is provided in a Word file and submitted as a supplementary file in step 4 of submission process. Authors should in no more than 100 words emphasize the scientific novelty of the presented research. Do not repeat for this purpose the content of your abstract.

### List of suggested reviewers

List of suggested reviewers is a Word file submitted as a supplementary file in step 4 of submission process. Authors should propose the names, full affiliation (department, institution, city and country) and e-mail addresses of five potential referees. Field of expertise and at least two references relevant to the scientific field of the submitted manuscript must be provided for each of the suggested reviewers. The referees should be knowledgeable about the subject but have no close connection with any of the authors. In addition, referees should be from institutions other than (and countries other than) those of any of the authors. Authors declare no conflict of interest with suggested reviewers. Authors declare that suggested reviewers are experts in the field of submitted manuscript.

## How to Submit

Users registered in the role of author can start submission by choosing USER HOME link on the top of the page, then choosing the role of the Author and follow the relevant link for starting the submission process. Prior to submission we strongly recommend that you familiarize yourself with the ACSi style by browsing the journal, particularly if you have not submitted to the ACSi before or recently.

## Correspondence

All correspondence with the ACSi editor regarding the paper goes through this web site and emails. Emails are sent and recorded in the web site database. In the correspondence with the editorial office please provide ID number of your manuscript. All emails you receive from the system contain relevant links. **Please do not answer the emails directly but use the embedded links in the emails for carrying out relevant actions.** Alternatively, you can carry out all the actions and correspondence through the online system by logging in and selecting relevant options.

## Proofs

Proofs will be dispatched via e-mail and corrections should be returned to the editor by e-mail as quickly as possible, normally within 48 hours of receipt. Typing errors should be corrected; other changes of contents will be treated as new submissions.

## Submission Preparation Checklist

As part of the submission process, authors are required to check off their submission's compliance with all of the following items, and submissions may be returned to authors that do not adhere to these guidelines.

1. The submission has not been previously published, nor is it under consideration for publication in any other journal (or an explanation has been provided in Comments to the Editor).
2. All the listed authors have agreed on the content and the corresponding (submitting) author is responsible for having ensured that this agreement has been reached.
3. The submission files are in the correct format: manuscript is created in MS Word but will be **submitted in PDF** (for reviewers) as well as in original MS Word format (as a supplementary file for technical editing); diagrams and graphs are created in Excel and saved in one of the file formats: TIFF, EPS or JPG; illustrations are also saved in one of these formats. The preferred position of graphic files in a document is to embed them close to the place where they are mentioned in the text (See **Author guidelines** for details).
4. The manuscript has been examined for spelling and grammar (spell checked).
5. The **title** (maximum 150 characters) briefly explains the contents of the manuscript.
6. Full names (first and last) of all authors together with the affiliation address are provided. Name of author(s) denoted as the corresponding author(s), together with their e-mail address, full postal address and telephone/fax numbers are given.
7. The **abstract** states the objective and conclusions of the research concisely in no more than 150 words.
8. Keywords (minimum three, maximum six) are provided.
9. **Statement of novelty** (maximum 100 words) clearly explaining new findings reported in the manuscript should be prepared as a separate Word file.
10. The text adheres to the stylistic and bibliographic requirements outlined in the **Author guidelines**.
11. Text in normal style is set to single column, 1.5 line spacing, and 12 pt. Times New Roman font is

recommended. All tables, figures and illustrations have appropriate captions and are placed within the text at the appropriate points.

12. Mathematical and chemical equations are provided in separate lines and numbered (Arabic numbers) consecutively in parenthesis at the end of the line. All equation numbers are (if necessary) appropriately included in the text. Corresponding numbers are checked.
13. Tables, Figures, illustrations, are prepared in correct format and resolution (see **Author guidelines**).
14. The lettering used in the figures and graphs do not vary greatly in size. The recommended lettering size is 8 point Arial.
15. Separate files for each figure and illustration are prepared. The names (numbers) of the separate files are the same as they appear in the text. All the figure files are packed for uploading in a single ZIP file.
16. Authors have read **special notes** and have accordingly prepared their manuscript (if necessary).
17. References in the text and in the References are correctly cited. (see **Author guidelines**). All references mentioned in the Reference list are cited in the text, and vice versa.
18. Permission has been obtained for use of copyrighted material from other sources (including the Web).
19. The names, full affiliation (department, institution, city and country), e-mail addresses and references of five potential referees from institutions other than (and countries other than) those of any of the authors are prepared in the word file. At least two relevant references (important recent papers with high impact factor, head positions of departments, labs, research groups, etc.) for each suggested reviewer must be provided. Authors declare no conflict of interest with suggested reviewers. Authors declare that suggested reviewers are experts in the field of submitted manuscript.
20. Full-colour illustration or graph from the manuscript is proposed for graphical abstract.
21. **Appendices** (if appropriate) as supplementary material are prepared and will be submitted at the same time as the manuscript.

## Privacy Statement

The names and email addresses entered in this journal site will be used exclusively for the stated purposes of this journal and will not be made available for any other purpose or to any other party.

ISSN: 1580-3155

---

## Koristni naslovi

---

Slovensko kemijsko društvo  
Slovenian Chemical Society



**Slovensko kemijsko društvo**

[www.chem-soc.si](http://www.chem-soc.si)

e-mail: [chem.soc@ki.si](mailto:chem.soc@ki.si)

---



**Wessex Institute of Technology**

[www.wessex.ac.uk](http://www.wessex.ac.uk)

---



**SETAC**

[www.setac.org](http://www.setac.org)

---



**European Water Association**

<http://www.ewa-online.eu/>

---



**European Science Foundation**

[www.esf.org](http://www.esf.org)

---



**European Federation of Chemical Engineering**

<https://efce.info/>

---



**I U P A C**

INTERNATIONAL UNION OF  
PURE AND APPLIED CHEMISTRY

**International Union of Pure and Applied Chemistry**

<https://iupac.org/>

---

---

## Novice evropske zveze kemijskih društev EuChemS najdete na:

---

 **EuChemS**  
European Chemical Society

**Brussels News Updates**

<http://www.euchems.eu/newsletters/>

---

**Kvaliteta vode Tip 1 do 3\***

\*v skladu s standardom ISO 3696 in ustreznimi ASTM ter CLSI



**DONAU LAB** Ljubljana  
Member of LPPgroup

Donau Lab d.o.o., Ljubljana  
Tbilisjska 85  
SI-1000 Ljubljana  
www.donaulab.si  
office-si@donaulab.com

# Sistemi za čisto in ultra čisto vodo QFRONT



**- 10 do 15 %**



# adrona







## Razvoj in inovacije za globalno uspešnost

Znanje, kreativnost zaposlenih in inovacije so ključnega pomena v okolju, kjer nastajajo Heliosovi pametni premazi. Z rešitvami, ki zadostijo široki paleti potreb, kontinuiranim razvojem ter s kakovostnimi produkti Helios predstavlja evropski center za inovacije, know-how in poslovni razvoj skupine Kansai Paint.

Part of  KANSAI  
PAINT







NATIONAL INSTITUTE OF CHEMISTRY **75**<sup>years</sup>

Hajdrihova 19,  
1000 Ljubljana  
Slovenia  
[www.ki.si](http://www.ki.si)



**research**  
**EXCELLENCE**

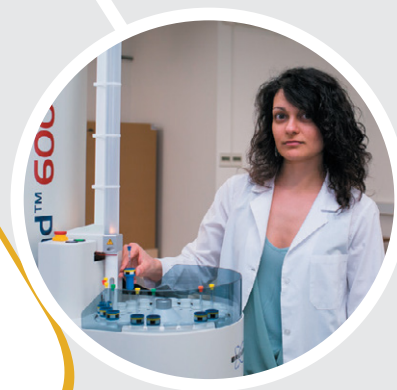


Basic and applied research in materials, life sciences, biotechnology, chemical engineering, structural and theoretical chemistry, analytical chemistry and environmental protection.

In line with EU research and innovation priorities: nanotechnology, genomics and biotechnology for health, sustainable development, climate change, energy efficiency and food quality and safety.

We expand knowledge and technology transfer to domestic and foreign chemical, automotive and nanobiotechnology industries.

We are aware of the power of youth, so we transfer our knowledge to younger generations and offer many opportunities for cooperation.



contact: [mladi@ki.si](mailto:mladi@ki.si)



# MAGNEZIJ Krka 300



## BODITE NEUSTAVLJIVI

Magnezij Krka 300 vsebuje **magnezijev citrat** in **vitamin B<sub>2</sub>**.

- ✓ Magnezij in vitamin B<sub>2</sub> prispevata k **zmanjševanju utrujenosti** in **izčrpanosti**.
- ✓ Magnezij prispeva tudi k **normalnemu delovanju mišic**.

[www.magnezijkrka.si](http://www.magnezijkrka.si)

Prehransko dopolnilo ni nadomestilo za uravnoteženo in raznovrstno prehrano. Skrbite tudi za zdrav življenjski slog.



 KRKA

# ActaChimicaSlovenica

## ActaChimicaSlovenica

Hetero-Diels-Alder reaction is among the most versatile tools in synthetic organic chemist's toolbox. Due to its potential for rapid generation of structural complexity in a stereospecific fashion, it has been frequently used to synthesize daunting members of the meroterpenoid class of natural products. One of the most recent examples is the total synthesis of (-)-epolone B (center structure). Page 247–267.



Year 2021, Vol. 68, No. 2

